

AD-A150 965

ANALYSIS OF SLABS-ON-GRADE FOR A VARIETY OF LOADING AND
SUPPORT CONDITION. (U) ILLINOIS UNIV AT URBANA DEPT OF
CIVIL ENGINEERING A M IOANNIDES ET AL. DEC 84

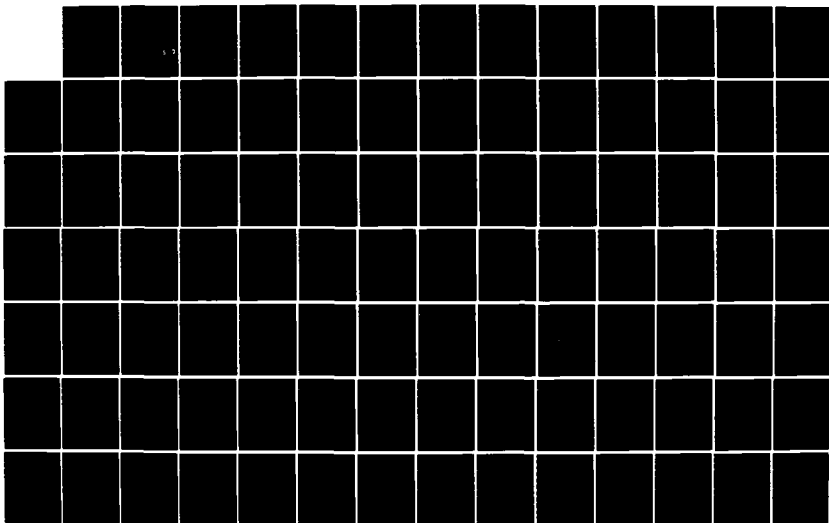
1/7

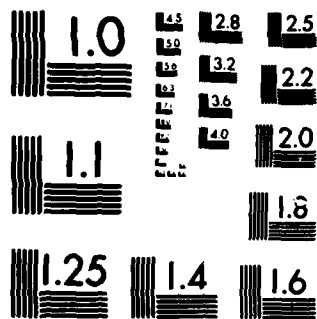
UNCLASSIFIED

AFOSR-TR-85-0083 AFOSR-84-0143

F/G 13/2

NL





MICROCOPY RESOLUTION TEST CHART
NATIONAL BUREAU OF STANDARDS-1963-A

REPRODUCED AT GOVERNMENT EXPENSE

AFOSR-TR- 85-0088

4

ANALYSIS OF SLABS-ON-GRADE
FOR A VARIETY OF LOADING AND SUPPORT CONDITIONS

(AFOSR-83-0143)

AD-A150 965

Submitted to

Air Force Office of Scientific Research (AFOSR)
Air Force Systems Command
United States Air Force
Bolling AFB, DC 20332

by

Department of Civil Engineering
University of Illinois at Urbana-Champaign
Urbana, Illinois 61801

Report Preparation by:

A. M. Ioannides
Dr. M. R. Thompson

J. Donnelly
Dr. E. J. Barenberg

Program Manager:

Lt. Col. Lawrence D. Hokanson

DTIC
ELECTE
MAR 4 1985
S B

December, 1984

Approved for Public Release; Distribution Unlimited

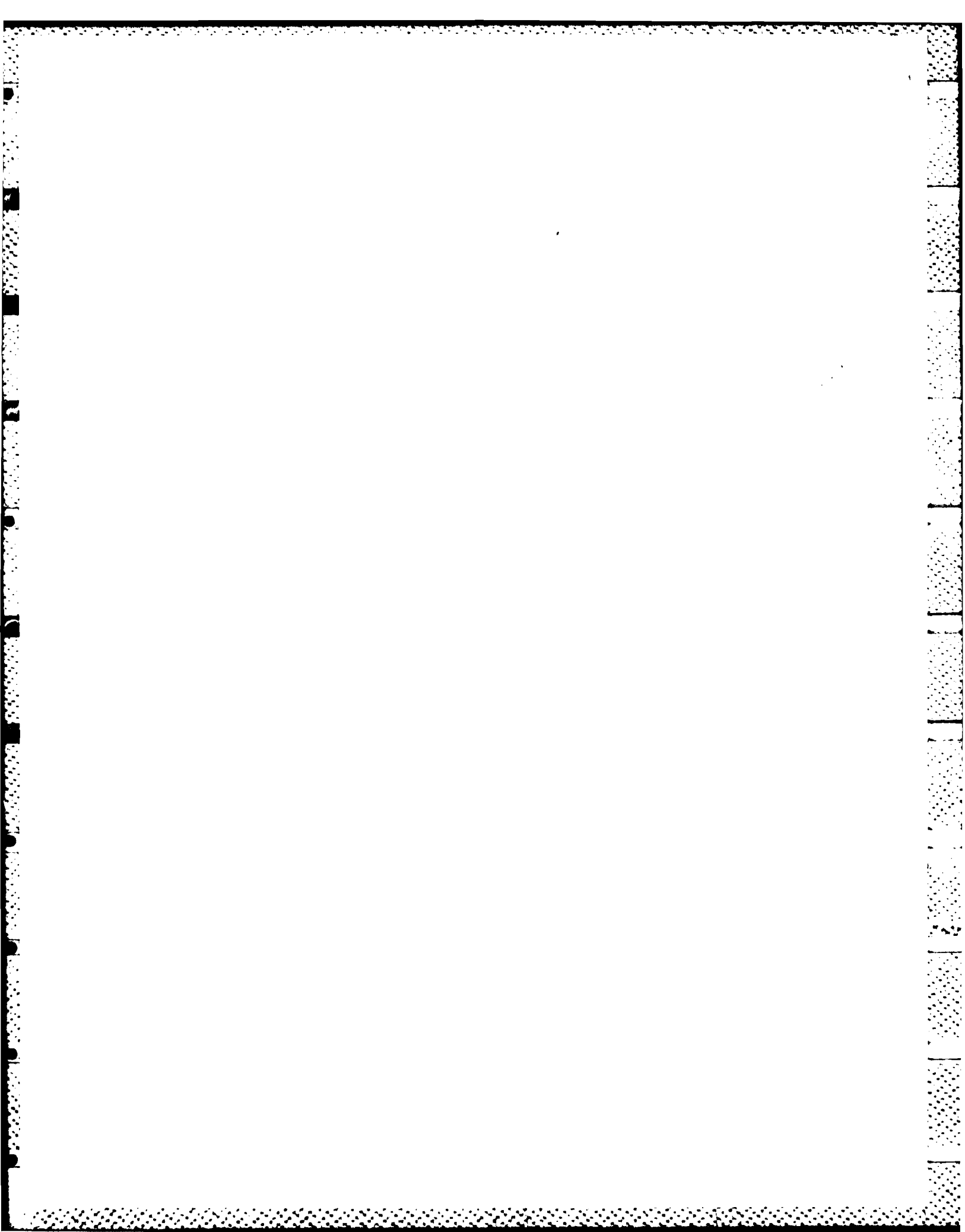
FILE COPY

85 02 12 196

Qualified requestors may obtain additional copies from the Defense Technical Information Service.

Conditions of Reproduction

Reproduction, translation, publication, use and disposal in whole or in part by or for the United States Government is permitted.



ACKNOWLEDGMENTS

This report was prepared as part of a Project entitled, "VALIDATION OF A STRESS-DEPENDENT FINITE ELEMENT SLAB MODEL". The Project is sponsored (Grant No. AFOSR-82-0143) by the Air Force Office of Scientific Research (AFOSR), Air Force Systems Command, Bolling AFB, DC.

Lt. Col. Lawrence D. Hokanson is the Program Manager.

DISCLAIMER

The contents of this report reflect the views of the authors who are responsible for the facts and the accuracy of the data presented herein. The contents do not necessarily reflect the official views or policies of the U. S. Air Force. This report does not constitute a standard, specification, or regulation.

(The reverse of this page is blank)

AIR FORCE OFFICE OF SCIENTIFIC RESEARCH (AFOSR)
NOTICE OF TRANSMITTAL TO DTIC
This technical report is approved and is
approved for publication under AFOSR 190-12.
Distribution is unlimited.
MATTHEW J. KEMPTER
Chief, Technical Information Division

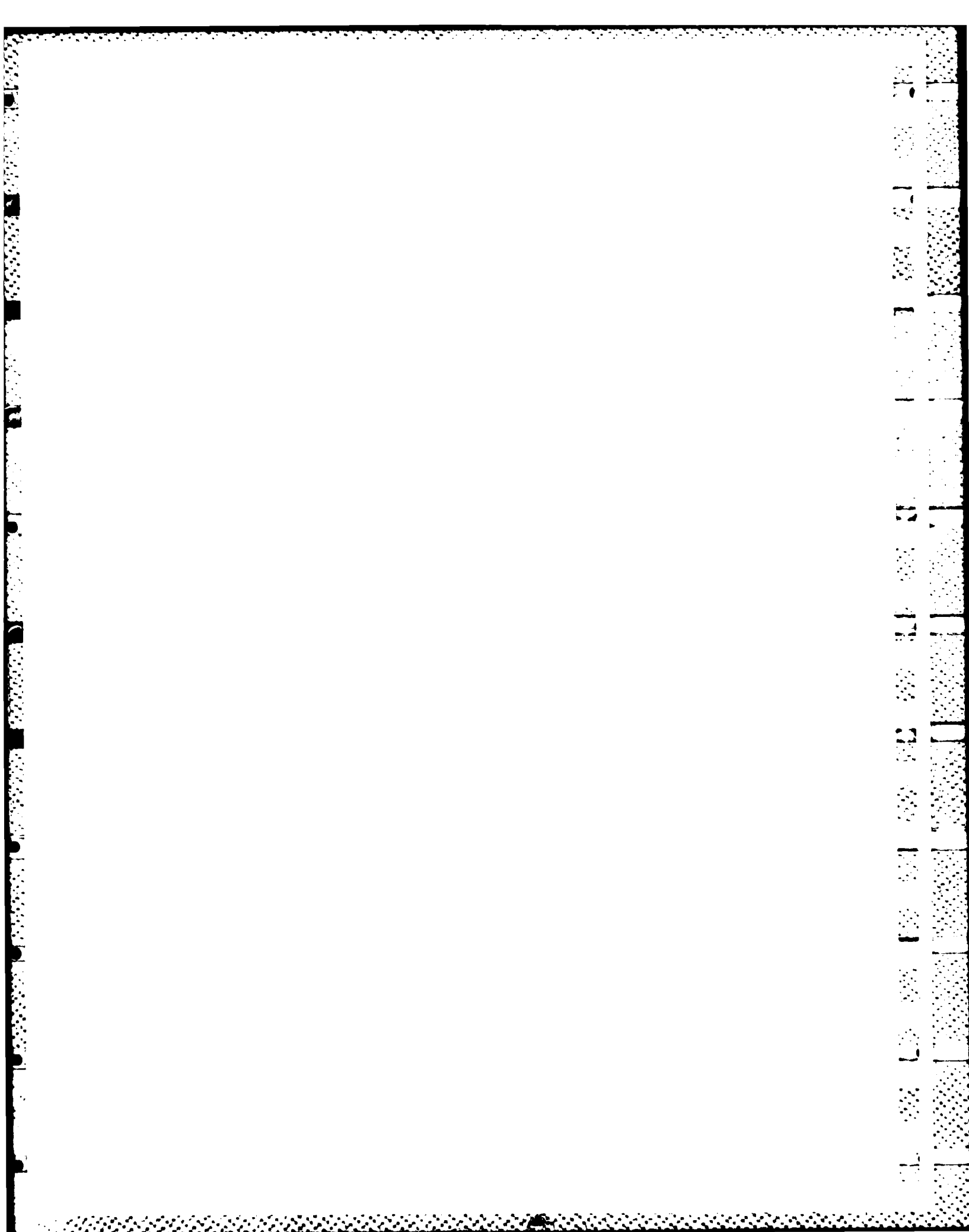


TABLE OF CONTENTS

CHAPTER	Page
1. INTRODUCTION	1
1.1 SCOPE OF STUDY	1
1.2 OBJECTIVES OF RESEARCH	4
1.3 THESIS ORGANIZATION	7
2. PAVEMENT SUPPORT CHARACTERIZATION MODELS	10
2.1 INTRODUCTION	10
2.2 THE DENSE LIQUID FOUNDATION	11
2.3 THE ELASTIC SOLID FOUNDATION	13
2.4 THE TWO-PARAMETER FOUNDATION	14
2.4.1 Filonenko - Borodich	17
2.4.2 Pasternak	17
2.4.3 Vlasov and Leont'ev	18
2.5 NONLINEAR ELASTIC SOLID MODELS	22
2.5.1 Fine-Grained Soils	22
2.5.2 Granular Materials	28
2.5.3 Other Materials	28
2.6 NONLINEAR DENSE LIQUID MODELS	31
2.6.1 The Plate Load Test	31
2.6.2 Hyperbolic Model	33
2.6.3 Ramberg and Osgood	35
2.6.4 Butterfield and Georgiadis	35
2.7 NONLINEAR TWO-PARAMETER MODELS	38

	Page
2.8 NON-HOMOGENEOUS ELASTIC HALF-SPACE	41
2.9 COMPARISON BETWEEN THE LAYERED ELASTIC AND PLATE THEORIES	43
3. COMPUTERIZED NUMERICAL ANALYSES OF SLABS-ON-GRADE	55
3.1 INTRODUCTION	55
3.2 THE FINITE ELEMENT METHOD	56
3.3 THE FINITE DIFFERENCE METHOD	57
3.4 NUMERICAL INTEGRATION TECHNIQUES	60
3.5 THREE-DIMENSIONAL MODELS	61
3.6 DISCRETE ELEMENT MODELS	66
3.7 DENSE LIQUID PROGRAMS	69
3.7.1 KENWINK	69
3.7.2 WESLIQID	70
3.7.3 FINITE	72
3.7.4 ILLI-SLAB	73
3.7.5 H-51	76
3.8 ELASTIC SOLID PROGRAMS	77
3.8.1 KENELS	77
3.8.2 WESLAYER	78
3.9 OTHER PROGRAMS	78
3.9.1 ILLI-PAVE	78
3.9.2 BISAR	79
3.9.3 CHEVRON--ELP15	81
3.9.4 RISC	82

	Page
3.9.5 WESTER	83
4. MAKING ILLI-SLAB USER FRIENDLY	85
4.1 INTRODUCTION	85
4.2 AIMS OF MODIFICATIONS	86
4.3 CONTOURING CAPABILITY	87
4.4 TOWARD MORE EFFICIENT MEMORY CORE UTILIZATION	91
4.5 CORRECTION OF SUBGRADE STIFFNESS MATRIX	93
4.6 SPECIFICATION OF LOADED AREAS IN TERMS OF GLOBAL COORDINATES	94
4.7 MULTIPLE SLABS CAPABILITY	96
4.8 FREE-FORM INPUT CAPABILITY	96
4.9 MISCELLANEOUS CHANGES	100
5. THE WESTERGAARD SOLUTIONS REEVALUATED IN THE LIGHT OF THE FINITE ELEMENT METHOD	102
5.1 INTRODUCTION	102
5.2 PROBLEMS INVESTIGATED	104
5.3 THE INTERIOR LOADING CONDITION	106
5.3.1 Comparison of the Present to the Original Version of ILLI-SLAB	106
5.3.2 Effect of Load Representation	111
5.3.3 Effect of Load Placement with Respect to Finite Element Mesh	115
5.3.4 Convergence Characteristics of ILLI-SLAB Upon Mesh Refinement	120
5.3.5 Convergence Characteristics of ILLI-SLAB Upon Slab Size Expansion	127

	Page
5.3.6 Effect of Element Aspect Ratio	135
5.3.7 Effect of Size of Loaded Area	135
5.4 THE EDGE LOADING CONDITION	143
5.4.1 Comparison of the Present to the Original Version of ILLI-SLAB	143
5.4.2 Alternative Westergaard Solutions	150
5.4.3 The Westergaard "New" Formulae for Edge Loading	160
5.5 THE CORNER LOADING CONDITION	163
5.5.1 A Review of Proposed Equations for Corner Loading	163
5.5.2 Equations for the Corner Loading Condition Based on the F.E.M.	166
5.5.3 Factors Affecting the Finite Element Solution for Corner Loading	176
5.5.4 Location of Maximum Stress	185
5.6 RECOMMENDATIONS FOR ILLI-SLAB USERS	187
6. DEVELOPMENT OF A STRESS DEPENDENT DENSE LIQUID MODEL	189
6.1 INTRODUCTION	189
6.2 SIMULATION OF REPEATED PLATE LOAD TESTS	191
6.3 ALGORITHM DEVELOPEMENT	193
6.4 SUBBASE EFFECTS ON THE VALUE OF K_R	204
6.4.1 Effect of a Granular Subbase	204
6.4.2 Effect of a Stabilized Subbase	207
6.5 MODEL IMPLEMENTATION	207
6.6 TYPICAL EFFECTS USING THE RESILIENT SUBGRADE MODEL ...	210

	Page
6.6.1 Cases Considered	210
6.6.2 Effect of Load Transfer	214
6.6.3 Effect of Resilient Modulus Characterization	214
6.6.4 Effect of Stress Dependence -- Iterative Scheme	216
7. ANALYSIS OF AXISYMMETRIC SLABS OF FINITE EXTENT ON AN ELASTIC SOLID FOUNDATION	222
7.1 INTRODUCTION	222
7.2 LITERATURE REVIEW	223
7.3 ANALYTICAL PROCEDURE USING CONCORDANT DEFLECTIONS	227
7.4 PROGRAM IMPLEMENTATION	232
7.5 PROGRAM VALIDATION	240
7.6 INVESTIGATION OF SUBGRADE CONTACT PRESSURES UNDER SLABS-ON-GRADE	248
8. A COMPUTERIZED CHART FOR EDGE LOADING OF PLATE ON ELASTIC SOLID FOUNDATION	263
8.1 INTRODUCTION	263
8.2 THEORY	264
8.3 NUMERICAL INTEGRATIONS	268
8.3.1 Evaluation of F_1 and F_2	268
8.3.2 Evaluation of H_1 and H_2	269
8.3.3 Evaluation of the Integral in Eqn. (8-2)	272
8.4 INVESTIGATION OF THE EDGE LOADING CONDITION FOR PLATE ON ELASTIC SOLID FOUNDATION	275

	Page
9. TWO-DIMENSIONAL FINITE ELEMENT MODEL FOR SLAB ON ELASTIC SOLID	290
9.1 INTRODUCTION	290
9.2 THEORY	291
9.3 REFINEMENTS OF THE CHEUNG-ZIENKIEWICZ MODEL	300
9.3.1 Partial Contact	300
9.3.2 Making the Subgrade Stiffness Matrix Banded .	303
9.3.3 Analysis of Two Slabs with Shear Transfer ...	307
9.3.4 Use of Symmetry	308
9.3.5 Higher Order Approximation to Contact Pressure Function	308
9.4 THE ELASTIC SOLID OPTION IN ILLI-SLAB	311
9.5 CONVERGENCE STUDIES WITH ILLI-SLAB ELASTIC SOLID	314
9.5.1 Scope of Analyses	314
9.5.2 Slab Size Effect	315
9.5.3 Mesh Fineness Effect	318
9.5.4 Effect of Size of Loaded Area	321
9.5.5 Effect of Element Aspect Ratio	321
9.6 INVESTIGATION OF THE k-SURFACE	324
10. ANALYSIS OF A PLATE ON AN ELASTIC SOLID USING THE METHOD OF FINITE DIFFERENCES	341
10.1 INTRODUCTION	341
10.2 FINITE DIFFERENCE FORMULATION	342
10.2.1 Theory	342
10.2.2 Boundary Conditions	349

	Page
10.2.3 Assembly of Equations	354
10.3 PROGRAM IMPLEMENTATION	355
10.3.1 Equation Assembly Subroutines	355
10.3.2 Stress Calculation	358
10.4 PROGRAM VERIFICATION	360
10.4.1 Scope of Investigation	360
10.4.2 Interior Loading	361
10.4.3 Corner Loading	367
10.5 DEVELOPMENT OF PREDICTIVE EQUATIONS FOR CORNER LOADING	373
11. FINITE ELEMENT ANALYSIS OF A PLATE ON A TWO-PARAMETER FOUNDATION	380
11.1 INTRODUCTION	380
11.2 FORMULATION FOR SUBGRADE STIFFNESS MATRIX	381
11.2.1 Assumed Displacement Function	381
11.2.2 The Concept of Strain Energy	382
11.2.3 Concentrated Boundary Reactions	387
11.2.4 The Winkler Term	390
11.2.5 The Shear Interaction x-Term	394
11.2.6 The Shear Interaction y-Term	397
11.3 NUMERICAL EVALUATION OF THE SUBGRADE STIFFNESS MATRIX	397
11.4 RESULTING STIFFNESS MATRICES	400
11.5 IMPLEMENTATION OF VLASOV MODEL INTO ILLI-SLAB	404
11.6 FACTORS INFLUENCING THE VLASOV MODEL PARAMETERS	405

	Page
11.7 MODEL BEHAVIOR	410
11.7.1 Parameter Selection	410
11.7.2 Mesh Fineness Effect	411
11.7.3 Effect of k for Constant G	414
11.7.4 Effect of G for Constant k	420
11.8 COMPARISON OF VLASOV AND ELASTIC SOLID MODELS	425
12. SUMMARY AND CONCLUSIONS	448
12.1 RESEARCH ACCOMPLISHMENTS	448
12.2 FUTURE RESEARCH DIRECTIONS	450
APPENDIX	
A INPUT GUIDES FOR PROGRAMS DEVELOPED	454
B FINITE ELEMENT MESHES USED	504
REFERENCES	525

LIST OF TABLES

Table		Page
2.1	TYPICAL RESILIENT PROPERTY DATA	30
2.2	COMPARISON OF LAYERED ELASTIC AND PLATE THEORIES	46
3.1	FINITE DIFFERENCE EXPRESSIONS	59
4.1	FREE-FORM DATA GROUPS AND KEY-WORDS	98
5.1(a)	REVALIDATION OF ILLI-SLAB	107
5.1(b)	COMPARISON WITH WESTERGAARD SOLUTIONS	108
5.2	EFFECT OF LOAD PLACEMENT WITH RESPECT TO F.E. MESH	119
5.3(a)	EFFECT OF F.E. MESH FINENESS	122
5.3(b)	COMPARISON BETWEEN ILLI-SLAB (WINKLER), 'SPRINGS' AND WESLIQID	123
5.4	THEORETICAL AND EMPIRICAL SIZE LIMITATIONS FOR THE WESTERGAARD SOLUTION	130
5.5	EFFECT OF SLAB SIZE	134
5.6	EFFECT OF ELEMENT ASPECT RATIO	136
5.7	EFFECT OF SIZE OF LOADED AREA	140
5.8	ORIGINAL ILLI-SLAB RESULTS FOR EDGE LOADING	144
5.9	ILLI-SLAB REVALIDATION: EDGE LOADING	149
5.10	ALTERNATIVE WESTERGAARD SOLUTIONS	151
5.11	COMPARISON WITH "NEW" EDGE LOADING FORMULAE	157
5.12	EQUATIONS PROPOSED FOR THE CORNER LOADING CONDITION	167
5.13	DEVELOPMENT OF CORNER LOADING FORMULAE	170
5.14	EFFECT OF SLAB SIZE: CORNER LOADING	178
5.15	EFFECT OF MESH FINENESS	181

Table		Page
5.16	EFFECT OF SIZE OF LOADED AREA	183
5.17	LOCATION OF MAXIMUM CORNER STRESS	186
6.1	MATERIALS PROPERTY SUMMARY	192
6.2	MODELS CONSIDERED	200
6.3	REGRESSION EQUATION PARAMETERS AND STATISTICS	203
6.4	PARAMETERS FOR DEMONSTRATION RUNS	211
6.5	RESULTS OF DEMONSTRATION RUNS	213
6.6	EFFECT OF LOAD TRANSFER	215
6.7	EFFECT OF RESILIENT MODULUS	217
6.8	EFFECT OF STRESS DEPENDENCE	219
6.9	COMBINED EFFECT OF PROPOSED CHANGES	221
7.1	EQUATIONS FOR MAXIMUM RESPONSES UNDER INTERIOR LOADING	225
7.2	EFFECT OF PLATE SIZE	242
7.3	EFFECT OF SIZE OF UNLOADED ELEMENTS	245
7.4	EFFECT OF SIZE OF LOADED ELEMENTS (I)	247
7.5	EFFECT OF SIZE OF LOADED ELEMENTS (II)	249
7.6	COMPARISON BETWEEN CFES AND CLOSED-FORM SOLUTIONS	250
7.7	COMPARISON WITH WESLAYER: SLAB SELF-WEIGHT ONLY	252
7.8	SUBGRADE STRESSES: EFFECT OF ELEMENT SIZE	254
7.9	EFFECT OF SOIL POISSON'S RATIO	255
7.10	COMPARISON WITH WESLAYER: AIRCRAFT LOADING ONLY	257
7.11	EFFECT OF ELEMENT SIZE	260
8.1	INCREMENTS USED IN NUMERICAL INTEGRATIONS	270
8.2	NUMBER OF INFLUENCE SQUARES FOR BENDING STRESS (EDGE)	276

Table		Page
8.3	PLATE ON ELASTIC SOLID: EDGE LOADING	280
8.4	NORMALIZED EDGE STRESSES	282
9.1	EFFECT OF SLAB SIZE	316
9.2	EFFECT OF MESH FINENESS	319
9.3	EFFECT OF SIZE OF LOADED AREA	322
9.4	EFFECT OF ELEMENT ASPECT RATIO	325
9.5	MAXIMUM RESPONSES FOR DENSE LIQUID AND ELASTIC SOLID	329
9.6	VARIATION OF k -SURFACE WITH SLAB LENGTH: INTERIOR LOADING .	335
9.7(a)	EQUIVALENT k VALUES: ELASTIC SOLID RUNS	340
9.7(b)	DENSE LIQUID RESPONSES USING EQUIVALENT k VALUES	340
10.1	EFFECT OF SLAB SIZE	362
10.2	EFFECT OF FINITE DIFFERENCE INTERVAL	365
10.3	EFFECT OF SLAB SIZE: CORNER LOADING	369
10.4	EFFECT OF GRID FINENESS: CORNER LOADING	371
10.5	DATA BASE FOR CORNER EQUATIONS	375
11.1	SHAPE FUNCTIONS FOR ACM ELEMENT	383
11.2	EXPANDED FORM OF EQUATIONS	392
11.3	STIFFNESS MATRICES FOR VLASOV FOUNDATION	401
11.4	EFFECT OF MESH FINENESS	412
11.5	EFFECT OF SUBGRADE MODULUS, k	415
11.6	EFFECT OF SHEAR PARAMETER, G	421
11.7	COMPARISON WITH ELASTIC SOLID (I)	426
11.8	MEMORY REQUIREMENTS	433
11.9	COMPARISON WITH ELASTIC SOLID (II)	434

Table	Page
11.10 COMPARISON WITH ELASTIC SOLID (III)	437
11.11 COMPARISON WITH ELASTIC SOLID (IV)	439
11.12 EFFECT OF μ_s ON ELASTIC SOLID RESPONSES	441

LIST OF FIGURES

Figure		Page
2.1	Comparison of Deflections of Infinite Beam Under Point Load	16
2.2	The Filonenko-Borodich Foundation Model	16
2.3	Medium-Thick Plate on Vlasov Foundation	19
2.4	Arithmetic Model for Stress Dependent Resilient Behavior of Fine-Grained Soils	23
2.5	Typical Stress Dependent Resilient Behavior of a Fine-Grained Soil [AASHTO A-7-6(36)]	24
2.6	Semi-Log Model for Stress Dependent Resilient Behavior of a Fine-Grained Soil [AASHTO A-7-6(36)]	26
2.7	Subgrade Soil Material Models for ILLI-PAVE Analyses	27
2.8	Resilient Modulus - θ Relation for a Sandy Gravel [AASHTO A-1-b(0)]	29
2.9	The Plate Load Test	32
2.10	The Hyperbolic Model	34
2.11	The Ramberg-Osgood Model for Loading and Unloading	36
2.12	Parameters for Butterfield and Georgiadis Empirical Equation	37
2.13	The Nonlinear Two-Parameter Model by Butterfield and Georgiadis	39
2.14	Comparison of Layered Elastic (L) and Plate (P) Theories ..	50
3.1	Typical Finite Element Mesh for Three-Dimensional Analysis	64
3.2	The Discrete Element Model of a Plate or Slab	67
3.3	Axisymmetric Solid of Revolution Used in ILLI-PAVE	80
4.1	Typical Contour Plots	88
4.2	Comparison of Free-Form and Fixed-Form Input Data Files ...	99

Figure		Page
5.1	ILLI-SLAB Revalidation (Interior Loading)	109
5.2	Finite Element Mesh I (Interior Loading)	110
5.3	Finite Element Mesh II (Interior Loading)	116
5.4	Finite Element Mesh III (Interior Loading)	117
5.5	Effect of Mesh Fineness: Mesh with 144 Elements	124
5.6	Effect of Mesh Fineness (Interior Loading)	126
5.7	Effect of Mesh Fineness on Deflection Bowl (WESLIQID)	128
5.8	Effect of Mesh Fineness on Bending Stresses (WESLIQID)	129
5.9	Finite Element Mesh for Slab Size Investigation	132
5.10	Effect of Slab Size (Interior Loading)	133
5.11	Effect of Element Aspect Ratio on Deflection Bowl (WESLIQID)	137
5.12	Effect of Element Aspect Ratio on Bending Stresses (WESLIQID)	138
5.13	Effect of Size of Loaded Area (Interior Loading)	142
5.14	Results by Tabatabaie Reproduced (Edge Loading)	145
5.15	Finite Element Mesh Used by Tabatabaie (Edge Loading)	146
5.16	Comparison of ILLI-SLAB with Westergaard's "New" Formula for Edge Stress	158
5.17	Effect of Slab Size on ILLI-SLAB Edge Loading Results	159
5.18	Finite Element Meshes I, Ia and Ib (Corner Loading)	169
5.19	Comparison of ILLI-SLAB and Westergaard Corner Deflections	171
5.20	Bending Stresses Under Corner Loading	172
5.21	Effect of Slab Size (Corner Loading)	179
5.22	Effect of Mesh Fineness (Corner Loading)	182

Figure		Page
5.23	Effect of Size of Loaded Area (Corner Loading)	184
6.1	Plate Pressure-Resilient Displacement Curves (Medium; Very Soft Subgrades)	194
6.2	Plate Pressure-Resilient Displacement Curves (Stiff; Soft Subgrades)	195
6.3	Resilient Modulus - Deflection Relations (Very Soft Subgrade)	196
6.4	Resilient Modulus - Deflection Relations (Soft Subgrade) ..	197
6.5	Resilient Modulus - Deflection Relations (Medium Subgrade)	198
6.6	Resilient Modulus - Deflection Relations (Stiff Subgrade) .	199
6.7	Effect of Granular Subbase Thickness on Resilient Modulus .	205
6.8	Effect of Granular Subbase on Resilient Modulus for Variable Plate Pressure	206
7.1	Slab Discretization for Method of Concordant Deflections ..	228
7.2	Equations for Simply Supported Plate	233
7.3	Effect of Slab Size	244
7.4	Effect of Unloaded Element Size	246
7.5	Comparison of CFES and WESLAYER Subgrade Stress Distributions (B-747F Aircraft; $E_s = 41,000$ psi)	258
7.6	Comparison of CFES and WESLAYER Subgrade Stress Distributions (B-747F Aircraft; $E_s = 7,000$ psi)	259
7.7	Comparison of Subgrade Stress Distributions Near Edge (B-747F Aircraft)	261
8.1	Edge Load on Semi-Infinite Slab-on-Grade	267
8.2	Comparison of Maximum Bending Stresses Under Interior and Edge Loads	284
8.3	Variation of Normalized Edge Stress	287
8.4	Derivation of Edge Stress Equations (Elastic Solid)	289

Figure		Page
9.1	Cheung and Zienkiewicz Finite Element Model	292
9.2	Variation of Influence Factor, f_{11}	294
9.3	Evaluation of Approximation Proposed by Cheung and Zienkiewicz	296
9.4	Analysis of Partial Contact	302
9.5	Load-Deflection Influence Patterns	306
9.6	Svec's Triangular Plate Bending Element	310
9.7	Derivation of Flexibility Coefficient for w_{11} in ILLI-SLAB	313
9.8	Effect of Slab Size (Interior Load)	317
9.9	Effect of Mesh Fineness (Interior Load)	320
9.10	Effect of Size of Loaded Area (Interior Load)	323
9.11	Deterioration of Accuracy as Aspect Ratio Increases	326
9.12	Radial Variation of Subgrade Stress (Interior Load)	327
9.13	Contours of k-Surface (Interior Loading)	331
9.14	Contours of k-Surface (Edge Loading)	332
9.15	Contours of k-Surface (Corner Loading)	333
9.16	Cross-Section in k-Surface (Interior Loading)	334
9.17	Effect of Slab Size on k (Interior Loading)	336
9.18	Radial Distribution of k-values (Interior Loading)	337
10.1	Typical Finite Difference Grid (NX=9; NY=6)	344
10.2	Geometric Representation of Finite Difference Equations ...	348
10.3	Computational Molecule for ϕ_{uvrs}	357
10.4	Effect of Slab Size (Interior Loading)	363
10.5	Effect of Grid Fineness (Interior Loading)	366

Figure		Page
10.6	Effect of Slab Size (Corner Loading)	370
10.7	Effect of Grid Fineness (Corner Loading)	372
10.8	Variation of Normalized Maximum Corner Deflection	376
10.9	Variation of Normalized Maximum Corner Subgrade Stress	377
10.10	Variation of Normalized Maximum Bending Stress Under Corner Loading	378
11.1	Relationship Between $f(\alpha R)$, ϵ and αR	409
11.2	Effect of Mesh Fineness on Maximum Bending Stress	413
11.3	Effect of Subgrade Modulus on Maximum Deflection and Bending Stress	418
11.4	Effect of Subgrade Modulus on Deflection and Bending Stress Profiles	419
11.5	Effect of Shear Parameter on Deflection and Bending Stress Profiles	424
11.6	Comparison of Deflection Profiles	429
11.7	Comparison of Subgrade Stress Profiles	430
11.8	Comparison of Bending Stress, σ_x , Profiles	431
11.9	Comparison of Bending Stress, σ_y , Profiles	432
11.10	Effect of Elastic Solid Poisson's Ratio on Maximum Deflection	443
11.11	Effect of Elastic Solid Poisson's Ratio on Maximum Subgrade Stress	444
11.12	Effect of Elastic Solid Poisson's Ratio on Maximum Bending Stress	445
11.13	Effect of Elastic Solid Poisson's Ratio on Response Profiles	446

LIST OF SYMBOLS

- A : loaded area
 a : radius of circular loaded area
 2a : short side of finite element
 2b : long side of finite element
 c : side length of square loaded area
 c : subscript, pertaining to corner loading
 D : plate flexural stiffness [$= Eh^3 / 12(1 - \nu^2)$]
 E : Young's modulus of plate
 e : subscript, pertaining to edge loading
 E_s : Young's modulus of elastic solid foundation
 E_R : Resilient modulus of foundation
 G : shear parameter for two-parameter foundation
 G_s : Shear modulus of elastic solid foundation
 [$= E_s / 2(1 + \nu_s)$]
 H : thickness of finite foundation layer
 h : plate thickness
 i : subscript, pertaining to interior loading
 k : modulus of subgrade reaction (dense liquid foundation)
 K_R : resilient modulus of subgrade reaction (stress dependent, resilient subgrade)
 L : side length of square plate
 l : radius of relative stiffness for dense liquid foundation ($= \sqrt[4]{D/k}$)

l_e : radius of relative stiffness for elastic solid foundation

$$[= \sqrt[3]{(1-\mu_s)D/G_s}]$$

NX : number of plate subdivisions in the x-direction

NY : number of plate subdivisions in the y-direction

P : applied load (force)

p : applied pressure

Q : surface subgrade reaction (force)

q : (maximum value of) surface subgrade reaction (pressure)

R : radius of circular plate

r : radial coordinate

u : horizontal displacement in the x-direction

v : horizontal displacement in the y-direction

w : vertical deflection

x : horizontal Cartesian coordinate

y : horizontal Cartesian coordinate

z : vertical Cartesian coordinate

α : finite element aspect ratio $[= 2a/2b]$

γ : two-parameter model vertical displacement attenuation parameter

Δ : spacing in finite difference grid

δ : (maximum value) vertical deflection

ϵ : strain

η : local orthogonal coordinate

- μ : Poisson's ratio for plate
- μ_s : Poisson's ratio for elastic solid
- ξ : local orthogonal coordinate
- σ : (maximum value of) plate bending stress
- $\psi(z)$: assumed vertical displacement shape in two-parameter foundation

CHAPTER 1

INTRODUCTION

1.1 SCOPE OF STUDY

This study is primarily concerned with analytical and numerical procedures applied to slab-on-grade type pavements, treated as plates on elastic foundation. For this reason, the terms "slab" and "plate" are used interchangeably throughout this work. This kind of analysis is encountered in many applications at the interface of structural and geotechnical engineering. There has been a proliferation of literature dealing with soil-structure interaction problems in recent years. Methods and techniques explored during this study, indeed the computer programs developed and insight gained from their utilization, have a strong bearing on such applications, and may be effectively employed with -perhaps- but a small amount of adaptation. Interesting and challenging as the question of soil-structure interaction may be, this study is only concerned with one category of field applications, namely the problem of a slab-on-grade, as encountered in the analysis and design of rigid pavements.

This is one of the few instances where the term "rigid" will be used to describe a pavement which owes the bulk of its structural value to its ability to carry the applied wheel loads through bending action. This is not coincidental. The term "rigid pavements" was coined several decades ago, in contrast to the other broad category of

"flexible pavements". The latter typically consisted of one or more layers of unbonded paving materials, such as crushed stone, gravel, sand etc., with a top wearing surface provided by a thin cover of asphalt concrete. Naturally, such pavements had limited bending stiffness, and deformed in direct compression when loaded. "Flexible" pavements are still as much in use today as "rigid" pavements are, but both these terms need reconsidering. "Rigid" pavements often exhibit substantial deformations, while "flexible" pavements may possess a high load bearing capacity, if only the proper design and construction methods are adhered to.

There are several additional reasons, entirely due to recent developments, that warrant the phasing out of the term "rigid pavements". When the term was coined in the early part of this century, the state-of-the-art in predicting the structural response of Portland Cement Concrete (PCC) slabs was in its infancy. A high degree of conservatism substituted for the lack of confidence in existing analytical methods. Coupled with the relatively light loads applied to PCC pavements in those days, and the small number of load repetitions, conservative designs led to almost imperceptible pavement deformations, thus warranting the term "rigid pavements". Modern-day analytical techniques -several of which are discussed herein- and experience gained in the field over the last half century, have eliminated a large portion of this conservatism. Furthermore, three other developments have rendered the term "rigid" less appropriate:

- (i) The ever increasing number and severity of applied loads, both in terms of total load, and tire pressure;
- (ii) The use of materials of lower bending stiffness than PCC, e.g. asphalt concrete (AC) and several types of stabilized materials;
- (iii) The availability of very sensitive and accurate deformation measuring devices.

Thus, not only are deflections in pavement slabs greater today, but the engineer is also better able to detect them.

Conceptually, the use of the terms "rigid" and "flexible" pavements has often led to the impression that a "flexible" pavement should respond in the manner prescribed by the layered elastic theory, while a "rigid" pavement should follow the rules of plate theory. This is reflected, it may be argued, in the existence of two distinct design approaches, and -more recently- in the development of two separate categories of computer programs. Such classification is useful and often indispensable. One must always be ready to admit, however, that the clearly defined and mutually exclusive categories are fictional, and exist only for convenience on paper.

There has been an effort in recent years to remedy this situation, through the development of a "unified" approach, that would bridge the gap between rigid and flexible pavements. Unfortunately, more often than not, this extremely ambitious, philosophically sound and practically desirable undertaking, has been reduced to the mere elimination of one of the two distinct categories, depending on the

personal preference and expertise of each individual investigator. All pavements analyzed are then forced to obey the "New Unified" approach, which -of course- they do even more reluctantly, if at all, than when they had two alternatives.

This study is a re-affirmation of the validity of the use of the plate theory for the analysis of slabs-on-grade, that is those pavements for which the capacity to develop and resist bending stresses is the prime feature. The "unified" approach -and this cannot evade engineers forever- will be one that will apportion plate theory its due credit. Until then, exploration of the methods and techniques used in this theory, such as is attempted herein, will remain useful and imperative.

1.2 OBJECTIVES OF RESEARCH

The main thrust in this research will be toward collecting, evaluating, and improving existing methods of analysis. Beginning with Westergaard's ground-breaking work in the 1920's, the scientific literature contains several important contributions in this field, which have remained largely unappreciated or forgotten. Some have been misquoted or misapplied in subsequent publications, while others, plagued by the complexity of mathematical rigor, never became popular with engineers. The automated digital computer has now replaced the slide-rule, and offers a unique possibility of taking full advantage of the work of such respectable investigators as Pickett, Bergstrom,

Losberg, and others. Mathematical calculations of prohibitive volume a few decades ago, now become a routine exercise -with much improved accuracy, too.

There are, in general, two methods of modeling subgrade support in a pavement system: the dense liquid (Winkler) or the elastic solid (Boussinesq). In the first part of this work, analyses employing the dense liquid foundation will be examined. This will include an exhaustive re-examination of Westergaard's work in the light of the Finite Element Method (F.E.M.).

The application of the F.E.M. to a plate on a Winkler subgrade will be reviewed, and a number of recommendations for its proper use will be formulated. Computer program ILLI-SLAB has been found to be a versatile, user friendly, multi-purpose and accurate tool, if used correctly. Several modifications to this program will be discussed, in an effort to enhance its easy and error-free application, and to aid appreciation of its results.

To account for the stress dependent behavior of soils and their increased stiffness under rapidly moving loads, the concept of the Resilient Modulus of Subgrade Reaction, K_R , will be introduced. Algorithms relating K_R to the level of vertical deflection, w , will be established for four broad categories of cohesive soils. An iterative scheme through which these have been incorporated into ILLI-SLAB will also be described.

The second part of this work will focus on elastic solid analyses of the same problem. This is dictated by the need to investigate

further the following two effects:

- (i) The effect of pavement system characteristics, as expressed by the radius of relative stiffness, on the relation between deflection and subgrade stress, i.e. the extent to which, if at all, the subgrade modulus, k , is an intrinsic soil property;
- (ii) Load placement effects, i.e. interior, edge or corner loading conditions.

Pickett's "Chart" for maximum edge stress using the elastic solid foundation will be recalculated using computerized numerical integration, and the result will be added to an expanded version of H-51, a program for the determination of edge stress for multiple wheel loads. In the original version of H-51, only the dense liquid subgrade is available. This exercise will also provide a chance to re-examine the basic assumptions, limitations and applicability of such charts.

In addition, three different formulations will be developed for the analysis of a finite-sized plate resting on an elastic solid foundation:

- (1) A method based on the concept of "concordant deflections" for axisymmetric, circular plates;
- (2) A finite difference approach for rectangular plates;
- (3) A finite element solution for rectangular plates.

Both (2) and (3) will be able to handle any number of loads at various locations. The finite element solution in (3) will be incorporated into ILLI-SLAB. Comparative analyses will be presented to establish

the limits of applicability of these methods. After this essential ground-work is completed, load placement effects will be evaluated.

Finally, a fourth formulation will be derived for the finite element analysis of a plate resting on a two-parameter Vlasov (or Pasternak) foundation. This will also be included in ILLI-SLAB, in an attempt to bridge the gap between the dense liquid and elastic solid solutions.

1.3 THESIS ORGANIZATION

The two major approaches to the problem of a plate on an elastic foundation, viz. the Winkler dense liquid and the Boussinesq elastic solid, have already been mentioned above. In addition, there are several variations to these, each attempting to remedy some shortcoming of the two fundamental idealizations. Several subgrade models are discussed in Chapter 2, with special emphasis upon those accounting for stress dependence of soil stiffness. As a contribution to the search for a "unified" design approach, the layered elastic and plate theories are also compared in that Chapter.

Since a basic direction of this research is the evaluation of the applicability of the digital computer in slab-on-grade analysis, Chapter 3 presents the three most important numerical procedures used in this study, i.e. the Finite Element Method (F.E.M.), the Method of Finite Differences (F.D.M.), and Numerical Integration techniques. Several currently available computer programs using these methods are

briefly described.

Four chapters are devoted to describing the improvement and extension of ILLI-SLAB capabilities achieved during this study. Chapter 4 describes those changes introduced to improve the program's accuracy and ease of application, and to facilitate meaningful interpretation of its results. The incorporation of three new foundation models, in addition to the original Winkler idealization, namely the Resilient, the Elastic Solid and the Vlasov subgrades is discussed in Chapters 6, 9 and 11, respectively.

In Chapter 5, a thorough re-evaluation of the time-honored Westergaard solutions for a slab supported by a Winkler medium is presented. The computer runs conducted also shed light upon the applicability and limitations of the F.E.M. in the analysis of pavement slabs on a dense liquid foundation.

The problem of a plate on an elastic solid foundation is approached from four different perspectives, each of which is described in a separate chapter (Chapters 7 through 10). The aim is to provide means for independent verification of the results of any individual program using this model, and to exhaust the capabilities of two-dimensional analysis. All three numerical methods mentioned above are used in this effort. Programs developed in this study vary in applicability, cost of execution and computer memory requirements. Thus, Chapter 7 describes a program that permits a very fine grid, but which can only be applied to axisymmetric slabs. The computerized chart described in Chapter 8 can analyze several cases at a minimal execution cost, but

its output is restricted to the maximum bending stress developing under edge loading. The more general finite element and finite difference formulations, described in Chapters 9 and 10, respectively, are necessarily more demanding in terms of computer resources.

Chapter 11 describes a finite element Vlasov model, in an attempt to bridge the gap between the Winkler and Boussinesq idealizations, at a reduced computer cost over the latter. The considerable limitations of this "panacea" are also discussed.

Finally, the major conclusions from this study are summarized in Chapter 12. Certain directions for future research are outlined, with the main emphasis placed upon the development of a versatile and usable three-dimensional finite element model for slabs-on-grade. An appendix to this work contains the updated input guides for the programs described herein, and other useful, peripheral information about these programs.

CHAPTER 2

PAVEMENT SUPPORT CHARACTERIZATION MODELS

2.1 INTRODUCTION

Slabs-on-grade type pavements belong to that broad category at the interface of structural and geotechnical engineering, commonly referred to as soil-structure interaction problems. As in numerous other engineering applications, the pavement slab is treated as an elastic plate, but it is the response of the supporting soil medium that is the governing consideration. For an accurate evaluation of this response, the complete stress-strain characteristics of the soil are required. The extreme variety of soil conditions encountered in engineering practice, however, all but precludes the development of generalized stress-strain relationships applicable to any large group of soils. The stress-strain behavior exhibited by most natural soils is markedly nonlinear, irreversible and time dependent, and these soils are, more often than not, anisotropic and inhomogeneous.

The inherent complexity of real soils, has led to the development of a number of idealized models, which attempt to provide a useful description of certain aspects soil response under a specific set of loading and boundary conditions. No justification will be provided here for the use of such assumptions as linear elasticity and homogeneity, although it is freely admitted that such a soil probably cannot exist even in the most sophisticated laboratory. Let it only be

said that linear elasticity is instrumental in reducing the analytical rigor of a complex boundary value problem, such as that of a slab-on-grade.

The next issue to be addressed is which model or idealization is best suited for any given application. The answer to this question need not be unique. In fact, comparisons between responses obtained using different models, might shed light on an area much larger than the sum of individual portions illumined by each separate analysis. Several factors must be considered. These include soil and pavement type, loading and boundary conditions, as well as economics -in terms of money and time required for the analysis, design and construction of the proposed facility. Thus, the scope of the engineer's choices is usually restricted, since several of these are proven unfeasible. Such constraints were -happily- not imposed upon the research reported herein. Thus, several models will be examined, fully cognizant that the tools used here are becoming increasingly available to engineers of today and tomorrow.

2.2 THE DENSE LIQUID FOUNDATION

In the calculation of stresses in slab-on-grade pavements, one of two fundamentally different hypotheses has been traditionally used, to idealize the properties of the subgrade. In the simplest of these theories, the supporting soil medium is considered as a bed of closely spaced, independent, linear springs. Each spring deforms in response to

the stress applied directly to it, while neighboring ones remain unaffected. It is thus assumed that the vertical stress $q(x,y)$ occurring at any point on the foundation surface is directly proportional to the deflection $w(x,y)$ at that point, i.e.

$$q(x,y) = k w(x,y) \quad (2-1)$$

where k is the modulus of subgrade reaction, assumed to be spatially independent. This idealization is commonly termed as a "dense liquid", and is almost universally ascribed to Winkler [1]. Vlasov and Leont'ev [2] note that the Russian academician Fuss first proposed this theory in 1801, and there are indications that it can be found earlier in the works of Euler, Bubnov and Zimmermann [3]. The first application of the dense liquid model was, indeed, one involving a liquid rather than a soil foundation. This was the analysis performed by Hertz [4], of a floating ice sheet, modeled as an infinite elastic plate. In this analysis, the Winkler assumption represents a simple consequence of Archimedes' principle. The use of the Winkler idealization in the study of beams and plates on an elastic foundation was highlighted by the classical treatises of Zimmermann [5], Schleicher [6], and Hetenyi [7]. In the area of pavement slabs-on-grade, the prominent name is that of Westergaard [8; 9; 10], who was responsible for the analytical work that has formed the basis for design practices for several decades.

2.3 THE ELASTIC SOLID FOUNDATION

In the second support characterization theory commonly employed, the soil is regarded as a linearly elastic, isotropic, homogeneous solid, of semi-infinite extent. The terms "elastic solid", "elastic continuum", or "Boussinesq's half-space" are often applied to this idealization. It is regarded as a more realistic representation of actual subgrade behavior than the dense liquid model, inasmuch as it takes into account the effect of shear interaction between adjacent support elements. Consequently, the distribution of surface displacements remains continuous. The deflection at any point occurs not just as a result of the stress acting at that particular point alone, but is influenced to a progressively decreasing extent by stresses at points further away.

Widespread use of the elastic solid foundation has been inhibited, however, by its mathematical complexity. Unlike the Winkler model, where the governing equations are of a differential form, problems associated with the elastic continuum generally require the solution of integral or integro-differential equations. Analytical solutions for an infinite plate on an elastic solid, loaded by an axisymmetric load, have been provided independently by Hogg [11] and Holl [12]. Equations similar to those by Westergaard [8], have been presented by Losberg [13] and by Arora and Khanna [14]. Closed-form solutions for plates of finite size, or for edge and corner loading are not available in the literature.

2.4 THE TWO-PARAMETER FOUNDATION

The dense liquid and elastic solid models, discussed in the preceeding sections, may be considered as two extreme idealizations of actual soil behavior. The first regards the subgrade as entirely discontinuous, while the second as completely continuous. The need to bridge the gap between the two is readily apparent. Experimental investigations indicate that surface displacements occur not only within the loaded area, as assumed for the Winkler model, but also outside it. They decrease, however, more rapidly than predicted by Boussinesq's theory [3]. Observations such as these, coupled with the mathematical complexity of the elastic solid model, have led researchers to look for a second parameter, in addition to the subgrade modulus, k , to describe elastic foundation response.

One way of approaching the problem is to provide additional terms in the relation between surface vertical deflection and subgrade reaction at any point (Eqn. 2-1). Thus, the reaction is assumed to be a function of the deflection itself and its derivatives. For example, in one-dimension it may be reasonable to assume that:

$$q(x) = \sum_{n=0}^N \alpha_n w^n \quad (2-2)$$

where:

α_n : characterization parameters;

w^n : the n th derivative of w with respect to x .

Only the first few terms of this series need be retained in general. Fletcher and Hermann [15] obtained solutions using one, two and three characterization parameters to model an elastic solid supporting an infinite beam subjected to a point load. Comparison of these solutions with the corresponding elastic solid solution (Fig. 2.1), indicates that use of two or three parameters improves the approximate solutions significantly.

In the historical development of two-parameter foundations, two other approaches have been used instead of the one suggested by Eqn. (2-2). The first introduces mechanical interaction between individual spring elements of the Winkler medium, while the other starts from the elastic solid model and imposes constraints or simplifications upon the distribution of displacements and stresses in the half-space. Examples of mechanical two-parameter models are provided by Filonenko-Borodich [16; 17], Hetenyi [7; 18], Pasternak [19] and Kerr [20; 21].

A fundamental problem with these and similar models is that the parameters chosen to describe the supporting medium have limited or no physical meaning. A variational approach to this problem by Vlasov and Leont'ev [2] and to a lesser extent Reissner's [22] approach, offer some new possibilities in this respect. An excellent review of related literature is presented by Kerr [20]. Brief descriptions of some two-parameter models are provided below.

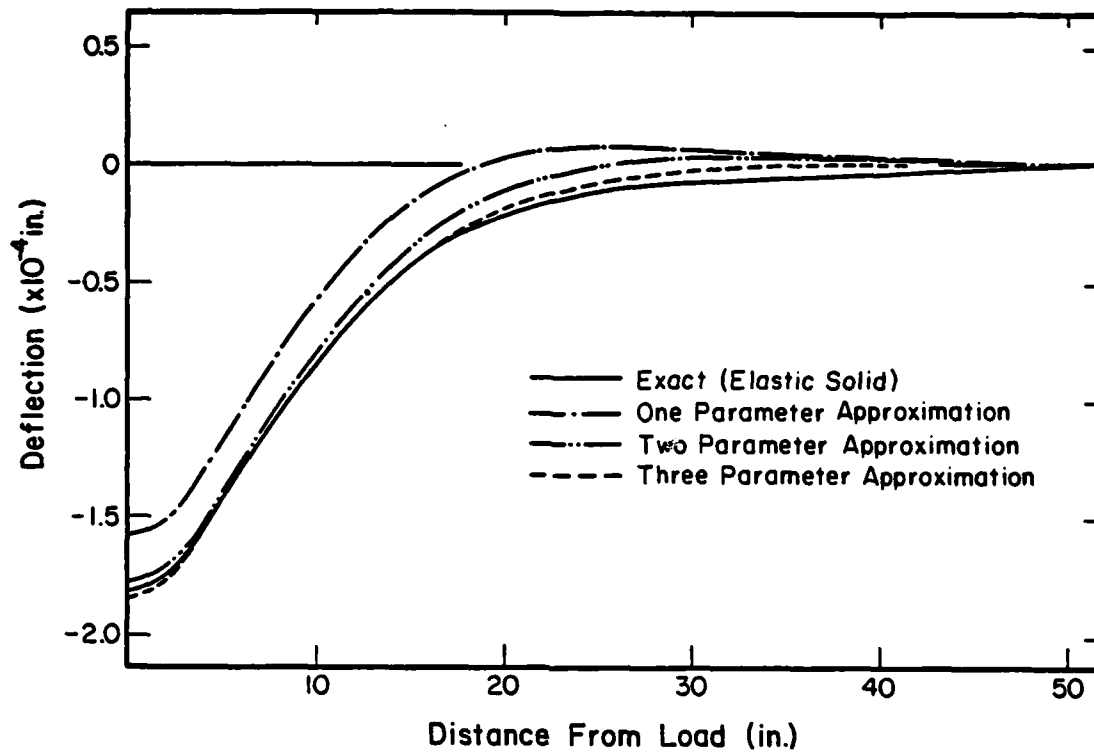


Fig. 2.1 Comparison of Deflections of Infinite Beam Under Point Load

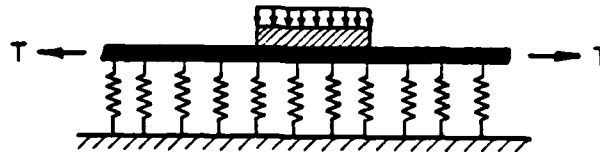


Fig. 2.2 The Filonenko-Borodich Foundation Model

2.4.1 Filonenko - Borodich

One of the earliest two-parameter models is the Filonenko-Borodich foundation [16; 17]. In addition to the vertical springs of the one-parameter model, this foundation includes a stretched elastic membrane (Fig. 2.2), connected to the top of the springs, and subjected to a constant tension field T (force/ unit length). The purpose is to develop some interaction between adjacent spring elements. The amount of interaction is a function of T . The relation between surface subgrade stress, $q(x,y)$, and deflection, $w(x,y)$, can be stated in the form:

$$q = kw - T \nabla^2 w \quad (2-3)$$

where ∇^2 is the Laplace operator in x and y .

2.4.2 Pasternak

Pasternak [19] considered the existence of shear interactions between the spring elements by tying the springs together at the top with a layer consisting of incompressible vertical elements that deform only in transverse shear. The relation between subgrade reaction and deflection is very similar to that of Filonenko-Borodich, with T replaced by G (shear parameter for the layer) so that:

$$q = kw - G \nabla^2 w \quad (2-4)$$

2.4.3 Vlasov and Leont'ev

A different approach, starting from an elastic solid foundation was used by Vlasov and Leont'ev [2]. The problem investigated was that of a plate supported by an elastic solid layer of thickness H , loaded by vertical pressure $p(x,y)$, as shown in Fig. 2.3. Since there is no horizontal loading, it may be assumed that the horizontal displacements (u,v) are negligible in comparison with the vertical displacement, w . According to the variational method used by Vlasov and Leont'ev, the unknown displacements of a point in the layer are replaced by a summation of the form:

$$w(x,y,z) = \sum_{k=1}^n W_k(x,y) \psi_k(z) \quad (2-5)$$

In this summation, $W_k(x,y)$ are generalized displacement functions to be determined. Each of these, calculated for a given section ($z=\text{constant}$) determines, in a generalized form, the magnitude of the vertical displacement $w(x,y)$ in this section. On the other hand, ψ_k are functions assumed to be known, chosen so that geometrical boundary conditions for $z=0$ and $z=H$ are satisfied. They represent the distribution of displacements with depth. Unknown generalized displacement functions $W_k(x,y)$ have dimensions of length, while assumed distribution functions ψ_k are dimensionless.

In writing Eqn. (2-5), the three-dimensional problem considered is reduced to a two-dimensional one, with a finite number of degrees-of-freedom in the z -direction, and an infinite number of degrees-of-

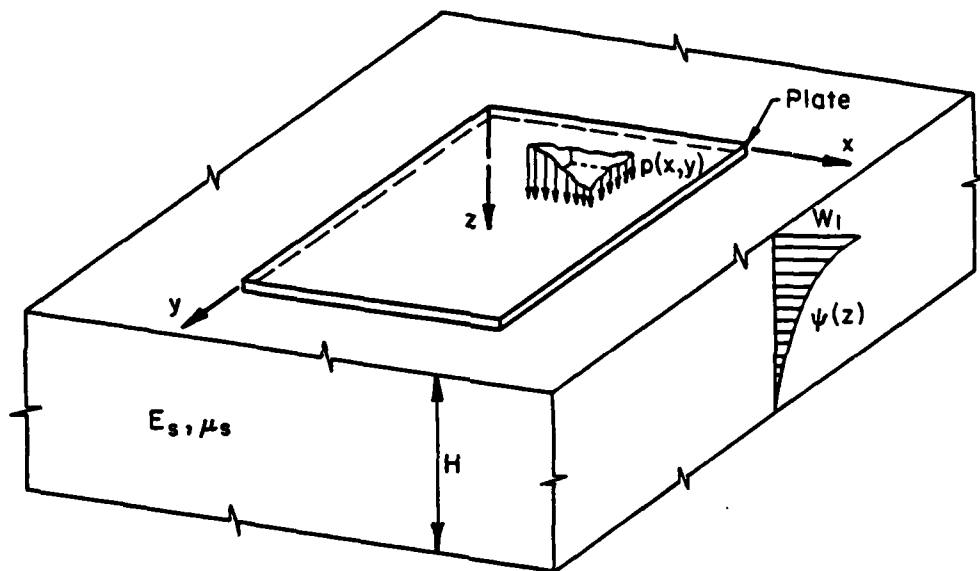


Fig. 2.3 Medium-Thick Plate on Vlasov Foundation

freedom in the x- and y-directions. In order to simplify the problem further, it is assumed that Eqn. (2-5) may be reduced to:

$$w(x,y,z) = W_1(x,y) \psi(z) \quad (2-6)$$

where:

W_1 : vertical displacement of the foundation surface,

$= w(x,y)$;

$$\psi(z) = \frac{\sinh(\gamma[H-z])}{\sinh(\gamma H)}$$

γ : a constant of dimension (1/length), describing the rate of the attenuation of vertical displacement with depth.

Applying the principle of virtual displacements to an elemental vertical column of the foundation ($dx \cdot l \cdot H$), and introducing Eqn. (2-6) into the stress-deformation relations of three-dimensional elasticity, results in the following equilibrium equation:

$$\frac{1-\mu_o}{2} r_{11} \nabla^2 w(x,y) - s_{11} w(x,y) + \frac{1-\mu_o}{E_o} q = 0 \quad (2-7)$$

where:

$$r_{11} = \int_0^H \psi^2(z) dz = \frac{1}{2\gamma} \left[\frac{\sinh(\gamma H) \cdot \cosh(\gamma H) - \gamma H}{\sinh^2(\gamma H)} \right]$$

$$= \frac{1}{2\gamma} \text{ (if } H=\infty \text{);}$$

$$s_{11} = \int_0^H \left\{ \frac{d}{dz} \psi(z) \right\}^2 dz = \frac{\gamma}{2} \left[\frac{\sinh(\gamma H) \cdot \cosh(\gamma H) + \gamma H}{\sinh^2(\gamma H)} \right]$$

$$= \frac{\gamma}{2} \quad (\text{if } H = \infty);$$

q : contact pressure at plate-foundation interface;

$$E_o = \frac{E_s}{1 - \mu_s^2}$$

$$\mu_o = \frac{\mu_s}{1 - \mu_s}$$

E_s , μ_s : Young's modulus and Poisson's ratio for the foundation, respectively.

Note that r_{11} has dimensions of length, while s_{11} of (1/length).

Introducing the notations,

$$G = \frac{E_o r_{11}}{2(1 + \mu_o)} \quad \text{and} \quad k = \frac{E_o s_{11}}{(1 - \mu_o^2)} \quad (2-8)$$

Eqn. (2-7) may be rewritten as:

$$G \nabla^2 w - kw + q = 0 \quad (2-9)$$

where k and G characterize the compressive and shear strain in the foundation, respectively. This equation is again essentially identical in form to those applying to the other two-parameter foundations, indicating the similarity of these models.

2.5 NONLINEAR ELASTIC SOLID MODELS

It was noted earlier that in-situ behavior is generally nonlinear and at least partly irreversible. Furthermore, typical highway and airport traffic loads are of a transient, repeated nature. Thus, the resilient behavior of a soil or material is an important property for pavement analysis and design. A commonly used measure of resilient response is the "resilient modulus", defined by:

$$E_R = \frac{\sigma_D}{\epsilon_r} \quad (2-10)$$

where:

E_R : resilient modulus;

σ_D : repeated deviator stress;

ϵ_r : recoverable axial strain.

Repeated unconfined compression or triaxial testing procedures are often used to evaluate the resilient moduli of fine-grained soils and granular materials. Resilient moduli are stress dependent. For fine-grained soils, resilient modulus decreases with increasing stress, while granular materials stiffen with increasing stress level.

2.5.1 Fine-Grained Soils

Two stress dependent behavior models have been proposed for describing the stress softening behavior of fine-grained soils. The arithmetic model is demonstrated in Figures 2.4 and 2.5, and the

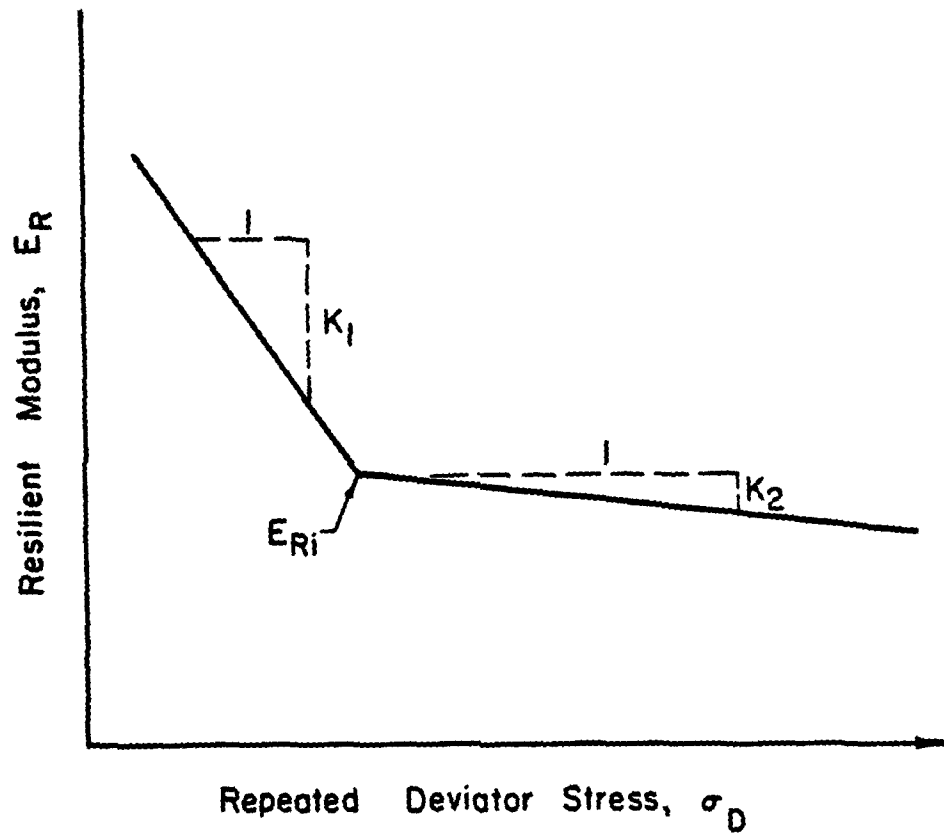


Fig. 2.4 Arithmetic Model for Stress Dependent Resilient Behavior of Fine-Grained Soils

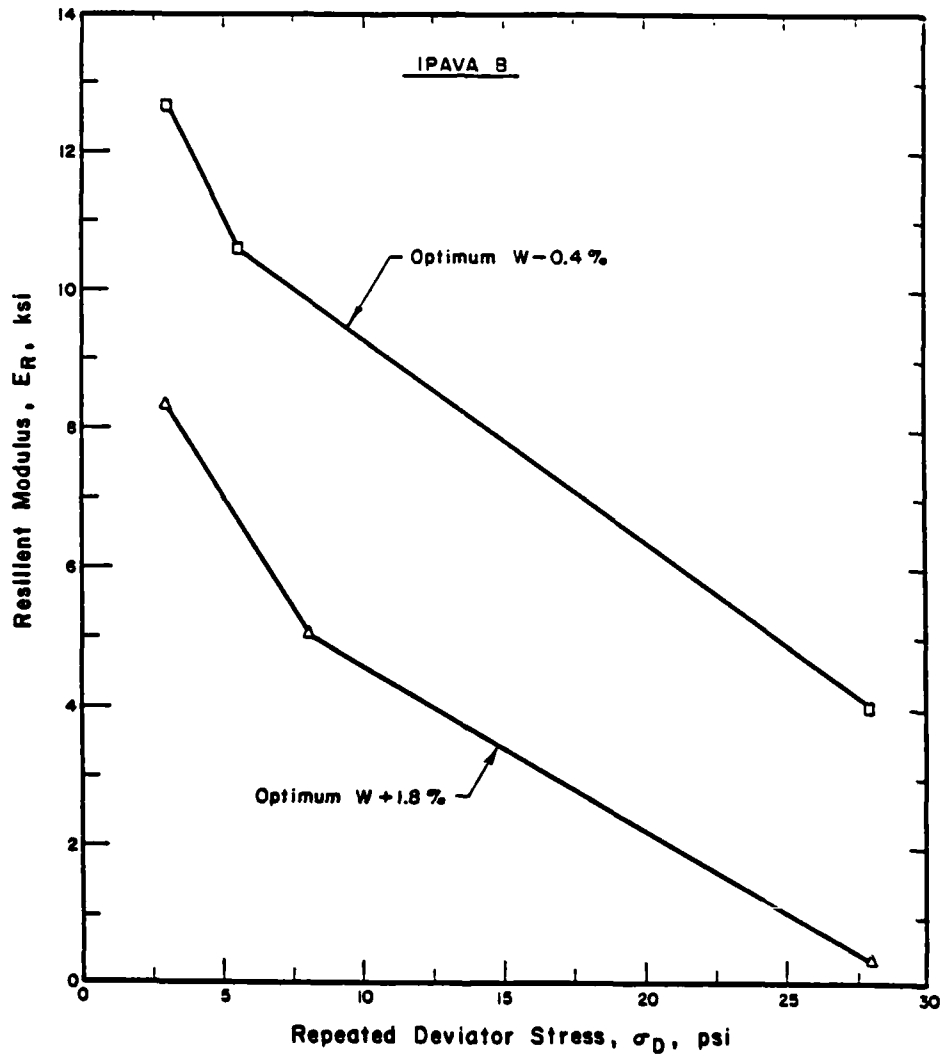


Fig. 2.5 Typical Stress Dependent Resilient Behavior of a Fine-Grained Soil [AASHTO A-7-6(36)]

semi-log model is shown in Fig. 2.6. Extensive resilient laboratory testing, nondestructive testing, and pavement analysis and design studies at the University of Illinois have indicated that the arithmetic model is adequate to describe soil response for pavement analysis activities [23; 24; 25].

In the arithmetic model (Fig. 2.4), the value of the resilient modulus at the break-point in the bilinear curve, E_{Ri} , is a good indicator of a soil's resilient behavior. The slope values, K_1 and K_2 , display less variability and influence pavement structural response to a smaller degree than E_{Ri} . Thompson and Robnett [23] developed procedures for predicting the resilient behavior of fine-grained soils based on soil classification, soil properties, and moisture content. They suggested the following regression equations relating E_{Ri} with static soil modulus, E_s , and unconfined compressive strength, q_u :

$$E_{Ri} = 3.46 + 1.9E_s$$

$$E_{Ri} = 0.86 + 307 q_u \quad (2-11)$$

in kips per square inch.

It is seen that E_{Ri} is substantially greater than static E_s due to the stiffer soil response to repeated, short-duration loads. The E_{Ri} -deviator stress relations developed for Illinois soils (Fig. 2.7) are representative of the soils exhibiting stress softening behavior. These relations are currently incorporated into finite element program

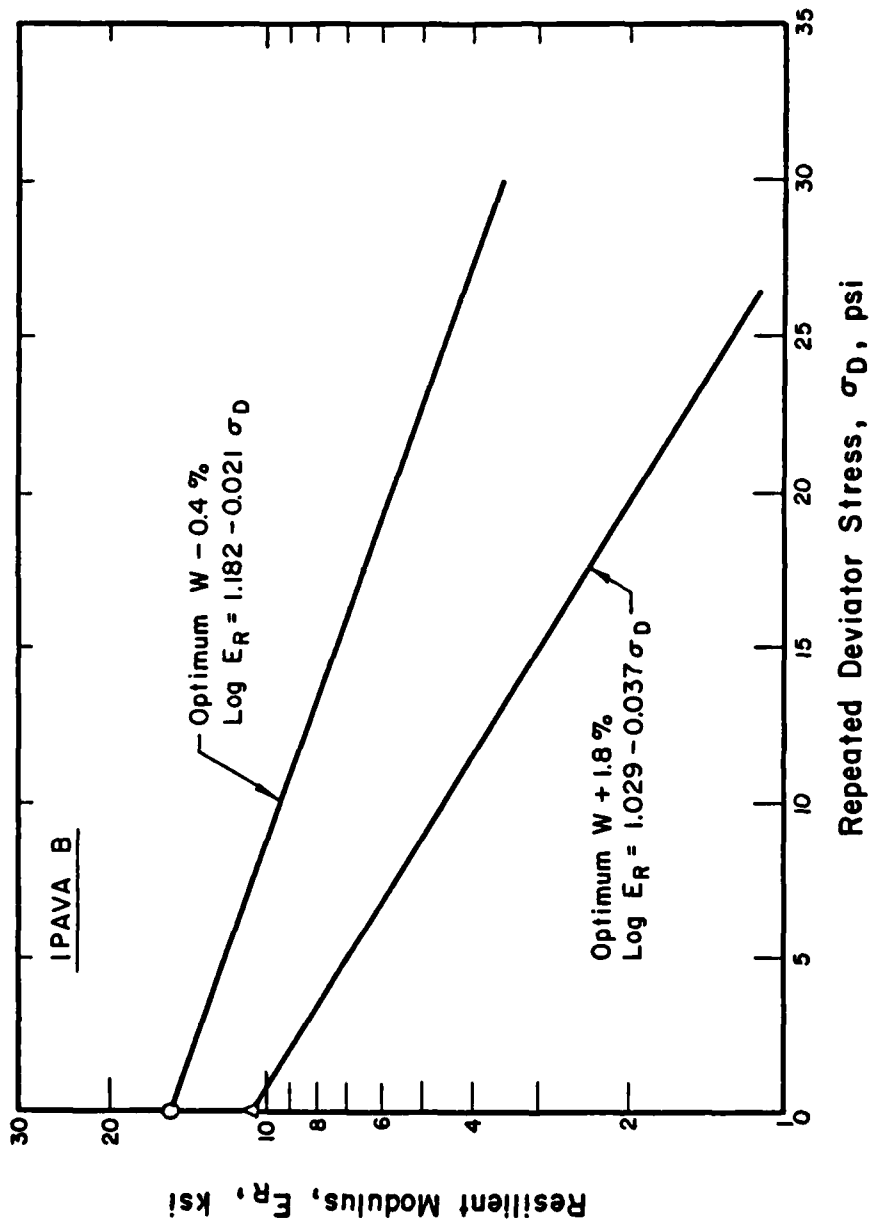


Fig. 2.6 Semi-Log Model for Stress Dependent Resilient Behavior of a Fine-Grained Soil [AASHTO A-7-6(36)]

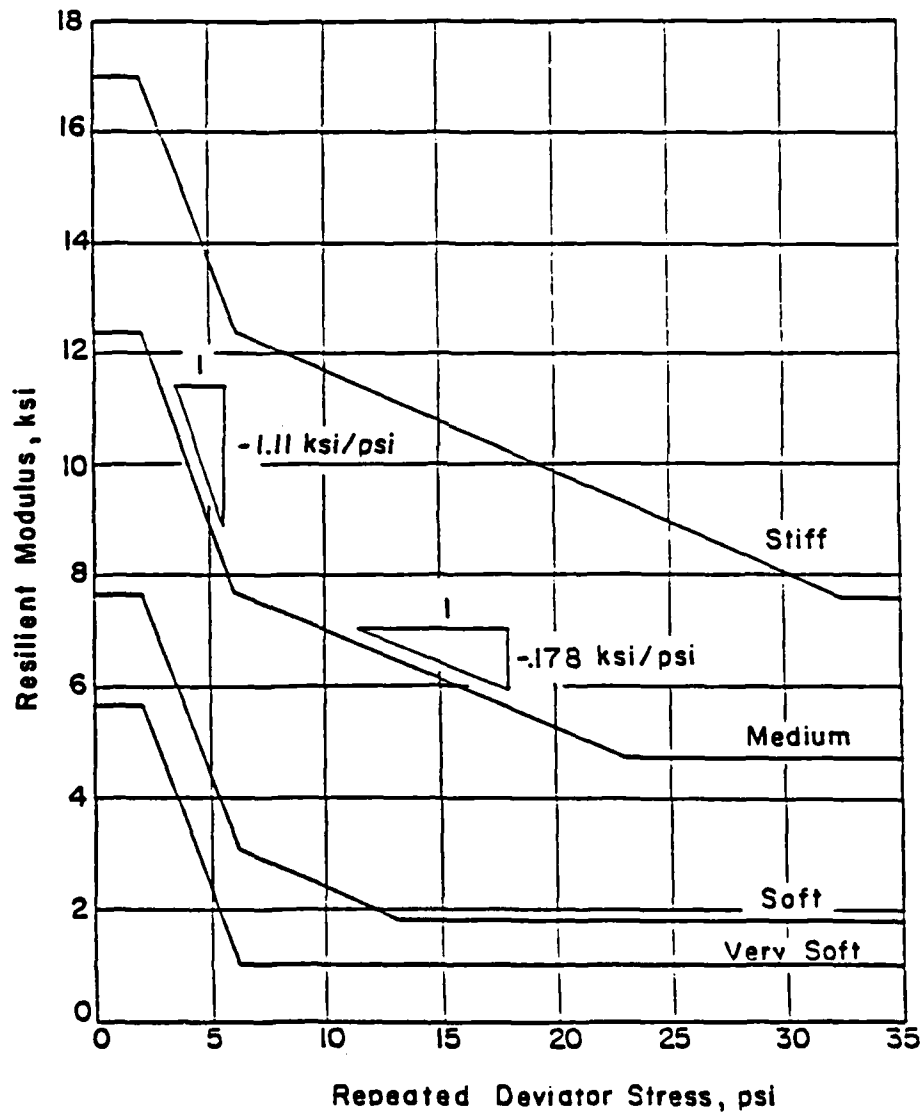


Fig. 2.7 Subgrade Soil Material Models for ILLI-PAVE Analyses

ILLI-PAVE, extensively used at the University of Illinois.

2.5.2 Granular Materials

In contrast to fine-grained soils, granular materials stiffen as the stress level increases. Repeated load triaxial testing is used to characterize the resilient behavior of granular materials. The resilient modulus, E_R , is a function of the applied stress state, as follows:

$$E_R = K\theta^n \quad (2-12)$$

where:

K, n : experimentally derived factors;

θ : first stress invariant = $\sigma_1 + 2\sigma_3$.

(Note: $\sigma_2 = \sigma_3$ in a standard triaxial compression test.)

Figure 2.8 is an E_R - θ relation for a sandy gravel (GW in the Unified System).

Rada and Witczak [26] have summarized and analyzed statistically extensive published resilient moduli data for a broad range of granular materials. The average values and ranges for K and n are presented in Table 2.1 for several granular materials and coarse-grained soils.

2.5.3 Other Materials

Stabilized materials such as soil-cement, cement-aggregate mixtures, soil-lime mixtures, lime-flyash-aggregate mixtures and

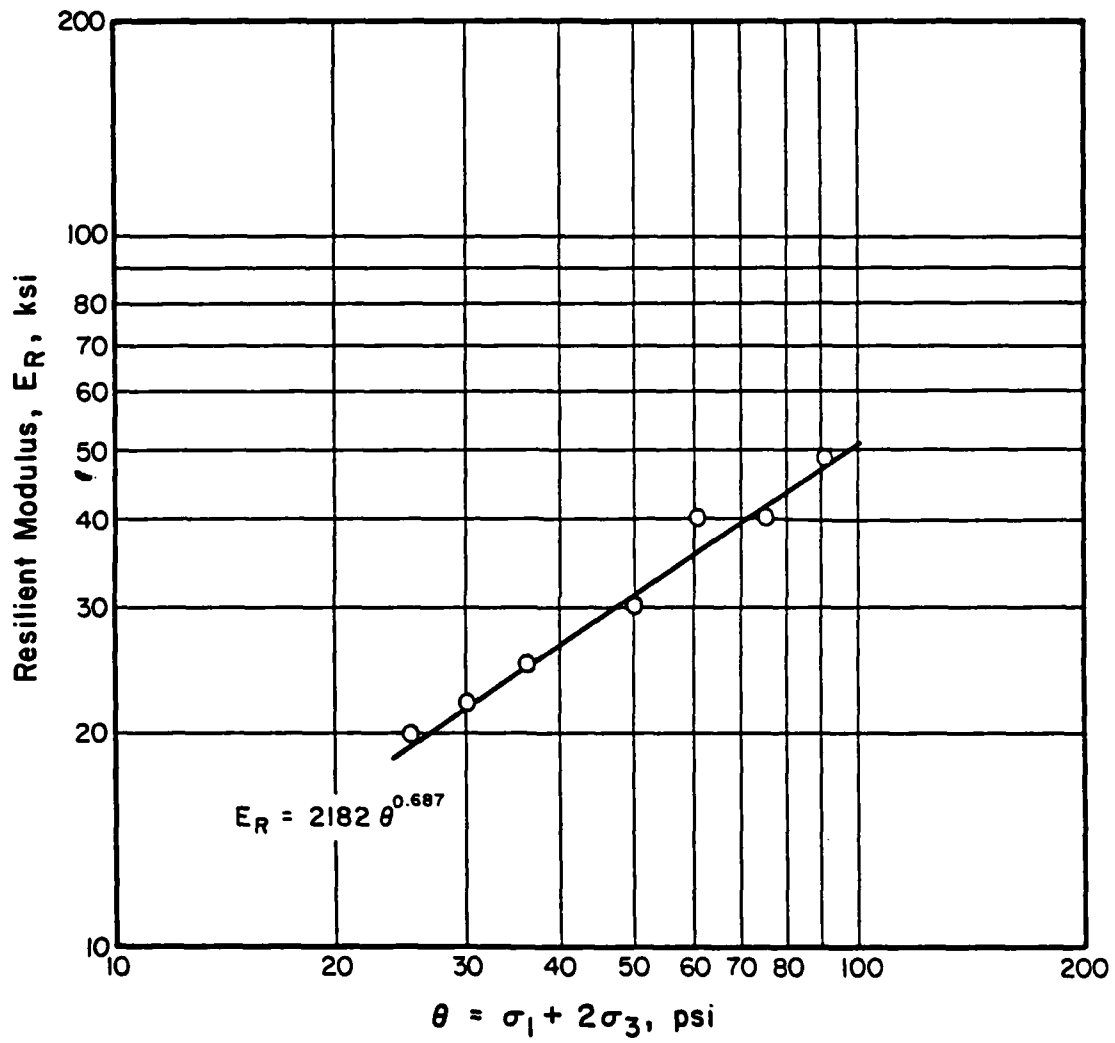


Fig. 2.8 Resilient Modulus - θ Relation for a Sandy Gravel
[AASHTO A-1-b(0)]

TABLE 2.1
TYPICAL RESILIENT PROPERTY DATA

Granular Material Type	Number of Data Points	K* (psi)		n*	
		Mean	Standard Deviation	Mean	Standard Deviation
Silty Sands	8	1620	780	0.62	0.13
Sand-Gravel	37	4480	4300	0.53	0.17
Sand-Aggregate Blends	78	4350	2630	0.59	0.13
Crushed Stone	115	7210	7490	0.45	0.23

* $E_R = K\theta^n$, where:

E_R : resilient modulus, psi;

K, n : experimentally derived factors from repeated triaxial testing data;

θ : first stress invariant = $\sigma_1 + 2\sigma_3$.

(After Rada and Witczak [26])

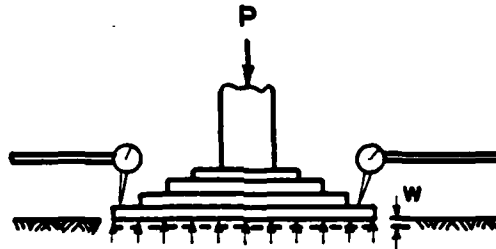
similar high strength and high modulus materials are frequently used as base and subbase layers. These materials are usually characterized as constant modulus (stress independent) materials in ILLI-PAVE, in accordance with common practice.

2.6 NONLINEAR DENSE LIQUID MODELS

2.6.1 The Plate Load Test

The modulus of subgrade reaction, k , is calculated using data from 30-in. diameter plate load tests (Fig. 2.9a). ASTM standards [27] include non-repetitive (ASTM D1196) and repetitive (ASTM D1195) static plate load tests. The Corps of Engineers (CE), however, only uses a non-repetitive static plate load test [28]. The US Air Force Engineering and Services Center routinely conducts plate bearing tests in its airfield pavement evaluation activities. Correlations between k , CBR and soil classification have been suggested by various agencies. These correlations are widely used, since plate load tests are expensive and time consuming.

A typical plate pressure versus plate deflection relation for a fine-grained soil shows a nonlinear, stress softening trend (Fig. 2.9b). The modulus of subgrade reaction is usually calculated using either the CE or the Portland Cement Association (PCA) procedure. In the CE procedure, k is determined for a plate pressure of 10 psi and the corresponding deflection. Using the PCA procedure [30], k is evaluated at a plate pressure corresponding to a 50-mil



(a) Typical Setup for the Plate Load Test

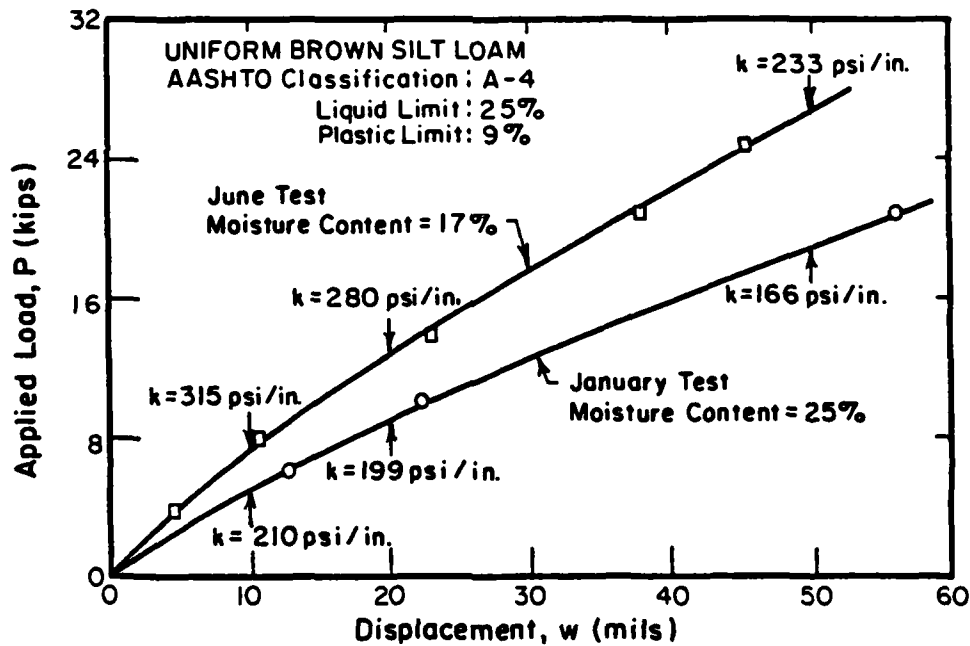
(b) Typical Plate Load Test Results
(After Teller and Sutherland [29])

Fig. 2.9 The Plate Load Test

(0.050-in.) plate deflection.

A more sophisticated representation of an elastic soil medium would consider the nonlinearity of soil stiffness, and approximate more closely the stress softening behavior of fine-grained subgrades. Two of the more widely used nonlinear models in geotechnical engineering are the hyperbolic and Ramberg-Osgood models. Both models were originally developed to reconstruct stress-strain curves, but may be adapted to pressure-deflection data [31].

2.6.2 Hyperbolic Model

The hyperbolic model [32] assumes the plate pressure-deflection (p-w) plot is a hyperbola (Fig. 2.10a) whose equation has the form:

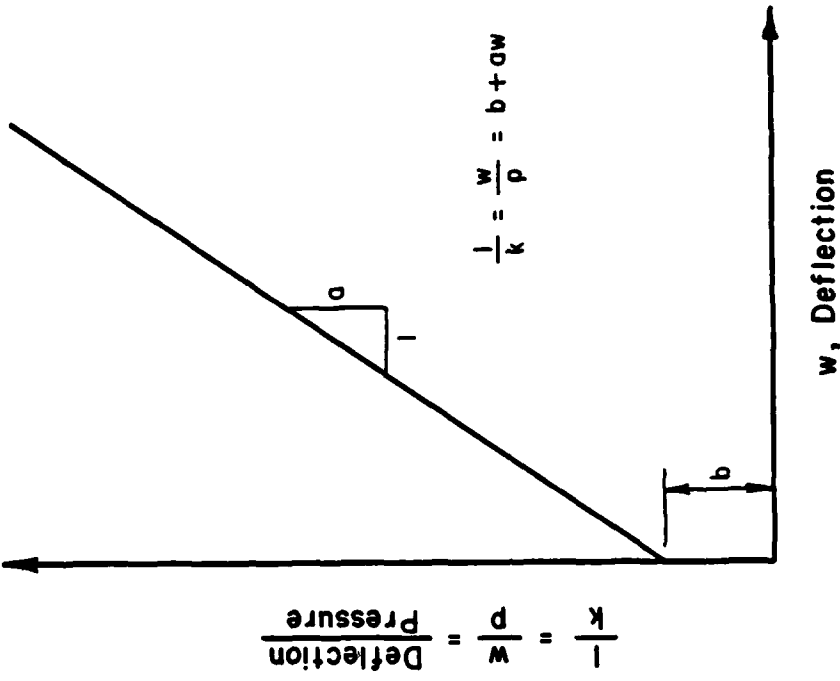
$$p = \frac{w}{b + aw} \quad (2-13)$$

where 'a' and 'b' are empirical constants.

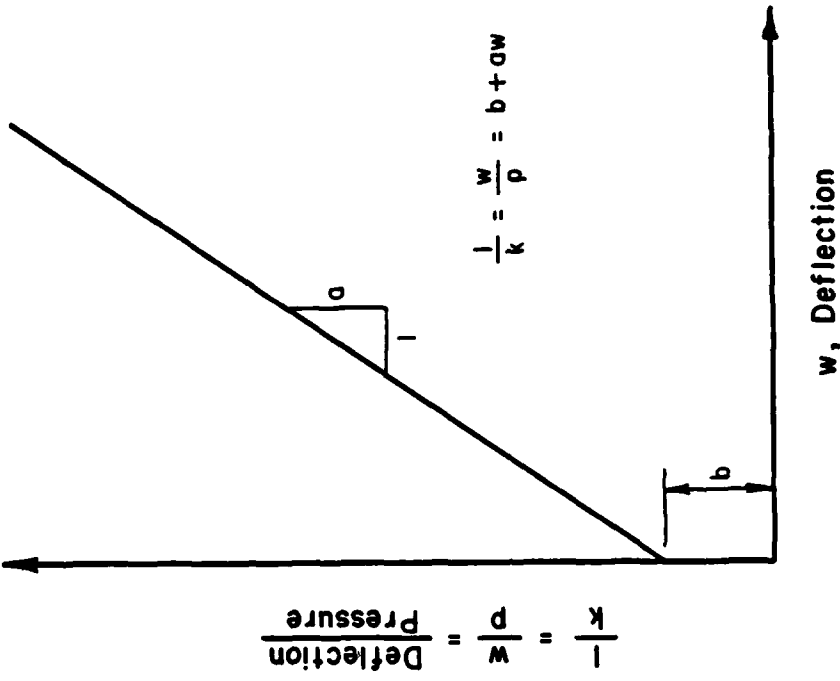
Rearranging this equation, the following relationship can be obtained:

$$\frac{1}{k} = \frac{w}{p} = b + aw \quad (2-14)$$

On transformed axes (Fig. 2.10b), this equation plots as a straight line with a slope of 'a' and an intercept of 'b'. The term (1/b) is equivalent to the initial stiffness, k_0 .



(a) Assumed Hyperbola



(b) Hyperbolic Model with Transformed Axes

Fig. 2.10 The Hyperbolic Model

2.6.3 Ramberg and Osgood

This model [33] is especially suited for cyclic loading situations, where both the loading and unloading curves are of interest. The function describing it may be expressed in the following form (Fig. 2.11):

$$\frac{w}{w_y} = \frac{p}{p_y} + a \left| \frac{p}{p_y} \right|^r \quad \text{for first loading}$$

$$\frac{w-w_o}{2w_y} = \frac{p-p_o}{2p_y} + a \left| \frac{p-p_o}{2p_y} \right|^r \quad \text{for reloading (2-15)}$$

where w_y and p_y are the deflection and plate pressure at yield, respectively, and w_o and p_o are the extreme values of w and p for the cycle. The values of the constants 'a' and 'r' must be determined experimentally.

2.6.3 Butterfield and Georgiadis

A third model used to account for the nonlinearity of the subgrade springs is an empirical equation developed by Butterfield and Georgiadis [34]. This is based on an idealization proposed by Burland and Lord [35], which uses three characterization parameters: an initial stiffness k_o , a final stiffness k_f and an applied pressure axis intercept p_u (Fig. 2.12). The applied pressure, p , is then expressed as:

$$p = p_u [1 - \exp \{ - (k_o - k_f) w / p_u \}] + k_f w \quad (2-16)$$

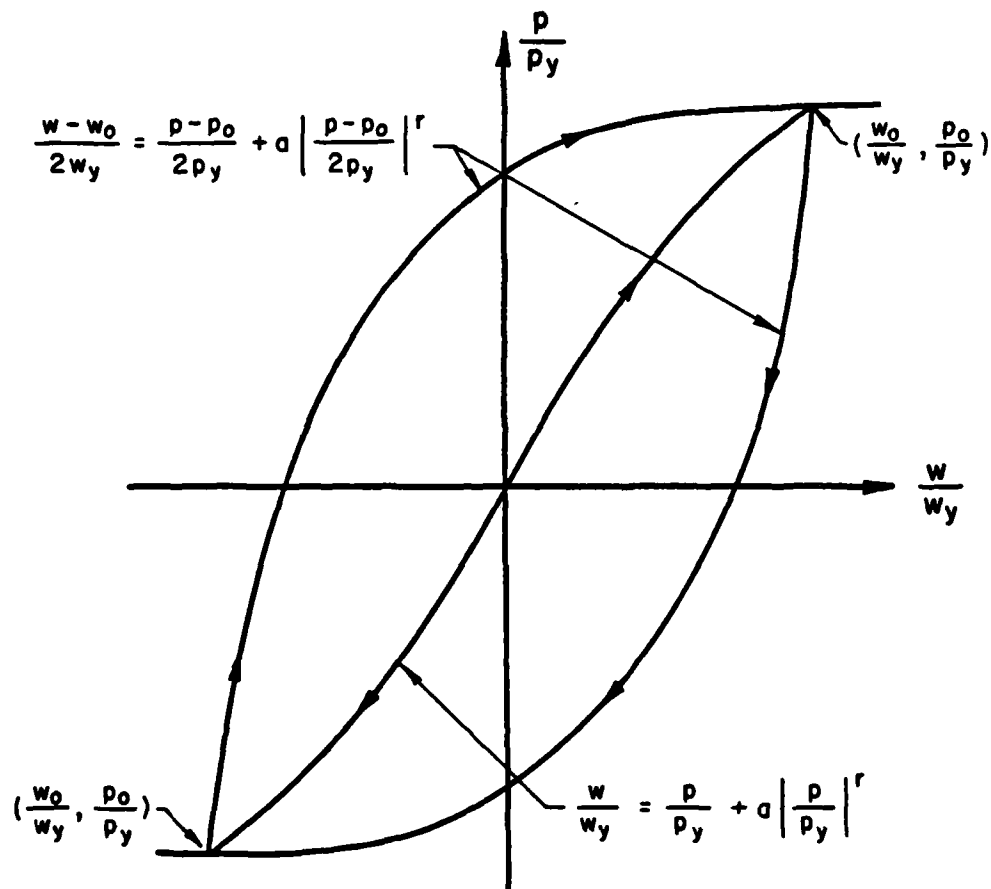


Fig. 2.11 The Ramberg-Osgood Model for Loading and Unloading

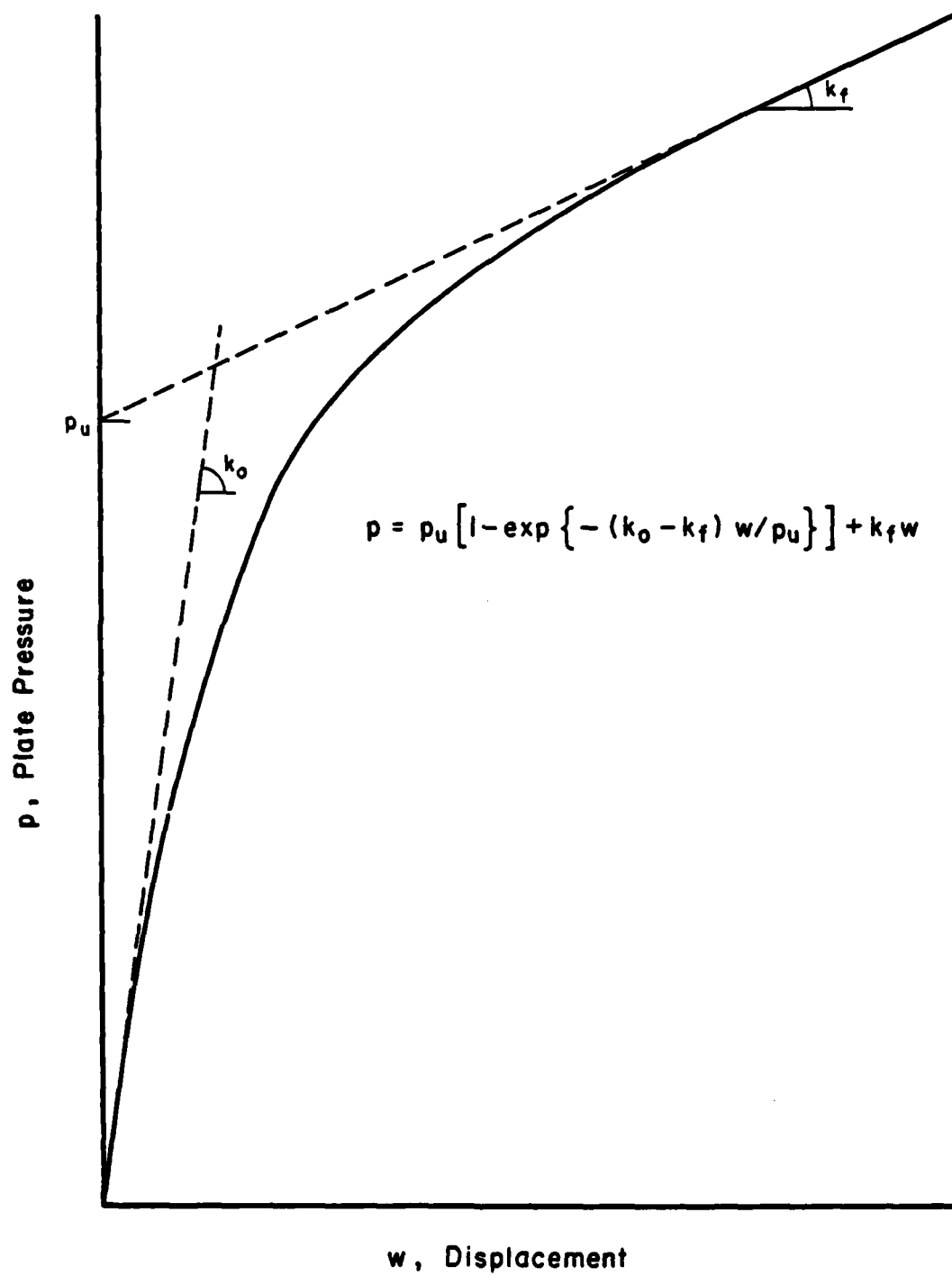


Fig. 2.12 Parameters for Butterfield and Georgiadis Empirical Equation

2.7 NONLINEAR TWO-PARAMETER MODELS

Expanding on an idealization first proposed by Engesser [36], and using the Pasternak Foundation, Butterfield and Georgiadis [34] also developed a plate pressure-deflection equation using two stiffness parameters: k for the compression springs, and G for the shear springs. They suggested that the pressure applied to a rigid square plate, side-length B , is balanced by two sets of reaction forces, R (Fig. 2.13). The first set is due to the subgrade reaction resulting from the displacement of the vertical springs, directly beneath the plate. The second is the summation of shear stress around the four edges of the plate, which is a function of the deflection in the unloaded region. Equilibrium considerations between applied and reactive forces, leads to:

$$p = \frac{P}{B^2} = q(w_0) + (4G^{0.5}/B) \int_0^{w_0} [q(w) \cdot dw / \sqrt{2 \int q(w) dw}] \quad (2-17)$$

where:

- p : applied plate pressure;
- P : total applied load;
- w_0 : plate displacement;
- $q(w_0) = k w_0$,
: subgrade reaction in loaded region;
- $q(w) = k w(x) = G (d^2w/dx^2)$,
: subgrade reaction in unloaded region.

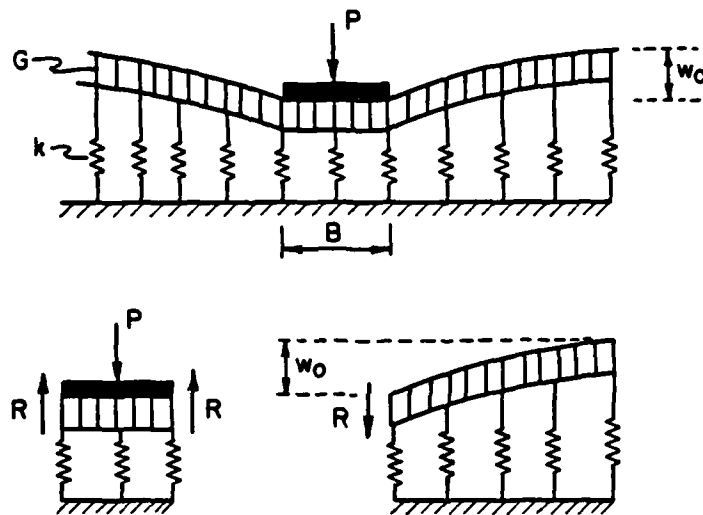


Fig. 2.13 The Nonlinear Two-Parameter Model by Butterfield and Georgiadis

Here parameters k and G are assumed to be nonlinear functions of plate deflection, w_0 , but otherwise independent of plate size. Therefore, Eqn. (2-17) is similar in form to an equation proposed by Engesser [36] for the case of a beam on an elastic foundation. In Engesser's equation, the modulus of subgrade reaction, k , is related to the breadth of the beam, B , as follows:

$$k = a + (b/B) \quad (2-18)$$

where ' a ' and ' b ' are empirical constants. Like Eqn. (2-17), this equation consists of a term depending on B , and another independent of it.

For a pair of plates of different sizes, B_1 and B_2 , but deflecting by the same amount, w_0 , Eqn. (2-17) may be written as [34]:

$$\begin{aligned} p_1 &= \alpha + \beta/B_1 \\ p_2 &= \alpha + \beta/B_2 \end{aligned} \quad (2-19)$$

whence constants α and β -and (k, G) by implication- may be determined.

Butterfield and Georgiadis [37] had earlier proposed another model which can be used to predict cyclic load behavior of plates of any size, from two in-situ tests: a conventional plate load test and a single load level cyclic plate test. From these two tests, the following empirical equations were developed:

$$k_u = k_o - C_2 \frac{P_c}{P_u} [1 + C_3 \log \{N/(P_c/P_u)\}] \quad \text{for unloading}$$

$$k_r = k_o - C_1 \frac{P_c}{P_u} \quad \text{for reloading (2-20)}$$

where:

k_o : initial stiffness;

k_f : final stiffness;

P_u : applied load axis intercept;

P_c : cyclic load level;

k_r : reloading stiffness;

k_u : unloading stiffness;

C_1, C_2, C_3 : experimentally determined constants;

N : number of cycles.

These equations can be used to predict the nonlinear response of a plate for any number of cycles at any load level.

2.8 NON-HOMOGENEOUS ELASTIC HALF-SPACE

The purpose of analyses discussed in this paragraph is to account for the inhomogeneity of typical in-situ soil masses. As a result of depositional processes, especially the effect of overburden pressure, soil stiffness generally increases with depth, with the possible exception of a dessicated crust of higher stiffness near the surface. The soil shear modulus, G_s , is commonly used as a measure of stiffness. Problems in which G_s varies with depth, either according

to a power law or exponentially, have been discussed by numerous investigators [3].

The analysis presented by Gibson [38] is particularly interesting, since it provides -as an unexpected bonus- a rigorous theoretical relation between the dense liquid and elastic solid models. Gibson examined the case of an incompressible medium ($\mu_s=0.5$) whose shear modulus G_s increases linearly with depth, i.e.

$$G_s(z) = G_s(0) + mz \quad (2-21)$$

In the special case when the modulus is zero at the surface ($G_s(0)=0$), he showed that a rectangular strip loading causes a uniform surface settlement of w_0 within the loaded area. This settlement is proportional to the applied pressure and can, therefore, be written as:

$$w_0 = q/k_s \quad (2-22)$$

where:

$$k_s = 2m \quad (2-23)$$

The factor k_s is similar in nature to the modulus of subgrade reaction, and it is shown in this case to be independent of the size or shape of the loaded area. Outside the loaded area, the surface does

not settle. This finding validates Winkler's concept for a semi-infinite elastic medium, provided that $\mu_g=0.5$ and $E_g(z)=3mz$. It was not established that these conditions are both necessary and sufficient, only that they are sufficient. It is conceivable that other combinations of $\mu_g(z)$ and $E_g(z)$ might lead to similar results.

2.9 COMPARISON BETWEEN THE LAYERED ELASTIC AND PLATE THEORIES

In the entirety of this work, the behavior of slabs-on-grade is investigated on the basis of plate theory. This approach has been used routinely in the design of such pavements ever since the publication of Westergaard's pioneer works in the 1920's. Recently, however, use of the layered elastic theory has been proposed for the analysis of both flexible and rigid pavements [39; 40; 41]. Such a "unified" procedure is philosophically and practically attractive, and would allow the characterization of the pavement as a multi-layered system. This is more realistic than the current use of the subgrade modulus, k , in a two-layer (or at most three-layer) system assumed when plate theory is employed.

Using the layered elastic theory, however, inevitably restricts the scope of all analyses to the case of interior loading, in which all layers extend to infinity in the two horizontal directions. Despite the fact that some layered elastic theory computer codes can currently accommodate multi-wheel loads, none of them can provide any information

on pavement response under edge and corner loads, or the efficiency of load transfer systems at the pavement joints. This latter aspect of behavior is evidently considered an overriding consideration by the Federal Aviation Administration. Advisory Circular AC 150/5320-6C dated December 7, 1978 [42] changed the design criterion for Portland Cement Concrete (PCC) airport pavements, from the maximum stress under an interior load, to that of the maximum stress when the load is placed near an edge. This approach to design is more realistic, as it can be shown that the maximum stress in PCC pavements occurs under edge loading. Furthermore, it is practically impossible to place an aircraft on most pavement slabs in a manner to produce anything approaching a true interior loading condition [43]. It has also been shown that nearly all distress in jointed concrete pavements is joint related [44].

Despite these limitations of universal usage of the layered elastic theory, the search for a "unified" approach remains a very attractive proposition. The investigation and comments that follow are intended as a contribution to this effort.

The possibility of analyzing the top layer of a pavement system as a plate, while retaining Burmister's multi-layer theory for the remainder has been investigated by Pickett and Ai [45]. These authors point out, however, that such a substitution "without modification would result in appreciable error in cases of practical importance, since it does not take into account the effects of shear in the pavement on deflection and does not properly take into account

horizontal shear at the interface between subgrade and pavement". A modification was, therefore, proposed so that their "hybrid" method gives results that are in agreement with the more rigorous theory used by Burmister over a wide range of conditions. On the other hand, Parker, et al. [40] contend that "the representation of the top layer as a thin elastic plate or as an elastic layer is really not that different when the top layer is a PCC slab. The major difference lies in the representation of the remainder of the structure."

To investigate this issue further, a comparison is attempted below between the layered elastic and plate theories for the case of interior loading on a semi-infinite pavement system. The system consists of a top layer or PCC slab resting on a Boussinesq half-space, characterized by E_s and μ_s . From the point of view of the layered elastic theory, this half-space is the special case of a multi-layered system consisting of one layer only. As far as plate theory is concerned, the problem is the standard one of a plate on an elastic solid foundation. The analyses were performed using ELP15 and WESTER computer programs, respectively. These programs are described briefly in Chapter 3. The equations presented by Losberg [13] are used in WESTER for the responses according to plate theory.

The parameters selected for the various system components ranged between very wide limits, in order to ensure that most practical conditions are included in the factorial of runs conducted. The results from these runs are tabulated in Table 2.2. The plots of non-dimensional maximum responses in Figure 2.14 indicate that the

TABLE 2.2
COMPARISON OF LAYERED ELASTIC AND PLATE THEORIES

RUN No.	E (psi)	E _s (psi)	h (in.)	l _e (in.)	a (in.)	P (psi)	(a/l _e)	DEFLECTION			SUBGRADE STRESS			BENDING STRESS		
								δ _p (mils)	δ _L (mils)	δ _L /δ _p	q _p (psi)	q _L (psi)	q _L /q _p	σ _p (psi)	σ _L (psi)	σ _L /σ _p
1	4000000.	5500.	2.16	9.99	1.00	3183.10	.10	55.66	65.25	1.17	18.25	23.08	1.26	3435.95	3299.00	.96
2	4000000.	1500.	1.40	9.98	5.01	126.82	.50	194.01	192.70	.99	14.58	14.87	1.02	3763.61	3720.00	.99
3	4000000.	5500.	2.16	9.99	7.50	56.59	.75	50.49	49.94	.99	12.67	12.85	1.01	1162.07	1118.00	.96
4	4000000.	3020.	1.77	10.00	10.00	31.83	1.00	87.31	85.96	.98	11.06	11.00	.99	1342.95	1251.00	.93
5	4000000.	1500.	1.40	9.98	20.01	7.95	2.00	147.80	134.70	.91	7.73	6.11	.79	1473.55	714.90	.49
6	3000000.	6000.	4.90	20.00	2.00	795.77	.10	25.48	30.11	1.18	4.55	5.82	1.28	667.92	627.30	.94
7	3000000.	5500.	4.75	19.96	4.00	198.94	.20	27.62	27.65	1.00	4.32	4.54	1.05	542.62	537.60	.99
8	4000000.	1500.	2.80	19.97	10.00	31.83	.50	97.02	96.37	.99	3.65	3.72	1.02	942.20	930.80	.99
9	3000000.	6000.	4.90	20.00	15.00	14.15	.75	23.12	22.87	.99	3.16	3.22	1.02	226.02	216.70	.96
10	4000000.	4351.	4.00	20.00	20.01	7.95	1.00	30.29	29.80	.98	2.76	2.75	1.00	262.95	244.10	.93
11	3000000.	5500.	4.75	19.96	29.99	3.54	1.50	21.70	20.86	.96	2.20	2.05	.93	133.57	100.50	.75
12	4000000.	1500.	2.80	19.97	39.99	1.99	2.00	73.91	67.37	.91	1.93	1.53	.79	368.28	179.00	.49
13	4000000.	5500.	6.50	30.06	3.00	353.68	.10	18.50	21.70	1.17	2.02	2.55	1.27	379.83	364.80	.96
14	4000000.	5500.	6.49	30.01	6.00	88.42	.20	18.37	18.34	1.00	1.91	1.99	1.04	290.99	288.90	.99
15	3000000.	3260.	6.00	30.01	15.00	14.15	.50	29.71	29.53	.99	1.62	1.67	1.03	205.48	202.30	.98
16	4000000.	3350.	5.50	30.00	22.99	6.02	.77	27.51	27.20	.99	1.39	1.41	1.01	176.19	169.90	.96
17	4000000.	3020.	5.31	29.99	29.99	3.54	1.00	29.10	28.65	.98	1.23	1.22	.99	149.26	139.10	.93
18	4000000.	5500.	6.49	30.01	45.00	1.57	1.50	14.44	13.89	.96	.97	.91	.93	71.64	54.25	.76
19	4000000.	5500.	6.50	30.06	60.00	.88	2.00	13.40	12.19	.91	.85	.68	.79	68.25	32.91	.48
20	6000000.	2754.	6.00	40.00	4.00	198.94	.10	27.76	32.23	1.16	1.14	1.40	1.23	445.46	443.60	1.00

TABLE 2.2 (continued)

RUN No.	E (psi)	E _s (psi)	h (in.)	t _e (in.)	a (in.)	P (psi)	(a/t _e)	DEFLECTION			SUBGRADE STRESS			BENDING STRESS		
								δ _p (mils)	δ _L	δ _L /δ _p	q _p (psi)	q _L	q _L /q _p	σ _p (psi)	σ _L	σ _L /σ _p
21	4000000.	4350.	8.00	40.00	8.00	49.74	.20	17.42	17.35	1.00	1.08	1.11	1.03	191.48	189.90	.99
22	4000000.	2914.	7.00	40.00	20.01	7.95	.50	24.93	24.77	.99	.91	.93	1.03	150.89	148.80	.99
23	4000000.	1836.	6.00	40.00	29.99	3.54	.75	37.78	37.38	.99	.79	.80	1.01	150.78	146.10	.97
24	4000000.	3020.	7.08	39.98	39.99	1.99	1.00	21.83	21.49	.98	.69	.69	.99	83.95	78.20	.93
25	4000000.	1836.	6.00	40.00	60.14	.88	1.50	32.43	31.25	.96	.55	.51	.93	83.68	63.94	.76
26	4000000.	1836.	6.00	40.00	79.79	.50	1.99	30.17	27.52	.91	.48	.38	.79	80.08	39.22	.49
27	4000000.	3055.	8.00	45.00	9.00	39.30	.20	22.05	21.91	.99	.85	.86	1.02	191.49	189.70	.99
28	3000000.	6000.	12.25	50.00	5.00	127.32	.10	10.19	12.05	1.18	.73	.93	1.28	106.87	100.40	.94
29	4000000.	3171.	9.00	50.01	10.00	31.83	.20	19.12	19.00	.99	.69	.70	1.02	151.30	149.90	.99
30	5000000.	5440.	10.00	50.00	25.01	5.09	.50	10.68	10.62	.99	.58	.60	1.03	73.93	72.78	.98
31	3000000.	6000.	12.25	50.00	37.50	2.26	.75	9.25	9.15	.99	.51	.51	1.02	36.16	34.67	.96
32	4000000.	3020.	8.85	49.98	50.06	1.27	1.00	17.46	17.19	.98	.44	.44	.99	53.66	49.97	.93
33	6000000.	3343.	8.00	49.99	50.06	1.27	1.00	15.77	15.53	.99	.44	.44	.99	65.69	61.31	.93
34	4000000.	3020.	8.85	49.98	74.99	.57	1.50	15.79	15.20	.96	.35	.33	.93	38.51	29.35	.76
35	5000000.	2790.	8.00	49.97	99.74	.32	2.00	15.89	14.49	.91	.31	.24	.79	45.05	21.99	.49
36	4000000.	5500.	13.00	60.12	6.00	88.42	.10	9.25	10.85	1.17	.50	.64	1.27	94.96	91.19	.96
37	4000000.	5500.	12.98	60.02	12.00	22.10	.20	9.18	9.17	1.00	.48	.50	1.04	72.75	72.20	.99
38	4000000.	3020.	10.62	59.97	20.01	7.95	.33	16.47	16.24	.99	.44	.46	1.04	84.25	84.37	1.00
39	4000000.	5500.	12.97	59.98	29.99	3.54	.50	8.81	8.76	.99	.40	.42	1.03	43.96	43.23	.98
40	6000000.	1930.	8.00	60.04	45.03	1.57	.75	23.94	23.69	.99	.35	.35	1.01	84.80	82.31	.97

TABLE 2.2 (continued)

RUN No.	E (psi)	E _s (psi)	h (in.)	l _e (in.)	a (in.)	p (psi)	(a/e)	DEFLECTION			SUBGRADE STRESS			BENDING STRESS		
								δ _p (mils)	δ _L (mils)	δ _L /δ _p	q _p (psi)	q _L (psi)	q _L /q _p	σ _p (psi)	σ _L (psi)	σ _L /σ _p
41	4000000.	5500.	12.97	59.98	60.14	.88	1.00	7.99	7.86	.98	.31	.31	1.00	24.96	23.10	.93
42	4000000.	5500.	12.98	60.02	90.00	.39	1.50	7.22	6.95	.96	.24	.23	.93	17.91	13.56	.76
43	4000000.	5500.	13.00	60.12	120.00	.22	2.00	6.70	6.10	.91	.21	.17	.79	17.06	8.23	.48
44	4000000.	1000.	8.60	70.20	7.00	64.96	.10	43.56	50.49	1.16	.37	.45	1.21	217.04	217.40	1.00
45	4000000.	1500.	9.82	70.03	14.00	16.24	.20	28.86	28.59	.99	.35	.35	1.00	127.10	125.40	.99
46	4000000.	1500.	9.82	70.03	34.99	2.60	.50	27.67	27.48	.99	.30	.30	1.02	76.72	75.80	.99
47	6000000.	2380.	10.00	69.99	52.61	1.15	.75	16.65	16.47	.99	.26	.26	1.01	54.16	52.52	.97
48	4000000.	1000.	8.60	70.20	70.00	.65	1.00	37.57	37.03	.99	.22	.22	.99	57.06	53.55	.94
49	4000000.	1500.	9.82	70.03	104.77	.29	1.50	22.70	21.90	.96	.18	.17	.93	31.33	24.09	.77
50	4000000.	1500.	9.82	70.03	141.05	.16	2.01	21.05	19.15	.91	.16	.12	.79	30.01	14.39	.48
51	4000000.	8500.	20.00	80.00	8.00	49.74	.10	4.50	5.32	1.18	.28	.36	1.28	40.09	37.50	.94
52	4000000.	1500.	11.20	79.87	40.10	1.98	.50	24.25	24.09	.99	.23	.23	1.02	58.79	58.08	.99
53	4000000.	8500.	20.00	80.00	60.14	.88	.75	4.08	4.03	.99	.20	.20	1.02	13.54	12.97	.96
54	6000000.	1593.	10.00	80.01	79.79	.50	1.00	20.69	20.40	.99	.17	.17	.99	42.19	39.59	.94
55	4000000.	1500.	11.20	79.87	162.87	.12	2.04	18.41	16.68	.91	.12	.09	.78	23.20	10.80	.47
56	4000000.	1500.	12.60	89.85	9.00	39.30	.10	22.69	26.32	1.16	.23	.28	1.22	100.96	100.80	1.00
57	4000000.	1500.	12.60	89.85	18.00	9.82	.20	22.49	22.27	.99	.21	.21	1.00	77.13	76.12	.99
58	4000000.	1500.	12.60	89.85	45.03	1.57	.50	21.56	21.41	.99	.18	.18	1.02	46.51	45.95	.99
59	4000000.	5500.	19.46	89.99	135.00	.17	1.50	4.81	4.63	.96	.11	.10	.93	7.97	6.03	.76
60	4000000.	1000.	12.30	100.40	10.00	31.83	.10	30.46	35.31	1.16	.18	.22	1.21	106.15	106.30	1.00

TABLE 2.2 (continued)

RUN No.	E (psi)	E _s (psi)	h (in.)	t _e (in.)	a (in.)	P (psi)	(a/t _e)	DEFLECTION			SUBGRADE STRESS			BENDING STRESS		
								δ _p (mils)	δ _L (mils)	δ _L /δ _p	q _p (psi)	q _L (psi)	q _L /q _p	σ _p (psi)	σ _L (psi)	σ _L /σ _p
61	4000000.	1500.	14.00	99.83	20.00	7.96	.20	20.25	20.05	.99	.17	.17	1.00	62.48	61.67	.99
62	4000000.	1500.	14.00	99.83	50.06	1.27	.50	19.40	19.27	.99	.15	.15	1.02	37.66	37.20	.99
63	6000000.	1410.	12.00	100.00	74.73	.57	.75	19.69	19.49	.99	.13	.13	1.00	37.80	36.74	.97
64	4000000.	1000.	12.30	100.40	100.00	.32	1.00	26.27	25.90	.99	.11	.11	.99	27.92	26.21	.94
65	3000000.	6000.	24.50	99.99	150.00	.14	1.50	3.97	3.82	.96	.09	.08	.93	5.03	3.78	.75
66	4000000.	1500.	14.00	99.83	199.47	.08	2.00	14.79	13.49	.91	.08	.06	.79	14.72	7.19	.49

Notes:

P = 10,000 lbs

ν_s = 0.45

μ = 0.15

P : Plate Theory ('WESTER') - Equations as per Losberg [13]

L : Layered Elastic Theory ('ELP15')

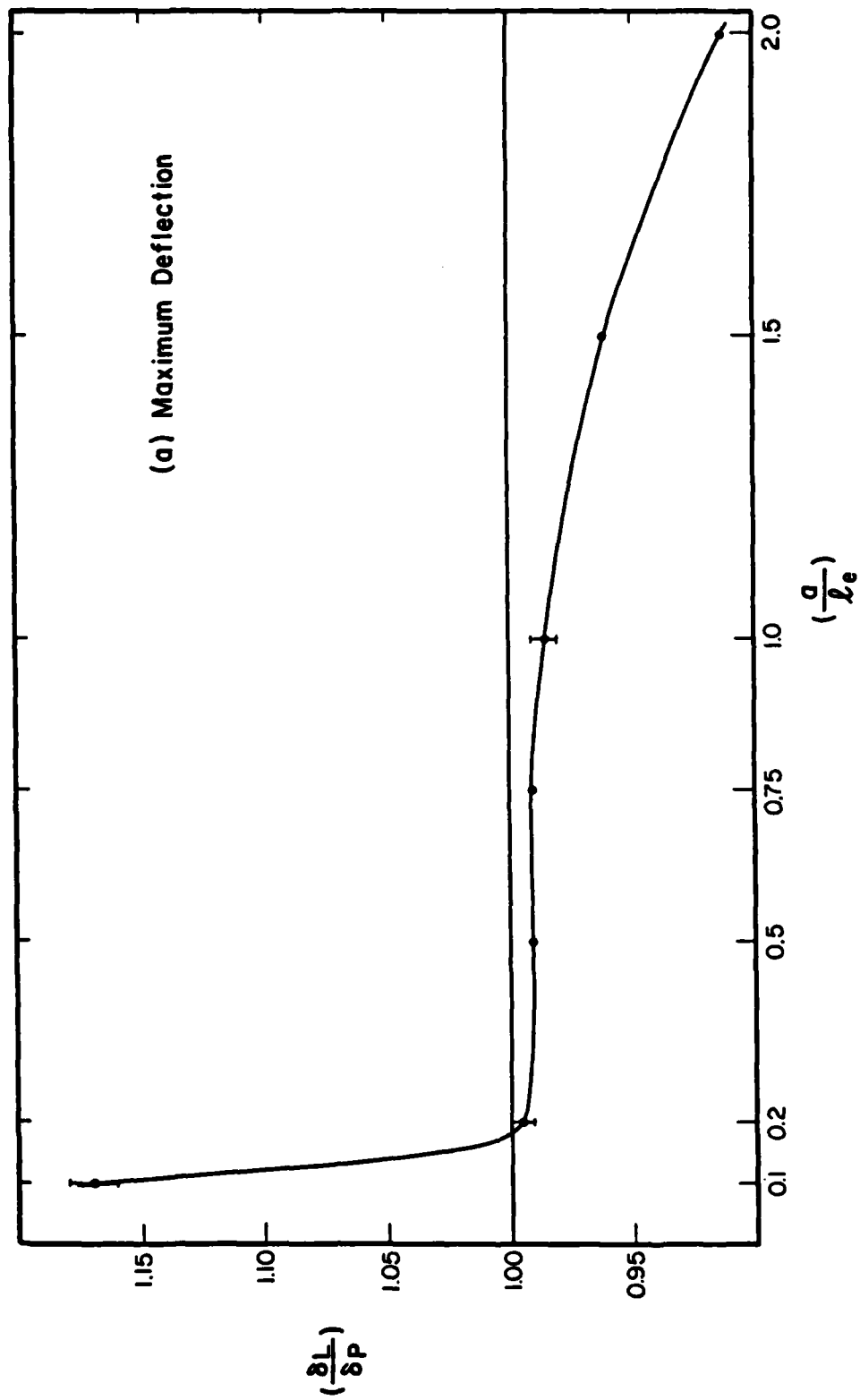


Fig. 2.14 Comparison of Layered Elastic (L) and Plate (P) Theories

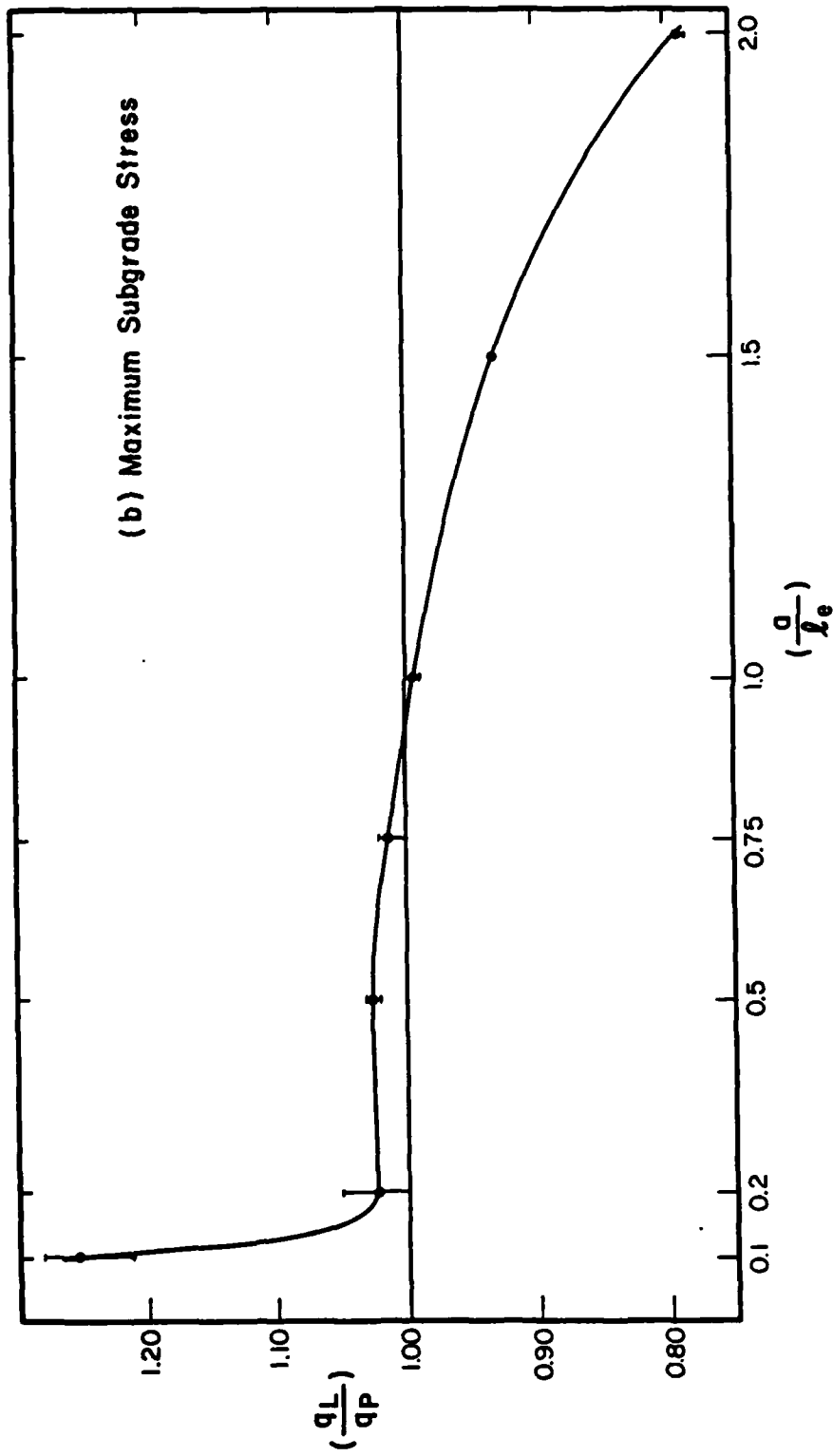


Fig. 2.14 (continued)

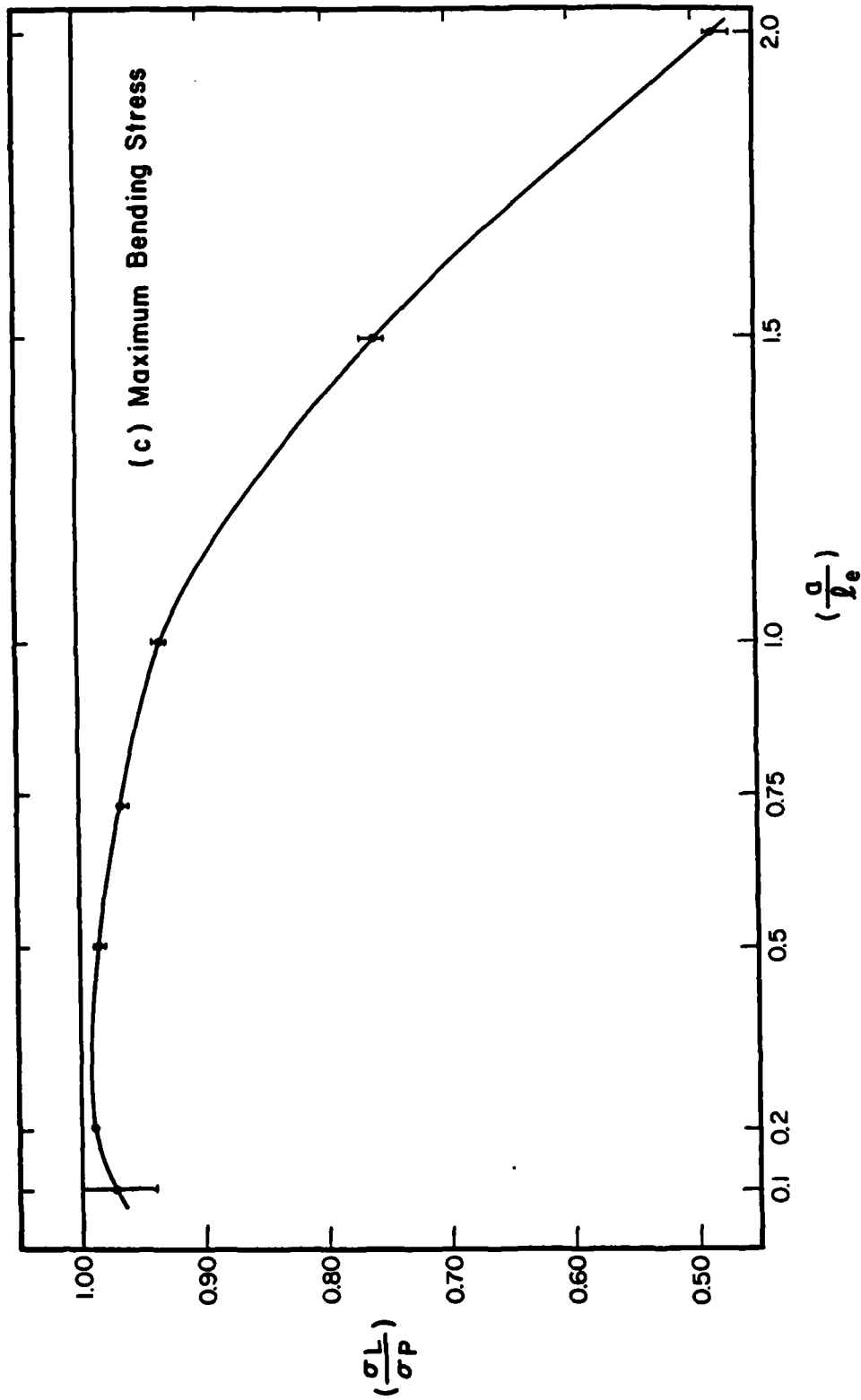


Fig. 2.14 (continued)

governing consideration in comparing the layered elastic and plate theories is the value of the ratio (a/ℓ_e) , of the radius of the applied load to the radius of relative stiffness of the pavement system.

Good agreement between the two theories is obtained when (a/ℓ_e) is between 0.2 and 1.0. Within this range, maximum deflection and bending stress as calculated by the layered elastic theory is about 97% of the corresponding plate theory values. On the other hand, maximum subgrade stress determined by the layered elastic theory is about 105% of that obtained using the plate theory. Considerable deterioration occurs in the agreement between the two theories outside this range. Values of (a/ℓ_e) greater than 1.0 are principally of academic interest only, but several cases may arise in practice where (a/ℓ_e) takes values below 0.2. In such cases, widely divergent results may be expected from the two theories.

Note that the comparison presented here refers only to the interior loading condition. Similar comparisons for edge and corner loading are not feasible, because of the inherent limitations of the layered elastic theory. Furthermore, the comparison is with the plate theory used in conjunction with an elastic solid foundation. It is generally admitted that the dense liquid and elastic solid models can only be correlated in a very limited number of special cases [46]. As a result, a comparison between the layered elastic theory and the plate theory used in conjunction with a dense liquid foundation would have very limited significance, and would not be of a general nature at

all. Such a comparison is attempted by Barker [41].

The fairly good agreement between the two theories within the prescribed range of (a/ℓ_e) values has only been established for the case of the semi-infinite half-space. A similar comparison for the multi-layered foundation case is feasible, at least theoretically, using WESLAYER or RISC finite element programs (see Chapter 3) for the plate theory investigation. Unfortunately, these programs are not available at the University of Illinois. Furthermore, the application of the finite element method in conjunction with a multi-layered subgrade has not yet been developed to the point where it is generally practical to use, since such programs make extravagant demands on computer resources.

CHAPTER 3

COMPUTERIZED NUMERICAL ANALYSES OF SLABS-ON-GRADE

3.1 INTRODUCTION

The determination of stresses and deflections in slab-on-grade pavements with joints and/or cracks has been a subject of major concern for several years. For many pavement structures it has been virtually impossible to obtain analytical (closed-form) solutions because of the complexity of geometry, boundary conditions, and material properties, unless certain simplifying assumptions are made. These, however, result in a modification of the characteristics of the problem. Since all the analytical solutions are based on an infinitely large slab with no, or at most one discontinuity, they cannot be applied to analysis of jointed or cracked slabs of finite dimensions, with or without load transfer systems at the joints and cracks.

With the advent of high speed digital computers, solution of these complex structural problems has been greatly facilitated. Three of the most powerful methods that have evolved are discussed briefly in this Chapter. These methods are applicable to a wide range of complex, boundary value problems in engineering. The present overview, however, is restricted to the use of the methods within the scope of this study.

In the second part of this Chapter, brief descriptions are given of several computer programs currently available for the determination of stresses and displacements in pavement systems. The emphasis is on

those programs that employ one of the three approaches outlined in the first part of this Chapter, and were available to the author during this study.

3.2 THE FINITE ELEMENT METHOD

In the Finite Element Method (F.E.M.) the system to be analyzed is represented by an assemblage of subdivisions or discrete bodies called "finite elements" [47; 48]. These elements are interconnected at specific locations called "nodes" or "nodal points". Functions are developed to approximate the distribution or variation of the actual displacements over each finite element. Such assumed functions are called "displacement functions" or "shape functions". Relationships are then established between these generalized displacements (usually denoted by $\{d\}$) and the generalized forces (usually denoted by $\{p\}$) applied at the nodes, using the principle of virtual work or some other variational principle. This element force-displacement relationship is expressed in the form of element stiffness matrices (usually denoted by $[k]$), each of which incorporates the material and geometrical properties of one element, viz.,

$$[k] \{d\} = \{p\} \quad (3-1)$$

The overall structural stiffness matrix, $[K]$ is then formulated by superimposing the individual element stiffness matrices using the

topological (element connectivity) properties of the structure. This "global" stiffness matrix is used to solve a set of simultaneous equations of the form:

$$[K] \{D\} = \{P\} \quad (3-2)$$

where:

$\{P\}$: applied nodal forces for the whole system;

$\{D\}$: resulting nodal displacements for the whole system.

3.3 THE FINITE DIFFERENCE METHOD

One of the earliest examples of the use of the Finite Difference Method (F.D.M.) to problems in the theory of elasticity is an analysis of torsional effects presented by Runge [49]. Since then, the method has been employed in numerous other applications in elasticity, plasticity and fluid mechanics. Prior to the 1960's the F.D.M. was probably the main numerical technique in geotechnical engineering. Extensive literature lists of geotechnical applications, including beams and plates on an elastic foundation, are given by Desai and Christian [50], and Selvadurai [3].

In the analysis of slabs-on-grade, it is generally recognized that the F.E.M. possesses certain advantages over the F.D.M. Nevertheless, the latter may be more suitable or convenient to use in some cases, but this possibility has remained largely unexplored. Since the amount of

computer memory core required for the solution of any given problem using the F.D.M. can be expected to be smaller than that required by the F.E.M., it is likely that the use of finite difference techniques may be particularly useful in problems requiring considerable computer effort. In any case, comparisons of numerical results from the two methods are bound to be enlightening, and will reinforce each other's credibility.

The basic concept in a finite difference solution of the slab-on-grade problem, is to replace the governing differential equation and the boundary conditions by the corresponding finite difference equations, describing the variation of the primary variable (deflection) over a small but finite spatial increment. Thus, the first derivative of deflection in the x-direction at any point, for example, may be written as:

$$\frac{du}{dx} = \lim_{\Delta x \rightarrow 0} \frac{\Delta u}{\Delta x} \approx \frac{\Delta u}{\Delta x} \quad (3-3)$$

Table 3.1 presents the finite difference expressions for the derivatives of a function $u(x,y)$, using what is commonly referred to in the literature as central-difference approximations. These are considered superior to the corresponding "forward-" or "backward-approximations". The result of such substitutions is to reduce the problem to the solution of a set of simultaneous equations, which can be routinely performed using pre-existing software on most digital computers.

TABLE 3.1
FINITE DIFFERENCE EXPRESSIONS

$$\bar{u}_{ij} = u_{ij}$$

$$\frac{\partial u}{\partial x}_{ij} = \frac{1}{2h} (u_{i+1,j} - u_{i-1,j})$$

$$\frac{\partial^2 u}{\partial x^2}_{ij} = \frac{1}{h^2} (u_{i+1,j} - 2u_{i,j} + u_{i-1,j})$$

$$\frac{\partial^3 u}{\partial x^3}_{ij} = \frac{1}{2h^3} (u_{i+2,j} - 2u_{i+1,j} + 2u_{i-1,j} - u_{i-2,j})$$

$$\frac{\partial^4 u}{\partial x^4}_{ij} = \frac{1}{h^4} (u_{i+2,j} - 4u_{i+1,j} + 6u_{i,j} - 4u_{i-1,j} + u_{i-2,j})$$

$$\frac{\partial^2 u}{\partial x \partial y}_{ij} = \frac{1}{4hk} (u_{i+1,j+1} - u_{i+1,j-1} - u_{i-1,j+1} + u_{i-1,j-1})$$

$$\frac{\partial^3 u}{\partial x^2 \partial y}_{ij} = \frac{1}{2h^2 k} (u_{i+1,j+1} - 2u_{i,j+1} + u_{i-1,j+1} - u_{i+1,j-1} +$$

$$2u_{i,j-1} - u_{i-1,j-1})$$

$$\frac{\partial^4 u}{\partial x^2 \partial y^2}_{ij} = \frac{1}{h^2 k^2} (u_{i+1,j+1} - 2u_{i+1,j} + u_{i+1,j-1} - 2u_{i,j+1} +$$

$$4u_{i,j} - 2u_{i,j-1} + u_{i-1,j+1} - 2u_{i-1,j} + u_{i-1,j-1})$$

where:

h : size of finite step in x-direction;

k : size of finite step in y-direction.

The most important criterion governing the adequacy of the finite difference approximation is the fineness of the finite difference grid. The requirement for a fine grid has to be tempered, of course, by the amount of computer memory space available. Useful discussions of the accuracy of finite difference solutions are given by Southwell [51], Allen [52] and Allen and Windle [53].

3.4 NUMERICAL INTEGRATION TECHNIQUES

A third category of computerized numerical procedures considered in this study includes solutions involving integrals of Bessel, elliptic or other functions over infinite or finite ranges. Use of digital computers reduces the evaluation of such integrals, from an enormous volume of hand-calculations, to a routine task requiring only a small effort on the part of the user. Furthermore, these computerized numerical integrations are performed over finite sub-ranges in a cumulative fashion. Computer results are, therefore, much more accurate than hand-calculations, since a larger number of smaller sub-ranges may be used without any penalty in terms of user effort.

This approach is fundamentally different from the F.D.M. or the F.E.M. In the latter two, the numerical procedure begins with the governing differential equations, and is thus an essential part of the final solution. The use numerical integration techniques, on the other hand, is only an incidental choice of how to evaluate the integrals in an expression derived after considerable manipulation of the governing

differential equation and the boundary conditions. In this sense, this third category of solutions is often more akin to an analytical (closed-form) approach, than to the F.D.M. and the F.E.M. Comparisons between these three techniques can, therefore, be particularly enlightening. Numerous computer programs have been developed for analyzing pavement systems using the three methods outlined in the preceeding sections. A brief review of some of these is presented below.

3.5 THREE-DIMENSIONAL MODELS

All programs reviewed in this Chapter, except those described in the present section, are basically two-dimensional models. The problem of a slab of finite dimensions on grade, however, involves processes that take place in three-dimensional space. Therefore, the response of the slab and the subgrade to loading, temperature and moisture changes etc., ideally requires a three-dimensional model for accurate simulation. Nevertheless, there are several advantages in simulating the three-dimensional effects using two-dimensional idealizations. First, considering the F.E.M., the difference in cost between a three-dimensional and two-dimensional calculation of the same mesh fineness can be several orders of magnitude, depending on the size of the problem. In the three-dimensional case, there is a higher chance that any given mesh will exceed the memory core capacity of the computer. Secondly, due to its much lower cost, it is practical in a

two-dimensional analysis to increase the mesh fineness in selected zones, thereby increasing the accuracy with which the smaller scale phenomena can be observed. Even more important is the fact that three-dimensional analysis is beyond the state-of-the art of most engineering design groups. If three-dimensional finite element analysis were to be recommended as part of a standard pavement analysis procedure, it is doubtful that many designers would make use of the procedure.

With respect to accuracy, Selvadurai [3] notes that close agreement between a two-dimensional analysis using plate theory and a more elaborate three-dimensional solution may be expected for plates of sufficiently small thickness. Morgenstern [54] has shown that the stresses and strains obtained from a plate theory solution converge, in a mean square sense, to a solution of three-dimensional elasticity, as the plate thickness approaches zero.

On the other hand, theoretical analyses involving three-dimensional models are very desirable, not only in the investigation of those aspects that simply cannot be handled by a two-dimensional approach, but also in providing helpful insight for the improvement and better interpretation of results from two-dimensional analyses. Thus, a two-dimensional analysis may be performed first, followed by a three-dimensional analysis of specific limited segments of the structure. Such a two-stage analysis provides a very reasonable engineering approach. Results from the two-dimensional analysis may be used as boundary conditions for segments to be analyzed using three-dimensional

analysis.

For example, the interaction between a loaded dowel and surrounding concrete constitutes a three-dimensional state of stress. This interaction depends on the dimensions and elastic properties of the dowel bar and concrete slab, as well as any looseness between the dowel bar and surrounding concrete. In the original development of ILLI-SLAB, Tabatabaie, *et al.* [55] performed a three-dimensional analysis in conjunction with two-dimensional analysis of a jointed slab, to establish a realistic dowel-concrete interaction. The solid SAP finite element program developed by Wilson [56] was employed for the three-dimensional analysis of a small section of the concrete slab near the joint and around a dowel bar (Fig. 3.1). Three-dimensional, 8-noded, isoparametric elements with three translational degrees-of-freedom (dof) per node, originally developed by Irons [57] were employed to represent the slab segment. The subgrade was idealized by spring elements. Dowel bars were modeled as beam elements with flexural and shear deformations. Spring or elastic elements were used to represent the contact condition between the dowel bar and surrounding concrete.

As a result of this and later analyses, the dowel bar is modeled in the two-dimensional ILLI-SLAB analysis by a bar element with two dof, a torsional rotation and a deflection. This is considered preferable to both the original model, in which the bar element had a flexural rotation and a deflection as its two dof, and to a third choice, that of a bar element with all three dof (torsional rotation, flexural rotation and deflection).

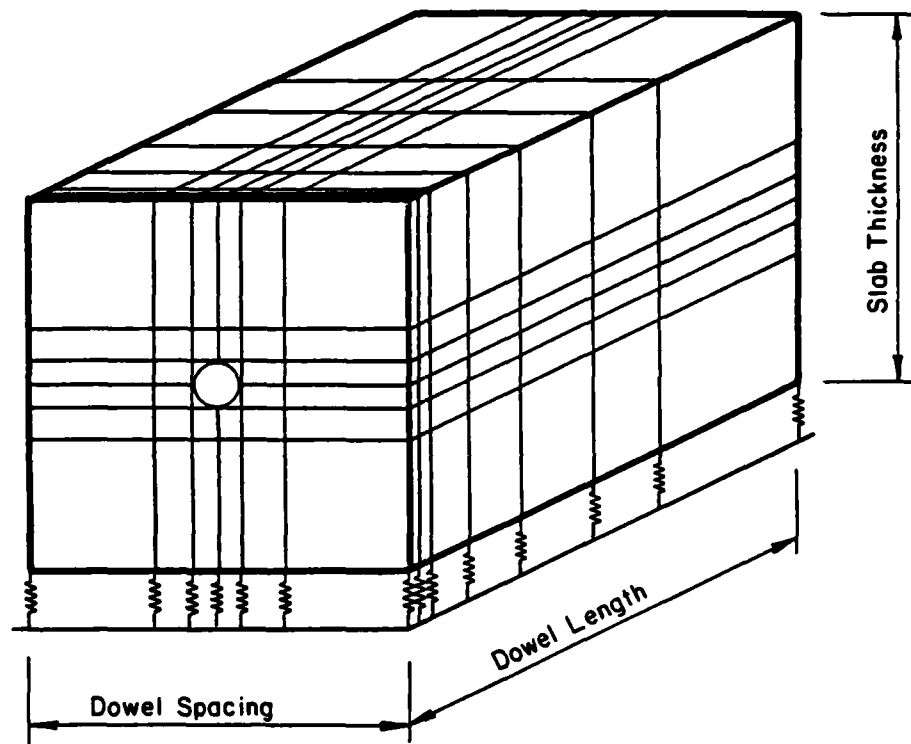


Fig. 3.1 Typical Finite Element Mesh for Three-Dimensional Analysis
(After Tabatabaie, et al, [55])

Another three-dimensional finite element program was developed by Wilson and Pretorius [58] for the analysis of pavements. The program uses a constant strain prismatic solid element, defined as a three-dimensional solid that has constant two-dimensional geometric shapes and infinite third dimension. Element properties can be varied at will in the transverse (x,z) plane, using twelve linearly elastic material types. These properties remain constant along the prisms in the longitudinal (y) direction. The system is essentially two-dimensional, with the third dimension introduced into the idealized structure by expressing the load as a Fourier series in this direction. Stresses and deformations caused by each Fourier term are summed, and the process is continued until further additions become insignificant. This program has been used to study the fatigue behavior of a cement-treated layer [59], reflection cracking through bituminous overlays [60], cracking in a treated pavement base layer [61], edge loading effects [62], and other problems. Execution times are in the range of 30 to 35 minutes; a typical two-dimensional ILLI-SLAB run takes 5 to 10 seconds.

Two programs with three-dimensional analysis capabilities are available at the University of Illinois: FINITE [63; 64] and GEOSYS [65]. Both are multi-purpose programs, i.e. include libraries of one-, two- and three-dimensional elements. FINITE is primarily designed as a tool for the structural engineer, while GEOSYS is geared more toward geotechnical problems. Due to their general nature, neither program is practical for routine analysis of pavement slabs. The major problems

are:

1. A tremendous quantity of input data is required, even for the simplest slab-on-grade three-dimensional analysis;
2. Execution times are prolonged. This translates to prohibitive costs, due to the present implementation of both FINITE and GEOSYS on the CDC-CYBER system.

This is not to underestimate the highly advanced structure and excellent performance of both these programs. Indeed, their data management systems, for example, are among the most efficient to date. The utilization of such techniques in slab-on-grade analysis programs would eliminate several problems now experienced with respect to computer storage requirements.

3.6 DISCRETE ELEMENT MODELS

The Discrete Element Method (D.E.M.) was developed for numerical analysis of plates on dense liquid foundations by Newmark and his co-workers [66; 67]. In this approach, the plate is replaced by an assemblage of deformable hinges (or joints), rigid bars and torsional (coil) springs, arranged in a system of orthogonal beams (Fig. 3.2). The torsional elements model plate twisting stiffness, C , while the hinges represent bending stiffness, D . Deflection at each hinge is the primary unknown. Equilibrium equations are derived from the free body of the hinge, with all internal and external moments, forces and reactions.

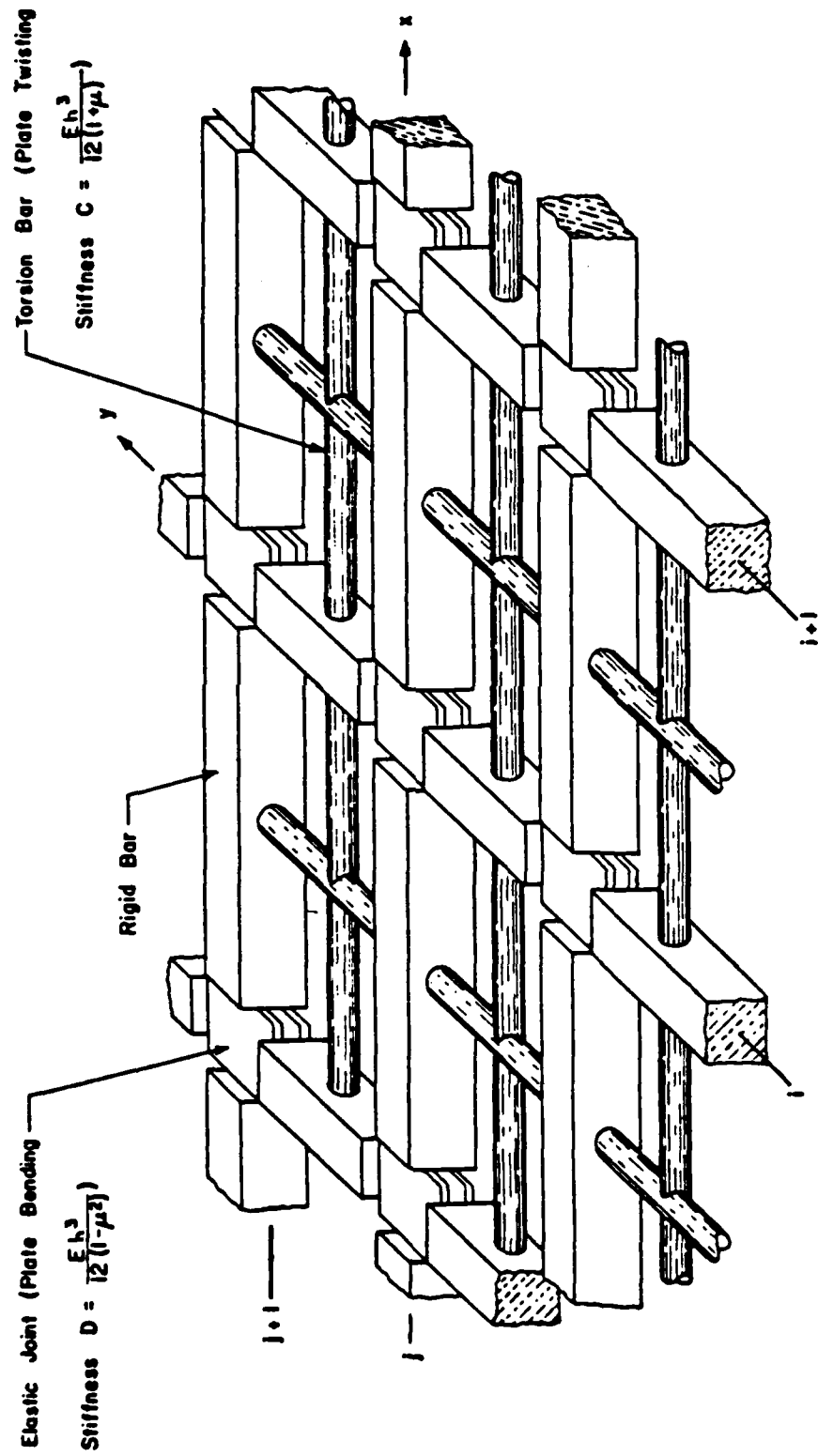


Fig. 3.2 The Discrete Element Model of a Plate or Slab

In Newmark's model subgrade support was provided by a set of independent vertical springs. The D.E.M. was later adapted by Mahanyi [68] for a two-parameter foundation, using a network of cables to model shear interaction between adjacent springs. Using Boussinesq's solution to evaluate subgrade reactions at each hinge, Saxena and Vesic [69; 70] expanded the method to include the elastic solid foundation, as well.

Computer programs developed at the University of Texas using the D.E.M. [71; 72; 73] are designated by the acronym SLAB, and have been extensively utilized. These programs can accommodate complex problems involving any combination of loads and boundary conditions, as well as a variety of discontinuities (cracks and joints) and subgrade support conditions. Thus, Hudson and Matlock [72] analyzed the case of partial subgrade support. Ayyash, *et al.* [74] used the program in a study of the effect of cracking on bending stiffness of a continuously reinforced concrete pavement (CRCP).

The discrete element model is helpful in visualizing the problem and forming the solution. It gives reasonable values for deflections, but may be inaccurate in determining stresses along slab edges. Furthermore, problems exist in the analysis of joints, cracks and gaps under the slab because of the nature of the method [75/1]. The major advantages of the finite element over the discrete element method are that elements of various sizes can easily be incorporated in the analysis and no special treatment is needed at a free edge [76].

3.7 DENSE LIQUID PROGRAMS

3.7.1 KENWINK

In this study, KENWINK denotes a finite element program developed at the University of Kentucky [76; 77]. The analysis is based on the classical theory of medium-thick plates and employs the 4-noded, 12-dof element, known as ACM or RPB12 in finite element literature. The subgrade is modeled as a Winkler foundation by attaching four spring elements at the corners of each plate bending element. The program was developed for determining deflections and stresses in a system composed of a single-layer pavement arranged in series of up to three rectangular slabs, with or without load transfer at the transverse joints. The externally applied loads are converted to a system of statically equivalent nodal loads, which often are not work equivalent to the applied loads.

The program can be used to investigate the effect of partial slab-subgrade contact. Problems involving partial contact are analyzed first by assuming the slab and subgrade are in full contact. If they are indeed in full contact, the problem is considered solved. Otherwise, an iterative procedure is employed. Reactive forces at nodes out of contact are set to zero and the process is repeated until assumed and calculated contact patterns are the same. This procedure considers the self-weight of the slab, allowing for some precompression of subgrade springs produced by this weight.

Load transfer between adjacent slabs is modeled by equating the sum of forces at each pair of nodes at a joint to the externally applied force(s) there, and by requiring that deflections at these nodes be related according to the prescribed load transfer efficiency at the joint. This procedure destroys the symmetry of the stiffness matrix and results in an upper half band which is greater than the lower half. It is thus necessary to store both the upper and lower bands, at a considerable memory core expense. Bar elements are not used in modeling dowel bars because dowels are considered unable to transmit moments from one slab to the other over the very small joint width [75/1; 78:Discussion].

3.7.2 WESLIQID

This program [75/1,3] constitutes an enhanced version of KENWINK. Only additions and/or changes to KENWINK made at Waterways Experiment Station in the preparation of WESLIQID will be described here.

WESLIQID can handle slab thicknesses and moduli of subgrade reaction which vary from node to node, and any number of slabs arranged in any arbitrary pattern. The only restriction is the amount of memory core required. The pavement can consist up to two layers, bonded or unbonded. WESLIQID retains the KENWINK model in which subgrade support springs are connected at the nodal points.

Once subgrade reactive forces at each node are determined, stresses and strains in the soil may be calculated using Boussinesq's or Burmister's equations, if the user supplies values of subgrade modulus,

E_s , and Poisson's ratio, μ_s . Superposition of individual nodal forces is employed in this computation.

Four options are provided for specifying load transfer at the joints. Three involve shear transfer only, while the fourth involves moment transfer. They are:

- (a) Efficiency of Shear Transfer: Load transfer efficiency is specified as a ratio of vertical deflections at two adjacent nodes on either side of the joint;
- (b) Spring Constant: According to Chou [75/1], using imaginary shear transfer springs along the joint is more realistic than specifying a load transfer efficiency, because springs take into consideration shear at the joint. The spring constant, defined as a force causing unit deflection, is specified by the user;
- (c) Diameter and spacing of dowels: Chou [75/1] considers this to be most straightforward and to yield results far superior to the other two options. This option applies only to cases where dowels are the only load transfer device. Dowel diameter, spacing and modulus of dowel support are specified by the user. Selection of the latter is a design decision depending upon the tightness with which dowels are held in the concrete, type of dowels, strength of concrete and method of construction;
- (d) Efficiency of moment transfer: This is defined as a fraction of the full moment which is determined by assuming that

AD-A150 965

ANALYSIS OF SLABS-ON-GRADE FOR A VARIETY OF LOADING AND
SUPPORT CONDITION. (U) ILLINOIS UNIV AT URBANA DEPT OF
CIVIL ENGINEERING. A H IOANNIDES ET AL. DEC 84

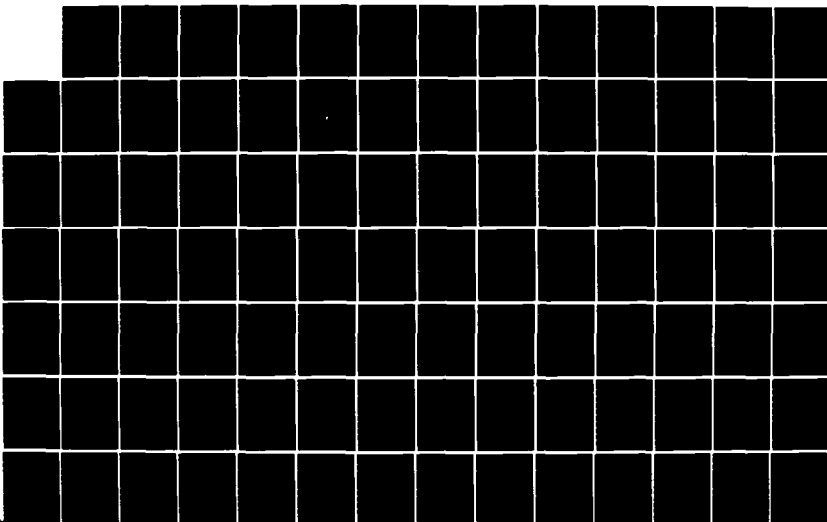
277

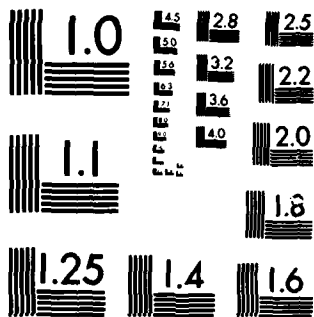
UNCLASSIFIED

AFOSR-TR-85-0083 AFOSR-82-0143

F/G 13/2

NL





MICROCOPY RESOLUTION TEST CHART
NATIONAL BUREAU OF STANDARDS-1963-A

rotations on both sides are the same, rather than as the ratio of rotations at two adjacent nodes on either side of the joint. A moment transfer efficiency of 100% implies equal rotations on both sides of the joint. A zero moment transfer efficiency requires that the moment of all nodal points along the joint is zero, although rotations may not be zero. Unless the efficiency is 0.0 or 1.0 at all joints, it is necessary to analyze the problem twice. First, an efficiency of 1.0 is assumed for all joints where real efficiency is not equal to zero, to determine the full moments. These moments are multiplied by the real moment transfer efficiency and are applied as external moments during a second analysis.

3.7.3 FINITE

This is a general purpose computer system for the analysis of linear and nonlinear structures, developed at the Universities of Illinois and Kansas [63; 64]. FINITE supports a wide variety of elements, from the simplest one- and two-dimensional symmetric elements, to nonsymmetric elements, some types of hybrid elements and elements with varying degrees-of-freedom at each node.

With respect to two-dimensional analyses presented herein, the term FINITE model refers to a representation of the slab on grade system using the RPB12 (or ACM) element for plate bending [47] with four supporting SPRING elements for the subgrade. This model is identical to that used in KENWINK and WESLIQID. In contrast to the latter two

models -which use statically equivalent loads- FINITE uses a work equivalent load vector [47] to convert applied external loads to nodal loads. The FINITE model is used to analyze a single slab with full contact and yields results identical to those obtained by the 'SPRINGS' option of revised ILLI-SLAB.

3.7.4 ILLI-SLAB

ILLI-SLAB was developed at the University of Illinois in the late 1970's for structural analysis of jointed, one- or two-layer concrete pavements with load transfer systems at the joints [79]. The ILLI-SLAB model is based on the classical theory of a medium-thick plate on a Winkler foundation [80], and can evaluate the structural response of a concrete pavement system with joints and/or cracks. It employs the 4-noded, 12-dof plate bending (ACM or RPBI2) element [47]. The Winkler type subgrade is modeled as a uniform, distributed subgrade through an equivalent mass formulation [81]. This is a more realistic representation than the four concentrated spring elements in WESLIQID and FINITE. A work equivalent load vector is used [47], as in FINITE.

Since ILLI-SLAB is a major tool for this research, a more detailed description of this program is appropriate. Assumptions regarding the concrete slab, stabilized base, overlay, subgrade, dowel bar, keyway, and aggregate interlock can be briefly summarized as follows:

- (i) Small deformation theory of an elastic, homogeneous medium-thick plate is employed for the concrete slab, stabilized base and overlay. Such a plate is thick enough to carry transverse

load by flexure, rather than in-plane force (as would be the case for a thin membrane), yet is not so thick that transverse shear deformation becomes important. In this theory, it is assumed that lines normal to the middle surface in the undeformed plate remain straight, unstretched and normal to the middle surface of the deformed plate; each lamina parallel to the middle surface is in a state of plane stress; and no axial or in-plane shear stress develops due to loading;

- (ii) The subgrade behaves as a Winkler foundation;
- (iii) In case of a bonded stabilized base or overlay, full strain compatibility exists at the interface; or for the unbonded case, shear stresses at the interface are neglected;
- (iv) Dowel bars at joints are linearly elastic, and are located at the neutral axis of the slab;
- (v) When aggregate interlock or a keyway is used for load transfer, load is transferred from one slab to an adjacent slab by shear. However, with dowel bars some moment as well as shear may be transferred across the joints.

Various types of load transfer systems, such as dowel bars, aggregate interlock, keyways, or a combination of these can be considered at pavement joints. The model can also accommodate the effect of a stabilized base or an overlay, either with perfect bond or no bond. Thus, ILLI-SLAB provides several options, that can be used in analyzing the following problem types:

1. Jointed concrete pavements with load transfer systems;
2. Jointed reinforced concrete pavements with cracks having reinforcement steel;
3. Continuously reinforced concrete pavements;
4. Concrete shoulders with or without tie bars;
5. Pavements slabs with a stabilized base or overlay, assuming either perfect bond or no bond between the two layers;
6. Concrete slabs of varying thicknesses and moduli of elasticity, and subgrades with varying moduli of support.

The program inputs are:

- (a) Geometry of the slab, including type of base or overlay, load transfer system, subgrade, and slab dimensions;
- (b) Elastic properties of concrete, stabilized base or overlay, load transfer system, and subgrade;
- (c) Loading.

The outputs given by the program are:

- (a) Nodal stresses in the slab, and stabilized base or overlay;
- (b) Vertical reactions at the subgrade surface;
- (c) Nodal deflections and rotations;
- (d) Reactions on the dowel bars;
- (e) Shear stresses at the joint for aggregate interlock and keyed joint systems.

The model has been verified by comparison with the available theoretical solutions and the results from experimental studies [55; 82; 83].

3.7.5 H-51

This program incorporates an analytical method for calculating the bending stress at the edge of a semi-infinite slab resting on a dense liquid foundation [84]. This computerized procedure was first developed by Kreger [85]. A similar procedure (called F-89) for the interior loading condition was also developed. Both are essentially computerized versions of the corresponding Pickett and Ray Charts [86]. In H-51, the table of number of influence squares for normalized load dimensions (a/l) and (b/l) ranging between 0 and 2 given by Pickett and Ray was originally used. This table was revised and expanded to (a/l) and (b/l) values up to 8 at Waterways Experiment Station. The load applied is considered to be uniformly distributed over elliptical areas, such as typical aircraft tire-prints. Only those landing gears possessing two lines of symmetry can be analyzed.

According to the procedure used, any loaded area is first approximated by a series of rectangular strips. The number of strips to be used is specified by the user, and controls the accuracy of the approximation. For each strip, the corresponding number of influence squares is determined from the table of number of squares directly, or by interpolation using subroutine TABINT. The stress developing at the edge is proportional to the sum of the squares under all strips. Given the load and pavement system properties, the program determines the edge stress. Alternatively, the program backcalculates required thickness for the development of a prescribed bending stress.

3.8 ELASTIC SOLID PROGRAMS

3.8.1 KENELS

This acronym is used here to denote the finite element program developed at the University of Kentucky [87] for the analysis of pavement slabs on an elastic solid foundation. It employs the same 12-dof plate bending element (RPB12 or ACM) as KENWINK and ILLI-SLAB for the slab. The formulation by Cheung and Zienkiewicz [88] is followed in the derivation of the subgrade stiffness matrix. A salient feature of the numerical method in KENELS is the adoption of an iterative scheme to reduce computer storage requirements. Two slabs can be analyzed, but a load transfer efficiency of 100% must be assumed at the joint. Partial contact can be accommodated, provided the nodes not in contact are known a priori. Only an old version of this program is available at the University of Illinois.

In a more recent revision of the program [89], a number of improvements were made:

- (i) Any number of slabs can be analyzed, the only restriction being computer storage capacity;
- (ii) Any load transfer efficiency can be specified at the joints, using one of three options, viz. efficiency of shear transfer, spring constant or dowel bars;
- (iii) The non-contact nodes are determined by a method of successive approximations.

These changes make KENELS very similar to WESLAYER, described below.

3.8.2 WESLAYER

This is the second of two finite element programs developed at Waterways Experiment Station [75/1,3] for the analysis of rigid multicomponent pavement structures with discontinuities. WESLAYER is an extension of the original edition of KENELS, and retains the fundamental concepts discussed above. The slab is modeled as a plate using the 12-dof plate bending element (RPB12 or ACM), while the foundation is assumed to be an elastic solid [88], or a layered elastic system. In the second case Burmister's solution is used to compute surface deflections, but this can be a computer time consuming exercise. Partial contact with or without initial gaps can be accommodated, using an iterative scheme. Because of the large computer storage space required, the program can handle only two slabs. Using the symmetry option, four slabs symmetrically loaded may also be analyzed. At the joints, WESLAYER considers only shear transfer, while moment transfer is assumed to be zero. Results from WESLAYER have been presented by Chou [46; 90].

This program is not available at the University of Illinois.

3.9 OTHER PROGRAMS

3.9.1 ILLI-PAVE

ILLI-PAVE is the name of the current version of a finite element program initially developed by Wilson [91], for plane strain analysis of elastic solids with stress dependent properties. This version

incorporates later modifications by Barksdale [92], Duncan, et al. [93], the research staff at the Construction Engineering Laboratory in Champaign, IL, and finally the Transportation Facilities Group, Department of Civil Engineering, at the University of Illinois [94]. It considers an axisymmetric solid of revolution as shown in Fig. 3.3, and employs nonlinear, stress dependent material models (see Section 2.5) and failure criteria for granular materials and fine-grained soils [94; 95; 96]. The principal stresses in the granular and subgrade layers are modified at the end of each iteration so that they do not exceed the strength of the materials as defined by the Mohr-Coulomb theory of failure.

Studies comparing measured and ILLI-PAVE calculated load-deformation responses, reported by Raad and Figueroa [94], Suddath and Thompson [97], Traylor [98], and Hoffman and Thompson [24] yielded favorable results. The ILLI-PAVE approach has been successfully utilized in developing a highway flexible pavement overlay design procedure based on nondestructive testing data analyses [25], as well as mechanistic thickness design procedures for secondary road flexible pavements [99] and soil-lime layers [100].

3.9.2 BISAR

The BISAR (Bitumen Structures Analysis in Roads) program is a general purpose program for computing stresses, strains and displacements in elastic multilayer systems, subjected to one or more normal or tangential, uniform, circular load(s) [101]. The analysis is

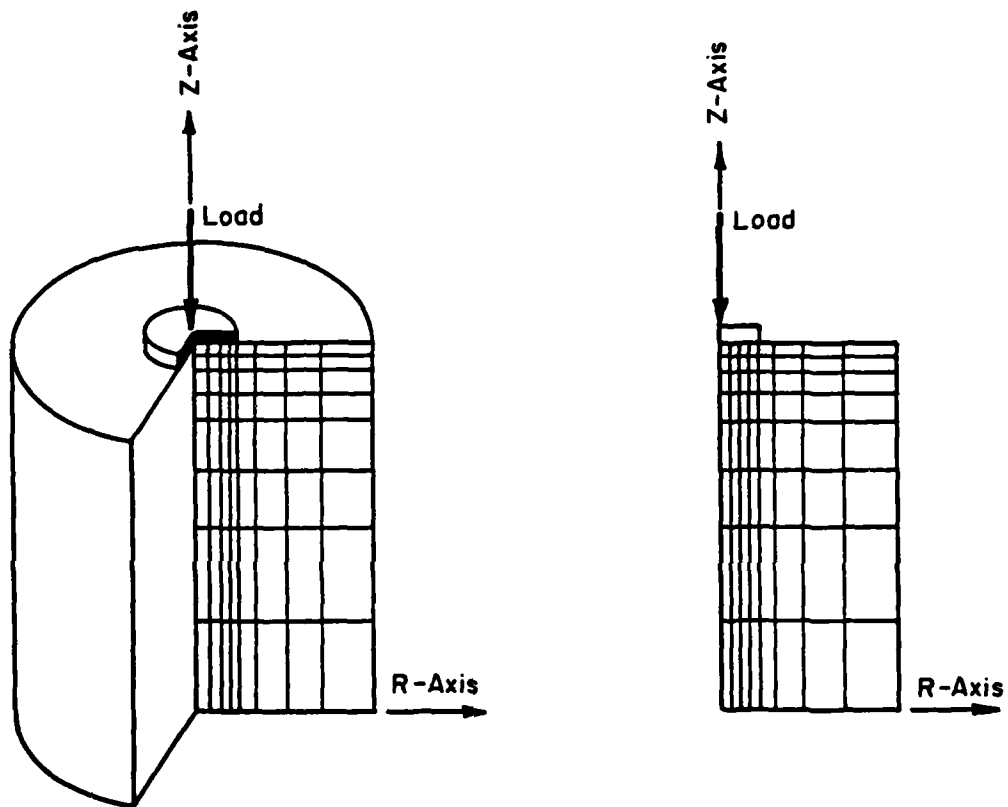


Fig. 3.3 Axisymmetric Solid of Revolution Used in ILLI-PAVE

based on an extension of the Burmister layered elastic theory, to take into account three-dimensional effects. The effect of each load is calculated individually using numerical integration techniques [102]. The combined effect of all applied loads is determined by summing individual stress, strain and displacement components, after these have been transformed to a common cartesian coordinate system. The program can accommodate several conditions at layer interfaces, including perfectly smooth, perfectly rough and intermediate degrees of roughness. The maximum number of layers that may be used is governed by practical considerations. The version available at the University of Illinois can accept up to 10 layers. This program is more widely used in Europe than in the United States, where its circulation is confined to research organizations.

An earlier edition of the program, called 'BISTRO', handled only the case of rough layer interfaces [103].

3.9.3 CHEVRON--ELP15

This program is used in the United States for layered elastic analysis. Its original version, 'CHEVRON', was developed by Chevron Research Corporation in 1963 [104; 105]. Since then, the program has been modified at the University of Illinois, mostly for practical reasons. The current version at the University of Illinois is called 'ELP15' and can be used to analyze an elastic layered system consisting of up to 15 layers. Only one circular loaded area can be accommodated and the analysis is performed according to the Burmister theory.

Numerical integration is used to evaluate the required Bessel functions and other integrals. ELP15 accepts free-form input using a routine which can fit nearly all compilers. An earlier version, 'LAYERS', was designed to handle 5 layers only. Three more recent versions, 'CHEVIT', 'ELSYM5' and 'MWELP15', accommodate multiple wheel loads [39; 106; 107]. The latter was developed at the University of Illinois.

3.9.4 RISC

The main idea behind the development of this program is coupling the finite element procedure based on plate theory (as used, for example, in ILLI-SLAB and WESLIQID), with a layered elastic analysis (such as is employed in ELP15 or BISAR). This purports to overcome a major shortcoming in conventional plate on elastic solid analysis, namely that the foundation must consist of a single layer [108]. RISC features the following characteristics:

1. The foundation (base, subbase, subgrade) is modeled as a layered elastic solid, consisting of up to 3 layers;
2. Partial contact is handled through an iterative procedure, but this tends to be time consuming;
3. Load transfer between adjacent slabs is accomplished using dowel bars, which are modeled as beam elements;
4. Thermal stresses are computed in a manner that accounts for the effect of slab self-weight and changes in slab geometry. These stresses can be determined for a system of several slabs, which may vary in size and thickness;

5. Stresses can be computed in the foundation layers, as well.

Execution times may be as high as 30 minutes in some cases, especially when stresses in the foundation are calculated. This reduces the scope of routine application of the advanced features of the program. An earlier version of the program was called 'RIGMUL' [109].

3.9.5 WESTER

This is a computerized compendium, assembled by the author, of available closed-form solutions to the problem of a plate on an elastic solid and a dense liquid foundation. Included are Westergaard's equations for the three fundamental cases of interior, edge and corner loading [8; 9; 10], and proposed modifications thereof; Losberg's solutions for the elastic solid foundation [13]; and Meyerhof's ultimate capacity expressions [110]. This program was coded during the course of this study, and several predictive equations developed herein have been incorporated into it. WESTER also employs an iterative scheme based on the Newton-Raphson approximation method, which backcalculates a dense liquid modulus, k , given an elastic solid modulus, E_s , and vice-versa, by matching one of the three statical influences (deflection, subgrade stress or bending stress). This procedure allows a direct comparison between the two subgrade models without the introduction of any restrictions with respect to the size of the loaded area or to the structural properties of the system [111]. Since equations are developed in this study for the edge and corner conditions using the elastic solid model, such comparisons can

now be performed for all three cases of loading. The input guide for WESTER is given in Appendix A.

CHAPTER 4

MAKING ILLI-SLAB USER FRIENDLY

4.1 INTRODUCTION

For the analysis of slabs-on-grade, the Finite Element Method (F.E.M.) has been a favorite among engineers in the last two decades. Its major attribute is flexibility in modeling a variety of pavement systems, loaded by any combination of loads, applied anywhere on the slab surface. Of the programs reviewed in the previous Chapter, ILLI-SLAB was selected for further study for a number of reasons, including its availability and extensive previous use at the University of Illinois. Despite some limitations in the applicability of the finite element model employed in ILLI-SLAB, of which both the researchers who originally developed it, as well as the present author, are fully cognizant, this program offers a practical tool that may be applied to several problem categories, with reasonable ease and confidence.

One of the basic aims of this research has been to reexamine the F.E.M. as used in ILLI-SLAB, and to improve the general characteristics of this program. This may be done by expanding its capabilities to include modeling of other types of foundations, in addition to the original dense liquid formulation, and by making any required modifications to improve its accuracy and ease of application, and enhance the beneficial interpretation of its results. This latter group

of changes are described in this Chapter. The introduction of three additional foundation models, namely the Resilient, the Elastic Solid, and the Vlasov subgrades, is discussed separately in subsequent chapters.

4.2 AIMS OF MODIFICATIONS

For the benefits of the Finite Element Method to be fully realized, it is highly desirable that programs using this method:

- (i) Accept easy to compile, user oriented input data, restricted to the absolute minimum required, and eliminating -where possible- potential pitfalls for the user;
- (ii) Employ carefully selected default values that will reduce the amount of input data required;
- (iii) Perform error checks, especially in the case of default values, so that errors concealed by the otherwise normal execution of the program will be avoided;
- (iv) Be free of code errors;
- (v) Organize the output so that it is neat, meaningful and user oriented;
- (vi) Incorporate skillful data-base management for the efficient utilization of available memory core;
- (vii) Provide basic and higher-level routines; and
- (viii) Present the results in summary and graphical form [112].

The modifications of ILLI-SLAB presented below aimed at providing these

capabilities.

4.3 CONTOURING CAPABILITY

During a study conducted in the Summer of 1981, computer program ILLI-SLAB was revised and the facility to generate contours of stresses and deflections was incorporated into it [113]. This was done through auxiliary program CONT, which accepts as input data results from ILLI-SLAB. Subroutine CONTOUR in this program passes these results to a number of NCAR subroutines. The software used in these subroutines was developed at the National Center for Atmospheric Research (NCAR), and was made available to the author with the restriction that NCAR be acknowledged as the source of the software in any resulting research or publications. For more information on the use of NCAR contouring software, the reader should refer to NCAR literature [114]. Sample contour plots (Run OHEWF in Table 6.5) are shown in Fig. 4.1. A very brief outline of the software, especially as used in the revised version of the ILLI-SLAB package, is given below.

The NCAR Graphics Software consists of graphics utilities such as contour plotting, three-dimensional surface drawing, and world map projections. These utilities perform graphic output using low level graphics subroutines in the NCAR System Plot Package (SPP). This consists of subroutines to draw, move, plot characters, clear the plotting surface, and similar subroutines. The output of the SPP is not a plot, but a file (called 'NCARMC') of "metacode" which contains the

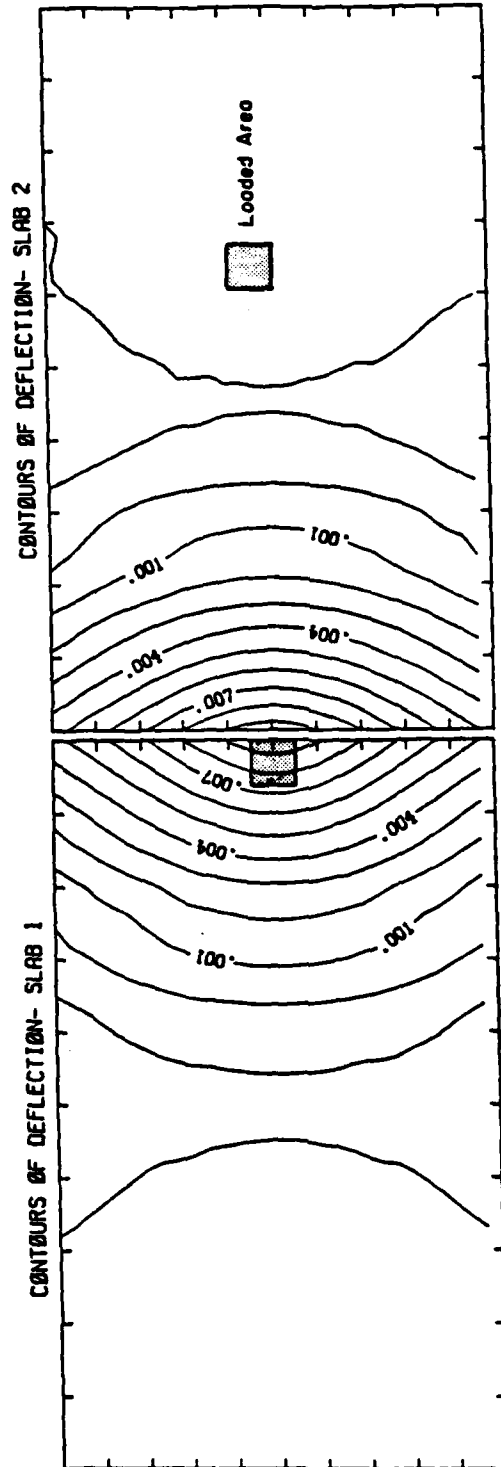


Fig. 4.1 Typical Contour Plots

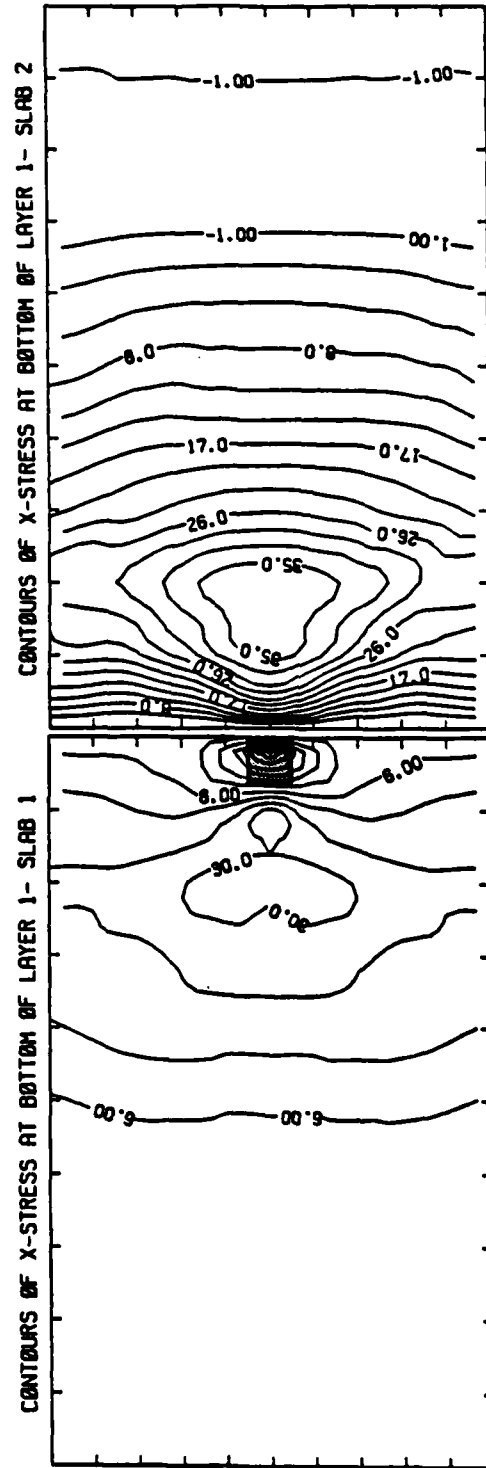


Fig. 4.1 (continued)

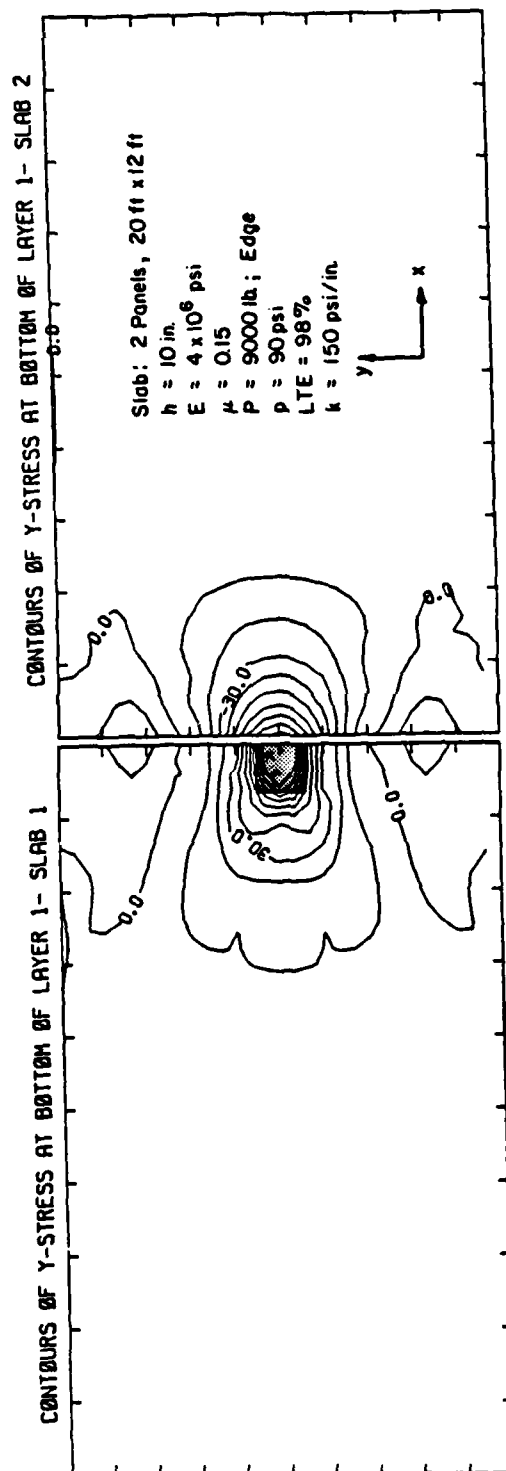


Fig. 4.1 (continued)

plotter instructions. NCARMC, the Metacode File, is device independent-i.e. it contains instructions to drive an "ideal" plotter or graphics device, such as a graphics terminal or a hard plotter. This file is interpreted by a Translator for a specific device. The Translator does the actual plotting.

The most important family of NCAR subroutines used in ILLI-SLAB is CONRAN. This is the name of a family of routines for the contouring of irregularly distributed data. The family consists of 4 versions: CONRAQ, CONRAN (used for two versions), and CONRAS. CONRAQ, the quick version, plots contours, perimeters, titles and messages. CONRAN, the standard version, adds line labeling, contour dash patterns, and plots relative highs and lows. This is the version that was selected for use with ILLI-SLAB. CONRAN, smooth version, adds splines under tension for smoothing of contour lines. CONRAS, super version, adds the elimination of contours when crowding with other contours or text occurs. CONRAQ is the fastest and smallest. The packages get progressively bigger and slower as features are added.

CONRAN plots contour lines using random, sparse or irregular data sets. The data is triangulated and then contoured. Contouring is performed using interpolation of the triangulated data.

4.4 TOWARD MORE EFFICIENT MEMORY CORE UTILIZATION

Users of ILLI-SLAB are often faced with the problem of exceeding available machine memory core. This may arise when several slabs are

used, or when one attempts to refine the finite element mesh. A finer mesh is desirable for improved accuracy, and when investigating the stability and convergence of the numerical solution. This problem has been addressed by the introduction of the capability to take advantage of any symmetry lines. In the modified ILLI-SLAB version, the user has the following options:

1. No lines of symmetry exist (ISYM=0);
2. The x-axis is a line of symmetry (ISYM=1);
3. The y-axis is a line of symmetry (ISYM=2);
4. The x- and y-axes are both axes of symmetry (ISYM=3).

Care was taken to introduce these options without imposing a burden on the user during the preparation of the input data. Particularly undesirable are requirements to provide node numbers for nodes along the line(s) of symmetry. In the new version of ILLI-SLAB, the various options related with symmetry are specified by using a single input variable (ISYM), which may even be omitted if no symmetry exists.

The possibility of breaking the program into two or more auxiliary programs to be loaded and executed separately and sequentially has also been investigated. Thus, the contouring subroutines have been separated from the main body of the program and placed in program CONT with appreciable savings. Another group of routines offered for such a separation are those related to the free-form input capability. An auxiliary program could be easily created from these routines to read free-form input data and prepare them for the main body of ILLI-SLAB.

4.5 CORRECTION OF SUBGRADE STIFFNESS MATRIX

One of the major advantages of ILLI-SLAB over similar programs is that the Winkler type foundation is not modeled by four concentrated springs at the corners of each slab element. Through an equivalent mass formulation, a uniform, distributed subgrade is provided, instead. The derivation of the stiffness matrix for this subgrade [55] follows the same steps as the one presented by Dawe [81] who first derived this matrix. In Dawe's equivalent mass formulation, the product of mass per unit area and plate thickness (ρh), replaces the subgrade modulus, k , or the resilient modulus of subgrade reaction, K_R , introduced in Chapter 6. Similar derivations using different sign conventions are also presented by Przemieniecki [115] and Zienkiewicz [47].

The subgrade stiffness matrix used in ILLI-SLAB was compared to each of the matrices presented in these publications, which were further compared to each other, with due allowance for differences in sign convention. The result of this was the corrected computer code as included in the modified version of ILLI-SLAB. A typographical error in the matrix in Ref. 47 was also detected: element (3,1) should be +461, as given in Ref. 116.

The stiffness matrix formulation in ILLI-SLAB was further verified by rederiving the subgrade stiffness matrix using the concept of strain energy, as opposed to the principle of virtual work employed by Tabatabaie [79]. As expected, both approaches yield identical results, reinforcing the credibility of ILLI-SLAB. The new derivation of the

subgrade stiffness matrix is presented in detail in Chapter 11.

The corrections made to the stiffness matrix are most obvious in the results of symmetric problems, where identical responses are obtained at corresponding points, as expected. Although the change in the results of a typical run may only range from 3% to 5% (see Chapter 5), it is important to have a balanced formulation, to ensure the good behavior and convergence of the numerical solution.

4.6 SPECIFICATION OF LOADED AREAS IN TERMS OF GLOBAL COORDINATES

In its original version, ILLI-SLAB required that input data for loaded areas be specified in terms of local (element) coordinates [117]. In this system, the origin is set at the lower left corner of each element, whose dimensions extend from 0 to $2a$ in the x -direction and $2b$ in the y -direction, for a typical element of dimensions $2a \times 2b$. The implication of this was that the user had to go through the following steps when specifying the loaded areas for a problem:

1. Determine the element numbers of the loaded elements, adhering to a fixed numbering sequence, i.e. from bottom to top, and from left to right. It should be noted that depending on the fineness of the mesh used, each loaded area (such as a wheel imprint) might apply a load on 4 or more elements. Thus, a large number of partially or fully loaded elements might be needed to define the loading pattern in all but the simplest situations;

2. For each of the loaded elements, determine the extent of the loaded subarea in terms of the local element coordinate system. These coordinates should then be specified, one subarea per card, together with the load intensity in each case;
3. In case of a change in the finite element mesh used, such as when making the mesh finer, the process must be repeated.

As a result of the complexity of this process, especially when used, as it was, with the fixed-form input format, a large portion of all problems encountered by ILLI-SLAB users was related to specifying loading pattern data. To overcome these difficulties, subroutine SUBAREA was coded to allow input data specification in terms of the global coordinate system. In this system, the origin is located at the lower left corner of the slab arrangement and the axes extend to the extreme corners of this arrangement in both the x- and y- directions. The advantages of this system are obvious:

1. Element numbering, although retained internally, does not enter into input data preparation;
2. Only as many loaded areas as actually exist need be specified. Global coordinates defining the extent of each applied load now acquire improved physical meaning for the user;
3. The global coordinate system is independent of the mesh used, being solely determined by the arrangement of slab(s) analyzed.

The output from ILLI-SLAB now includes both the loaded areas as specified, and the loaded subareas generated by subroutine SUBAREA. The user familiar with the original version of ILLI-SLAB will recognize that

the latter are identical to the input data the user would have had to prepare for the original version. A comparison of the two sets of information illustrates the significant improvement in input data specification achieved by subroutine SUBAREA.

4.7 MULTIPLE SLABS CAPABILITY

It is often desirable to model a series of slabs interconnected by load transfer devices in the x- and the y-direction, especially in the analysis of cracked continuously reinforced concrete (CRC) pavements. The original version of ILLI-SLAB provided for a maximum 3X2 array of slabs, but this was found to be inadequate in some cases. Therefore, the ability to accommodate any array of slabs as specified by the user was introduced. This choice is perfectly flexible, and leads to no waste in terms of computer storage utilization, independent of the number of slabs actually used. An arbitrary upper limit of a 10X10 array of 100 slabs is set for practical reasons, but even this may be increased by changing one variable in the program.

4.8 FREE-FORM INPUT CAPABILITY

With the addition of several new subroutines, ILLI-SLAB can now accept free-form input data using a Problem Oriented Language (POL) consisting of simple, easy-to-remember English-like statements. This has been made possible by accessing the SCAN library of routines

developed at the Civil Engineering Systems Laboratory (CESL), Department of Civil Engineering, University of Illinois at Urbana-Champaign [118; 119; 120]. SCAN has been used as a teaching and research tool for a number of years at the University of Illinois. It is also the front end of the POLO System, including FINITE [63], and is used in a number of production systems at CESL.

Free-form input data for ILLI-SLAB are classified into ten Groups, each defined by a Key-Word. Four of these Groups belong to Block 1 and the remainder to Block 2. Data in Block 1 must be read in first, since they determine the amount of memory core required for a given run. Apart from this restriction in sequence, data can be read in any order desired by the user. Brief descriptions of the Data Groups are given in Table 4.1.

Only those parameters that are different from the default values need be provided when using the free-form input capability. This saves time in preparing the input data file and executing the program. The free-form subroutines are set up to issue diagnostic error messages before execution in the event of improper input data. These greatly facilitate debugging the input data file and are particularly useful to the new user of ILLI-SLAB.

Use of the free-form input capability is described in complete detail in the updated User's Manual in Appendix A. Figure 4.2 shows a comparison between the fixed-form and the free-form input data files for a typical run (Run DR003 in Table 6.5).

TABLE 4.1

FREE-FORM DATA GROUPS AND KEY-WORDS

	<u>GROUP</u>	<u>KEY-WORD</u>	<u>EXPLANATION</u>
BLOCK 1	1	TITLE	The title for a given problem; this will appear on the first page of the output.
	2	NUMBER	Declaration of number of nodes, layers, and loaded areas.
	3	TYPE	Specification of subgrade and load transfer types (if any).
	4	CONTOUR	Specification of countouring requests, if any, and of pertinent variables.
BLOCK 2	5	COORDINATES	Specification of nodal coordinate along the x- and y-axes.
	6	PROPERTIES	Specification of properties of top and bottom layers (if any) and of the subgrade.
	7	LOADED	Specification of loaded area limits and of load intensity.
	8	LOAD	Specification of load transfer pertinent variables.
	9	ITERATIVE	Specification of iterative scheme to be used (if any), including num- ber of iterations, convergence tol- erances and output type.
	10	SYMMETRY	Specification of lines of symmetry (if any)

```

0
TITLE "***** RUN DR003: COMPARISON OF TWO TYPES OF INPUT FORMAT *****"
NUMBER OF NODES IN X DIRECTION 11 11
NUMBER OF NODES IN Y DIRECTION 8
NUMBER OF LOADED AREAS 1
NUMBER OF LAYERS 1
TYPE OF SUBGRADE SOFT
TYPE OF LOAD TRANSFER IN X DIRECTION AGGREGATE INTERLOCK
COORDINATES OF NODES IN X DIRECTION 0 80 140 170
190 210 220 225 230 235 240 240 245 250 255 260 270
290 310 340 400 480
IN Y DIRECTION 0 5 10 15 20 30 60 120
PROPERTIES OF TOP LAYER
THICKNESS 10
TOP LAYER ELASTIC MODULUS 4000000
POISSON RATIO 0.15
OF SUBGRADE
MODULUS 430.9
LOADED AREAS
1 IN X DIRECTION FROM 230 TO 240 AND IN Y DIRECTION FROM 0 TO 5
WITH PRESSURE 270
SYMMETRY X
LOAD TRANSFER IN X DIRECTION
AGGREGATE INTERLOCK FACTOR 1000000
ITERATIVE SCHEME
NUMBER OF ITERATIONS 6
TOLERANCE FOR SUBGRADE MODULUS 0.05
TOLERANCE FOR NUMBER OF NODES 0.05
OUTPUT TYPE FULL

```

```

1
***** RUN DR003: COMPARISON OF TWO TYPES OF INPUT FORMAT *****
1      1
11     11
8
1      0      430.9
2      6 0.05 0.05      1
000000 50
0
0.0      80.0      140.0      170.0      190.0      210.0      220.0      225.0
230.0      235.0      240.0      240.0      245.0      250.0      255.0      260.0
270.0      290.0      310.0      340.0      400.0      480.0
0.0      5.0      10.0      15.0      20.0      30.0      60.0      120.0
10.0 4.000E+06      0.150
1.0E+06
270.0      230.0      240.0      0.0      5.0
000000

```

Fig. 4.2 Comparison of Free-Form and Fixed-Form Input Data Files

4.9 MISCELLANEOUS CHANGES

In addition to providing a user oriented input data capability, it is desirable to have a user oriented presentation of the results from a given run. The presentation of results in a graphical form as achieved by using the contouring subroutines is a major step in this direction. Attention was also paid to the actual printed output from ILLI-SLAB. Early in this study, a particular effort was made to improve the output format by introducing of appropriate carriage control characters, eliminating unnecessary lines of output (such as stresses in layer 2 when only one layer is used!) and replacing them by other meaningful output information. The changes incorporated in the revised version of ILLI-SLAB aim at providing a well-organized, clear echo of the input file -so that the parameters and loading conditions used can be checked- as well as giving the user a neat, usable output. Thus, the appearance of the title page has been enhanced. The date of the last update of the program is also shown on this page. The output now includes a listing of nodal coordinates as generated by the program. Of most interest to the user, however, is the summary of maximum values of deflection and stresses, and the nodal numbers at which these occur. This is given at the end of the output. The output from ILLI-SLAB is now particularly suited for the Page Printer System (PPS), which produces good quality printouts on 8.5 X 11-in. forms, punched for a standard three-ring binder. Such printouts may be directly included in a report.

A second group of changes involved the elimination of several code errors ("bugs") that were revealed during this study. Comparisons with FINITE show that at least the major routines of ILLI-SLAB, such as stiffness matrix assembly, inversion, solution and determination of stresses and deflections, are now free of code errors.

CHAPTER 5

THE WESTERGAARD SOLUTIONS REEVALUATED IN THE
LIGHT OF THE FINITE ELEMENT METHOD

5.1 INTRODUCTION

Computer programs developed using the Winkler foundation have traditionally been compared to and validated by the Westergaard closed-form solutions. These solutions are available for three particular loading conditions only, and assume a slab of infinite or semi-infinite dimensions. In practice, empirical guidelines have been developed for the slab size requirement before the Westergaard solution becomes applicable. These guidelines may now be verified and/or reviewed using the Finite Element Method (F.E.M.). Furthermore, several investigators have noted repeatedly in the past that although the Westergaard solution agreed fairly well with their observations for the interior loading condition, it failed to give even a close estimate of the response in the cases of edge and corner loading. Similar remarks have been made in validation studies of ILLI-SLAB. It is considered that the time-honored Westergaard solutions deserve a more thorough reexamination, using the tool of finite element analysis now available.

On the other hand, useful conclusions may also be drawn with respect to the use of the F.E.M. in the analysis of pavement slabs on a dense liquid foundation, by studying the convergence characteristics of the computer results, and comparing these to analytical solutions. From

this applied viewpoint, the analyses presented in this Chapter were conducted for the following reasons:

(1) Modifications discussed in Chapter 4 to essential features of ILLI-SLAB, viz. the subgrade stiffness matrix, as well as the addition of several higher-level routines (e.g. free-form input, contouring, subgrade types, stress dependence, etc.) have created the need for a revalidation of the program. Such revalidations have been carried out in the past since the publication of Ref. 55 in 1979, by various graduate students as part of their studies and research at the University of Illinois. These, however, have been incomplete and have remained scattered in the private files of each worker. As a result, no benefit could be derived from them by ILLI-SLAB users at large;

(2) It was noted earlier that ILLI-SLAB incorporates a uniform, distributed subgrade, while similar programs, e.g. KENWINK [76], WESLIQID [75/1], or FINITE [64], provide four concentrated springs under each plate element. There has been no study up to now, comparing the results of these two subgrade idealizations. The basic difficulty of having a computer program which would incorporate both models is now overcome, since ILLI-SLAB also provides, as an option, the 'SPRINGS' subgrade, intended for research purposes only;

(3) The most efficient utilization of the capabilities of ILLI-SLAB, as well as of the other programs, greatly depends upon the extent of the user's familiarity with simple, yet very important factors affecting the program's performance. The analyses presented herein aim at providing some guidelines that can be applied by the user when

ILLI-SLAB is employed in pavement design and analysis problems.

Typical results will be presented and comparisons made between ILLI-SLAB and other available finite element programs. The purpose of such comparisons is primarily to provide a further means for validating the ILLI-SLAB code, rather than to assert the superiority of one particular program. Different models may perform better than others depending on the problem considered. It is obvious that the restricted scope of the analyses presented in this Chapter does not exhaust the capabilities of each model.

5.2 PROBLEMS INVESTIGATED

In the present study the following questions are addressed using well-designed factorials of ILLI-SLAB runs:

- (i) How does the revised version of ILLI-SLAB compare to that used in the validation presented in Ref. 55? The conclusion of this validation was that ILLI-SLAB agreed with Westergaard very well;
- (ii) How should the circular loaded area assumed by Westergaard be modeled in ILLI-SLAB? What is the effect on response of different ways of loaded area representation?
- (iii) Since ILLI-SLAB can accommodate partially loaded elements, what is the effect of load placement with respect to the finite element mesh? Is there any particular configuration which can be recommended to the general ILLI-SLAB user?

- (iv) Finite element theory requires that in the limit of mesh refinement, the finite element solution should approach the correct closed-form solution (if available). Is this true of ILLI-SLAB? If not, why not?
- (v) How does slab size affect the manner in which ILLI-SLAB results approach the Westergaard solution? Are the empirically developed slab size criteria verified by the F.E.M, or do they require redefinition?
- (vi) What is the effect of element aspect ratio? How important is it to have square elements?
- (vii) How is the relation between Westergaard and finite element solutions affected by the extent of the loaded area?
- (viii) How does the 'SPRINGS' subgrade compare with the 'WINKLER' (uniform) subgrade?
- (ix) To what extent are the disputed edge and corner solutions by Westergaard verified or contradicted by the F.E.M.?

To provide answers to these questions, the three fundamental cases of loading considered by Professor Harald Malcom Westergaard (1888-1950), viz. interior, edge and corner loading, are investigated. The interior loading condition is discussed first. This condition has been extensively studied and is well understood. Theoretical solutions are available and they have been found to be much closer to observed pavement behavior than for any other loading condition. This condition also lends itself to a factorial of simple runs using finite element programs at a relatively low cost.

5.3 THE INTERIOR LOADING CONDITION

5.3.1 Comparison of the Present to the Original Version of ILLI-SLAB

The original ILLI-SLAB code contained several errors, notably in the stiffness matrix for the subgrade. These have now been corrected, but a credibility problem is created for the excellent agreement with Westergaard theory reported in Ref. 55. In order to verify the results obtained during that study, the same factorial of ILLI-SLAB runs was performed using the updated version of the program. The results are compared to those reported by Tabatabaie, et al. [55] in Table 5.1a.

The original factorial [55] consisted of 3 slab thicknesses, h , of 12, 16 and 20 in. and 3 moduli of subgrade reaction, k , of 50, 200 and 500 psi/in. A 25-ft. square slab was used in the analysis. As will be shown in a later paragraph, this slab may be slightly smaller than the minimum requirement for the development of the Westergaard infinite slab condition, in view of a large radius of relative stiffness. The modulus of elasticity, E , and Poisson's ratio, μ , of the concrete slab were assumed to be 5×10^6 psi and 0.15, respectively. A single load of 50 kips was modeled as a 15 X 15 in. area with a load intensity of 222.2 psi. The results were compared in Ref. 55 with the Westergaard solution in which the 50-kip load is distributed over a circular area 15 in. in diameter (WESI in Table 5.1a). Some results tabulated in Table 5.1a are also plotted in Fig. 5.1. The mesh used for these runs is shown in Fig. 5.2.

TABLE 5.1
(a) REVALIDATION OF ILLI-SLAB

RUN No.	k (psi/in.)	h (in.)	l (in.)	DEFLECTION (mils)			BENDING STRESS (psi)		
				Original ILLI-SLAB	Revised ILLI-SLAB	WEST	Original ILLI-SLAB	Revised ILLI-SLAB	WEST
1	50	12	61.95	36.3	35.8	32.3	562.9	562.4	528.0
2	200		43.81	16.9	16.6	16.1	488.0	487.2	461.9
3	500		34.84	10.3	10.1	10.1	443.2	442.3	418.2
4	50	14	69.55	29.4	29.1	25.7	431.1	430.9	399.1
5	200		49.18	13.8	13.5	12.8	376.3	375.8	350.5
6	500		39.11	8.3	8.2	8.0	341.9	341.3	318.4
7	50	16	76.87	24.6	24.4	21.0	340.4	340.3	311.5
8	200		54.36	11.5	11.3	10.5	300.4	300.1	274.3
9	500		43.23	6.9	6.8	6.6	273.5	272.5	249.8
10	50	20	90.88	18.9	18.8	15.1	226.4	226.4	203.9
11	200		64.26	8.5	8.4	7.5	205.4	205.3	180.1
12	500		51.10	5.1	5.0	4.7	187.4	187.1	164.4

Notes:Finite Element SolutionSlab: 25'x25' ($\frac{l}{b}=3.3$ to 8.6)E = 5×10^6 psi $\mu = 0.15$

p = 222.2 psi

A = 15"x15" interior

Mesh: Fig. 3.2

Theoretical Solution (WEST)

P = 50,000 lb.

p = 282.94 psi

a = 7.5"

Equations used:

Special Theory - Infinite Slab-Circular Load

$$\sigma_1 = 0.275 (1 + \mu) \frac{P}{h^2} (4 \log_{10} \frac{l}{b} + 1.069)$$

$$\delta_1 = \frac{P}{8kl^2} \left[\left(1 - \frac{a^2}{l^2}\right) (0.217 - 0.367 \log_{10} \frac{a}{l}) \right]$$

$$b = \sqrt{1.6a^2 + h^2} - 0.675h \text{ for } a < 1.724$$

$$= a \text{ for } a > 1.724$$

TABLE 5.1 (continued)

(b) COMPARISON WITH WESTERGAARD SOLUTIONS

RUN No.	DEFLECTION (mils)			BENDING STRESS (psi)					
	WESI	WESII	REVISED ILLI-SLAB	WESI		WESII		WESIII	Revised ILLI-SLAB
				ORD. THEORY	SP. THEORY	ORD. THEORY	SP. THEORY		
1	32.3	32.2	35.8	520.3	528.1	497.3	508.4	495.2	562.4
2	16.1	16.0	16.6	454.5	462.3	431.6	442.7	429.5	487.2
3	10.1	10.0	10.1	411.1	418.9	388.3	399.4	386.2	442.3
4	25.7	25.6	29.1	398.4	399.1	381.5	386.4	379.9	430.9
5	12.8	12.7	13.5	350.0	350.7	333.2	338.0	331.6	375.8
6	8.0	8.0	8.2	318.1	318.8	301.3	306.1	299.8	341.3
7	21.0	21.0	24.4	315.7	311.5	302.8	303.0	301.6	340.3
8	10.5	10.4	11.3	278.7	274.5	265.8	265.9	264.6	300.1
9	6.6	6.6	6.8	254.2	250.0	241.3	241.5	240.2	272.5
10	15.1	15.1	18.8	213.5	203.9	205.3	199.7	204.5	226.4
11	7.5	7.5	8.4	189.8	180.1	181.5	175.9	180.8	205.3
12	4.7	4.7	5.0	174.1	164.5	165.9	160.3	165.1	187.1

Notes:

See Table 5.1(a) for values of k, h, l and Notes on F. E. Solution and WESI.

Theoretical SolutionsWESII, WESIII

P = 50,000 lb.

p = 222.2 psi

a = 8.46" (WESII)

c = 15" (WESIII)

Equations Used:

WESI, WESII: $\sigma_i = \frac{3}{2\pi} (1+\mu) \frac{P}{h^2} \left[\left(\ln \frac{2c}{a} \right) - \gamma + \frac{1}{2} + \frac{\pi}{32} \left(\frac{a}{c} \right)^2 \right]$
(Ordinary Theory
Circular Load)

$$\delta_i = \frac{P}{8ki^2} \left[1 + \frac{1}{2\pi} \left(\left(\ln \frac{a}{c} \right) + \gamma - \frac{5}{4} \right) \left(\frac{a}{c} \right)^2 \right]$$

For Special Theory, substitute b for a in Equation for σ_i .

WESIII: Substitute c' for a in Equation for σ_i , where

(Ordinary Theory
Square Load) $c' = \frac{\frac{\pi}{4} - 1}{\sqrt{2}} c$; c = side of square load

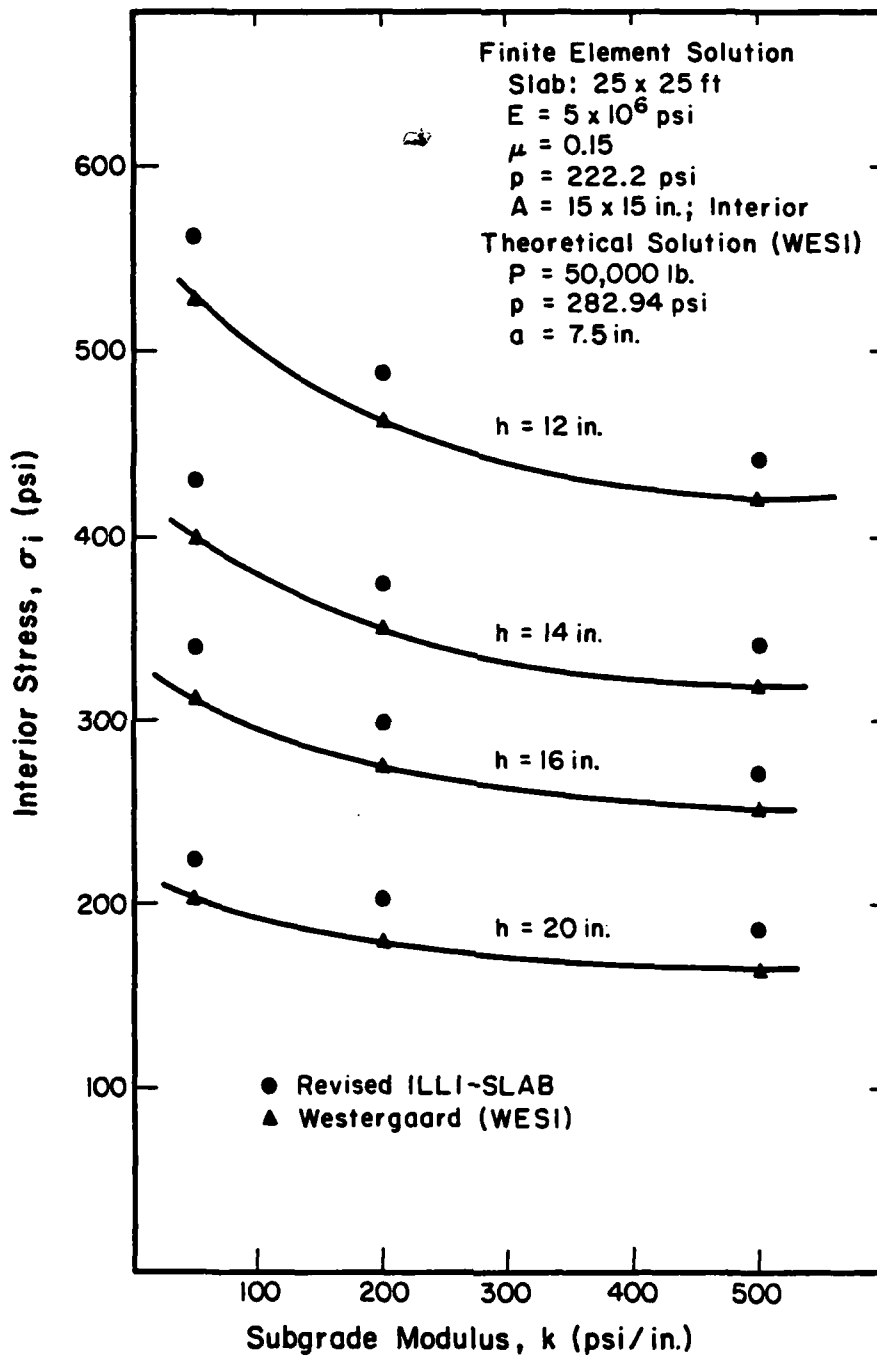


Fig. 5.1 ILLI-SLAB Revalidation (Interior Loading)

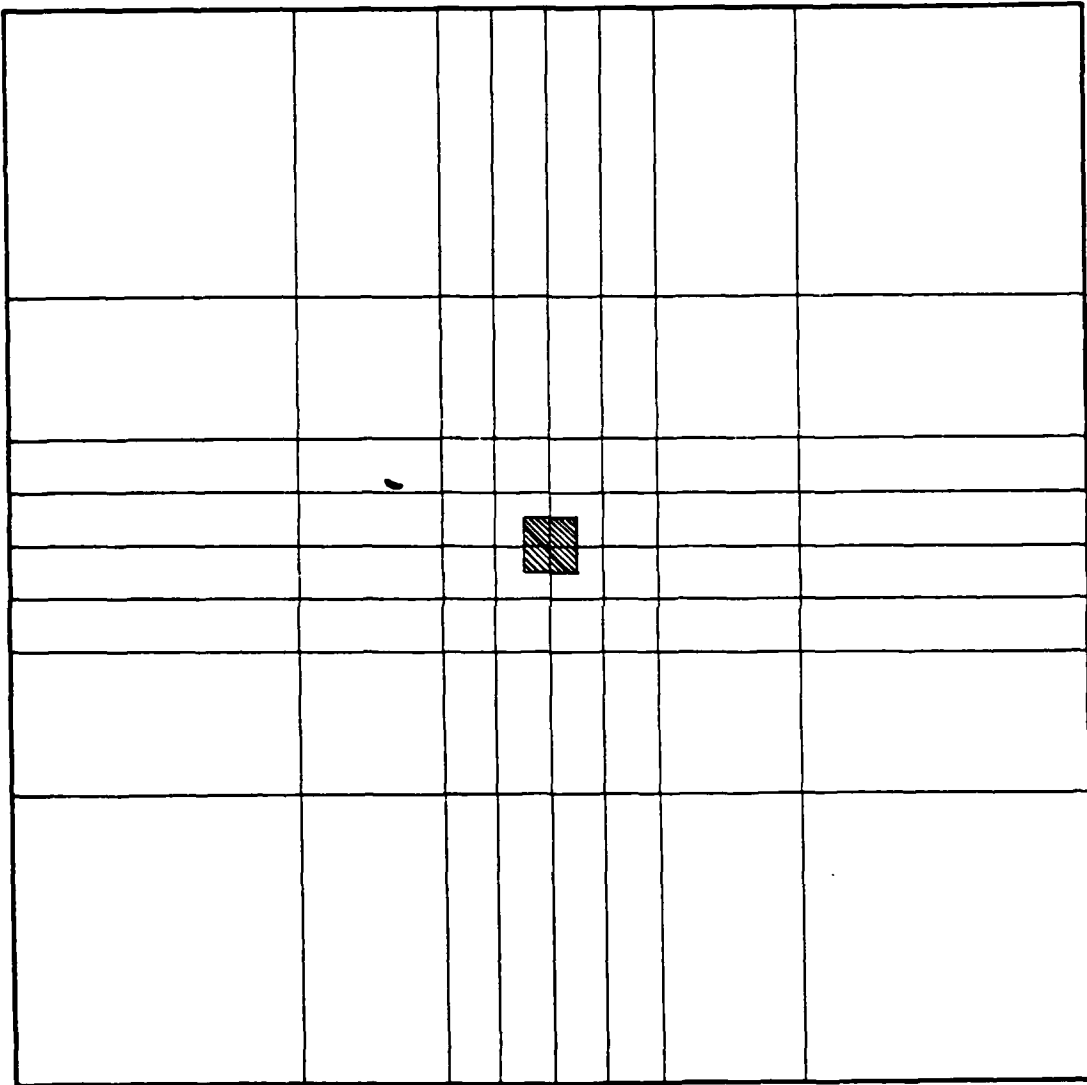


Fig. 5.2 Finite Element Mesh I (Interior Loading)

For the cases considered the results of the updated version are slightly improved compared to those of the original version. The difference between the two versions is very small, from an engineering viewpoint. Any conclusions reached by previous studies using the original version are considered valid.

5.3.2 Effect of Load Representation

In Table 5.1b comparisons of the finite element solution are presented with three different Westergaard idealizations, WESI, WESII and WESIII. The difference is the way the square or rectangular loaded area in ILLI-SLAB is modeled for Westergaard's analysis. WESI is the same representation as used in Ref. 55 and was retained here for consistency. It essentially matches the total load, P , and the diameter of the loaded area (which is assumed to be equal to the side of the square loaded area in the finite element solution). As a result, the load intensity used in the finite element solution (222.20 psi) is different from that in the Westergaard idealization (282.94 psi).

A more rigorous representation is attempted in WESII where the total load, P , and the load intensity, p , are matched, while the diameter of the equivalent circular load is chosen to retain the same area. This leads to a larger diameter than the side of the square element (16.92 in. cf. 15.0 in.).

Finally, in WESIII the load is treated as a square of the same size and load intensity as in the finite element analysis. Such a solution is only available for the maximum bending stress under interior loading.

The following equations were used in Ref. 55 for the maximum interior bending stress (σ_i) and deflection (δ_i), as the Westergaard solution:

$$\sigma_i = 0.275 (1+\mu) \frac{P}{h^2} (4 \log_{10} \frac{\ell}{b} + 1.069)$$

$$\delta_i = \frac{P}{8k\ell^2} \left[1 - \frac{a^2}{\ell^2} (0.217 - 0.367 \log_{10} \frac{a}{\ell}) \right] \quad (5-1)$$

$$b = \sqrt{1.6 a^2 + h^2} - 0.675h \text{ for } a < 1.724h$$

$$= a \text{ for } a > 1.724h$$

$$\ell = \sqrt[4]{Eh^3 / 12(1-\mu^2)k}$$

: radius of relative stiffness (dense liquid foundation);

E, μ , h: Slab modulus, Poisson's ratio, and thickness, respectively.

This equation for deflection is misquoted in Ref. 55 without the factor of 8, evidently due to a typographical error. Also, in the calculation of b, the factor 1.724h is wrongly stated as 1.74h.

In the expression for the interior stress, an equivalent radius, b, was introduced by Westergaard [8] to account for the effect of shear stresses in the vicinity of the applied load. This effect is neglected in the "ordinary theory" of medium-thick plates, in which the true radius, a, is used. The validity of Westergaard's semi-empirical adjustment and of the resulting "special theory" has been debated by various investigators (see, for example, Scott [121]), but a discussion

of this issue would be beyond the scope of this study. It is considered, however, that the results of a finite element solution as obtained from ILLI-SLAB, should be compared to Westergaard's "ordinary theory", because both ignore the effect of shear stresses. Such a comparison is much more meaningful as will be shown below.

The following general form of the Westergaard equations [122] was used in this study (WESII):

$$\sigma_i = \frac{3}{2\pi} (1+\nu) \frac{P}{h^2} \left[\left\{ \ln \frac{2\ell}{a} \right\} - \gamma + \frac{1}{2} + \frac{\pi}{32} \left(\frac{a}{\ell} \right)^2 \right]$$

$$\delta_i = \frac{P}{8k\ell^2} \left[1 + \frac{1}{2\pi} \left\{ \ln \frac{a}{2\ell} \right\} + \gamma - \frac{5}{4} \right] \left(\frac{a}{\ell} \right)^2$$

$$\gamma : \text{Euler's Constant } (=0.577 \ 215 \ 664 \ 901 \ 532 \ 860 \ 61\dots) \quad (5-2)$$

These equations differ from those in Eqn. (5-1) inasmuch as the former are a specialized and simplified (hence, not as rigorous) version of the latter. Furthermore, the general equation for interior stress includes Westergaard's "supplementary" σ_2 stress [122]. Although this usually makes only a small contribution, it is included here for completeness.

To obtain the interior stress in the case of a square loaded area (WESIII), the radius of the circular load, a , in Eqn. (5-2) is replaced by a constant c' , related to the length of the side of the square, c , as follows:

$$c' = \frac{e^{\frac{\pi}{4}} - 1}{\sqrt{2}} \quad c = 0.573804... c \quad (5-3)$$

The resulting expression is not stated explicitly by Westergaard, but follows directly from his theory [123; 10]. Timoshenko and Woinowsky-Krieger [80] provide a theoretical justification for this solution by showing that, loaded by the same total load P , a square side c and a circle radius a , give the same maximum interior stress.

Table 5.1b shows that the WESII representation yields, in general, lower deflections and bending stresses than WESI (with deflections being much less sensitive). WESI appears to agree better with the finite element solution than WESII. It is shown below that this "improvement" is only apparent, indicating that using WESI may tend to conceal some of the differences between Westergaard and the finite element analysis.

Note in Table 5.1b that both finite element deflections and bending stresses are slightly higher than Westergaard's. Deflections are much less sensitive to changes in load representation and are closer to theory than are bending stresses. This agrees with the observation that deflections are much less sensitive to changes in the finite element discretization. Computer program validations which quote only comparisons of theoretical and calculated deflections [88] may be misleading.

As will be noted in subsequent paragraphs, the difference between ILLI-SLAB and Westergaard responses may be attributed to:

1. The 25-ft. square slab may be too small to develop the Westergaard infinite slab condition, thus leading to higher

calculated deflections. This should also lead to somewhat lower calculated stresses, however, a feature not observed in Table 5.1b;

2. The placement of the load on top of a single node (Fig. 5.2) leads to higher calculated stresses and deflections;
3. The use of elements with aspect ratios much different from unity. Note that the mesh in Fig. 5.2 was used in Ref. 55 and was retained here for consistency;
4. The relatively large size of the loaded area. This is deemed to be the most important factor in this case.

5.3.3 Effect of Load Placement with Respect to Finite Element Mesh

The effect of load placement with respect to the finite element mesh was investigated for one of the cases presented in Table 5.1 ($k = 200$ psi/in. and $h = 14$ in.). Three different mesh configurations were used:

- Mesh I (Fig. 5.2) is the one used for all runs in Table 5.1 and has the load placed on top of one central node, without any corner nodes;
- Mesh II (Fig. 5.3) introduces 4 corner nodes in addition to the central node, thus turning the 9X9 mesh in Fig. 5.2 into an 11X11 mesh, requiring 71% more memory spaces to execute. It is, however, considered a closer representation of reality;
- Mesh III (Fig. 5.4) has the 4 corner nodes but the central node is missing. It is thus a 10X10 mesh, requiring only 32% more memory spaces than Mesh I to execute.

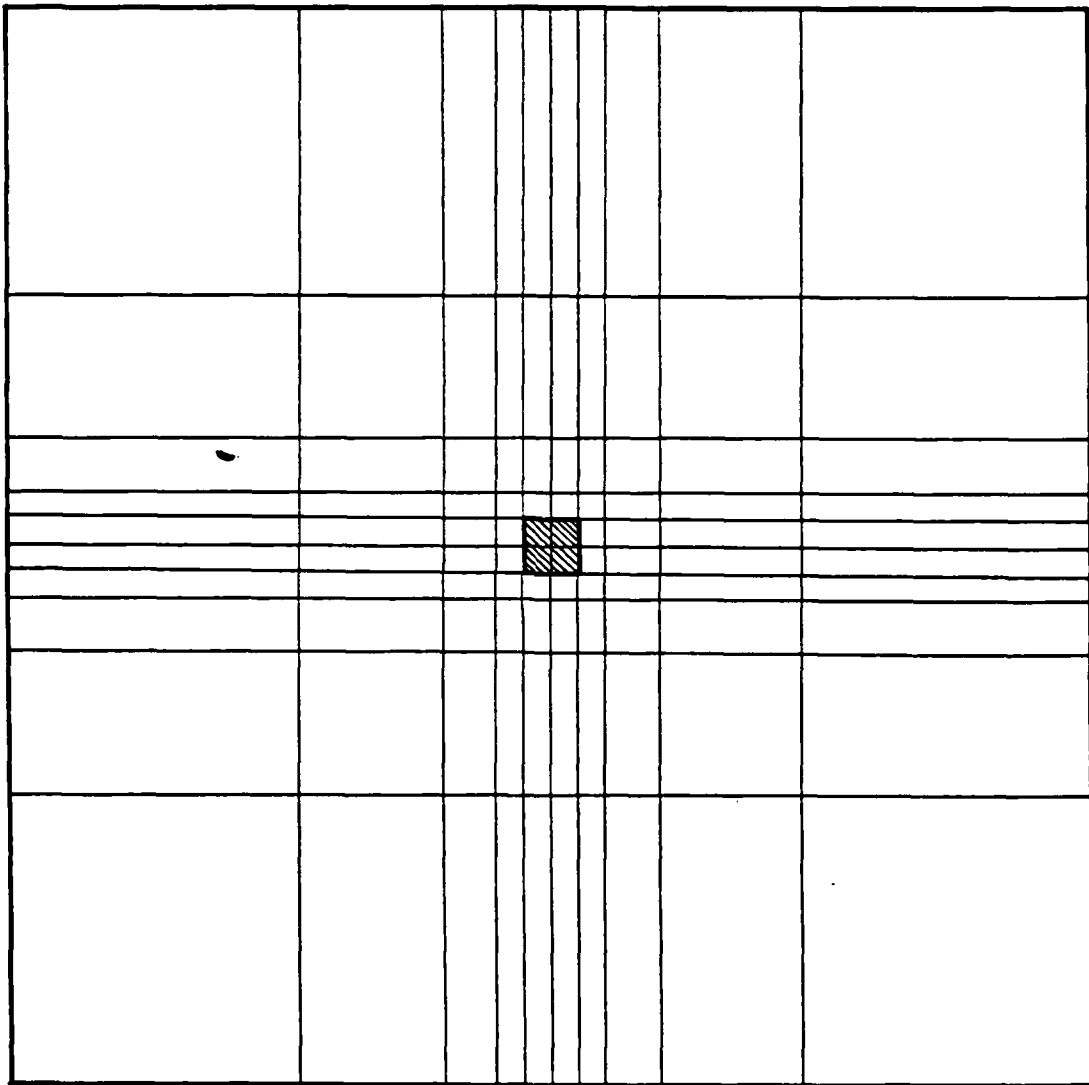


Fig. 5.3 Finite Element Mesh II (Interior Loading)

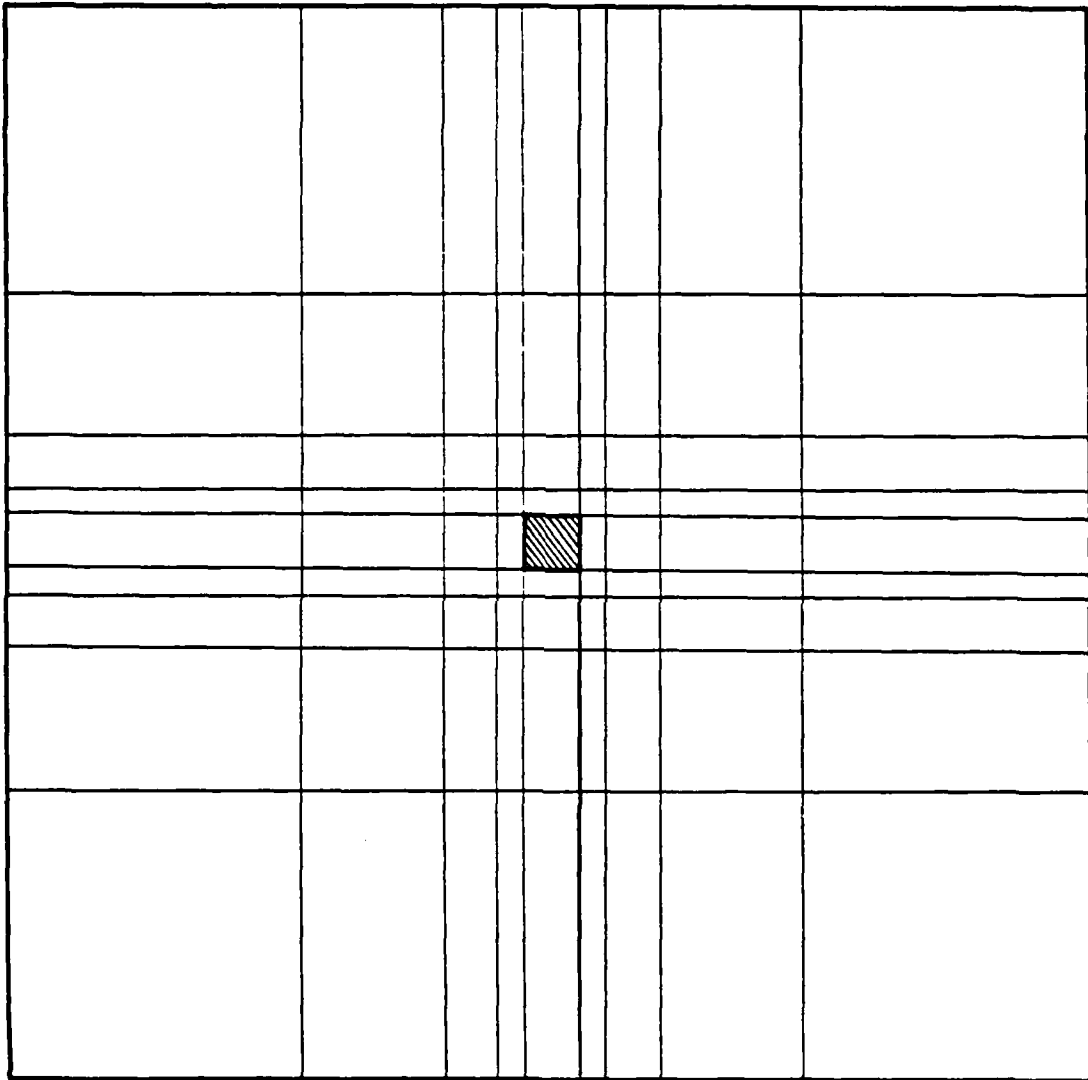


Fig. 5.4 Finite Element Mesh III (Interior Loading)

Comparisons among the results of these configurations and the results of the Westergaard idealizations WESI, WESII and WESIII are shown in Table 5.2. It is observed that the deflections are again largely insensitive to these changes, but they do follow the same pattern as calculated bending stresses. Of the three meshes, Mesh II yields the best results compared to Westergaard's (close and slightly conservative). Mesh I offers an attractive alternative, especially for those cases where a coarser mesh must be used. The results obtained with this mesh are slightly more conservative. Table 5.2 indicates that where possible, Configuration III must be avoided. Despite the extra effort involved in using this mesh as compared to Mesh I, its results underestimate the closed-form solution considerably.

This behavior may be explained with reference to the way the applied load is internally discretized by the finite element procedure in ILLI-SLAB. It was noted above that the 'WINKLER' option employs a work equivalent load vector. Thus, each applied element load is represented internally by twelve generalized force components (i.e. direct forces or moments) acting at the four nodes of the element. The work done by these nodal loads during a virtual displacement is equal to the work performed by the applied load going through the same virtual displacement. (By comparison, the 'SPRINGS' option converts each applied load to four direct force nodal components only, which are statically equivalent to the applied element load. The 'WINKLER' option is considered to offer a more accurate representation.) For best results, it is important to locate several nodes within the loaded area

TABLE 5.2

EFFECT OF LOAD PLACEMENT WITH RESPECT TO F.E. MESH

RUN No.	MESH USED	MEMORY SPACES	DEFLECTION		BENDING STRESS	
			mils	% WESII	psi	% WESIII
5	MESH I	20171	13.5	106	375.8	113
21	MESH II	34507	13.4	106	348.3	105
22	MESH III	26711	13.1	103	257.5	78
WESI	-	-	12.8	-	350.0	-
WESII	-	-	12.7	-	333.2	-
WESIII	-	-	unavailable	-	331.6	-

Notes:

(a) See also Table 5.1(b) for more details

(b) Mesh I: 9x9 mesh (Fig. 5.2)
 Mesh II: 11x11 mesh (Fig. 5.3)
 Mesh III: 10x10 mesh (Fig. 5.4)

(c) Finite Element Solution

Slab: 25'x25'

c = 15"

E = 5×10^6 psi

k = 200 psi/in.

 μ = 0.15

h = 14"

p = 222.2 psi

l = 49.18"

A = c"xc" interior

 $\frac{c}{l}$ = 0.305Theoretical Solutions

Ordinary Theory

WESI

WESII

WESIII

P = 50,000 lb.

P = 50,000 lb.

P = 50,000 lb.

p = 282.94 psi

p = 222.2 psi

p = 222.2 psi

a = 7.5" (circular)

a = 8.46" (circular)

c = 15" (square)

(Mesh II). This is often not possible, so the best alternative is to have a node as close to the centroid of the applied load as possible (Mesh I), so that the load discretization will be more accurate. It should also be noted that in Mesh III twelve components are used in the internal load representation, compared to 48 in Mesh I and II. A node must also be provided close to the anticipated maximum response location, if this does not coincide with the centroid of the applied load (e.g. for bending stress under corner loading). The design of a good mesh is often a trade-off between extra computer core usage and accuracy.

5.3.4. Convergence Characteristics of ILLI-SLAB Upon Mesh Refinement

In the present as well as the original version, ILLI-SLAB employs the 12 degree-of-freedom (dof) plate element [47] which is referred to in the literature as the RPB12 or ACM element. The dimensions of this rectangular (or square) element are $2a$ by $2b$. It is a 4-node, 3-dof per node plate bending element formulated using classical medium-thick plate theory. Deformations due to transverse shear are neglected in this formulation. Because all terms of a complete fourth order polynomial are not present in the assumed displacement shape (15 terms would be required), the element is non-conforming, i.e. slopes normal to interelement boundaries are not continuous. However, the element is capable of correctly reproducing constant strain (curvature) states. Therefore, convergence to the exact solution is assumed as the element mesh is refined. What is not guaranteed is that convergence will be

monotonic, i.e. consistently from above or from below.

To check the convergence characteristics of ILLI-SLAB, a factorial of runs was designed which would permit the examination of the effect of mesh refinement without interference from limitations due to finite slab size and element aspect ratio. It will be noted in a later paragraph that minimum slab size, L , for the development of the Westergaard infinite slab condition with respect to bending stresses seems to be about 3.5 times the radius of relative stiffness, ℓ , of the slab. For the 12X12-ft. slab used, parameters were chosen that gave ℓ equal to 23.16 in., i.e. an (L/ℓ) ratio of 6.2. Thus, no slab size problems can be expected, at least as far as bending stresses are concerned.

The slab thickness, h , was chosen as 15 in. despite the fact that this meant a higher radius of relative stiffness than would be obtained with a thinner slab. The objective here was to allow the investigation of element sizes smaller than h , since it had been pointed out by previous ILLI-SLAB users that elements this small produced a stiffening effect. The other parameters used for this factorial are shown in Table 5.3a. Square elements were used to eliminate any aspect ratio effects, but their size varied from run to run depending on how many were available to fill the 12X12-ft. slab used. The ratio of element size, $2a$, to slab thickness, h , varied between 5.8 when 4 elements were used, to 0.8 when 144 elements were used. The mesh used for the latter case is shown in Fig. 5.5. Also shown in Table 5.3a are the results from two Westergaard idealizations of the problem, one where P and p were matched using a circular load (WESII), and another for a square load

TABLE 5.3

(a) EFFECT OF F.E. MESH FINENESS

RUN No.	No. of Elements	$(\frac{2a}{h})$	DEFLECTION		BENDING STRESS	
			(mils)	% WESII	psi	% WESIII
32	4	4.8	1.06	91	4.53	27
33	16	2.4	1.23	106	9.68	59
34	64	1.2	1.25	108	14.22	86
35	144	0.8	1.24	107	16.34	99
WESII	-	-	1.16	-	16.61	-
WESIII	-	-	unavailable	-	16.54	-

Notes:Finite Element Solution: Revised ILLI-SLABTheoretical Solutions

Slab: 12'x12' (= 6.28 square)
Elements: 2ax2a

See Table 5.1(b) for
equations used.

Ordinary Theory

P = 2500 lb

p = 100 psi

a = 2.82" (circular:
WESII)

c = 5" (square:
WESIII)

E = 0.5×10^6 psi

μ = 0.15

p = 100 psi

A = c"xc" interior

c = 5"

h = 15"

k = 500 psi/in.

ℓ = 23.16"

$\frac{c}{\ell}$ = 0.216

TABLE 5.3 (continued)

(b) COMPARISON BETWEEN ILLI-SLAB (WINKLER), 'SPRINGS' AND WESLIQID

ILLI-SLAB	RUN No. SPRINGS	WESLIQID	No. of Elements	DEFLECTION				BENDING STRESS			
				ILLI-SLAB mils	ILLI-SLAB %	'SPRINGS' mils	'SPRINGS' %	WESLIQID mils	WESLIQID %	ILLI-SLAB psi	WESLIQID psi
32	62		4	1.06	91	0.82	71	1.15	99	4.53	27
33	63	83	16	1.23	106	1.19	103	1.15	99	9.68	59
34	64		64	1.25	108	1.24	107	1.21	104	14.22	86
35	65	85	144	1.24	107			1.22	105	16.34	99
		86	576					1.22	105		
		87	784					1.22	105		
				1.16				16.61			
WESII				unavailable				16.54			
WESIII											

Notes:

Slab and load characteristics as in Table 5.3(a).

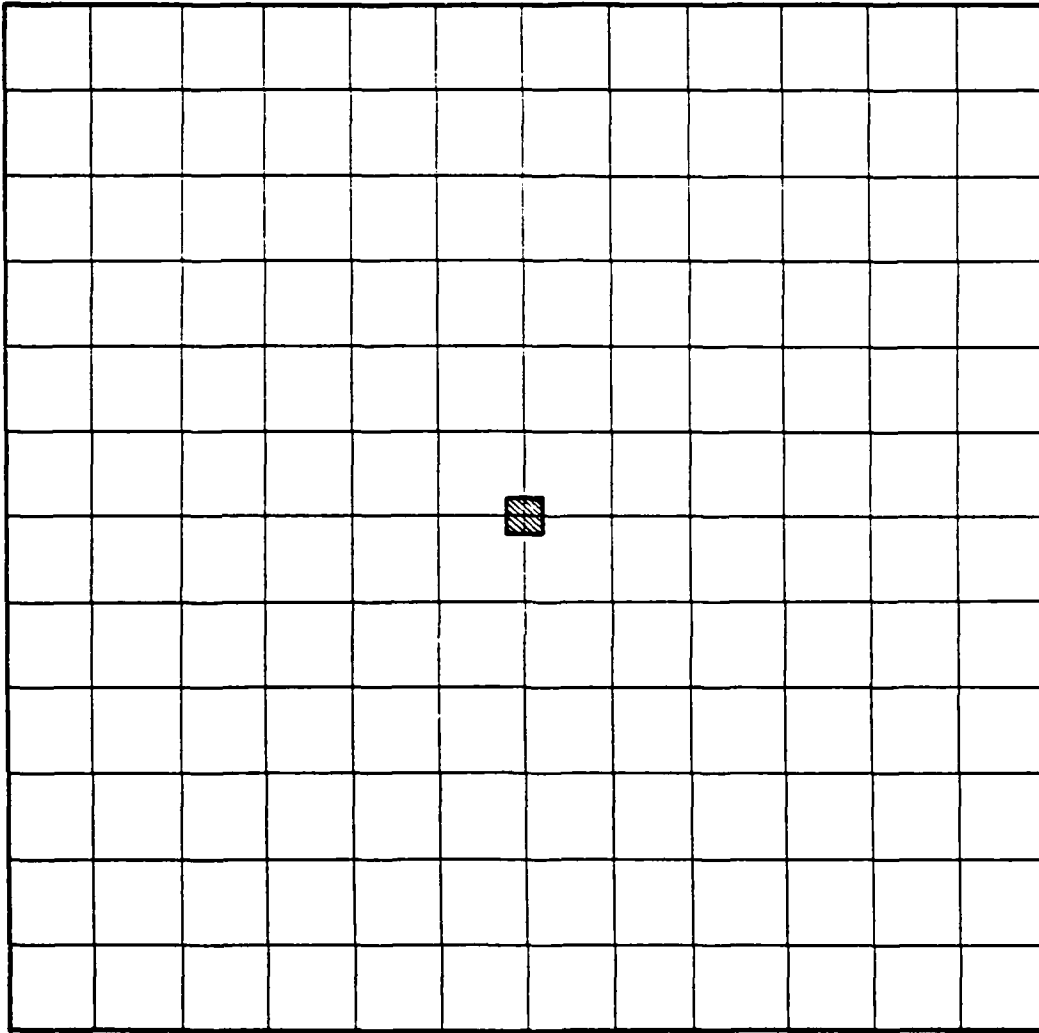


Fig. 5.5 . Effect of Mesh Fineness: Mesh with 144 Elements

(WESIII).

The results shown in Table 5.3a are presented graphically in Fig. 5.6. It is noted that for the cases studied, as the mesh is refined both maximum deflection and bending stress converge monotonically from below to a theoretical value that would be obtained in the limit of refinement. In the case of deflection, this is slightly higher than the Westergaard value for the corresponding problem. This is probably due to the lack of an exact solution for a square load, as well as as the finite size of the slab ($L/\ell=6.2$; see below). In this study, deflections are compared to the theoretical values for an equivalent circular load of the same area as the square load (WESII). The observed discrepancy is very small. It is also noted that the convergence rate of deflection is much faster than that of bending stress, the limit solution being reached at values of $(2a/h)$ as large as 2 to 3.

On the other hand, maximum bending stress converges to the corresponding Westergaard solution, but at a smaller value of $2a/h$ ($=0.8$). Note that this comparison is with Westergaard's ordinary theory for a square load (WESIII). The stress from a special theory analysis would be 12.8 psi and this could lead to unjustified conclusions with respect to the F.E.M. The true cause of this discrepancy is, of course, that the special theory and the F.E.M. based on medium-thick plate theory are not directly comparable, since the first accounts (in a semi-empirical fashion) for the effect of shear stresses in the vicinity of the load, while the latter does not.

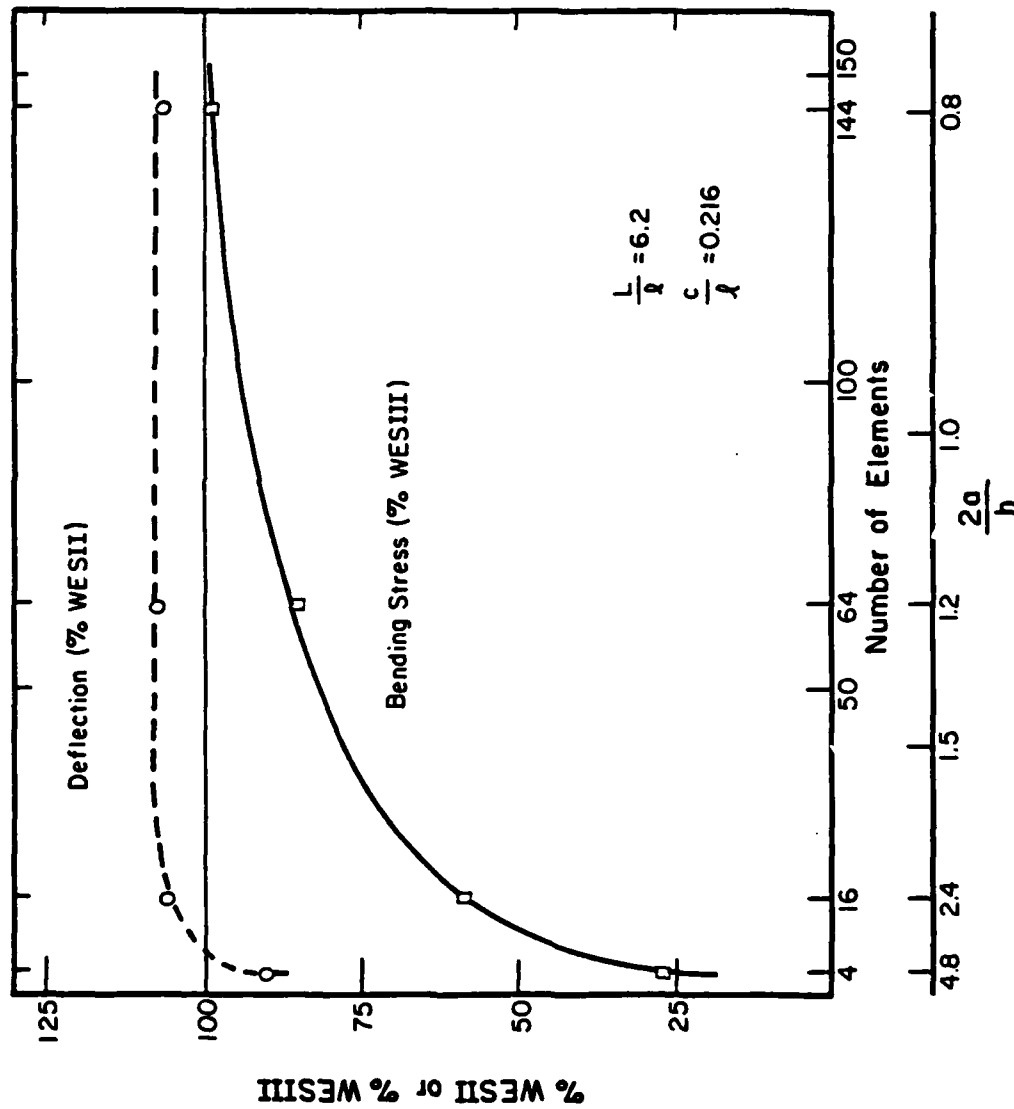


Fig. 5.6 Effect of Mesh Fineness (Interior Loading)

The problem was further investigated by using a similar factorial of WESLIQID runs, and using the 'SPRINGS' option in revised ILLI-SLAB. As mentioned previously, this option is identical to the FINITE model. In Table 5.3b, the results from these runs are compared to those from ILLI-SLAB.

It is observed that all three models exhibit basically the same behavior, i.e. they monotonically converge from below to the same limit values. The effect of mesh refinement on the distribution of deflections and stresses is shown in Figures 5.7 and 5.8, respectively. Deflections are fairly insensitive, especially outside a region of about twice the size of the loaded area. Stress differences persist relatively longer.

5.3.5 Convergence Characteristics of ILLI-SLAB Upon Slab Size Expansion

As mentioned earlier, the closed-form Westergaard solution assumes a slab of infinite dimensions, although in practice empirical guidelines have been developed for the least slab dimension required to achieve the Westergaard "infinite slab" condition. These guidelines are summarized in Table 5.4, for a typical single, circular load [124]. It is the purpose of this part of the present study to examine if and how ILLI-SLAB converges to the Westergaard solution as the slab size is increased and establish whether the empirical guidelines in Table 5.4 are verified by the F.E.M.

The same parameters were used for this factorial of runs as in the study of mesh refinement, giving again a radius of relative stiffness,

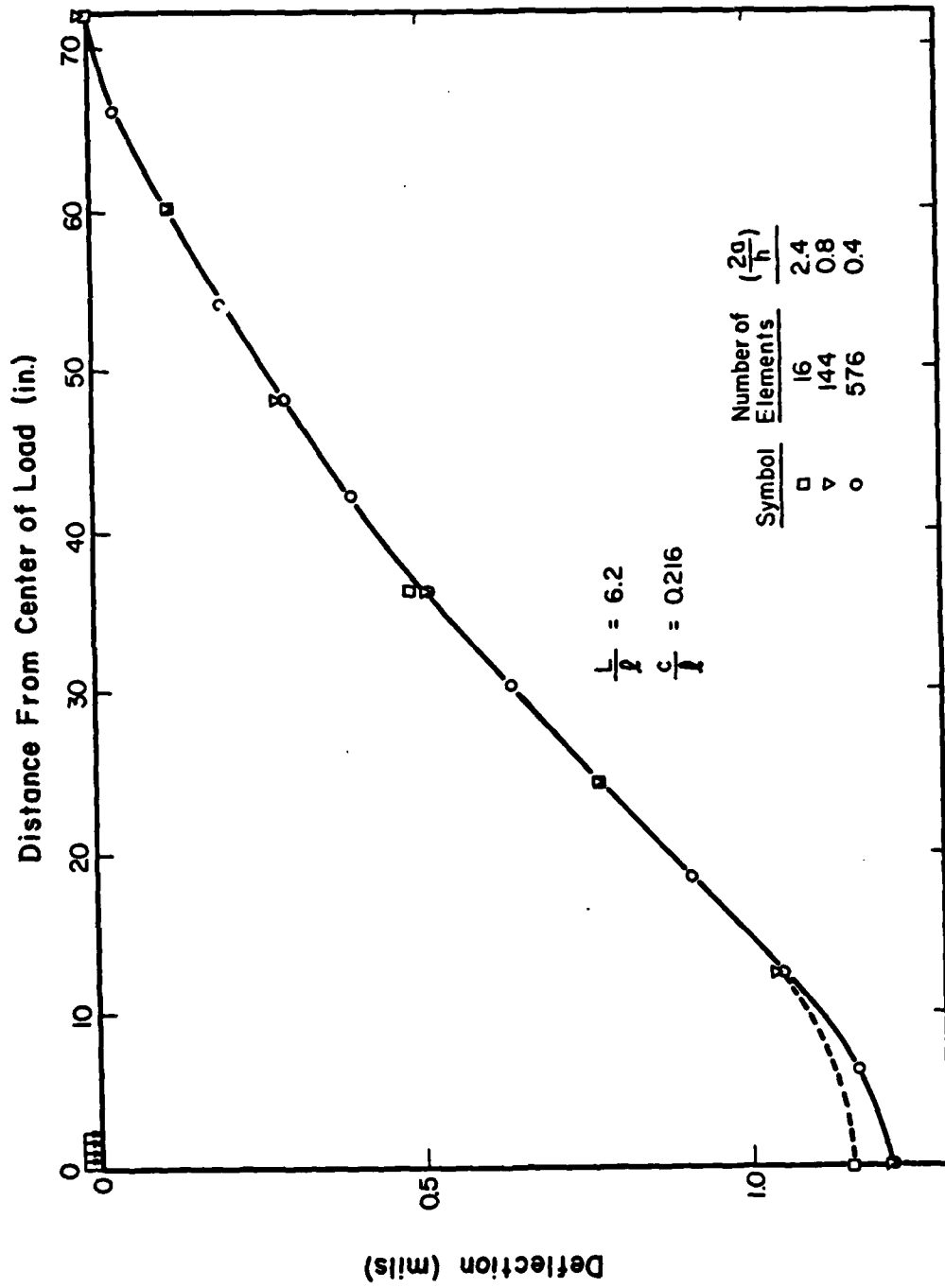


Fig. 5.7 Effect of Mesh Fineness on Deflection Bowl (WESLIQID)

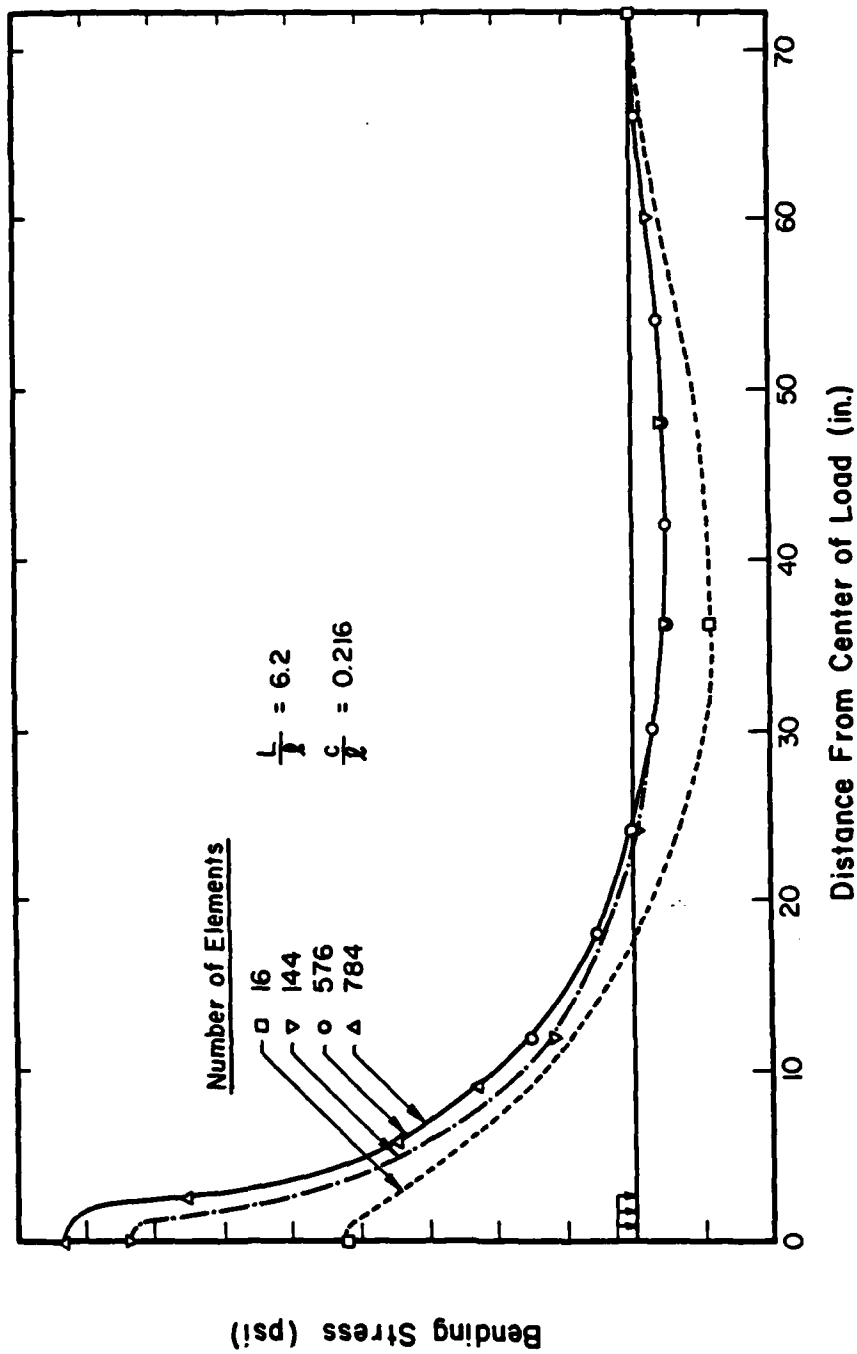


Fig. 5.8 Effect of Mesh Fineness on Bending Stresses (WESLIQID)

TABLE 5.4
THEORETICAL AND EMPIRICAL SIZE LIMITATIONS FOR
THE WESTERGAARD SOLUTION

Loading Condition	Minimum Side Length	
	Theoretical	Practical
Interior	11ℓ	6ℓ
Edge	11ℓ	6ℓ
Corner	Unavailable	

ℓ : radius of relative stiffness

Size Limitations apply for typical
single, circular load

(After Barenberg [124])

ℓ , of 23.16 in. The element size was kept at 18 in. (i.e. $2a/h=1.2$). The mesh used for these runs shown in part in Fig. 5.9. The pattern shown is repeated in all 4 directions to give the required slab size.

The results from this investigation are given in Table 5.5, where they are compared to the corresponding Westergaard values. The same results are presented graphically in Fig. 5.10. Both maximum deflection and bending stress converge to a theoretical value for an infinite slab. The convergence of deflection is from above, indicating that a smaller slab settles more than a bigger one in a "punch-like" fashion. Bending stress converges from below, as expected. The rate of convergence, defined as the slab size at which the solution is essentially that for an infinite slab, is different for deflection ($L/\ell=8.0$) than for bending stress ($L/\ell=3.5$). Surprisingly, deflection appears to be much more sensitive to slab size changes for (L/ℓ) values of less than 3, because of the above-mentioned "punch-like" effect. The limit value approached by the deflection is the Westergaard solution.

The value to which bending stress converges upon slab size expansion is exactly that which would be expected for the given mesh fineness ($2a/h=1.2$) as shown in Table 5.3a. This indicates that, fineness effects apart, stress converges to the theoretical value for (L/ℓ) values of about 3.5. In Table 5.5, the stress is not expected to approach the Westergaard solution by any appreciable amount upon further slab expansion, simply because the discrepancy observed arises from mesh fineness effects, as shown in Table 5.3a.

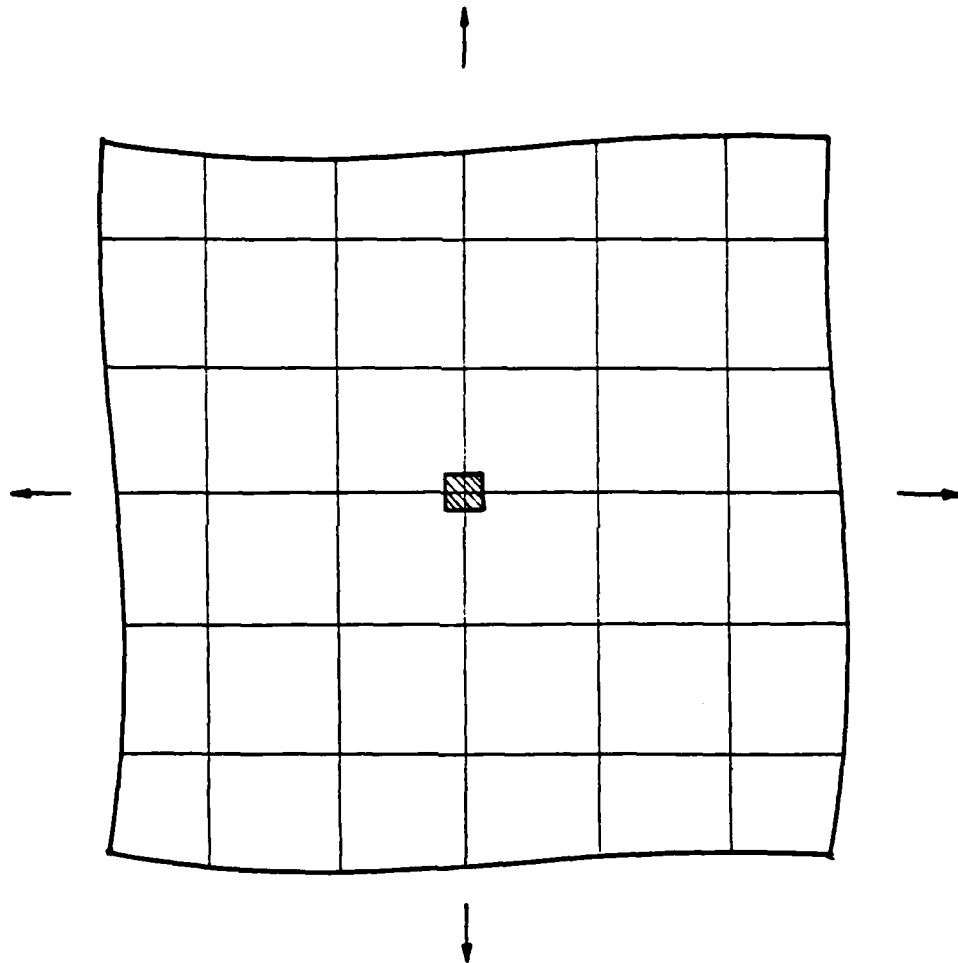


Fig. 5.9 Finite Element Mesh for Slab Size Investigation

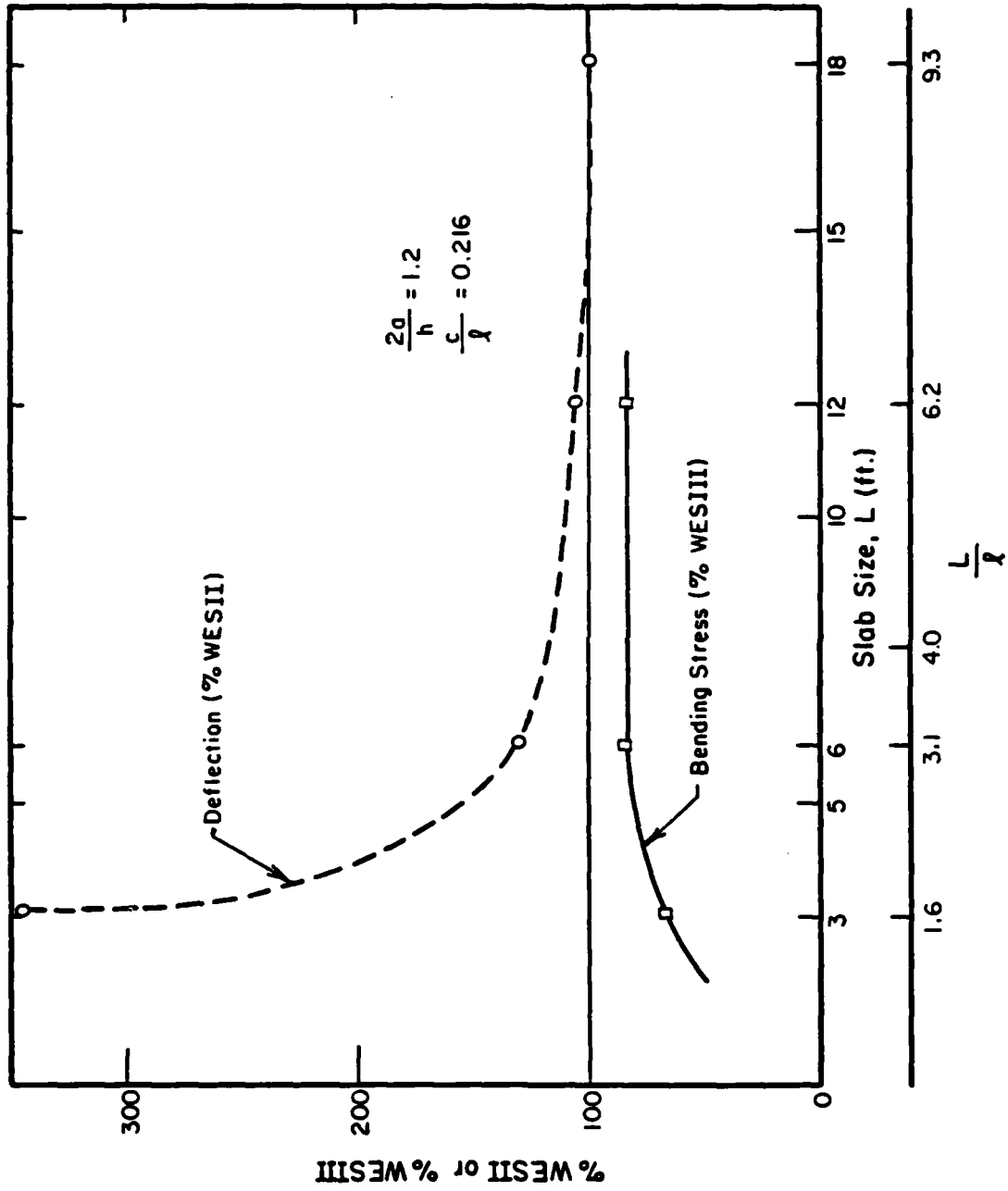


Fig. 5.10 Effect of Slab Size (Interior Loading)

TABLE 5.5
EFFECT OF SLAB SIZE

RUN No.	ILLI-SLAB	SPRINGS	L (ft)	L/l	DEFLECTION				BENDING STRESS				
					'WINKLER'		'SPRINGS'		'WINKLER'		'SPRINGS'		
					mils	%	mils	%	psi	%	psi	%	
					WESII	WESII	WESII	WESII	WESII	WESIII	WESIII	WESIII	WESIII
41		71	3	1.6	4.01	346	4.09	353	9.88	60	11.09	67	
42		72	6	3.1	1.52	131	1.56	134	14.13	85	14.14	85	
43 or 34		73	12	6.2	1.25	108	1.24	107	14.22	86	14.13	85	
44			18	9.3	1.18	102			14.10	85			
					WESII		1.16		16.61				
					WESIII		unavailable		16.54				

Notes:

Finite Element Solution

Revised ILLI-SLAB 'WINKLER' and 'SPRINGS'

Slab: L'xL'

Element Size: 18"x18" ($\frac{2a}{h} = 1.2$)E = 0.5×10^6 psi

h = 15"

 $\mu = 0.15$

k = 500 psi/in.

p = 100 psi

l = 23.16 in.

A = c"xc"; interior

 $\frac{c}{l} = 0.216$

c = 5"

Theoretical Solutions

See Table 5.1(b) for equations used
Ordinary Theory

P = 2500 lb

p = 100 psi

a = 2.82" (circular: WESII)

c = 5" (square: WESIII)

It is interesting to note in Table 5.5 the similarity in behavior patterns between ILLI-SLAB options 'WINKLER' and 'SPRINGS'. This reinforces the observations above.

5.3.6 Effect of Element Aspect Ratio

The effect of element aspect ratio, defined as the ratio between the length of the long side of the element to the length of the short side, was investigated by the factorial of runs shown in Table 5.6 using WESLIQID. Theoretically, best results are obtained when the aspect ratio is kept close to unity, i.e. the elements are as close to square as possible. This postulate is borne out in Table 5.6.

Figures 5.11 and 5.12 show how the aspect ratio affects deflection and stress distributions. It is observed that deflection is largely insensitive -as always- to any changes. The bending stress distribution is also insensitive except in a small region surrounding the loaded area. The radius of this region is approximately twice the radius of the loaded area. Within this region, a departure of aspect ratio from unity may cause significant errors.

5.3.7 Effect of Size of Loaded Area

In his attempt to develop equations for a loaded area of finite size, Westergaard used an approach which essentially consists of first deriving a solution for a point load. Then, the loaded area is split into a number of small subareas, each subarea being replaced by a statically equivalent point load acting at its center. A summation is

TABLE 5.6

EFFECT OF ELEMENT ASPECT RATIO

RUN NO.	ASPECT RATIO	DEFLECTION		BENDING STRESS	
		mils	% WESII	psi	% WESIII
91 or 86	1	1.22	105	16.67	100
92	2	1.21	104	16.07	97
93	3	1.21	104	15.19	92
94	4	1.20	103	14.29	86
96	6	1.18	102	12.65	76
WESII			1.16		16.61
WESIII			unavailable		16.54

Notes:Finite Element Solution (WESLIQID)

Slab: 12'x12' (= 6.28 square)

Elements: 2ax2b

 $E = 0.5 \times 10^6$ $\mu = 0.15$ $p = 100$ psi $2a = 6''$ $2b = 2a \times$ (Aspect Ratio) $A = c'' \times c''$ interior $c = 5''$ $h = 15''$ $k = 500$ psi/in. $l = 23.16''$ $\frac{c}{l} = 0.216$ $\frac{2a}{h} = 0.4$ Theoretical Solutions

See Table 5.1 (b) for equations used.

Ordinary Theory

 $P = 2500$ lb. $p = 100$ psi $a = 2.82''$ (circular: WESII) $c = 5''$ (square: WESIII)

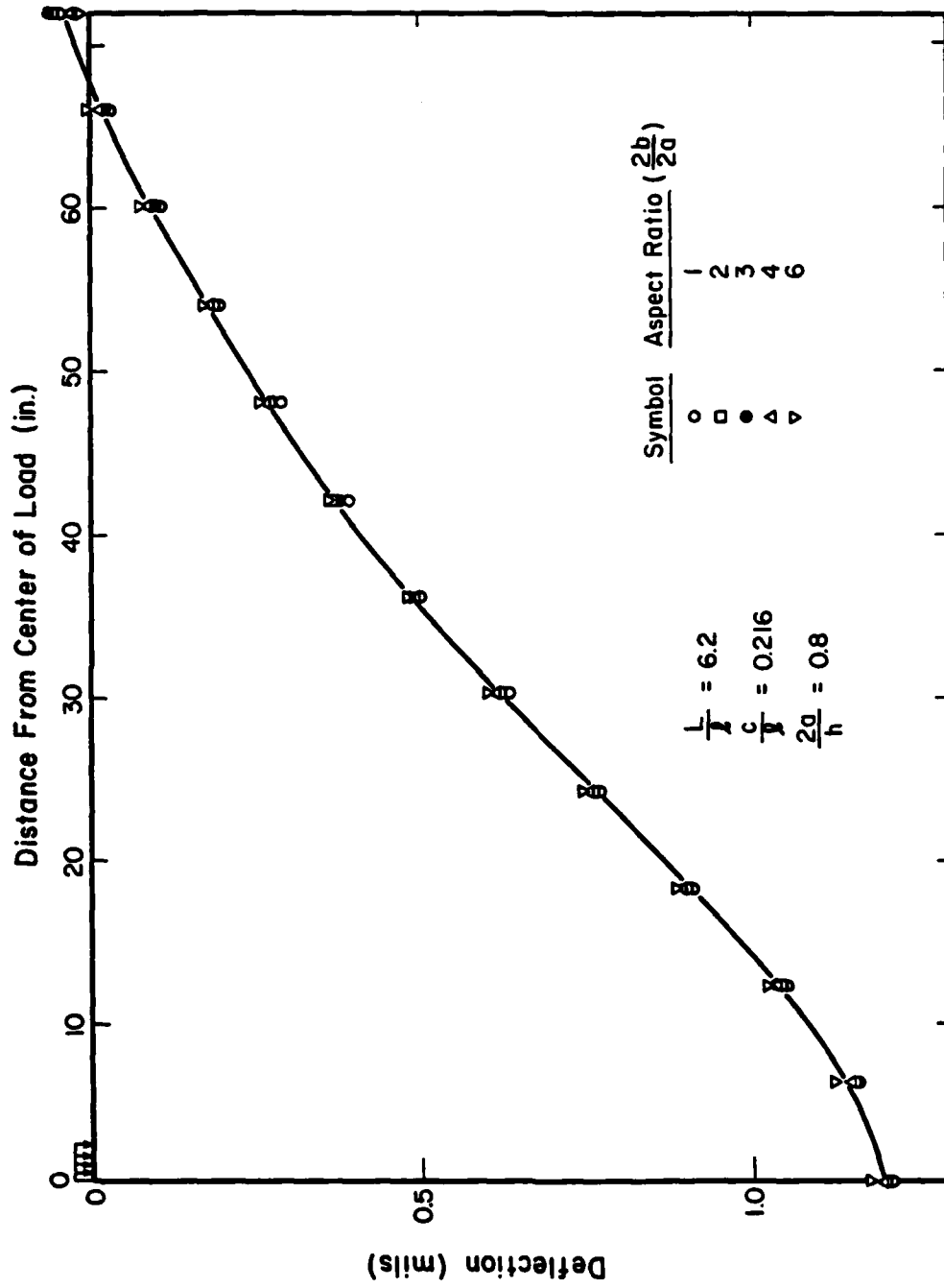


Fig. 5.11 Effect of Element Aspect Ratio on Deflection Bowl (WESLIQID)

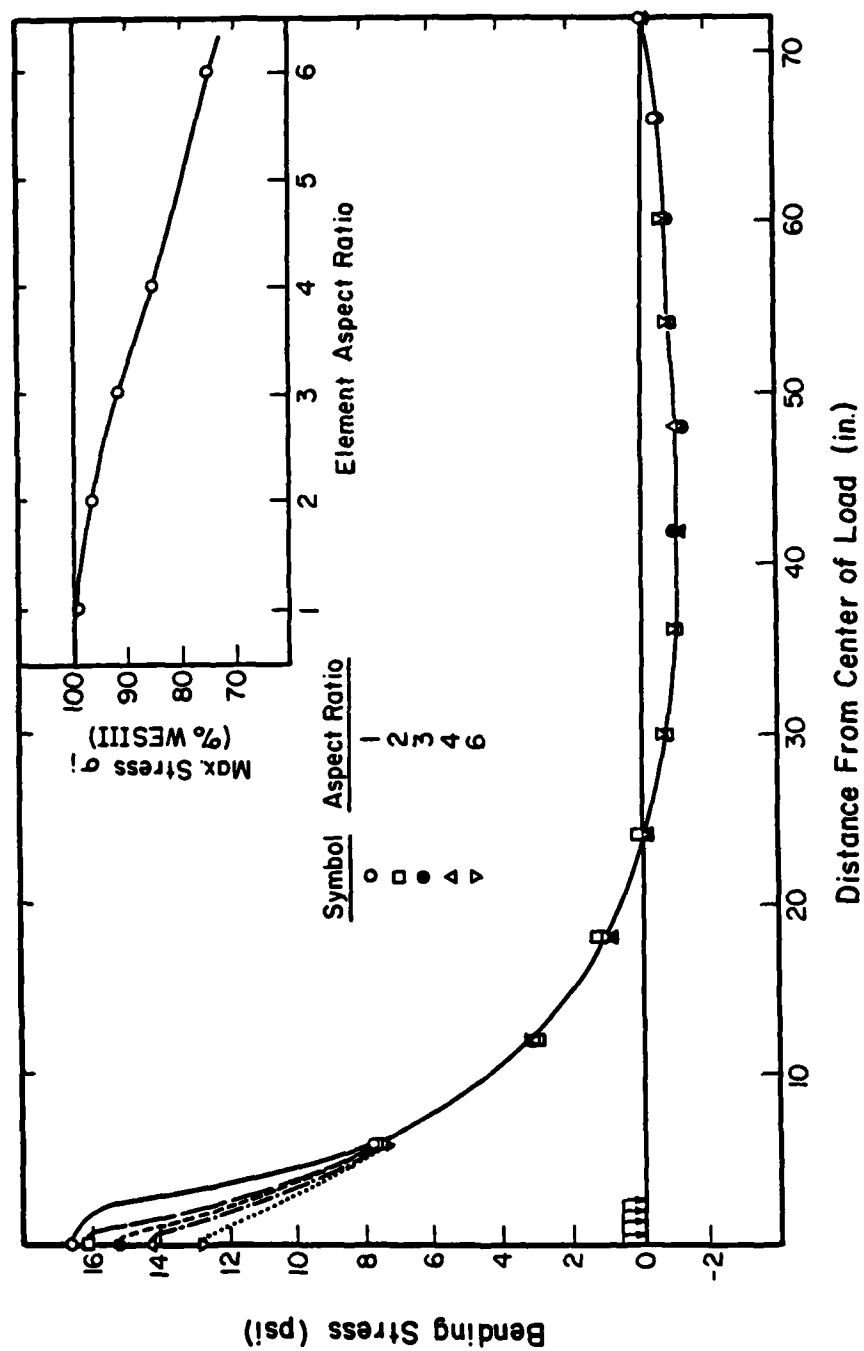


Fig. 5.12 Effect of Element Aspect Ratio on Bending Stresses (WESLIQID)

performed over these subareas. In the limit of refinement, this summation tends to an exact integration [84]. Westergaard suggests that his equations are valid for any size of loaded area and that, in fact, his "New Formulas" [10] assume that "the average width and length of the footprint of the tire is greater than the thickness of the slab in all significant cases".

Losberg [13] showed that the stress and deflection equations presented by Westergaard and widely used in practice, are only the first one or two terms of a rapidly converging infinite series. Westergaard's supplementary stress, σ_2 mentioned above, for example, is an additional term of this series. The rate of convergence can be expected to vary depending, among other things, upon the size of the loaded area.

Timoshenko and Woinowsky-Krieger [80] state that the equations apply only when the radius of the loaded area is "small in comparison with ℓ ". Scott [121] attributes this restriction to the fact that "in the derivation of the equation a term of approximate value $0.1 a^2/\ell^2$ was omitted". This cannot be the real cause of the restriction imposed by Timoshenko and Woinowsky-Krieger, since in most cases (even when the radius of the loaded area, a , is not "small in comparison with ℓ ") this term is, indeed, negligible.

In this study, the effect of the size of the loaded area was investigated using the F.E.M.. Table 5.7 shows a factorial of ILLI-SLAB runs and comparisons with Westergaard's ordinary theory solutions. To eliminate slab size, mesh fineness and aspect ratio effects, a large ($L/\ell=9.33$) and fine ($2a/h=0.6$) mesh was used, consisting of square

TABLE 5.7
EFFECT OF SIZE OF LOADED AREA

RUN No.	p (psi)	c (in.)	c/l	DEFLECTION		BENDING STRESS	
				mils	% WESII	psi	% WESIII
109	1000	1.58	0.068	1.18	101	18.77	80
110	400	2.50	0.108	1.18	101	18.52	89
108	200	3.54	0.153	1.18	101	18.12	97
107	175	3.78	0.163	1.18	101	18.01	99
106	150	4.08	0.176	1.17	101	17.87	100
105	125	4.47	0.193	1.17	101	17.68	103
101	100	5.00	0.216	1.17	101	17.40	105
102	75	5.77	0.249	1.17	102	16.96	108
103	50	7.07	0.305	1.16	101	16.17	112
104	25	10.00	0.432	1.15	102	14.23	115
111	13.72	13.50	0.583	1.13	101	11.98	114
112	10.23	15.63	0.675	1.11	101	10.77	111
113	8.29	17.37	0.750	1.10	101	9.92	110
114	7.72	18.00	0.777	1.10	101	9.64	109

Notes:

- (a) The theoretical values WESII and WESIII (not explicitly given here) were obtained for a circular and a square load respectively using the equations given in Table 5.1(b), for $P = 2500$ lb and p as shown above.

(b) Finite Element Solution

Slab: 18'x18' ($\frac{L}{\ell} = 9.33$)

Element Size: 9"x9" ($\frac{2a}{h} = 0.6$)

Number of Elements = 576

$E = 0.5 \times 10^6$ psi

$\mu = 0.15$

$A = c'' \times c''$ interior

$h = 15''$

$k = 500$ psi/in.

$\ell = 23.16''$

elements (aspect ratio=1.0). The load is applied over the central node, in a manner similar to Mesh I (Fig. 5.2). The results in Table 5.7 are plotted in Fig. 5.13.

It is observed that Westergaard stress values agree with finite element results for a loaded area whose side length, c (if square) is about 0.2 times the radius of relative stiffness, ℓ ; if the load is circular, its radius, a , must be about 0.1ℓ . As (c/ℓ) or (a/ℓ) increase, finite element stresses become progressively higher than Westergaard's.

Although the consequences of Westergaard's truncation mentioned above must be borne in mind when attempting such comparisons, the results in Table 5.7 also suggest an effect related to the internal discretization of the applied load, discussed briefly in paragraph 5.3.3. As the size of the loaded area increases, the centroids of the four individual element loads progressively move away from the central node, which may also explain part of the discrepancy. This raises the question of whether a separate mesh fineness ratio should be established for loaded elements, which would be more stringent than the value of $(2a/h)$ of 0.8 established above. Such a requirement would probably tax computer resources excessively, and lead to compromises with respect to overall mesh fineness and/or element aspect ratio. This would create more problems than it would solve, and will not be pursued further here. It may be noted, however, that further refinement of the mesh within the loaded region may lead to lower bending stresses, if the trend exhibited by Mesh II in Table 5.2 is repeated. Additional comments with respect

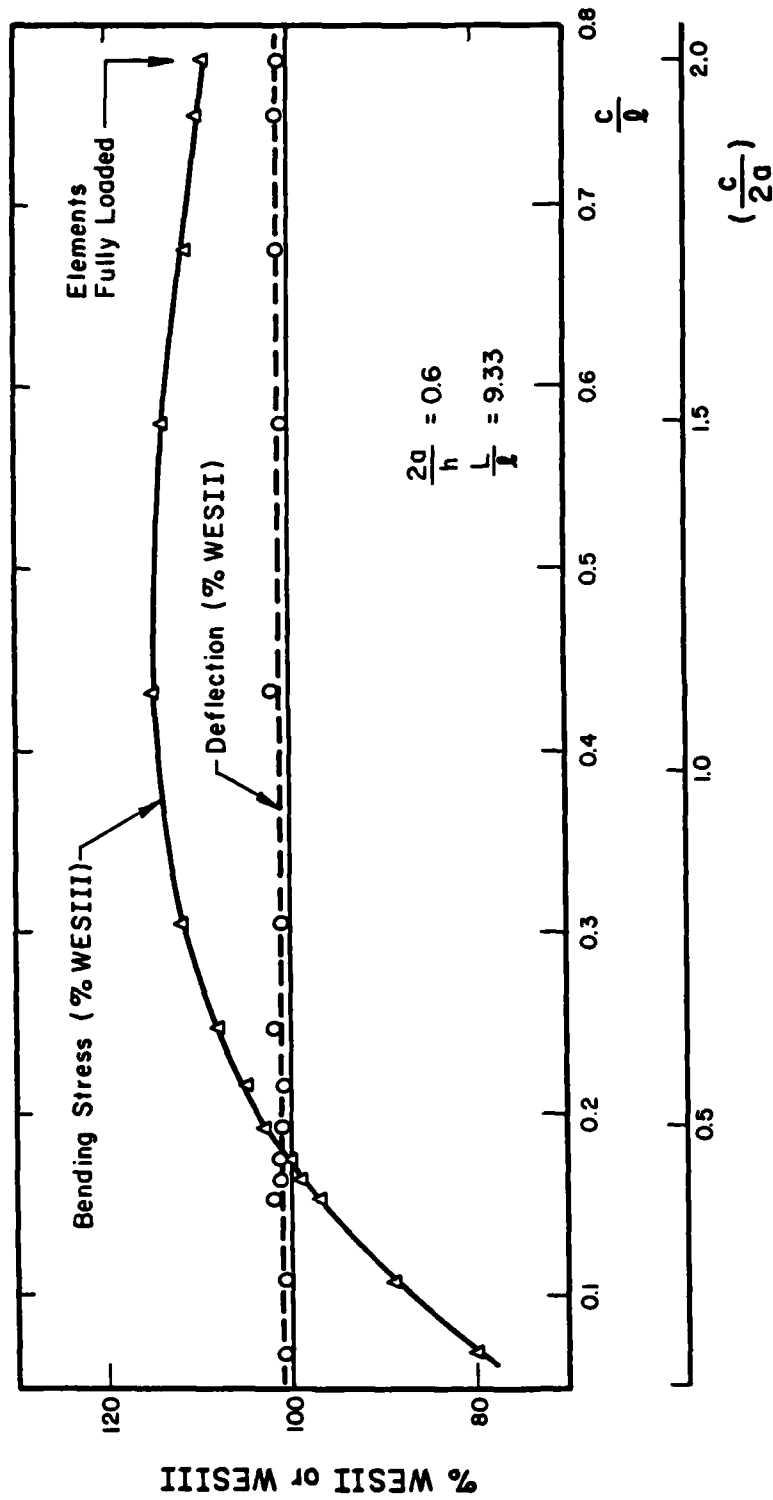


Fig. 5.13 Effect of Size of Loaded Area (Interior Loading)

to the loaded area size effect are made in Section 7.5 and elsewhere.

5.4 THE EDGE LOADING CONDITION

5.4.1 Comparison of the Present to the Original Version of ILLI-SLAB

This comparison, involving the edge loading condition, is a continuation of a similar investigation presented in Paragraph 5.3.1 for interior loading. The objective here is to check the "good agreement" between theory and ILLI-SLAB reported in Ref. 55 and compare the original and revised versions of the program.

The results reported in Ref. 55 are reproduced in Table 5.8 and Fig. 5.14. According to Tabatabaie, et al., the finite element solutions for a 25-ft. square slab ($E = 5 \times 10^6$ psi; $\mu=0.15$) loaded by a single edge load of 50 kips distributed over a 15-in. square area, are compared to Westergaard's infinite slab solutions for the same load distributed over a circular area, radius 7.5 in. The finite element mesh used is reproduced in Fig. 5.15. The equations used as the Westergaard solution for the maximum edge deflection (δ_e) and bending stress (σ_e), are quoted in Ref. 55 as follows:

$$\delta_e = \frac{1}{\sqrt{6}} (1+0.4\mu) \frac{P}{kl^2}$$

$$\sigma_e = 0.497 (1+\mu) \frac{P}{h^2} [4 \log_{10} \left(\frac{l}{b}\right) + 0.359] \quad (5-4)$$

$$b = \sqrt{1.6 a^2 + h^2} \quad -0.675h \text{ for } a < 1.724h$$

TABLE 5.8
ORIGINAL ILLI-SLAB RESULTS FOR EDGE LOADING

RUN NO.	k (psi/in.)	h (in.)	l (in.)	P/kl ²	δ_e (mils)		σ_e (psi)	
					Theory	ILLI-SLAB (ORIGINAL)	Theory	ILLI-SLAB (ORIGINAL)
1	50	12	61.95	0.261	112.7	110.3	813	975
2	200	12	43.81	0.130	56.4	49.7	694	816
3	500	12	34.84	0.082	35.7	29.6	615	708
4	50	16	76.87	0.169	73.2	78.9	484	593
5	200	16	54.36	0.085	36.6	34.3	417	516
6	500	16	43.23	0.054	23.2	20.3	372	455
7	50	20	90.88	0.121	52.4	63.7	318	395
8	200	20	64.26	0.061	26.2	26.0	275	356
9	500	20	51.10	0.038	16.6	15.3	246	320

Notes:

Finite Element Solution

Original Version of ILLI-SLAB
Slab: 25 x 25 ft.
E = 5 x 10⁶ psi
u = 0.15
P = 50,000 lbs; p = 222.2 psi
A = 15 x 15 in.; edge
Mesh: Fig. 5.15

Theoretical Solution

P = 50,000 lb.
p = 282.94 psi
a = 7.5 in.
 $\delta_e = \frac{1}{\sqrt{6}} (1 + 0.4u) P/kl^2$
 $\sigma_e = 0.497(1+u) \frac{P}{h^2} [4 \log(l/b) + 0.359]$
 $b = \sqrt{1.6 a^2 + h^2} - 0.675h$ for $a < 1.724h$
= a for $a > 1.724h$

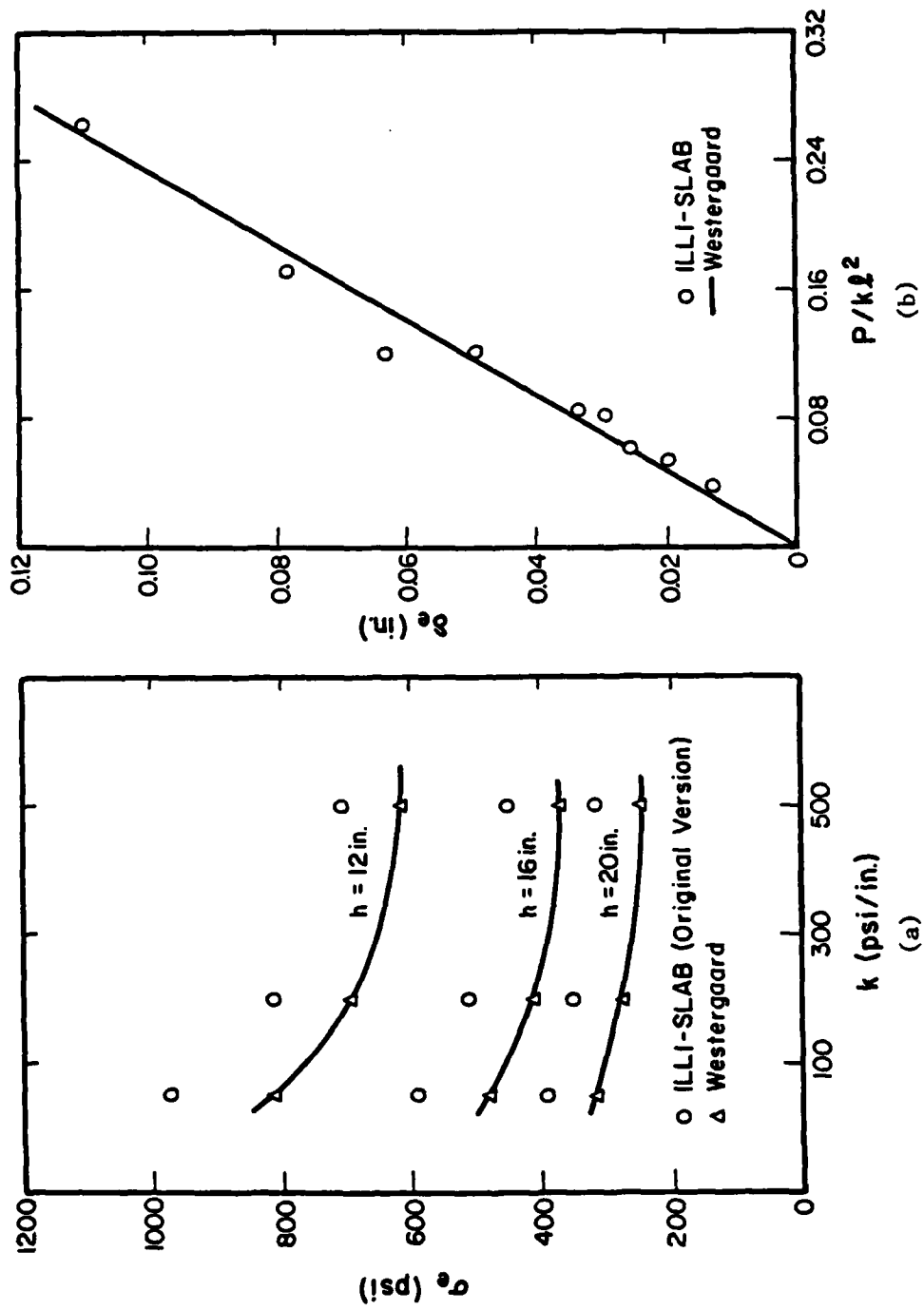


Fig. 5.14 Results by Tabatabaie Reproduced (Edge Loading)

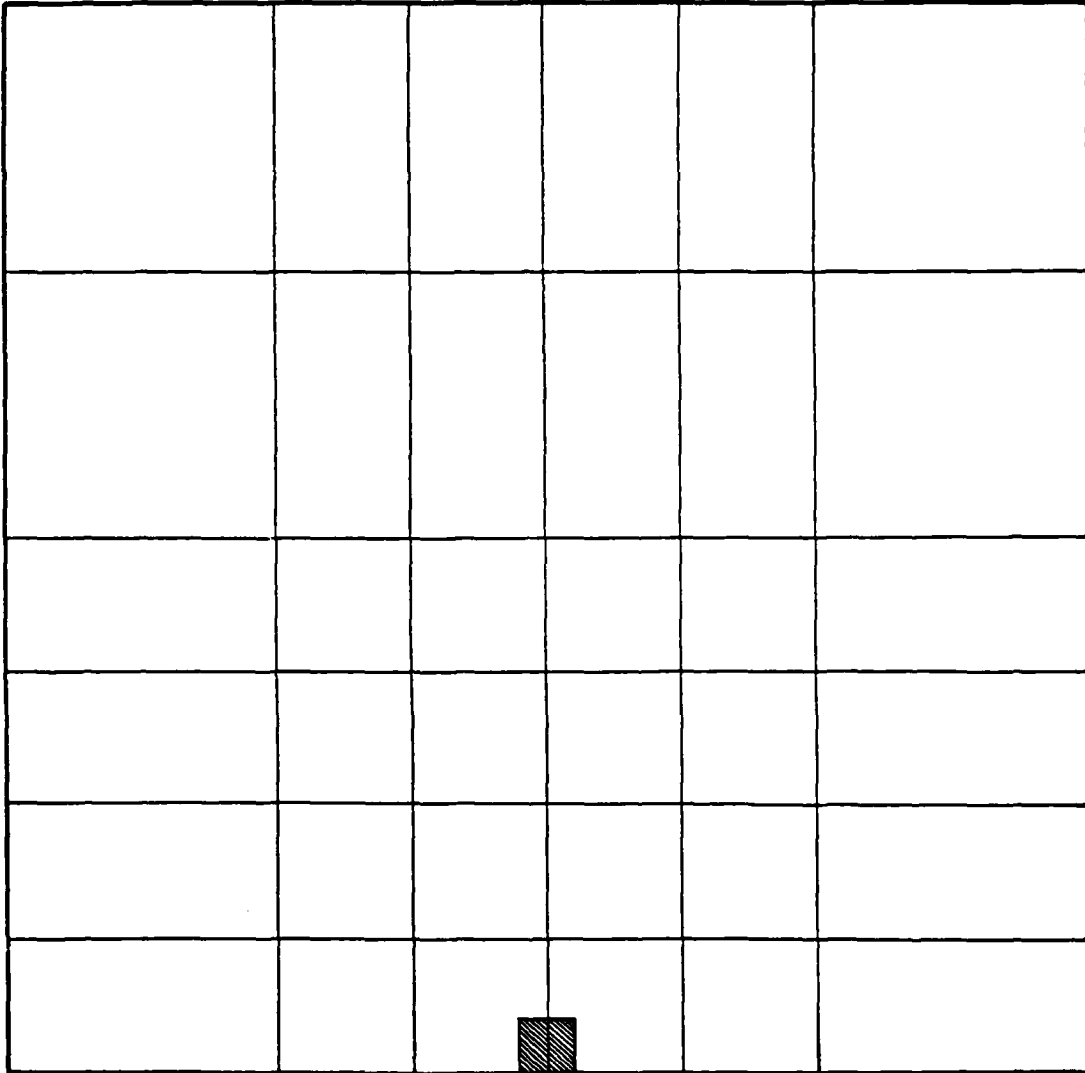


Fig. 5.15 Finite Element Mesh Used by Tabatabaie (Edge Loading)

$$b = a$$

$$\text{for } a > 1.724h$$

The following observations may be made regarding the comparison presented in Ref. 55:

- (i) In the vicinity of $(P/k\ell^2) = 0.12$, finite element deflection decreases as $(P/k\ell^2)$ increases. According to the Westergaard theory, deflection is directly proportional to $(P/k\ell^2)$, as indicated by the straight line in Fig. 5.14(b);
- (ii) Stresses obtained by the finite element program are substantially greater than those predicted by theory. The discussion of the interior condition has indicated that this may result from a relatively large loaded area, but this factor would not justify the 15 to 30% discrepancy observed here;
- (iii) Theoretical results are obtained for a circular load, radius 7.5 in., loaded with a pressure of 282.94 psi, while the finite element solution uses a 15-in. square area under 222.2 psi of pressure. A more rigorous comparison would be obtained if the total load, P , and pressure, p , are matched, i.e. if the areas of the square and circle are made equal;
- (iv) The Westergaard equation used for stress determination is not rigorous, since the term 0.359 implicitly assumes $\mu = 0.15$, and μ also appears explicitly. Furthermore, the source of the term $0.497(1+\mu)$ is unknown; this term cannot be derived from the equation presented by Westergaard [9] and does not appear elsewhere in the literature, with the exception of Yang [125].

The term $1.74h$ should be $1.724h$ according to Westergaard [8]. Finally, it was shown earlier in connection with the interior condition, that ILLI-SLAB stress results should be compared with Westergaard's "ordinary theory". Both ILLI-SLAB and the "ordinary theory" ignore the effect of shear stresses in the vicinity of the load. The comparison presented by Tabatabaie et al. is with the "special theory", which employs equivalent radius, b ;

- (v) The equation proposed by Westergaard [9], of which the equation quoted in Ref. 55 is a specialized version, subject to the comments in (iv), above, applies to a semi-circular load with its diameter tangent to the slab edge. The finite element solution models a circular load tangent to the slab edge. The difference in the results of these two conditions may be expected, based on theory [10] to be very small. It will be shown below that this is surprisingly not so.

To make a direct comparison between the results of the original and revised versions of ILLI-SLAB, the same runs were performed using the revised version and the same finite element mesh (Fig. 5.15). Table 5.9 shows that both versions produce very similar results, suggesting that the source of discrepancy between the theoretical and numerical solution should be sought elsewhere.

TABLE 5.9
ILLI-SLAB REVALIDATION: EDGE LOADING

RUN NO.	k (psi/in)	h (in.)	δ_e (mils)		σ_e (psi)	
			Original ILLI-SLAB	Revised	Original ILLI-SLAB	Revised
1	50	12	110.3	109.7	975	974
2	200	12	49.7	49.2	816	813
3	500	12	29.6	29.3	708	705
4	50	16	78.9	78.5	593	593
5	200	16	34.3	34.1	516	515
6	500	16	20.3	20.2	455	454
7	50	20	63.7	63.3	395	395
8	200	20	26.0	25.8	356	356
9	500	20	15.3	15.1	320	319

Notes:

Finite Element Solutions

Slab: 25 x 25 ft. ($\frac{L}{\lambda} = 3.3$ to 8.6)

$E = 5 \times 10^6$ psi

$\mu = 0.15$

$p = 222.2$ psi

$A = 15 \times 15$ in.; edge

Mesh: Fig. 5.15

5.4.2 Alternative Westergaard Solutions

A number of alternative Westergaard solutions are considered in this section, in order to determine which one, if any, is most suitable for comparison with the ILLI-SLAB finite element solution. The following effects are investigated:

- (a) Matching P and p , rather than P and the dimension of the loaded area;
- (b) Using semi-circular rather than circular load distribution;
- (c) Using "ordinary" rather than "special" theory;
- (d) Using Westergaard's "New" formulae;

In Table 5.10, six different Westergaard solutions are compared. The first solution is the one presented in Table 5.8 and is reproduced here for comparison purposes. It is obtained using Eqn. (5-4) quoted in Ref. 55, using a pressure of 282.94 psi. In all the other solutions in Table 5.10, a pressure of 222.2 psi is maintained, i.e. P and p are matched. The investigation of the interior condition, earlier, illustrated that the latter is a more appropriate representation of the loaded area used in the finite element solution, than is obtained by matching the total load, P and the side of the square with the diameter of the circle. Solutions in Table 5.10 are code-named WESI through WESV. Solution WESI is obtained using Eqn. (5-4) but with pressure 222.2 psi.

A more general version of Westergaard's stress equation is used in WESII [9]. This is as follows:

TABLE 5.10

ALTERNATIVE WESTERGAARD SOLUTIONS

RUN NO.	k (psi/in.)	h (in.)	DEFLECTION, δ_e (mils)				BENDING STRESS, σ_e (psi)			
			TBT	WESI	WESII	WESIII	TBT	WESI	WESII	WESIII
1	50	12	112.7			104.8	99.7	813	778	661
2	200	12	56.4			50.8	47.3	694	659	541
3	500	12	35.7			31.3	28.4	615	580	462
4	50	16	73.2			69.0	66.4	484	468	413
5	200	16	36.6	Same as TBT			33.7	31.8	417	401
6	500	16	23.2			20.8	19.4	372	357	302
7	50	20	52.4			49.8	48.2	318	310	281
8	200	20	26.2			24.4	23.3	275	267	238
9	500	20	16.6			15.2	14.3	246	239	210

Notes:

TBT:	Eqn. (5-4)	Circular	"Special" Theory	p = 282.94 psi
WESI:	Eqn. (5-4)	Circular	"Special" Theory	p = 222.2 psi
WESII:	Westergaard's Original Equations	Semi-circular	"Special" Theory	p = 222.2 psi
WESIII:	Westergaard's Original Equations	Semi-circular	"Ordinary" Theory	p = 222.2 psi
WESIV:	"New" Formulae	Semi-circular	"Ordinary" Theory	p = 222.2 psi
WESV:	"New" Formulae	Circular	"Ordinary" Theory	p = 222.2 psi

$$\sigma_e = 0.529 (1+0.54\mu) \frac{P}{h^2} \left\{ \log_{10} \left(\frac{Eh^3}{4kb_2} \right) - 0.71 \right\}$$

$$b_2 = \sqrt{1.6 a_2^2 + h^2} - 0.675h \text{ for } a_2 < 1.724h$$

$$= a_2 \text{ for } a_2 > 1.724h \quad (5-5)$$

In this equation, which employs the "special" theory, a_2 is assumed to be the radius of a semi-circular load with its diameter tangent to the slab edge.

The same equation is used in WESIII. This solution, however, employs the "ordinary" theory, i.e. the true radius, a_2 , is used instead of the equivalent radius, b_2 , independent of the value of (a_2/h) . Since Westergaard's original [9] equation for edge deflection applies to a concentrated load and is independent of radius and pressure, deflections given by Ref. 55, WESI, WESII, and WESIII are identical.

In solution WESIV, Westergaard's "New" formulae [10] are used for the semi-circular loaded area. The justification for these equations will be presented below. At this stage, it is enough to quote the equations as used here:

$$\delta_e = \frac{P \sqrt{2+1.2\mu}}{\sqrt{Eh^3k}} \left\{ 1 - (0.323 + 0.17\mu) \left(\frac{a_2}{l} \right) \right\}$$

$$\sigma_e = \frac{3(1+\mu)P}{\pi(3+\mu)h^2} \left\{ \ln \frac{Eh^3}{100ka_2^4} + 3.84 - \frac{4}{3}\mu + 0.5(1+2\mu) \left(\frac{a_2}{l} \right) \right\} \quad (5-6)$$

where a_2 is the radius of the semi-circular load.

Finally, in WESV, the "New" formulae [10] for the circular loaded area tangent to the slab edge are used. Again, suffice it at this point to quote the equations as used, without further justification:

$$\delta_e = \frac{P\sqrt{2+1.2\mu}}{\sqrt{Eh^3k}} \{1 - (0.76 + 0.4\mu) \left(\frac{a}{\ell}\right)\}$$

$$\sigma_e = \frac{3(1+\mu)P}{\pi(3+\mu)h^2} \left\{ \ell \ln \frac{Eh^3}{100ka^4} + 1.84 - \frac{4}{3}\mu + \frac{1}{2}(1-\mu) \right. \\ \left. + 1.18 (1+2\mu) \left(\frac{a}{\ell}\right) \right\} \quad (5-7)$$

Several interesting observations may be made in reference to Table 5.10:

- (a) The range of results obtained is extremely wide. Careful use of the Westergaard theory cannot, therefore, be overemphasized;
- (b) As a corollary to (a), the theory may be applied correctly or wrongly, especially when comparisons with the F.E.M. are intended. Furthermore, it will be shown below that there are, indeed, erroneous Westergaard equations which should be avoided;
- (b) Using a pressure of 222.2 psi, i.e. matching P and p with the corresponding values in the finite element solution, leads to stresses that are about 5% lower than those obtained using a pressure of 282.94 psi, for which P and the dimension of the loaded area are matched (compare WESI and Ref. 55). Since finite element results are, in general, even higher than the

latter [see Fig. 5.14(a)], such a comparison may lead to the conclusion that matching P and the dimension of the loaded area is a more appropriate representation of the load. As in the case of the interior condition, this "improvement" in load representation is only apparent, and may conceal some of the discrepancy between theory and the F.E.M. which needs to be investigated and explained;

- (d) Further reduction in stresses calculated (of the order of another 15%) is obtained when Westergaard's original equation for a semi-circular loaded area is used, instead of the version presented in Ref. 55 for a circular load (compare WESII and WESI). Even after allowing for the limitations of Eqn. (5-4), it is very surprising to determine that changing from a semi-circular to a circular area not only leads to a 15% difference in calculated stresses, but also suggests that the circular load is more severe than the semi-circular load. Having the finite element results in mind, it may seem that using the correct original equation in the manner it was meant to be applied, leads to increased discrepancy with the finite element solution;
- (e) The situation becomes more perplexing when Westergaard's "ordinary" theory is used, rather than his "special" theory. This change causes another 5% reduction in stresses (compare WESIII and WESII). The stresses obtained by WESIII are a staggering 35% smaller than the finite element results (see

Table 5.9), and there does not seem to be any way of compromising them at this point. As indicated by the interior condition investigation, increasing the slab size and/or the finite element mesh fineness, leads to increased finite element stresses, i.e. the discrepancy with theory increases. Decreasing the size of the loaded area may, in certain cases, lead to lower finite element stresses, but not to the extent of closing the 35% gap;

- (f) A way out of this deadlock, is provided by the "New" formulae, presented in their general form by Westergaard [10]. These may be applied to either a semi-circular or a circular loaded area. In both WESIV and WESV, the "New" formulae in conjunction with "ordinary" theory are employed, since a comparison with ILLI-SLAB results is eventually intended. The most obvious effect to observe is that the "New" formulae typically lead to stresses 55% higher and deflections 8% lower than the values obtained using the original formulae (compare WESIV with WESIII). What is important to note here is that the original formulae are supposed to be derived from the "New" formulae. This is true only for the edge deflection equation;
- (g) Comparing WESIV and WESV, the semi-circular load is seen to be more severe than the circular load, i.e. leads to higher stresses and deflections, as expected. If both the circular and semi-circular loads are reduced to an equivalent point load acting at the respective center of gravity, this expectation is

shown to be justified, since the center of gravity of the circle is further toward the interior of the slab, than that of the semi-circular. Clearly the interior condition is less severe than the edge condition;

- (h) The above argument also leads to the conclusion that the difference in response from a circular and a semi-circular load should be fairly small, proportional to the difference in the distance between the respective centers of gravity and the slab edge. Comparing WESIV and WESV, stress difference is about 1% and deflection difference about 5%. These differences are much more compatible with expected values, than the stress difference obtained using the original equation (compare WESI and WESII).

The results in Table 5.10 clearly suggest that the "New" formulae lead to correct results, while the original stress equation is erroneous. Table 5.11 shows a comparison between WESV, ILLI-SLAB, and H-51 results. Stresses exhibit almost perfect agreement (Fig. 5.16), even at the low (L/ℓ) values. Deflections are more sensitive to slab size effects, as shown in Fig. 5.17. This graph shows that an (L/ℓ) value of about 5.0 is required for the development of Westergaard stresses and about 8.0 is required for Westergaard deflections. The trends in Fig. 5.17 are similar to those observed for the interior condition. Note, however, that the requirement for the development of maximum edge stress ($L/\ell=5.0$) is higher than for maximum interior stress ($L/\ell=3.5$). Further improvement of the finite element solution should

TABLE 5.11
COMPARISON WITH "NEW" EDGE LOADING FORMULAE

RUN NO.	k (psi/in.)	h (in.)	$(\frac{L}{h})$	DEFLECTION, δ_e		BENDING STRESS, σ_e		
				WESV (mils)	ILLI-SLAB (mils)	ILLI-SLAB (psi)	H-51 (psi)	ILLI-SLAB WESV
1	50	12	4.84	99.7	109.7	980	974	951 0.99
2	200	12	6.85	47.3	49.2	822	813	808 0.99
3	500	12	8.61	28.4	29.3	720	705	711 0.98
4	50	16	3.90	66.4	78.5	607	593	591 0.98
5	200	16	5.52	31.8	34.1	517	515	504 1.00
6	500	16	6.94	19.4	20.2	459	454	452 0.99
7	50	20	3.30	48.2	63.3	417	395	396 0.95
8	200	20	4.67	23.3	25.8	359	356	348 0.99
9	500	20	5.87	14.3	15.1	321	319	317 0.99

Notes:

Revised ILLI-SLAB Solution

Slab: 25 x 25 ft. $(\frac{L}{h}) = 3.30$ to 8.61

$E = 5 \times 10^6$ psi

$\mu = 0.15$

$P = 50,000$ lbs

$p = 222.2$ psi

$A = 15 \times 15$ in.; edge

Mesh: Fig. 5.15

Westergaard Solution (WESV)

"New" Formulae

Circular Load

"Ordinary" Theory

$p = 222.2$ psi

$E = 5 \times 10^6$ psi

$\mu = 0.15$

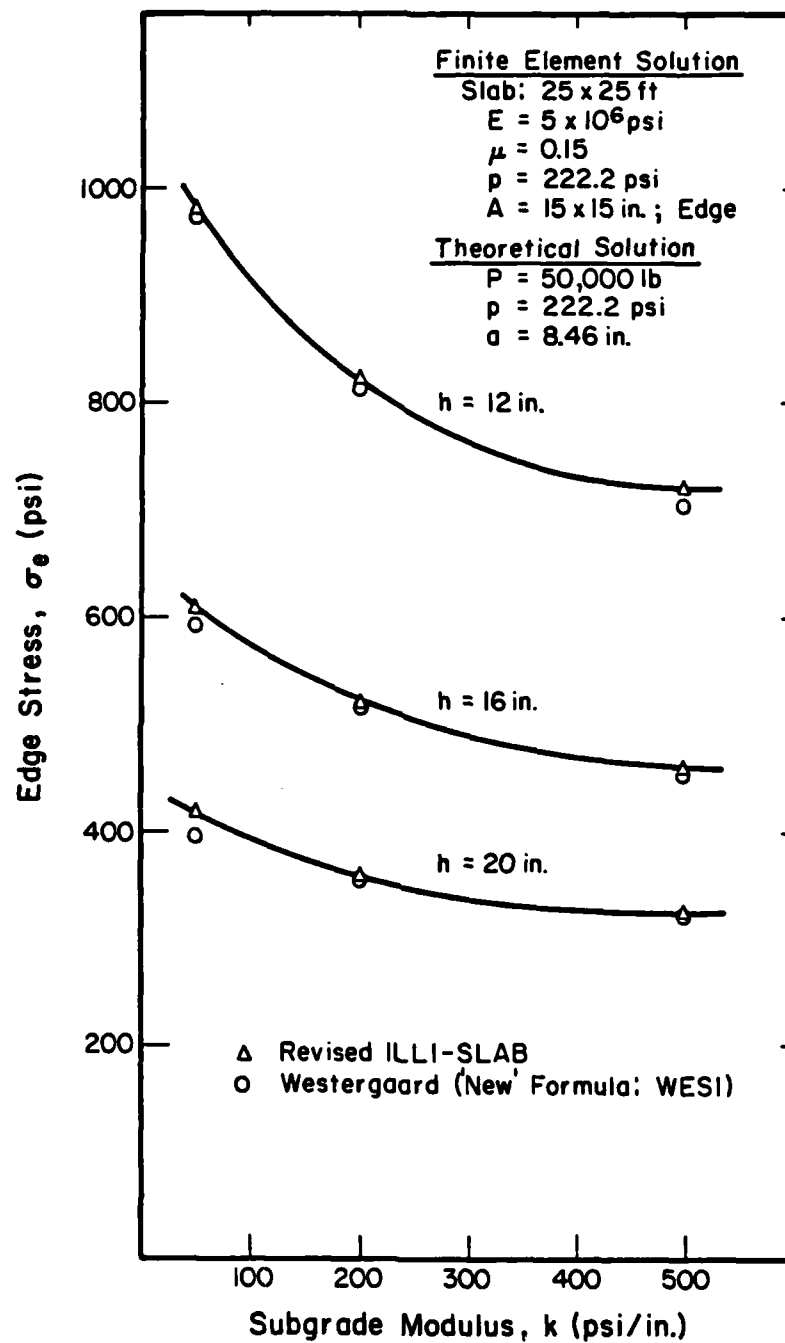


Fig. 5.16 Comparison of ILLI-SLAB with Westergaard's "New" Formula for Edge Stress

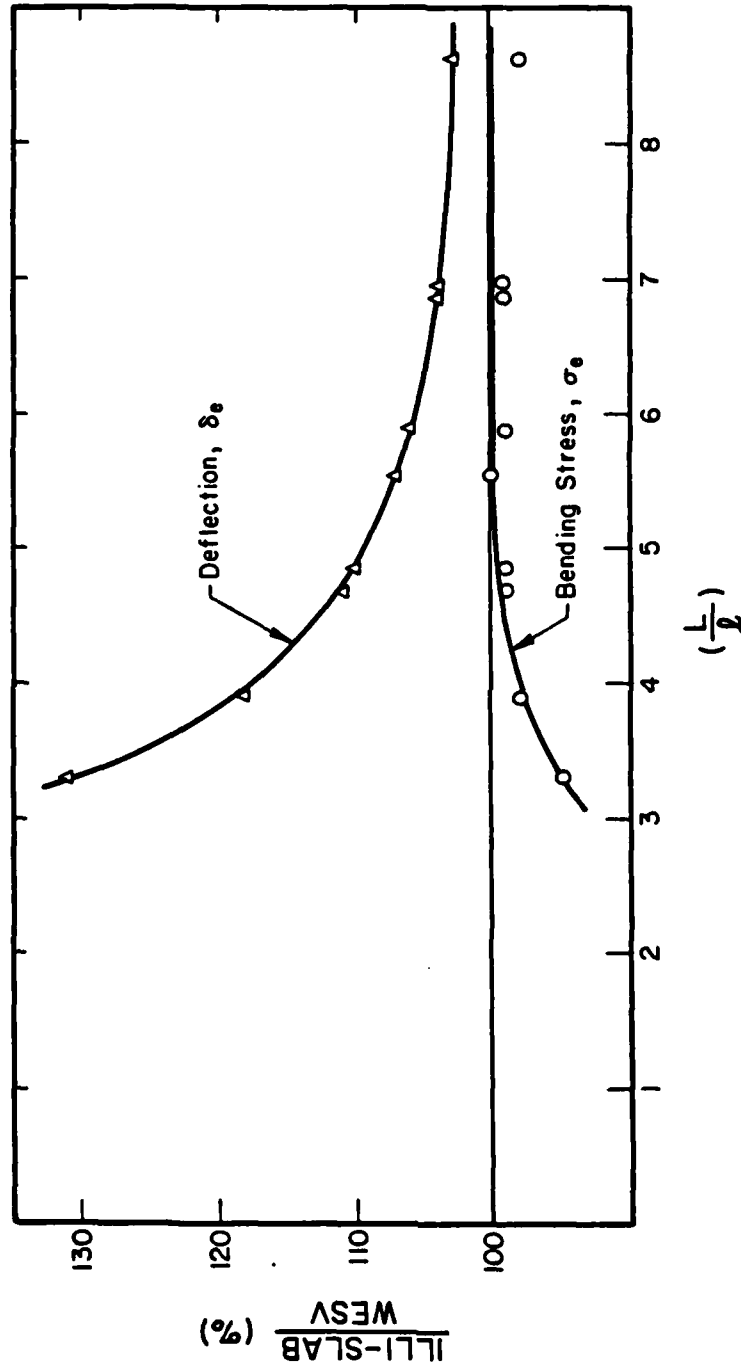


Fig. 5.17 Effect of Slab Size on ILLI-SLAB Edge Loading Results

not be expected from further slab size increases, but rather from using a finer mesh.

5.4.3 The Westergaard "New" Formulae for Edge Loading

It was noted above that the "New" equations presented by Westergaard [10] were used to obtain solutions WESIV and WESV in Table 5.10. The form of the equations as used in this investigation was also quoted above. In his 1948 paper, Westergaard presented generalized solutions for maximum stress and deflection produced by an elliptical and a semi-elliptical loaded area placed at a slab edge. Setting the lengths of both the major and minor semi-axes of the ellipse to a or a_2 leads to the corresponding solutions for a circle radius a , or a semi-circle radius a_2 , given by Equations (5-6) and (5-7), above.

Losberg [13] presented simplified versions of these solutions by introducing "simplifications of the same type as Westergaard [126] himself introduced in his original formula for the case of edge loading" to eliminate the "complicated functional relationship" in which μ appears in these equations. Losberg [13] stated that his simplified equations "are well applicable, for the small μ -values here concerned". These equations are quoted below:

(a) Semi-circular load:

$$\delta_e = \frac{1}{\sqrt{6}} (1+0.4\mu) \frac{P}{k\ell^2} \left[1 - 0.323 (1+0.5\mu) \left(\frac{a_2}{\ell} \right) \right]$$

$$\sigma_e = \frac{-6P}{h^2} (1+0.5\mu) \left[0.489 \log_{10} \left(\frac{a_2}{\ell} \right) - 0.091 - 0.027 \left(\frac{a_2}{\ell} \right) \right] \quad (5-8)$$

(b) Circular load:

$$\delta_e = \frac{1}{\sqrt{6}} (1+0.4\mu) \frac{P}{k\ell^2} [1 - 0.760 (1+0.5\mu) (\frac{a}{\ell})]$$

$$\sigma_e = \frac{-6P}{h^2} (1+0.5\mu) [0.489 \log_{10} (\frac{a}{\ell}) - 0.012 - 0.063(\frac{a}{\ell})] \quad (5-9)$$

Comparisons made during this study show that Losberg's simplified equations lead to results that are typically about 1% greater than those obtained by the general Equations (5-6) and (5-7).

It was pointed out by previous investigators [127; 13] that in the case of interior deflection and stress, as well as edge deflection, when the "New" formulae are specialized for a circular (or a semi-circular) loaded area, they become identical to the corresponding original [8; 9] equations. As results from this study show, however, edge stresses calculated from the "New" formula are about 55% higher than those computed using the original formula. The excellent agreement between finite element and H-51 results and the "New" formula, confirms Losberg's observation that "the original formula for edge loading according to Westergaard [8] is, at least from a theoretical viewpoint, completely erroneous". It is, therefore, recommended that for meaningful conclusions, the F.E.M. as used in ILLI-SLAB should only be compared to the "New" formulae.

The Pickett and Ray charts [86] for the edge loading condition on a dense liquid subgrade are based on a pair of integral equations identical to those presented by Westergaard [10]. The results from these charts, therefore, agree with the "New" formulae as indicated by

H-51 results in Table 5.11. It is interesting to note that although in several design codes reference is made to the original equation, the fact that multiple-wheel loads are considered indicates that design charts in these codes have been obtained using the Pickett and Ray charts, i.e. the "New" formulae.

The question of the source of the discrepancy between Westergaard's original and "New" formulae for edge loading remains unanswered. It is too early to dismiss the original formulae as altogether false and useless. Bergstrom, et al. [127] reported that values calculated using these equations are "in relatively close agreement with test results". They furthermore proceeded to suggest that there are "no reasons to use the new formula for edge loading". On the other hand, Scott [121] suggests that "experimental indications are that the edge stresses experienced in practice are higher than the Westergaard (original) equation indicates". Laboratory model tests by Carlton and Behrmann [128] produced edge stresses 10 to 12% lower than the "New" formula predicts, reinforcing the expectation that in-situ values probably lie between the two Westergaard equations.

The theoretical background for the original edge stress equation is also open to debate. The derivation of this equation is not presented in any of Westergaard's papers. Attempts by Losberg [13] to arrive at the formula in question through integration of the expressions for the concentrated load [126], did not produce agreement with Westergaard's result. If the probability of a gross theoretical blunder by such a meticulous investigator as Westergaard can be cast aside, for the time

being, a possible explanation for this discrepancy is some assumption regarding subgrade support that is implicit in the original formula but is never explicitly stated. It will be shown in Chapter 9 that the equivalent subgrade modulus for edge loading is about 20% higher than the value for interior loading, assuming the soil behaves as a Boussinesq solid. Model tests [128] suggest edge loading k -values may be up to twice as high as for interior loading. The edge loading condition is one where the fundamental limitation of the Winkler medium (i.e. that deflection is assumed to be zero outside the loaded area) becomes much more significant than for the interior condition. It is possible that Westergaard attempted to account for this limitation by increasing, for example, the value of the subgrade modulus in a zone near the edge. This would lead to a decrease in maximum edge stress, as per the original equation. The decreased deflections obtained using the "New" formulae are the results of the distribution of the load over a finite area. Further investigation of the theory leading to the original equation, with reference to field observations, is required before the riddle can be resolved.

5.5 THE CORNER LOADING CONDITION

5.5.1 A Review of Proposed Equations for Corner Loading

The last loading condition considered in this investigation is corner loading. Of the three fundamental cases of loading investigated by Westergaard [8], corner loading is undoubtedly the most obscure and

debatable. The theoretical background for maximum corner deflection and stress equations is particularly weak, and their semi-empirical and approximate nature have led to numerous revisions and modifications in the years following their original publication. This loading condition becomes even more complicated when curling and warping effects of temperature and moisture changes are considered, or when one attempts to account for the fundamental weakness of the Winkler medium, viz. that unloaded regions do not deflect. These effects will not be considered during this study. Rather, the effort will be concentrated on investigating the ideal condition of full contact between the slab and the Winkler medium, as per Westergaard's original theory.

In the early 1920's a short and simple piece of analytical work was heralded as "the most important single step in the investigation of the mechanics of road slabs" [129]. This was the first attempt to solve the problem of the "corner break" by two prominent engineers of the day working independently: A. T. Goldbeck of the Bureau of Public Roads and Clifford Older of the Illinois Highway Department. By assuming that in the corner region the slab acts as a cantilever of uniform strength, i.e. that in this region the subgrade reaction is negligible compared to the applied load, the following equation for the maximum stress (σ_c) was proposed for a concentrated load, P, acting at the corner of a slab, thickness h [130; 131]:

$$\sigma_c = \frac{3P}{h^2}$$

(5-10)

A few years later, Westergaard [8] took up the problem again, trying to account for the effect of a load distributed over some area, whose resultant could be represented by a point load P acting at a small distance a_1 from the corner, along the bisector of the corner angle. Using a "simple approximate process" involving the use of the principle of minimum potential energy [132] he hoped to achieve an "improved approximation" to corner stress. Thus, he first arrived at the following equation for corner deflection:

$$\delta_c = \frac{P}{k\ell^2} [1.1 - 0.88 \left(\frac{a_1}{\ell}\right)] \quad (5-11)$$

He quotes this equation as being "approximately applicable for plausible ranges of a_1 and ℓ " (presumably, (a_1/ℓ) not much greater than 0.1). From this, he obtained bending moments by integration and concluded that the maximum stress "would be represented with satisfactory accuracy" by the following equation:

$$\sigma_c = \frac{3P}{h^2} [1 - \left(\frac{a_1}{\ell}\right)0.6] \quad (5-12)$$

Furthermore, the distance to the point of maximum stress along the corner angle bisector was found to be, "roughly":

$$x_1 = 2\sqrt{a_1 \ell} \quad (5-13)$$

In an attempt to reconcile observed slab behavior with theory, several empirical adjustments to the Westergaard corner equation were proposed in the years that followed. These were summarized and discussed by Kelley [133] and Pickett [134] and are reproduced in Table 5.12.

5.5.2 Equations for the Corner Loading Condition Based on the F.E.M.

In this section, an attempt is described to use the F.E.M. to establish a set of equations that would accurately predict the response of a slab, in full contact with a Winkler foundation, to a single load distributed over a small area at its corner. For this reason, several runs were performed using ILLI-SLAB. The equations proposed by previous investigators (Table 5.12) suggest that, from a theoretical viewpoint, the parameters involved in the determination of slab response can be lumped into three non-dimensional ratios to be investigated, viz.

$$\left(\frac{\delta_c k l^2}{P} \right), \left(\frac{\sigma_c h^2}{P} \right) \quad \text{and } (a/l) \text{ or } (a_1/l) \text{ for a circular,} \\ \text{or } (c/l) \text{ for a square load.}$$

On the other hand, as far as the F.E.M. is concerned, the guidelines derived from the investigation of the interior and edge loading conditions may be used to determine reasonable ranges of slab size, mesh fineness and size of loaded area for such runs.

A typical Portland Cement Concrete (PCC) pavement was selected for analysis. A 20-ft square slab was used, having a modulus, E , of

TABLE 5.12

EQUATIONS PROPOSED FOR THE CORNER LOADING CONDITION

Deflection:

$$\delta_c = \frac{P}{k\ell^2} \left\{ 1.1 - 0.88 \frac{a_1}{\ell} \right\} \quad \text{Westergaard [8]}$$

Stress:

$$\sigma_c = \frac{3P}{h^2} \quad \text{Goldbeck [130]; Older [131]}$$

$$\sigma_c = \frac{3P}{h^2} \left[1 - \left(\frac{a_1}{\ell} \right)^{0.6} \right] \quad \text{Westergaard [8]}$$

$$\sigma_c = \frac{3P}{h^2} \left[1 - \left(\frac{a}{\ell} \right)^{0.6} \right] \quad \text{Bradbury [135]}$$

$$\sigma_c = \frac{3P}{h^2} \left[1 - \left(\frac{a_1}{\ell} \right)^{1.2} \right] \quad \text{Kelley [133], Teller and Sutherland [29]}$$

$$\sigma_c = \frac{3.2P}{h^2} \left[1 - \left(\frac{a_1}{\ell} \right) \right] \quad \text{Spangler [136]}$$

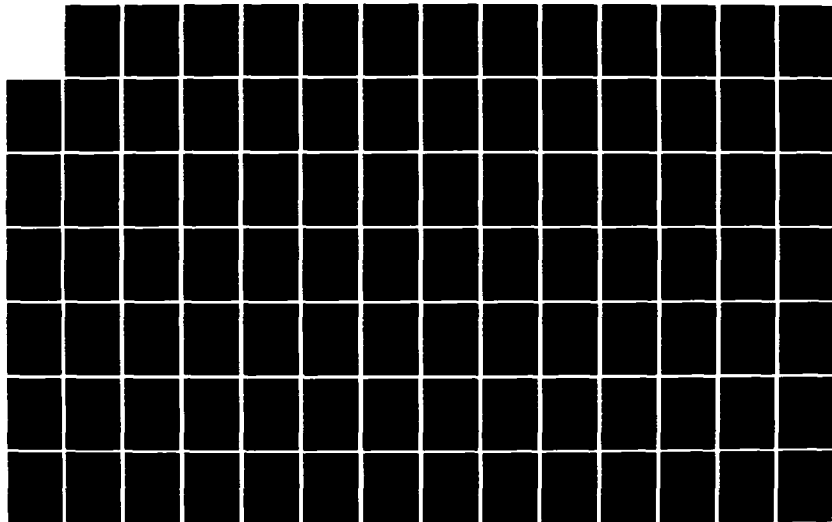
$$\sigma_c = \frac{4.2P}{h^2} \left[1 - \frac{\sqrt{(a/\ell)}}{0.925 + 0.22(\frac{a}{\ell})} \right] \quad \text{Pickett [134]}$$

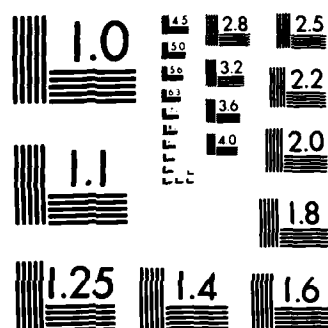
Distance to point of max. stress along corner angle bisector:

$$X_1 = 2\sqrt{(a_1\ell)} \quad \text{Westergaard [8]}$$

where a : radius of circular load tangent to both edges at corner;
 a_1 : distance to point of action of resultant along corner
 angle bisector,
 $= \frac{\sqrt{2}}{2} a$

AD-A150 965 ANALYSIS OF SLABS-ON-GRADE FOR A VARIETY OF LOADING AND 377
SUPPORT CONDITION. (U) ILLINOIS UNIV AT URBANA DEPT OF
CIVIL ENGINEERING A M IOANNIDES ET AL. DEC 84
UNCLASSIFIED AFOSR-TR-85-0083 AFOSR-82-0143 F/G 13/2 NL





MICROCOPY RESOLUTION TEST CHART
NATIONAL BUREAU OF STANDARDS-1963-A

3×10^6 psi and a Poisson's ratio of 0.15. Slab thickness, h , ranged between 6 and 12 inches, while values of subgrade modulus, k , between 100 and 400 psi/in. were assumed. The slab was loaded by a single square load located at one of its corners. The total applied load of 10 kips was distributed over square areas whose size, c , varied from 2.5 to 7.5 inches. The corresponding pressures were 1600 and 177.8 psi, respectively.

Mesh I was used for these seven runs (Fig. 5.18). Based on the findings of the investigation for the interior and edge conditions presented earlier, the mesh was made finer using square elements in a region around the load, at least twice as large of the loaded area itself. Using the side length, $2a$, of square elements in this region, a local fineness ratio ($2a/h$) may be defined. In these runs, ($2a/h$) ranged between 0.4 and 0.8.

The results obtained from these analyses are presented in Table 5.13 and are plotted in a non-dimensional fashion in Figures 5.19 and 5.20. Other available closed-form solutions are also shown in these figures for comparison. The latter were obtained using a circular load of the same area as the square one in ILLI-SLAB, but are plotted with the corresponding (c/ℓ) values along the ordinate. Though not mathematically rigorous, this facilitates direct comparison of the results. Selecting a circle and a square whose respective centroids are at the same distance from the corner, and adjusting the applied pressure on each to retain the same total load, might provide a more rigorous comparison. This is not deemed important for the purpose of the present

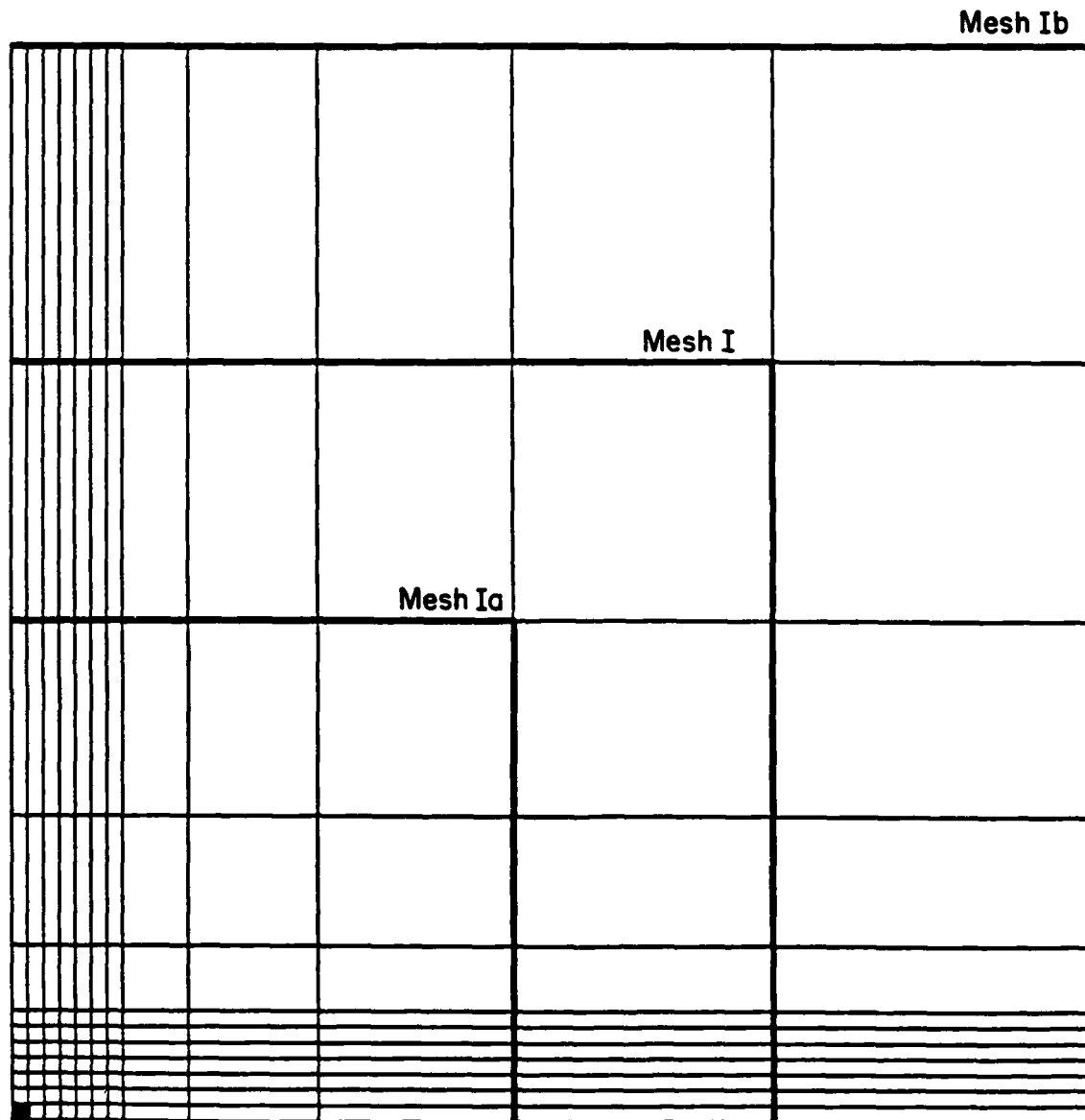


Fig. 5.18 Finite Element Meshes I, Ia and Ib (Corner Loading)

TABLE 5.13
DEVELOPMENT OF CORNER LOADING FORMULAE

RUN NO.	h (in.)	k (psi/in.)	c (in.)	p (psi.)	(L/l)	(c/l)	DEFLECTION, δ_c		BENDING STRESS, σ_c		Location X_1 (in.)
							mils	$\frac{\delta_c k l^2}{p}$	psi	$\frac{\sigma_c h^2}{p}$	
C001	9	200	2.5	1600	7.72	0.0805	59.5	1.149	307.5	2.491	18.03
C002	9	200	5.0	400	7.72	0.1609	56.6	1.093	270.9	2.194	25.50
C003	9	200	7.5	177.8	7.72	0.2414	53.8	1.039	242.7	1.966	30.41
C004	9	100	5.0	400	6.49	0.1353	81.4	1.111	282.1	2.285	25.50
C005	9	400	5.0	400	9.19	0.1914	39.3	1.073	259.9	2.105	20.62
C006	6	200	5.0	400	10.47	0.2181	100.4	1.055	563.6	2.029	18.03
C007	12	200	5.0	400	6.22	0.1297	37.5	1.115	159.9	2.303	25.50

Notes: Finite Element Solution: Revised ILLI-SLAB

Slab Size, L = 240 in. (square)

E = 3×10^6 psi

$\mu = 0.15$

Local $\frac{2a}{h} = 0.6 - 0.8$

P = 10,000 lbs

Mesh Used: Mesh I (Fig. 5.18)

σ_c : Max. bending stress, i.e. minor (tensile) principal stress

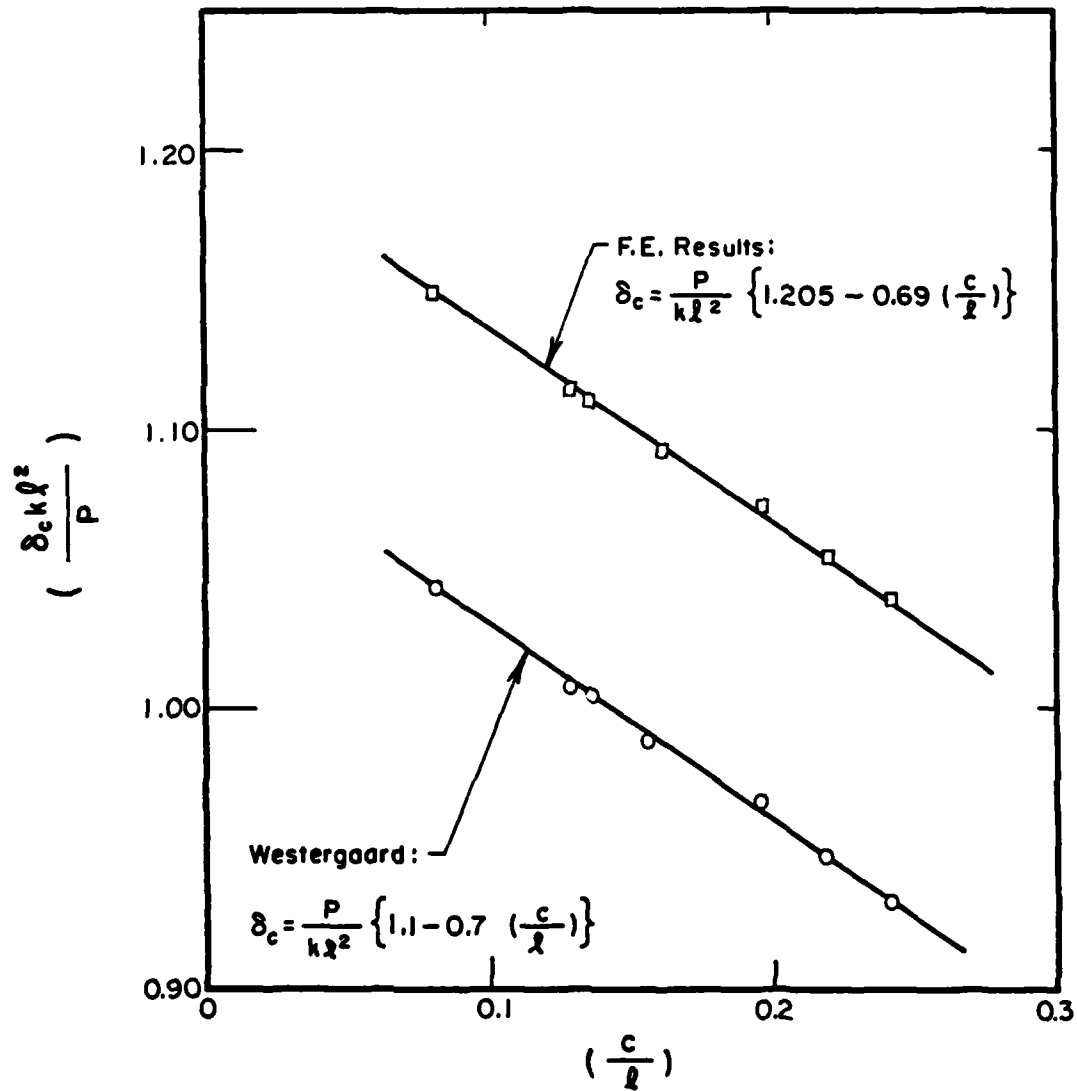


Fig. 5.19 Comparison of ILLI-SLAB and Westergaard Corner Deflections

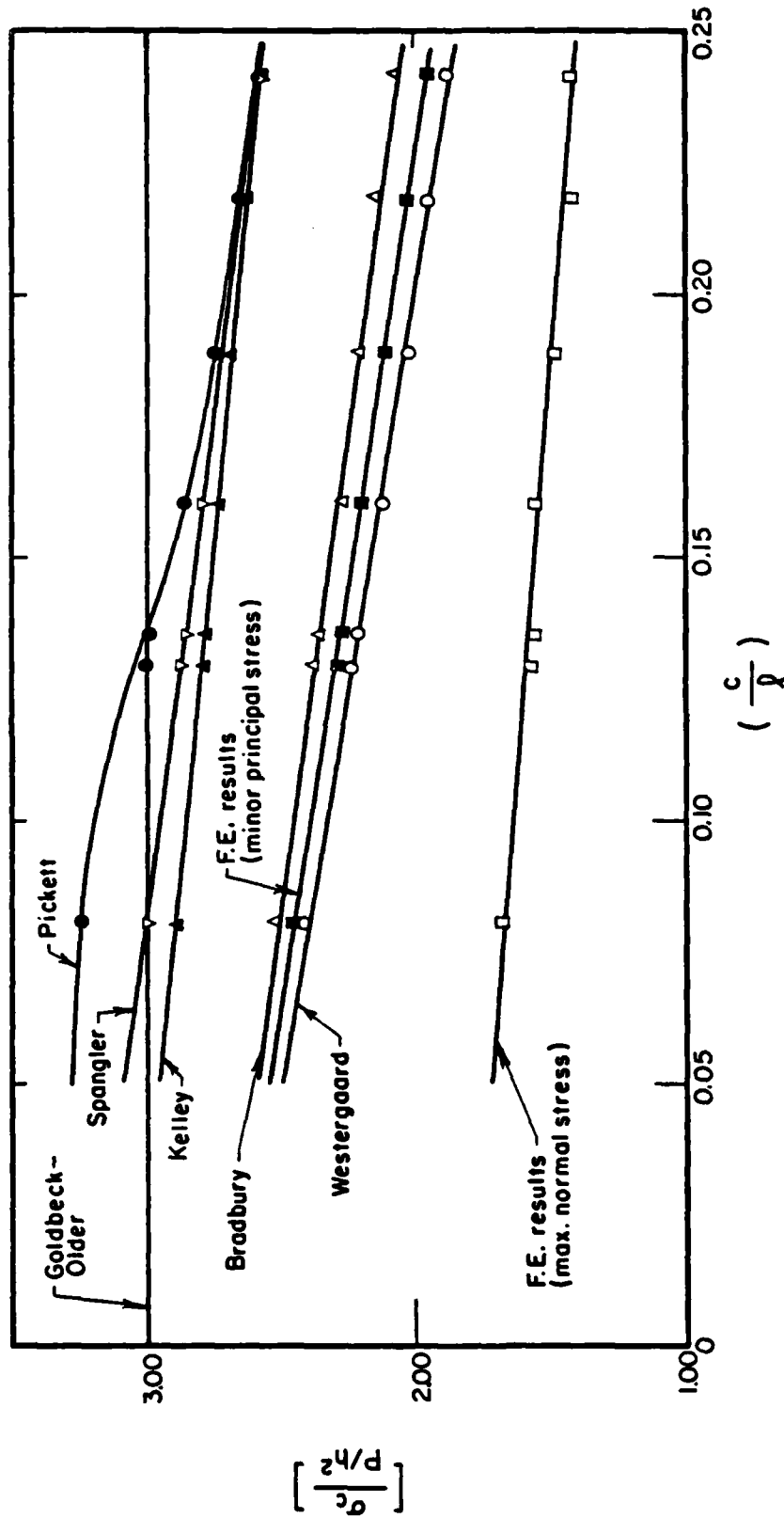


Fig. 5.20 Bending Stresses Under Corner Loading

discussion. ILLI-SLAB stresses are values of the minor (tensile) principal stress occurring at the top fiber of the slab.

Curves were fitted to ILLI-SLAB data with a special effort to keep the general form of the equations the same as that of the Westergaard formulae. Thus, a straight line may be used to describe the deflections obtained using the F.E.M. (Fig. 5.19). This line has the following equation:

$$\delta_c = \frac{P}{k\ell^2} \{1.205 - 0.69(\frac{c}{\ell})\} \quad (5-14)$$

where c is the side length of square loaded area. Expressed in terms of the Westergaard ratio (a_1/ℓ), this equation can be approximated by:

$$\delta_c = \frac{P}{k\ell^2} \{1.2 - 0.88(\frac{a_1}{\ell})\} \quad (5-15)$$

where:

$$a_1 = \sqrt{2} a; \text{ and}$$

a : radius of circle of same area, as square in the finite element solution.

The similarity to Westergaard's equation indicates that Westergaard's approximation was fairly good. The finite element results obtained are typically about 10% higher than those predicted by Westergaard. Part of this discrepancy is due to the lack of a theoretical solution for a square loaded area, as well as limitations of the finite element solution with respect to mesh fineness and slab size.

The investigation of the interior condition indicated that the theoretical limitation may account for an error of about 1%; the finite element analysis limitations will be discussed in more detail below.

In the case of ILLI-SLAB corner stresses, a curve of the following form was sought in order to retain the Westergaard form:

$$\sigma_c = X \frac{P}{h^2} \left\{ 1.0 - \left(\frac{c}{\ell} \right)^Y \right\}$$

$$\text{or } \sigma_c = X \frac{P}{h^2} \left\{ 1.0 - \left(\frac{a_1}{\ell} \right)^Y \right\} \quad (5-16)$$

Curve fitting suggested the following equation:

$$\sigma_c = 3.0 \frac{P}{h^2} \left\{ 1.0 - \left(\frac{c}{\ell} \right)^{0.72} \right\} \quad (5-17)$$

The average error of this fit is 0.86%. This is calculated as follows:

$$\text{Average Error (\%)} = \frac{1}{N} \sum_{i=1}^N \frac{|\text{ILLI-SLAB Result} - \text{Proposed Equation}|}{\text{Proposed Equation}} \times 100\% \quad (5-18)$$

Expressed in terms of Westergaard's variables, the best fit equation is:

$$\sigma_c = 3.0 \frac{P}{h^2} \left\{ 1.0 - \left(\frac{a_1}{\ell} \right)^{0.64} \right\} \quad (5-19)$$

with an average error of 0.31%. Westergaard's equation, which uses (X,Y) of (3.0, 0.6) gives 3.46% average error.

At this point, a number of comments will be made with regard to Fig. 5.20 of corner stress results. The closed-form solutions should be compared to the value of the minor (tesile) principal stress from the finite element analysis. This is because, in contrast to the edge or interior stress, maximum corner stress occurs on a plane that is not free of shear. The maximum normal stress obtained from finite element analysis [137] significantly underestimates the critical stress.

The Goldbeck-Older equation is obviously a rough approximation of the theoretical solution, much more so at high values of (c/ℓ) . This is to be expected, in view of the Goldbeck-Older assumption of a concentrated load acting on a cantilever. Assuming that finite element results give a fairly accurate picture of the theoretical solution, the Westergaard equation represents a considerable improvement over the Goldbeck-Older one. The F.E.M. gives results which fall between those predicted by Westergaard [8] and those predicted by Bradbury [135]. What is very interesting to observe, however, is that the empirical modifications to the Westergaard formula proposed in the last 60 years -with the exception of Bradbury's- have tended to increase the discrepancy between empirically predicted and theoretical (ILLI-SLAB) stresses. In fact, these modified expressions are much closer to the Goldbeck-Older equation to than the theoretical solution. The explanation for this observation probably lies in the very fact that these modifications were empirical, based on each investigator's

experience. Scott [121] points out that "experimental indications are that the corner stresses experienced in practice are higher than the Westergaard equation indicates". Note, however, that in the model tests mentioned above, maximum corner stresses measured "were only 65 to 75% as great as those determined from the Westergaard equation" [128]. The very significant limitations of the Winkler subgrade idealization for corner loading, are reflected in Fig. 5.20. As a result, discrepancies between measured responses and theory may be expected.

5.5.3 Factors Affecting the Finite Element Solution for Corner Loading

The investigation of the interior and edge loading conditions has identified three major factors which affect the convergence of the finite element solution obtained using a slab of finite size, to the corresponding theoretical values:

- (a) Slab Size;
- (b) Mesh Fineness; and
- (c) Size of loaded area.

These three effects on the accuracy of the solution for corner loading will be considered in this section, in terms of three non-dimensional parameters; (L/ℓ) , $(2a/h)$ and (c/ℓ) . In order to bring forth the influence of these parameters more clearly, several runs were performed in addition to those in Table 5.13. In some a total load of 27 kips was used, instead of the 10-kip load used in the remainder. The additional finite element meshes used are shown in Figures B.1 through B.9 in Appendix B.

(a) Slab Size: Westergaard's infinite slab assumption is, of course, never valid in practice. Theoretical and empirical criteria have been developed to indicate whether infinite slab response may be expected for slabs of finite size under interior or edge loading (Table 5.4). No such criteria have been developed for the corner condition. Furthermore, the interior and edge investigations discussed earlier, showed that comparison of theoretical and finite element solutions are meaningful only if infinite slab response is achieved.

The pertinent results from this study are tabulated in Table 5.14 and are presented graphically in Fig. 5.21, where both deflections and stresses are shown as percentages of the values given by the best fit equations developed above. The validity of any conclusions drawn from such a comparison is not considered to be greatly affected by the numerical accuracy of the proposed formulae. The patterns observed in Fig. 5.21 are the same as those observed for the other loading conditions. Deflections converge from above, while stresses converge from below to their large slab size values. Once again, stresses converge faster, requiring a minimum (L/ℓ) value of about 4.0, and are less sensitive to changes in (L/ℓ) than deflections. The latter are extremely sensitive even to small changes for (L/ℓ) smaller than about 3.0. Infinite slab deflection requires an (L/ℓ) ratio of at least 5.0.

(b) Mesh Fineness: The ratio $(2a/h)$ was shown earlier to be a good indication of the effect of mesh fineness on the finite element solution. As used here, $2a$ is the side length of square elements in the vicinity of the loaded area. In view of computer storage limitations, a

TABLE 5.14
EFFECT OF SLAB SIZE: CORNER LOADING

RUN NO.	Mesh	c (in)	p (psi)	$(\frac{2a}{h})$	$(\frac{L}{q})$	DEFLECTION, δ_c		BENDING STRESS, σ_c	
						mils	%DCI	psi	%SCI
C010	Ia				5.08	56.7	100	270.9	100
C002	I	5.0	400.0	0.56	7.72	56.6	100	270.9	100
C011	Ib				10.94	56.6	100	270.9	100
DCI or SCI					-	56.7	-	270.8	-
CT2	V				1.609	327.0	247	448.9	77
CT4	VII				2.253	200.7	152	528.5	91
CT1	IV	10.0	270.0	1.11	3.219	148.9	112	580.8	100
CT3	VI				3.862	141.3	107	588.7	101
DCI or SCI					-	132.4	-	581.1	-

Notes:

Equations based on F.E.M.

$$DCI = \frac{P}{k\ell} \{1.205 - 0.69(\frac{c}{q})\}$$

$$SCI = 3.0 \frac{P}{h^2} \{1.0 - (\frac{c}{q})^{0.72}\}$$

$$p = 10,000 \text{ or } 27,000 \text{ lb.}$$

$$h = 9 \text{ in.}$$

$$k = 200 \text{ psi/in.}$$

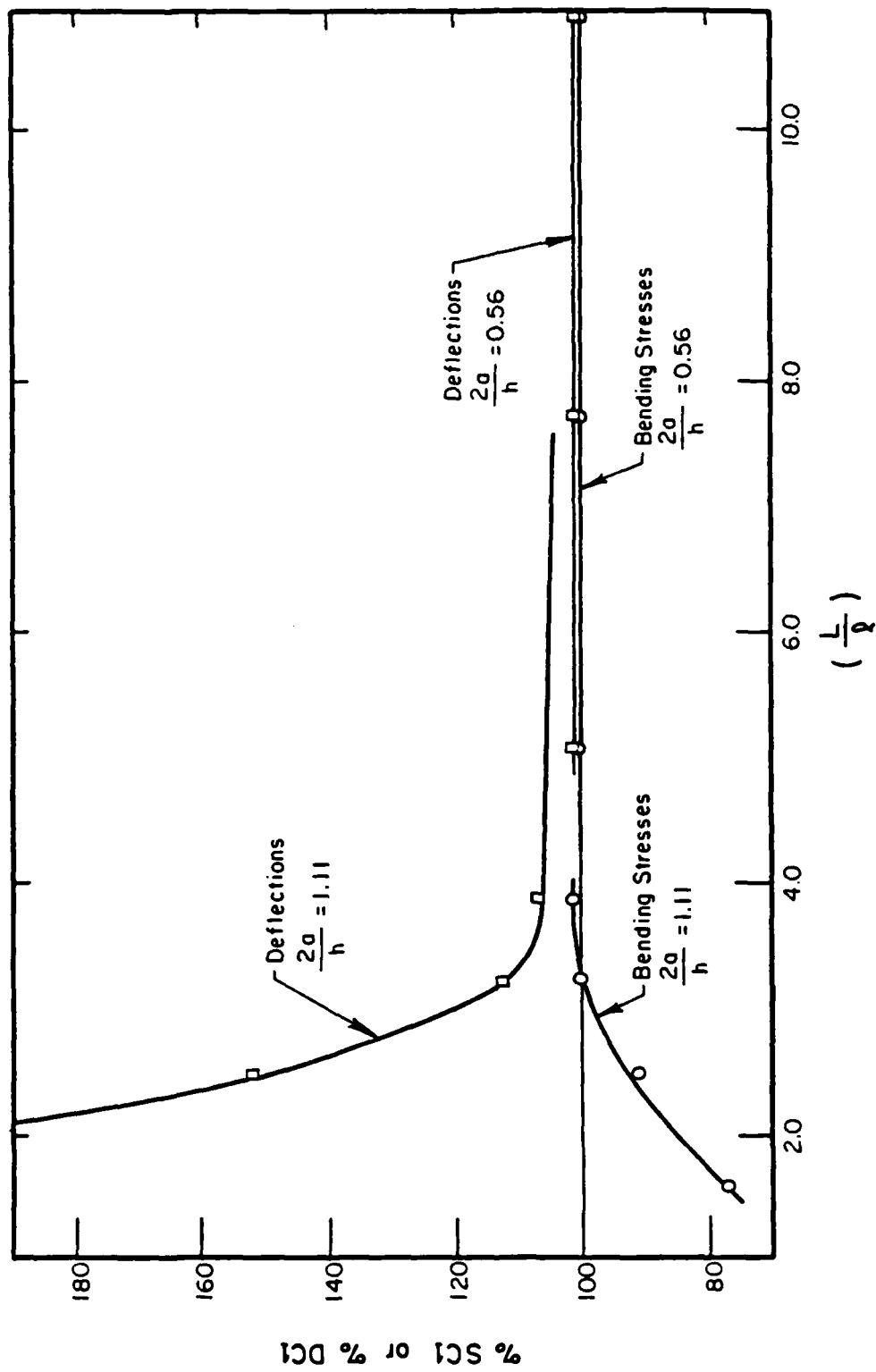


Fig. 5.21 Effect of Slab Size (Corner Loading)

non-uniform mesh had to be employed in certain cases, but care was taken to abide by the recommendations arrived at in connection with the interior condition, with regard to the extent of a fine zone of square elements surrounding the loaded area.

Results from the mesh fineness runs conducted are shown in Table 5.15. In Fig. 5.22, these results are plotted in terms of the corresponding values obtained from the proposed Equations (5-14) and (5-17). The pattern observed earlier for the other loading conditions is repeated here in the case of deflections: as the mesh becomes finer, deflections converge monotonically from below. The stress convergence pattern is slightly more complicated. In general, it would seem that stresses converge from below (as for the interior condition), and that small deviations from this conclusion can be attributed to numerical problems. A fineness ratio ($2a/h$) of about 0.8 is required for accurate stress determination. Deflections are less sensitive to this effect, and can be accurately obtained even if ($2a/h$) is as large as 3.0 or 4.0. These fineness requirements are very similar to those determined for the interior condition.

(c) Size of Loaded Area: The sensitivity of interior finite element stresses to the size of the loaded area, expressed in terms of the non-dimensional ratio (c/ρ) of the side length of the square load to the radius of relative stiffness, make this an important factor to consider. An indication of this effect is given in Table 5.16, and in Fig. 5.23, in which the same results are given as a fraction of the values obtained by the proposed best fit equations. Deflections are not very sensitive

TABLE 5.15

EFFECT OF MESH FINENESS

Run No.	Mesh	c (in.)	p (psi)	(L/2)	$(\frac{2a}{h})$	DEFLECTION, δ_c		BENDING STRESS, σ_c	
						mils	% DC1	psi	% SC1
C015	XIII				3.33	56.4	99	233.7	86
C009	III				1.67	56.5	100	270.6	100
C008	II	5.0	400.0	7.72	1.11	56.5	100	272.6	101
C002	I				0.56	56.6	100	270.9	100
DC1 or SC1					—	56.7	--	270.8	--
CT7	X				5.56	146.9	111	466.5	80
CT6	IX				3.70	148.1	112	503.5	87
CT5	VIII	10.0	270.0	3.22	2.22	148.7	112	585.7	101
CT8	XI				1.67	148.9	112	578.9	100
CT1	IV				1.11	148.9	112	580.1	100
DC1 or SC1					—	132.4	--	581.1	--

Notes:Equations Based on F.E.M.

$$DC1 = \frac{P}{kl^2} \{ 1.205 - 0.69 \left(\frac{c}{l} \right) \}$$

$$SC1 = 3.0 \frac{P}{h^2} \{ 1.0 - \left(\frac{c}{l} \right)^{0.72} \}$$

$$P = 10,000 \text{ or } 27,000 \text{ lbs}$$

$$h = 9 \text{ in.}$$

$$k = 200 \text{ psi/in.}$$

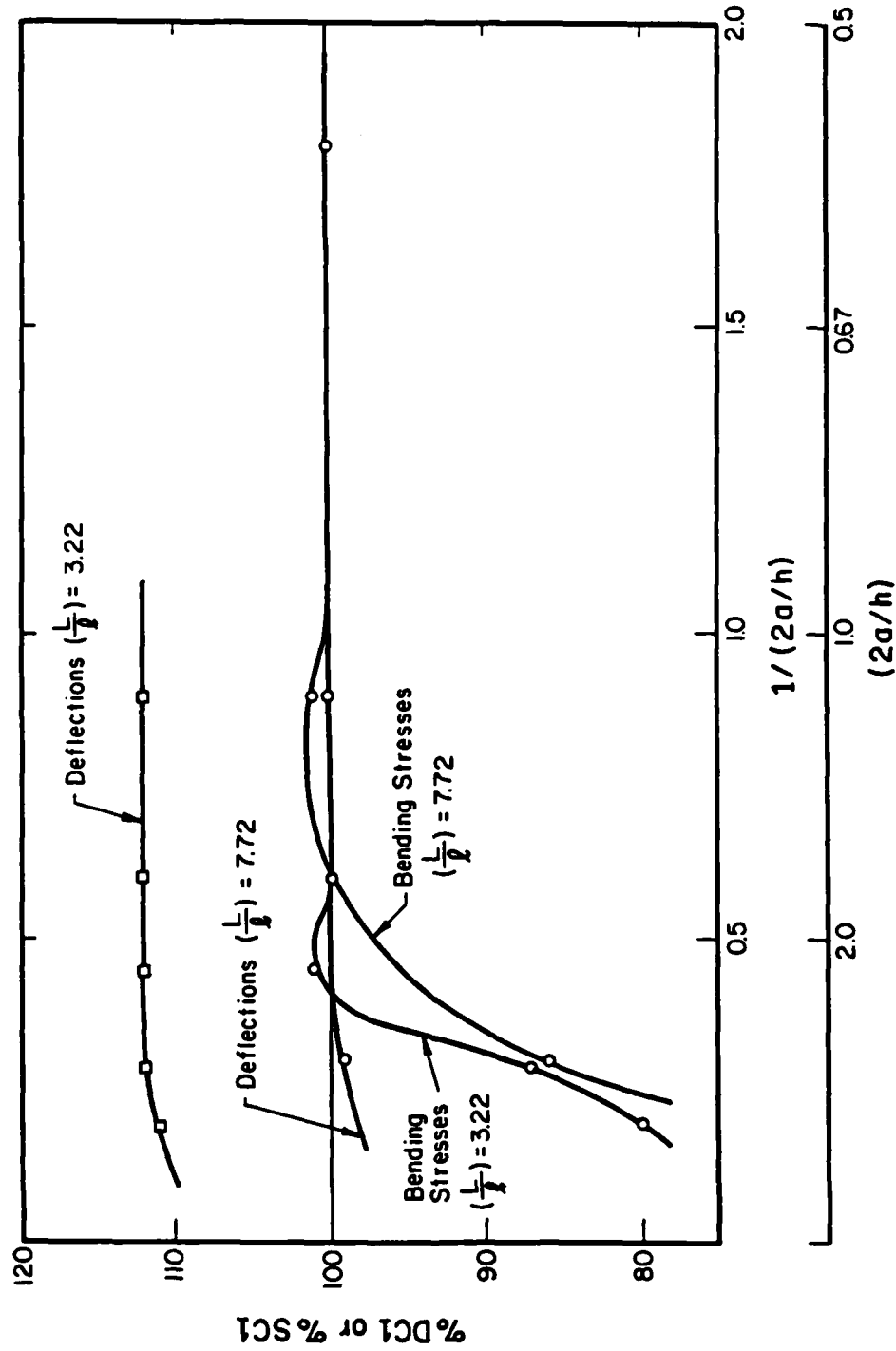


Fig. 5.22 Effect of Mesh Fineness (Corner Loading)

TABLE 5.16
EFFECT OF SIZE OF LOADED AREA

Run No.	(c/l)	DEFLECTION, δ_c			BENDING STRESS, σ_c		
		DC1	ILLI-SLAB	% DC1	SC1	ILLI-SLAB	% SC1
		(mils)			(psi)		
C001	0.0805	59.5	59.5	100	306.5	307.5	100
C002	0.1609	56.7	56.6	100	270.8	270.9	100
C003 (*)	0.2414	53.8	53.8	100	241.3	242.7	101
C016	0.3219	50.9	51.1	100	215.2	219.2	102
C017	0.4828	44.2	41.4	94	169.2	159.5	94
OC001	0.1288	33.3	33.2	100	155.3	153.7	99
OC002 (**)	0.2575	122.6	122.6	100	515.8	510.5	99

Notes:

Equations Based on F.E.M.

$$DC1 = \frac{P}{kl^2} \left\{ 1.205 - 0.690 \left(\frac{c}{l} \right) \right\}$$

$$SC1 = 3.00 \frac{P}{h^2} \left\{ 1.0 - \left(\frac{c}{l} \right)^{0.72} \right\}$$

	(*)	(**)
p	44.4 - 1600 psi	270 psi
P	10,000 lb	6750 or 27,000 lb
h	9 in.	10 in.
k	200 psi/in.	150 psi/in.
l	31.07 in.	38.83 in.
μ	0.15	0.15
E	3×10^6	4×10^6
Slab	20 ft x 20 ft	25 ft x 25 ft
Mesh	I	XII
$\left(\frac{l}{l} \right)$	7.72	7.73
$\left(\frac{2a}{h} \right)$	0.56	2.00

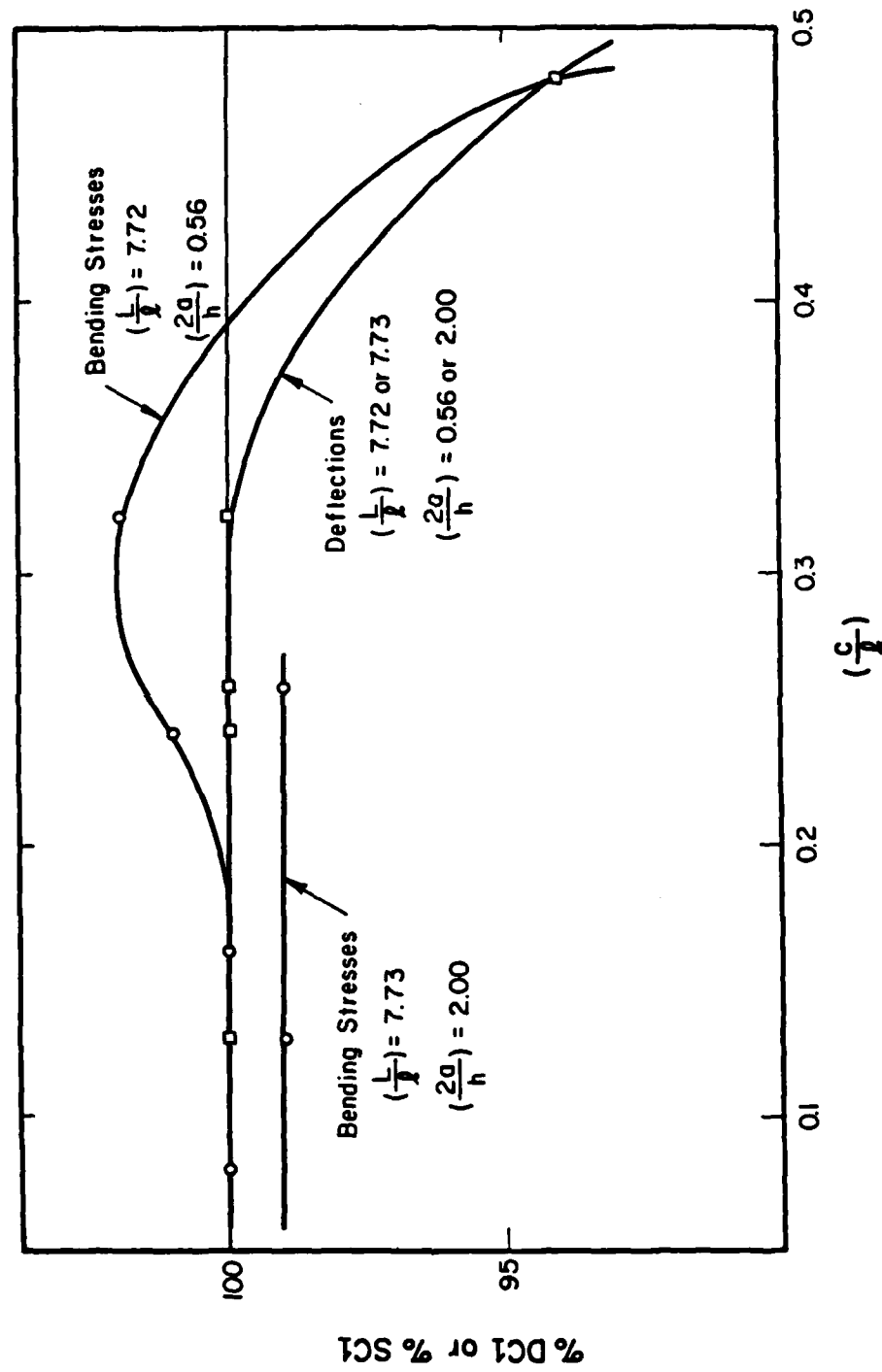


Fig. 5.23 Effect of Size of Loaded Area (Corner Loading)

to changes in (c/ℓ) , but stresses diverge from the predicted values as (c/ℓ) exceeds about 0.2. The trend exhibited by the stresses here is again the reverse of the one observed earlier for interior stresses. The effect of (c/ℓ) on corner stresses is not as great as on interior stresses. Comments made with respect to this effect in paragraphs 5.3.3 and 5.3.7 are also generally applicable to corner loading.

5.5.4 Location of Maximum Stress

The last aspect of slab response investigated in this study for corner loading is the location of the maximum stress, expressed as a distance from the slab corner. It was noted above that Westergaard called this distance X_1 and proposed the semi-empirical and approximate Eqn. (5-13) for its calculation.

The results from a selected number of runs are shown in Table 5.17, where X_1 as obtained from Eqn. (5-13) is compared with the location of the minor (tensile) principal stress given by ILLI-SLAB. This shows that ILLI-SLAB usually gives a somewhat greater value than Westergaard. On the other hand, model tests suggest values about 85% of Westergaard's [128]. An attempt was made to fit through the values of X_1 obtained by extrapolation from ILLI-SLAB, a curve of the form:

$$X_1 = F(c)^G (\ell)^H$$

The result was the following equation:

TABLE 5.17

LOCATION OF MAXIMUM CORNER STRESS

Run No.	l (in.)	c (in.)	Eqvt a (in.)	Location of σ_c, X_1 (in.)		
				Eqn. (5-13)	ILLI-SLAB At node By Extrapol.	PROPOSED EQUATION
C001	31.07	2.5	1.41	15.74	18.03	18.50
C002	31.07	5.0	2.82	22.26	25.50	22.93
C003	31.07	7.5	4.23	27.27	30.41	26.00
C004	36.95	5.0	2.82	24.28	25.50	25.45
C005	26.13	5.0	2.82	20.42	20.62	20.67
C006	22.92	5.0	2.82	19.12	18.03	19.11
C007	38.56	5.0	2.82	24.80	25.50	26.10
C011	31.07	5.0	2.82	22.26	25.50	22.93
CT3	31.07	10.0	6.56	33.96	28.28	28.42

Notes:

$$\text{Eqvt } a = \frac{c}{\sqrt{\pi}}$$

$$\text{Eqn. (5-13): } X_1 = 2 \sqrt{a_1} \bar{x}$$

$$a_1 = \sqrt{2} \ a$$

Proposed Equation:

$$X_1 = 1.80 \ c^{0.32} \ l^{0.59}$$

$$X_1 = 1.80 c^{0.32} \ell^{0.59} \quad (5-20)$$

The average error [Eqn. (5-18)] of this fit was 7.37%. Expressed in terms of Westergaard's variables, the best fit is:

$$X_1 = 1.90 (a_1)^{0.31} (\ell)^{0.60} \quad (5-21)$$

with an average error of 7.36%. Using (F,G,H)-values of (2.10,0.50,0.50) yielded an average error of 9.69%, while Westergaard's [8] equation with (2.00, 0.50, 0.50) produces an average error of 11.28%. The best-fit equations indicate that the influence of the radius of relative stiffness, ℓ , is much greater than that of the size of the loaded area. Westergaard's equation suggests that these two parameters contribute equally in the determination of X_1 .

5.6 RECOMMENDATIONS FOR ILLI-SLAB USERS

The following recommendations for future users of ILLI-SLAB can be formulated as a result of investigations presented in this Chapter:

1. The load(s) must be placed over the finite element mesh with at least one node at the anticipated location of maximum response. For example, in the case of interior loading, a central node must be provided. Otherwise, the results must be carefully interpreted. Any peaks in response missed by the finite element analysis because of node spacing, must be

reconstructed;

2. The finest mesh practicable must be used. Accuracy of 99% can be expected if the element size, $2a$, is about 0.8 times the thickness of the slab. There is no gain in making the mesh any finer than this, although correct answers will be obtained with finer meshes too. Computer resources are more efficiently utilized if element aspect ratios are improved, as per Recommendation 4, below, instead. A fine zone equal to twice the size of the loaded area(s) is recommended, with progressive decrease in fineness outside this area;
3. The convergence characteristics of the work equivalent uniform subgrade 'WINKLER' model (option IST=6 in modified ILLI-SLAB) are slightly better than those of the 'SPRINGS' option (IST=7 in modified ILLI-SLAB). The latter option should only be used for research purposes;
4. Element aspect ratio should be kept close to unity, particularly in a region around the loaded area(s), extending to three times the radius of the loaded area. Within this region, this recommendation is a requirement. If at all possible, no element aspect ratio should be greater than 4 or 5, anywhere in the mesh.

These recommendations apply to all three fundamental loading conditions, viz. interior, edge and corner loading. Some of the meshes used in this study were designed before these guidelines were established, and illustrate that a compromise is often necessary.

CHAPTER 6

DEVELOPMENT OF A STRESS DEPENDENT DENSE LIQUID MODEL

6.1 INTRODUCTION

Extensive use of ILLI-SLAB since its development at the University of Illinois in the late 1970's, has indicated the desirability for expanding its capabilities to include modeling of subgrade support systems that do not behave in the linear, discontinuous fashion assumed by Winkler [83]. Three additional models have been incorporated into ILLI-SLAB during the course of this research, namely the Resilient, Elastic Solid and Vlasov foundations. This Chapter describes the development and implementation of the first of these.

In the original version of ILLI-SLAB [78; 82], the modulus of subgrade reaction, k , obtained from the plate load test, is used for subgrade characterization. This is in conformity with general engineering practice, as well as several other finite element models. The value of k can be varied from node to node according to a pattern specified by the user at the beginning of each analysis. Note that k is independent of stress/deflection level, being essentially a linear, low stress modulus. Most subbase-subgrade support systems, however, display a stress-level dependent load-deflection response. Typically, a softer (lower k) response is exhibited at higher magnitudes of stress or deflection (Fig. 2.9b).

The purpose of this Chapter is to introduce the concept of the Resilient Modulus of Subgrade Reaction, K_R , develop deflection dependent support relations, and incorporate these into ILLI-SLAB to accommodate deflection dependent subgrade behavior. Various models reviewed in Chapter 2 are reexamined, with special attention paid to those that can be used to simulate nonlinear subgrade response. Thompson and Robnett [23] have proposed a resilient modulus characterization for the elastic solid foundation. This not only introduces soil nonlinearity, but also -perhaps more importantly- accounts for the apparent increase in subgrade stiffness, produced by rapidly moving, repeated loads. In this Chapter a similar resilient modulus characterization for the dense liquid foundation is developed.

Data for the development of the necessary algorithms are obtained using ILLI-PAVE to simulate repeated plate loading tests. Equations are derived relating the resilient modulus of subgrade reaction, K_R , and deflection. Note that this is no longer the modulus, k , derived from the static plate load test, but a modulus characterizing subgrade response to a repeated (impulse-type) test. The latter loading condition is considered more appropriate for the type of moving loads applied by modern-day aircraft traffic.

The stress dependent subgrade algorithms developed are incorporated into ILLI-SLAB through an iterative scheme. This change is also described in this Chapter. Typical results from the new resilient subgrade model in ILLI-SLAB are finally presented, and the effects of the proposed changes are evaluated.

6.2 SIMULATION OF REPEATED PLATE LOAD TESTS

To account for stress dependent behavior of typical fine-grained subgrade soils, the concept of the Resilient Modulus of Subgrade Reaction, K_R , is introduced [83; 31]. This new subgrade support parameter is analogous to reaction modulus, k , from the static plate load test, but is defined by:

$$K_R = \frac{\text{applied plate pressure}}{\text{resilient (recoverable) plate deflection}} \quad (6-1)$$

Ideally, K_R should be calculated from an impulse-type plate load test. In this investigation, finite element program ILLI-PAVE was employed instead, to generate data necessary for developing K_R versus deflection algorithms.

ILLI-PAVE incorporates subgrade material relations developed from repeated, impulse-type, triaxial tests [23]. Therefore, this program was used to simulate repeated plate load tests on various subgrades. The rigid plate condition was represented by a 4-in. thick steel loading plate ($E_{\text{steel}} = 30 \times 10^6$ psi). Plate diameters of 30, 21, and 15 in. were considered. Various plate pressures were applied. For each loading condition, a resilient (recoverable) deflection was determined from the ILLI-PAVE analysis.

The four subgrade types introduced earlier (very soft, soft, medium, and stiff) were investigated. Pertinent subgrade properties and characteristics are summarized in Table 6.1. Resilient modulus, E_R ,

TABLE 6.1
MATERIALS PROPERTY SUMMARY

PARAMETER	SUBGRADE				
	<u>Very Soft</u>	<u>Soft</u>	<u>Medium</u>	<u>Stiff</u>	<u>Gravel</u>
Unit Weight (pcf)	110.0	115.0	120.0	125.0	135.0
Coefficient Earth Pressure at Rest	0.82	0.82	0.82	0.82	0.6
Poisson's Ratio	0.45	0.45	0.45	0.45	0.38
E_{Ri} (ksi)	1.00	3.02	7.68	12.34	--
E_R - Model (psi)*	--	--	--	--	$5000 \theta^{.50}$
Friction Angle (degree)	0.0	0.0	0.0	0.0	40.0
Cohesion, psi	3.1	6.5	11.4	16.4	0.0

* $E_R = K \theta^n$ (E_R , K, and θ in psi)

versus repeated stress level relations for these subgrades are shown in Fig. 2.7.

In this study, applied plate pressures ranged from 2 psi to πc psi, where c is subgrade cohesion. Pressures larger than πc are not of practical interest, since at higher pressures significant permanent deformation (rutting) will occur in the subgrade. Plate pressure versus resilient displacement data obtained using ILLI-PAVE are presented in Figures 6.1 and 6.2. From these, resilient modulus of subgrade reaction (K_R) versus plate deflection relations for the various subgrades may be developed. These are shown in Figures 6.3 through 6.6. The subgrades show a definite softening behavior (reduced K_R) with increasing pressures. The softening behavior is most pronounced for the soft subgrade (Fig. 6.4), for which K_R at a pressure of πc is approximately 60% of K_R at 2 psi. Furthermore, for a given plate pressure and subgrade type, a decrease in plate size results in a stiffer plate response (K_R increases).

6.3 ALGORITHM DEVELOPMENT

The ILLI-PAVE plate pressure-deflection data were analyzed using different theories and empirical equations described in Chapter 2 and summarized in Table 6.2. The Ramberg-Osgood model and Butterfield and Georgiadis' cyclic plate-bearing model may be better suited for the case where both the loading and unloading pressure-deflection curves are of interest. However, these models did not provide a good fit for

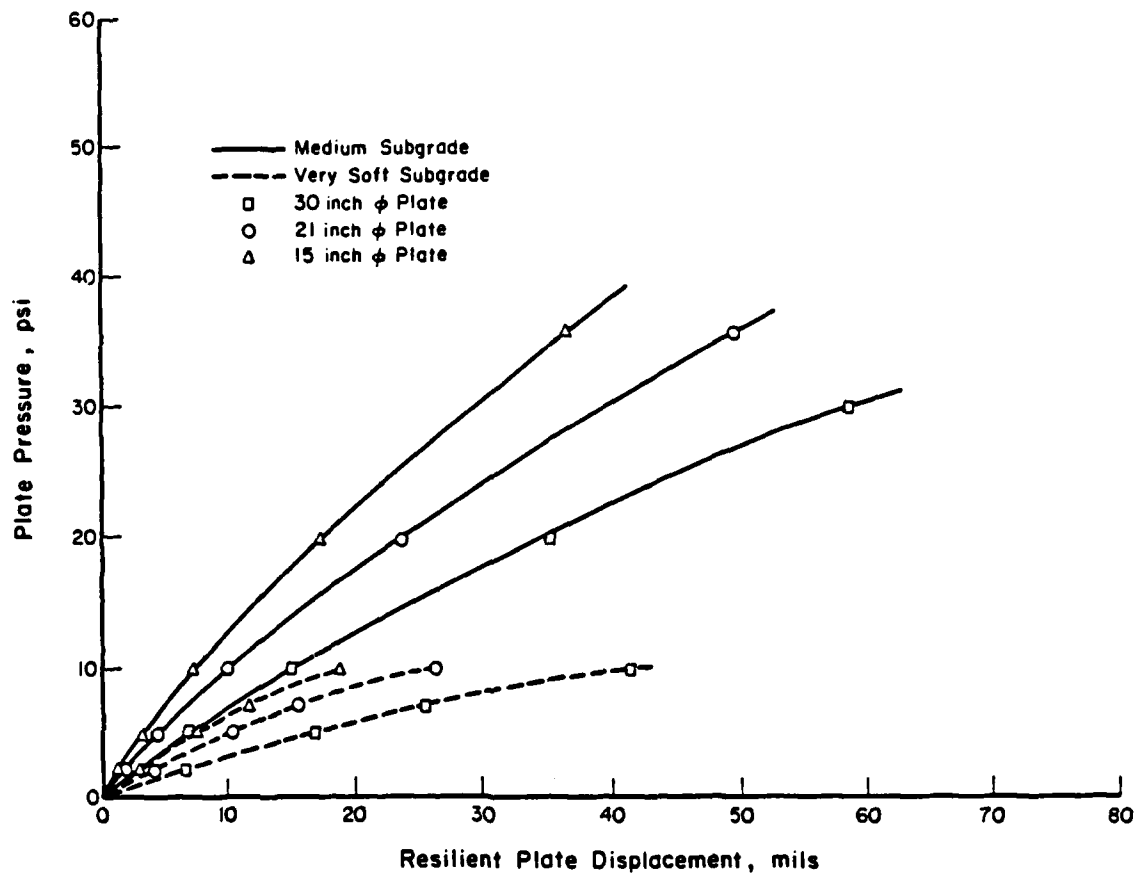


Fig. 6.1 Plate Pressure-Resilient Displacement Curves
(Medium; Very Soft Subgrades)

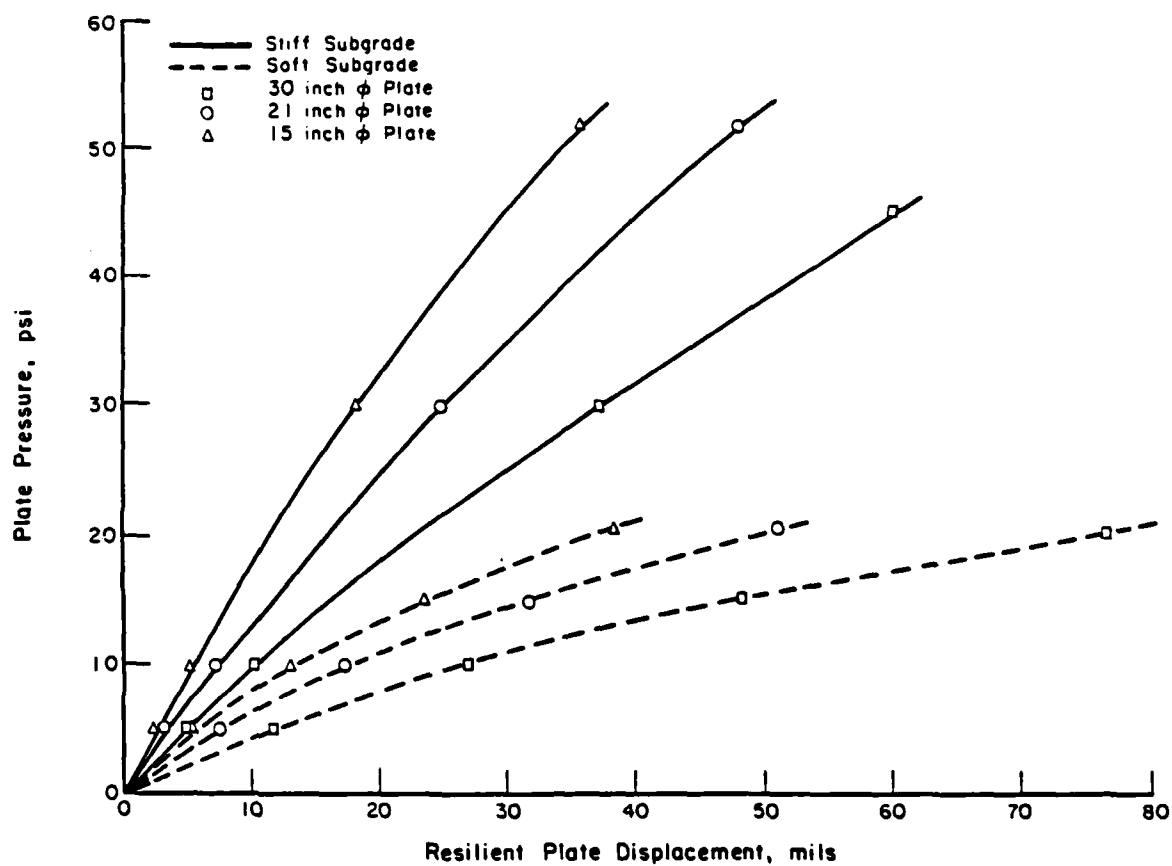


Fig. 6.2 Plate Pressure-Resilient Displacement Curves
(Stiff; Soft Subgrades)

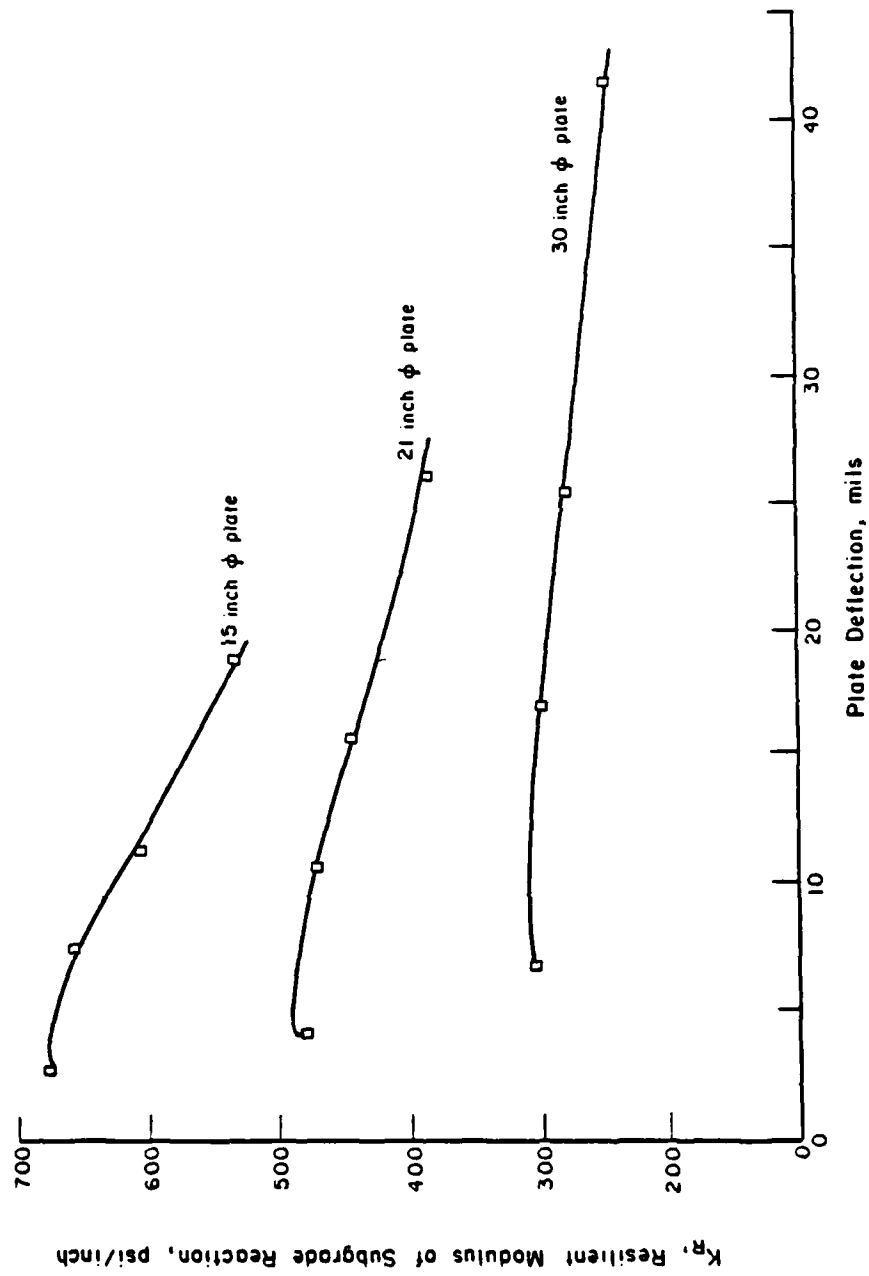


Fig. 6.3 Resilient Modulus - Deflection Relations (Very Soft Subgrade)

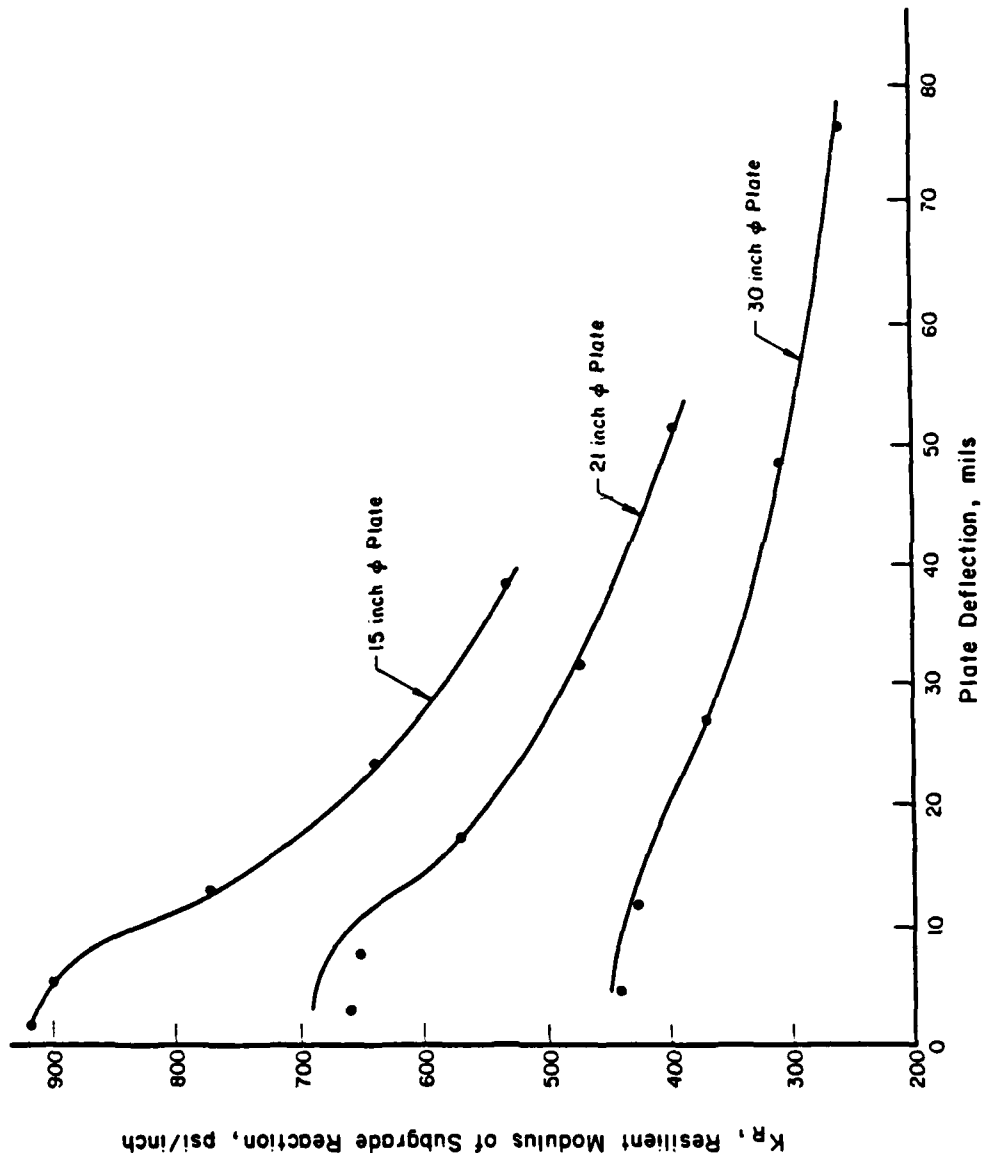


Fig. 6.4 Resilient Modulus - Deflection Relations (Soft Subgrade)

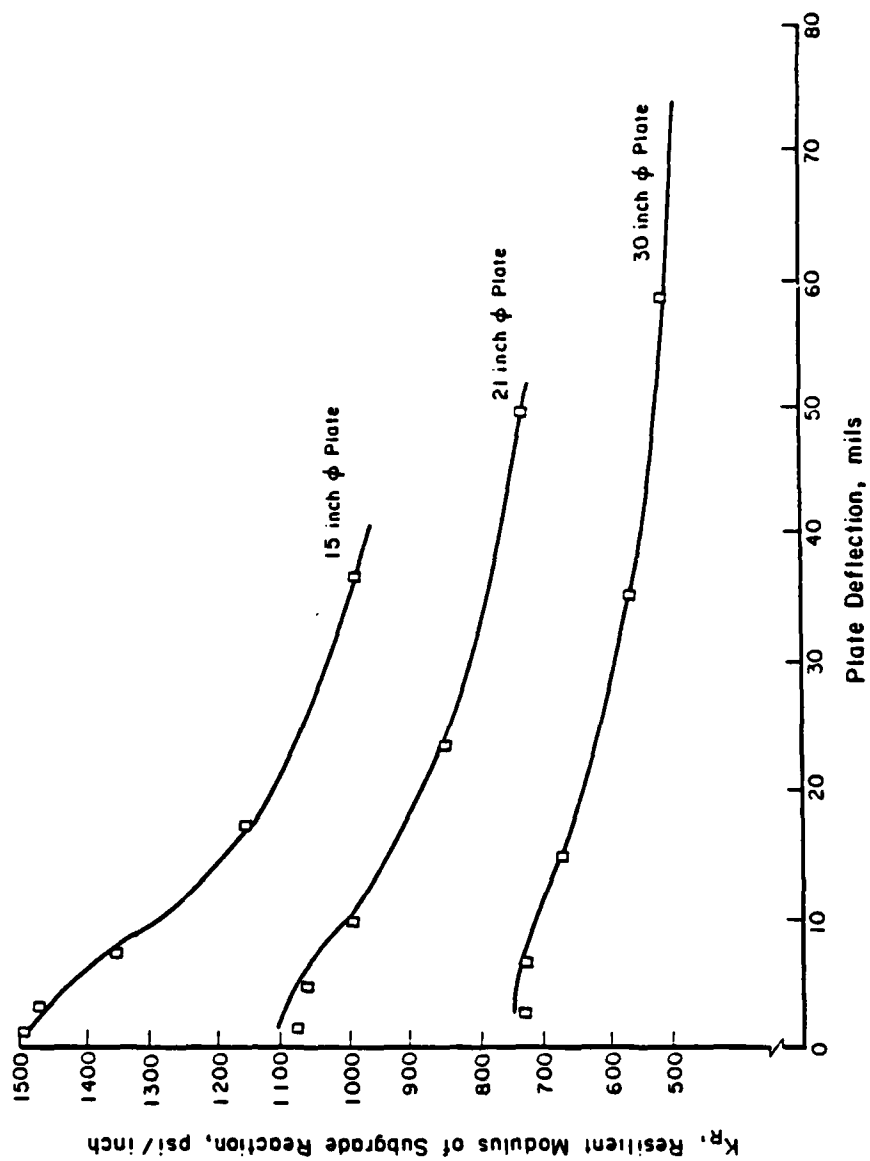


Fig. 6.5 Resilient Modulus - Deflection Relations (Medium Subgrade)

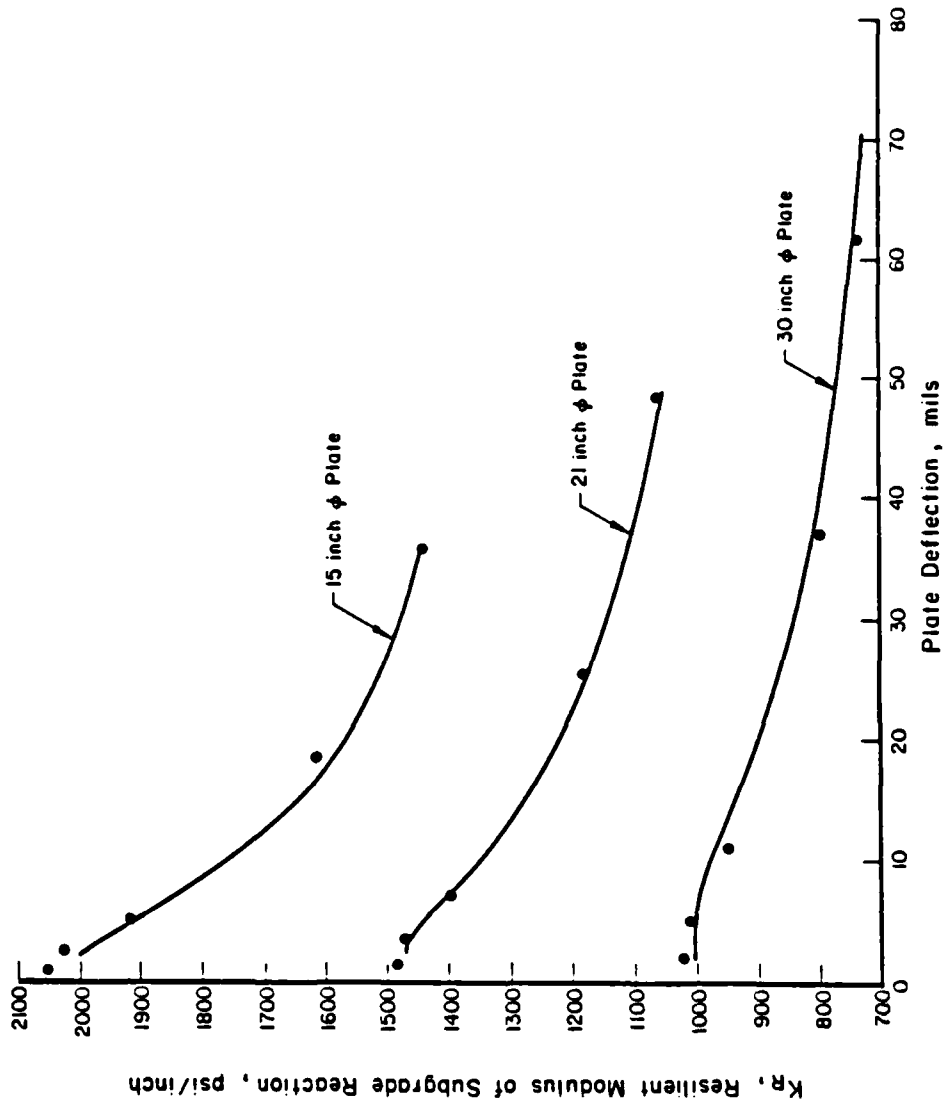


Fig. 6.6 Resilient Modulus - Deflection Relations (Stiff Subgrade)

TABLE 6.2

MODELS CONSIDERED

MODEL	EQUATIONS	SYMBOLS
Ramberg-Osgood	$\frac{w}{2w_y} = \frac{p}{p_y} + a \left \frac{p}{p_y} \right ^r$ $\frac{w - w_o}{2w_y} = \frac{p - p_o}{2p_y} + a \left \frac{p - p_o}{2p_y} \right ^r$	<p>w : plate deflection</p> <p>p : plate pressure</p> <p>w_y, p_y : values of w and p at yield</p> <p>a, r : experimentally determined constants</p> <p>w_o, p_o : extreme values of w and p for any cycle</p>
Butterfield and Georgiadis Cyclic Model	$k_u = k_o - C_2 \frac{p}{p_u} \frac{C}{p_u}$ $k_r = k_o - C_1 \frac{p}{p_u} \frac{C}{p_u}$	<p>k_o : initial stiffness</p> <p>k_f : final stiffness</p> <p>p_u : load axis intercept</p> <p>p_c : cyclic load level</p> <p>k_r : reloading stiffness</p> <p>k_u : unloading stiffness</p> <p>C₁, C₂, C₃ : experimentally determined constants</p> <p>N : number of cycles</p>
Hyperbolic Model	$p = \left[\frac{1}{b + aw} \right] w$	<p>a, b : experimentally determined constants</p>
Butterfield and Georgiadis Two-parameter Model	$p = q(w_o) + (4G^{0.5}/B) \int_0^w [q(w) \cdot dw / \sqrt{2/q(w)} dw]$	<p>q(w_o) = kw_o</p> <p>q(w) = kw = G (3²w/3x²)</p> <p>w_o : central deflection</p> <p>k : compression spring stiffener</p> <p>G : shear spring stiffness</p> <p>B : side length of rigid square plate</p>
Butterfield and Georgiadis Empirical Equation	$p = p_u (1 - \exp -(k_o - k_r) w / p_u) + k_r w$	<p>p_u : pressure axis intercept</p>

ILLI-PAVE resilient data. The hyperbolic model and Butterfield and Georgiadis' two parameter model did not adequately describe these data either.

The empirical equation proposed by Butterfield and Georgiadis provided the best fit. This equation was modified for presenting ILLI-PAVE plate pressure-resilient displacement data. A normalized deflection parameter (w/D_y) was substituted into the equation in place of w , where D_y represents the deflection at a plate pressure of πc psi (πc is the upper bound for plate pressures considered in the ILLI-PAVE analyses). The resulting equation is:

$$P = A_1 \left[1 - \exp \left\{ -A_2 \left(\frac{w}{D_y} - A_3 \right) \right\} \right] + A_4 \left(\frac{w}{D_y} - A_3 \right) + 2 \quad (6-2)$$

where:

p : plate pressure (psi);

w : plate deflection (in.);

D_y : deflection factor for a given subgrade type (very soft; soft; medium; stiff);

A_1, A_2, \dots : subgrade constants.

If this equation is divided through by the plate deflection, w , the p/w term is K_R , the resilient modulus of subgrade reaction (psi/in.). The final K_R algorithm is:

$$K_R = (1/w) \{ A_1 [1 - \exp \{ -A_2 ([w/D_y] - A_3) \}] + A_4 ([w/D_y] - A_3) + 2 \} \\ = A_5 / D_y, \text{ if } [w/D_y] < A_3 \quad (6-3)$$

Regression analyses were used to develop four equations (one for each type of subgrade). The equation parameters for a 30-in. diameter plate are summarized in Table 6.3. Values of the correlation coefficient, R , standard error of estimate and coefficient of variation for the equations are also presented in Table 6.3. To be consistent with the subgrade resilient modulus-stress level relations (see Fig. 2.7), K_R is assumed to be a constant for pressures less than 2 psi.

Note that the resilient modulus of subgrade reaction, K_R , obtained from these algorithms, has values much greater than the corresponding static subgrade modulus, k , for any given soil. This is consistent with the observation that soils exhibit a much stiffer response when loaded by rapidly moving loads, rather than static loads. A similar observation was made earlier in relation to the values of E_{Ri} and static E for fine-grained soils (Section 2.5.1). This phenomenon can be explained in terms of the viscoelastic behavior of soil, and the variation in strength due to changes in the strain rate. Ladd and Foott [138] point out that "the exact variation is a function of the plasticity and creep susceptibility of the soil. The effect is due to undrained creep which occurs during shear, giving increased pore pressures, decreased effective stresses, and decreased strengths. The slower the strain rate, the more time there is for this creep to occur, and the lower the strength."

TABLE 6.3
REGRESSION EQUATION PARAMETERS AND STATISTICS

Subgrade Type	A ₁	A ₂	A ₃	A ₄	A ₅	D _y	R*	SEE**	Coefficient of Variation, %
Very Soft	15.0	0.80	0.1680	0.62	11.9	0.0400	0.993	3.9	1.4
Soft	9.5	2.60	0.0594	10.25	33.7	0.0782	0.995	9.1	2.5
Medium	7.0	3.74	0.0377	28.10	53.1	0.0734	0.997	9.1	1.4
Stiff	5.0	5.30	0.0282	45.90	71.0	0.0707	0.995	13.9	1.5

* Correlation Coefficient

** SEE = Standard error of estimate (psi/in.)

$$K_R = A_1 \left[1 - \exp \left\{ - A_2 \left(\frac{W}{D} - A_3 \right) \right\} \right] + A_4 \left(\frac{W}{D} - A_3 \right) + 2$$

in psi/in.

6.4 SUBBASE EFFECTS ON THE VALUE OF K_R

6.4.1 Effect of a Granular Subbase

A layer of granular material is frequently used as a subbase in Portland Cement Concrete (PCC) pavement construction. The structural contribution of the granular material layer is generally acknowledged by assigning an increased design k to the granular layer-subgrade system [30; 42].

Plate load tests, employing a 30-in. diameter plate on a granular subbase-subgrade soil support system, were simulated using ILLI-PAVE. The properties of the granular subbase (gravel) are listed in Table 6.1. Three different granular subbase thicknesses (8, 16 and 24 in.) were considered. The applied plate pressure was $2c$ (c = subgrade cohesion). Figure 6.7 shows the effect of granular layer thickness on K_R for each of the four subgrades. It may be concluded that the introduction of a granular subbase up to 6-in. thick, has a pronounced beneficial effect on K_R . For higher thicknesses of subbase, the K_R -thickness effect decreases with an increase in the thickness of the granular subbase. Subbase thickness has only a slight effect within the 8 to 24-in. thickness range considered. Comments made in the previous section with regard to the seemingly high K_R -values, apply here as well.

Plate pressure effects were also evaluated for an 8-in. granular subbase layer thickness and a 'SOFT' subgrade type. Plate pressures of c , $2c$, and πc psi were considered. Comparative data for the no-subbase and subbase conditions are shown in Fig. 6.8. Plate pressure has only

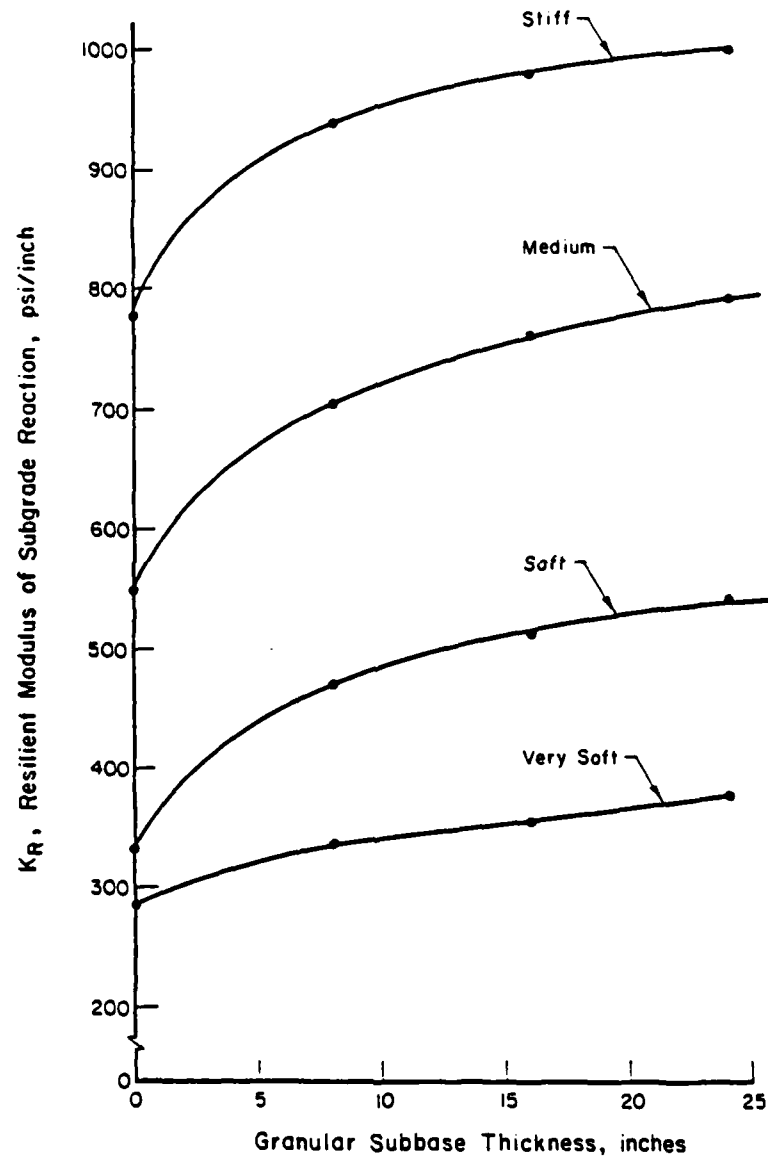


Fig. 6.7 Effect of Granular Subbase Thickness on Resilient Modulus

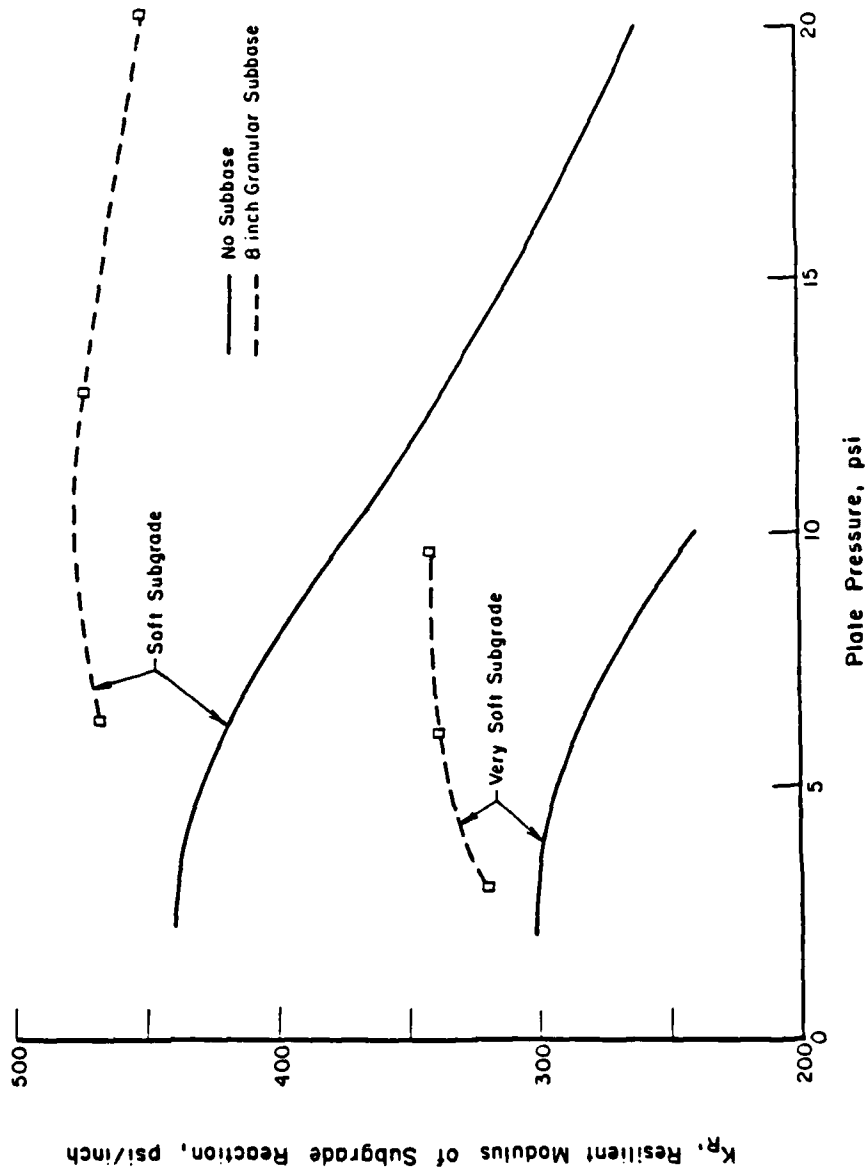


Fig. 6.8 Effect of Granular Subbase on Resilient Modulus for Variable Plate Pressure

a nominal effect. The stress stiffening behavior of the granular material counteracts to some extent the stress softening behavior of the fine-grained subgrade.

6.4.2 Effect of a Stabilized Subbase

The effect of a high strength and high modulus subbase for a PCC pavement can be considered by increasing k for the stabilized subbase-subgrade system. This procedure is recommended by the Portland Cement Association [30] and the Federal Aviation Administration [42].

The ILLI-SLAB program considers the stabilized subbase as a second plate beneath the PCC layer. This is a more desirable procedure than using an increased k , since the flexural properties of the subbase and its degree of bonding with the PCC slab can be considered. Therefore, its behavior is assumed to be stress independent.

6.5 MODEL IMPLEMENTATION

It is desirable to incorporate the relationships derived above into ILLI-SLAB through an iterative procedure which compares support values (K_R) corresponding to calculated deflections with previously determined values. New support values may be assigned for a subsequent iteration, until compatibility is achieved between support system stress and/or deflection and the user prescribed support relation/pattern. Furthermore, it is desirable to have the capability to assign variable support values to selected (or all) nodes according to a user prescribed

relation/ pattern. This is achieved with the introduction of subroutine ITERATE [112].

The general expression for the relation between K_R and w as developed in this study (30-in. diameter plate) is given by Eqn. (6-3) in which $A_1, A_2, A_3, A_4, A_5, D_y$ are regression parameters determined from plate load tests simulated using ILLI-PAVE. By specifying these parameters, ILLI-SLAB users may define any other stress dependent subgrade, as well. During this study, parameter sets for the following broad subgrade types (Fig. 2.7) have been developed and are now a part of the revised version of ILLI-SLAB:

1. VERY SOFT ($K_R = 300$ psi/in.)
2. SOFT ($K_R = 425$ psi/in.)
3. MEDIUM ($K_R = 725$ psi/in.)
4. STIFF ($K_R = 1000$ psi/in.).

The figures in parentheses are recommended initial (small deflection) values, for fast convergence. As noted in Section 6.3, above, K_R is significantly higher than the corresponding static k -value, reflecting the increased subgrade stiffness in response to rapidly moving loads. Other dense liquid subgrade options available in modified ILLI-SLAB are:

5. OTHER : The user specifies individual regression parameters to obtain a different K_R versus deflection relation.
6. WINKLER: This is the stress independent, uniform Winkler subgrade, available in the original version of ILLI-SLAB.
7. SPRINGS: Support is provided by 4 springs at the corner of the element (stress independent). This option allows direct

comparison-validation with FINITE.

Option 0 specifies that support varies from node to node and requires that the user proceed to assign one of the above 7 options to each of the nodes. In the case where most nodes have one type of support, the EXCEPT option in the free-form mode allows specification of exceptions only, rather than of each node.

Subroutine ITERATE is structured to allow easy modification of the regression equations and/or addition of other subgrade options. When one of the stress dependent subgrade types are used, subroutine ITERATE provides a procedure for checking convergence, updating support values and proceeding with another iteration, if necessary. The user controls this procedure by three variables:

1. ITMAX: Specifies the maximum (total) number of iterations desired. Usually 3 iterations are sufficient. A value of ITMAX=6 is recommended;
2. TOL1: Convergence tolerance for updated K_R compared with K_R from the previous iteration. A value of TOL1=0.05, i.e. 5%, is recommended;
3. TOL2: Convergence tolerance for the percentage of nodes at which TOL1 is not satisfied. Again, a value of TOL2=0.05, i.e. 5%, is recommended.

Through a fourth parameter (IOT), the user is allowed to specify the output type desired. Thus, one may opt to have only partial output during intermediate iterations (stresses not calculated or printed), reserving full output of deflections and stresses for the last

iteration; or one may choose to have full output for each iteration.

6.6 TYPICAL EFFECTS USING THE RESILIENT SUBGRADE MODEL

6.6.1 Cases Considered

To illustrate the capabilities of ILLI-SLAB and the impact of the introduction of the Resilient Subgrade model, a number of demonstration runs were performed [112]. Results obtained from these runs are presented and discussed in this Section.

Two typical pavement cross-sections are considered in this investigation (Table 6.4). The first is a 10-in. Portland Cement Concrete (PCC) Pavement, consisting of panels that are 20-ft. square, or 20-ft. by 12-ft., with or without load transfer between adjacent slabs. These dimensions are typical of airport and highway pavements, respectively. The contour plots shown in Fig. 4.1 were obtained from one of the demonstration runs using a highway pavement. The second pavement section is a 12-in. pavement consisting of a stabilized layer with a modulus, E , of 1.5×10^6 psi. This pavement is divided into 15-ft. by 12-ft. panels and is typical of pavements proposed for the USAF Alternate Launch and Recovery Surfaces (ALRS) Program.

The two pavement sections are loaded by a 9-kip highway load, or one of three typical USAF aircraft loading patterns: the F-4, the C-130, or the F-111. A typical soft subgrade is assumed, using two alternative ways of characterization. The first is the conventional static subgrade modulus, k , which was assigned a value of 120 to 150 psi/in. using the

TABLE 6.4
PARAMETERS FOR DEMONSTRATION RUNS

(a) PCC Pavement Section

Slab: 20' x 20' panels (airport)

or 20' x 12' panels (highway)

$h = 10''$

$E = 4 \times 10^6 \text{ psi}$

$\mu = 0.15$

$k = 150 \text{ psi/in. or 'SOFT'}$

(b) ALRS Pavement Section

Slab: 12' x 15'

$h = 12''$

$E = 1.5 \times 10^6 \text{ psi}$

$\mu = 0.15$

$k = 120 \text{ psi/in. or 'SOFT'}$

(c) Loading Patterns

(i)	Highway:	10-in.	x	10-in.	@ 90 psi
(ii)	F - 4:	10-in.	x	10-in.	@ 270 psi
(iii)	C-130:	2 21-in.	x	21-in.	@ 100 psi
(iv)	F-111:	20.2-in.	x	15.5-in.	@ 150 psi

`WINKLER' option in ILLI-SLAB. The second is the proposed resilient modulus, K_R , which was set at 425 psi/in. using the `SOFT' option. Associated with the latter option, is stress dependence, provided by the iterative scheme described above.

The finite element meshes used for the demonstration runs are shown in Appendix B, Figures B.10 through B.20. These meshes were designed before the finalization of the aspect ratio guidelines, presented in Chapter 5. Since this is primarily a comparative study, however, the high aspect ratios used are believed to have a negligible effect. Also note that results from the highway and F-4 loads may be expected to be in the ratio of 1:3, except for a small slab size and mesh effect. For the cases involving load transfer, a second "mirror image" panel was added to the right of the panels shown in these figures. Note that the ALRS runs involving load transfer are of academic interest only, since load transfer systems are not recommended for such sections.

The major results from the demonstration runs are summarized in Table 6.5. In an effort to clarify the picture presented by these results, three distinct effects are identified:

- (a) Effect of Load Transfer;
- (b) Effect of Resilient Modulus; and
- (c) Effect of Stress Dependence--Iterative Scheme.

These effects are discussed separately below.

TABLE 6.5
RESULTS OF DEMONSTRATION RUNS

RUN	PAVEMENT	LOADING	SUBGRADE	LOAD POSITION	SPECIFIED AIF	ACTUAL LTE	MAX. DEFLECTION (psi/node)			MAX. BENDING STRESS (psi/node)		
							NIT-1	NIT-2	NIT-3	NIT-1	NIT-2	NIT-3
ONEW	PCC	Wey	k=150 psi/in.	Edge	10 ⁶	98	9.1/43	--	--	151/43	--	--
ONEW	PCC	Wey	k=150 psi/in.	Edge	0	--	18.1/43	--	--	245/43	--	--
ONESF	PCC	Wey	'SOFT'	Edge	10 ⁶	96	4.9/43	x	x	140/43	x	x
ONESF	PCC	Wey	'SOFT'	Edge	0	--	9.6/43	x	x	223/43	x	x
DR001	PCC	F-4	k=150 psi/in.	Edge	10 ⁶	98	24.1/81	--	--	470/81	--	--
DR002	PCC	F-4	k=150 psi/in.	Edge	0	--	47.7/81	--	--	773/81	--	--
DR003	PCC	F-4	'SOFT'	Edge	10 ⁶	96	13.5/81	x	x	423/81	x	x
DR004	PCC	F-4	'SOFT'	Edge	0	--	26.4/81	27.3/81	x	680/81	690/81	x
DR005	PCC	C-130	k=150 psi/in.	Edge	10 ⁶	98	40.4/85	--	--	561/78	--	--
DR006	PCC	C-130	'SOFT'	Edge	0	--	38.6/85	42.3/85	x	740/85	776/85	x
DR007	PCC	C-130	'SOFT'	Edge	10 ⁶	97	19.7/78	20.3/78	x	456/78	464/78	x
DR008	PCC	F-111	'SOFT'	Edge	0	--	39.6/81	42.6/81	x	806/81	834/81	x
DR009	ALRS	F-4	k=120 psi/in.	Edge	10 ⁶	98	37.1/65	--	--	302/65	--	--
DR010	ALRS	F-4	k=120 psi/in.	Edge	0	--	73.6/65	--	--	509/65	--	--
DR011	ALRS	F-4	'SOFT'	Edge	10 ⁶	97	17.3/65	17.5/65	x	270/65	272/65	x
DR012	ALRS	F-4	'SOFT'	Edge	0	--	34.1/65	36.0/65	x	446/65	455/65	x
DR013	ALRS	C-130	k=120 psi/in.	Edge	10 ⁶	99	59.1/67	--	--	366/61	--	--
DR014	ALRS	C-130	'SOFT'	Edge	10 ⁶	98	23.9/67	25.1/61	x	294/61	301/61	x
DR015	ALRS	C-130	'SOFT'	Edge	0	--	47.2/67	53.6/67	x	475/67	507/67	x
DR016	ALRS	F-111	'SOFT'	Edge	0	--	50.3/65	56.1/65	x	518/65	545/65	x
OH1W	PCC	Wey	k=150 psi/in.	Interior	0	--	5.6/1	--	--	130/1	--	--
OH15F	PCC	Wey	'SOFT'	Interior	0	--	3.1/1	x	x	119.1	x	x
DR017	PCC	F-4	'SOFT'	Interior	0	--	8.8/1	x	x	356/1	x	x
OH1J8	PCC	C-130	'SOFT'	Interior	0	--	14.1/25	x	x	408/25	x	x
DR019	PCC	F-111	'SOFT'	Interior	0	--	14.8/1	x	x	462/1	x	x

Notes: (a) For f.e. meshes, see Appendix B, Figures B.10 through B.20.

(b) For relevant parameters, see Table 6.4.

(c) Parameters for option 'SOFT':

ITMAX = 6
TOL1 = 5%
TOL2 = 5%

(d) Actual LTE's calculated after first iteration.

(e) NIT: Iteration Number
x: Convergence achieved at an earlier iteration.

6.6.2 Effect of Load Transfer

To investigate the impact of load transfer systems, load transfer by aggregate interlock was provided in some runs and these are compared to those in which only one panel was used. It was intended to investigate the two extreme cases, that of no load transfer (LTE = 0%) and that of full load transfer (LTE = 100%). For the latter, an aggregate interlock factor (AIF) of 1×10^6 was specified, producing load transfer efficiencies (LTE) between 96% and 99% (see Table 6.5).

Under conditions of full load transfer, maximum deflection is reduced to half its value for the condition of no load transfer. The effect of load transfer on maximum bending stress is shown as a stress ratio in Table 6.6. The Table indicates that full load transfer stress is about 0.6 times the no load transfer value. It is also observed that the proposed change to a resilient modulus subgrade characterization has only a minor effect in this respect. As expected, the load transfer effect is more pronounced (albeit only very slightly) in the case of the less stiff ALRS pavement.

6.6.3 Effect of Resilient Modulus Characterization

As explained earlier, it is considered that a resilient modulus subgrade characterization would be more appropriate for airfield pavement systems under transient loads, than the conventional static plate load test subgrade modulus. The k-value used to characterize the subgrade in finite element programs like ILLI-SLAB may be replaced by a stress dependent K_R -value, which at low stress levels is substantially

TABLE 6.6
EFFECT OF LOAD TRANSFER

<u>PAVEMENT</u>	<u>LOADING</u>	<u>SUBGRADE</u>	<u>STRESS RATIO</u>
PCC	Hwy	k=150 psi/in. 'SOFT'	0.61 0.63
	F-4	k=150 psi/in. 'SOFT'	0.61 0.62
	C-130	'SOFT'	0.62
ALRS	F-4	k=120 psi/in. 'SOFT'	0.59 0.61
	C-130	'SOFT'	0.62

Notes:

(a) All runs for edge loading condition

$$(b) \text{ STRESS RATIO} = \frac{\sigma_{\text{max. for LTE} = 100\%}}{\sigma_{\text{max. for LTE} = 0}}$$

where LTE = Load Transfer Efficiency

$$= \frac{\text{Deflection across joint on unloaded side}}{\text{Max. deflection along joint on loaded side}}$$

(c) The corresponding DEFLECTION RATIO is 0.50 for
LTE = 100%.

(d) All comparisons for first iteration.

greater than the static k . In the cases analyzed in this investigation, the 'WINKLER' subgrade was assumed to have a static k value of 120 to 150 psi/in. This is considered equivalent to the stress dependent 'SOFT' subgrade option in ILLI-SLAB. The low stress level K_R -value for this subgrade is 425 psi/in., according to the algorithms described above.

The effect of this change is shown in Table 6.7 in the form of deflection and stress ratios, comparing the responses of the 'SOFT' and 'WINKLER' subgrades. Deflection ratios vary between 0.40 and 0.56, while stress ratios have values between 0.80 and 0.93. Thus, the proposed resilient modulus subgrade characterization leads to lower calculated deflections and stresses, with stresses being affected to a smaller extent than deflections. Table 6.7 also shows the impact of the proposed change is more significant as the load becomes more severe (C-130 instead of F-4) and/or the pavement system is less stiff (ALRS rather than PCC pavement; no load transfer).

6.6.4 Effect of Stress Dependence -- Iterative Scheme

Associated with the stress dependent options in ILLI-SLAB, including 'SOFT' employed in these demonstration runs, is an iterative scheme. In this scheme, after each iteration a check is performed for the compatibility of calculated deflections and assumed support pattern (i.e. K_R -values). If this compatibility is poor, a new iteration is performed after updating the support pattern until specified convergence tolerances are achieved. Usually no more than three iterations were

TABLE 6.7

EFFECT OF RESILIENT MODULUS

PAVEMENT	LOADING	SPECIFIED LTE (%)	DEFLECTION RATIO	STRESS RATIO
PCC	Hwy	0	0.53	0.91
		100	0.54	0.93
	F-4	0	0.55	0.88
		100	0.56	0.90
	C-130	100	0.49	0.81
ALRS	F-4	0	0.46	0.87
		100	0.47	0.89
	C-130	100	0.40	0.80

Notes: (a) All runs for edge loading condition

(b) DEFLECTION RATIO = $\frac{\text{Max. deflection for 'SOFT'}}{\text{Max. deflection for 'WINKLER'}}$

(c) STRESS RATIO = $\frac{\text{Max. stress for 'SOFT'}}{\text{Max. stress for 'WINKLER'}}$

(d) All comparisons for first iteration.

required to achieve convergence within a tolerance of 5%.

Table 6.8 is an attempt to filter out the effect of the iterative scheme, by presenting in terms of deflection and stress ratios, the responses after the first and after the last iterations. Deflection ratios range between 1.00 and 1.14 while stress ratios fall between 1.00 and 1.07. Thus, the effect of the iterative scheme is to increase the maximum deflections and stresses obtained after the first iteration, thereby counterbalancing some of the change produced by the resilient modulus described above.

Since the application of the iterative scheme increases execution time, it is important to draw some conclusions as to when such an increased expense is justified by the changes in response produced. Table 6.8 shows that the iterative scheme effect becomes substantial (i.e. 10% or more) for the more severe loading patterns (edge rather than interior; F-111, C-130 rather than F-4), on the less competent pavement systems (ALRS rather than PCC section; LTE = 0% rather than LTE = 100%). The iterative scheme has no effect in the case of the 9-kip highway load, and only one iteration is required to achieve the 5% specified tolerance.

In general, the effect of the iterative scheme is not dramatic. This may be partly attributed to the fact that the algorithms used in the present version of ILLI-SLAB were developed by simulating rigid plate load tests using ILLI-PAVE. The plates used in these tests are much stiffer than any ordinary pavement slabs, and their radius of relative stiffness, l , is much higher than the values encountered in

TABLE 6.8

EFFECT OF STRESS DEPENDENCE

PAVEMENT	LOADING	SPECIFIED LTE (%)	DEFLECTION RATIO	STRESS RATIO
PCC	F-4	0	1.03	1.01
		100	1.00	1.00
	C-130	0	1.10	1.05
		100	1.03	1.02
	F-111	0	1.04	1.07
ALRS	F-4	0	1.06	1.02
		100	1.01	1.00
	C-130	0	1.14	1.07
		100	1.05	1.03
	F-111	0	1.12	1.05

Notes:

(a) All runs for 'SOFT' subgrade; edge loading condition.

(b) DEFLECTION RATIO = $\frac{\text{Max. deflection for last iteration}}{\text{Max. deflection for first iteration}}$

(c) STRESS RATIO = $\frac{\text{Max. stress for last iteration}}{\text{Max. stress for first iteration}}$

(d) Convergence Tolerances: TOL1 = 5%
TOL2 = 5%

(e) Iterative Scheme has no effect for 9-kip highway loading.

pavement slabs. Westergaard [9] as well as other investigators have pointed out the effect of the radius of relative stiffness on subgrade-pavement system response. Subroutine ITERATE is flexible enough to accommodate refined K_R algorithms accounting for such effects, when they are developed.

Finally, Table 6.9 presents the combined effects of the resilient modulus and of the iterative scheme. The deflection ratios range between 0.42 and 0.57 and are, in general, substantially lower than the corresponding stress ratios, which lie between 0.82 and 0.93. This indicates that the impact of the proposed changes is much more significant with respect to deflections rather than stresses. Furthermore, the effects are more pronounced in the case of the more severe load patterns and/or the less competent pavement systems.

TABLE 6.9

COMBINED EFFECT OF PROPOSED CHANGES

PAVEMENT	LOADING	SPECIFIED LTE (%)	DEFLECTION RATIO	STRESS RATIO
PCC	9-kip	0	0.53	0.91
		100	0.54	0.93
	F-4	0	0.57	0.89
		100	0.56	0.90
	C-130	100	0.50	0.83
ALRS	F-4	0	0.49	0.89
		100	0.47	0.90
	C-130	100	0.42	0.82

Notes: (a) All runs for edge loading condition.

(b) DEFLECTION RATIO = $\frac{\text{Max. deflection after changes}}{\text{Max. deflection before changes}}$

(c) STRESS RATIO = $\frac{\text{Max. stress after changes}}{\text{Max. stress before changes}}$

(d) Changes consist of:

(i) Subgrade Characterization by resilient modulus, K_R (= 425 psi/in.: 'SOFT'), instead of static subgrade modulus k (= 120 or 150 psi/in.);

(ii) Stress dependence-iterative scheme.

CHAPTER 7

ANALYSIS OF AXISYMMETRIC SLABS OF FINITE EXTENT
ON AN ELASTIC SOLID FOUNDATION

7.1 INTRODUCTION

In the analyses of pavement slabs presented above, an important simplifying assumption has been made to render the problem tractable. This is that the deflection at any point is related to the subgrade stress at that point alone through a constant, the modulus of subgrade reaction, k . Thus, the soil was treated as a Winkler medium, named after the pioneer of this concept, which is also referred to as a dense liquid foundation. The latter term is used to distinguish this from the other common model, viz. the elastic solid, or Boussinesq foundation. The preceeding chapters indicate that the fundamental work by Westergaard and others, and more recently the Finite Element Method (F.E.M.) yield adequate solutions to the problem of a slab on dense liquid, which take into account such effects as load placement, size of slab, existence of joints, etc. On the other hand, analyses involving the elastic solid foundation are still at a comparatively elementary stage, despite the general consensus among engineers that the Boussinesq foundation is a much more realistic representation of the subgrade than the Winkler medium.

This Chapter describes the development of a computer program called CFES (Circular Finite Extent Slab) and analyses performed for an

axisymmetric slab of finite extent resting on an elastic solid foundation. The model presented herein is the first of a series of elastic solid formulations, derived during this research. Additional models will be discussed in chapters to follow.

7.2 LITERATURE REVIEW

The computer program developed in this study uses the concept of "concordant deflections" [139]. This is a numerical method in which the deflections of the slab are matched to the deflections of the subgrade surface at a number of discrete points. For this purpose, the slab is divided into a number of elements and the matching is done at the centers of these elements. The solution presented here follows closely the procedure outlined by Bergstrom, et al. [127], who analyzed slabs consisting of four elements only. They concluded that this approach gave accurate results for engineering purposes. The method has also been used by Barden [140], and Rananathan [141]. Its application to the case of a beam on an elastic foundation is discussed by Scott [121]. The accuracy of earlier applications of similar methods [142; 143] to determine bending and subgrade stresses is critically examined by Brown [144].

Closed-form solutions to the problem of a plate on an elastic solid are limited. The special case of an axisymmetric slab of infinite dimensions has been treated by Hogg [11] and Holl [12; 145]. These investigations carried the numerical calculations to such a stage that,

for the first time, their results could be applied with relative ease to the calculation of stresses and displacements in pavement slabs. Thus, Hogg obtained expressions for the displacement and curvature of a plate under a concentrated load, and for the curvature at the center of the same plate loaded with a circular load. Graphs of these quantities were also presented. Hogg later considered the case of a finite layer with a rough base as well [146], and presented the exact mathematical solution for the plate displacement under a point load in the form of an infinite integral and tabulated results.

Holl's solution is a generalized approach to the problem, in which the subgrade properties enter in the form of a "kernel" or "influence function". This function describes the deflection basin created by the application of a unit point load, and its forms for both the dense liquid and the elastic solid are presented [12]. On the basis of the work by Hogg and Holl, Losberg [13] developed a set of equations for maximum responses of a plate on an elastic solid under a circular interior load. These are similar in form to those presented earlier by Westergaard [8] for the corresponding dense liquid case (Table 7.1). In both cases, the equations consider only the first one or two terms of an infinite series. Several other authors also quote Losberg's equations [147; 125]. A similar set of formulae have been obtained by Arora and Khanna [14] by comparison to the dense liquid solutions.

Other approaches to the problem of a plate on an elastic solid foundation are also described in the literature [148; 149; 150]. Solutions to certain special cases are summarized by Poulos and Davis

TABLE 7.1

EQUATIONS FOR MAXIMUM RESPONSES UNDER INTERIOR LOADING

A. DENSE LIQUID

$$\delta = \frac{P}{8k\ell^2} \left[1 + \left(\frac{1}{2\pi} \right) \left\{ \ln \left(\frac{a}{2\ell} \right) + \gamma - 1.25 \right\} \left(\frac{a}{\ell} \right)^2 \right]$$

$$q = k \delta$$

$$\sigma = \frac{3P(1+\mu)}{2\pi h^2} \left[\ln \left(\frac{2\ell}{a} \right) + 0.5 - \gamma + \frac{\pi}{32} \left(\frac{a}{\ell} \right)^2 \right]$$

B. ELASTIC SOLID

$$\delta = \frac{P\ell_e^2}{D3\sqrt{3}} \left[1 - a_e^2 \left(0.1413 - 0.1034 \ln a_e \right) \right]$$

$$q = \frac{P}{\ell_e^2 3\sqrt{3}} \left[1 - 0.5513 a_e + 0.1257 a_e^2 \right]$$

$$\sigma = \frac{-6P(1+\mu)}{h^2} \left[0.1833 \log_{10} a_e - 0.0490 - 0.0120 a_e^2 \right]$$

Note: $a_e = \frac{a}{\ell_e}$

[151]. Charts for the determination of the response of an axisymmetric slab of infinite size have been presented by Pickett, et al. [86; 84]. For the case of edge loading, Pickett and his co-workers [152; 153] later presented a similar chart for maximum bending stress, which has not been as extensively used as their previous charts. A computerized version of this chart is described in Chapter 8. Pickett, et al. [84] also presented a finite difference approach, not adequately investigated to this day. Chapter 10 describes the implementation of this method in a computer program, and examines the scope of this analysis.

A finite element solution for the analysis of a slab of finite extent on a Boussinesq foundation was first presented by Cheung and Zienkiewicz [88], using the assumption of stepwise uniform foundation reactions. This concept is also used in the method of "concordant deflections" described below. The finite element method has not advanced much, however, mainly because of the following two reasons:

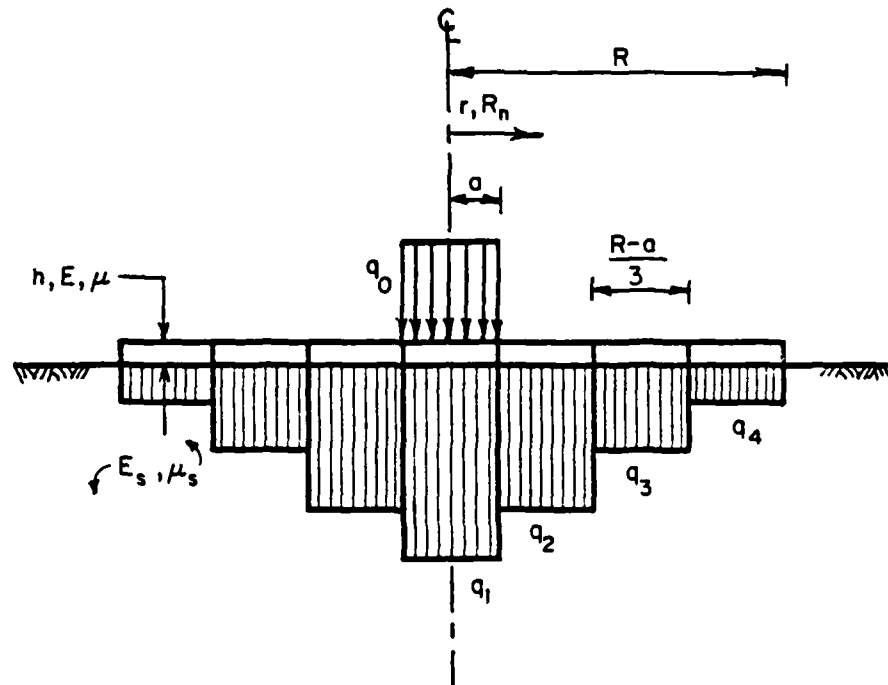
- (a) Computer storage is problematic for all but the coarsest meshes;
- (b) The assumption of stepwise uniform reactions, coupled with (a), sometimes leads to unrealistic contact pressure distributions [154].

This method is examined further in Chapter 9.

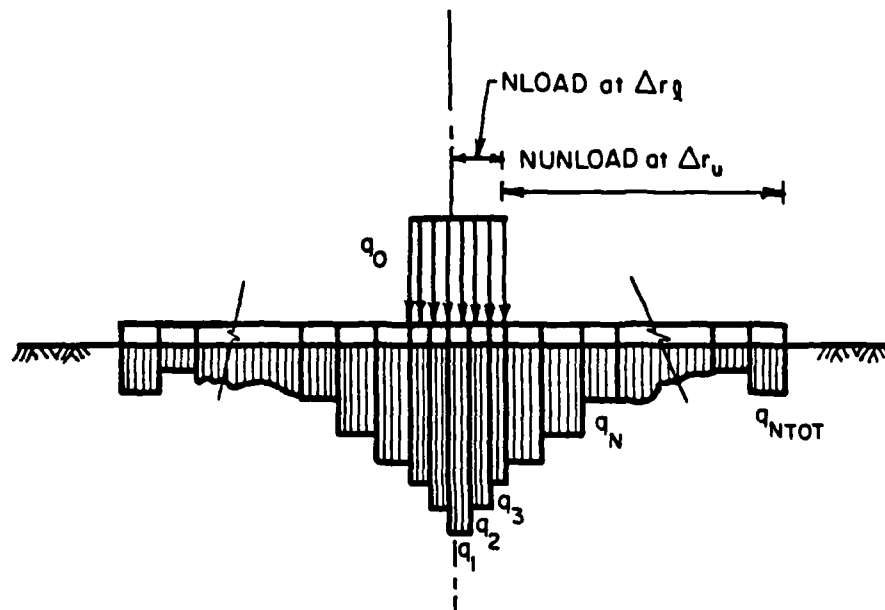
7.3 ANALYTICAL PROCEDURE USING CONCORDANT DEFLECTIONS

In many complex structural engineering problems, an adequate solution can be obtained by dividing the structure into small elements. Figure 7.1(a) illustrates the application of this approach to the problem of a plate resting on an elastic solid foundation [127]. The plate is divided into four elements, the outer three of which are ring-shaped while the central element is circular and has the same radius as the loaded area. The subgrade reaction within each element is assumed to be stepwise uniform, and the corresponding intensities are denoted by q_1 to q_4 , respectively. In the computer program developed in this study [Fig. 7.1(b)] any number of elements can be used, and the load may extend beyond the central core.

Plate and foundation are analyzed separately, and then deflections at the center of each element are matched, according to the method of "concordant deflections". In Bergstrom's scheme [127], the plate is loaded by reactions q_1 to q_4 in an upward direction and by the applied load of intensity q_0 in the downward direction. Similarly, the soil is subjected to the downward reactions q_1 to q_4 only. Four equations are needed for the determination of the magnitude of these reactions. One is the equation of equilibrium between the four reactions and the applied load. The other three are compatibility equations, expressing the equality between the vertical deflections of the plate and those of the soil at the centers of the elements.



(a) Bergstrom's Finite Extent Slab



(b) The Slab in CFES

Fig. 7.1 Slab Discretization for Method of Concordant Deflections

The equation of equilibrium is as follows:

$$\sum_{n=1}^3 2\pi R_n \frac{R-a}{3} q_n = \pi a^2 (q_0 - q_4) \quad (7-1)$$

where:

R : radius of circular plate;

a : radius of circular interior load;

R_n : radius of the median circle in element n ;

q_n : reaction at element n .

The equations of compatibility are derived on the assumption that the plate is always in contact with the subgrade along the median circles of the ring-shaped elements and at the center of the plate. At this point the following notation is introduced:

$w_{n,p}$: denotes the deformation of the plate at the median circle of the element n due to the externally applied loads, and the subgrade reactions. The plate is assumed to be simply supported along its outer edge;

$w_{n,m}$: denotes the deformation of the surface of the soil due to the reactions alone, plate removed.

Using this notation, the general form of the compatibility equation is:

$$w_{4,m} - w_{n,p} = w_{4,p} - w_{n,p} \quad (7-2)$$

For the case shown in Fig. 7.1(a), index n ranges between 1 and 3, thus generating the required three equations of compatibility. Together with the equation of equilibrium given above, they form a system of four simultaneous equations, which upon solution yield the four unknown magnitudes of the subgrade reactions. In writing the equations of compatibility, pairs of deflection differences are matched rather than absolute deflection values, because plate deflections are not absolute in the same sense as are subgrade displacements [121]. Plate deflections are relative to the deflection of the plate edge, assumed to be simply supported in the determination of $w_{n,p}$.

The deformations entering Eqn. (7-2) are determined from an examination of elementary cases of loading, which have been dealt with in the literature. In the case of the elastic solid foundation, loaded by a circular load, Schleicher [155] derived the following expressions for the vertical deflection:

$$\begin{aligned} r \leq a: \quad w_{r,m} &= \frac{4}{\pi} p \frac{a}{C} E\left(\frac{r}{a}, \frac{\pi}{2}\right) \\ r > a: \quad w_{r,m} &= \frac{4}{\pi} p \frac{r}{C} \left[E\left(\frac{a}{r}, \frac{\pi}{2}\right) - \left(1 - \frac{a^2}{r^2}\right) F\left(\frac{a}{r}, \frac{\pi}{2}\right) \right] \end{aligned} \quad (7-3)$$

where:

a : radius of circular load;

p : circular load intensity;

r : radial distance of point under consideration from center of load;

$$C = \frac{E_s}{1-\mu_s};$$

E_s : soil modulus of elasticity;

μ_s : soil Poisson's ratio;

$$F(k, \frac{\pi}{2}) = \int_0^{\pi/2} \frac{d\phi}{\sqrt{1-k^2 \sin^2 \phi}}$$

: complete elliptic integral of first kind;

$$E(k, \frac{\pi}{2}) = \int_0^{\pi/2} \sqrt{1-k^2 \sin^2 \phi} \, d\phi$$

: complete elliptic integral of second kind.

The upper expression in Eqn. (7-3) applies to points located within the loaded area, while the lower is used for a point outside the circular load. The contribution to vertical deflections of the reaction acting on the circular core element is obtained from Eqn. (7-3) directly. The contributions of reactions acting on ring-shaped elements can be computed by superposition, from the difference between loads applied to two adjacent circular elements. In CFES, the computer program developed in this study, elliptic integrals $F(k, \frac{\pi}{2})$ and $E(k, \frac{\pi}{2})$ are evaluated using numerical integration. Subroutine GQU3Z from UOILIB, a library of software developed at the University of Illinois, is used for this purpose. Simpson's 96-point integral rule is employed.

In calculating plate deformations, it is assumed that the plate is simply supported along its circumference. In order to simplify the calculations, the reaction within each ring-shaped element is replaced by a concentrated line acting along the median circle. The effect of

this approximation was found to be insignificant [127]. Thus, the deflection equations in Fig 7.2 may be used [80]. Any meaningful value may be assigned to the elasticity constants for the plate and the soil. A similar procedure gives the values of bending moments (and stresses) in the plate, once reactions are determined. The corresponding moment equations in Fig 7.2 are used [156].

Most matrix algebra operations in CFES are performed using LINPACK routines, a mathematical software package for the solution of linear systems developed between 1976 and 1979 by a project centered at Argonne National Laboratory for Environment Damaging and Research.

7.4 PROGRAM IMPLEMENTATION

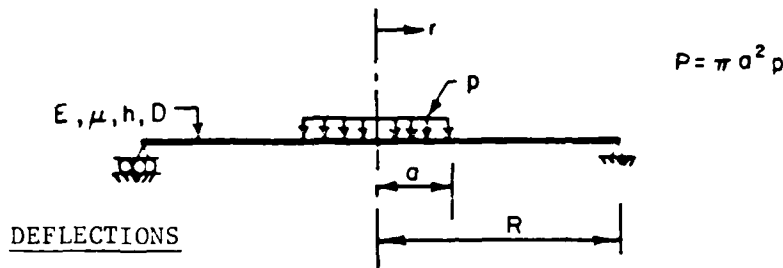
In accordance to the procedure described above, a set of simultaneous equations is sought, which upon solution will yield the primary unknowns, i.e. subgrade reaction under each element. This set of equations will be of the form:

$$[Q] \{REACT\} = \{X\} \quad (7-4)$$

where:

[Q] : Coefficient matrix, (NTOT*NTOT) in dimensions, where NTOT is the total number of loaded plus unloaded elements;

- (a) Uniformly distributed load over central portion of a simply supported plate



$r > a$:

$$w = \frac{P}{16\pi D} \left\{ \frac{(3 + \mu)}{(1 + \mu)} (R^2 - r^2) + 2 r^2 \ln \frac{r}{R} + a^2 \left[\ln \frac{r}{R} - \frac{(1 - \mu)}{2(1 + \mu)} \frac{(R^2 - r^2)}{R^2} \right] \right\}$$

$r = 0$:

$$w = \frac{P}{16\pi D} \left[\frac{(3 + \mu)}{(1 + \mu)} R^2 + a^2 \ln \frac{a}{R} - \frac{(7 + 3\mu)}{4(1 + \mu)} a^2 \right]$$

BENDING MOMENTS

$r = 0$:

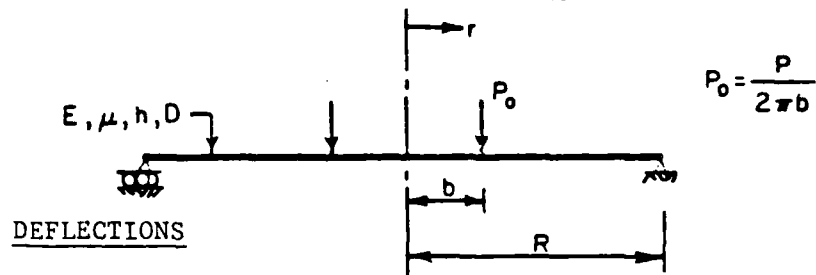
$$M_r = M_\theta = \frac{P}{4\pi} \left[(1 + \mu) \ln \frac{R}{a} + 1 - \frac{(1 - \mu) a^2}{4R^2} \right]$$

$r > a$:

$$M_r = \frac{(1 + \mu)}{4\pi} P \ln \frac{R}{r} + \frac{(1 - \mu)}{16\pi} P a^2 \left(\frac{1}{r^2} - \frac{1}{R^2} \right)$$

$$M_\theta = \frac{P}{4\pi} \left[(1 + \mu) \ln \frac{R}{r} + 1 - \mu \right] - \frac{(1 - \mu)}{16\pi} P a^2 \left(\frac{1}{r^2} + \frac{1}{R^2} \right)$$

Fig. 7.2 Equations for Simply Supported Plate

(b) Ring load applied to a simply supported plate $r < b:$

$$w = \frac{P}{8\pi D} \left[(b^2 + r^2) \ln \frac{b}{R} + (R^2 - b^2) \frac{(3 + \mu) R^2 - (1 - \mu) r^2}{2(1 + \mu) R^2} \right]$$

 $r \geq b:$

$$w = \frac{P}{8\pi D} \left[(R^2 - r^2) \left(1 + \frac{1}{2} \frac{(1 - \mu)}{(1 + \mu)} \frac{(R^2 - b^2)}{R^2} \right) + (b^2 + r^2) \ln \frac{r}{R} \right]$$

BENDING MOMENTS $r \leq b:$

$$M_r = M_\theta = (1 - \mu) P \frac{(R^2 - b^2)}{8\pi R^2} - \frac{(1 + \mu)}{4\pi} P \ln \frac{b}{R}$$

 $r > b:$

$$M_r = \frac{P}{4\pi} (1 + \mu) \ln \frac{R}{r} - \frac{P}{8\pi} (1 - \mu) b^2 \left(\frac{1}{R^2} - \frac{1}{r^2} \right)$$

$$M_\theta = \frac{P}{4\pi} \left[(1 + \mu) \ln \frac{R}{r} + (1 - \mu) \right] - \left[\frac{P}{8\pi} (1 - \mu) b^2 \left(\frac{1}{r^2} + \frac{1}{R^2} \right) \right]$$

$$\sigma_{r,\theta} = \frac{6 M_{r,\theta}}{h^2}$$

Fig. 7.2 (continued)

{REACT}: vector of NTOT subgrade reactions,

$$= \begin{Bmatrix} q_1 \\ q_2 \\ \vdots \\ q_{NTOT} \end{Bmatrix} ;$$

{X} : right-hand side vector, NTOT long.

The first equation in this set is the equilibrium equation.

Equation (7-1) may be rewritten as:

$$\pi \left(\frac{\Delta r_\ell}{2} \right)^2 q_1 + \sum_{i=2}^{i=NTOT} 2\pi r_i \Delta r_i q_i =$$

$$\pi \left(\frac{\Delta r_\ell}{2} \right)^2 p_1 + \sum_{j=2}^{j=NLOAD} 2\pi r_j \Delta r_\ell p_j \quad (7-5)$$

where:

Δr_ℓ : width of each loaded element (Note: the inner core width (radius) is $\Delta r_\ell / 2$);

Δr_i : width of element i. This varies depending on the position of the element, and may be equal to Δr_ℓ or Δr_u , where Δr_u is the width of each unloaded element;

r_i : radial distance to the median circle of element i;

q_i : subgrade reaction under element i;

p_j : externally applied pressure on element j.

Note that the first term on the left-hand side of Eqn. (7-5) refers to the reaction under the inner core, while the summation gives the reactions under each of the ring elements. Similarly, on the right-hand side of Eqn. (7-5), the first term indicates the load applied on the inner core, while the summation is the contribution of

loads applied ring-shaped elements. In Bergstrom's formulation [127] this last summation is omitted.

Since all applied pressures p_i are known, the right-hand side of Eqn. (7-5) is the first element in vector $\{X\}$ of Eqn. (7-4). Writing the left-hand side of Eqn. (7-5) in the form of Eqn. (7-4), readily indicates that the first row of coefficient matrix $[Q]$ consists of $\pi \left(\frac{\Delta r_i}{2} \right)^2$ as its first element, and $(2\pi r_i \Delta r_i)$ as its second through $NTOT$ -th elements. An additional $(NTOT-1)$ equations in Eqn. (7-4) are derived from the compatibility relations as described below.

Since in the analytical procedure plate and subgrade are considered separately, the following flexibility type expressions apply:

$$[SOIL] \begin{Bmatrix} q_1 \\ q_2 \\ \vdots \\ q_{NTOT} \end{Bmatrix} = \begin{Bmatrix} w_{1,m} \\ w_{2,m} \\ \vdots \\ w_{NTOT,m} \end{Bmatrix}$$

$$\text{or } [SOIL]_{NTOT \times NTOT} \{q_A\}_{NTOT} = \{w_m\}_{NTOT} \quad (7-6)$$

$$\text{and } [SLAB] \begin{Bmatrix} (p_1 - q_1) \\ (p_2 - q_2) \\ \vdots \\ (p_{NTOT} - q_{NTOT}) \end{Bmatrix} = \begin{Bmatrix} w_{1,p} \\ w_{2,p} \\ \vdots \\ w_{NTOT,p} \end{Bmatrix}$$

$$\text{or } [SLAB]_{NTOT \times NTOT} \{q_B\}_{NTOT} = \{w_p\}_{NTOT} \quad (7-7)$$

where:

$[SOIL]$: flexibility matrix for soil;

[SLAB] : flexibility matrix for plate;

$\{w_m\}$: vector of soil deflections;

$\{w_p\}$: vector of plate deflections.

Note that $\{q_A\}$ is identical to $\{REACT\}$ in Eqn. (7-4), whereas $\{q_B\}$ is a vector of net pressures on the plate. Unloaded elements in $\{q_B\}$ will reduce to $-q_i$. None of vectors $\{q_A\}$, $\{q_B\}$, $\{w_m\}$ and $\{w_p\}$ are known at this stage.

Each of the rows of flexibility matrix [SOIL] consists of terms evaluated using one of the two expressions in Eqn. (7-3), depending on the position of the element indicated by the subscript of q_i in $\{q_A\}$ (i.e. the column number in [SOIL]). As indicated earlier, when the lower expression in Eqn. (7-3) is used, the flexibility matrix element is obtained by superposition, as the difference between the effect of the reaction q_i applied over i elements, plus the effect of a reaction $-q_i$ applied over $(i-1)$ elements. Item $SOIL(k, l)$ gives the contribution to deflection $w_{k,m}$ at element k , due to a reaction q_l at element l .

Similarly, each term in a given row of flexibility matrix [SLAB] is evaluated through the application of one of the 4 deflection expressions in Fig. 7.2. Item $SLAB(k, l)$ gives the contribution to deflection $w_{k,p}$ at element k , due to a net pressure $(p_l - q_l)$ at element l .

Applying the compatibility Eqn. (7-2) to any element n , the following expression is derived:

$$w_{1,m} - [\text{SOIL},n] \{q_A\} = w_{1,p} - [\text{SLAB},n] \{q_B\}$$

$$\text{or } w_{1,m} - w_{1,p} = -[\text{SLAB},n] \{q_B\} + [\text{SOIL},n] \{q_A\} \quad (7-8)$$

where $[\text{SOIL},n]$ and $[\text{SLAB},n]$ indicate the n th row of $[\text{SOIL}]$ or $[\text{SLAB}]$. Note that both $[\text{SLAB}]$ and $[\text{SOIL}]$ are known at this stage. Now, Eqn. (7-7) may be rewritten as:

$$[\text{SLAB}] \{\text{ELPRS}\} - [\text{SLAB}] \{q_A\} = \{w_p\}$$

$$\text{or } \{\text{WEXTSLB}\} - [\text{SLAB}] \{q_A\} = \{w_p\} \quad (7-9)$$

where:

$\{\text{ELPRS}\}$: the vector of externally applied element pressures
(known);

$\{\text{WEXTSLB}\} = [\text{SLAB}] \{\text{ELPRS}\},$
: plate deflections due to externally applied pressures
(known).

Introducing Eqn. (7-9) into Eqn. (7-8) yields:

$$w_{1,m} - w_{1,p} = -\text{WEXTSLB}(n) [\text{SLAB},n + \text{SOIL},n] \{q_A\} \quad (7-10)$$

where:

$\text{WEXTSLB}(n)$: n th element in vector $\{\text{WEXTSLB}\};$

$[\text{SLAB},n + \text{SOIL},n]$: row vector that results from the addition of
the n th rows of $[\text{SLAB}]$ and $[\text{SOIL}]$.

Note that Eqn. (7-10) applies to all values of n , since $(w_{1,m} - w_{1,p})$ is a constant. Thus, the right-hand side of Eqn. (7-10) derived for one value of n is equal to that derived for any other. For example, Eqn. (7-10) may be rewritten as:

$$-WEXTSLB(1) + [SLAB, 1 + SOIL, 1] \{q_A\} = \\ WEXTSLB(n) + [SLAB, n + SOIL, n] \{q_A\}$$

$$\text{or } [SLAB, 1 + SOIL, 1] - [SLAB, n + SOIL, n] \{q_A\} = \\ WEXTSLB(1) - WEXTSLB(n) \quad (7-11)$$

where $n \neq 1$.

This form gives rise to $(NTOT-1)$ equations, as required. Noting again that $\{q_A\}$ and $\{REACT\}$ are identical, Eqn. (7-11) may be used directly to complete the equation set in Eqn. (7-4). Upon solution, this set yields the vector of subgrade reactions under each element.

Having solved for the reactions in Eqn. (7-4), the vectors of plate and soil deflections may be recovered by application of Eqns. (7-6) and (7-7). Note that $\{w_m\}$ and $\{w_p\}$ are not identical, but

$$w_m(i) - w_p(i) = \text{constant}$$

for all i . This constant is equal to soil deflection at the circumference of the plate, which is assumed to be simply supported when the plate is analyzed separately. Thus, as noted above, only

$\{w_m\}$ are absolute deflections, while $\{w_p\}$ are merely relative deflections.

The final task is to calculate bending moments and stresses in the plate. This is achieved by performing the summations:

$$M_{ri} = \sum_{j=1}^{NTOT} \Delta M_{r i,j}$$

$$\text{and } M_{\theta i} = \sum_{j=1}^{NTOT} \Delta M_{\theta i,j} \quad (7-12)$$

where:

$M_{ri}, M_{\theta i}$: radial and circumferential moments at the median circle of element i , respectively;

$\Delta M_{ri,j}, \Delta M_{\theta i,j}$: contribution to these moments of the net pressure $(p_j - q_j)$ acting over element j , obtained from the moment expressions in Fig. 7.2.

7.5 PROGRAM VALIDATION

In order to check the performance of the program a series of validation runs were conducted, the results of which are presented in this section. The following effects were investigated:

(a) Plate Size : According to theory, plate response should approach asymptotically the response of an infinite plate, as plate

size is increased. The infinite plate response is given by the equations in Table 7.1;

(b) Element Size: Theoretically, the exact solution should be approached as the plate is divided into more and more elements;

(c) Element Distribution: CFES allows any number of elements to be used under the load, as well as beyond the load. Thus, the total number of elements used in a given run is the sum of NLOAD (number of loaded elements) and NUNLOAD (number of unloaded elements). The size of loaded elements (Δr_l) need not be the same as the size of unloaded elements, (Δr_u). This allows increased element fineness under the load;

(d) Size of Loaded Area: The applicability of CFES and/or the closed-form equations in Table 7.1, for a range of loaded area sizes was examined. This factor was found to be important in Chapter 5 in connection with the dense liquid finite element solution.

For the plate size investigation, a plate with a medium radius of relative stiffness ($\ell_e = 47$ in.) was selected. A fairly small loaded area was used to eliminate any possible area effects. Table 7.2 shows that central deflection and subgrade stress converge to an infinite plate response from above. This "punch-like" behavior is characteristic of short slabs, and has also been observed in dense liquid solutions. On the other hand, central bending stress converges from below, as expected, and is much less sensitive to the plate size effect than deflection and subgrade stress. Both bending stress and deflection converge to about 100% of the values predicted by the

TABLE 7.2
EFFECT OF PLATE SIZE

NUNLOAD	R (in.)	(R/ℓ_e)	δ (mils)	q (psi)	σ (psi)
3	67.68	1.44	11.4	0.32	82.04
5	110.76	2.35	10.2	0.30	85.47
7	153.84	3.27	9.9	0.30	84.67
11	240.00	5.10	9.6	0.29	84.22
22	476.94	10.13	9.5	0.29	84.26
33	713.88	15.16	9.5	0.29	84.26
CLOSED-FORM SOLUTION			9.6	0.25	84.57

Notes:

Parameters Used:

$$E = 3 \times 10^6 \text{ psi}$$

$$E_s = 2000 \text{ psi}$$

$$\mu = 0.15$$

$$\mu_s = 0.45$$

$$h = 8 \text{ in.}$$

$$\ell_e = 47.09 \text{ in.}$$

$$P = 2941.7 \text{ lbs}$$

$$a = 3.06 \text{ in.}$$

$$p = 100 \text{ psi}$$

$$\text{NLOAD} = 1$$

$$\Delta r_l = 6.12 \text{ in.}$$

$$\Delta r_u = 21.54 \text{ in.}$$

equations in Table 7.1. A discrepancy is observed in the case of subgrade stress. As will be shown below, about 60% of this discrepancy is due to inadequate unloaded element fineness, and the rest to inadequate loaded element fineness. This effect apart, Fig. 7.3 shows that for deflection and subgrade stress an (R/ℓ_e) ratio of about 5.0 is required for the infinite plate response. The required value of (R/ℓ_e) for bending stress is only about 2.0.

To investigate the effect of element size, one of the cases in Table 7.2 was selected and the number of unloaded elements (NUNLOAD) varied. The results are tabulated in Table 7.3. Note that in all these runs, one loaded element was used (NLOAD=1). Significant improvement in the solution is observed as the element size becomes smaller. Subgrade stress converges from above (Fig. 7.4) and is much more sensitive to element size than deflection and bending stress. The latter converge from below. Expressed in terms of the non-dimensional ratio $(\Delta x_u/\ell_e)$, the element size requirements for a good solution may be stated as follows:

For subgrade stress : $(\Delta x_u/\ell_e) \approx 0.2$

For deflection : $(\Delta x_u/\ell_e) \approx 0.6$

For bending stress : $(\Delta x_u/\ell_e) \approx 1.5$

Next, the effect of varying the number of loaded elements (NLOAD) was considered for one of the cases in Tables 7.2 and 7.3. Table 7.4 shows the results obtained in this way. It is seen that subgrade

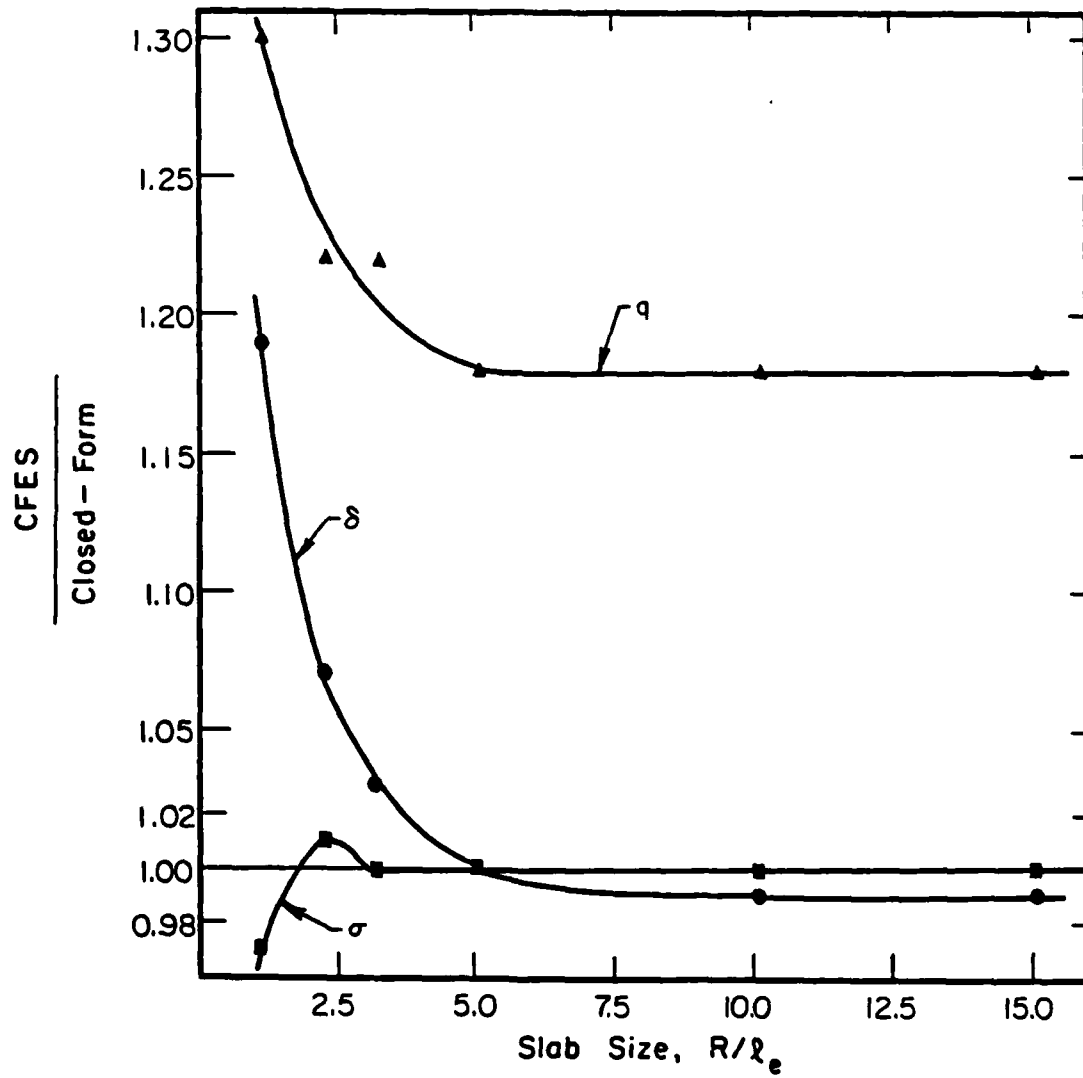


Fig. 7.3 Effect of Slab Size

TABLE 7.3
EFFECT OF SIZE OF UNLOADED ELEMENTS

NUNLOAD	Δr_u (in.)	$(\Delta r_u / \ell_e)$	δ (mils)	q (psi)	σ (psi)
3	78.98	1.68	9.2	0.76	84.69
6	39.49	0.84	9.5	0.39	83.94
9	26.33	0.56	9.6	0.31	84.13
11	21.54	0.46	9.6	0.29	84.22
15	15.80	0.34	9.6	0.27	84.33
20	11.80	0.25	9.6	0.26	84.40
CLOSED-FORM SOLUTION			9.6	0.25	84.57

Notes:

Parameters Used:

$$E = 3 \times 10^6 \text{ psi}$$

$$E_s = 2000 \text{ psi}$$

$$\mu = 0.15$$

$$\mu_s = 0.45$$

$$h = 8 \text{ in.}$$

$$\ell_e = 47.09 \text{ in.}$$

$$P = 2941.7 \text{ lbs}$$

$$a = 3.06 \text{ in.}$$

$$p = 100 \text{ psi}$$

$$\text{NLOAD} = 1$$

$$\Delta r_\ell = 6.12 \text{ in.}$$

$$R = 240 \text{ in.}$$

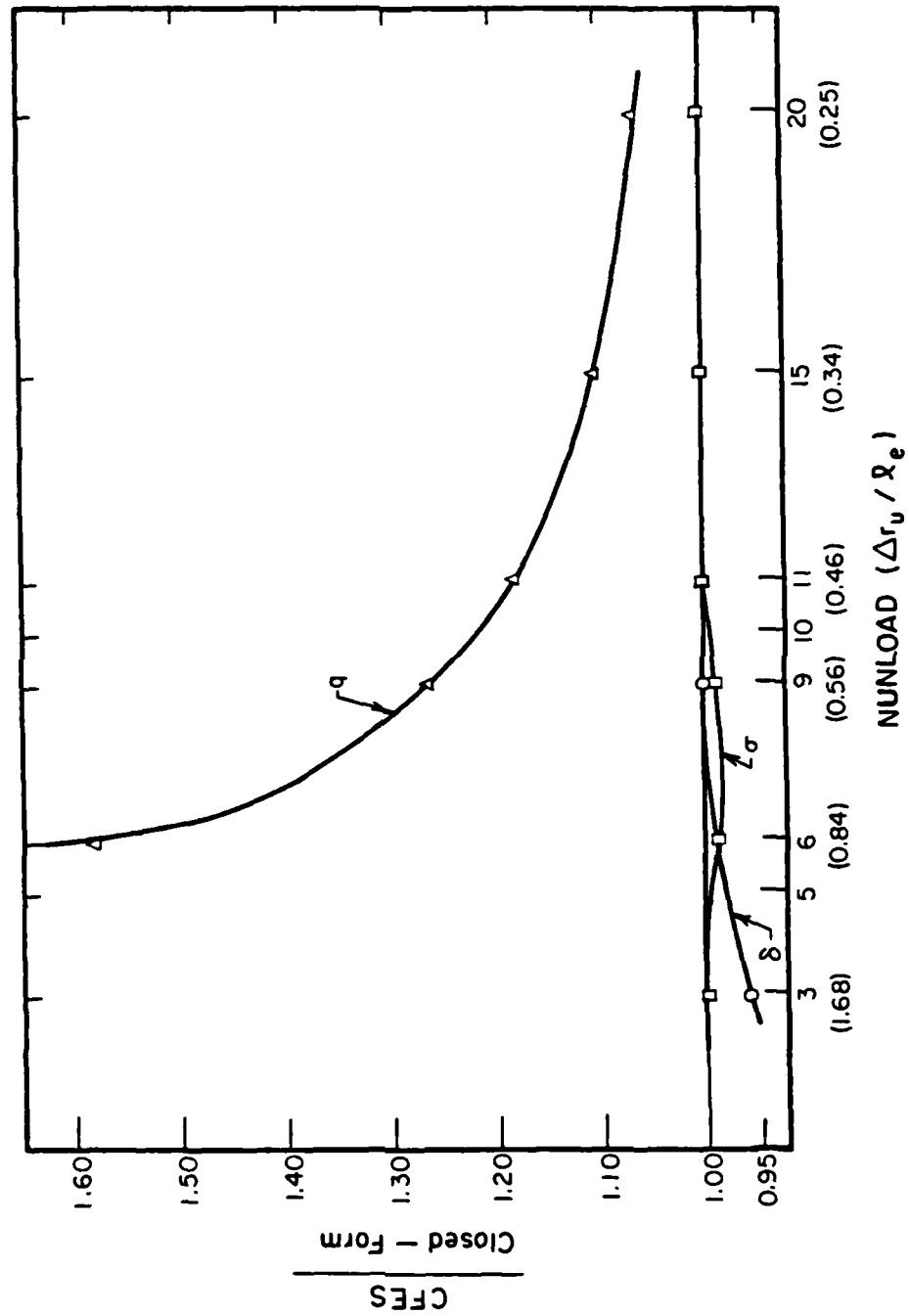


Fig. 7.4 Effect of Unloaded Element Size

TABLE 7.4
EFFECT OF SIZE OF LOADED ELEMENTS (I)

NLOAD	Δr_{ℓ} (in.)	$(\Delta r_{\ell} / \ell_e)$	δ (mils)	q (psi)	σ (psi)
1	6.12	0.13	9.6	0.29	84.22
2	2.04	0.04	9.6	0.27	85.17
3	1.22	0.03	9.6	0.27	84.73
4	0.87	0.02	9.6	0.27	84.53
5	0.68	0.01	9.6	0.27	84.53
CLOSED-FORM SOLUTION			9.6	0.25	84.57

Notes:

Parameters Used:

$$E = 3 \times 10^6 \text{ psi}$$

$$E_s = 2000 \text{ psi}$$

$$\mu = 0.15$$

$$\mu_s = 0.45$$

$$h = 8 \text{ in.}$$

$$\ell_e = 47.09 \text{ in.}$$

$$P = 2941.7 \text{ lbs}$$

$$a = 3.06 \text{ in.}$$

$$p = 100 \text{ psi}$$

$$\text{NUNLOAD} = 11$$

$$\Delta r_u = 21.54 \text{ in.}$$

$$R = 240 \text{ in.}$$

stress converges from above at a $(\Delta r_\ell / \ell_e)$ value of about 0.08. Thus, a more stringent fineness requirement applies to the loaded region (cf. paragraph 5.3.7). This effect was also studied for a plate with low relative stiffness ($\ell_e = 28$ in.) and the results are shown in Table 7.5. The general conclusions reached above are confirmed. Deflection and bending stress are again largely insensitive to the size of loaded elements.

To test the validity of the guidelines established above, a large slab ($R/\ell_e = 13.25$) divided into small elements ($\frac{\Delta r_\ell}{\ell_e} = 0.025$; $\frac{\Delta r_u}{\ell_e} = 0.26$) was used to investigate the agreement between CFES and the equations in Table 7.1 for a range of loaded area sizes. The ratio (a/ℓ_e) -where a is the radius of the loaded area- varied between 0.044 and 0.44. As shown in Table 7.6, agreement is perfect throughout this range, for all three responses.

7.6 INVESTIGATION OF SUBGRADE CONTACT PRESSURES UNDER SLABS-ON-GRADE

To demonstrate the applicability of the program developed in this study to practical problems related to the design of slab-on-grade type pavements, analyses were performed to examine the distribution of surface subgrade stresses under such pavements. Results presented by Chou [46] indicated that "at the slab edge the subgrade pressure abruptly increases manyfold" and that "this phenomenon becomes more significant when the E/E_g ratio increases." According to Chou, this effect is relatively more pronounced for a "slab under its own weight",

TABLE 7.5
EFFECT OF SIZE OF LOADED ELEMENTS (II)

NLOAD	Δr_{λ} (in.)	$(\Delta r_{\lambda} / \ell_e)$	δ (mils)	q (psi)	σ (psi)
1	25.00	0.883	21.2	8.84	392.75
2	8.33	0.294	21.2	9.44	401.33
4	3.57	0.126	21.2	9.26	395.97
6	2.27	0.080	21.2	9.23	394.56
9	1.47	0.052	21.2	9.21	393.82
13	1.00	0.035	21.2	9.21	393.47
18	0.71	0.025	21.2	9.21	393.30
CLOSED-FORM SOLUTION			21.2	9.21	394.21

Notes:

Parameters Used:

$$E = 4 \times 10^6 \text{ psi}$$

$$E_s = 24000 \text{ psi}$$

$$\mu = 0.15$$

$$\mu_s = 0.45$$

$$h = 10 \text{ in.}$$

$$\ell_e = 28.30 \text{ in.}$$

$$P = 9087.4 \text{ lbs}$$

$$a = 12.50 \text{ in.}$$

$$p = 100 \text{ psi}$$

$$\text{NUNLOAD} = 50$$

$$\Delta r_u = 7.25 \text{ in.}$$

$$R = 375 \text{ in.}$$

TABLE 7.6
COMPARISON BETWEEN CFES AND CLOSED-FORM SOLUTIONS

NLOAD	a (in.)	Δr_{ℓ} (in.)	Δr_u (in.)	δ (mils)		q (psi)		σ (psi)	
				CFES	THEORY	CFES	THEORY	CFES	THEORY
2	1.25	0.83	7.48	0.2	0.2	0.12	0.12	10.16	10.07
4	2.50	0.71	7.45	0.9	0.9	0.46	0.45	32.90	32.82
6	3.75	0.68	7.43	2.0	2.0	0.99	0.99	64.10	64.05
8	5.00	0.67	7.40	3.5	3.5	1.72	1.71	101.56	101.54
12	7.50	0.65	7.35	7.8	7.8	3.67	3.66	189.60	189.67
16	10.00	0.65	7.30	13.7	13.8	6.20	6.20	288.65	288.97
18	12.50	0.71	7.25	21.2	21.2	9.21	9.21	393.30	394.21

Notes:

Parameters Used:

$E = 4 \times 10^6$ psi
 $\nu = 0.15$
 $h = 10$ in.
 $E_s = 24000$ psi
 $\mu_s = 0.45$
 $\ell_e = 28.30$ in.
 $p = 100$ psi
 $R = 375$ in.
 $NUNLOAD = 50$

i.e. a slab loaded over its entire surface, although it is observed in cases of interior loading as well. Chou also pointed out that the increase in contact pressure under the edge of a fairly stiff slab, is similar in nature to the theoretically infinite stresses that develop under the edges of a rigid punch.

Chou's results were obtained using WESLAYER, a finite element program for a plate on elastic solid foundation. A piecewise uniform approximation to the subgrade stress is assumed in WESLAYER, as in CFES. The F.E.M. has been successfully applied to numerous structural engineering problems, including the analysis of pavements on dense liquid foundation. In the case of a plate on an elastic solid foundation, however, severe implementation problems arise. Accurate application of the method requires a large number of elements which, in turn, taxes the computer system, often beyond its capacity. As a result, a coarse mesh is usually adopted: Chou used seven elements for the half-width of his 25 X 25-ft. slab. Additional comments are made by this author in a discussion of Chou's paper [46]. Since CFES can easily accommodate 50 or 60 elements (or more) along the slab radius, it is considered ideal for the investigation of the phenomenon described by Chou.

For the case of a plate loaded by its self-weight alone, Table 7.7 shows a comparison of the results presented by Chou and those obtained using CFES with a mesh of similar coarseness. WESLAYER generally underestimates subgrade stress compared to CFES, except at the plate edge. Note that CFES calculates the subgrade stress at a point just

TABLE 7.7

COMPARISON WITH WESLAYER: SLAB SELF-WEIGHT ONLY

Node or Element	E/E _s =10 ($l_e=17.37$ in.)		E/E _s =100 ($l_e=37.42$ in.)		E/E _s =1000 ($l_e=80.61$ in.)		E/E _s =1000 ($l_e=173.67$ in.)	
	WESLAYER	CFES	WESLAYER	CFES	WESLAYER	CFES	WESLAYER	CFES
1	1.40	1.78	1.41	1.77	1.05	1.25	0.75	0.97
2	1.40	1.78	1.40	1.75	1.04	1.25	0.75	0.98
3	1.40	1.79	1.37	1.72	1.04	1.25	0.77	1.02
4	1.39	1.79	1.32	1.65	1.03	1.26	0.82	1.08
5	1.36	1.76	1.28	1.57	1.08	1.32	0.94	1.21
6	1.36	1.61	1.40	1.48	1.42	1.43	1.39	1.43
7	1.14	1.81	1.16	2.23	1.18	2.88	1.16	3.17
8	3.20		5.50		7.87		9.00	

Notes: Parameters Used:E = 4×10^6 psi $\mu = 0.15$

h = 16 in.

 $\mu_s = 0.5$ $\gamma = 150$ pcf
concrete

p = 1.77 psi

R = 150 in.

a = 150 in.

NLOAD = 7

NUNLOAD = 0

 $\Delta r_2 = 23.08$ in.

inside the slab edge, not at the edge itself. The discussion of the F.E.M. for a dense liquid in Chapter 5, showed that both large element size and high element aspect ratios, as used by Chou, may lead to underestimation of stresses and deflections.

To better examine the effect of element size in the case of CFES, the most severe case in Table 7.7 was analyzed using an increasing number of elements. The results in Table 7.8 show that the edge subgrade stress increases considerably with the number of elements used, as the last stress calculation point moves toward the physical edge of the plate. Note, however, that the stress at 5-in. from the plate edge is fairly low and does not vary much with element size. This suggests that the effect of high subgrade stresses at the edge is limited to a very narrow zone. Subgrade stress at the center is fairly insensitive to changes in the number of elements used.

Furthermore, it should be noted the extreme values of (E/E_s) examined by Chou are only of academic interest. Slabs having a radius of relative stiffness of 174 in. or an (R/ℓ_e) ratio of 0.86 are very rarely encountered in practice. Ranges of 15 to 50 in. for ℓ_e and 2 to 4 or more for (R/ℓ_e) would be more realistic. It is in the case of the more extreme values that high edge stresses are predicted by theory.

Table 7.9 shows the results of an examination of the effect of the soil Poisson's ratio on subgrade stress under a fully loaded plate. In the range of μ_s values of 0.2 to 0.5 considered, subgrade stress is insensitive to μ_s .

TABLE 7.8
SUBGRADE STRESSES: EFFECT OF ELEMENT SIZE

NLOAD	q_{center} (psi)	q_{edge} (psi)	$q_{\text{5-in. from edge}}$ (psi)
7	0.97	3.17	3.66
15	0.95	4.58	4.62
30	0.95	6.44	4.66
45	0.94	7.87	3.46
60	0.94	9.08	3.52

Notes:

(a) Parameters Used:

$$E = 4 \times 10^6 \text{ psi}$$

$$E/E_s = 10,000$$

$$\mu = 0.15$$

$$\mu_s = 0.5$$

$$h = 16 \text{ in.}$$

$$l_e = 173.67 \text{ in.}$$

$$\gamma_{\text{concrete}} = 150 \text{ pcf}$$

$$p = 1.77 \text{ psi}$$

$$R = 150 \text{ in.}$$

$$a = 150 \text{ in.}$$

$$\text{NUNLOAD} = 0$$

(b) Self-weight only;

q_{edge} is the stress at the last point of computation,
just inside the slab edge;

$q_{\text{5-in. from edge}}$ obtained by extrapolation or
interpolation.

TABLE 7.9
EFFECT OF SOIL POISSON'S RATIO

μ_s	l_e (in.)	q_{center} (psi)	q_{edge} (psi)
0.5	173.67	0.94	7.87
0.4	180.35	0.94	7.88
0.3	185.23	0.93	7.90
0.2	188.56	0.93	7.90

Notes:

(a) Parameters Used:

$E = 4 \times 10^6$ psi	$p = 1.77$ psi
$\mu = 0.15$	$R = 150$ in.
$h = 16$ in.	$a = 150$ in.
$E/E_s = 10,000$	NUNLOAD = 0
$\gamma_{concrete} = 150$ pcf	NLOAD = 45

(b) Self-weight only:

q_{edge} is the stress at the last point of computation, just inside the slab edge.

Results obtained by Chou for aircraft interior loading alone were also examined. Table 7.10 shows these together with comparable CFES results using a similar mesh. The B747-F configuration is modeled in CFES by a single circular load of radius 17.7 in. loaded by a pressure of 185.5 psi, i.e. the size of loaded area, pressure and total applied load used by Chou are retained. This representation is slightly more severe than that used in WESLAYER, and may be expected to give somewhat higher stresses and deflections at the interior of the slab. As shown in Figures 7.5 and 7.6, WESLAYER generally underestimates subgrade stress compared to CFES, with the exception again of the edge region. To satisfy equilibrium, integration of subgrade stress distributions from both CFES and WESLAYER should give the total applied load of 182.6 kips. An integration performed for the CFES results confirmed that this program satisfies equilibrium. On the other hand, complete subgrade stress distribution under the entire slab was not available for WESLAYER. The areas under the WESLAYER curves in Figures 7.5 and 7.6, however, are substantially smaller than the corresponding areas under the CFES curves. This suggests that WESLAYER may not satisfy equilibrium, or that some other error is involved in Chou's results.

To fine-tune the response in the edge region, additional analyses were performed using more elements (Table 7.11). It is observed that as element size decreases, edge subgrade stress increases. Note again, however, that high edge subgrade stresses occur only in a narrow zone (Fig. 7.7) for plates of high relative stiffness. As Chou pointed out, the effect is not as pronounced here, as for the uniformly distributed

TABLE 7.10

COMPARISON WITH WESLAYER: AIRCRAFT LOADING ONLY

Radial Distance (in.)	$E_s=41000$ psi ($\ell_e=37.11$ in.)	$E_s=15000$ psi ($\ell_e=51.88$ in.)	$E_s=7000$ psi ($\ell_e=66.89$ in.)
-----------------------------	--	--	---

(a) Distributions of q by WESLAYER

0	10.6	7.1	5.0
25.0	9.0	6.3	4.6
50.0	6.5	5.1	4.1
75.0	3.5	3.1	3.0
100.0	1.75	2.2	2.0
125.0	0.75	1.5	1.5
150.0	-2.7	0.0	2.75

(b) Distributions of q by CFES

0	20.32	11.55	7.38
11.8	19.07	11.06	7.14
28.7	12.90	8.49	5.86
50.8	7.31	5.86	4.45
72.8	4.04	3.98	3.36
94.9	2.16	2.62	2.50
116.9	0.99	1.56	1.81
139.0	-1.27	-0.17	1.29

Notes:

Parameters Used:

$$E = 4 \times 10^6 \text{ psi} \qquad a = 17.70 \text{ in.}$$

$$\mu = 0.15 \qquad p = 185.5 \text{ psi}$$

$$\mu_s = 0.5 \qquad \text{or B-747F aircraft}$$

$$h = 16 \text{ in.} \qquad \text{NLOAD} = 2$$

$$R = 150 \text{ in.} \qquad \text{NUNLOAD} = 6$$

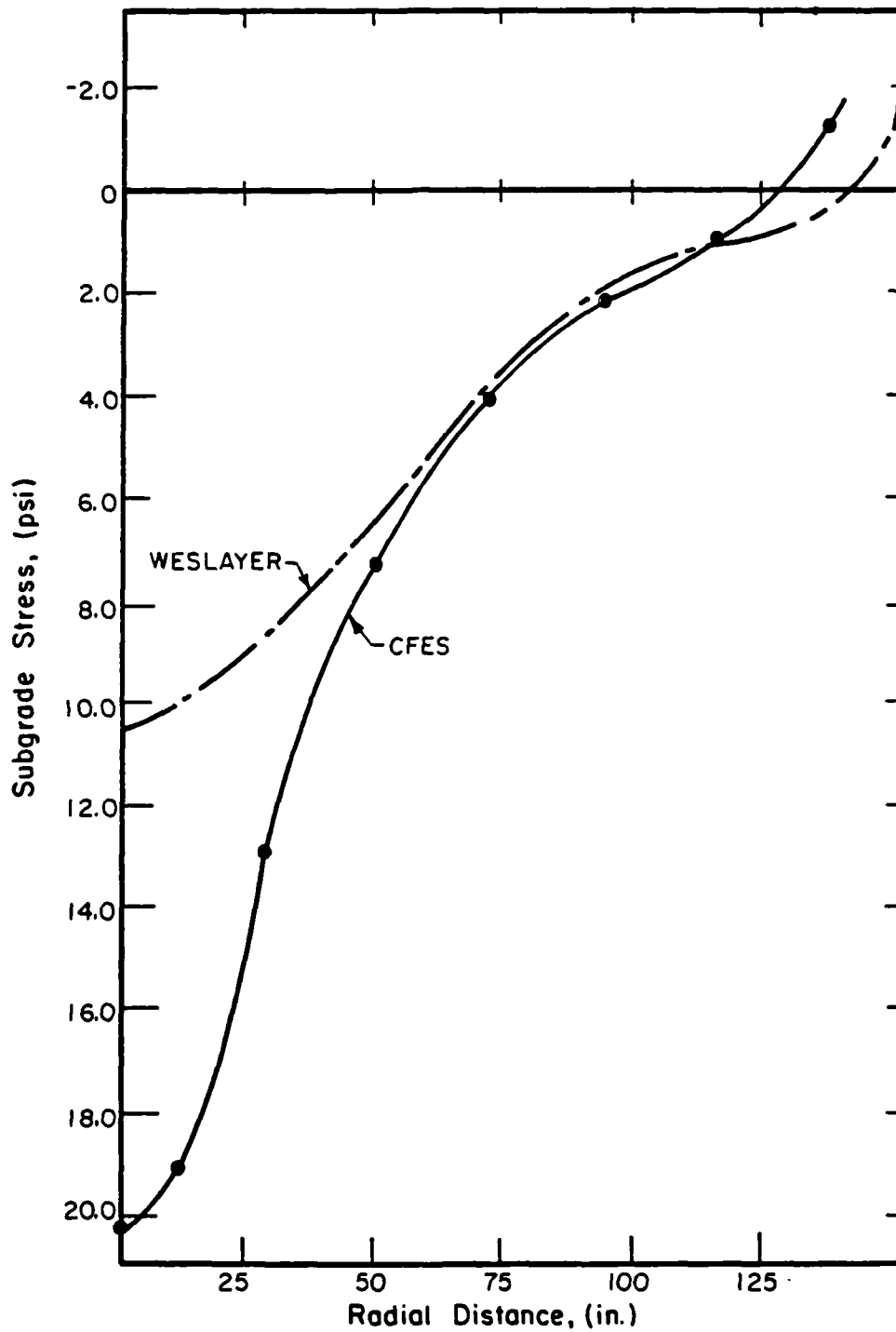


Fig. 7.5 Comparison of CFES and WESLAYER Subgrade Stress Distributions
(B-747F Aircraft; $E_s=41,000$ psi)

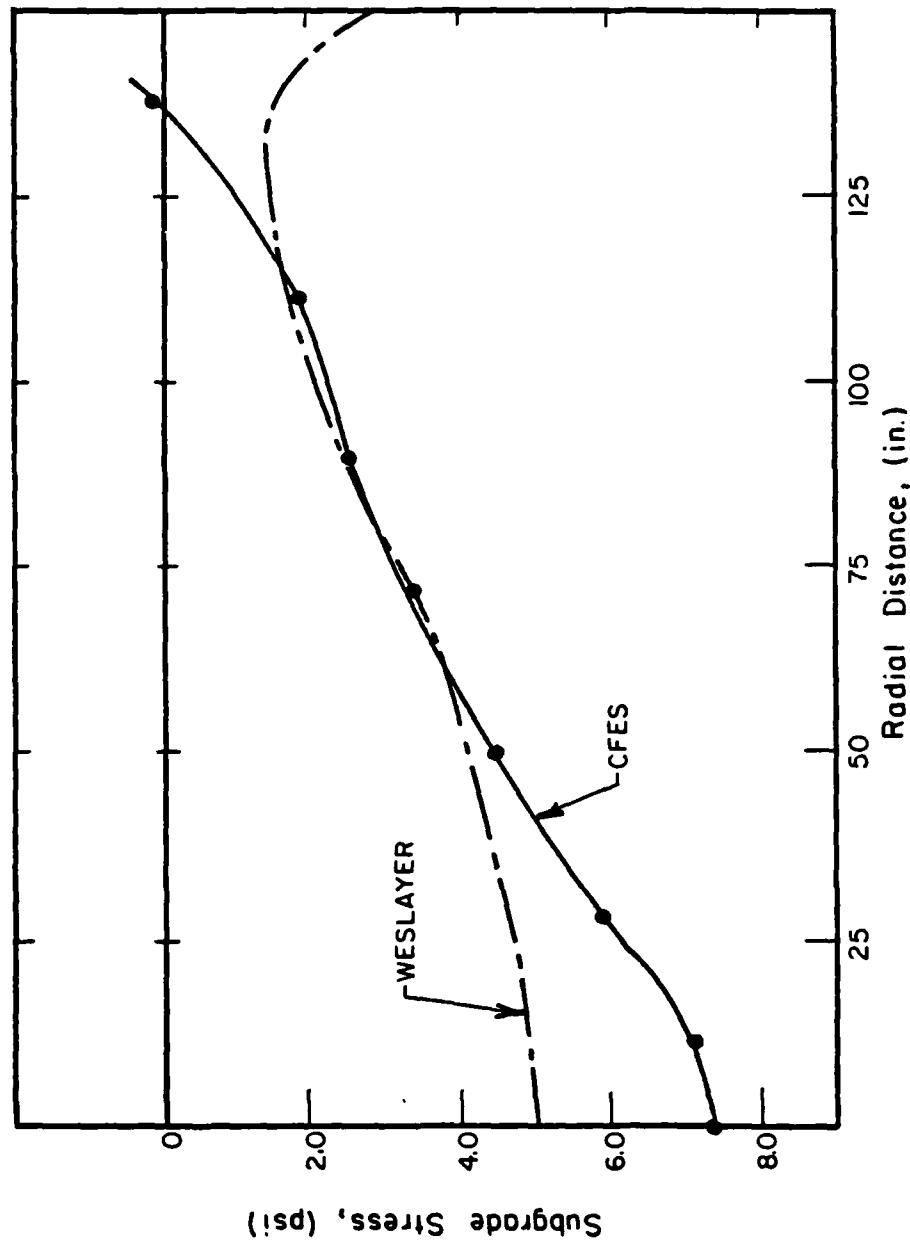


Fig. 7.6 Comparison of CFES and WESLAYER Subgrade Stress Distributions
(B-747F Aircraft; $E_s = 7,000$ psi)

TABLE 7.11
EFFECT OF ELEMENT SIZE

NLOAD	NUNLOAD	$E_s = 41000 \text{ psi}$ ($\lambda_e = 37.11 \text{ in.}$)		$E_s = 7000 \text{ psi}$ ($\lambda_e = 66.89 \text{ in.}$)	
		q_{center} (psi)	q_{edge} (psi)	q_{center} (psi)	q_{edge} (psi)
2	6	20.32	-1.27	7.38	1.49
4	15	19.92	-2.62	7.30	1.27
4	30	19.91	-3.99	7.31	1.44
4	45	19.91	-5.01	7.31	1.62

Notes:

(a) Parameters Used:

$E = 4 \times 10^6 \text{ psi}$ $R = 150 \text{ in.}$ $a = 17.70 \text{ in.}$
 $\mu = 0.15$ $\mu_s = 0.5$ $p = 185.5 \text{ psi}$
 $h = 16 \text{ in.}$ or B-747F aircraft

(b) Aircraft Loading only;

q_{edge} is the stress at the last point of computation
 just inside the slab edge.

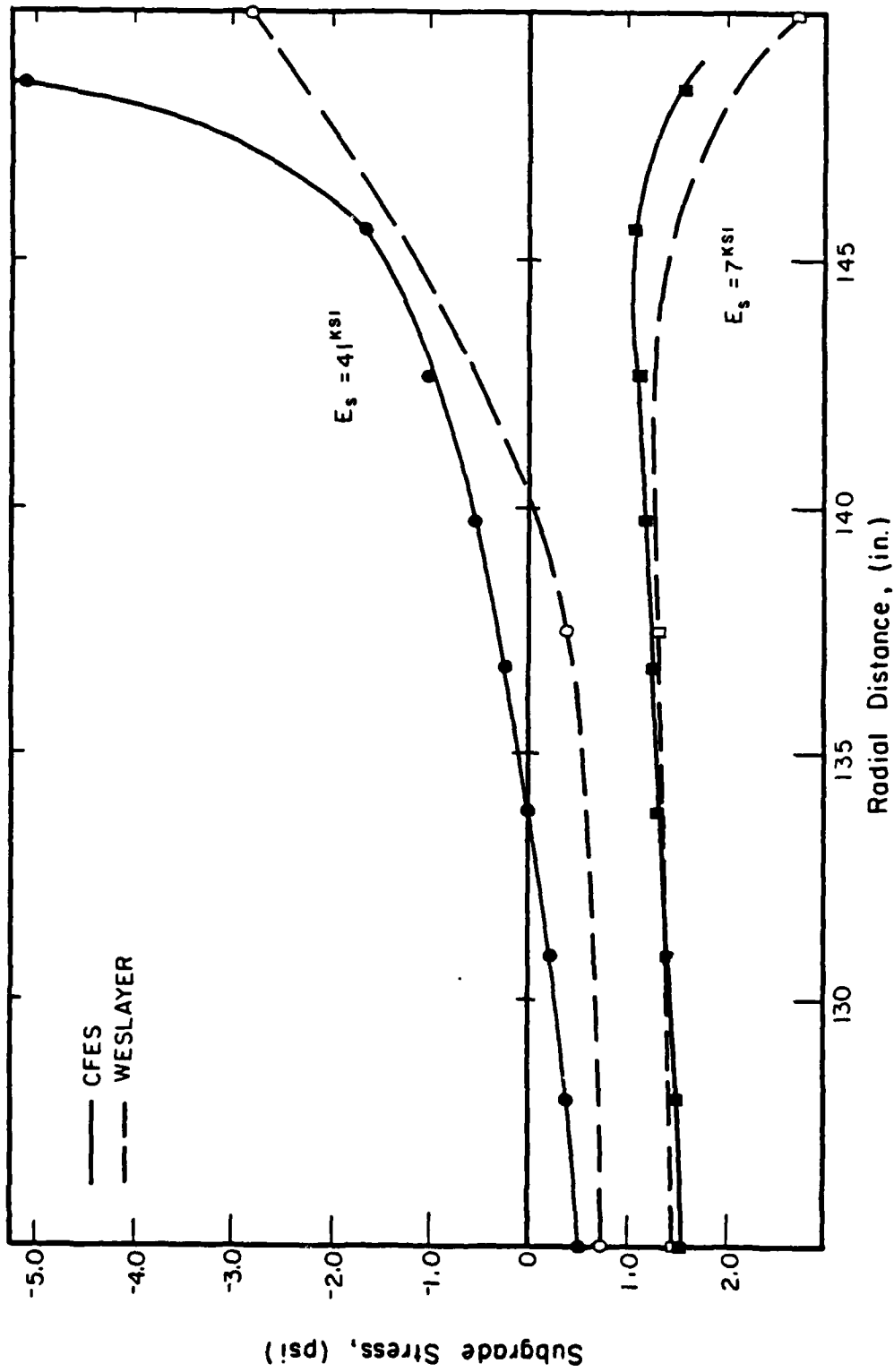


Fig. 7.7 Comparison of Subgrade Stress Distributions Near Edge
(B-747F Aircraft)

load (self-weight only).

Other possible applications of CFES include the analysis of foundation rafts and footings, floor slabs, etc. The program is extremely easy to use, permits multiple analyses to be performed in a single run and accepts free-form input data, consisting of one line per analysis. The input guide for CFES is presented in Appendix A. The output from CFES consists of distributions of surface deflections, subgrade stresses, bending moments and bending stresses in the slab. Typical execution times (50-60 elements) are of the order of 5 CPU seconds on the CDC-CYBER 174 system.

CHAPTER 8

A COMPUTERIZED CHART FOR EDGE LOADING
OF PLATE ON ELASTIC SOLID FOUNDATION

8.1 INTRODUCTION

In this Chapter, the study of the problem of a plate on an elastic solid foundation, initiated in Chapter 7, will be continued. It was noted earlier that the elastic solid or Boussinesq half-space provides a more realistic representation of the subgrade than the Winkler model. It is also generally accepted that the edge loading condition is more critical, at least with respect to slab bending stresses, than the interior condition. The use of load transfer systems has increased the need for analyses of slabs loaded near edges or joints.

The investigation presented in this Chapter belongs to the group of computerized numerical analyses, called "Numerical Integration Techniques" in Chapter 3. It constitutes an attempt to provide an analytical solution to the problem of an infinite plate on an elastic solid foundation loaded by an edge load. Note that the word "infinite" is used loosely in the case of a plate under edge or corner loading, in conformity with earlier literature. A closed-form solution for edge loading has evaded researchers for several decades, even to the present day. The availability of high speed computers, however, capable of performing an extremely large number of numerical integrations with relative ease, has opened new possibilities in this respect. The

AD-A150 965

ANALYSIS OF SLABS-ON-GRADE FOR A VARIETY OF LOADING AND
SUPPORT CONDITION. (U) ILLINOIS UNIV AT URBANA DEPT OF
CIVIL ENGINEERING A M IOANNIDES ET AL. DEC 84

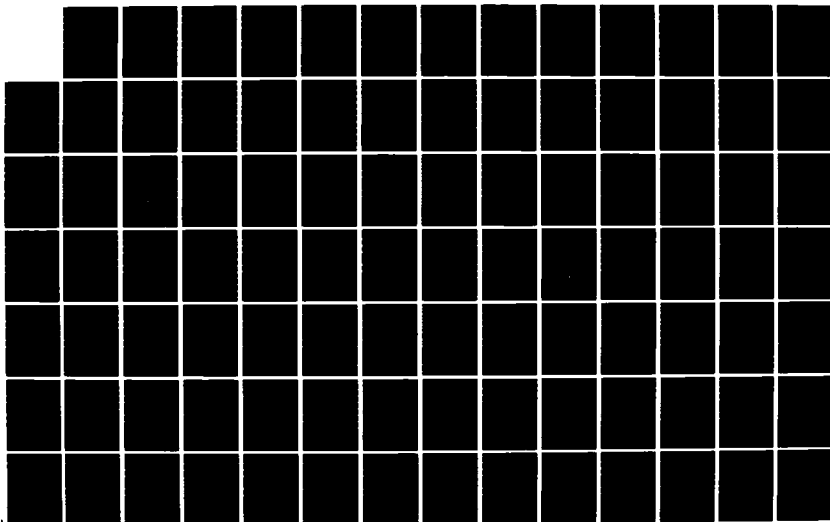
4/7

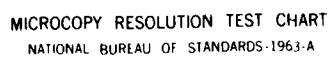
UNCLASSIFIED

AFOSR-TR-85-0083 AFOSR-85-0143

F/G 13/2

NL





MICROCOPY RESOLUTION TEST CHART
NATIONAL BUREAU OF STANDARDS-1963-A

advantage of having a closed-form solution for edge loading on a plate supported by an elastic solid foundation cannot be overestimated. Comparisons between such a solution and the corresponding solutions available for the interior case, will permit the evaluation of the amount of increase in bending stress as the load moves from the interior to the edge.

8.2 THEORY

The theoretical background for this study is provided by the work of Pickett and his co-workers, who were the first to present a solution to the problem of "the bending of a large pavement slab by loadings near a straight boundary edge" [152; 153]. They hoped to "bring the solution for this problem to the same stage of completion as the Westergaard solution, i.e. the deflections and moments expressed as single Fourier integrals. The single integrals can then be evaluated for various loading conditions, as has been done for the Westergaard solution" [84; 86]. The following assumptions were made in the analysis:

- (i) The slab is of uniform thickness;
- (ii) The straight edge is free of externally applied moments and shear;
- (iii) The other boundaries are so far from the loaded region that they may be considered to be at infinity;

- (iv) Perfect contact exists between the slab and the elastic half-space;
- (v) The Lagrange plate equation (medium-thick plate theory) is applies to the slab, and the theory of elasticity (elastic solid foundation) is valid for the subgrade;
- (vi) Loading is symmetrical about the y-axis, i.e. a perpendicular to the free edge.

With respect to assumption (vi), Pickett, et al. [152] note that this is not "an important restriction since the slab is considered to extend to infinity in both the positive and negative x-directions. In such cases both moments and deflections at a given point are equally affected by loads in a positive or a negative x-direction from the given point." Based on the foregoing assumptions, Pickett et al. derived the following equation for the edge deflection and moment:

$$w_{y=0} = \frac{2P}{\pi^2 D} \int_0^{\infty} \cos \alpha x \left[H_1 + \left\{ \mu H_1 + \frac{H_2}{(\alpha \ell)^2} \left(\frac{1+\mu}{(1-\mu)(3-\mu)} - \frac{(\alpha \ell)^2 F_2 + \frac{1+\mu}{(1-\mu)(3-\mu)} (\mu F_1 + F_2)}{(3+\mu) \frac{\pi}{4} + \mu F_1 + F_2} \right) \right\} \frac{\sin \alpha a}{\alpha a} \right] d(\alpha \ell) \quad (8-1)$$

$$M_{y=0} = \left(\frac{1+\mu}{3+\mu} \right) \frac{2P}{\pi^2} \int_0^{\infty} \cos \alpha x \left[(3-\mu)(\alpha \ell)^2 H_1 + (1+\mu) H_2 - \frac{\{ (3-\mu)F_1 + (1+\mu)F_2 \} \{ \mu(\alpha \ell)^2 H_1 + H_2 \}}{(3+\mu) \frac{\pi}{4} + \mu F_1 + F_2} \right] \frac{\sin \alpha a}{\alpha a} d(\alpha \ell) \quad (8-2)$$

where:

P : total load on pavement;

α, β : dummy variables;

$$H_1 = \int_0^\infty \frac{\sin \beta b}{K_1 \gamma \beta b} d\beta$$

$$H_2 = \int_0^\infty \frac{\beta \sin \beta b}{K_1 \gamma b} d\beta$$

$$F_1 = \alpha \int_0^\infty \frac{K_2}{K_1 \gamma^2} d\beta$$

$$F_2 = \frac{1}{\alpha} \int_0^\infty \frac{K_2 \beta^2}{K_1 \gamma^2} d\beta$$

$$K_1 = 2 + (\gamma \ell)^3$$

$$K_2 = \frac{1+\mu}{1-\mu} - \frac{\alpha^2 - \beta^2}{\gamma^2}$$

$$\gamma = \sqrt{\alpha^2 + \beta^2}$$

ℓ : radius of relative stiffness ($=\ell_e$),

$$= \sqrt[3]{\frac{Eh^3 (1-\mu_s^2)}{6 E_s (1-\mu^2)}}$$

a, b : limits of loaded area, covering the region bounded by $x=a$, $x=-a$, $y=0$, and $y=b$ (Fig. 8.1)

The evaluation of the four functions, F_1 , F_2 , H_1 and H_2 and the integral in Eqn. (8-2) was the major focus of the present study. Having determined the four functions, it would be a routine process to evaluate the integral in Eqn. (8-1) for edge deflection, as well. However, the determination of edge stresses was considered more urgent.

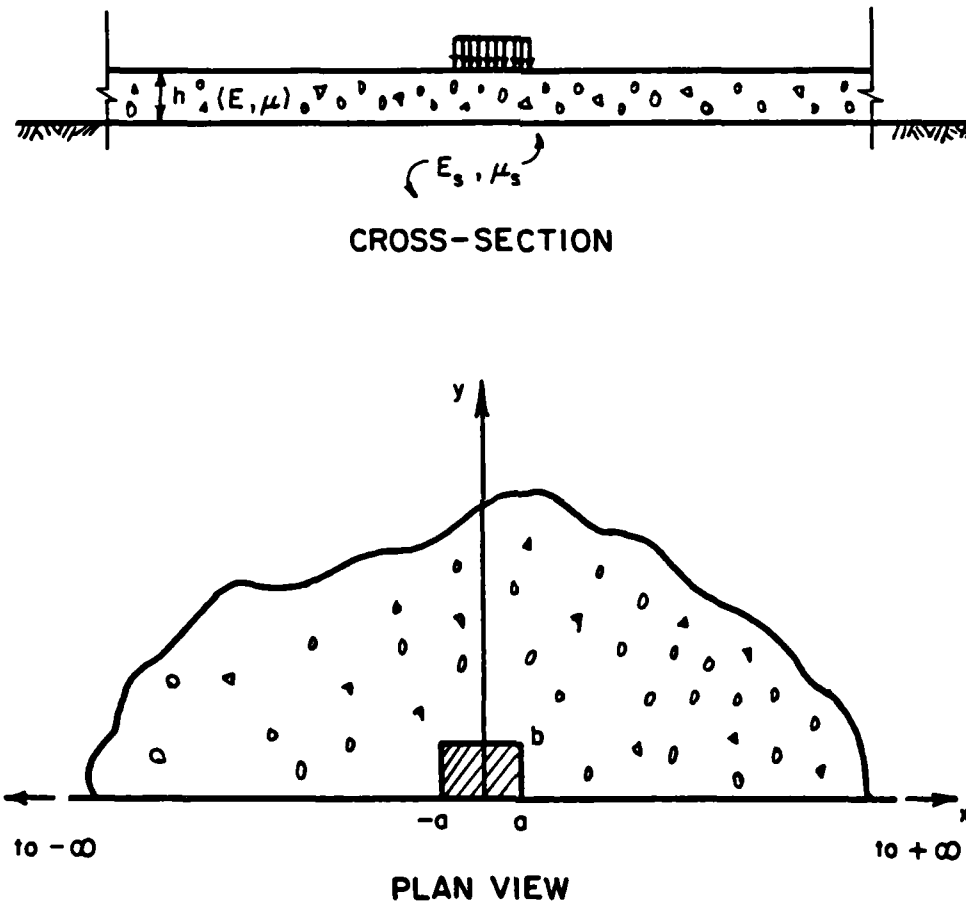


Fig. 8.1 Edge Load on Semi-Infinite Slab-on-Grade

8.3 NUMERICAL INTEGRATIONS

8.3.1 Evaluation of F_1 and F_2

It is shown by Pickett, et al. [152] that by setting:

$$\beta = \alpha x$$

F_1 and F_2 may be rewritten as:

$$F_1 = \int_0^{\infty} K_3 \, dx$$

$$\text{and } F_2 = \int_0^{\infty} x^2 K_3 \, dx \quad (8-3)$$

where:

$$K_3 = \frac{\frac{1+\mu}{1-\mu} - \frac{1-x^2}{1+x^2}}{(1+x^2) [2 + (\alpha l)^3 (1+x^2)^{3/2}]}$$

A computer program (called 'NUMERIN') was written to evaluate the infinite integrals in Eqn. (8-3), using subroutine GQU3Z from the University of Illinois software library UOILIB. This routine evaluates the integral of $f(x)$ from $x=a$ to $x=b$ using a composite Gaussian quadrature based on a 96-point formula. This numerical integration procedure has been used successfully in connection with other models, as well (e.g. CFES).

Since K_3 is a function of (αl) , values of F_1 and F_2 must be determined for a fairly wide range of this parameter. Pickett, et al. [152] recommended values of (αl) between 0 and 32, but the increments in (αl) they used are so large that interpolation is bound to lead to errors. In the present study, the increments shown in Table 8.1 were used. Thus, F_1 and F_2 were evaluated at 125 values of (αl) , compared to the 24 values given by Pickett, et al.

The numerical integration of the infinite integrals in Eqn. (8-3) proceeded as follows: the integrand was evaluated for increments in x of 10 and its cumulative value was calculated. The process was stopped when the ratio of the integral values for two consecutive increments fell between 0.999999 and 1.000001. Such a stringent convergence criterion was considered necessary to ensure an accurate solution when the functions are substituted in Eqn. (8-2), where a second infinite integral must be evaluated. The values obtained in this way were compared to those presented by Pickett, et al. and, in most cases, there was fair agreement. However, agreement between values evaluated in this study, and those that were obtained by interpolation from Pickett, et al., was inevitably much less satisfactory.

8.3.2 Evaluation of H_1 and H_2

The convergence of these functions is much slower and the convergence criterion had to be modified accordingly. Pickett, et al. [152] show that by setting:

TABLE 8.1

INCREMENTS USED IN NUMERICAL INTEGRATIONS

INCREMENTS IN (αl)
(for all four functions)

(αl)	INCREMENT
0.05 → 1.00	0.05
1.0 → 4.0	0.1
4.0 → 10.0	0.2
10.0 → 32.5	0.5

INCREMENTS IN (b/l) FOR H_1

(b/l)	INCREMENT
0.05 → 1.00	0.05
1.0 → 2.0	0.1
2.0 → 8.0	0.2

INCREMENTS IN (b/l) FOR H_2

(b/l)	INCREMENT
0.05 → 0.30	0.05
0.3 → 2.0	0.1
2.0 → 8.0	0.2

$$\beta = z/b$$

the functions H_1 and H_2 can be put in the form:

$$\begin{aligned} H_1 &= (b/\ell)^3 \int_0^\infty \frac{\sin z}{z[(K_4)^4 + 2(b/\ell)^3 K_4]} dz \\ H_2 &= (b/\ell) \int_0^\infty \frac{z \sin z}{(K_4)^4 + 2(b/\ell)^3 K_4} dz \end{aligned} \quad (8-4)$$

where:

$$K_4 = [(\alpha b)^2 + z^2]^{0.5} = [(\alpha \ell \frac{b}{\ell})^2 + z^2]^{0.5}$$

The same computer program was used to evaluate these functions for the increments of $(\alpha \ell)$ and (β/ℓ) in Table 8.1. Again, a much larger range and number of values were calculated in this study than are given by Pickett, et al. In order to speed up the convergence of the infinite integrals the following additional conditions were allowed to end the numerical integration:

- (a) If the absolute value of the contribution of the last range of 10 in z was less than 1.0×10^{-10} ;
- (b) If the value of z was greater than 999.0 and the absolute value of the contribution of the last range in z was less than 1.0×10^{-6} .

For H_2 , the increment in z was increased from 10 to 100 for values of z greater than 99.9. Comparisons with the values given by Pickett, et al. indicated again that agreement was generally very good.

8.3.3 Evaluation of the Integral in Eqn. (8-2)

Having evaluated and stored on magnetic tape values of the four functions under the infinite integral in Eqn. (8-2) for a broad range of the dependent variables, the next step was to evaluate this infinite integral itself. Since the critical location of interest is at $x=0$, Eqn. (8-2) was specialized for this location. Making use of symmetry, only half of loaded area need be considered. Thus,

$$P = p \cdot a \cdot b$$

where p is the applied uniform pressure. Furthermore, noting that:

$$\alpha a = \frac{\alpha l}{l} \cdot \frac{a}{l} \cdot l = (\alpha l) \left(\frac{a}{l} \right)$$

Eqn. (8-2) yields for $x=0$:

$$M_{y=0} = \left(\frac{1+\mu}{3+\mu} \right) \frac{2p (a/l)(b/l)l^2}{\pi^2} \int_0^\infty \left[(3-\mu)(\alpha l)^2 H_1 + (1+\mu)H_2 \right. \\ \left. - \frac{\{(3-\mu)F_1 + (1+\mu)F_2\} \{\mu(\alpha l)^2 H_1 + H_2\}}{\{(3+\mu)\frac{\pi}{4} + \mu F_1 + F_2\}} \right] \frac{\sin \alpha l \frac{a}{l}}{\alpha l \frac{a}{l}} d(\alpha l) \quad (8-5)$$

In order to evaluate the infinite integral in this equation, another computer program (called 'NUMER25') was coded. The previously determined functions F_1 , F_2 , H_1 and H_2 were read in as input data, a total of 14,988 words in all! Where necessary, one- or two-way

interpolation was used to determine the required values of these functions using a modified version of subroutine TABINT from computer program H-51 [85]. The numerical integration involved was again performed using subroutine GQU3Z.

Following a suggestion by Pickett, et al. [152], the integral in Eqn. (8-5) was evaluated as given for (αl) between 0 and 32, while for the range of (αl) from 32 to infinity the following asymptotic expression for the integral was used:

$$\int_{32}^{\infty} \dots d(\alpha l) = (3-\mu) \frac{\pi \cos \alpha x \sin \alpha a}{2ab l \alpha^3} [1 - e^{-\alpha b} (1 + \frac{\alpha b}{2} + \dots)] \quad (8-6)$$

Setting $x=0$ and noting that:

$$\alpha a = (\alpha l) \left(\frac{a}{l}\right)$$

$$l \alpha^2 b = \frac{\alpha l^2}{l^2} \left(\frac{b}{l}\right) \cdot l \cdot l = (\alpha l)^2 \left(\frac{b}{l}\right)$$

$$\alpha b = (\alpha l) \left(\frac{b}{l}\right)$$

Eqn. (8-6) may be rewritten as:

$$\int_{32}^{\infty} \dots d(\alpha l) = \frac{(3-\mu)\pi \sin [\alpha l \cdot (a/l)]}{2\alpha l (a/l) (\alpha l)^2 (b/l)} \left[1 - e^{-(\alpha l)(b/l)} \left\{ 1 + \frac{(\alpha l)(b/l)}{2} + \dots \right\} \right] \quad (8-7)$$

In evaluating the integral between $\alpha l = 0$ and $\alpha l = 32$ using 'NUMER25', this range was subdivided into 8 intervals and the 96 point formula in subroutine GQU3Z was applied over each of these. For the rest of the integral range between 32 and infinity, an increment in (αl) of 40 was used, consisting again of 8 intervals. The process was stopped when the absolute value of the last contribution to the integral was less than 1.0×10^{-4} , or the ratio of the integral values for two consecutive increments of 40 in (αl) lay between 0.999 and 1.001. In view of the interpolation and other accumulated round-off errors involved here, more stringent convergence criteria would only increase execution times, with no substantial improvement in accuracy. The contribution of the integral between 32 and infinity was, in general, less than 1% of the total value of the integral.

It is desirable to introduce at this stage the notation which had been used earlier by Pickett and Ray [86], to express the edge moment as a number of squares in an influence chart, i.e.

$$M = p \frac{l^2}{10000} N \quad (8-8)$$

where N is the number of influence squares in the chart under the tire print(s). Comparison of this expression with Eqn. (8-5), leads to:

$$N = \left(\frac{1+\mu}{3+\mu} \right) \frac{20000}{\pi^2} (a/l) (b/l) \int_0^{\infty} \dots d(\alpha l) \quad (8-9)$$

A table of N values was thus compiled (Table 8.2) for (a/l) and (b/l) values ranging between 0 and 8. This range was selected so that Table 8.2 would be compatible with the table already included in computer program H-51 [85], for the dense liquid foundation. A modified version of the program was thus developed (called 'H51ES') for analyzing infinite slabs under edge loading with dense liquid and/or elastic solid subgrades. The input data deck for the new version is identical to that for the original H-51, except for the addition of an indicator of subgrade type, and a new card containing E_s and μ_s , provided only when the elastic solid foundation model is used. Appendix A includes a detailed input guide for H51ES.

8.4 INVESTIGATION OF THE EDGE LOADING CONDITION FOR PLATE ON ELASTIC SOLID FOUNDATION

In order to demonstrate the capabilities of H51ES, a series of runs were performed. The purpose of these runs was two-fold:

- (i) Determine values of the ratio (σ_e/σ_i) of the maximum edge to the maximum interior bending stress for an elastic solid foundation;
- (ii) Derive a closed-form expression for σ_e for a plate on an elastic solid foundation.

For the case of a dense liquid foundation, Westergaard's "New" formula [10] for maximum edge stress may be written as [13]:

TABLE 8.2

NUMBER OF INFLUENCE SQUARES FOR BENDING STRESS (EDGE)

b/t	a/t											
	0.00	.10	.20	.30	.40	.50	.60	.80	1.00	1.20	1.40	1.60
0.00	0.00	0.00	0.00	0.00	0.00	0.00	0.00	0.00	0.00	0.00	0.00	0.00
0.10	0.00	53.80	84.94	104.79	117.53	125.37	129.60	130.67	125.52	116.93	106.61	95.69
0.20	0.00	93.33	153.76	193.68	219.91	236.46	245.85	249.80	241.13	225.41	206.07	185.33
0.30	0.00	123.76	209.56	268.55	308.37	334.15	349.40	357.76	347.09	325.62	298.48	269.01
0.40	0.00	148.04	255.31	331.57	384.44	419.56	441.09	455.07	443.74	417.80	384.02	346.86
0.50	0.00	167.88	293.26	384.80	449.77	493.96	521.89	542.36	531.50	502.24	462.91	419.04
0.60	0.00	184.36	325.06	429.95	505.89	558.64	592.89	620.35	610.87	579.31	535.42	485.74
0.80	0.00	209.90	374.77	501.35	595.84	663.69	709.66	751.47	746.65	712.95	662.51	603.67
1.00	0.00	228.41	411.04	553.99	662.97	743.15	799.17	854.53	855.69	822.20	767.94	702.71
1.20	0.00	242.08	437.94	593.27	713.46	803.47	867.80	935.14	942.58	910.70	854.58	785.11
1.40	0.00	252.30	458.11	622.86	751.71	849.47	920.52	998.04	1011.46	981.91	925.25	853.16
1.60	0.00	260.02	473.37	645.31	780.85	884.69	961.11	1047.10	1065.91	1038.96	982.59	909.02
1.80	0.00	265.89	484.99	662.45	803.18	911.78	992.48	1085.40	1108.92	1084.55	1028.95	954.70
2.00	0.00	270.39	493.90	675.62	820.37	932.71	1016.81	1115.36	1142.89	1120.96	1066.37	991.97
2.20	0.00	273.86	500.78	685.79	833.69	948.96	1035.75	1138.87	1169.79	1150.05	1096.58	1022.37
2.40	0.00	276.54	506.12	693.70	844.06	961.64	1050.58	1157.40	1191.14	1173.36	1121.00	1047.17
2.60	0.00	278.64	510.29	699.89	852.18	971.60	1062.25	1172.06	1208.17	1192.08	1140.80	1067.47
2.80	0.00	280.30	513.57	704.76	858.59	979.47	1071.50	1183.74	1221.82	1207.21	1156.91	1084.14
3.00	0.00	281.61	516.17	708.64	863.69	985.74	1078.88	1193.11	1232.83	1219.49	1170.11	1097.90
3.20	0.00	282.65	518.26	711.74	867.78	990.78	1084.81	1200.68	1241.78	1229.54	1180.98	1109.33
3.40	0.00	283.50	519.94	714.25	871.09	994.86	1089.63	1206.86	1249.12	1237.83	1190.01	1118.90
3.60	0.00	284.19	521.32	716.30	873.80	998.21	1093.58	1211.94	1255.19	1244.73	1197.57	1126.96
3.80	0.00	284.76	522.46	717.99	876.04	1000.97	1096.85	1216.17	1260.26	1250.53	1203.96	1133.82
4.00	0.00	285.23	523.40	719.40	877.90	1003.29	1099.60	1219.72	1264.54	1255.44	1209.41	1139.71
8.00	0.00	288.42	529.75	728.90	890.52	1018.98	1118.30	1244.26	1294.60	1290.65	1249.36	1183.97

TABLE 8.2 (continued)

b/z	1.80	2.00	2.20	2.40	2.60	a/z	2.80	3.00	3.20	3.40	3.60	3.80	4.00	8.00
0.00	0.00	0.00	0.00	0.00	0.00	0.00	0.00	0.00	0.00	0.00	0.00	0.00	0.00	0.00
0.10	84.86	74.56	65.03	56.41	48.73	41.98	36.10	31.02	26.66	22.94	19.78	17.10	14.60	2.60
0.20	164.64	144.85	126.49	109.85	94.99	81.90	70.50	60.64	52.15	44.91	38.76	33.55	28.99	5.19
0.30	239.39	210.92	184.42	160.34	138.79	119.78	103.20	88.84	76.48	65.92	56.95	49.34	42.76	7.76
0.40	309.20	272.83	238.87	207.90	180.16	155.63	134.21	115.64	99.64	85.97	74.33	64.47	55.91	10.31
0.50	374.21	330.69	289.90	252.61	219.13	189.49	163.56	141.06	121.66	105.07	90.94	78.95	68.85	12.85
0.60	434.56	384.61	337.62	294.54	255.78	221.41	191.30	165.14	142.57	123.24	106.77	92.79	80.37	15.37
0.80	542.03	481.22	423.57	370.42	322.39	279.65	242.10	209.41	181.15	156.91	136.22	118.64	103.35	20.35
1.00	633.22	563.93	497.73	436.35	380.63	330.89	287.05	248.79	215.66	187.19	162.86	142.15	124.25	25.25
1.20	709.92	634.16	561.24	493.25	431.26	375.71	326.63	283.69	246.44	214.37	186.91	163.51	142.07	30.07
1.40	773.95	693.38	615.28	542.06	475.03	414.77	361.36	314.53	273.81	238.70	208.59	182.90	158.81	34.81
1.60	827.10	743.03	661.01	583.75	512.72	448.66	391.74	341.70	298.12	260.47	228.13	200.49	174.47	39.47
1.80	871.04	784.49	699.58	619.22	545.09	478.02	418.27	365.63	319.69	279.93	245.74	216.46	188.04	44.04
2.00	907.26	819.03	732.03	649.36	572.84	503.41	441.42	386.69	338.84	297.35	261.62	230.97	200.52	48.52
2.20	937.10	847.77	759.30	674.93	596.61	525.37	461.62	405.23	355.84	312.96	275.96	244.19	212.91	52.91
2.40	961.70	871.70	782.22	696.64	616.98	544.38	479.27	421.58	370.97	326.96	288.93	256.24	224.21	57.21
2.60	982.01	891.65	801.53	715.10	634.49	560.86	494.72	436.02	384.46	339.55	300.70	267.25	235.42	61.42
2.80	998.85	908.35	817.84	730.85	649.56	575.19	508.28	448.82	396.51	350.90	311.39	277.33	245.53	65.53
3.00	1012.88	922.38	831.68	744.34	662.60	587.70	520.23	460.20	407.32	361.17	321.14	286.59	254.54	69.54
3.20	1024.63	934.24	843.48	755.95	673.92	598.67	530.80	470.35	417.05	370.47	330.04	295.10	263.45	73.45
3.40	1034.54	944.33	853.60	766.00	683.81	608.33	540.19	479.44	425.83	378.94	338.20	302.96	271.26	77.26
3.60	1042.96	952.97	862.35	774.75	692.49	616.89	548.57	487.62	433.79	386.67	345.69	310.21	278.96	80.96
3.80	1050.17	960.43	869.95	782.42	700.16	624.50	556.09	495.01	441.03	393.74	352.59	316.93	285.57	84.57
4.00	1056.40	966.91	876.61	789.19	706.97	631.31	562.86	501.71	447.63	400.24	358.96	323.17	291.07	88.07
8.00	1104.53	1018.47	931.18	846.35	766.33	692.52	625.58	565.64	512.50	465.78	424.96	389.42	358.36	138.36

$$\sigma_e = -6 \frac{P}{h^2} (1 + 0.5\mu) \left[0.489 \log_{10} \left(\frac{a}{\ell} \right) - 0.012 - 0.063 \left(\frac{a}{\ell} \right) \right] \quad (8-10)$$

where:

P : total applied load;

h : slab thickness;

μ : slab Poisson's ratio;

a : radius of circular load placed tangentially at slab edge;

ℓ : radius of relative stiffness for slab on dense liquid,

$$\ell = \sqrt[4]{\frac{Eh^3}{12(1-\mu^2)k}}$$

E : slab Young's modulus;

k : modulus of subgrade reaction.

It may be expected that the corresponding equation for σ_e in the elastic solid foundation case will have a similar form. Thus, if the last term on the right-hand side of Eqn. (8-10) is neglected for the time being, an equation of the following form may be sought:

$$\sigma_e = A \left(\frac{P}{h^2} \right) \left[B \log_{10} \left(\frac{a}{\ell_e} \right) + C \right] \quad (8-11)$$

where:

ℓ_e : radius of relative stiffness for slab on elastic solid.

Letting $\mu=0.15$ and assuming A is similar to the corresponding dense liquid term, gives A equal to 6.45. Therefore, plotting

$$\left(\frac{\sigma_e h^2}{6.45P} \right) \text{ versus } \log_{10}(a/\ell_e),$$

will yield a straight line, whose slope is B and intercept is C.

For the purpose of this study, (a/ℓ_e) values between 0.1 and 2.0 were considered. Note that the larger values of (a/ℓ_e) are of academic interest only, since loads commonly encountered are relatively much smaller. Values of ℓ_e ranged from 20 to 80 in., and a broad range of other parameters was selected. The results from the runs performed are shown in Tables 8.3 and 8.4.

The following observations may be made with respect to these results:

- (i) The governing parameter in determining the edge stress is (a/ℓ_e) . The value of this parameter uniquely defines the value of the normalized edge stress $(\frac{\sigma_e h^2}{6.45 P})$, independent of the individual values of a , ℓ_e , h^2 , P , etc. This confirms that the general form of the equation of σ_e for an elastic solid is similar to that for a dense liquid foundation. In the latter case, (a/ℓ) controls the normalized edge stress.
- (ii) The value of the ratio $(\frac{\sigma_e}{\sigma_i})$ is solely a function of (a/ℓ_e) independent of the individual values of the parameters entering into the analysis. This is a corollary of (i) above, since both σ_e and σ_i , in their normalized forms, are only functions of (a/ℓ_e) .

Figure 8.2 shows the variation of (σ_e/σ_i) with (a/ℓ_e) for an elastic solid, or (a/ℓ) for a dense liquid foundation. It is observed that for both foundation types, the edge stress becomes less than the corresponding interior stress at high normalized load areas. For the

TABLE 8.3
PLATE ON ELASTIC SOLID: EDGE LOADING

RUN No.	E (psi)	E _s (psi)	h (in.)	l _e (in.)	a (in.)	P (psi)	(a/l _e)	BENDING STRESS (psi)				ELASTIC SOLID	
								σ _i	σ _{e,0}	σ _{e,0S}	σ _{e,N}	σ _i	σ _e
1	4000000.	4351.	4.00	20.00	2.00	793.65	.10	1001.46	1557.22	1342.04	2043.96	1001.86	1745.20
2	3000000.	5500.	4.75	19.96	4.00	198.93	.20	542.00	798.72	646.13	1046.18	542.61	876.49
3	2000000.	7343.	6.00	20.00	10.00	31.83	.50	203.41	248.34	152.70	341.67	205.42	269.90
4	3000000.	6000.	4.90	20.00	15.00	14.15	.75	219.29	204.62	61.23	323.32	226.04	255.63
5	4000000.	4351.	4.00	20.00	20.00	7.96	1.00	245.07	128.44	-86.74	302.36	263.07	257.22
6	3000000.	5500.	4.75	19.96	30.00	3.54	1.50	104.69	-88.40	-240.99	57.57	133.54	91.02
7	2000000.	7343.	6.00	20.00	39.99	1.99	2.00	48.12	-134.16	-229.79	-16.47	80.15	32.12
8	6000000.	2754.	6.00	40.00	3.99	200.00	.10	445.69	693.18	597.54	909.87	445.87	771.63
9	4000000.	4350.	8.00	40.00	8.00	49.70	.20	191.24	281.88	228.08	369.20	191.45	309.30
10	4000000.	2914.	7.00	40.00	20.00	7.96	.50	149.46	182.48	112.22	251.06	150.94	198.71
11	4000000.	1836.	6.00	40.00	30.00	3.54	.75	146.24	136.44	40.81	215.60	150.74	170.46
12	4000000.	1836.	6.00	40.00	60.00	.88	1.50	65.79	-54.83	-150.46	36.52	83.80	57.31
13	4000000.	1836.	6.00	40.00	79.79	.50	1.99	48.20	-133.48	-229.12	-16.09	80.08	32.28
14	4000000.	5500.	13.00	60.12	6.00	88.42	.10	94.92	147.62	127.25	193.77	94.96	165.33
15	4000000.	5500.	12.98	60.02	12.00	22.10	.20	72.66	107.11	86.67	140.29	72.74	117.53
16	4000000.	5500.	13.00	60.12	29.99	3.54	.50	43.40	53.04	32.67	72.95	43.83	57.78
17	6000000.	1930.	8.00	60.04	44.60	1.60	.74	82.99	78.24	24.44	122.87	85.48	97.10
18	4000000.	5500.	13.00	60.12	60.14	.88	1.00	23.19	12.13	-8.24	28.60	24.90	24.36
19	4000000.	5500.	12.98	60.02	90.00	.39	1.50	14.07	-11.69	-32.12	7.83	17.91	12.26
20	4000000.	5500.	13.00	60.12	119.74	.22	1.99	10.28	-28.35	-48.72	-3.38	17.05	6.90

TABLE 8.3 (continued)

RUN No.	E (psi)	E _s (psi)	h (in.)	l _e (in.)	a (in.)	P (psi)	(a/l _e)	BENDING STRESS (psi)				ELASTIC SOLID	
								σ_1	σ_{e0}	σ_{eOS}	σ_{eN}	σ_1	σ_e
21	4000000.	1062.	10.00	80.00	16.00	12.43	.20	122.41	180.43	146.00	236.33	122.54	197.98
22	4000000.	2914.	14.00	80.01	16.00	12.43	.20	62.46	92.06	74.50	120.58	62.53	101.02
23	4000000.	2914.	14.00	80.01	20.00	7.96	.25	56.27	80.75	63.19	106.02	56.37	87.58
24	4000000.	1500.	11.20	79.87	40.10	1.98	.50	58.21	70.95	43.50	97.68	58.79	77.37
25	4000000.	8500.	20.00	80.00	60.14	.88	.75	13.13	12.22	3.61	19.34	13.54	15.30
26	6000000.	1593.	10.00	80.01	79.79	.50	1.00	39.33	20.82	-13.61	48.64	42.20	41.36
27	4000000.	1500.	11.20	79.87	120.01	.22	1.50	18.84	-15.87	-43.12	10.38	24.03	16.40
28	4000000.	1500.	11.20	79.87	160.22	.12	2.01	13.78	-38.75	-66.20	-4.87	23.03	9.16
29	4000000.	1500.	12.60	89.85	18.00	9.82	.20	77.04	113.53	91.84	148.70	77.12	124.58
30	4000000.	1500.	12.60	89.85	45.03	1.57	.50	46.05	56.17	34.49	77.31	46.51	61.16

Notes:

DENSE LIQUID

- σ_1 : interior stress (Eqn. 5-2);
 σ_{e0} : edge stress, circular load, original equation (Eqn. 5-5);
 σ_{eOS} : edge stress, semi-circular load, original equation (Eqn. 5-6);
 σ_{eN} : edge stress, circular load, "New" equation (Eqn. 8-10).

ELASTIC SOLID

- σ_1 : interior stress (Table 7.1);
 σ_e : edge stress from H5LES.

TABLE 8.4

NORMALIZED EDGE STRESSES

RUN No.	ℓ_e (in.)	(a/ℓ_e)	(σ_e / σ_1)			$(\frac{\sigma_e h^2}{6.45 p})$				
			E.S.	D.L.O	D.L.OS	D.L.N	E.S.	D.L.O	D.L.OS	D.L.N
1	20.0004	.1001	1.7420	1.5550	1.3401	2.0410	.4329	.3863	.3329	.5070
2	19.9572	.2004	1.6153	1.4737	1.1921	1.9302	.3066	.2794	.2260	.3660
3	20.0000	.5000	1.3139	1.2209	.7507	1.6798	.1506	.1386	.0852	.1907
4	19.9989	.7500	1.1309	.9331	.2792	1.4744	.0952	.0762	.0228	.1204
5	20.0004	1.0000	.9777	.5241	-.3540	1.2338	.0638	.0319	-.0215	.0750
6	19.9572	1.5032	.6815	-.8444	-2.3020	.5500	.0318	-.0309	-.0843	.0201
7	20.0000	1.9997	.4008	-2.7878	-4.7751	-.3422	.0179	-.0749	-.1283	-.0092
8	39.9977	.0997	1.7306	1.5553	1.3407	2.0415	.4307	.3869	.3335	.5078
9	40.0038	.2001	1.6155	1.4740	1.1927	1.9306	.3069	.2797	.2263	.3663
10	40.0045	.4999	1.3165	1.2210	.7509	1.6798	.1510	.1386	.0853	.1907
11	39.9977	.7500	1.1308	.9330	.2790	1.4743	.0951	.0762	.0228	.1203
12	39.9977	1.5001	.6839	-.8334	-2.2871	.5552	.0320	-.0306	-.0840	.0204
13	39.9977	1.9948	.4031	-2.7691	-4.7531	-.3338	.0180	-.0745	-.1279	-.0090
14	60.1169	.0998	1.7412	1.5552	1.3406	2.0414	.4332	.3868	.3334	.5077
15	60.0244	.1999	1.6156	1.4740	1.1928	1.9307	.3070	.2798	.2264	.3665
16	60.1169	.4988	1.3181	1.2221	.7527	1.6807	.1514	.1390	.0856	.1911
17	60.0402	.7429	1.1360	.9427	.2945	1.4806	.0963	.0776	.0243	.1219
18	60.1169	1.0004	.9784	.5232	-.3553	1.2333	.0638	.0318	-.0216	.0749
19	60.0244	1.4993	.6845	-.8308	-2.2836	.5564	.0320	-.0305	-.0839	.0204
20	60.1169	1.9918	.4047	-2.7576	-4.7395	-.3286	.0181	-.0743	-.1276	-.0088

TABLE 8.4 (continued)

RUN No.	t_e (in.)	(a/t_e)	(σ_e / σ_1)				$(\frac{\sigma_e}{6.45 p})$			
			E.S.	D.L. ₀	D.L. _{OS}	D.L. _N	E.S.	D.L. ₀	D.L. _{OS}	D.L. _N
21	80.0003	.2000	1.6156	1.4740	1.1927	1.9307	.3069	.2797	.2264	.3664
22	80.0090	.2000	1.6156	1.4740	1.1928	1.9307	.3070	.2798	.2264	.3664
23	80.0090	.2500	1.5537	1.4352	1.1230	1.8843	.2661	.2454	.1920	.3222
24	79.8660	.5020	1.3159	1.2189	.7474	1.6782	.1505	.1380	.0846	.1900
25	79.9953	.7518	1.1301	.9306	.2752	1.4728	.0949	.0758	.0224	.1199
26	80.0079	.9973	.9802	.5293	-.3460	1.2367	.0641	.0323	-.0211	.0754
27	79.8660	1.5027	.6825	-.8426	-2.2995	.5508	.0319	-.0309	-.0842	.0202
28	79.8660	2.0061	.3976	-2.8121	-4.8037	-.3532	.0178	-.0754	-.1287	-.0095
29	89.8492	.2004	1.6154	1.4737	1.1922	1.9303	.3066	.2794	.2261	.3660
30	89.8492	.5011	1.3150	1.2198	.7489	1.6789	.1505	.1383	.0849	.1903

Notes:

- E.S. : Elastic Solid;
D.L.₀ : Dense Liquid, circular load, original equation;
D.L._{OS} : Dense Liquid, semi-circular load, original equation;
D.L._N : Dense Liquid, circular load, "New" equation.

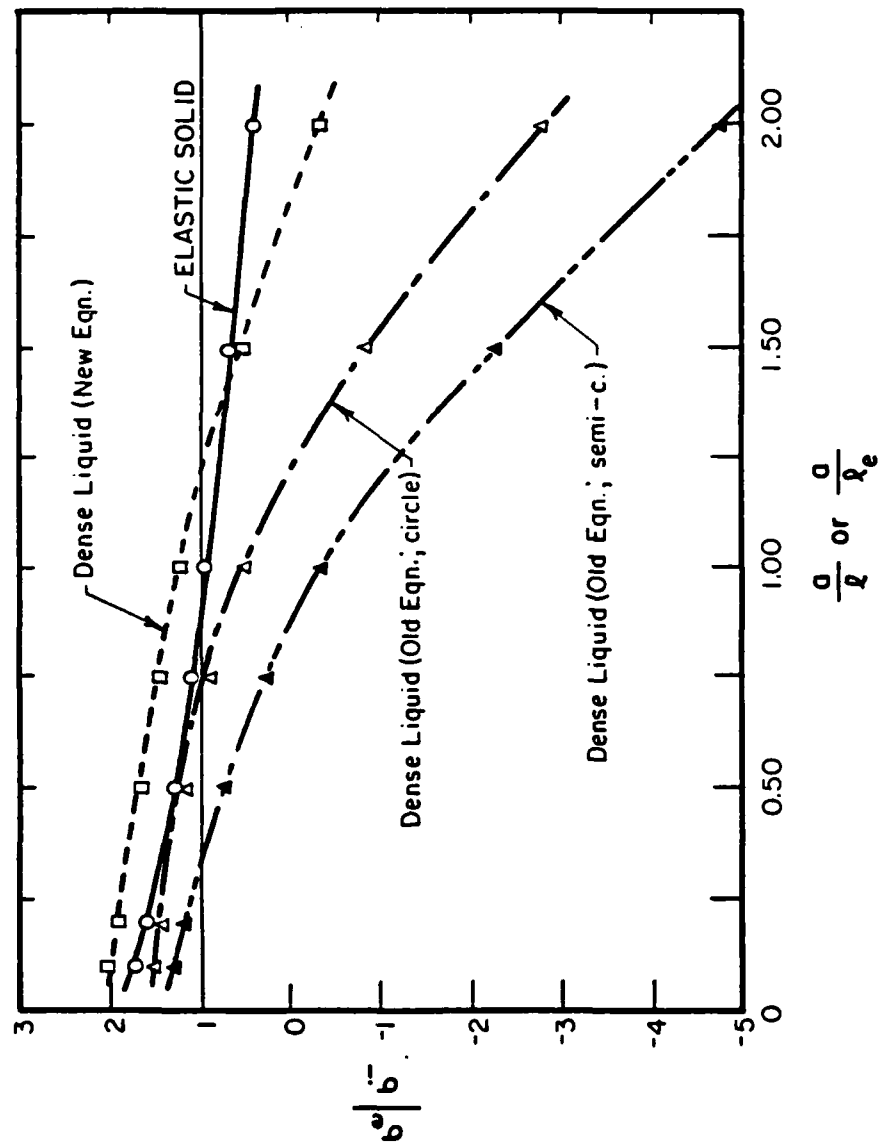


Fig. 8.2 Comparison of Maximum Bending Stresses Under Interior and Edge Loads

range of loaded area sizes commonly encountered in practice, the elastic solid ratio of (σ_e/σ_i) is generally about 25% smaller than the corresponding dense liquid ("New" equation) value.

The curves in Fig. 8.2 show the variation of the "Load Placement Effect Factor" (LPEF) for the case of an infinite slab. Costigan [157] notes that for a dense liquid foundation "the upper limit for LPEF approaches that calculated by Westergaard's equations". Thus, smaller slabs may be expected to give lower LPEF values. This is further demonstrated by the slab size investigations conducted during this research, for both the dense liquid and elastic solid subgrades. The (L/λ) or (L/λ_e) requirement for the development of the infinite-slab interior stress has been found to be about 3.0 to 3.5 (Fig. 5.10; Fig. 7.3; Fig. 9.8; Fig. 10.4). The corresponding value for the edge stress is considerably higher, at about 5.0 (Fig. 5.17). This will lead to a lower value of (σ_e/σ_i) or LPEF than indicated in Fig. 8.2 for slabs shorter than 5.0 times the radius of relative stiffness. The value of LPEF of 1.4 to 1.5 recommended by Thompson and Dempsey [158] and other investigators, probably refers to such shorter (or cracked) slabs.

For the case of an F-4 aircraft load, Costigan [157] used ILLI-SLAB to derive the following equation for LPEF (dense liquid):

$$\text{LPEF} = 1.7016 + 0.000963 h^2 - 0.00746 \text{LTE} \quad (8-12)$$

where LTE denotes the load transfer efficiency at the slab joints. Equation (8-12) accounts for the effect of load transfer, but is only

applicable to the case it was derived for, since the major factor of (a/ℓ) does not enter it explicitly. To compare Eqn. (8-12) with the results in Fig. 8.2, one of the cases analyzed by Costigan may be considered. Let:

$$E = 7 \times 10^5 \text{ psi}$$

$$\mu = 0.3$$

$$h = 12 \text{ in.}$$

$$k = 200 \text{ psi/in.}$$

$$a = 5.7 \text{ in.}$$

$$p = 265 \text{ psi.}$$

For this system, $\ell = 27.3 \text{ in.}$ and $(a/\ell) = 0.21$. Equation (8-12) gives $LPEF=1.84$ for this case, compared to $LPEF=1.92$ obtained from Fig. 8.2. Thus, Costigan's expression slightly underestimates the infinite-slab $LPEF$.

In view of no better alternative, Costigan [157] recommended that in situ edge stress be estimated from the interior stress calculated using ILLI-PAVE and Eqn. (8-12). The elastic solid curve in Fig. 8.2 is now an improved choice for the determination of $LPEF$ in such a calculation.

The variation of the normalized edge stress with (a/ℓ_e) or (a/ℓ) is shown in Fig. 8.3. The elastic solid edge stress does not fall below 0 even when (a/ℓ_e) is as high as 2.0, indicating that tension always develops at the bottom. On the other hand, a sign reversal in the edge stress is obtained for the dense liquid foundation, when (a/ℓ) exceeds about 1.7.

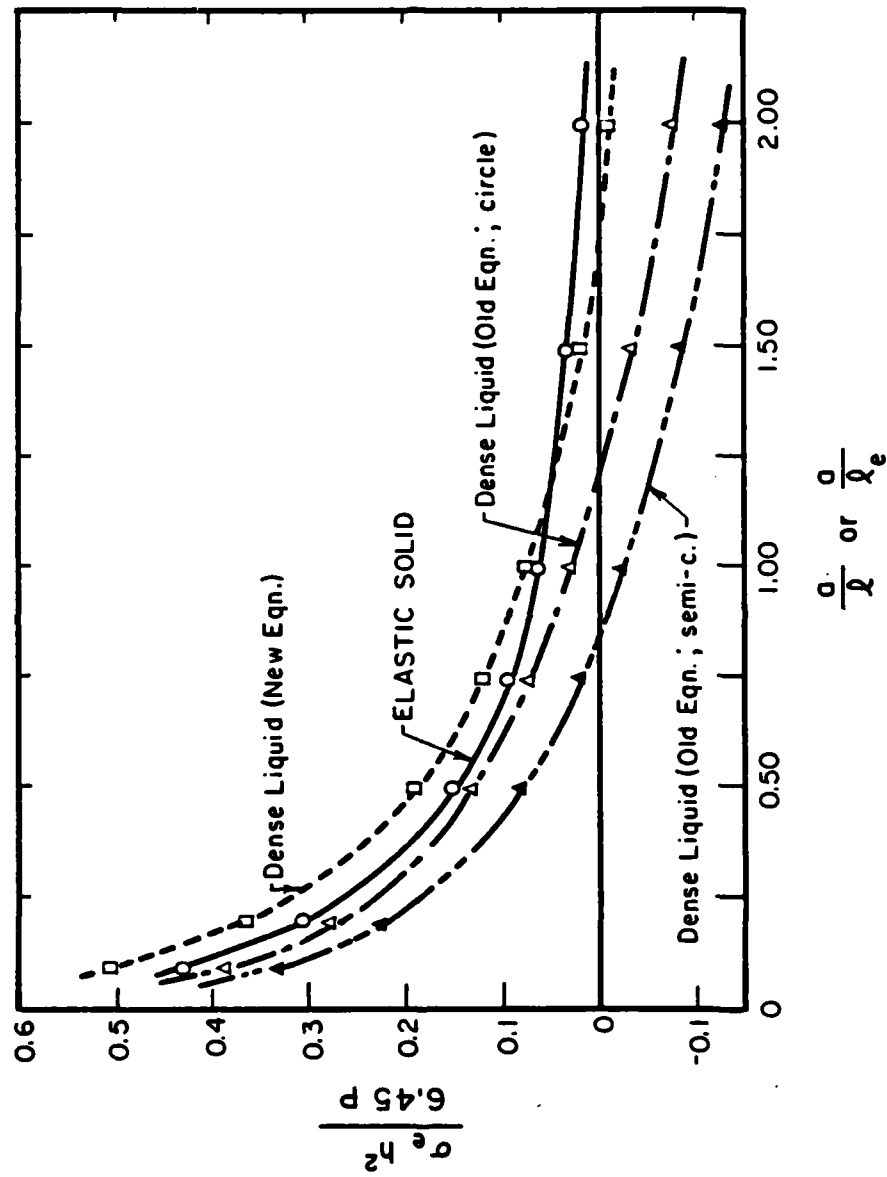


Fig. 8.3 Variation of Normalized Edge Stress

It is also observed in Fig. 8.3 that the dense liquid edge stress predicted by the original Westergaard equation [8] is much lower than that calculated from the "New" formula [10], as well as the corresponding elastic solid value. This confirms that the original equation is flawed, since the elastic solid edge stress may be expected to be smaller than that for the dense liquid, in which no shear interactions between adjacent foundation elements exist. An extensive discussion of this issue has been presented in Chapter 5.

Figure 8.4 shows a plot of normalized edge stress versus (a/λ_e) on semi-log paper. The data points may be fitted with a bilinear equation as follows:

$$0.1 < (a/\lambda_e) < 0.7:$$

$$\sigma_e = 6.45 \frac{P}{h^2} [0.040 - 0.385 \log_{10} (a/\lambda_e)]$$

$$0.7 < (a/\lambda_e) < 2.0:$$

$$\sigma_e = 6.45 \frac{P}{h^2} [0.0712 - 0.1864 \log_{10} (a/\lambda_e)] \quad (8-13)$$

These expressions may be used to predict elastic solid edge stress for values of (a/λ_e) between 0.1 and 2.0.

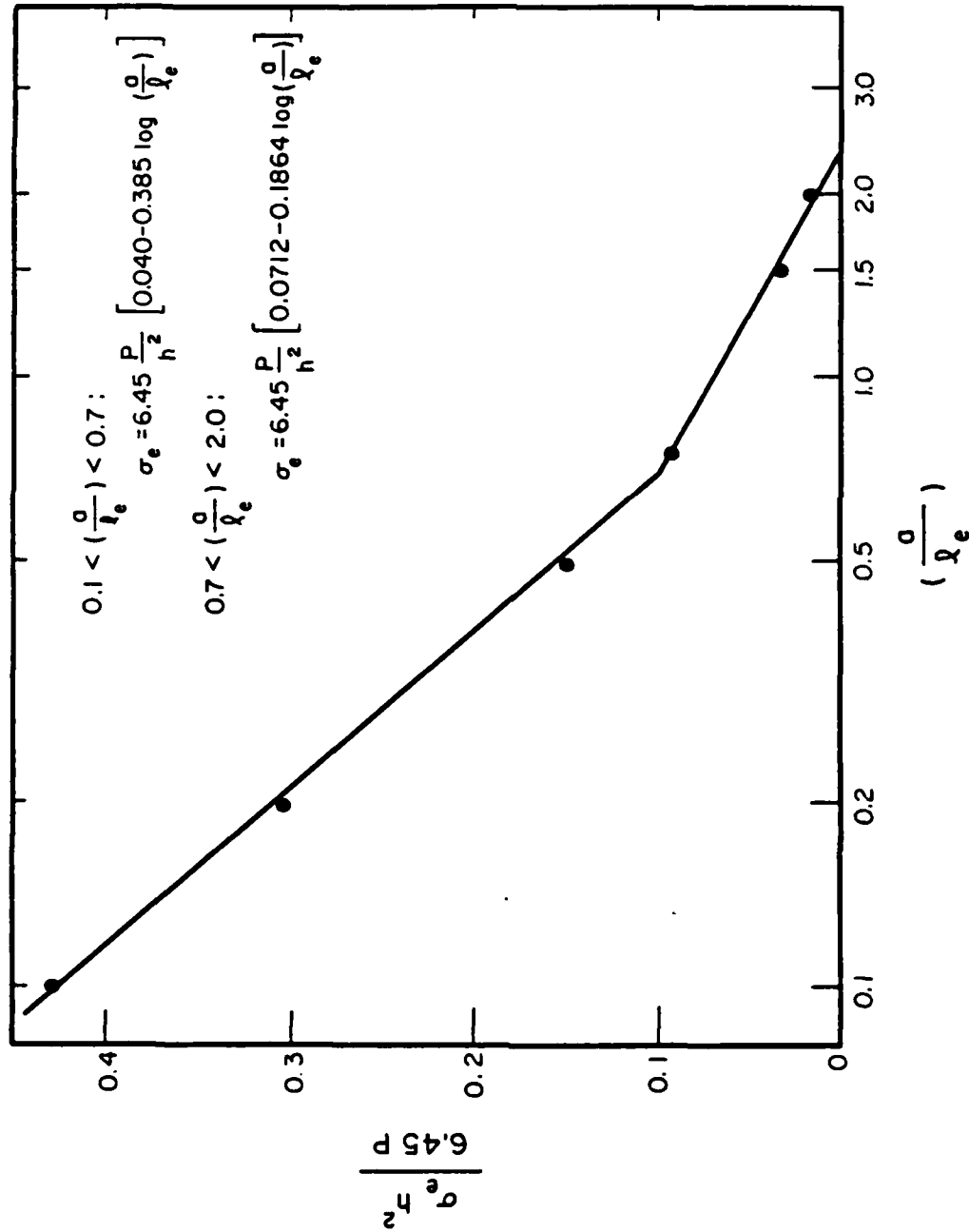


Fig. 8.4 Derivation of Edge Stress Equations
(Elastic Solid)

CHAPTER 9

TWO-DIMENSIONAL FINITE ELEMENT MODEL
FOR SLAB ON ELASTIC SOLID

9.1 INTRODUCTION

The two procedures described above, CFES and H5LES, provide some means for investigating the problem of a plate on an elastic solid foundation. Unfortunately, the applicability of these programs is restricted to certain slab configurations and loading patterns. Furthermore, results obtained from the edge load analysis in H5LES are not descriptive of all aspects of slab and subgrade response, since only maximum bending stress is determined. It is to situations like this that the other two numerical analysis techniques referred to in Chapter 3, owe their popularity. Both finite element and finite difference approaches possess a certain flexibility of application, albeit to different degrees depending on the problem considered, that makes them ideal for slab-on-grade studies. Both methods were examined during this research.

This Chapter discusses the application of the Finite Element Method (F.E.M.) to the solution of the problem of a plate on an elastic solid foundation, and describes the development and implementation of such a model within ILLI-SLAB.

9.2 THEORY

In their paper "Plates and Tanks on Elastic Foundations- An Application of Finite Element Method", Cheung and Zienkiewicz [88] were the first to propose a method for incorporating the elastic solid subgrade in a two-dimensional plate bending finite element model. They assumed a piecewise uniform approximation to the subgrade reaction, and formed the subgrade stiffness matrix by inverting the flexibility matrix obtained using Boussinesq's theory. This concept had also been used by Pickett, et al. [84] in a finite difference solution of the same problem.

According to Cheung and Zienkiewicz [88], the plate is divided into rectangular elements of dimensions $2a \times 2b$. In a rectangular area $2a \times 2b$ surrounding any node i , the subgrade reaction is assumed to be constant and its resultant, a vertical force Q_i , to be acting at node i (Fig. 9.1). The reaction pressure is, therefore, $Q_i/4ab$ and varies from node to node.

Now, the vertical displacement, w_{ni} , at a point n on the surface of the elastic half-space, due to a concentrated load F_i acting at another point i , also on the surface of the half-space, is given by [159]:

$$w_{ni} = \frac{F_i (1 - \mu_s^2)}{\pi E_s r_{ni}} \quad (9-1)$$

where:

E_s, μ_s : Young's modulus and Poisson's ratio for the subgrade;

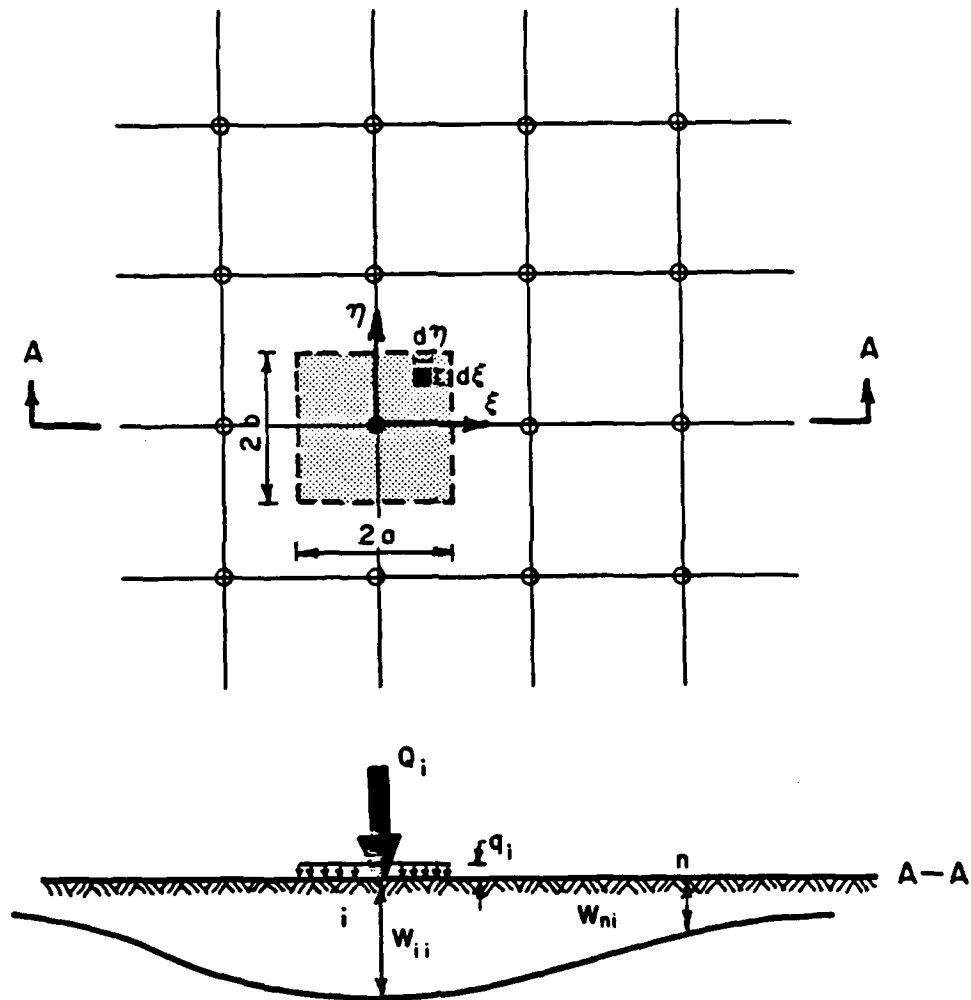


Fig. 9.1 Cheung and Zienkiewicz Finite Element Model

r_{ni} : distance between points i and n .

Deflection, w_{ii} , at node i due to a uniform pressure, q_i , over the rectangular area of influence around this node can be obtained from Eqn. (9-1) as follows:

$$\begin{aligned} \text{Force acting on elemental area } d\xi \times d\eta &= q_i \cdot d\xi \cdot d\eta \\ &= \frac{Q_i}{2a \times 2b} \cdot d\xi \cdot d\eta \end{aligned}$$

$$\text{Distance to corner of elemental area from } i = \sqrt{\xi^2 + \eta^2}$$

Therefore, integrating over $2a \times 2b$:

$$\begin{aligned} w_{ii} &= 2 \int_{\xi=0}^{\xi=a} 2 \int_{\eta=0}^{\eta=b} \frac{Q_i}{2a \times 2b} \frac{(1-\mu_s^2)}{\pi E_s} \frac{1}{\sqrt{\xi^2 + \eta^2}} d\xi d\eta \\ &= \frac{Q_i (1-\mu_s^2)}{2a \pi E_s} f_{ii} \end{aligned} \quad (9-2)$$

where:

$$f_{ii} = \frac{2}{\alpha} \left[\ln(\alpha + \sqrt{1+\alpha^2}) + \alpha \ln\left(\frac{1+\sqrt{1+\alpha^2}}{\alpha}\right) \right] = 2\alpha \int_0^1 \int_0^\alpha \frac{d\xi d\eta}{\sqrt{\xi^2 + \eta^2}}$$

$\alpha = 2b/2a$: element aspect ratio.

This equation is quoted by Giroud [160]. The variation of f_{ii} with α is shown in Fig. 9.2. Alternative forms of f_{ii} are given by Harr [161] and Cheung and Nag [162].

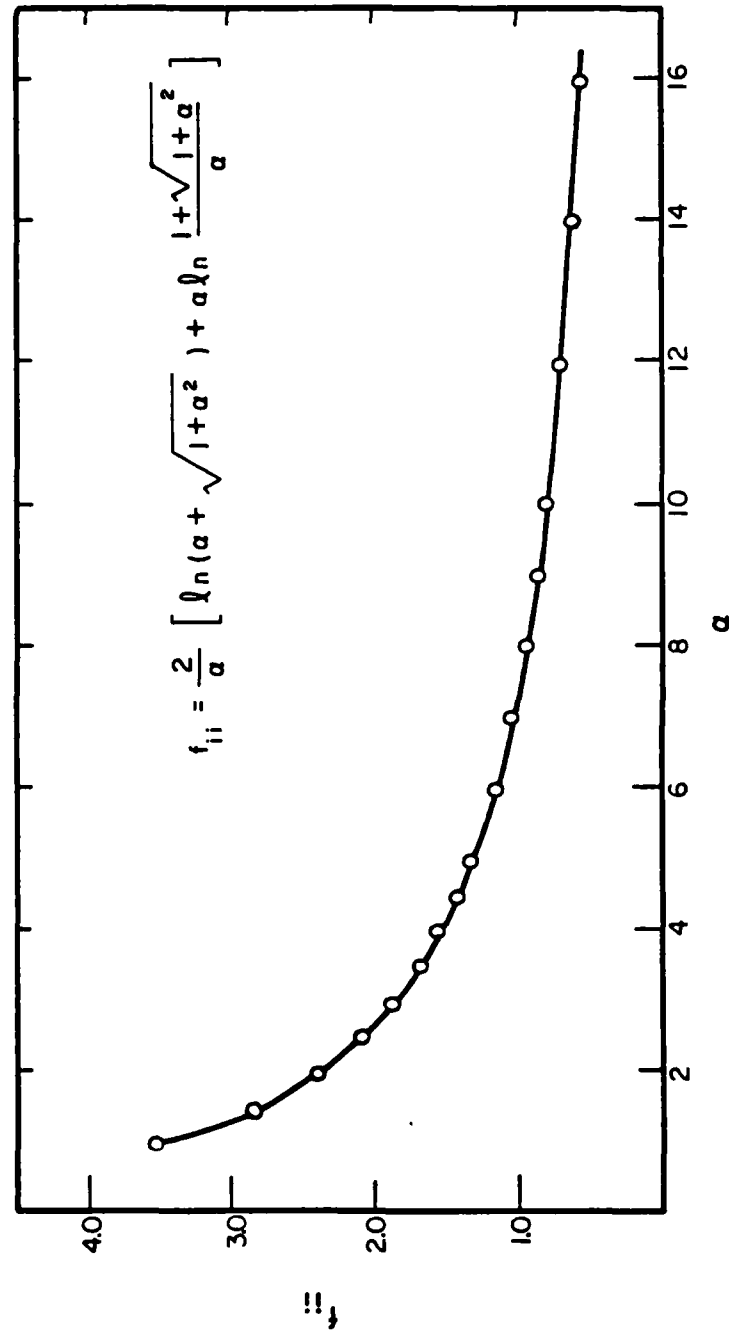


Fig. 9.2 Variation of Influence Factor, f_{ii}

To calculate the deflection w_{ni} at node n due to the rectangular loaded area of influence surrounding node i , a similar integration can be performed. Cheung and Zienkiewicz [88] claim that an adequate approximation can be obtained (error less than about 5%) if the resultant total load Q_i is used in Eqn. (9-1), instead of the uniformly loaded rectangular area. Note that this applies only to square areas of influence ($\alpha = 1.0$). Significant deterioration of the approximation occurs for other values of the aspect ratio (Fig. 9.3).

According to Cheung and Zienkiewicz [88], therefore, for a given mesh, the vertical deflections can be written as:

$$\{w\} = [F_f]\{Q\} \quad (9-3)$$

where:

- $\{w\}$: vector of surface vertical deflections;
- $[F_f]$: flexibility matrix for foundation;
- $\{Q\}$: vector of nodal subgrade reaction forces.

The off-diagonal terms of the flexibility matrix are obtained from Eqn. (9-1), and the diagonal terms from Eqn. (9-2). Note that, in view of the form of these equations, the mesh must be such that all elements are of equal size ($2a \times 2b$), except the ones adjacent to the plate edges which must be half this size [163].

The subgrade stiffness matrix, $[K_f]$, can be obtained by inverting the flexibility matrix:

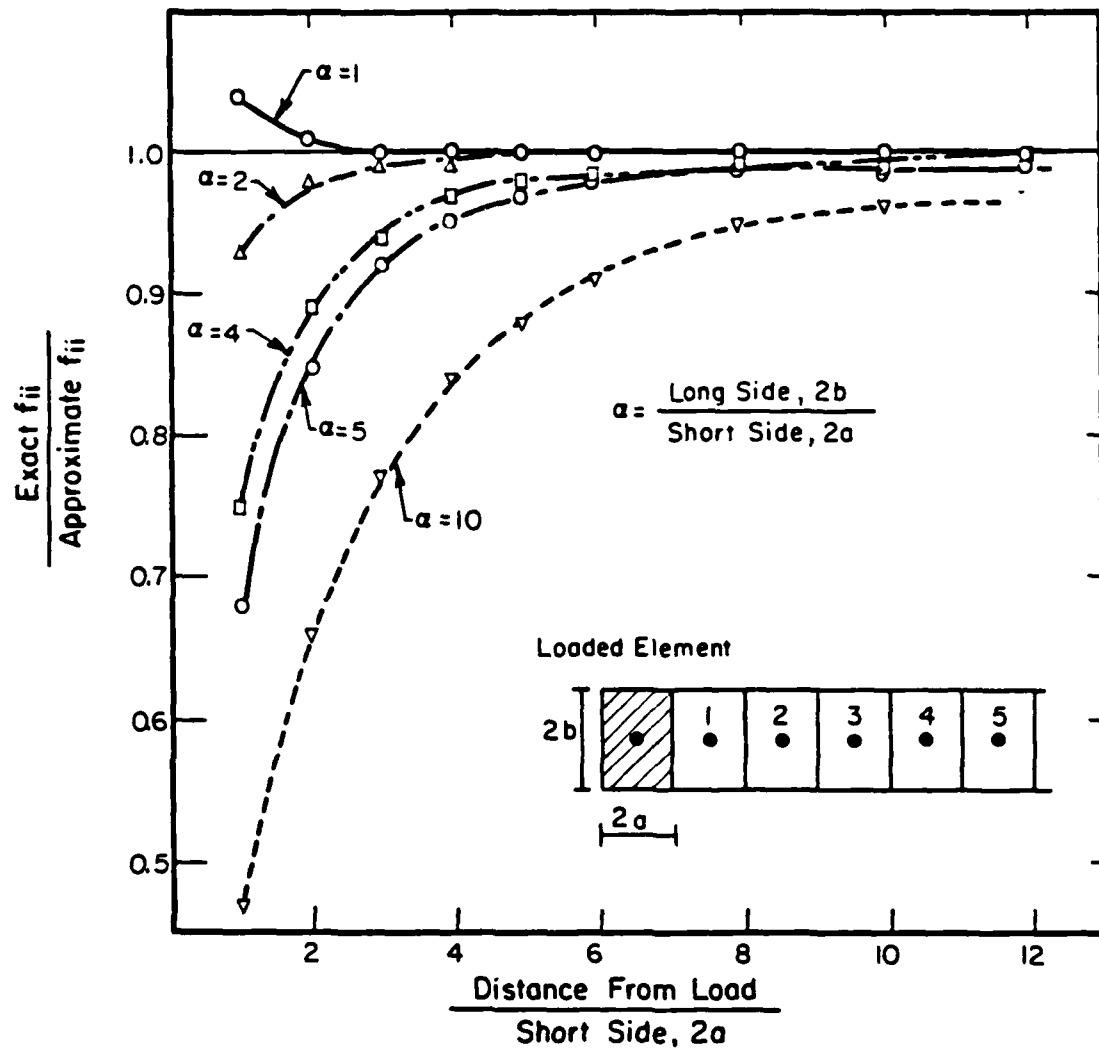


Fig. 9.3 Evaluation of Approximation Proposed by Cheung and Zienkiewicz

$$\{Q\} = [K_f]\{w\} \quad (9-4)$$

where:

$$[K_f] = [F_f]^{-1}$$

This stiffness matrix is added to the stiffness matrix of the slab to obtain the system stiffness matrix. Before this addition, however, the subgrade stiffness matrix $[K_f]$ and vertical displacement vector $\{w\}$ must be "expanded-to-size" by inserting appropriate rows and columns of zeroes, so that they are compatible with the slab stiffness matrix. Eqn. (9-4) may, therefore, be rewritten as:

$$\{Q'\} = [K_f']\{d_f'\} \quad (9-5)$$

where:

$\{Q'\}$: vector of generalized subgrade reaction forces,

i.e. $\{Q\}$ "expanded-to-size";

$[K_f']$: subgrade stiffness matrix "expanded-to-size";

$\{d_f'\}$: subgrade generalized displacement vector,

i.e. $\{w\}$ "expanded-to-size".

For any given element:

$$[K_f']_{12 \times 12} = \begin{bmatrix} K'_{f(1,1)} & K'_{f(1,2)} & \cdots & K'_{f(1,4)} \\ K'_{f(2,1)} & \cdots & \cdots & \cdots \\ \vdots & \cdots & \cdots & \cdots \\ K'_{f(4,1)} & K'_{f(4,2)} & \cdots & K'_{f(4,4)} \end{bmatrix}$$

12 X 12

where:

$$K'_{f(i,j)} = \left[K'_{f(i,j)} \right]_{3 \times 3} = \begin{bmatrix} K'_{f(0,0)} & 0 & 0 \\ 0 & 0 & 0 \\ 0 & 0 & 0 \end{bmatrix}_{3 \times 3}$$

K_f : corresponding stiffness matrix element in subgrade stiffness matrix, before "expansion-to-size";

$$\text{and } \{d'_f\}_{12 \times 1} = \begin{Bmatrix} d'_{f_1} \\ d'_{f_2} \\ d'_{f_3} \\ d'_{f_4} \end{Bmatrix}_{12 \times 1}$$

$$d'_{f_1} = \{d'_{f_1}\}_{3 \times 1} = \begin{Bmatrix} w_i \\ 0 \\ 0 \end{Bmatrix}_{3 \times 1}$$

w_i : corresponding vertical displacement in vector of vertical displacements, $\{w\}$, before "expansion-to-size";

$$\text{and } \{Q'\}_{12 \times 1} = \begin{Bmatrix} Q'_1 \\ Q'_2 \\ Q'_3 \\ Q'_4 \end{Bmatrix}_{12 \times 1}$$

$$Q'_1 = \{Q'_1\}_{3 \times 1} = \begin{Bmatrix} Q_1 \\ 0 \\ 0 \end{Bmatrix}_{3 \times 1}$$

Q_i : corresponding vertical reaction force in vector of vertical reaction forces, $\{Q\}$, before "expansion-to-size".

Note that the two rotational displacements and forces in $\{d_{fi}'\}$ and $\{Q_i'\}$ are zero because the Boussinesq equation involves only vertical forces and deflections and no angular continuity is assumed between the plate and the foundation.

Now, if $\{P\}$ is the vector of externally applied nodal loads, the following equation applies for the system:

$$\begin{aligned}\{P\} - \{Q\} &= [K_p] \{d_p\} \\ \text{or } \{P\} &= [K_p] \{d_p\} + [K_f'] \{d_f'\} \\ \text{or } \{P\} &= [[K_p] + [K_f']] \{d_{tot}\} \quad (9-6) \\ \text{i.e.}\end{aligned}$$

$$\{P\} = [K_{tot}] \{d_{tot}\}$$

whence:

$$\{d_{tot}\} = [K_{tot}]^{-1} \{P\} \quad (9-7)$$

where:

$[K_p]_{12 \times 12}$: stiffness matrix for the plate;

$$[K_{tot}] = [[K_p] + [K_f']]$$

: system stiffness matrix;

$\{d_p\}_{12 \times 1}$: displacement vector for the plate;

$\{d_{tot}\}$: system displacement vector.

Note that vertical displacements in $[d_p]$ and $[d_f']$ are equal for compatibility, and that rotational displacements in $[d_f']$ are zero.

Having solved for $\{d_{tot}\}$, subgrade vertical displacement vector $\{d_f'\}$ may be retracted by setting the rotational displacements in $\{d_{tot}\}$ to zero. It is necessary, however, to calculate these rotational displacements in the first place, since they are essential in calculating bending stresses in the slab. Eliminating the rotations yields the vector of subgrade vertical displacements, $\{w\}$. Thus, the subgrade reaction forces $\{Q\}$ are obtainable from Eqn. (9-4).

Cheung and Zienkiewicz [88] concluded that the "Winkler type spring approximation introduced to avoid mathematical difficulties need no longer be used where continuous foundations are presented." Almost two decades later, the "spring approximation" is still by far the most widely used subgrade representation. This is due to the computational drawbacks of the elastic solid approach, some of which are addressed below.

9.3 REFINEMENTS OF THE CHEUNG-ZIENKIEWICZ MODEL

9.3.1 Partial Contact

Cheung and Nag [162] proposed the following iterative procedure to account for the loss of contact between the slab and the subgrade:

- (i) Perform the analysis as described in Section 9.2;
- (ii) If all the contact pressures are compressive the problem is terminated; otherwise,

- (iii) Determine which nodes are associated with tensile or zero contact pressures and make the corresponding rows and columns in the original flexibility matrix zero;
- (iv) Invert the new flexibility matrix and repeat step (i).

Convergence is usually reached after three to four cycles. After each iteration the nodes which have been eliminated will always yield zero contact pressures. According to the results of an analysis of a square plate under a central point load presented by these authors, there is a 0.7% increase in the maximum contact pressure when tensile stresses in the subgrade are eliminated.

Huang [164] expanded this concept to include gaps produced by pumping and permanent deformation and/or temperature warping, as well as precompressions due to the self-weight of the slab. As shown in Fig. 9.4(a), the total gap, s_i , at any node i is:

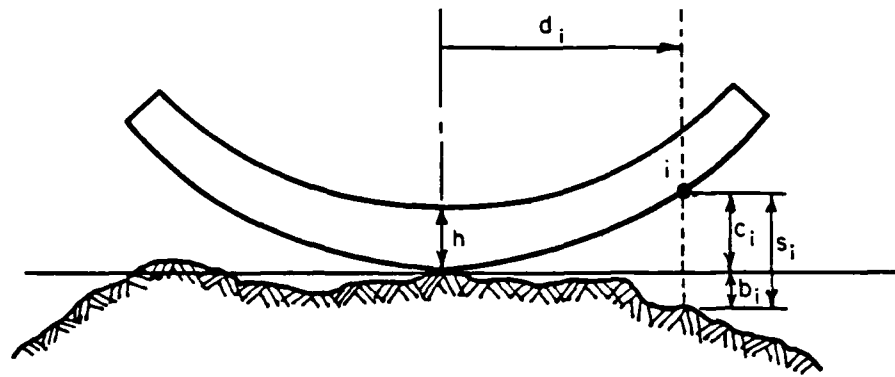
$$s_i = b_i + c_i \quad (9-8)$$

where:

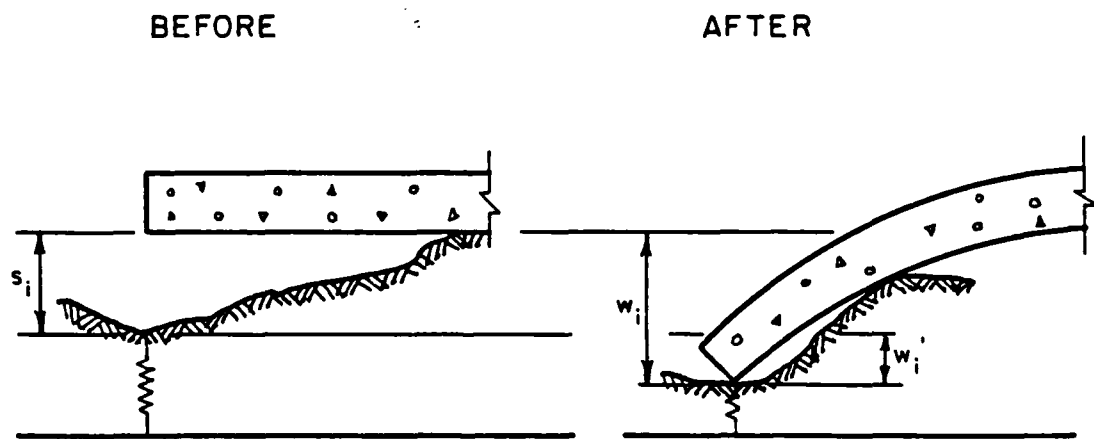
b_i : gap due to pumping and plastic deformation;

c_i : gap due to temperature warping.

It is first assumed that the slab is in full contact with the subgrade, and the set of nodal displacements w_i thus determined is compared against s_i . If w_i is smaller than s_i , the plate and the foundation are not in contact at node i , and this node is eliminated as proposed by Cheung and Nag [162]. Otherwise, a set of modified nodal



(a) Definitions



(b) Checking Partial Contact

Fig. 9.4 Analysis of Partial Contact

displacements, w_i' , is obtained as shown in Fig. 9.4(b) using:

$$w_i' = w_i - s_i \quad (9-9)$$

The process is repeated until the same contact condition is obtained for two successive iterations. For most cases, only four or five iterations are needed.

9.3.2 Making the Subgrade Stiffness Matrix Banded

A major difficulty in using the Cheung and Zienkiewicz [88] elastic solid model is the large computer storage required, in view of the fact that the subgrade stiffness matrix is symmetric but not banded. An iterative scheme was proposed by Huang [87] to convert this matrix into a banded one and thus reduce the number of storage spaces required.

The principle of this scheme is very simple. It follows from above that

$$[[K_p] + [K_f']] \{d_{tot}\} = \{P\} \quad (9-6)$$

$$\text{or } [K_{tot}] \{d_{tot}\} = \{P\}$$

Since $[K_f']$ is symmetric but not banded, $[K_{tot}]$ is also symmetric but not banded. However, a pseudo half-bandwidth, m , may be arbitrarily assigned. Any coefficients outside the half-band are transferred to the right-hand side of the equation, as shown in Eqn. (9-10) (see next

page) which is solved by iteration. First, assume displacements $\{d_{tot}\}$ on the right-hand side are zero and compute a set of nodal displacements $\{d_{tot}\}$ by solving Eqn. (9-10). Enter the displacements thus computed into the right-hand side of Eqn. (9-10) and find a new set of displacements. The process is repeated until displacements converge to a specified tolerance. Huang recommended using a large pseudo half-bandwidth when the "number of equations is large while the (real) half-bandwidth is small".

An alternative method to overcome the computer storage limitation by using a banded matrix was proposed by Cheung [165]. Modification of the foundation stiffness matrix is based on the assumption that the deflection at a point is affected substantially only by forces acting at nearby points. This makes the model less accurate, but also reduces computer storage dramatically. Cheung claims that "if a maximum computer storage is given, the simplified method can divide the system into much finer meshes and will provide an approximate solution with accuracy better than the conventional method."

A study of various load-deflection patterns (Fig. 9.5) was conducted by Cheung, and square pattern (d) was proposed for general use. In this pattern, a deflection occurring at node (i,i) is assumed to be influenced by nodal loads distributed in a square influence area $2N \times 2N$. Cheung reported that several test runs were made and the results for $N=4$ seem to be adequate. The maximum stress and contact pressure in these analyses agreed within 0.5% with the conventional method. As N increases, the accuracy of the approximation improves.

(9-10)

$$\begin{bmatrix} k_{tot1,1} & \dots & k_{tot1,m} & 0 \\ \vdots & \ddots & \vdots & \vdots \\ k_{tot1,i} & \dots & p_{1,i+m-1} & \vdots \\ \vdots & \ddots & \vdots & p_{n,n} \end{bmatrix} = \begin{Bmatrix} d_{tot1} \\ \vdots \\ d_{tot1} \\ \vdots \\ d_{totn} \end{Bmatrix} - \begin{Bmatrix} p_1 \\ \vdots \\ p_i \\ \vdots \\ p_n \end{Bmatrix} \begin{bmatrix} p_{1,m+1} \dots p_{1,n} \\ \vdots \\ 0 \\ \vdots \end{bmatrix} \begin{Bmatrix} d_{tot1} \\ \vdots \\ d_{totn} \end{Bmatrix}$$

Symmetric

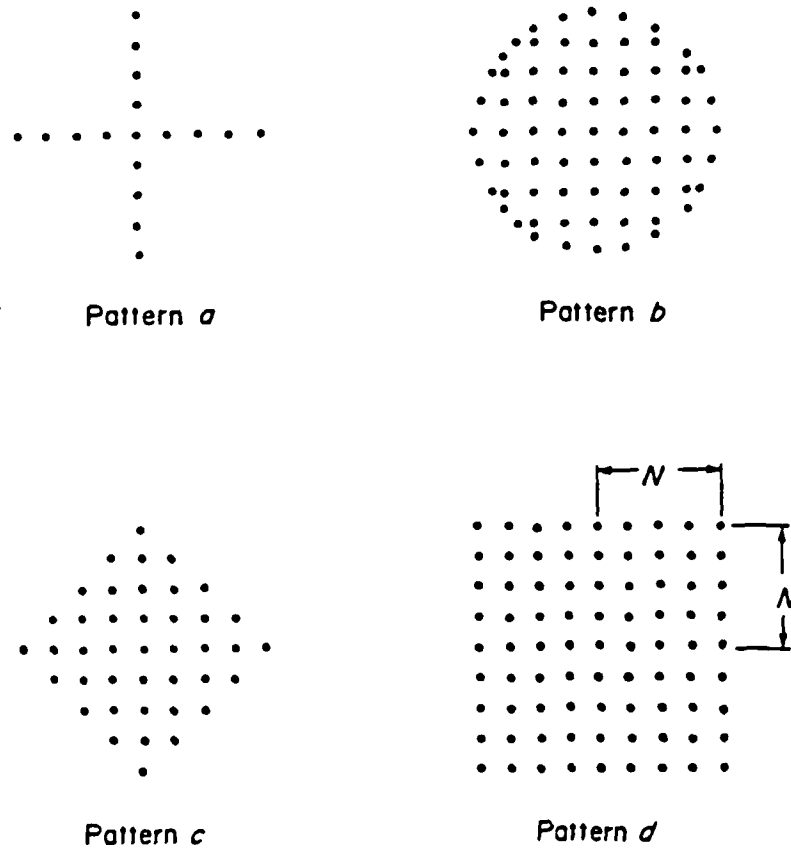


Fig. 9.5 Load-Deflection Influence Patterns

The conventional (elastic solid) method is simply the case where N is large enough to cover all nodes in the system. Setting $N=1$, a model similar to the dense liquid is obtained. Cheung's method is also similar to that proposed by Huang [87], when only one iteration is allowed in the latter.

9.3.3 Analysis of Two Slabs with Shear Transfer

Huang's iterative scheme [87; 164] is particularly useful for analyzing two slabs interconnected by a load transfer device, so that both have the same vertical deflections along the joint, while the moments about the joint are still zero. This situation is very similar to the case where dowel bars are used to connect adjacent slabs, allowing the transfer of shear but not of moment. Each slab can be considered separately. To begin with, consider one slab only and determine a first set of nodal displacements from Eqn. (9-10). Next, consider the second slab, and impose the joint deflections and reaction forces calculated for the first slab. Thus, the nodal displacements of the second slab can be computed. Then, return to the first slab and impose the joint deflections and reaction forces determined from the second slab, to calculate a new set of displacements for the first slab. The process is repeated until the nodal displacements converge. When imposing deflections from one slab onto another, an underrelaxation factor of 0.5 was recommended to insure stability [87].

9.3.4 Use of Symmetry

Using a concept very similar to that employed in ILLI-SLAB, Huang [166] presented results obtained by analyzing only one quarter of a symmetrical slab under an interior load. Using symmetry implies that rotations θ_x (when x-axis is a line of symmetry) and/or θ_y (when y-axis is a line of symmetry) are zero. This condition is imposed by setting the corresponding elements in the diagonal of the stiffness matrix to "infinity", say 10^{20} .

Furthermore, the subgrade stiffness matrix for the subgrade $[K_f']$ must also be modified when symmetry is used, because a force at any node in the full slab will cause a deflection at all nodes in the portion of the slab analyzed using symmetry. The effect of the "mirror image" nodes is accounted for by adding their flexibility coefficients to the one for the corresponding node in the portion of the slab analyzed. Thus, the flexibility coefficient of a typical node in the interior of a quarter slab analyzed using symmetry along the x- and y-axis is multiplied by 4, since in the full slab four such corresponding nodes would exist. Huang also suggested employing a scheme which would allow using a coarser mesh (bigger elements) away from the load.

9.3.5 Higher Order Approximation to Contact Pressure Function

The most important assumption in the model proposed by Cheung and Zienkiewicz [88] is that the contact pressure under the slab is uniformly distributed over rectangular areas around each node. This is a very crude approximation to the contact pressure function and may lead

to unrealistic contact pressure distributions, since contact pressure is highly dependent on the finite element mesh fineness. In order to obtain a better approximation to the contact pressure function, Svec and McNeice [167] assumed that this function may be represented by a polynomial of the form:

$$q(\xi, \eta) = \sum_{m,n} b_{m,n} \xi^m \eta^n \quad (9-11)$$

where:

(ξ, η) : local orthogonal coordinates.

A third degree (cubic) polynomial involving ten coefficients was selected in order to provide a reasonable approximation, even over large elements. The ten coefficients are obtained by discretizing and inverting the Boussinesq equation. It has been shown, however, that normal slopes along the boundary of a loaded region on an elastic half-space are infinite [168]. Consequently, only vertical displacements of the half-space can be dealt with. Therefore, a new triangular plate bending element was developed [169] which has ten nodes and includes the vertical displacements at these nodes among its generalized coordinates. The element has 33 degrees-of-freedom and a deflection field represented by a polynomial of the seventh degree (Fig. 9.6). It has compatible boundary slopes and displacements and satisfies the convergence requirements [170].

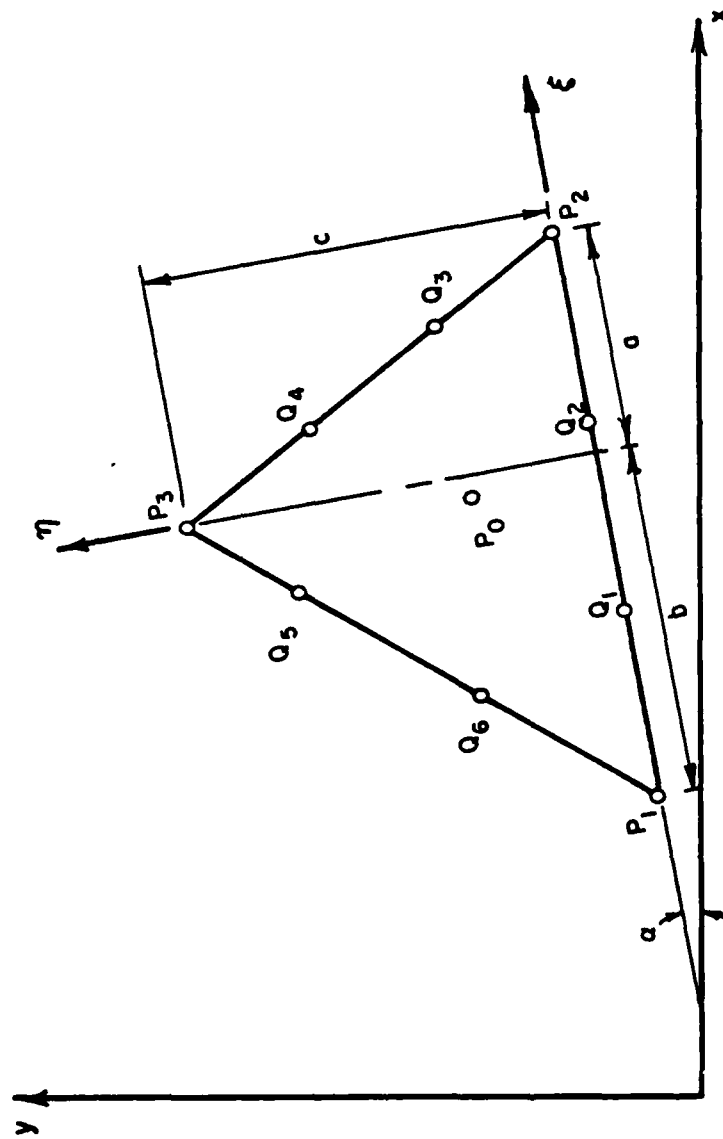


Fig. 9.6 Svec's Triangular Plate Bending Element

9.4 THE ELASTIC SOLID OPTION IN ILLI-SLAB

The elastic solid option has been added to ILLI-SLAB through subroutine ELSOLID. The advantage of having both the elastic solid and the dense liquid models in a single finite element program is self-evident. Direct comparisons can be made between the two models with respect to execution costs, computer storage requirements, accuracy, factors affecting the efficiency of the finite element mesh, as well as comparisons between the pavement system responses in each case. Since it is desirable that meshes consisting of elements of unequal size should be admitted, an equation for the deflection under the corner of a uniformly loaded rectangular area over an elastic solid foundation, given by Giroud [160] was used to derive an expression for deflection w_{ii} , at node i due to a uniform pressure q_i over the rectangular area of influence surrounding this node. Thus,

$$w_{ii} = \frac{1-\mu_s^2}{E_s \pi} q_i \sum_{j=1}^m \text{SIDES}_j f_j(\alpha) \quad (9-12)$$

where:

q_i : pressure over rectangular area of influence around node i ;

$\alpha = \text{SIDEL}_j / \text{SIDES}_j \geq 1.0$;

SIDEL_j : long side of contributory quadrant j ;

SIDES_j : short side of contributory quadrant j ;

$$f_j(\alpha) = \{ \ln(\alpha + \sqrt{1 + \alpha^2}) + \alpha \ln\left(\frac{1 + \sqrt{1 + \alpha^2}}{\alpha}\right) \}$$

The summation is over the m contributory quadrants surrounding node i . Depending on whether i is an interior, edge or corner node m takes the value of 4, 2 or 1, respectively (Fig. 9.7).

Noting that:

$$q_i = \frac{Q_i}{\sum_{j=1}^m (\text{SIDEL}_j * \text{SIDES}_j)}$$

Eqn. (9-12) may be rewritten as:

$$w_{ii} = \frac{1 - \mu_s^2}{E_s \pi} \left\{ \frac{1}{\sum_{j=1}^m (\text{SIDEL}_j + \text{SIDES}_j)} * \sum_{j=1}^m \text{SIDES}_j f_j(\alpha) \right\} Q_i \quad (9-13)$$

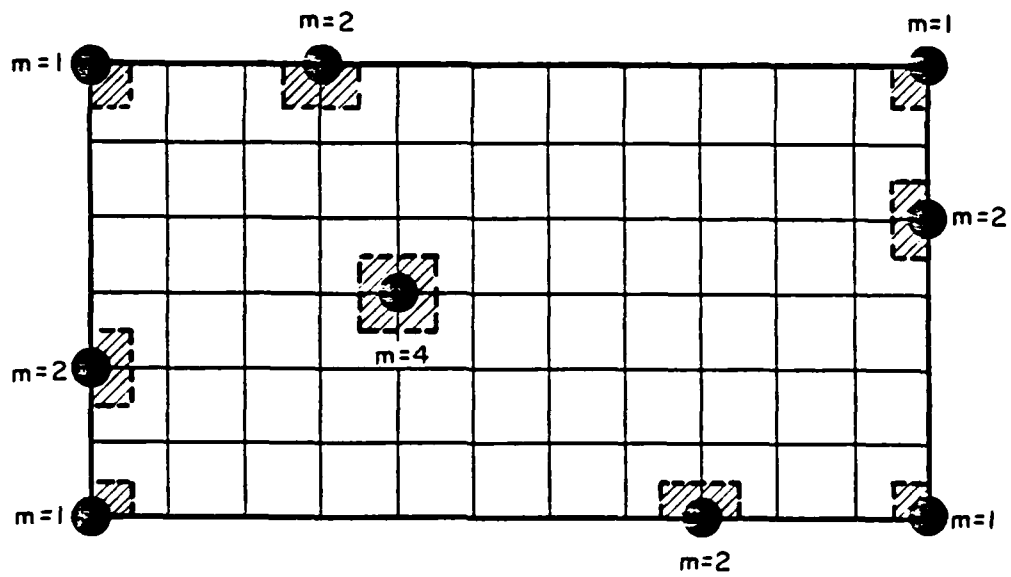
where:

Q_i : resultant reaction force at node i (includes the contribution of all m quadrants).

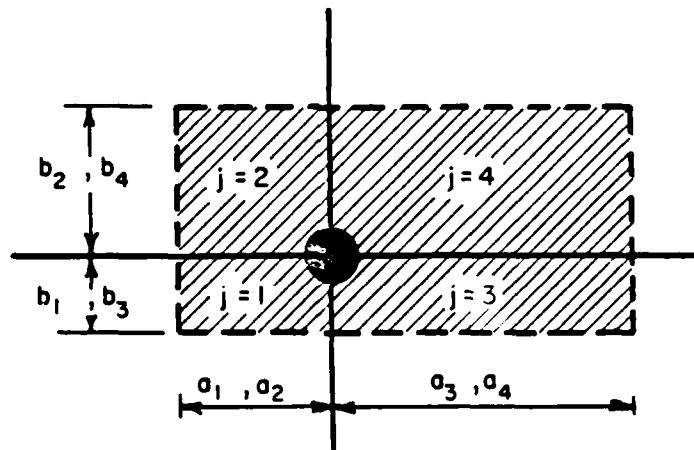
Similarly, Eqn. (9-1) for deflection w_{ni} may be written as:

$$w_{ni} = \frac{1 - \mu_s^2}{E_s \pi} \left\{ \frac{1}{r_{ni}} \right\} Q_i \quad (9-14)$$

Both Equations (9-13) and (9-14) are now in the form required by Eqn. (9-3). It should be noted that although arbitrary aspect ratios are nominally permitted, the approximation involved in Eqn. (9-14)



(a) Limits of Summation



(b) Contributory Quadrants Surrounding a Typical Interior Node

Fig. 9.7 Derivation of Flexibility Coefficient for w_{ii} in ILLI-SLAB

strictly applies to square elements only.

The upper triangle of the flexibility matrix for the subgrade is stored in array FLEX. The inverse of FLEX is added to the upper triangle of the stiffness matrix for the plate elements in array SMES. Most matrix operations are performed using LINPACK routines, a mathematical software package for the solution of linear systems developed between 1976 and 1979 by a project centered at Argonne National Laboratory for Environment Damaging and Research.

At present, only one slab is allowed with the elastic solid option. This must have a constant thickness and elastic modulus and must consist of only one layer. The symmetry capability is not yet operable with this option. To use this option, the user specifies IST=8 in the fixed-form input, or SUBGRADE TYPE BOUSSINESQ in the free-form input. Both types of input are described in detail in Appendix A.

9.5 CONVERGENCE STUDIES WITH ILLI-SLAB ELASTIC SOLID

9.5.1 Scope of Analyses

In order to validate the elastic solid finite element model in ILLI-SLAB, examine the limits of its applicability and establish guidelines for potential users, several of runs were performed. The results from these are discussed in this section. Four effects were investigated:

- (a) Convergence to the closed-form solution which applies to an infinite slab (see Table 7.1), upon expansion of slab size;

- (b) Improvement in the accuracy as mesh fineness increases;
- (c) Comparison between closed-form and finite element solutions for a range of loaded area sizes; and
- (d) Importance of deterioration in accuracy for element aspect ratios other than one.

These effects have been identified as most significant in similar studies with other models. The interior loading condition was selected because closed-form solutions exist only for this case. The responses quoted below are those occurring under the center of the circular load.

9.5.2 Slab Size Effect

The non-dimensional ratio (L/ℓ_e), of slab length to the radius of relative stiffness, is used to characterize this effect, using square slabs divided into square elements, and loaded by one small square interior load. The slab used here has a rather low ℓ_e value (26.02 in.) for practical reasons. The range of (L/ℓ_e) examined is 1.384 to 6.918.

Table 9.1 shows the results obtained using ILLI-SLAB, as well as the closed-form solution. A non-dimensional plot of the same results is shown in Fig. 9.8. As expected, deflection and subgrade stress converge to the infinite slab response from above, exhibiting a typical "punch-like" behavior at small slab sizes. On the other hand, bending stress converges from below, and is much less sensitive to such changes. As will be shown below, discrepancies observed between the large (L/ℓ_e) and infinite slab responses can be attributed to mesh fineness effects. These discrepancies aside, bending stress converges to the

TABLE 9.1
EFFECT OF SLAB SIZE

L (in.)	(L/λ_e)	δ (mils)	q (psi)	σ (psi)
36	1.384	0.366	0.314	8.055
72	2.767	0.295	0.264	8.633
108	4.151	0.280	0.251	8.503
144	5.534	0.272	0.243	8.407
180	6.918	0.268	0.239	8.376
CLOSED-FORM SOLUTION		0.265	0.247	11.497

Notes:

Parameters Used:

$$E = 3 \times 10^6 \text{ psi}$$

$$E_s = 40,000 \text{ psi}$$

$$\mu = 0.15$$

$$\mu_s = 0.45$$

$$h = 12 \text{ in.}$$

$$\lambda_e = 26.02 \text{ in.}$$

Load:

$$A = 3 \text{ in.} \times 3 \text{ in.}$$

$$p = 100 \text{ psi}$$

Interior

$$\text{Element Size, } 2a = 18 \text{ in.}$$

$$\left(\frac{2a}{h}\right) = 1.5$$

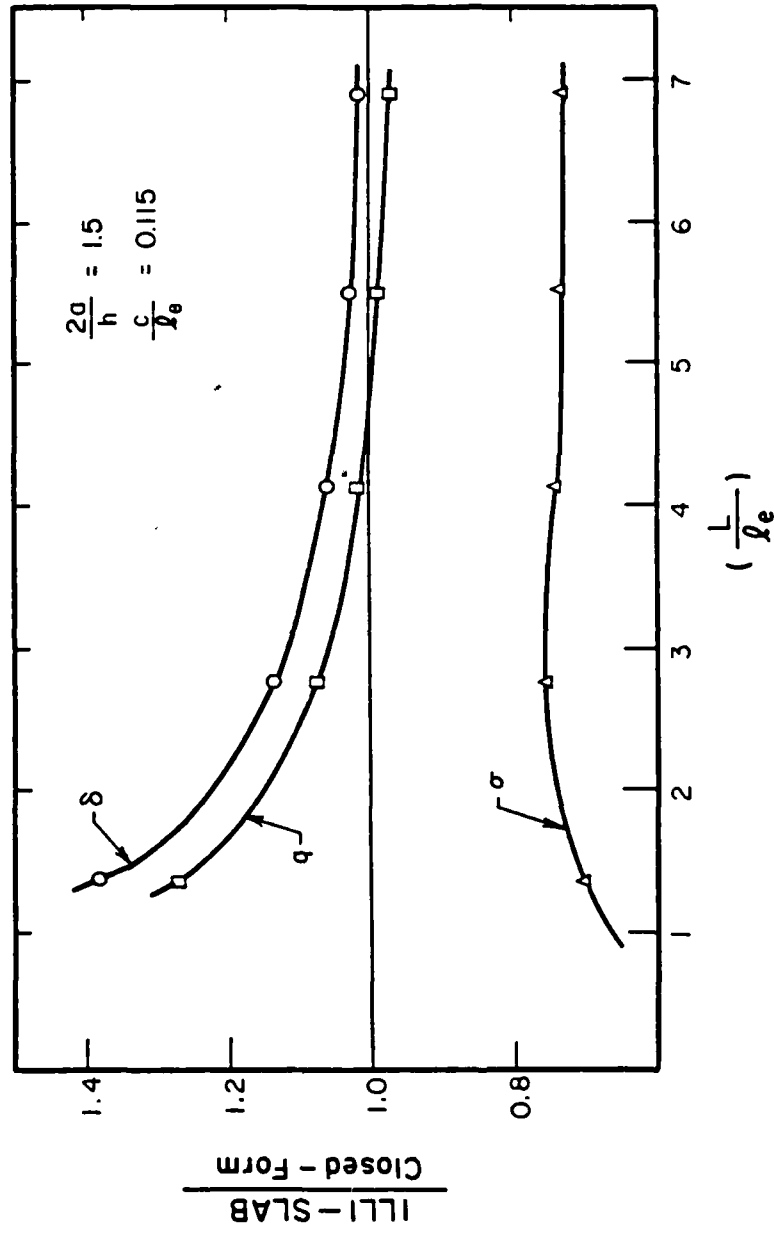


Fig. 9.8 Effect of Slab Size (Interior Load)

large slab value at (L/ℓ_e) of about 3.0. For deflection and subgrade stress, a much higher value (about 7.0) is required. These values are comparable with those obtained for the dense liquid finite element solution.

9.5.3 Mesh Fineness Effect

This effect is characterized by the non-dimensional ratio $(2a/h)$, where $2a$ is the length of the (square) elements and h is the slab thickness. For one of the cases solved above $(L/\ell_e=4.151)$, responses were calculated using finer and coarser meshes.

A comparison between numerical and closed-form solutions is given in Table 9.2. The non-dimensional graphical representation of these results in Fig. 9.9, shows that all three responses converge from below. Bending stress is much more sensitive to mesh fineness than deflection or subgrade stress. A finer mesh would eliminate the discrepancies observed in Fig. 9.8. Similarly, the discrepancies shown in Fig. 9.9 can be explained in terms of the slab size effect. The required values of $(2a/h)$ for good results are as follows:

Deflection : $(2a/h) = 1.5$

Subgrade Stress: $(2a/h) = 0.9$

Bending Stress : $(2a/h) = 0.8.$

TABLE 9.2
EFFECT OF MESH FINENESS

No. of Elements	(2a/h)	δ (mils)	q (psi)	σ (psi)
4	4.5	0.263	0.183	3.384
16	2.25	0.278	0.234	6.874
36	1.5	0.280	0.251	8.503
64	1.125	0.281	0.258	9.529
100	0.9	0.281	0.261	10.262
CLOSED-FORM SOLUTION		0.265	0.247	11.497

Notes:

Parameters Used:

$$E = 3 \times 10^6 \text{ psi}$$

$$E_s = 40,000 \text{ psi}$$

$$\mu = 0.15$$

$$\mu_s = 0.45$$

$$h = 12 \text{ in.}$$

$$l_e = 26.02 \text{ in.}$$

Load:

$$A = 3 \text{ in.} \times 3 \text{ in.}$$

$$p = 100 \text{ psi}$$

Interior

$$\text{Slab Length, } L = 108 \text{ in.}$$

$$\left(\frac{L}{l_e}\right) = 4.151$$

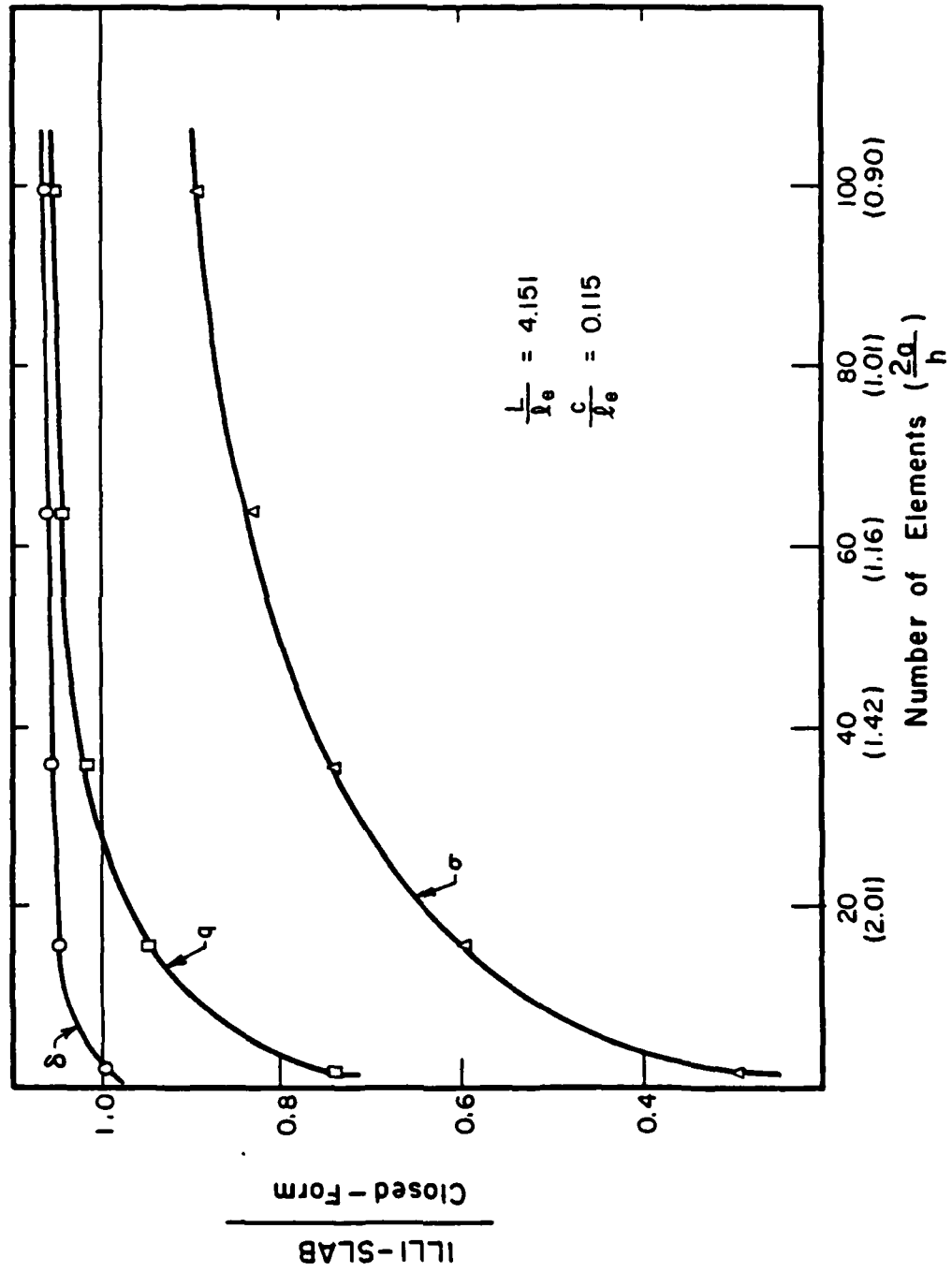


Fig. 9.9 Effect of Mesh Fineness (Interior Load)

9.5.4 Effect of Size of Loaded Area

Using the non-dimensional ratio (c/l_e) of the length of the (square) load divided by the radius of relative stiffness to quantify this effect, several runs were performed for another of the cases in Table 9.1. Total applied load, P , was held constant, but was distributed on an increasingly larger square area.

The results are tabulated in Table 9.3 and plotted in Fig. 9.10. It is observed that all three responses increase in comparison to their closed-form counterparts, with bending stress being much more sensitive to this effect. Similar behavior was observed for the dense liquid model in ILLI-SLAB. It is believed that this is associated with the fact that closed-form solutions consist only of the first one or two terms of an infinite series; and with a mesh fineness effect in the loaded region, in view of the way the F.E.M. converts applied distributed loads, to concentrated, nodal force components. Note that the absolute values of the three responses, decrease as (c/l_e) increases, as expected.

9.5.5 Effect of Element Aspect Ratio

Element aspect ratio, α , defined as the ratio of the long side of the element to its short side, is particularly important in the elastic solid model, due to the approximation discussed above. In a series of runs performed to investigate this effect, the slab was divided into a number of identical elements of a given aspect ratio. This may have a more pronounced effect than a typical mesh which uses only a few high

TABLE 9.3
EFFECT OF SIZE OF LOADED AREA

c (in.)	(c/ℓ_e)	δ (mils)		q (psi)		σ (psi)	
		ILLI-SLAB	CLOSED-FORM	ILLI-SLAB	CLOSED-FORM	ILLI-SLAB	CLOSED-FORM
1	0.0384	0.268	0.265	0.240	0.253	8.457	15.266
3	0.1153	0.268	0.265	0.239	0.247	8.376	11.497
5	0.1922	0.267	0.264	0.237	0.241	8.226	9.747
7	0.2690	0.267	0.263	0.235	0.235	8.018	8.598
10	0.3843	0.265	0.262	0.231	0.227	7.621	7.386

Notes:

Parameters Used:

$$E = 3 \times 10^6 \text{ psi}$$

$$E_s = 40,000 \text{ psi}$$

$$\mu = 0.15$$

$$\mu_s = 0.45$$

$$h = 12 \text{ in.}$$

$$\ell_e = 26.02 \text{ in.}$$

Load (Interior):

$$A = c \text{ in.} \times c \text{ in.}$$

$$P = 900 \text{ lbs}$$

$$\text{Element Size, } 2a = 18 \text{ in.; } (2a/h) = 1.5$$

$$\text{Slab Length, } L = 180 \text{ in.; } (L/\ell_e) = 6.918$$

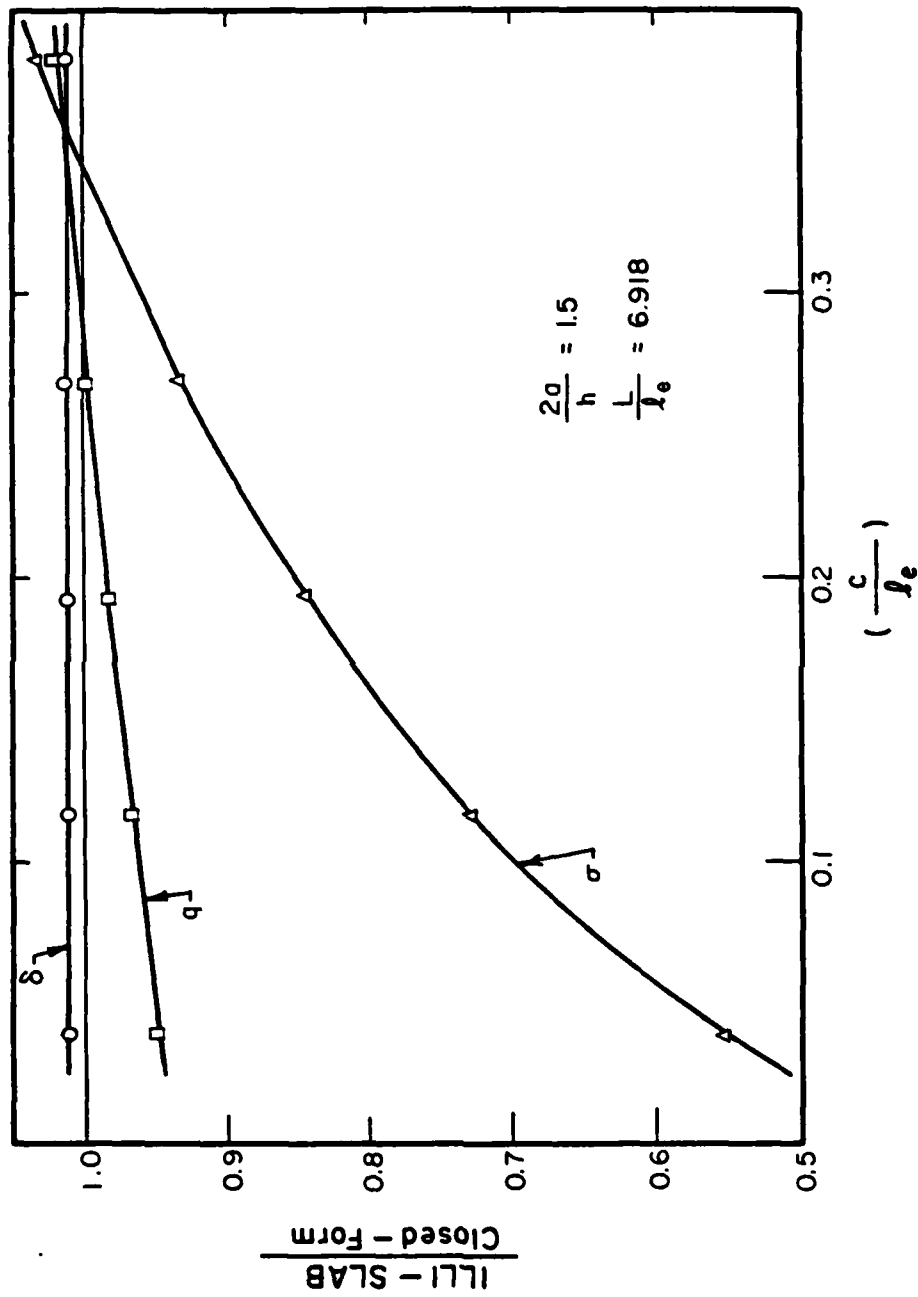


Fig. 9.10 Effect of Size of Loaded Area (Interior Load)

aspect ratio elements.

Table 9.4 shows the results from these runs, and Fig. 9.11 presents them in a non-dimensional plot. The deterioration in accuracy of subgrade stress and bending stress is very significant. Figure 9.12 shows that this effect persists far beyond the loaded region. If at all possible, aspect ratios greater than 2 should be avoided, especially close to the loads or in the region of expected critical response.

9.6 INVESTIGATION OF THE k-SURFACE

With the addition of the Elastic Solid option in ILLI-SLAB, this program becomes the first and only program to incorporate both fundamental subgrade idealizations (viz. Winkler and Boussinesq foundations) in a usable package. This opens up new possibilities for comparative studies, and the investigation presented below is intended to illustrate the broad scope of such analyses. Gibson's analytical work [38] provides a unique theoretical interpretation of the relation between a dense liquid and an elastic solid (see Chapter 2). Numerous other attempts to reproduce the results of one idealization using the other have failed. When one of the three major responses (maximum deflection, subgrade stress or bending stress) is made the same for both models, the other two remain substantially different. It is now generally accepted that no universal correlation exists between Winkler and Boussinesq [46]. In the analyses presented below the F.E.M. is employed in an attempt to explain this phenomenon.

TABLE 9.4
EFFECT OF ELEMENT ASPECT RATIO

2b (in.)	ASPECT RATIO $(\frac{2b}{2a})$	L (in.)	δ (mils)	q (psi)	σ_x (psi)	σ_y (psi)
18	1.0	180	0.268	0.239	8.376	8.376
22.5	1.25	180	0.268	0.234	7.665	8.167
30	1.67	180	0.268	0.225	6.634	7.748
36	2.0	216	0.265	0.215	5.933	7.386
45	2.5	180	0.268	0.204	5.044	6.865
54	3.0	216	0.265	0.191	4.319	6.362
72	4.0	144	0.277	0.186	3.000	5.687
72	4.0	288	0.261	0.173	3.223	5.471
CLOSED-FORM SOLUTION			0.265	0.247	11.497	

Notes:

Parameters Used:

$$E = 3 \times 10^6 \text{ psi}$$

$$E_s = 40,000 \text{ psi}$$

$$\mu = 0.15$$

$$\mu_s = 0.45$$

$$h = 12 \text{ in.}$$

$$l_e = 26.02 \text{ in.}$$

Load:

$$A = 3 \text{ in.} \times 3 \text{ in.}$$

$$p = 100 \text{ psi}$$

Interior

$$\text{Element Width, } 2a = 18 \text{ in.}$$

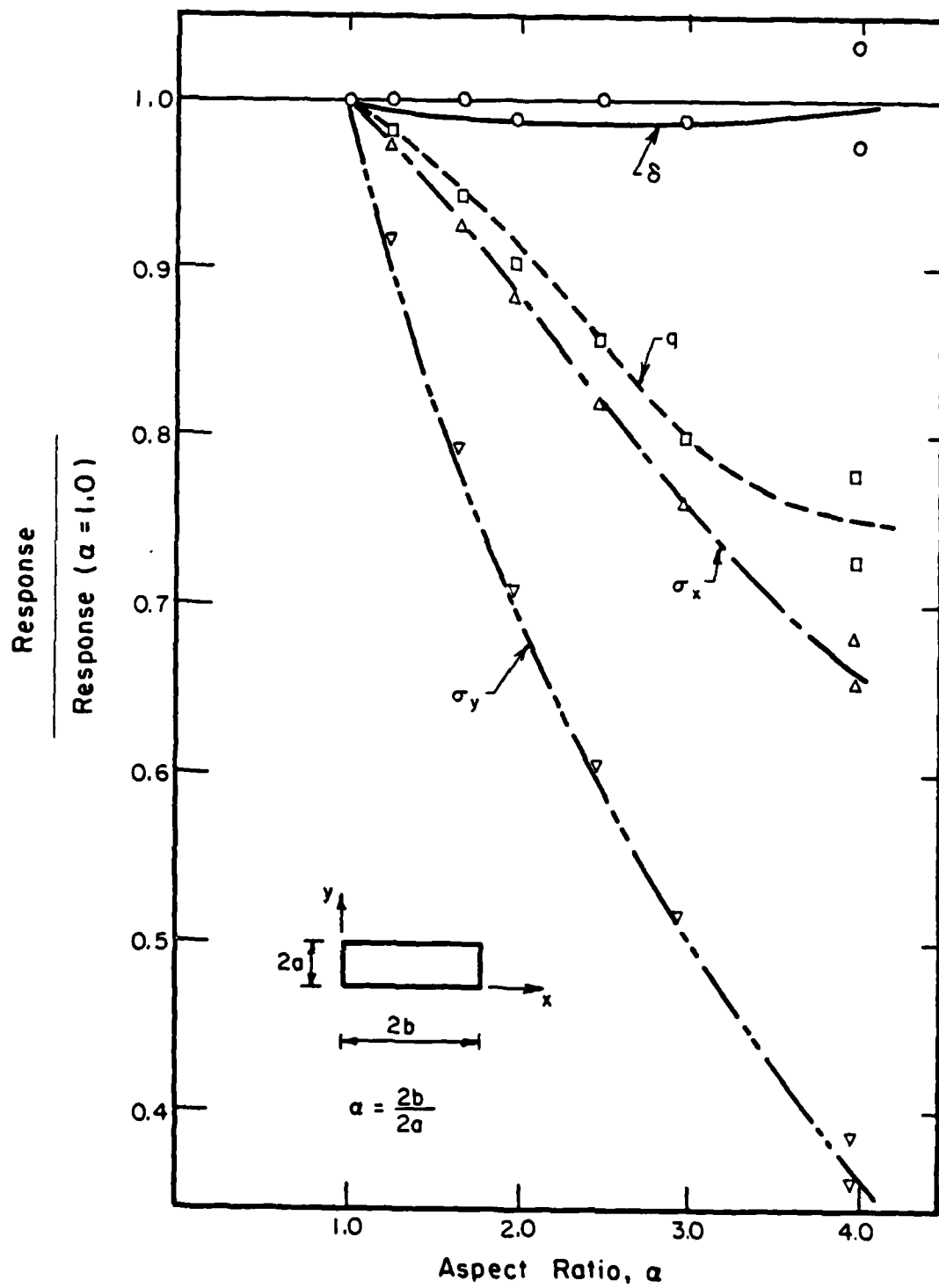


Fig. 9.11 Deterioration of Accuracy as Aspect Ratio Increases

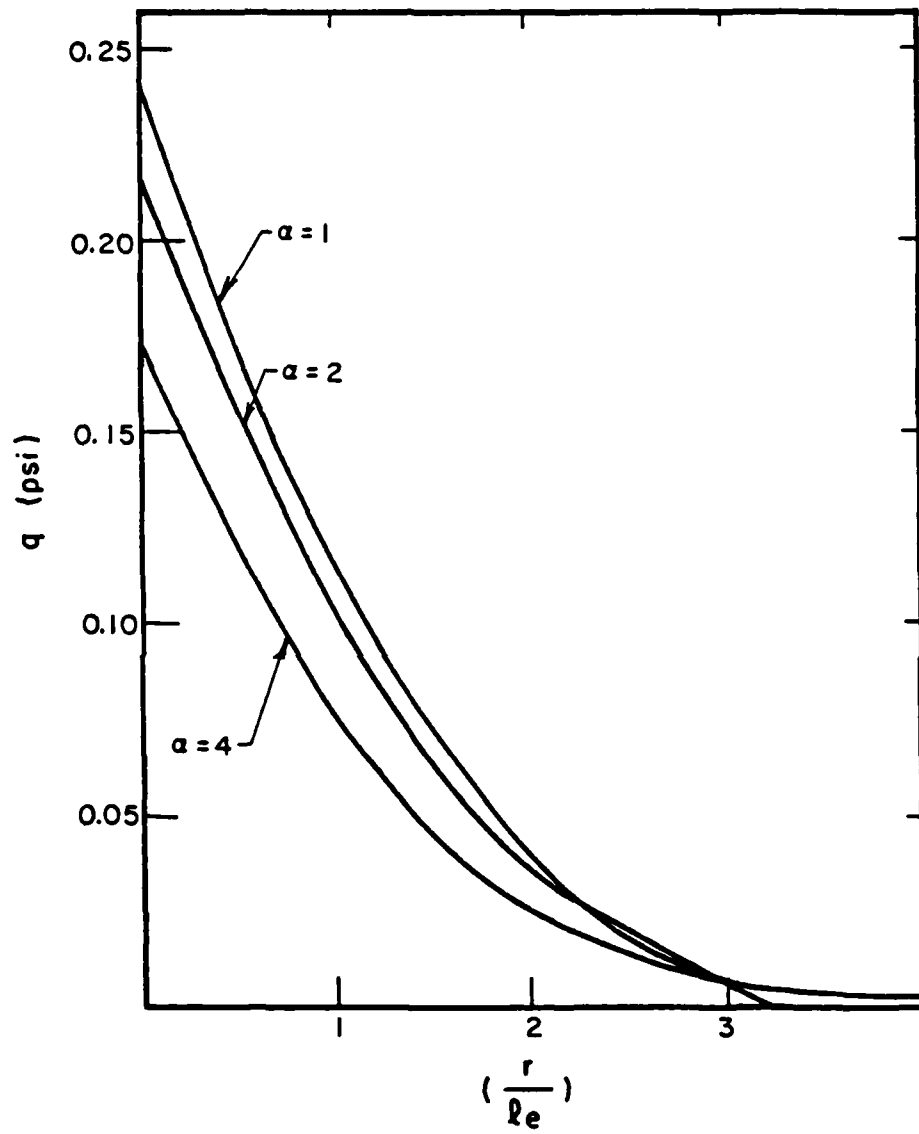


Fig. 9.12 Radial Variation of Subgrade Stress (Interior Load)

The concept of the k-surface will be introduced at this point. This is an imaginary surface showing the spatial distribution (x,y) of the subgrade modulus, k , under a slab resting on an elastic solid foundation. This distribution is such that the response of the slab is identical for the two models. Using a constant, k , at all points under the slab, as is the conventional practice, yields a k-surface that forms a horizontal plane. It might be reasonably expected that with appropriate modifications of this surface, the dense liquid and elastic solid may be better correlated.

The value of $k(x,y)$ may be obtained, by definition, from:

$$k(x,y) = \frac{q(x,y)}{w(x,y)} \quad (9-15)$$

where $q(x,y)$ and $w(x,y)$ are the values of subgrade stress and deflection calculated for any given location, using the plate on elastic solid theory. Thus, it is possible to perform an elastic solid run on ILLI-SLAB and back-calculate nodal values of k by applying Eqn. (9-15). Since ILLI-SLAB allows node-by-node specification of subgrade modulus values, the Winkler option may then be employed in an attempt to reproduce the Boussinesq results.

One of the cases in the mesh fineness study was selected for this investigation. For this case $(2a/h)$ is 0.9 and (L/ℓ_e) is 4.151, so that mesh fineness and slab size effects are reduced, as far as possible. The remaining parameters are shown in Table 9.5. The process outlined above was applied to each of the three fundamental cases of loading:

TABLE 9.5

MAXIMUM RESPONSES FOR DENSE LIQUID AND ELASTIC SOLID

LOAD PLACEMENT	Deflection (mils)			Subgrade Stress (psi)			Bending Stress (psi)		
	E.S.	D.L.	$\frac{D.L.}{E.S.}$	E.S.	D.L.	$\frac{D.L.}{E.S.}$	E.S.	D.L.	$\frac{D.L.}{E.S.}$
Interior	0.281	0.284	1.01	0.261	0.263	1.01	10.26	10.32	1.01
Edge	0.485	0.540	1.11	1.798	1.999	1.11	19.76	20.32	1.03
Corner	0.794	0.966	1.22	8.824	10.739	1.22	8.15	12.07	1.48

Notes:Slab: 108 x 108 in. ($L/\ell_e = 4.151$)Mesh: 10 x 10 @ 10.8 in. ($2a/h = 0.9$)

h = 12 in.

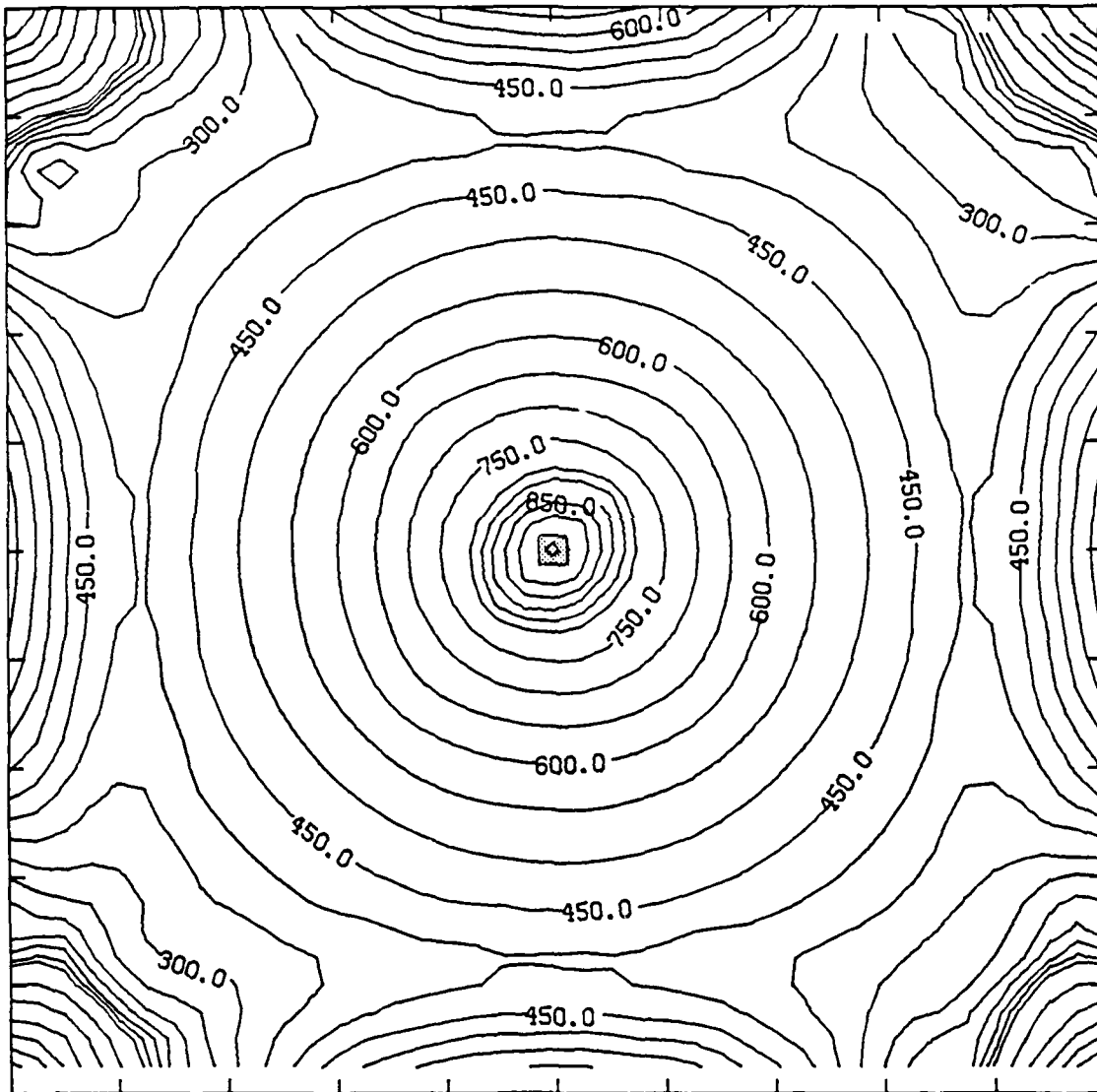
E = 3×10^6 psi $\mu = 0.15$ $E_s = 4 \times 10^4$ psi $\mu_s = 0.45$ $\ell_e = 26.02$ in.

k = q/w (back-calculated) D.L.: Dense Liquid

A = 3 x 3 in. @ 100 psi E.S.: Elastic Solid

interior, edge, and corner. The results of the Elastic Solid option were reproduced fairly accurately by the Winkler option for these cases. Table 9.5 presents comparisons of the maximum responses obtained. It is interesting to note that in all three cases the dense liquid foundation leads to higher stresses and deflections than the elastic solid subgrade. Furthermore, the interior condition is the easiest case to reproduce, while the corner case gives the most unsatisfactory comparison, especially as far as bending stresses are concerned. This clearly illustrates the primary deficiency of the discontinuous Winkler model, namely its assumption that soil elements beyond the slab edges do not provide any support. Figures 9.13 through 9.15 show contours of the k -surface in each of the three cases investigated. Figure 9.16 shows two cross-sections in this surface for interior loading. The edge and corner effects on the k -values are extremely pronounced in all these figures.

To investigate the persistence of these effects for interior loading as slab size increases, several additional runs using progressively smaller slabs were performed. The results are tabulated in Table 9.6. The variation of k at the interior, the edge and along the cross-section A-A is examined in Figures 9.17 and 9.18. It is observed that as (L/λ_e) increases, the k -value at the interior increases, while at the edge it decreases (Fig. 9.17). At a value of (L/λ_e) of about 3.75, the interior- k first becomes greater than the edge- k (Fig. 9.18a). The normalized profiles of k along cross-section A-A become flatter and the edge effect is gradually eliminated, as slab size increases (Fig.



CONTOUR FROM -3250.0 TO 925.00 CONTOUR INTERVAL IRREGULAR
X INTERVAL= 10.800 Y INTERVAL= 10.800

Fig. 9.13 Contours of k-Surface (Interior Loading)

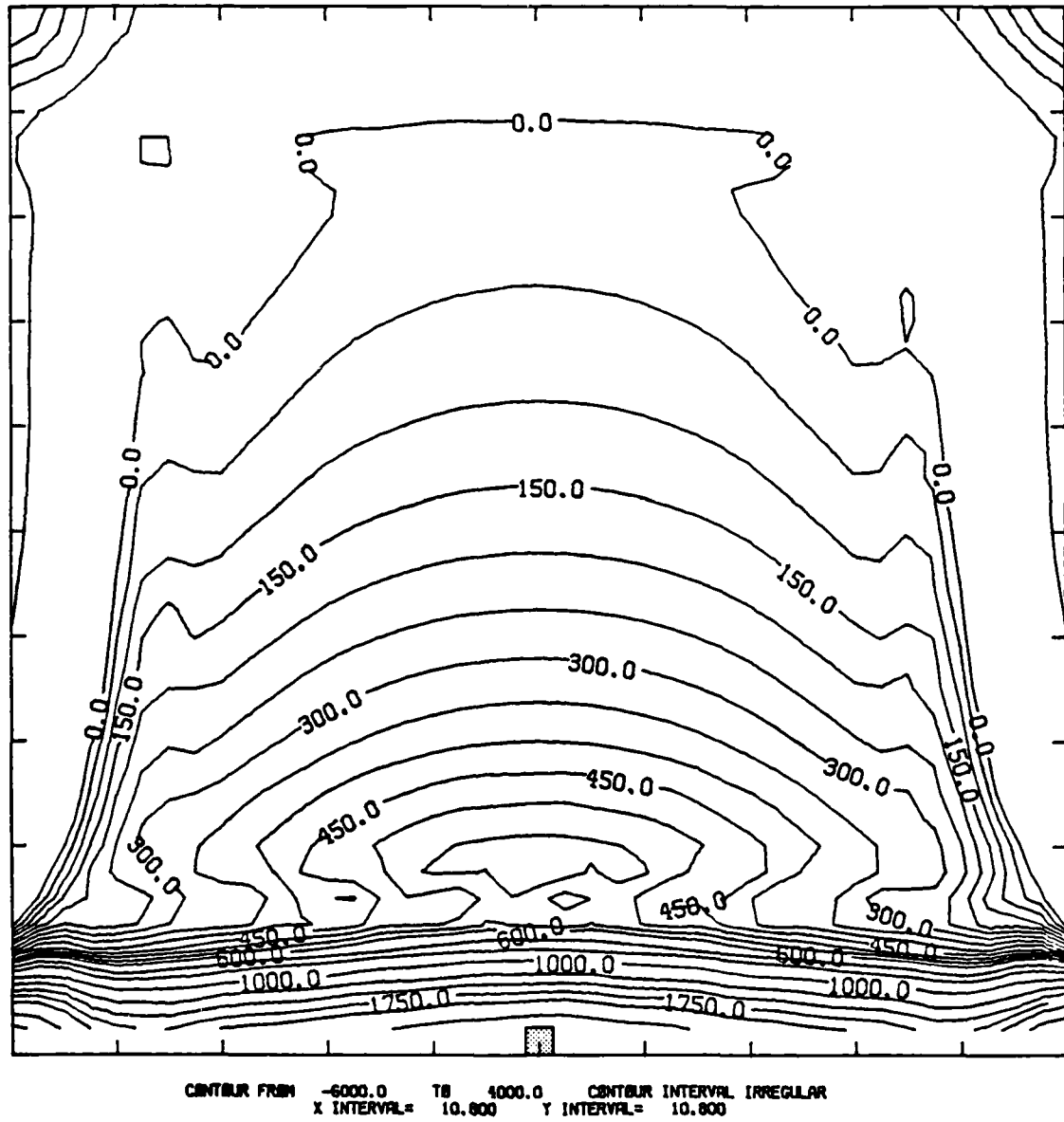
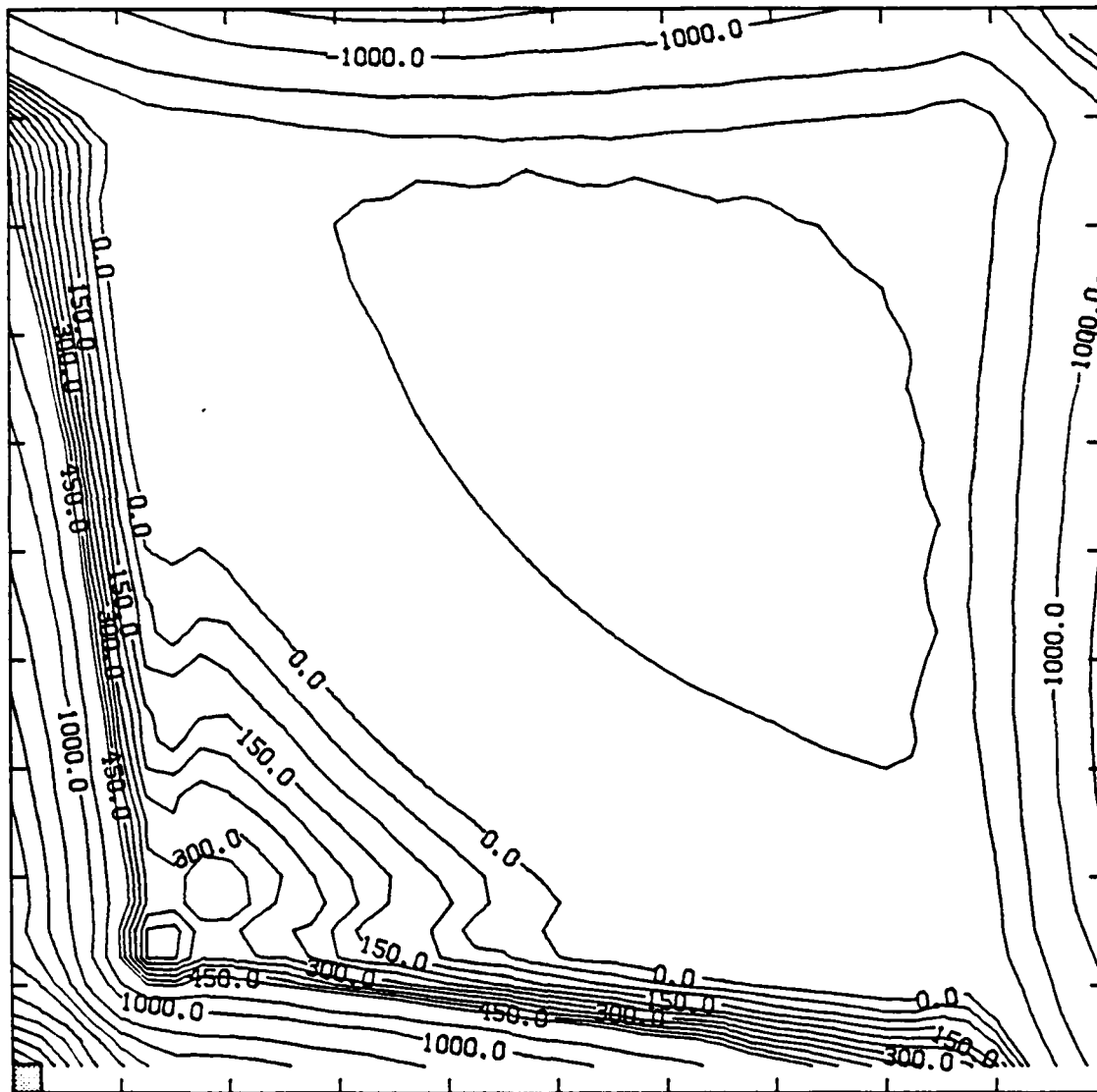


Fig. 9.14 Contours of k-Surface (Edge Loading)



CONTOUR FROM -1750.0 TO 11000.0 CONTOUR INTERVAL IRREGULAR
X INTERVAL= 10.800 Y INTERVAL= 10.800

Fig. 9.15 Contours of k-Surface (Corner Loading)

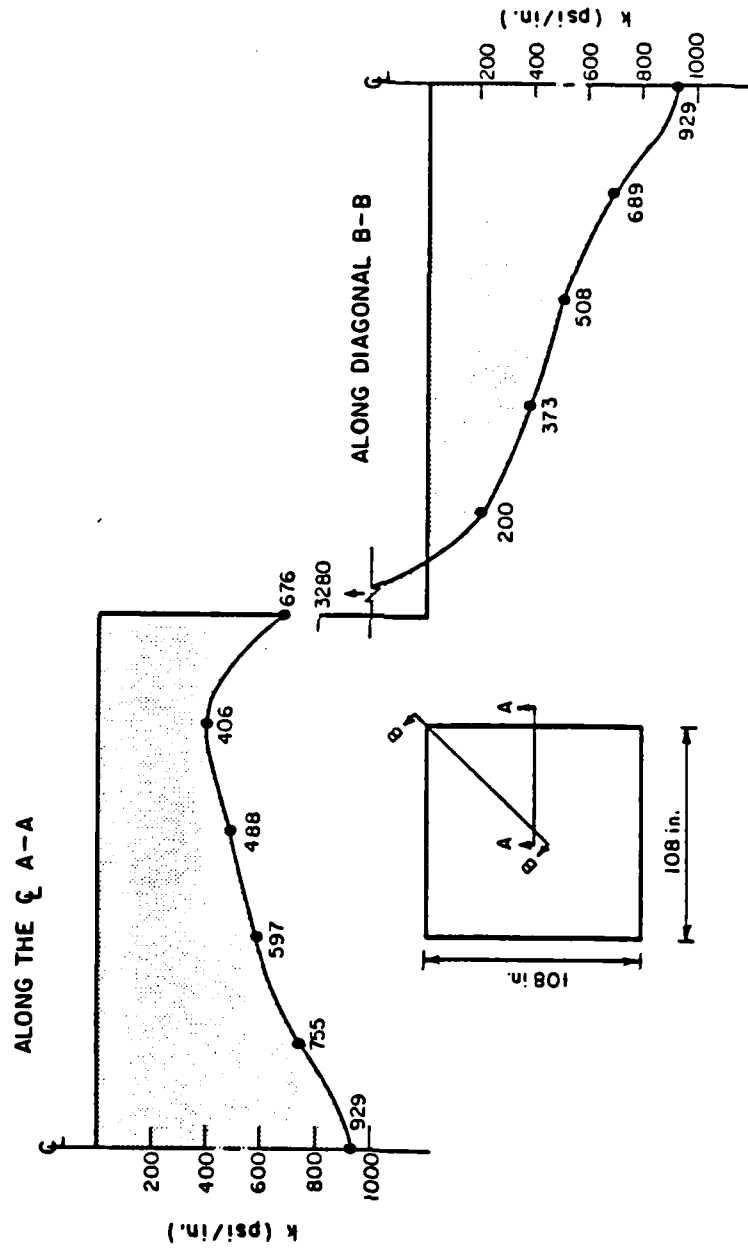


Fig. 9.16 Cross-Section in k -Surface (Interior Loading)

TABLE 9.6
VARIATION OF k-SURFACE WITH SLAB LENGTH: INTERIOR LOADING

$L/\ell_e = 1.66$		$L/\ell_e = 2.49$		$L/\ell_e = 3.32$		$L/\ell_e = 4.15$	
NODE	k (psi/in.)	NODE	k (psi/in.)	NODE	k (psi/in.)	NODE	k (psi/in.)
Slab Center							
13	899	25	914	41	928	61	929
18	786	32	760	50	760	72	755
23	2142	39	639	59	611	83	597
		46	1588	68	519	94	488
Slab Edge				77	1108	105	406
						116	676

Notes:

Slab: $L \times L$ in. ($\ell_e = 26.02$ in.)

2a: 10.8 in. ($2a/h = 0.9$)

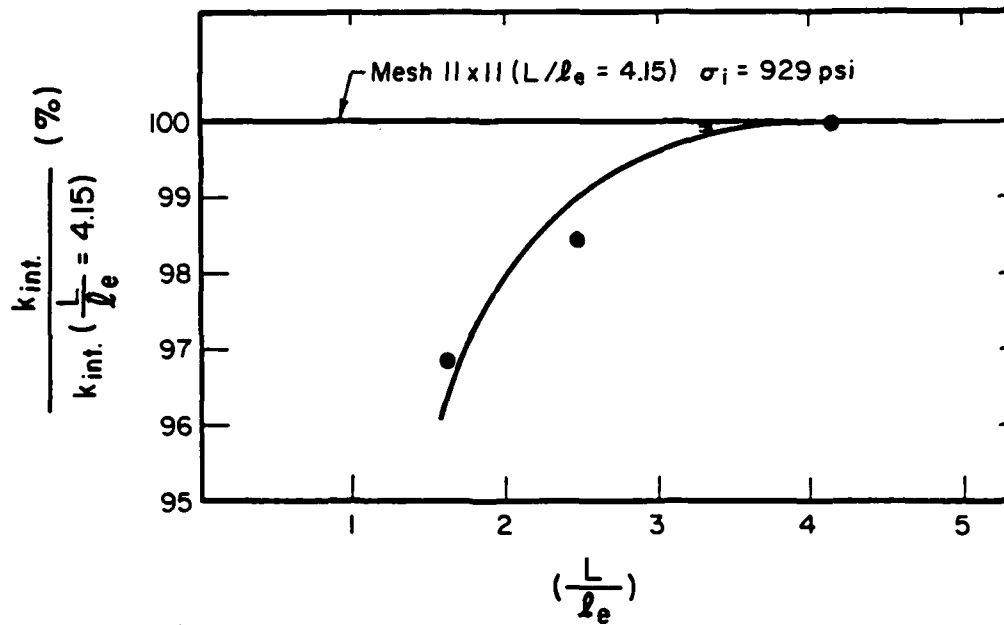
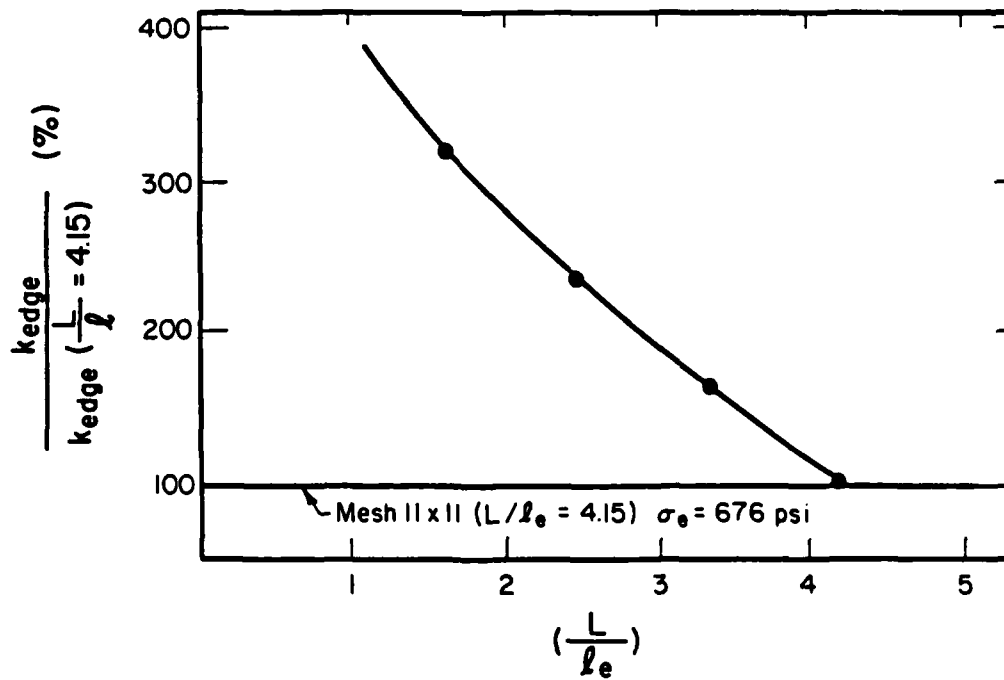
$E = 3 \times 10^6$ psi $\mu = 0.15$

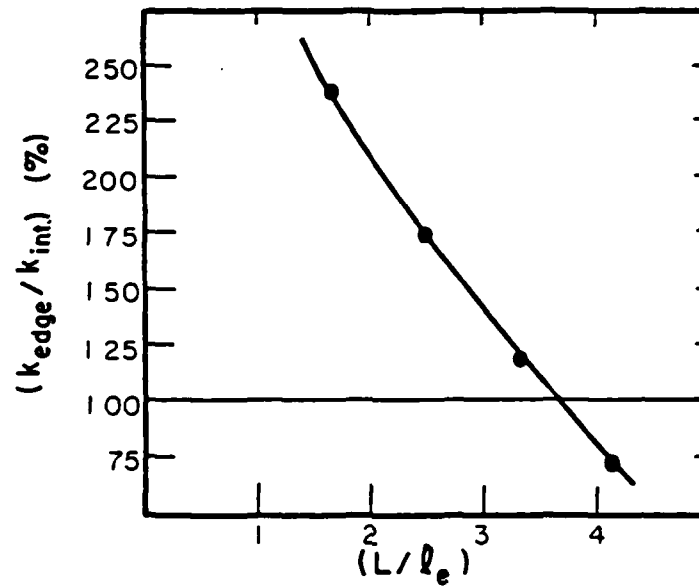
$E_s = 4 \times 10^4$ psi $\mu_s = 0.45$

$h = 12$ in.

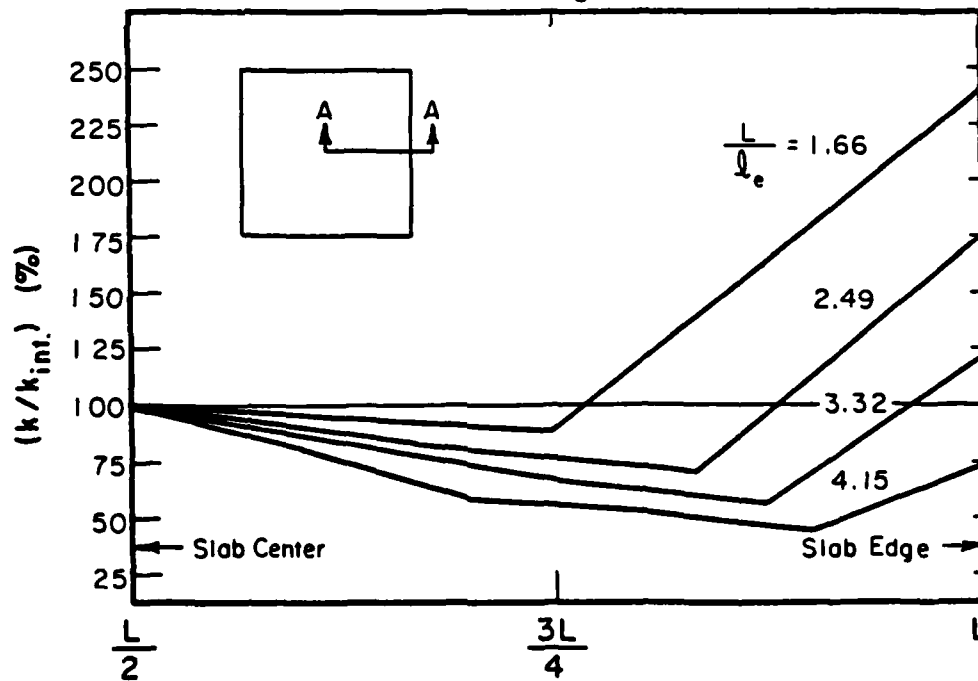
$k = q/w$ (back-calculated)

$A = 3 \times 3$ in. @ 100 psi - interior

(a) Variation of k at the Interior(b) Variation of k at the EdgeFig. 9.17 Effect of Slab Size on k (Interior Loading)



(a) Comparison of k at the Interior and k at the Edge



(b) Normalized Cross-Sections of k -Surface

Fig. 9.18 Radial Distribution of k -values (Interior Loading)

9.18b).

These analyses show that to a large extent, the dense liquid and the elastic solid theories are merely alternative ways of relating deflection and subgrade stress (Equations 9-15 and 9-1 respectively). As Holl [12] pointed out, the distinction between the two reduces down to the selection of the appropriate "kernel function". The differences between the two models may be substantially decreased if the load is applied far away from all free edges. This explains the fact that the interior loading condition on an infinite slab is the easiest to reproduce using the dense liquid model. On the other hand, pronounced differences persist for edge and corner loading. No simple way exists at present of resolving these differences.

Carlton and Behrmann [128] suggested using a flat k-surface, with the value of k determined from the deflection basin obtained under a slab on an elastic solid. Using results from laboratory model tests, they calculated an "equivalent k value" from the relationship:

$$k = P/V \quad (9-16)$$

where:

P : total applied load;

V : volume of deflection basin.

A calculation as indicated by Eqn. (9-16) may easily be performed using ILLI-SLAB elastic solid results. The volume of the deflection basin is simply the sum of nodal deflections times the area of influence

surrounding each node. For the three cases analyzed above, this approach yielded the equivalent k values shown in Table 9.7(a). An increase in equivalent k is observed as the load moves from the interior to the edge and then to the corner of the slab. Carlton and Behrmann [128] noted that the equivalent k value for interior loading was found to be "approximately half the value of k measured at the edge and at the corner," the latter two being practically the same. ILLI-SLAB results suggest a more gradual increase in k .

Introducing the equivalent k values back-calculated using Eqn. (9-16) into dense liquid analyses, leads to the maximum responses given in Table 9.7(b). Agreement between dense liquid and elastic solid results obtained using a flat k -surface is much less satisfactory than when variable nodal k values are employed (Table 9.5). Note, however, that when negative deflections are included in the determination of the deflection basin volume, the equivalent k value from a dense liquid analysis is nearly identical to the value assumed for that run. Since the volume of the deflection basin, V , is equal to the volume of the subgrade stress basin (which by definition is equal to the total applied load, P) divided by k , this simply confirms that ILLI-SLAB satisfies equilibrium, as expected. Thus, Eqn. (9-16) (also used by Bergstrom, et al. [127]) is a valid method of estimating an equivalent k under the slab. This finding is significant with respect to non-destructive pavement evaluation methods which generate a deflection profile (e.g. Falling Weight Deflectometer, Road Rater, etc.).

TABLE 9.7
(a) EQUIVALENT k VALUES: ELASTIC SOLID RUNS

LOAD PLACEMENT	EQUIVALENT k (psi/in.)	k/k _{corner}	k/k _{edge}
Interior	464	0.66	0.83
Edge	561	0.79	1.00
Corner	707	1.00	1.26

(b) DENSE LIQUID RESPONSES USING EQUIVALENT k VALUES

LOAD PLACEMENT	ASSUMED k (psi/in.)	BACK-CALCULATED k (psi/in.)	DEFLECTION (mils)	SUBGRADE STRESS (psi)	BENDING STRESS (psi)
Interior	464	467	0.304	0.141	11.02
Edge	561	559	0.910	0.511	22.45
Corner	707	694	1.860	1.315	14.76

Notes: Mesh: 10 x 10 @ 10.8 in.

L = 108 x 108 in.

h = 12 in.

E = 3×10^6 psi; $\mu=0.15$

A = 3 x 3 in. @ 100 psi

$E_s = 4 \times 10^4$ psi

$\mu_s = 0.45$

E.S.: Elastic Solid (see Table 9.5)

D.L.: Dense Liquid

Equivalent k from Eqn. (9-16)

CHAPTER 10

ANALYSIS OF A PLATE ON AN ELASTIC SOLID
USING THE METHOD OF FINITE DIFFERENCES

10.1 INTRODUCTION

It was noted earlier that the application of the Finite Element Method (F.E.M.) to the solution of the problem of a plate on an elastic solid foundation creates two major problems:

- (i) Computer storage and execution time requirements are considerably more demanding than those for a dense liquid model. Compromises are often necessary in terms of mesh fineness and accuracy, in order to remain within the allowable limits of the computer;
- (ii) Certain aspects of slab-subgrade behavior examined using the F.E.M. have never been investigated before, and some unexpected results may be obtained. Engineering intuition is not always reliable in judging which of the results are valid, and which are due to the mechanics of the numerical procedure or due to the trade-offs mentioned above. An independent method of verifying finite element results is very desirable.

The Finite Difference Method (F.D.M.) offers a possible solution to both these problems. It is generally found that, at the price of a certain amount of flexibility, the F.D.M. is less exacting in computer resources than the F.E.M. Furthermore, comparing solutions obtained

using these two methods is often enlightening and reinforces the credibility of both.

The development of a Finite Difference program for a plate on an Elastic Solid (called 'FIDIES') is described in this Chapter. This formulation brings the F.D.M. to the foreground of pavement analysis once again, after a long period of neglect. Results presented in this Chapter confirm that the F.D.M. still remains a viable tool for slab-on-grade analysis. The input guide for FIDIES is included in Appendix A.

10.2 FINITE DIFFERENCE FORMULATION

10.2.1 Theory

The finite difference solution employed in FIDIES, follows closely the development by Pickett, et al. [84]. It utilizes the Boussinesq equation for the deflection due to a concentrated load on the surface of an elastic solid, and assumes a piecewise uniform subgrade stress distribution, similar to that used by Bergstrom, et al. [127], and Cheung and Zienkiewicz [88].

According to Boussinesq [159], the vertical displacement, w_{ni} , at a point n on the surface of the elastic half-space, due to a concentrated load Q_i acting at another point i , also on the surface of the half-space, is given by:

$$w_{ni} = \frac{Q_i (1 - \mu_s^2)}{\pi E_s r_{ni}} \quad (10-1)$$

where:

E_s, μ_s : Young's modulus and Poisson's ratio for the half-space;

r_{ni} : distance between points i and n .

In the finite difference solution, the upper surface of the elastic solid is divided into squares, Δ by Δ in size, for convenience, as shown in Fig. 10.1. The deflection at the center of one of these squares, due to a pressure q acting on the same or on any other square, may be obtained by setting Q_i in Eqn. (10-1) equal to $q \cdot dA$ and integrating over the area of the loaded square. The result may be expressed as follows [84]:

$$w_{mn} = \frac{(1-\mu_s)}{2\pi G_s \Delta} \gamma_{ij} Q_{uv} \quad (10-2)$$

where:

$$\gamma_{ij} = \frac{\Delta}{Q_{uv}} \int_{(i-1/2)\Delta}^{(i+1/2)\Delta} \int_{(j-1/2)\Delta}^{(j+1/2)\Delta} \left[q \int_0^{\infty} \frac{J_0(\alpha r)}{F(\alpha H)} d\alpha \right] dx dy \quad (10-3)$$

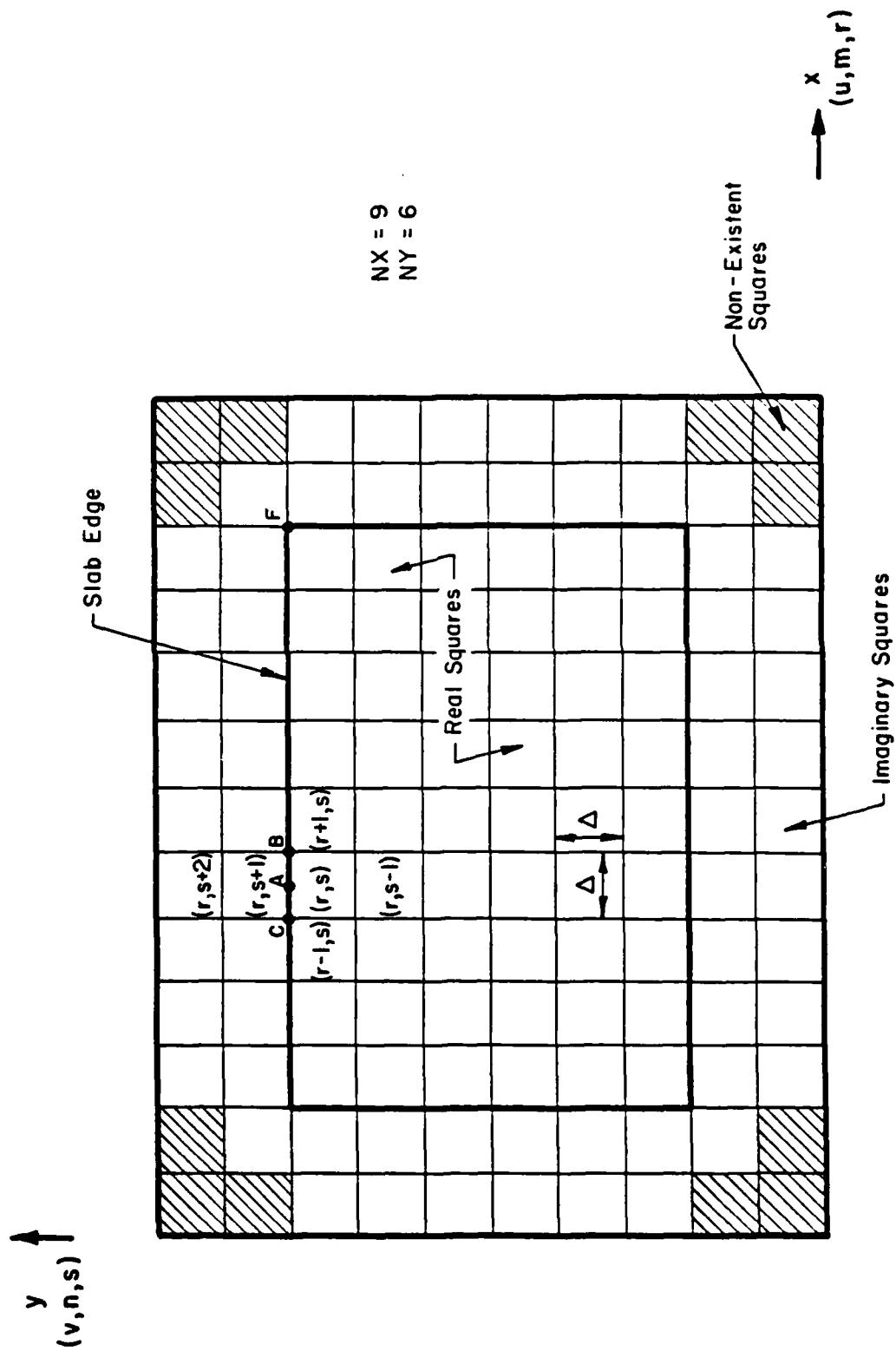
m, u : indices of the column number of a real (plate) square;

n, v : indices of the row number of a real (plate) square;

Q_{uv} : total load on the loaded square designated as a uv -square;

w_{mn} : deflection at center of the mn -square;

$F(\alpha H)$: a function that depends on the thickness H of the elastic solid and the conditions at its base. For $H=\infty$ (semi-infinite half-space) $F(\alpha H)=1.0$;

Fig. 10.1 Typical Finite Difference Grid ($NX=9$; $NY=6$)

$J_0(\alpha r)$: Bessel function of first kind and order zero;

$$G_s : \text{shear modulus for subgrade,}$$

$$= \frac{E_s}{2(1+\mu_s)}$$

The numbers:

$$i = |m-u|$$

$$\text{and } j = |n-v|$$

when multiplied by Δ give the x and y distances between the center of the two squares. Note that when the load is on the square whose deflection is under consideration, both i and j are zero, since $m=u$ and $n=v$.

Specializing Eqn. (10-3) for $H=\infty$ and for $q=\text{constant}$ over the uv-square, the expression for coefficient γ_{ij} becomes [84]:

$$\begin{aligned} \gamma_{ij} = & (i+1/2) \ln \frac{\sqrt{(2i+1)^2 + (2j+1)^2} + 2j + 1}{\sqrt{(2i+1)^2 + (2j-1)^2} + 2j - 1} \\ & + (j+1/2) \ln \frac{\sqrt{(2i+1)^2 + (2j+1)^2} + 2i + 1}{\sqrt{(2i-1)^2 + (2j+1)^2} + 2i - 1} \\ & + (i-1/2) \ln \frac{\sqrt{(2i-1)^2 + (2j-1)^2} + 2j - 1}{\sqrt{(2i-1)^2 + (2j+1)^2} + 2j + 1} \\ & + (j-1/2) \ln \frac{\sqrt{(2i-1)^2 + (2j-1)^2} + 2i - 1}{\sqrt{(2i+1)^2 + (2j-1)^2} + 2i + 1} \end{aligned}$$

By superposition of all forces Q_{uv} on the upper surface of the elastic solid, the deflection of the center of the mn -square is:

$$w_{mn} = \frac{1-\mu_s}{2\pi G \Delta} \sum_u \sum_v \gamma_{ij} Q_{uv} \quad (10-5)$$

Note that Q_{uv} is the subgrade reaction force between the uv -square of the plate and the uv -square of the foundation. The summation in Eqn. (10-5) is carried out over all squares of the plate. These are of the same size and lie directly above those of the elastic solid.

Now, the Lagrange equation for the equilibrium of a plate on an elastic foundation, applied to uv -square yields:

$$D \nabla^4 w = p_{uv} - q_{uv} \quad (10-6)$$

where:

p_{uv} : applied pressure;

q_{uv} : subgrade reaction.

In finite difference form (see Table 3.1), this expression becomes:

$$\begin{aligned} \frac{D}{\Delta^4} [& 20w_{uv} - 8(w_{u+1,v} + w_{u-1,v} + w_{u,v+1} + w_{u,v-1}) \\ & + 2(w_{u+1,v+1} + w_{u-1,v+1} + w_{u+1,v-1} + w_{u-1,v-1}) \\ & + w_{u+2,v} + w_{u-2,v} + w_{u,v+2} + w_{u,v-2}] \\ & = \frac{p_{uv}}{\Delta^2} - \frac{q_{uv}}{\Delta^2} \end{aligned} \quad (10-7)$$

where:

P_{uv}, Q_{uv} : applied external load and subgrade reaction forces on uv-square, respectively;

$w_{k,\ell}$: deflection at center of square in kth row and ℓ th column of plate mesh.

Equation (10-7) may be represented as the standard thirteen-point central finite difference molecule shown in Fig. 10.2(a). This provides a simple geometric presentation of the equilibrium equation.

Substituting Q_{uv} from Eqn. (10-5) and multiplying both sides of Eqn. (10-7) by $\frac{2\pi G_s \Delta^3}{(1-\mu_s)D}$ gives:

$$\begin{aligned}
 2\pi \left(\frac{\Delta}{\ell_e}\right)^3 w_{mn} + \sum_u \sum_v \gamma_{ij} [20w_{uv} - 8(w_{u+1,v} + w_{u-1,v} + w_{u,v+1} + w_{u,v-1}) \\
 + 2(w_{u+1,v+1} + w_{u-1,v+1} + w_{u+1,v-1} + w_{u-1,v-1}) \\
 + (w_{u+2,v} + w_{u-2,v} + w_{u,v+2} + w_{u,v-2})] \\
 = \sum_u \sum_v \gamma_{ij} \frac{\Delta^2}{D} P_{uv}
 \end{aligned} \tag{10-8}$$

where:

ℓ_e : radius of relative stiffness,

$$= \sqrt[3]{\frac{(1-\mu_s)D}{G_s}}$$

Since only plate deflections are of interest, the deflection w_{mn} in Eqn. (10-8) will be restricted to those squares covered by the slab. Note, however, that Equations (10-5) and (10-8) are general,

$$\begin{array}{c}
 v+2 \\
 v+1 \\
 v \\
 v-1 \\
 v-2
 \end{array}
 \begin{array}{ccccc}
 & & +1 & & \\
 & +2 & -8 & +2 & \\
 +1 & -8 & +20 & -8 & +1 \\
 & +2 & -8 & +2 & \\
 & & +1 & &
 \end{array}
 \left[\frac{D}{\Delta^4} \right] = \frac{P_{uv}}{\Delta^2} - \frac{Q_{uv}}{\Delta^2}$$

u-2 u-1 u u+1 u+2

(a) Computational Molecule for Eqn. (10-7)

$$\begin{array}{c}
 s+2 \\
 s+1 \\
 s \\
 s-1
 \end{array}
 \begin{array}{ccc}
 & 1 & \\
 \mu & -1-2\mu & \mu \\
 \mu & -1-2\mu & \mu \\
 & 1 &
 \end{array}
 \begin{array}{c}
 \\
 \\
 \text{Top Edge} \\
 \\
 \end{array}$$

r-1 r r+1

(b) Computational Molecule for Eqn. (10-12)

$$\begin{array}{c}
 s+2 \\
 s+1 \\
 s \\
 s-1
 \end{array}
 \left[\begin{array}{ccc}
 & +1 & \\
 & -3 & \\
 +3 & & \\
 & -1 &
 \end{array} \right] + [(2-\mu) \begin{array}{ccc}
 & +1 & -2 & +1 \\
 -1 & +2 & -1 &
 \end{array}] = 0$$

r-1 r r+1 r-1 r r+1

(c) Computational Molecule for Eqn. (10-16)

Fig. 10.2 Geometric Representation of Finite Difference Equations

i.e. they could be applied to all squares, including those extending beyond the plate edges. On the other hand, subgrade reaction force Q_{uv} refers only to the squares that slab and subgrade have in common. Therefore, the summations in Equations (10-5) and (10-8) are carried out over these common squares alone. It is important to notice that, as is often the case with the F.D.M., Eqn. (10-8) contains deflections of "imaginary squares", beyond the slab boundaries. These deflections are not equal to the deflections of the corresponding squares of the subgrade. The additional equations required for the determination of real and imaginary square deflections, are derived from the application of boundary conditions.

10.2.2 Boundary Conditions

It would appear that there should be three boundary conditions at a free edge (e.g. $y=a$), i.e.

$$\begin{aligned} M_y(x,a) &= 0 \\ M_{xy}(x,a) &= 0 \\ V_y(x,a) &= 0 \end{aligned} \tag{10-9}$$

where:

M_{xy} : Twisting moment about x-axis on positive y-face;

V_y : Transverse shear force (in z-direction) on positive y-face.

In view of the assumption, however, of no transverse shear strain employed in medium-thick plate theory, the order of the governing

equation -Eqn. (10-6)- has been lowered. Thus, only two boundary conditions can be satisfied at a free edge, as is also the case for a clamped or a simply supported edge. A shear deformation theory of plates would allow all three physically correct boundary conditions.

Using virtual work methods, the number of boundary conditions may be reduced to two. This leads to the following Kirchhoff conditions:

$$\begin{aligned} M_y(x, a) &= 0 \\ [V_y + \frac{\partial}{\partial x} M_{xy}](x, a) &= 0 \end{aligned} \quad (10-10)$$

In terms of derivatives of w , the free edge boundary conditions are:

$$\left[\frac{\partial^2 w}{\partial y^2} + \mu \frac{\partial^2 w}{\partial x^2} \right]_{y=a} = 0 \quad (10-11a)$$

$$\left[\frac{\partial^3 w}{\partial y^3} + (2-\mu) \left(\frac{\partial^3 w}{\partial x^2 \partial y} \right) \right]_{y=a} = 0 \quad (10-11b)$$

For illustration purposes, the finite difference expressions corresponding to these boundary conditions will be derived below for the top edge of the slab. For a square (r, s) along the top edge of the slab (Fig. 10.1), the following finite difference expression for Eqn. (10-11a) may be derived from Table 3.1:

$$\begin{aligned} w_{r,s+2} - w_{r,s+1} - w_{r,s} + w_{r,s-1} + \mu \{ w_{r+1,s+1} - 2w_{r,s+1} \\ + w_{r-1,s+1} + w_{r+1,s} - 2w_{r,s} + w_{r-1,s} \} = 0 \end{aligned} \quad (10-12)$$

Equation (10-12) may be rewritten in the computational molecule form shown in Fig. 10.2(b). Similar expressions apply for the 3 other edges. Note that indices r and s refer again to the column and row position in the finite difference grid of any square, real or imaginary. The boundary conditions, of course, are applied successively to all real edge squares only.

In view of the presence third derivatives in Eqn. (10-11b), this condition requires special treatment. Consider first the twist term $\frac{\partial}{\partial x}(M_{xy})$, where, by definition:

$$M_{xy} = -D(1-\mu) \frac{\partial^2 w}{\partial x \partial y}$$

With points as defined in Fig. 10.1, the following finite difference expressions may be written:

$$\text{at B: } M_{xy} = \frac{-D(1-\mu)}{2} \frac{\left\{ w_{r,s} - w_{r,s+1} - w_{r+1,s} + w_{r+1,s+1} \right\}}{4 \left(\frac{\Delta}{2} \right)}$$

$$\text{at C: } M_{xy} = \frac{-D(1-\mu)}{2} \frac{\left\{ -w_{r,s} + w_{r-1,s} + w_{r,s+1} - w_{r-1,s+1} \right\}}{4 \left(\frac{\Delta}{2} \right)}$$

Therefore,

$$\frac{\partial}{\partial x} (M_{xy})_A = \frac{1}{2 \left(\frac{\Delta}{2} \right)} \left[(M_{xy})_B - (M_{xy})_C \right]$$

$$\text{or } \frac{\partial}{\partial x} (M_{xy})_A = \frac{-D(1-\mu)}{\Delta^3} \{2w_{r,s} - w_{r+1,s} - w_{r-1,s} - 2w_{r,s+1} + w_{r+1,s+1} + w_{r-1,s+1}\} \quad (10-13)$$

Now, consider the shear term:

$$V_y = -D \frac{\partial}{\partial y} \left[\frac{\partial^2 w}{\partial x^2} + \frac{\partial^2 w}{\partial y^2} \right] \quad (10-14)$$

Thus, at the center of a square (r,s) along the top edge of the slab (Fig. 10.1) the following expressions apply:

$$\frac{\partial^2 w}{\partial x^2} = \frac{1}{\Delta^2} \{-2w_{r,s} + w_{r+1,s} + w_{r-1,s}\}$$

$$\frac{\partial^2 w}{\partial y^2} = \frac{1}{\Delta^2} \{-2w_{r,s} + w_{r,s+1} + w_{r,s-1}\}$$

whence:

$$\left(\frac{\partial^2 w}{\partial x^2} + \frac{\partial^2 w}{\partial y^2} \right)_{r,s} = \frac{1}{\Delta^2} \{-4w_{r,s} + w_{r+1,s} + w_{r-1,s} + w_{r,s+1} + w_{r,s-1}\}$$

Similarly, at $(r, s+1)$:

$$\left(\frac{\partial^2 w}{\partial x^2} + \frac{\partial^2 w}{\partial y^2} \right)_{r,s+1} = \frac{1}{\Delta^2} \{-4w_{r,s+1} + w_{r+1,s+1} + w_{r-1,s+1} + w_{r,s+2} + w_{r,s}\}$$

Therefore, at point A on the slab edge:

$$\begin{aligned}
 (V_y)_A &= \frac{-D}{2(\frac{\Delta}{2})} \left[\left(\frac{\partial^2 w}{\partial x^2} + \frac{\partial^2 w}{\partial y^2} \right)_{r,s+1} - \left(\frac{\partial^2 w}{\partial x^2} + \frac{\partial^2 w}{\partial y^2} \right)_{r,s} \right] \\
 &= \frac{-D}{\Delta^3} \{ 5w_{r,s} - w_{r+1,s} - w_{r-1,s} - w_{r,s-1} - 5w_{r,s+1} + w_{r+1,s+1} \\
 &\quad + w_{r-1,s+1} + w_{r,s+2} \} \quad (10-15)
 \end{aligned}$$

To obtain the finite difference expression for boundary condition Eqn. (10-11b), the sum of the twist and shear terms is obtained:

$$\begin{aligned}
 (V_y)_A + \frac{\partial}{\partial x} (M_{xy})_A &= w_{r,s+2} - 3w_{r,s+1} + 3w_{r,s} - w_{r,s-1} \\
 &\quad + (2-\mu) \{ w_{r+1,s+1} - 2w_{r,s+1} + w_{r-1,s+1} \\
 &\quad - w_{r+1,s} - 2w_{r,s} - w_{r-1,s} \} = 0 \quad (10-16)
 \end{aligned}$$

The computational molecule for Eqn. (10-16) is shown in Fig. 10.2(c). The corresponding expressions applying to the 3 other edges are derived in a similar fashion.

In addition to the equations from the two free-edge boundary conditions discussed above, another four equations may be written, each describing the requirement of no force at each of the four free corners of the plate. Consider for example the upper right corner, F in Fig. 10.1. The corner reaction force is defined as:

$$\begin{aligned}\text{Corner force, } R_F &= 2M_{xy} \\ &= 2D(1-\mu)\frac{\partial^2 w}{\partial x \partial y}\end{aligned}$$

Setting this to zero and denoting point F by (i,j) -although F is not at the center of a square and is, therefore, not a nodal point- the following finite difference expression may be written:

$$\frac{\partial^2 w}{\partial x \partial y} = \frac{1}{4(\frac{\Delta}{2})^2} \{w_{i+1,j+1} - w_{i+1,j-1} - w_{i-1,j+1} + w_{i-1,j-1}\} = 0$$

In terms of the elements surrounding the corner element (r,s), this may be rewritten as:

$$\{w_{r,s} - w_{r+1,s} - w_{r,s+1} + w_{r+1,s+1}\} = 0 \quad (10-17)$$

This equation states that the one real and three imaginary squares touching the corner lie in a plane. Similar equations may be written for the other three corners.

10.2.3 Assembly of Equations

For a slab consisting of NX elements in the x-direction and NY elements in the y-direction, there are (NX+2)*(NY+2)-12 unknown deflections, (NX*NY) of which belong to real squares and the remaining refer to imaginary squares. The application of Eqn. (10-8) to each real square yields (NX*NY) equations. Each of the two Kirchhoff boundary conditions, applied to every real square along the plate

edges, gives another $2(NX+NY)$ equations. Finally, 4 equations can be written from the free corner condition. Thus, as many equations can be set up as there are unknown deflections. These are solved using standard methods for the solution of simultaneous equations.

10.3 PROGRAM IMPLEMENTATION

10.3.1 Equation Assembly Subroutines

The formulation described above was coded into a new computer program, called 'FIDIES', a few pertinent features of which are discussed below. Following the notation used by Pickett, *et al.* [84], Eqn. (10-8) may be rewritten for each mn-square in the form:

$$2\pi \left(\frac{\Delta}{\ell_e}\right)^3 w_{mn} + \sum_r \sum_s \beta_{mnrs} w_{rs} = \sum_u \sum_v \gamma_{ij} \frac{\Delta^2}{D} P_{uv} \quad (10-18)$$

where β_{mnrs} denotes the sum of the coefficients for w_{rs} . Note that the summation for r and s is over all squares, both real and imaginary, included in Eqn. (10-8), whereas both m,n and u,v are defined for real squares only. In Eqn. (10-18), w_{rs} is the unknown deflection of any one of the $(NX+2)*(NY+2)-12$ squares. The parameter β_{mnrs} is the sum of the coefficients of this unknown, except for $2\pi(\Delta/\ell_e)^3$ which applies to the particular mn-square. It can be computed using the equation:

$$\beta_{mnrs} = \sum_u \sum_v \gamma_{ij} \phi_{uvrs} \quad (10-19)$$

where ϕ_{uvrs} is given by the computational molecule of Fig. 10.3. Its value is zero for all u and v , except the thirteen shown in the figure. Some of the thirteen ϕ 's may not appear for a given β , since u and v are restricted to the real squares of the slab.

Using Eqn. (10-4), all required values of γ_{ij} are computed at the beginning of each run by subroutine DETGAMA. Note that γ_{ij} is only defined for real squares. Each of its values is stored in array GAMMA at location (M,N) where $M=i+1$ and $N=j+1$. It gives the deflection at the center of the square (m,n) , due to a unit load applied on square (u,v) , where $i = |m-u|$ and $j = |n-v|$. Thus, M ranges from 1 to NX , and N takes values between 1 and NY . The corresponding i values range from 0 to $(NX-1)$, and those of j range from 0 to $(NY-1)$. The storage location of γ_{ij} in array GAMMA is (M,N) ; note that this is not necessarily the same as (m,n) used by Pickett, et al. [84].

Next, the required equations are assembled by subroutine EQNS. The following set of equations is created:

$$[COEFF]_{NALL*NALL} \{DEFL\}_{NALL*1} = \{CONST\}_{NALL*1} \quad (10-20)$$

For the $(NX*NY)$ equations that are obtained by the application of Eqn. (10-8) over each real square, matrix $[COEFF]$ contains values of β_{mnrs} and the value $2\pi (\Delta / \lambda_e)^3$, while the vector $\{CONST\}$ contains values of the summation on the right-hand side of Eqn. (10-8). These values are computed by repeated calls to subroutine DETBETA, which evaluates the expression for β_{mnrs} given by Eqn. (10-19), and Eqn.

$\begin{array}{c} v \\ u \end{array}$	s-2	s-1	s	s+1	s+2
r-2			+1		
r-1		+2	-8	+2	
r	+1	-8	+20	-8	+1
r+1		+2	-8	+2	
r+2			+1		

Fig. 10.3 Computational Molecule for ϕ_{uvrs}

(10-8). The remaining equations assembled in subroutine EQNS are obtained by the application of the boundary conditions, discussed above.

The matrix algebra operations required for the solution of equation set in Eqn. (10-20), are performed using subroutines from LINPACK. This is a package of mathematical software developed in the early 1970's by a project centered at the Argonne National Laboratory for Environmental Research and Damaging.

10.3.2 Stress Calculation

Once deflections of all real and imaginary squares have been determined, bending moments developing in the slab are determined from their respective finite difference expressions. These are as follows:

$$M_x = -D \left[\frac{\partial^2 w}{\partial x^2} + \mu \frac{\partial^2 w}{\partial y^2} \right]$$

$$M_y = -D \left[\frac{\partial^2 w}{\partial y^2} + \mu \frac{\partial^2 w}{\partial x^2} \right]$$

$$\text{and } M_{xy} = -D \left[(1-\mu) \frac{\partial^2 w}{\partial x \partial y} \right] \quad (10-21)$$

The finite difference expressions for the derivatives in Eqn. (10-21) are given in Table 3.1. The following stress-moment relations are then used to obtain the corresponding slab bending stresses:

$$\begin{aligned}
 \sigma_x &= 6M_x/h^2 \\
 \sigma_y &= 6M_y/h^2 \\
 \tau_{xy} &= 6M_{xy}/h^2
 \end{aligned}
 \tag{10-22}$$

Finally, the principal stresses in the slab are calculated from:

$$\sigma_1, \sigma_3 = \frac{1}{2} (\sigma_x + \sigma_y) \pm \frac{1}{2} [(\sigma_x - \sigma_y)^2 + 4 \tau_{xy}^2]^{1/2}
 \tag{10-23}$$

These calculations are performed in subroutine STRESS.

Subroutine REAXION is finally used for the back-calculation of subgrade reactions, using Eqn. (10-5). This equation may be rearranged and rewritten in matrix form as follows:

$$\frac{1-\mu_s}{2\pi G_s \Delta} [\text{GAMMA}] \{Q\}_{\text{NREAL} \times 1} = \{w\}_{\text{NREAL} \times 1}
 \tag{10-24}$$

In this expression, array [GAMMA] contains values of γ_{ij} and vector $\{w\}$ is the vector of the real deflections calculated earlier. When this equation set is solved using LINPACK routines, vector $\{Q\}$ is returned with the values of element forces. Dividing the contents of $\{Q\}$ by Δ^2 , yields the corresponding subgrade stresses.

Applied loads are specified in terms of the global coordinate system, in a manner similar to the one used in the current version ILLI-SLAB (see Section 4.6). In this system, the origin of the x- and y-coordinates is fixed at the lower left corner of the slab. The

AD-A150 965

ANALYSIS OF SLABS-ON-GRADE FOR A VARIETY OF LOADING AND
SUPPORT CONDITION. (U) ILLINOIS UNIV AT URBANA DEPT OF
CIVIL ENGINEERING A M IOANNIDES ET AL. DEC 84

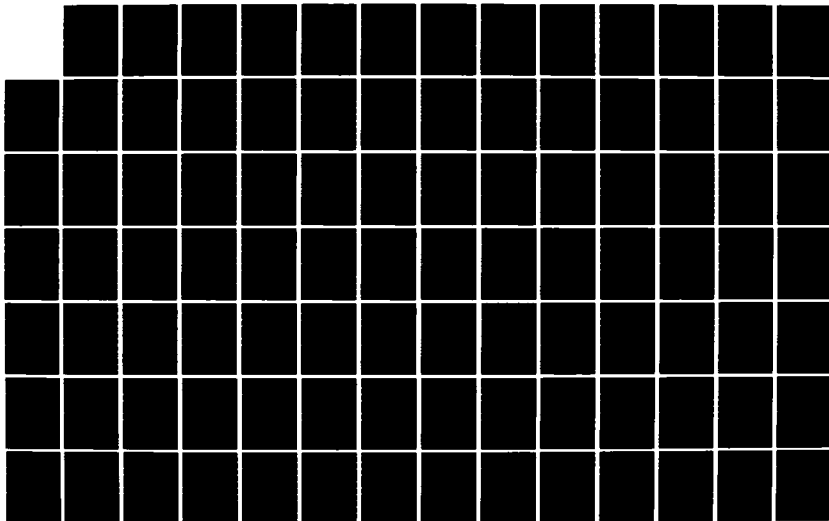
5/7

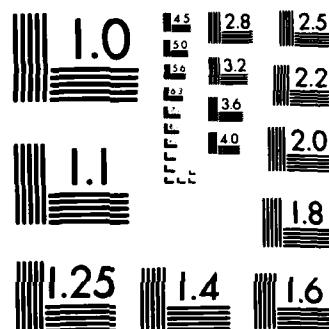
UNCLASSIFIED

AFOSR-TR-85-0083 AFOSR-87-0143

F/G 13/2

NL





MICROCOPY RESOLUTION TEST CHART
NATIONAL BUREAU OF STANDARDS-1963-A

loaded areas are thus independent of the way the slab is subdivided into N_X by N_Y squares. Subroutine SUBAREA generates element loads from the applied load inputs. Note that in the present version of FIDIES each externally applied distributed element load is converted into a concentrated force applied at the center of the element. Its magnitude is the product of the applied pressure times the area over which this is applied, irrespective of the location of this area within the element. For areas that are not symmetrically placed within the element, the applied and element loads are not exactly statically equivalent. For fine meshes, however, this error will be small.

10.4 PROGRAM VERIFICATION

10.4.1 Scope of Investigation

Previous studies have shown that the performance of a program such as FIDIES may be investigated in terms of three non-dimensional ratios:

- (i) The Slab Size Ratio, (L/ℓ_e) ;
- (ii) The Mesh Fineness Ratio, (Δ/h) ; and
- (iii) The Size of the Loaded Area Ratio, (c/ℓ_e) .

These factors are discussed below for the cases of interior and corner loading. Closed-form solutions are only available for the first of these cases (Table 7.1). The investigation of the corner loading condition will prepare the way for the development of similar equations for this case as well. The correctness of the code in FIDIES was also confirmed by comparison to results presented by Pickett, et al. [84].

10.4.2 Interior Loading

(a) Effect of Slab Size: The slab selected for this study had a small radius of relative stiffness ($\ell_e=26$ in.), and was analyzed using a rather coarse mesh ($\Delta/h=1.5$). This is the same slab and mesh used for the corresponding finite element study in Chapter 9. A number of runs were performed for square slabs, whose size L ranged from 54 in. to 234 in. Care was taken to maintain the applied load symmetrically placed on the central square. Results from these runs are shown in Table 10.1, together with the corresponding infinite-slab closed-form solutions. Figure 10.4 shows the same results in a normalized plot.

It is observed that deflections and subgrade stresses converge to the corresponding large slab value from above, and seem to be slightly more sensitive to slab size changes than bending stresses. The latter converge from below. These trends are similar to those obtained using the F.E.M. (Fig. 9.8), although finite element responses are nearer to the closed-form solutions. This indicates a higher sensitivity to grid fineness in the case of the F.D.M., and/or the limitations of the way the applied loads are handled in FIDIES. This may be expected since in ILLI-SLAB each applied load is represented by twelve generalized force components, while in FIDIES a single point load replaces each applied load.

The discrepancies between the closed-form solution and the large slab values, which the numerical results converge to upon slab size expansion, will be investigated further below. Ignoring these

TABLE 10.1
EFFECT OF SLAB SIZE

L (in.)	(L/ l_e)	δ (mils)	q (psi)	σ (psi)
54	2.075	0.3798	0.3352	6.174
90	3.459	0.3086	0.3005	7.009
126	4.842	0.2964	0.2920	6.998
162	6.226	0.2904	0.2860	6.926
198	7.610	0.2867	0.2829	6.898
234	8.993	0.2847	0.2816	6.892
Closed-Form		0.2649	0.2467	11.497

Notes:

Parameters Used:

$E = 3 \times 10^6$ psi $E_s = 4 \times 10^4$ psi $\Delta = 18$ in.
 $\mu = 0.15$ $\mu_s = 0.45$ $A = 3 \times 3$ in.
 $h = 12$ in. @ 100 psi;
 interior
 $l_e = 26.02$ in.

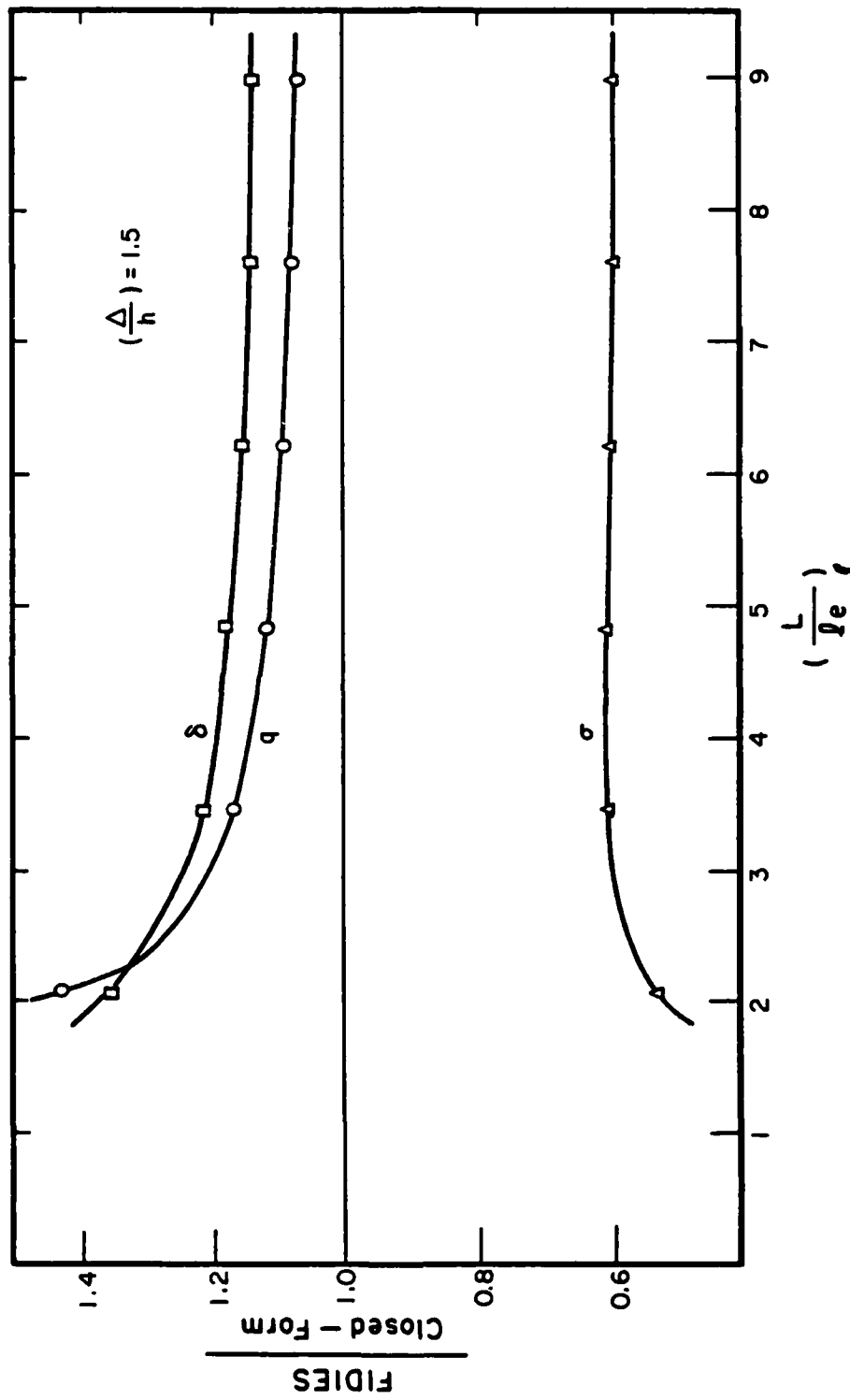


Fig. 10.4 Effect of Slab Size (Interior Loading)

discrepancies, it may be concluded that the following slab sizes are required for the development of an infinite-slab condition:

Deflection : $(L/\ell_e) \approx 6.5$
 Subgrade Stress: $(L/\ell_e) \approx 6.0$
 Bending Stress : $(L/\ell_e) \approx 3.5.$

These values are comparable to those obtained using the elastic solid option in ILLI-SLAB (see paragraph 9.5.2).

(b) Effect of Finite Difference Interval: One of the cases considered above ($L/\ell_e=3.459$) was selected and additional analyses were performed using a range of values for the finite difference interval, Δ . The results from these runs are summarized in Table 10.2, and are plotted in a non-dimensional form in Fig. 10.5.

Considerable improvement in the accuracy of the solution is observed as the slab is subdivided into smaller finite difference intervals. It appears that subgrade and bending stresses converge to the corresponding fine-mesh values from below, while deflection approaches this value from above. This latter trend appears to be contrary to that obtained using the F.E.M. (Fig. 9.9), although in both cases the sensitivity of deflection is very small. The bending stress, on the other hand, is particularly sensitive to the fineness effect.

A considerable portion of the discrepancy between closed-form and numerical solutions noted earlier, disappears as Δ decreases. Since (L/ℓ_e) is fairly low, however, some discrepancy persists in Fig. 10.5

TABLE 10.2
EFFECT OF FINITE DIFFERENCE INTERVAL

Δ (in.)	(Δ/h)	No. of Elements	δ (mils)	q (psi)	σ (psi)
30	2.5	9	0.3165	0.2804	4.762
18	1.5	25	0.3086	0.3005	7.009
12.857	1.071	49	0.3028	0.3000	8.331
10	0.833	81	0.2994	0.2974	9.268
8.182	0.682	121	0.2973	0.2950	9.996
6.923	0.385	169	0.2960	0.2929	10.593
Closed-Form			0.2649	0.2467	11.497

Notes:

Parameters Used:

$$E = 3 \times 10^6 \text{ psi} \quad E_s = 4 \times 10^4 \text{ psi} \quad L = 90 \text{ in.} \left(\frac{L}{l_e} = 3.459 \right)$$

$$\mu = 0.15 \quad \mu_s = 0.45$$

$$h = 12 \text{ in.}$$

$$l_e = 26.02 \text{ in.}$$

$$A = 3'' \times 3'' @ 100 \text{ psi};$$

interior

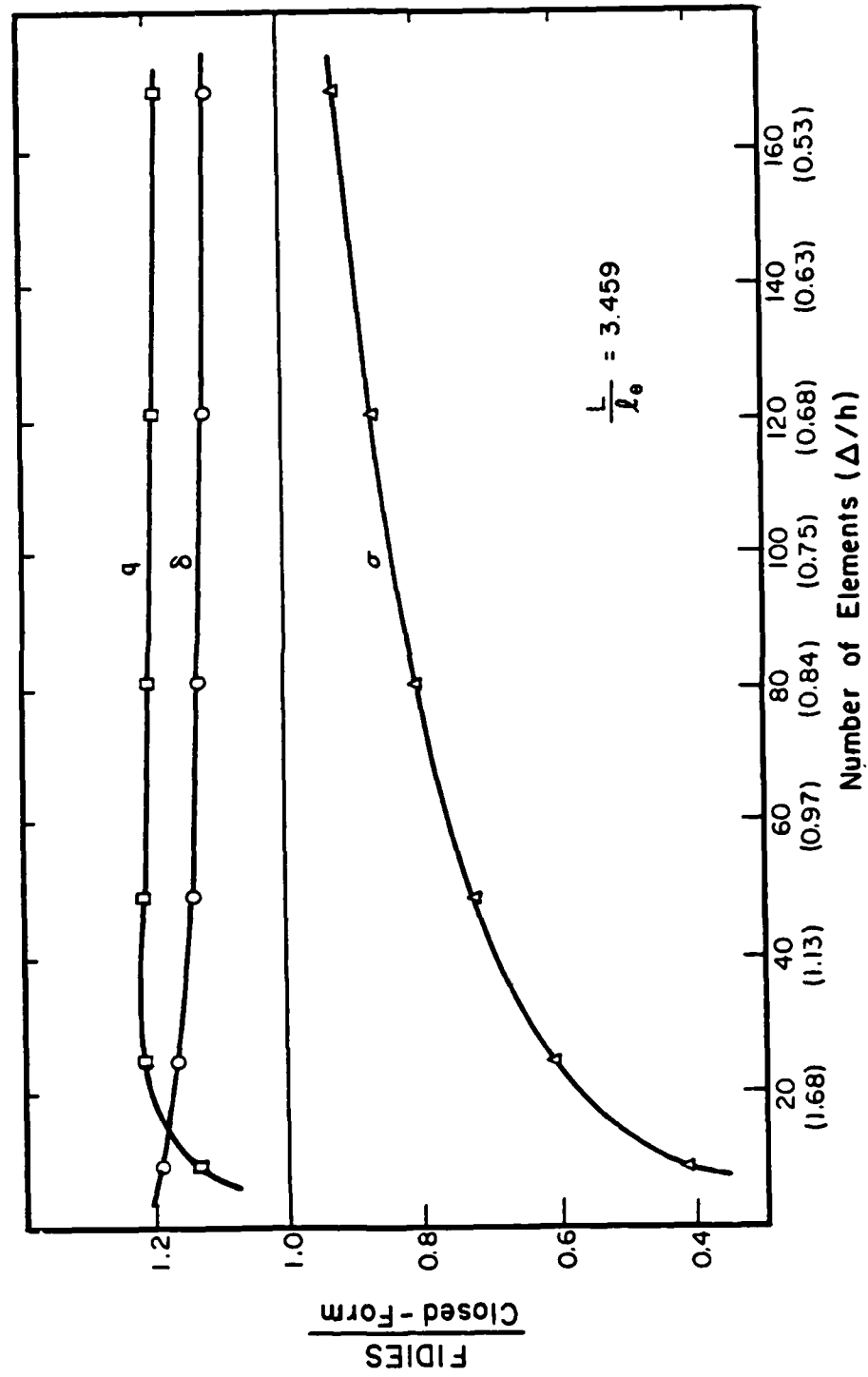


Fig. 10.5 Effect of Grid Fineness (Interior Loading)

even when a large number of elements is used. Another possible cause of this will be discussed below. The following fineness requirements may be established at this point:

Deflection : $\Delta / h \approx 0.90$

Subgrade Stress: $\Delta / h \approx 0.85$

Bending Stress : $\Delta / h \approx 0.55.$

Compared to the corresponding mesh fineness requirements obtained from the F.E.M. (see paragraph 9.5.3), these values are considerably more stringent and confirm a higher sensitivity of FIDIES to this effect.

(c) Effect of Size of Loaded Area: It was noted earlier that all externally applied loads are replaced in the finite difference analysis by approximately statically equivalent point loads acting at the centroid of each element over which the external loads are prescribed. This may not be an accurate representation, especially in the case of large elements and eccentrically placed loads. As a result some discrepancy between the closed-form and numerical solutions may be expected to persist even for large slabs divided into numerous elements. The comments made with respect to this effect in paragraph 9.5.4, and Fig. 9.10 obtained using the F.E.M., must be borne in mind.

10.4.3 Corner Loading

(a) Effect of Slab Size: For practical reasons, a slab with a low radius of relative stiffness ($\rho_e = 20$ in.) was selected for this

study, as well. Square slabs were used in all runs, ranging in size between 60 in. and 156 in. A single corner load was applied, covering an entire corner square. The grid fineness ratio (Δ/h) for these runs was 0.86.

The results from the FIDIES runs conducted are shown in Table 10.3. Note that for corner loading, the maximum bending stress is not a direct stress but a principal stress. Since no closed-form solution is currently available for this case, the responses were normalized with respect to those obtained using the largest slab in this study. Normalized plots are shown in Fig. 10.6. The trends displayed are similar to those in Fig. 10.4 for interior loading, and Fig. 5.29 for the dense liquid corner loading. Deflection and subgrade stress converge from above, and seem to be equally sensitive to the slab size effect as bending stress, whose convergence is from below. All three responses reach their large-slab values at a value (L/ℓ_e) of about 5.0. This is comparable to the corresponding dense liquid requirements established in paragraph 5.5.3, and somewhat lower than the interior loading values developed above.

(b) Effect of Finite Difference Interval: The 10-ft. square slab ($L/\ell_e=6.0$) used above was selected for the grid fineness study. Again, a corner square was loaded but, in this case, it was not possible to use only fully and/or symmetrically loaded elements. As a result, a poorer correlation may be expected.

The results obtained from these FIDIES runs are tabulated in Table 10.4, and plotted in a normalized fashion, in Fig. 10.7. Once more,

TABLE 10.3
EFFECT OF SLAB SIZE: CORNER LOADING

NX=NY	(L/ℓ_e)	δ (mils)	$\delta/\delta_{13 \times 13}$ (%)	q (psi)	q/q _{13x13} (%)	σ -tensile- (psi)	$\sigma/\sigma_{13 \times 13}$ (%)
5	3.0	13.246	103.947	85.130	104.014	127.905	95.794
6	3.6	12.929	101.460	82.896	101.284	131.710	98.644
7	4.2	12.808	100.510	82.153	100.376	132.997	99.608
8	4.8	12.765	100.173	81.924	100.097	133.393	99.904
9	5.4	12.750	100.055	81.862	100.021	133.498	99.983
10	6.0	12.745	100.016	81.848	100.004	133.510	99.999
11	6.6	12.744	100.008	81.846	100.001	133.522	100.001
12	7.2	12.744	100.008	81.845	100.00	133.522	100.001
13	7.8	12.743	100.000	81.845	100.000	133.521	100.000

Notes:

$$E = 2 \times 10^6 \text{ psi}$$

$$E_s = 87,724 \text{ psi}$$

$$\mu = 0.15$$

$$\mu_s = 0.5$$

$$h = 14 \text{ in.}$$

$$\ell_e = 20 \text{ in.}$$

$$\Delta = 12 \text{ in.}$$

$$\Delta/h = 0.86$$

$$c/\Delta = 1.00$$

$$A = 12 \text{ in.} \times 12 \text{ in. @ } p = 200 \text{ psi (corner)}$$

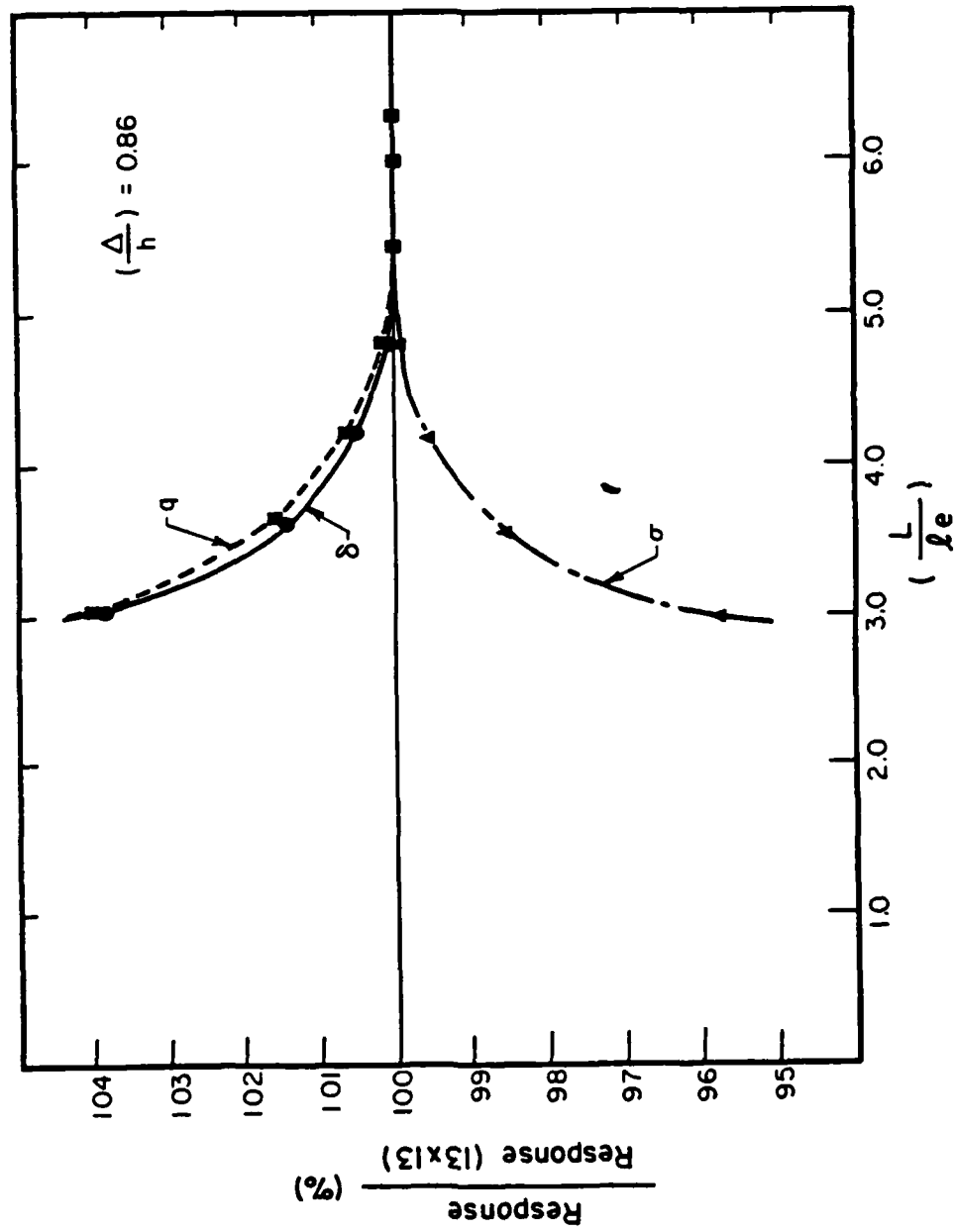


Fig. 10.6 Effect of Slab Size (Corner Loading)

TABLE 10.4
EFFECT OF GRID FINENESS: CORNER LOADING

NX=NY	Δ (in.)	$\frac{c}{\Delta}$	δ (mils)	$\delta/\delta_{13 \times 13}$ (%)	q (psi)	$q/q_{13 \times 13}$ (%)	σ (psi)	$\sigma/\sigma_{13 \times 13}$ (%)
6	20.0	0.60	10.125	81.430	44.399	48.244	86.399	74.881
7	17.1	0.70	10.952	88.081	54.011	58.688	100.854	87.409
8	15.0	0.80	11.646	93.663	63.468	68.964	112.867	97.820
9	13.3	0.90	12.238	98.424	72.768	79.070	122.887	106.504
10	12.0	1.00	12.745	102.501	81.848	88.936	133.520	115.720
11	10.9	1.10	12.537	100.828	84.493	91.810	124.508	107.909
12	10.0	1.20	12.447	100.105	87.955	95.572	119.904	103.919
13	9.2	1.30	12.434	100.000	92.030	100.000	115.382	100.000

Notes:

$$E = 2 \times 10^6 \text{ psi}$$

$$\mu = 0.15$$

$$h = 14 \text{ in.}$$

$$L = 120 \text{ in.}$$

$$A = 12 \text{ in.} \times 12 \text{ in.} @ p = 200 \text{ psi (corner)}$$

$$E_s = 87,724 \text{ psi}$$

$$\mu_s = 0.5$$

$$\ell_e = 20 \text{ in.}$$

$$L/\ell_e = 6.0$$

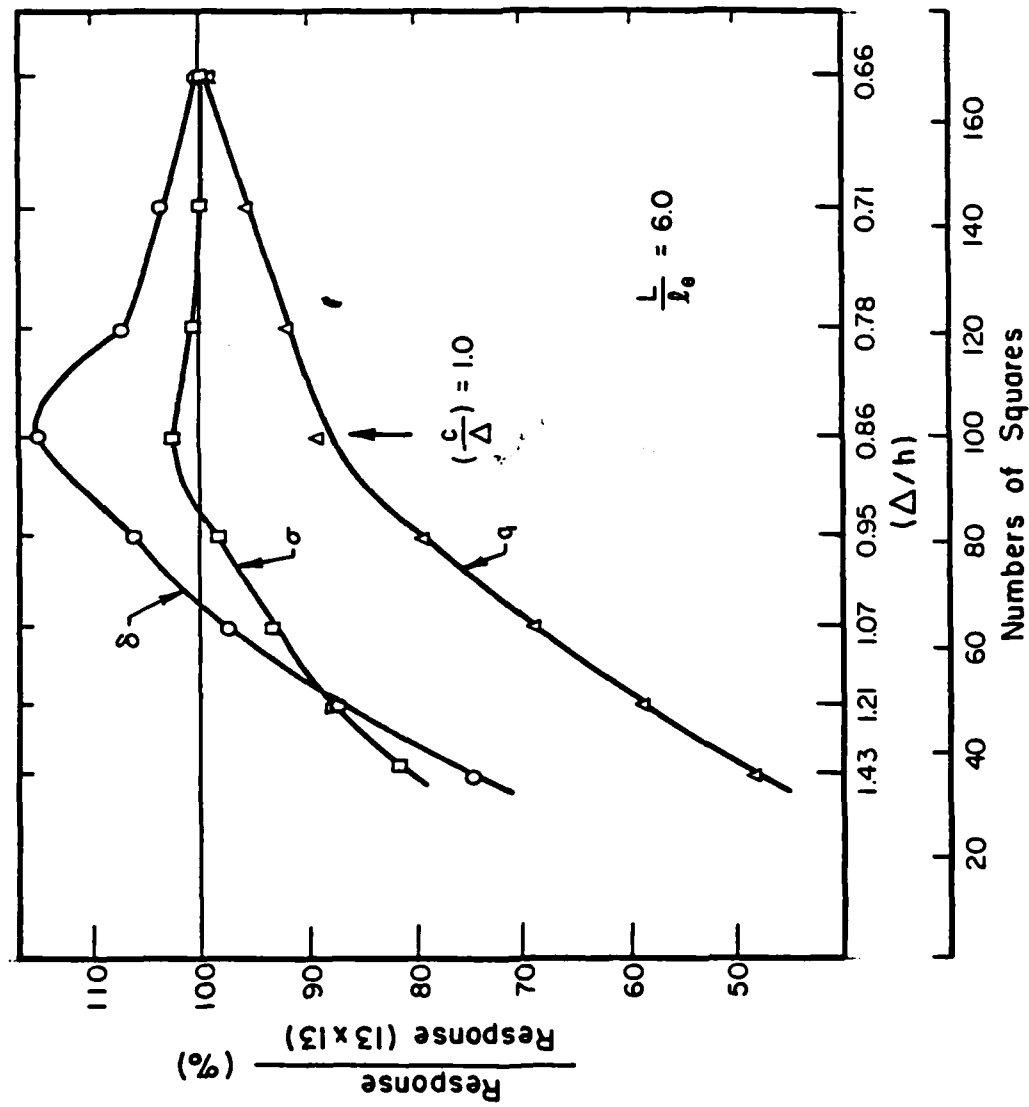


Fig. 10.7 Effect of Grid Fineness (Corner Loading)

the normalization is with respect to the responses obtained using the finest grid. The trends exhibited in Fig. 10.7 are unexpected, with "humps" occurring when the load covers the entire square. This reflects the effect of the way loads are handled in FIDIES. Despite this, all three responses seem to converge from below, with subgrade stress being most sensitive to the fineness effect, while bending stress is most sensitive to the effect of partially or unsymmetrically loaded squares. The following approximate requirements may be extracted from these plots:

Deflection : $\Delta/h = 0.90$

Subgrade Stress: $\Delta/h = 0.60$

Bending Stress : $\Delta/h = 0.75$

10.5 DEVELOPMENT OF PREDICTIVE EQUATIONS FOR CORNER LOADING

It was shown in Chapter 5, how the F.E.M. as employed in ILLI-SLAB may be used to derive predictive equations for the maximum deflection, and magnitude and location of the maximum bending stress developing in a slab supported by a dense liquid foundation, loaded by a corner load. Closed-form equations for the case of an elastic solid subgrade have been restricted up to now to interior loading. In Chapter 8, the computerized chart developed during this research, was used to obtain an equation for the bending stress under an edge load, applied to a plate supported by an elastic solid. This was achieved by assuming the elastic solid equation sought, would be of the same general form as the

corresponding dense liquid formula by Westergaard [10]. Using similar reasoning, the finite difference program FIDIES developed in this Chapter will be employed to derive predictive equations to describe the response under corner loading of a plate resting on an elastic solid subgrade.

Referring to the Westergaard corner equations (Table 5.12), it is reasonable to lump the parameters entering the equations sought into the following dimensionless groups:

$$\frac{\delta_c D}{P \ell_e^2} \quad \frac{q_c \ell_e^2}{P} \quad \text{and} \quad \frac{\sigma_c h^2}{P}$$

Plotting these groups against (c/ℓ_e) , a set of straight lines may be expected. Parameter c is the side-length of the applied square load, and is equal to Δ for fully loaded grid elements in FIDIES.

The data base used for the development of the equations consists of the results of several FIDIES runs, tabulated in Table 10.5. An effort was made to select parameters for these runs that would range between fairly wide limits. It was also attempted to keep the grid fineness ratio (Δ/h) and the slab size ratio (L/ℓ_e) at values which, according to the preceding discussion, would eliminate, as much as possible, these two effects.

The values of the non-dimensional groups identified above are plotted in Figures 10.8 through 10.10. The expectation for straight line plots is borne out in these graphs. The following three equations

TABLE 10.5
DATA BASE FOR CORNER EQUATIONS

E (psi)	E_s (psi)	μ_s	h (in.)	$\Delta=c$ (in.)	NX= NY	P (kips)	δ (mils)	q (psi)	σ (psi)
2×10^6	50,000	0.5	12.00	10.20	12	20	16.022	65.375	147.470
3×10^6	89,403	0.5	16.00	12.00	13	30	10.948	66.645	130.719
1×10^6	25,387	0.5	8.00	6.33	13	10	24.365	79.843	174.277
2×10^6	60,000	0.5	14.00	11.34	12	10	6.075	26.851	53.853
3×10^6	90,000	0.5	14.00	11.23	12	20	8.126	54.253	108.475
2.5×10^6	50,000	0.5	14.00	11.79	13	20	13.126	45.265	115.104
1.0×10^6	26,991	0.45	14.00	11.00	12	10	13.957	26.260	57.171
3.0×10^6	80,000	0.45	6.00	4.80	12	10	10.896	139.805	308.389
2.0×10^6	60,576	0.50	10.00	8.08	12	10	8.449	52.925	105.498
4.3×10^6	83,000	0.35	12.00	9.60	13	40	20.936	121.740	336.962
3.8×10^6	99,000	0.35	6.00	4.80	12	20	18.850	268.982	632.954
1.0×10^6	38,090	0.45	6.00	4.80	10	10	24.816	156.676	283.020
1.0×10^6	33,197	0.45	12.00	9.60	12	30	41.402	112.498	219.770

Notes: $\Delta/h = 0.75 - 0.85$

$L/\ell_e = 5.25 - 6.00$

$\mu = 0.15$

Load applied on a corner square

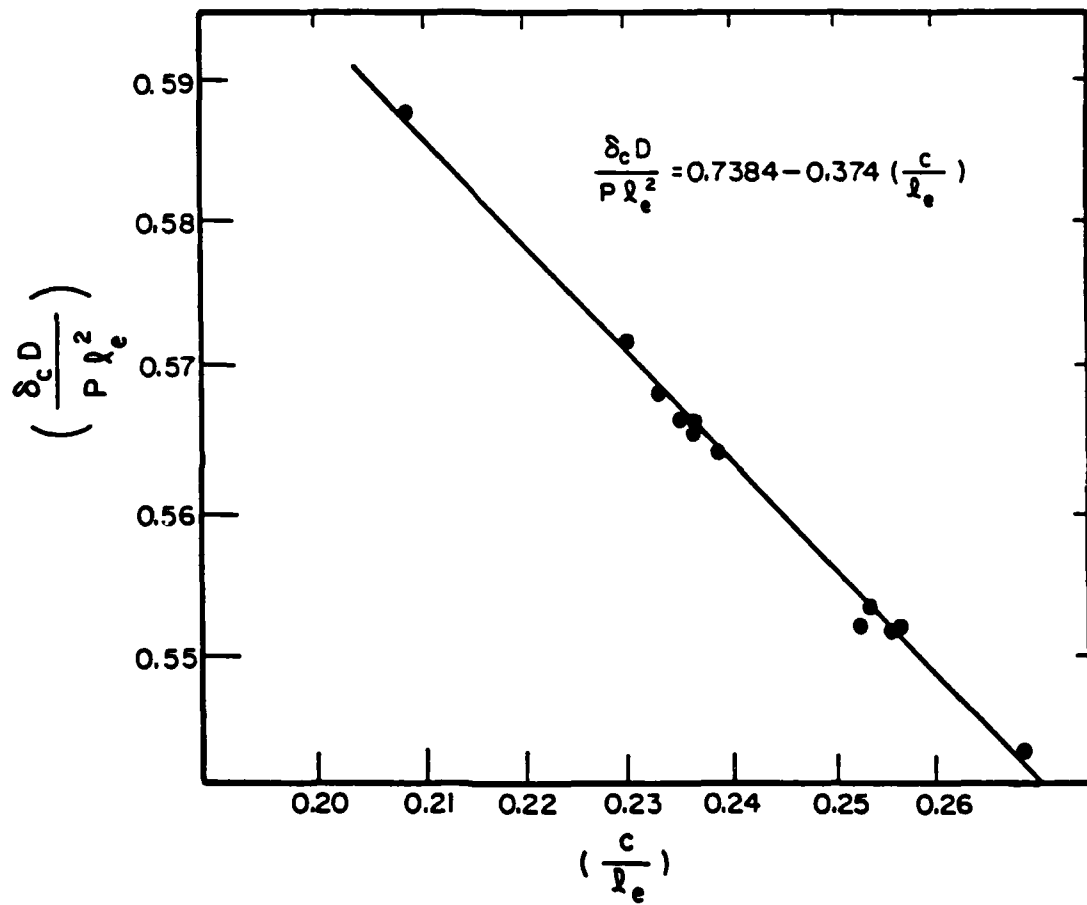


Fig. 10.8 Variation of Normalized Maximum Corner Deflection

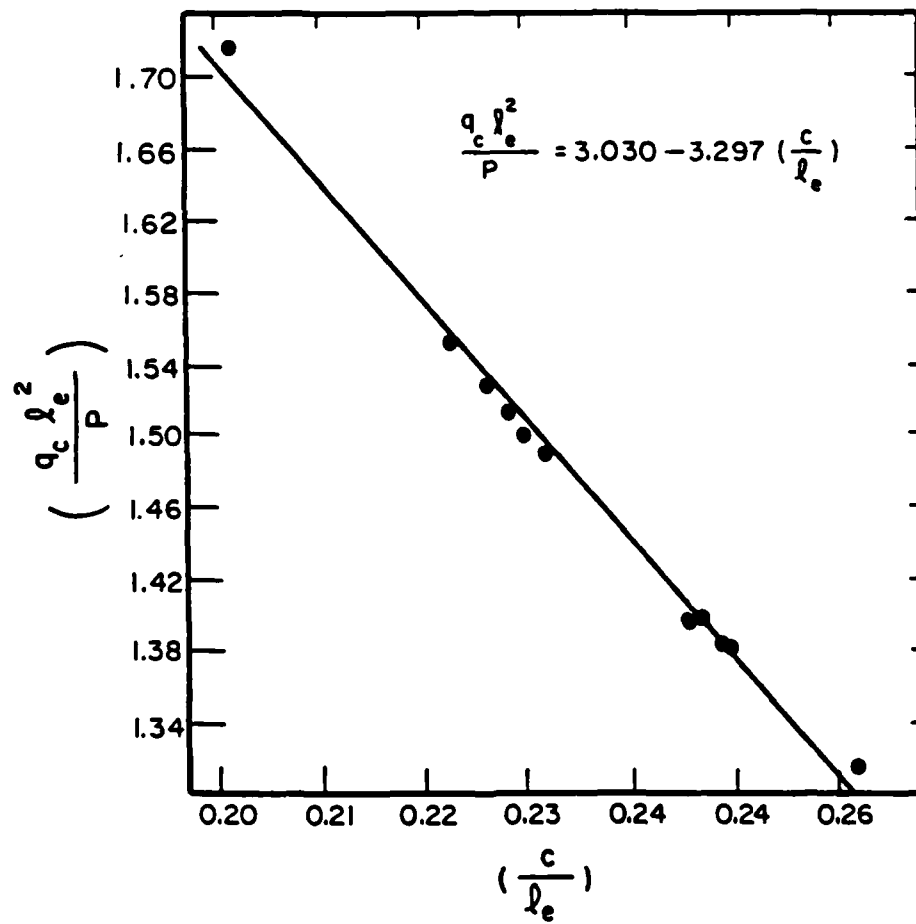


Fig. 10.9 Variation of Normalized Maximum Corner Subgrade Stress

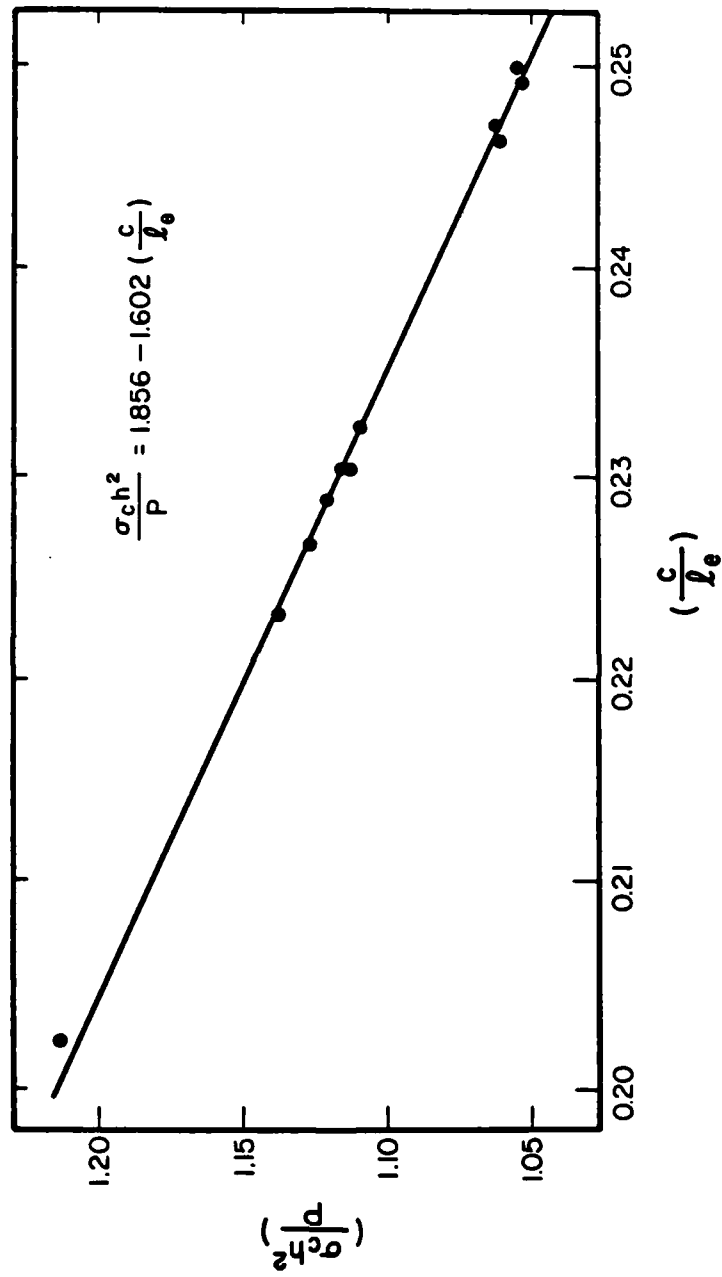


Fig. 10.10 Variation of Normalized Maximum Bending Stress Under Corner Loading

may be used to describe the best fit straight lines obtained in this way:

$$\begin{aligned}\delta_c &= \frac{Pl_e^2}{D} [0.7384 - 0.374 (c/l_e)] \\ q_c &= \frac{P}{l_e^2} [3.0300 - 3.297 (c/l_e)] \\ \sigma_c &= \frac{P}{h^2} [1.8560 - 1.602 (c/l_e)]\end{aligned}\tag{10-25}$$

These equations have been derived for

$$0.20 < c/l_e < 0.26$$

but may hold, at least approximately, within a reasonably broader range. Note that, due to the manner in which the applied loads are handled in FIDIES, best correlation is obtained when the corner element is fully, or at least symmetrically, loaded. These predictive equations may be verified by the F.E.M., using the elastic solid option in ILLI-SLAB.

CHAPTER 11

FINITE ELEMENT ANALYSIS OF A PLATE
ON A TWO-PARAMETER FOUNDATION

11.1 INTRODUCTION

The desirability of developing two-parameter soil models stems from two observations made in the preceding analyses. The first is the inherent deficiency of the simple Winkler model to faithfully reproduce the behavior of continuous soil masses. The second is that any attempt to introduce the more realistic elastic solid model is plagued by the mathematical complexities of this idealization, which translate -on a practical level- into excessive requirements for computer storage and computational effort. A model that would bridge the gap between the completely discontinuous springs subgrade and the completely continuous Boussinesq half-space is, therefore, an attractive proposition.

Of the two-parameter models described in Chapter 2, that proposed by Vlasov and Leont'ev [2] will be more closely investigated in this Chapter, using the Finite Element Method (F.E.M.). Previous studies [2; 22; 68] have suggested that the Vlasov model offers the possibility of selecting subgrade parameters which have some physical significance, and may eventually be related to the engineering properties of the soil. In order to examine the applicability of Vlasov's two-parameter model in the analysis of slabs-on-grade, a finite element formulation was used to derive the subgrade stiffness matrices for this model. The

formulation, which has now been incorporated into ILLI-SLAB, is described in detail below.

11.2 FORMULATION FOR SUBGRADE STIFFNESS MATRIX

11.2.1 Assumed Displacement Function

In accordance with the derivation for the original version of ILLI-SLAB, which employs the 4-noded 12-dof plate bending element (known as ACM or RPB12), the following displacement function is assumed:

$$w = a_1 + a_2x + a_3y + a_4x^2 + a_5xy + a_6y^2 + a_7x^3 + a_8x^2y + a_9xy^2 + a_{10}y^3 + a_{11}x^3y + a_{12}xy^3$$

$$\text{or } w_{1 \times 1} = [X]_{1 \times 12} \{a\}_{12 \times 1} \quad (11-1)$$

The nodal displacements, $\{d\}$, consisting of w , $\theta_x (= -\frac{\partial w}{\partial y})$ and $\theta_y (= \frac{\partial w}{\partial x})$ at each node may then be written as:

$$\{d\}_{12 \times 1} = [A]_{12 \times 12} \{a\}_{12 \times 1}$$

whence,

$$w_{1 \times 1} = [X]_{1 \times 12} [A]^{-1}_{12 \times 12} \{d\}_{12 \times 1}$$

$$\text{or } w_{1 \times 1} = [N]_{1 \times 12} \{d\}_{12 \times 1} \quad (11-2)$$

The twelve shape functions in row vector $[N]$ are given in Table 11.1.

In deriving the stiffness matrix for the Winkler type subgrade, Tabatabaie [79] used the principle of virtual work. In the present formulation the concept of strain energy is used instead, to provide a check on the Winkler subgrade stiffness matrix in ILLI-SLAB, and obtain the additional stiffness matrices required to define a Vlasov type foundation.

11.2.2 The Concept of Strain Energy

Consider a body acted upon by a stress σ (or force P) which results in a small strain $\delta\epsilon$ (or displacement $\delta\omega$). The increment in strain energy stored in this body is defined as:

$$\begin{aligned}\delta U &= \sigma \delta\epsilon \\ \text{or } \delta U &= P \delta\omega\end{aligned}\tag{11-3}$$

Thus, considering the example of a linear spring for which $P = k\omega$, Eqn. (11-3) gives:

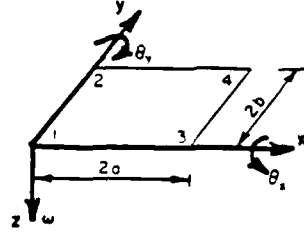
$$\begin{aligned}\delta U &= P \delta\omega \\ &= k\omega \delta\omega\end{aligned}$$

The total strain energy stored in the spring as this deforms from $\omega=0$ to $\omega=w$, say, is obtained by integration as follows:

TABLE 11.1

SHAPE FUNCTIONS FOR ACM ELEMENT

CONVENTION:



Nodal dof:

$$\begin{Bmatrix} w \\ \theta_2 \\ \theta_3 \end{Bmatrix}$$

ASSUMED DEFLECTION SHAPE:

$$w = a_1 + a_2x + a_3y + a_4x^2 + a_5xy + a_6y^2 + a_7x^3 + a_8x^2y + a_9xy^2 + a_{10}y^3 + a_{11}x^3y + a_{12}xy^3$$

SHAPE FUNCTIONS:

$$N_1 = 1 - \frac{3x^2}{4a^2} - \frac{xy}{4ab} - \frac{3y^2}{4b^2} + \frac{x^3}{4a^3} + \frac{3x^2y}{8a^2b} + \frac{3xy^2}{8ab^2} + \frac{y^3}{4b^3} - \frac{x^3y}{8a^3b} - \frac{xy^3}{8ab^3}$$

$$N_2 = -y + \frac{xy}{2a} + \frac{y^2}{b} - \frac{xy^2}{2ab} - \frac{y^3}{4b^2} + \frac{xy^3}{8ab^2}$$

$$N_3 = x - \frac{x^2}{a} - \frac{xy}{2b} + \frac{x^3}{4a^2} + \frac{x^2y}{2ab} - \frac{x^3y}{8a^2b}$$

$$N_4 = \frac{xy}{4ab} + \frac{3y^2}{4b^2} - \frac{3x^2y}{8a^2b} - \frac{3xy^2}{8ab^2} - \frac{y^3}{4b^3} + \frac{x^3y}{8a^3b} + \frac{xy^3}{8ab^3}$$

$$N_5 = \frac{y^2}{2b} - \frac{xy^2}{4ab} - \frac{y^3}{4b^2} + \frac{xy^3}{8ab^2}$$

$$N_6 = \frac{xy}{2b} - \frac{x^2y}{2ab} + \frac{x^3y}{8a^2b}$$

$$N_7 = \frac{3x^2}{4a^2} + \frac{xy}{4ab} - \frac{x^3}{4a^3} - \frac{3x^2y}{8a^2b} - \frac{3xy^2}{8ab^2} + \frac{x^3y}{8a^3b} + \frac{xy^3}{8ab^3}$$

$$N_8 = \frac{-xy}{2a} + \frac{xy^2}{2ab} - \frac{xy^3}{8ab^2}$$

$$N_9 = \frac{-x^2}{2a} + \frac{x^3}{4a^2} + \frac{x^2y}{4ab} - \frac{x^3y}{8a^2b}$$

$$N_{10} = \frac{-xy}{4ab} + \frac{3x^2y}{8a^2b} + \frac{3xy^2}{8ab^2} - \frac{x^3y}{8a^3b} - \frac{xy^3}{8ab^3}$$

$$N_{11} = \frac{xy^2}{4ab} - \frac{xy^3}{8ab^2}$$

$$N_{12} = \frac{-x^2y}{4ab} + \frac{x^3y}{8a^2b}$$

$$\begin{aligned}
 U &= \int_{\omega=0}^{\omega=w} \delta U \\
 &= \int_{\omega=0}^{\omega=w} k\omega \, d\omega
 \end{aligned}$$

$$\text{or } U = k w^2 / 2 \quad (11-4)$$

Now, consider a plate element $2a \times 2b$ at the interior of a finite element mesh. The increment in strain energy is obtained from Eqn. (11-3):

$$U = \int_0^{2a} \int_0^{2b} (q \cdot \delta w) \, dx \, dy \quad (11-5)$$

where q is the subgrade reaction (force per unit area).

It was shown in Chapter 2 that for the Vlasov foundation, subgrade reaction, q , is related to surface deflection, w , through:

$$q = kw - G \nabla^2 w \quad (11-6)$$

where:

G : foundation constant describing the shear interaction between adjacent springs (assumed to be equal in x - and y -directions).

Note that if G is set to zero, the Vlasov foundation reduces to the Winkler dense liquid. Substituting Eqn. (11-6) into Eqn. (11-5) yields:

$$\delta U = \int_0^{2a} \int_0^{2b} \left\{ kw - G \frac{\partial^2 w}{\partial x^2} - G \frac{\partial^2 w}{\partial y^2} \right\} \delta w \, dx \, dy \quad (11-7)$$

Integration of δU will yield the required total strain energy for the plate element. The first term in Eqn. (11-7) may readily be integrated as per Eqn. (11-4). Now, consider the first shear interaction term:

$$I_x = -G \int_{x=0}^{2a} \int_{y=0}^{2b} \frac{\partial^2 w}{\partial x^2} \delta w \, dx \, dy$$

Integrating by parts, this gives:

$$\begin{aligned} I_x = & -G \int_{y=0}^{2b} \left(\frac{\partial w}{\partial x} \delta w \right) \Big|_{x=0}^{2a} dy \\ & + G \int_{x=0}^{2a} \int_{y=0}^{2b} \frac{\partial w}{\partial x} \frac{\partial}{\partial x} (\delta w) \, dx \, dy \end{aligned} \quad (11-8)$$

Note that the first term in this equation is a line integral, evaluated at the two plate element edges that are parallel to the y-axis. Similarly, the second shear interaction term in Eqn. (11-7) yields:

$$\begin{aligned} I_y = & -G \int_{x=0}^{2a} \int_{y=0}^{2b} \frac{\partial^2 w}{\partial y^2} \delta w \, dx \, dy \\ = & -G \int_{x=0}^{2a} \left(\frac{\partial w}{\partial y} \delta w \right) \Big|_{y=0}^{2b} dx \\ & + G \int_{x=0}^{2a} \int_{y=0}^{2b} \frac{\partial w}{\partial y} \frac{\partial}{\partial y} (\delta w) \, dx \, dy \end{aligned} \quad (11-9)$$

Eqn. (11-9) also contains a line integral evaluated at the two plate element edges that are parallel to the x -axis. For a region at the interior of the plate, the line integrals in Equations (11-8) and (11-9) from adjacent regions will cancel in pairs. Only the line integrals along the plate edges remain, which give rise to concentrated edge reactions along these boundaries. The concentrated reactions will be considered further below.

Substituting Equations (11-4), (11-8), and (11-9) into Eqn. (11-7), the following expression for the total strain energy of an interior plate bending element is obtained:

$$U = \int_0^{2a} \int_0^{2b} \left\{ \frac{1}{2} k w^2 + \frac{1}{2} G \left(\frac{\partial w}{\partial x} \right)^2 + \frac{1}{2} G \left(\frac{\partial w}{\partial y} \right)^2 \right\} dx dy \quad (11-10)$$

since the first variation of $\frac{1}{2} \left(\frac{\partial w}{\partial n} \right)^2$ is:

$$\begin{aligned} \delta \left[\frac{1}{2} \left(\frac{\partial w}{\partial n} \right)^2 \right] &= \frac{\partial w}{\partial n} \delta \left(\frac{\partial w}{\partial n} \right) \\ &\equiv \frac{\partial w}{\partial n} \frac{\partial}{\partial n} (\delta w) \end{aligned}$$

In Eqn. (11-10), the first term describes the Winkler contribution. The two additional terms result from the shear interaction between adjacent spring elements. The formulation for the stiffness matrix corresponding to each of these three terms will be presented separately below.

11.2.3 Concentrated Boundary Reactions

It was noted above that concentrated reactions arise at the boundaries of a rectangular plate resting on a Vlasov foundation. These are due to the deformation of the subgrade beyond the plate edges, i.e. the interaction between foundation elements covered by the plate and those that are not. Such interaction also exists in the Boussinesq idealization, but not in the Winkler model.

Kerr [171] shows that boundary reactions, R_e , are proportional to the difference in slope of the foundation surface (w'_+ and w'_-) on either side of the boundary:

$$\begin{aligned} R_e &= G (w'_- - w'_+) \\ &= Gw'_- - Gw'_+ \\ &= R_{e-} + R_{e+} \end{aligned} \tag{11-11}$$

The stiffness matrix formulation presented above implicitly includes the first term in Eqn. (11-11). Therefore, only the second term -which involves the slope of the foundation surface just beyond the plate edge- need be considered further. The effect of this term may be accounted for by installing an additional spring element at each edge and corner node. The problem then reduces to determining the spring constant for these elements.

To obtain a first approximation for the spring constant, consider the corresponding one-dimensional case of a semi-infinite plate. For the uncovered part of the foundation the subgrade reaction according to

Eqn. (11-6) is:

$$q(x) = kw - G \frac{\partial^2 w}{\partial x^2} = 0$$

Therefore, the deflected foundation surface beyond the slab is given by:

$$w = w_e \exp [-\sqrt{k/G} \cdot x] \quad (11-12)$$

where:

w_e : deflection at the boundary between uncovered parts;

x : distance from the boundary.

Differentiating Eqn. (11-12):

$$dw/dx = -\sqrt{k/G} w_e \exp [-\sqrt{k/G} \cdot x]$$

Thus, the slope of the foundation surface just outside the covered part is:

$$(dw/dx)_{x=0+} = w'_+ = -\sqrt{k/G} \cdot w_e \quad (11-13)$$

Substituting Eqn. (11-13) into the second term of Eqn. (11-11):

$$\begin{aligned} R_{e+} &= +G \sqrt{k/G} \cdot w_e \\ &= \sqrt{kG} \cdot w_e \end{aligned} \quad (11-14)$$

where the term \sqrt{kG} is the approximate spring stiffness sought.

A different approximate adjustment for boundary reactions is employed by Yang [172], who follows a formulation presented by Vlasov and Leont'ev [2]. This approach results in an iterative procedure when incorporated into a finite element code, which is not as attractive as the addition of boundary spring elements since it inevitably prolongs execution time.

To obtain an idea of how good the approximation involved in Eqn. (11-14) is, comparisons may be attempted with more refined approaches. For example, an exact formulation for the Vlasov foundation may be derived along the lines proposed by Cheung and Zienkiewicz [88] for the Boussinesq half-space. The following expression for the effect of a point load, P , on a Vlasov subgrade may be used [2]:

$$w(r) = \frac{2Py(1+\mu_o)}{\pi E_o} K_o(\alpha r) \quad (11-15)$$

where:

γ : vertical displacement attenuation coefficient;

$K_o(\alpha r)$: modified zero-order Bessel function of the second kind;

α : $\sqrt{k/G}$;

$$E_o = \frac{E_s}{1-\mu_s^2}$$

$$\mu_o = \frac{\mu_s}{1-\mu_s}$$

The foundation stiffness matrix resulting from the flexibility matrix obtained using Eqn. (11-15) will not be banded and, therefore, will suffer from the same storage limitations as the matrix for the elastic solid. For research purposes, however, this may be worthwhile, since it may facilitate a better selection of the boundary spring stiffness.

An alternate approach would consider the effect of fictitious plates of zero thickness added to the four boundaries of the real plate, with due allowance for the possibility of slope discontinuity at these boundaries. A more elaborate discussion of this issue would be beyond the scope of this work. It may be expected, however, that the effect of the concentrated reactions will be more pronounced for short slabs of high relative stiffness, with loads applied close to the edges.

11.2.4 The Winkler Term

From Eqn. (11-10) the total strain energy contribution of this term is given by:

$$U = \frac{1}{2} k \int_0^{2a} \int_0^{2b} w^2 dx dy \quad (11-16)$$

Equation (11-2) may be rewritten as:

$$\begin{aligned} w_{1X1} &= \sum_{k=1}^{12} N_k d_k \\ &= N_1 d_1 + N_2 d_2 + \dots + N_{12} d_{12} \end{aligned} \quad (11-17)$$

Thus,

$$w^2 = \left\{ \sum_{k=1}^{12} N_k^2 d_k^2 \right\} + 2 \left\{ \sum_{k=1}^{12} N_k d_k \left(\sum_{\ell=k+1}^n N_\ell d_\ell \right) \right\} \quad (11-18)$$

Equation (11-18) is written out fully in Table 11.2(a). Substituting Eqn. (11-18) into Eqn. (11-16):

$$U = \frac{1}{2} k \int_0^{2a} \int_0^{2b} \left[\left\{ \sum_{k=1}^{12} N_k^2 d_k^2 \right. \right. \\ \left. \left. + 2 \left\{ \sum_{k=1}^{12} N_k d_k \left(\sum_{\ell=k+1}^{12} N_\ell d_\ell \right) \right\} \right\} \right] dx dy \quad (11-19)$$

To obtain term $K_{i,j}$ of the element stiffness matrix for the Winkler contribution, where both i and j range from 1 to 12, Castigliano's theorem is employed. This states that:

"The partial derivative of the total strain energy of any structure with respect to any one of the applied forces, is equal to the displacement of the point of application of that force, in the direction of the force."

Since stiffness term $K_{i,j}$ expresses the displacement at i due to a unit force at j , all other nodal forces being set to zero, the following two steps are required for its derivation:

TABLE 11.2

EXPANDED FORM OF EQUATIONS

$$\begin{aligned}
 & \text{(a)} \\
 w^2 &= \left\{ \sum_{k=1}^{12} N_k^2 d_k^2 \right\} + 2 \left\{ \sum_{k=1}^{12} N_k d_k \left(\sum_{l=k+1}^{12} N_l d_l \right) \right\} \quad (11-18) \\
 &= N_1^2 d_1^2 + N_2^2 d_2^2 + \dots + \dots + N_{12}^2 d_{12}^2 \\
 &\quad + 2 \{ N_1 d_1 \cdot N_2 d_2 + N_1 d_1 \cdot N_3 d_3 + \dots + N_1 d_1 \cdot N_{12} d_{12} \\
 &\quad \quad + N_2 d_2 \cdot N_3 d_3 + \dots + N_2 d_2 \cdot N_{12} d_{12} \\
 &\quad \quad + \dots + \\
 &\quad \quad \quad + N_{11} d_{11} \cdot N_{12} d_{12} \}
 \end{aligned}$$

$$\begin{aligned}
 & \text{(b)} \\
 \left(\frac{\partial w}{\partial x} \right)^2 &= \left\{ \sum_{k=1}^{12} \left(\frac{\partial N_k}{\partial x} \right)^2 d_k^2 \right\} + 2 \left\{ \sum_{k=1}^{11} \frac{\partial N_k}{\partial x} \cdot d_k \left(\sum_{l=k+1}^{12} \frac{\partial N_l}{\partial x} \cdot d_l \right) \right\} \quad (11-28) \\
 &= \left(\frac{\partial N_1}{\partial x} \right)^2 d_1^2 + \left(\frac{\partial N_2}{\partial x} \right)^2 d_2^2 + \dots + \dots + \left(\frac{\partial N_{12}}{\partial x} \right)^2 d_{12}^2 \\
 &\quad + 2 \left\{ \frac{\partial N_1}{\partial x} d_1 \cdot \frac{\partial N_2}{\partial x} d_2 + \frac{\partial N_1}{\partial x} d_1 \cdot \frac{\partial N_3}{\partial x} d_3 + \dots + \frac{\partial N_1}{\partial x} d_1 \cdot \frac{\partial N_{12}}{\partial x} d_{12} \right. \\
 &\quad \quad + \frac{\partial N_2}{\partial x} d_2 \cdot \frac{\partial N_3}{\partial x} d_3 + \dots + \frac{\partial N_2}{\partial x} d_2 \cdot \frac{\partial N_{12}}{\partial x} d_{12} \\
 &\quad \quad + \dots + \\
 &\quad \quad \quad \left. + \frac{\partial N_{11}}{\partial x} d_{11} \cdot \frac{\partial N_{12}}{\partial x} d_{12} \right\}
 \end{aligned}$$

(i) Differentiate U with respect to d_i ;

(ii) Set all d 's to zero, except d_j which is set to one.

Thus, only terms involving d_i in Eqn. (11-19) need be considered.

Setting $k=i$ in this equation yields:

$$w^2(d_i) = N_i^2 d_i^2 + 2 \{ N_i d_i \sum_{\substack{\ell=1 \\ \ell \neq i}}^{12} N_\ell d_\ell \} \quad (11-20)$$

Differentiating Eqn. (11-16) with respect to d_i :

$$\frac{\partial U}{\partial d_i} = \frac{1}{2} k \int_0^{2a} \int_0^{2b} \frac{\partial}{\partial d_i} (w^2) dx dy = K_{i,j} \quad (11-21)$$

and from Eqn.(11-20):

$$\frac{\partial}{\partial d_i} (w^2) = 2 N_i^2 d_i + 2 \{ N_i \sum_{\substack{\ell=1 \\ \ell \neq i}}^{12} N_\ell d_\ell \} \quad (11-22)$$

For the off-diagonal terms $K_{i,j}$ ($i \neq j$), all d 's are set to zero, except d_j which is set equal to one. Thus, Eqn. (11-22) gives:

$$\frac{\partial}{\partial d_i} (w^2) = 2 N_i \cdot N_j \cdot 1 \quad (11-23)$$

which is the only term to survive in the summation of Eqn. (11-22).

Therefore, from Equations (11-21) and (11-23):

$$K_{i,j} = \frac{1}{2}k \int_0^{2a} \int_0^{2b} 2 N_i \cdot N_j \, dx \, dy \quad (11-24)$$

Similarly, for the diagonal terms $K_{i,i}$:

$$\frac{\partial}{\partial d_i}(w^2) = 2 N_i^2 \cdot 1$$

which follows from the first term on the right-hand side of Eqn. (11-22). The resulting stiffness term is then:

$$K_{i,i} = \frac{1}{2}k \int_0^{2a} \int_0^{2b} 2N_i^2 \, dx \, dy \quad (11-25)$$

Equations (11-24) and (11-25) may be rewritten for the general case of both diagonal and off-diagonal terms, as:

$$K_{i,j} = k \int_0^{2a} \int_0^{2b} N_i \cdot N_j \, dx \, dy \quad (i=1,12; j=1,12) \quad (11-26)$$

from which the Winkler term stiffness matrix may be obtained.

11.2.5 The Shear Interaction x-Term

The total strain energy contribution of this term is again obtained from Eqn. (11-10):

$$U = \frac{1}{2}G \int_0^{2a} \int_0^{2b} \left(\frac{\partial w}{\partial x}\right)^2 \, dx \, dy \quad (11-27)$$

Differentiating Eqn. (11-17) with respect to x yields:

$$\begin{aligned}\frac{\partial w}{\partial x} &= \frac{\partial N_1}{\partial x} d_1 + \frac{\partial N_2}{\partial x} d_2 + \dots + \frac{\partial N_{12}}{\partial x} d_{12} \\ &= \sum_{k=1}^{12} \frac{\partial N_k}{\partial x} d_k\end{aligned}$$

from which:

$$\begin{aligned}\left(\frac{\partial w}{\partial x}\right)^2 &= \left\{ \sum_{k=1}^{12} \left(\frac{\partial N_k}{\partial x}\right)^2 d_k^2 \right\} \\ &+ 2 \left\{ \sum_{k=1}^{11} \frac{\partial N_k}{\partial x} d_k \left(\sum_{\ell=k+1}^{12} \frac{\partial N_\ell}{\partial x} d_\ell \right) \right\}\end{aligned}\quad (11-28)$$

Equation (11-28) is presented in an expanded form in Table 11.2(b).

From Equations (11-27) and (11-28):

$$\begin{aligned}U &= \frac{1}{2} G \int_0^{2a} \int_0^{2b} \left[\sum_{k=1}^{12} \left(\frac{\partial N_k}{\partial x}\right)^2 d_k^2 \right. \\ &\quad \left. + 2 \left\{ \sum_{k=1}^{11} \frac{\partial N_k}{\partial x} d_k \left(\sum_{\ell=k+1}^{12} \frac{\partial N_\ell}{\partial x} d_\ell \right) \right\} \right] dx dy\end{aligned}\quad (11-29)$$

Proceeding in the same way as for the Winkler term, stiffness element $K_{i,j}$ is obtained by applying Castigliano's theorem. As indicated earlier, only terms involving d_i need be considered. Substituting

$k=i$ in Eqn. (11-28), therefore, gives:

$$\left(\frac{\partial w}{\partial x}\right)^2(d_i) = \left(\frac{\partial N_i}{\partial x}\right)^2 \cdot d_i^2 + 2\left\{ \frac{\partial N_i}{\partial x} \cdot d_i \left(\sum_{\substack{\ell=1 \\ \ell \neq i}}^{12} \frac{\partial}{\partial x} N_\ell \cdot d_\ell \right) \right\} \quad (11-30)$$

Differentiating with respect to d_i :

$$\frac{\partial}{\partial d_i} \left(\frac{\partial w}{\partial x}\right)^2(d_i) = 2 \left(\frac{\partial N_i}{\partial x}\right)^2 d_i + 2\left\{ \frac{\partial N_i}{\partial x} \left(\sum_{\substack{\ell=1 \\ \ell \neq i}}^{12} \frac{\partial}{\partial x} N_\ell \cdot d_\ell \right) \right\} \quad (11-31)$$

The off-diagonal stiffness terms $K_{i,j}$ ($i \neq j$) are obtained from the summation in Eqn. (11-31), by setting all d 's to zero, except d_j (i.e. $\ell=j$), which is set to one:

$$K_{i,j} = \frac{1}{2} G \int_0^{2a} \int_0^{2b} 2 \frac{\partial N_i}{\partial x} \frac{\partial N_j}{\partial x} dx dy \quad (11-32)$$

Similarly, the diagonal terms are obtained from the first term on the right-hand side of Eqn. (11-31):

$$K_{i,i} = \frac{1}{2} G \int_0^{2a} \int_0^{2b} 2 \left(\frac{\partial N_i}{\partial x}\right)^2 dx dy \quad (11-33)$$

In either case, Equations (11-32) and (11-33) may be written in the following general form:

$$K_{i,j} = \frac{1}{2} G \int_0^{2a} \int_0^{2b} \frac{\partial N_i}{\partial x} \cdot \frac{\partial N_j}{\partial x} dx dy \quad (i=1,12; j=1,12) \quad (11-34)$$

Equation (11-34) may be used to obtain all terms on the element stiffness matrix due to the shear interaction x-term.

11.2.6 The Shear Interaction y-Term:

The derivation of the element stiffness matrix for this term proceeds along lines identical to those described in paragraph 11.2.5, above. By analogy to Eqn. (11-34) this stiffness matrix may be obtained from the following general expression:

$$K_{i,j} = G \int_0^{2a} \int_0^{2b} \frac{\partial N_i}{\partial y} \cdot \frac{\partial N_j}{\partial y} dx dy \quad (i=1,12; j=1,12) \quad (11-35)$$

11.3 NUMERICAL EVALUATION OF THE SUBGRADE STIFFNESS MATRIX

It was shown above that the subgrade stiffness matrix for the Vlasov foundation consists of three terms:

$$[K_{sub}] = [K_{Winkler}] + [K_{x-Term}] + [K_{y-Term}] \quad (11-36)$$

The general form of the equations that can be used for the evaluation of any element in these matrices is given by Equations (11-26), (11-34) and (11-35). In all three of these expressions subscripts i and j range from 1 to 12.

A small computer program, called 'STIFNES', was written to perform the operations necessary for the evaluation of the three stiffness

matrices. Note that Equations (11-26), (11-34) and (11-35) may be rewritten as:

$$K_{i,j} = \int_0^{2a} \int_0^{2b} FN_1 \cdot FN_2 \, dx \, dy \quad (11-37)$$

where FN_1 and FN_2 are two shape functions, or their derivatives. For the present formulation, FN_1 is the sum of (NTERMS1) terms, and FN_2 is the sum of (NTERMS2) terms. For example, referring to Table 11.1, if FN_1 is shape function N_{10} , NTERMS1=2. Also note that each term in any function may be written in general as:

$$C \frac{x^N y^M}{a^I b^J}$$

where the 5 constants (C,N,M,I,J) are describe each term uniquely.

In 'STIFNES', the terms constituting FN_1 are read in and stored in array $FN_1(NTERMS1,5)$. Similarly, those for FN_2 are stored in array $FN_2(NTERMS2,5)$. The necessary operations may then be performed using these arrays as follows:

(i) Multiplication: To obtain the product ($FN_1 \cdot FN_2$), each term of FN_1 is multiplied by each term of FN_2 . The product, therefore, consists of NTERMS (=NTERMS1*NTERMS2) terms. Each of the terms in the product, is uniquely described by a set of 5 constants (C,N,M,I,J), as above. These terms are stored in array $PRD(NTERMS,5)$. Note that the terms in the product are related to those in FN_1 and FN_2 as follows:

- (a) Each constant C-term is the product of the 2 corresponding C-terms in FN1 and FN2;
- (b) Each of the other 4 constant terms, is the sum of the two corresponding constants in FN1 and FN2.

(ii) Integration: Each of the terms in the product array PRD(NTERMS,5) must then be integrated as per Eqn. (11-37). The integral of each is stored in the same location in PRD. The integration of each term involves the following computer operations:

$$C = \frac{C}{(N+1)(M+1)}$$

$$N = N+1 - I$$

$$M = M+1 - J$$

I,J remain unchanged.

To obtain the required stiffness matrix element $K_{i,j}$, the C-integral terms in PRD are summed as follows:

$$SUM = SUM + PRD(K, 1) \quad (K = 1, NTERMS).$$

The "area multipliers" (i.e. the terms involving the plate element dimensions 2a and 2b) are the same for all terms for a given K, and are obtained from PRD(2,1) and PRD(3,1).

11.4 RESULTING STIFFNESS MATRICES

The resulting subgrade stiffness matrices are presented in Table 11.3. The following observations may be made regarding these results:

- (i) The stiffness matrix derived here for the Winkler term is identical to that derived by Tabatabaie [79; 55] who used the principle of virtual work, instead of the concept of strain energy employed here;
- (ii) The problem of a plate on a Vlasov foundation is analogous to that of a freely vibrating plate with a harmonic frequency of one and plate mass density of k , while the plate is subjected to a pair of orthogonal in-plane compressive stresses equal to G with no in-plane shear [172]. With this analogy in mind, the sum of the shear interaction stiffness matrices of the foundation beneath the plate is similar to the "initial stress" matrix for the buckling and large deflection analysis of a plate, in which the two orthogonal in-plane stresses equal G , and in-plane shears stress vanishes. Similarly, the Winkler term stiffness matrix is identical to the "consistent mass" matrix of a freely vibrating plate element where the mass density is replaced by the subgrade modulus k and the natural frequency is set to unity;
- (iii) Stiffness matrices similar to those derived here have been presented by Severn [173], but these contain several numerical

and typographical errors. The matrices developed in this study are much more accurate and free of such errors. A matrix similar to the shear interaction stiffness matrix is implicitly given by Yang [174]. The corresponding beam stiffness matrices have been presented by Zhaohua and Cook [175].

11.5 IMPLEMENTATION OF VLASOV MODEL INTO ILLI-SLAB

The two additional stiffness matrices derived above can easily be incorporated into ILLI-SLAB. The coefficients in these matrices are simply added to the Winkler and the plate element stiffness matrices. Determination of subgrade stresses, however, requires some additional attention.

According to the assumed relation between deflection, w , and subgrade stress, q :

$$q = kw - G \left(\frac{\partial^2 w}{\partial x^2} + \frac{\partial^2 w}{\partial y^2} \right) \quad (11-6)$$

But,

$$w = [N] \{d\} \quad (11-2)$$

where:

$[N]_{1 \times 12}$:row vector of shape functions for the plate bending element;

$\{d\}_{12 \times 1}$:generalized nodal displacements.

It follows, therefore, that:

$$\frac{\partial^2 w}{\partial x^2} = \left[\frac{\partial^2 N}{\partial x^2} \right] \{d\}$$

$$\text{and } \frac{\partial^2 w}{\partial y^2} = \left[\frac{\partial^2 N}{\partial y^2} \right] \{d\}$$

whence:

$$q = kw - G \left[\frac{\partial^2 N}{\partial x^2} + \frac{\partial^2 N}{\partial y^2} \right] \{d\}$$

The second derivatives of the shape functions can be easily derived from Table 11.1 by differentiation. In ILLI-SLAB, these are evaluated for each element and the subgrade stress at each of the 4 nodes is calculated. In general, elements that share a node can be expected to predict different individual subgrade stresses at that node. Thus, an average nodal subgrade stress is determined.

A brief review of the literature pertaining to the determination of the parameters k and G in the Vlasov model is given below.

11.6 FACTORS INFLUENCING THE VLASOV MODEL PARAMETERS

The two parameters in the Vlasov model are the modulus of subgrade reaction, k (psi/in.) and the foundation shear parameter, G (lb/in.).

The modulus of subgrade reaction is the spring constant as used in the Winkler model, and may be correlated with test results from the CBR or the plate load tests. The shear parameter accounts for the interaction between adjacent spring elements, but is generally not equivalent to the shear modulus defined by the theory of elasticity. This theory, however, may provide a good initial estimate of the parameters in the Vlasov model.

Reissner [22] suggested that k and G are functions of the deflection profile and the effective depth of the foundation, and proposed the following equations for their determination:

$$k = E_s/H \qquad G = H G_s/3 \qquad (11-38)$$

where:

$$G_s = \frac{E_s}{2(1+\mu_s)}$$

: elastic shear modulus for subgrade;

H : effective depth of the foundation.

Jones and Xenophontos [176] established a rigorous theoretical basis for the vertical deformation profile $\psi(z)$, assumed in Eqn. 2.6. They also deduced that several other important factors influence the value of the attenuation parameter γ , namely the applied load, and the shape and flexural rigidity of the plate.

Harr, et al. [177] also suggested that the radius of relative stiffness of the plate-foundation system affects the parameters k and

G. These authors recommended introducing the radius of relative stiffness, ℓ_e , of the corresponding elastic solid foundation into the assumed displacement shape as follows:

$$\psi(z) = \frac{\sinh \bar{\gamma} \frac{H-z}{\ell_e}}{\sinh \bar{\gamma} \frac{H}{\ell_e}} \quad (11-39)$$

where $\bar{\gamma}$ is a dimensionless attenuation parameter.

The dimensionless parameters K and ξ introduced by Mahany [68] contain the factors that author considered most important:

$$\begin{aligned} K &= \frac{k b^4}{D} \\ &= 6\gamma \frac{(1-\mu^2)}{(1-\mu_o^2)} \frac{E_o}{E} \frac{b^4}{h^3} \quad (\text{if } H=\infty) \\ \xi &= \frac{G}{2k b^2} \\ &= \frac{(1-\mu_o)}{4\gamma^2 b^2} \quad (\text{if } H=\infty) \end{aligned} \quad (11-40)$$

where b is the half-length of the short side of the plate.

The plate aspect ratio is also identified as significant. These equations permit, to some extent, the determination of the attenuation parameter, γ , given the other constants.

A method for the experimental determination of k and G is also described by Mahanyi [68]. Following a suggestion by Pasternak [19], a rigid circular plate, radius R , is loaded by a point load P at its center, and the deflection, w , is measured. A second measurement of the rotation, ϕ , is also made with the load applied with an eccentricity, e , smaller than $R/4$. This restriction prevents any tension from arising within the contact area. These values of ϕ and w are then substituted into the following equation, to determine the corresponding value of a function $f(\alpha R)$:

$$f(\alpha R) = \frac{w}{\phi} \frac{1}{R^2} \frac{4M}{P} \left(1 - \frac{\phi \pi R^2}{M}\right) \quad (11-41)$$

where:

$$M = P \cdot e$$

Entering Fig. 11.1 with the value of $f(\alpha R)$ thus obtained, one determines parameters ϵ , αR , and α by implication. The following equations may then be used to determine k and G :

$$k = \frac{P}{\pi R^2 w \epsilon}$$

$$G = \frac{k}{\alpha^2} \quad (11-42)$$

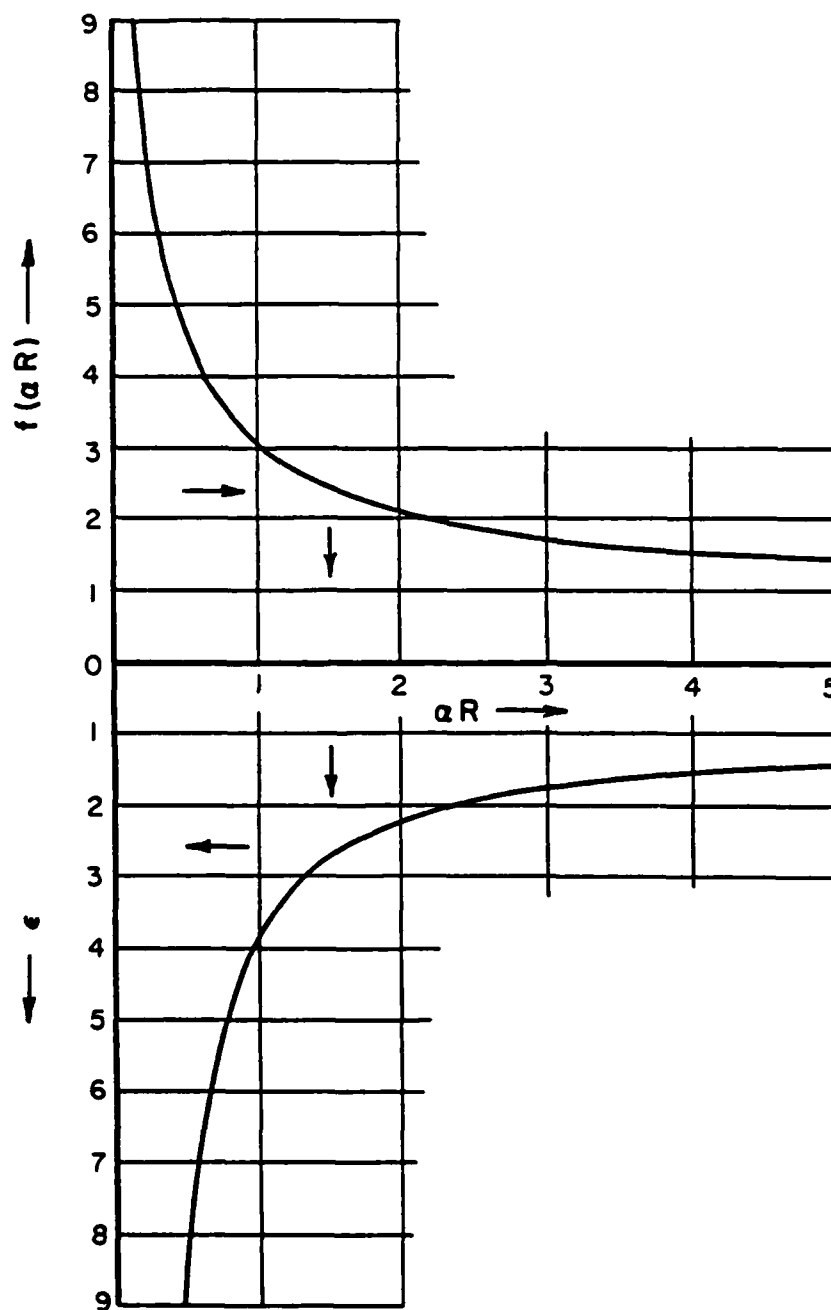


Fig. 11.1 Relationship Between $f(\alpha R)$, ϵ and αR
(After Mahanyi [68])

11.7 MODEL BEHAVIOR

11.7.1 Parameter Selection

To investigate the major aspects of the behavior of the Vlasov finite element model in ILLI-SLAB, a number of computer runs were performed [178]. The results of these analyses will be presented and discussed in the remainder of this Chapter. Only the interior loading condition will be examined. The effect of the concentrated edge reactions was ignored in these runs. This is considered to have only a minor effect on the qualitative conclusions reached below, since in most cases analyzed edge reactions should be fairly small.

On the basis of several numerical analyses, Mahanyi [68] concluded that:

- (a) As K increases plate deflection and bending stress decreases;
- (b) As ξ increases deflection at the interior decreases, while deflection at the edge increases;
- (c) The effect of plate Poisson's ratio and aspect ratio depends on K and ξ , and is not negligible.
- (d) The effect of the additional soil parameter G is "to cause a distribution of the load on the subsoil, bringing the problem closer to the actual behavior of soil."

In the present study, a square slab with square elements was used to avoid any problems related to plate or element aspect ratios. The slab was loaded by a single, interior, square load. The interior loading condition was selected because it is considered to be the

simplest. Results corresponding to this condition are generally indicative -at least in a qualitative way- of the response of the system under other conditions too. The main consideration for the selection of slab thickness was one pertaining to adequate mesh fineness. Previous analyses using the Winkler and Boussinesq models have shown that the mesh fineness ratio ($2a/h$) should be close to 0.8 for best results. Other pertinent parameters were selected to give a slab length ratio (L/ℓ) within practical limits. In these analyses, predominant emphasis was placed on the deflection and bending stress responses of the system.

11.7.2 Mesh Fineness Effect

To validate the model and provide guidelines for its effective use, convergence upon mesh refinement was first investigated. Table 11.4 shows the results from a series of runs in which the slab was divided into a number of elements, ranging from 16 to 400. The runs for the finer meshes were performed on a HARRIS 800-2 virtual-memory computer.

It is observed that deflections are much less sensitive to mesh fineness than bending stresses. Furthermore, convergence is from above for deflections, and from below for bending stresses. Figure 11.2 shows the bending stress results in a graphical form. A mesh fineness ratio ($2a/h$) of 0.8 would produce a bending stress about 95% of the "exact" solution.

TABLE 11.4
EFFECT OF MESH FINENESS

No of Elts	2a (in.)	$\frac{2a}{h}$	δ (mils)	%	σ (psi)	%	Memory Words
4X 4	45.0	3.00	2.326	(100)	20.096	(63)	3699
6X 6	30.0	2.00	2.325	(100)	23.767	(75)	8875
8X 8	22.5	1.50	2.322	(100)	26.149	(82)	17491
10X10	18.0	1.20	2.320	(100)	27.853	(88)	30411
12X12	15.0	1.00	2.319	(100)	29.126	(92)	48499
14X14	12.9	.86	2.318	(100)	30.096	(95)	72619
16X16	11.3	.75	2.317	(100)	30.838	(97)	103635
18X18	10.0	.67	2.316	(100)	31.405	(99)	142411
20X20	9.0	.60	2.316	(100)	31.831	(100)	189811

Notes:

Slab : 180 X 180 in.
 E = 3,000,000 psi
 μ = 0.15
 k = 72 psi/in.
 G = 36,000 lb/in.
 h = 15 in.
 A = 6 X 6 in. @ 100 psi; interior

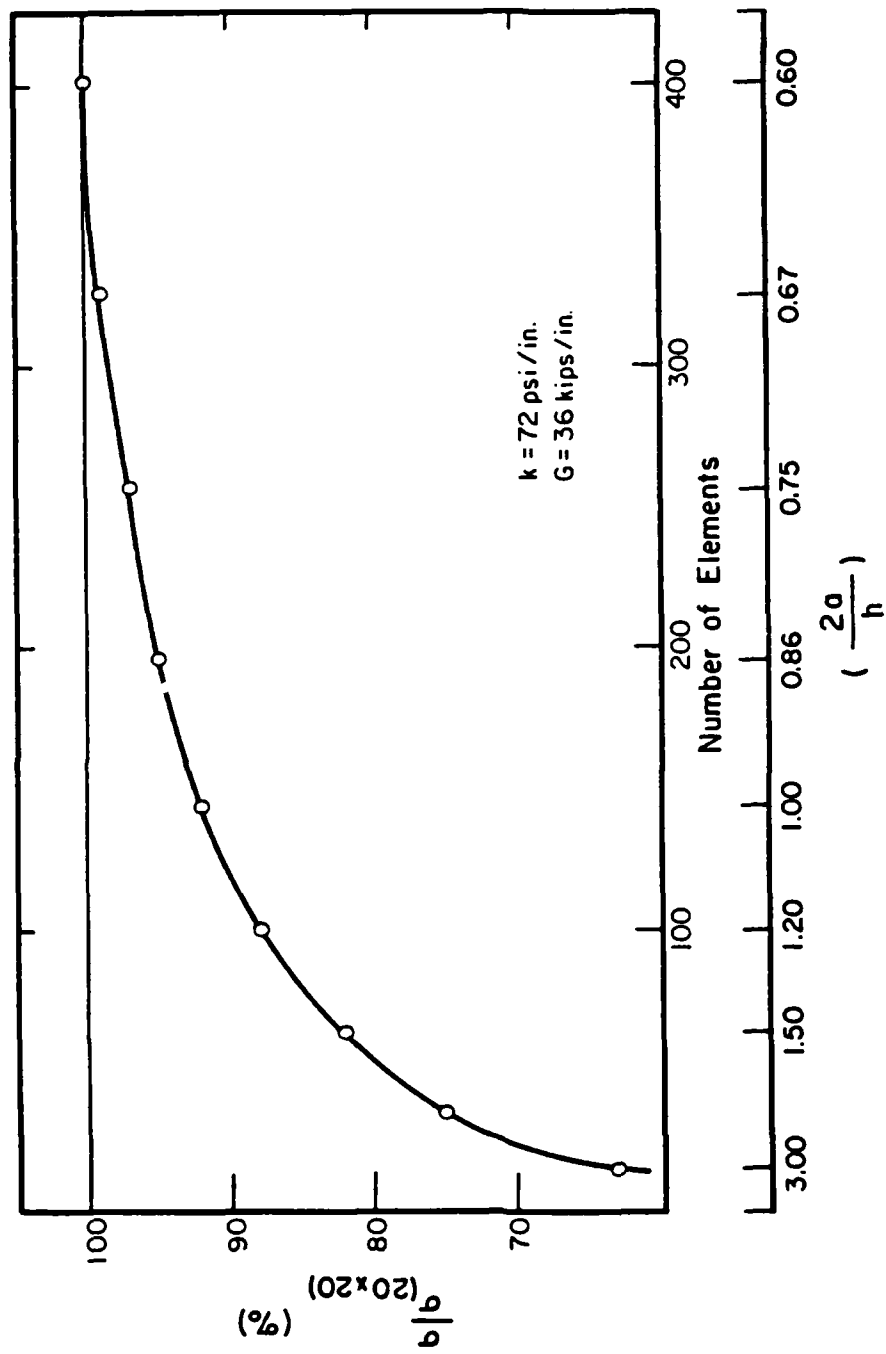


Fig. 11.2 Effect of Mesh Fineness on Maximum Bending Stress

11.7.3 Effect of k for Constant G

The aim of the analyses performed here is to examine the relative effect of the two parameters in the Vlasov model, and to evaluate the conclusions reached by Mahanyi [68]. For one particular slab under interior loading, a series of runs were performed in which the value of the modulus of subgrade reaction was varied between fairly wide limits. The runs were otherwise identical to each other.

Typical results are presented in Table 11.5. These confirm, as expected, Mahanyi's observation that as k increases, maximum plate deflection and bending stress decrease (Fig. 11.3). It is also observed that as k increases, the deflection and bending stress at the plate edge both decrease (Fig. 11.4). For low values of k , the deflection profile is fairly flat, indicating the predominance of G , whose effect -as indicated by Mahanyi- is to transfer some of the response from the interior to the edges. On the other hand, increasing the value of k tends to concentrate the bulk of the deflection under the interior load; the edges deflect progressively less, and eventually lift up and lose contact with the soil. A similar trend is observed for bending stresses, but the effects are considerably less pronounced.

The following comments relate to the subgrade stress data in Table 11.5c. As k increases, maximum subgrade stress increases, while subgrade stress at the plate edge decreases. The subgrade stress profile is fairly flat at low values of k , but stresses at the interior become progressively more important as k increases. This is a consequence of the gradual lift-up of the plate edges mentioned above.

TABLE 11.5
EFFECT OF SUBGRADE MODULUS, k
(a) ON DEFLECTIONS (mils)

k	Node Number					
pci	61	62	63	64	65	66
0	1111,211	1111,211	1111,210	1111,210	1111,210	1111,211
10	11.959	11.832	11.599	11.341	11.088	10.851
20	6.391	6.265	6.035	5.781	5.532	5.299
50	3.023	2.899	2.677	2.433	2.197	1.977
72	2.320	2.199	1.981	1.745	1.517	1.305
100	1.861	1.741	1.530	1.302	1.084	.881
125	1.616	1.499	1.292	1.071	.860	.666
150	1.447	1.331	1.129	.914	.711	.524
200	1.225	1.112	.917	.715	.525	.351
300	.979	.871	.689	.506	.337	.185
500	.744	.643	.481	.324	.187	.065
1000	.513	.422	.288	.170	.075	-.005

Notes:

Slab : 180 X 180 in.
 Mesh : 10 X 10 @ 18 in.
 E = 3,000,000 psi
 μ = 0.15
 G = 36,000 lb/in.
 h = 15 in.
 A = 6 X 6 in. @ 100 psi; interior

Node Numbering

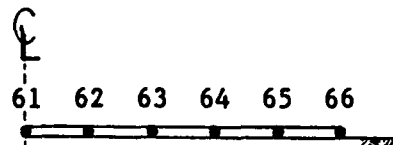


TABLE 11.5 (continued)

(b) ON BENDING STRESSES, σ_x (psi)

k pci	Node Number					
	61	62	63	64	65	66
0	28.941	15.696	9.705	7.023	5.628	4.972
10	28.772	15.531	9.550	6.879	5.494	4.840
20	28.610	15.373	9.401	6.741	5.364	4.713
50	28.157	14.931	8.895	6.357	5.005	4.362
72	27.853	14.634	8.707	6.101	4.767	4.129
100	27.496	14.287	8.382	5.802	4.489	3.859
125	27.203	14.001	8.115	5.557	4.262	3.638
150	26.930	13.735	7.868	5.331	4.053	3.436
200	26.437	13.257	7.425	4.928	3.682	3.077
300	25.621	12.468	6.698	4.274	3.084	2.503
500	24.430	11.323	5.662	3.358	2.264	1.725
1000	22.681	9.667	4.218	2.142	1.223	.774

TABLE 11.5 (continued)

(c) ON SUBGRADE STRESSES, (psi)

k pci	Node Number					
	61	62	63	64	65	66
0	.190	.142	.128	.121	.118	.118
10	.198	.149	.133	.123	.118	.115
72	.243	.186	.158	.134	.115	.100
500	.438	.341	.248	.165	.095	.035

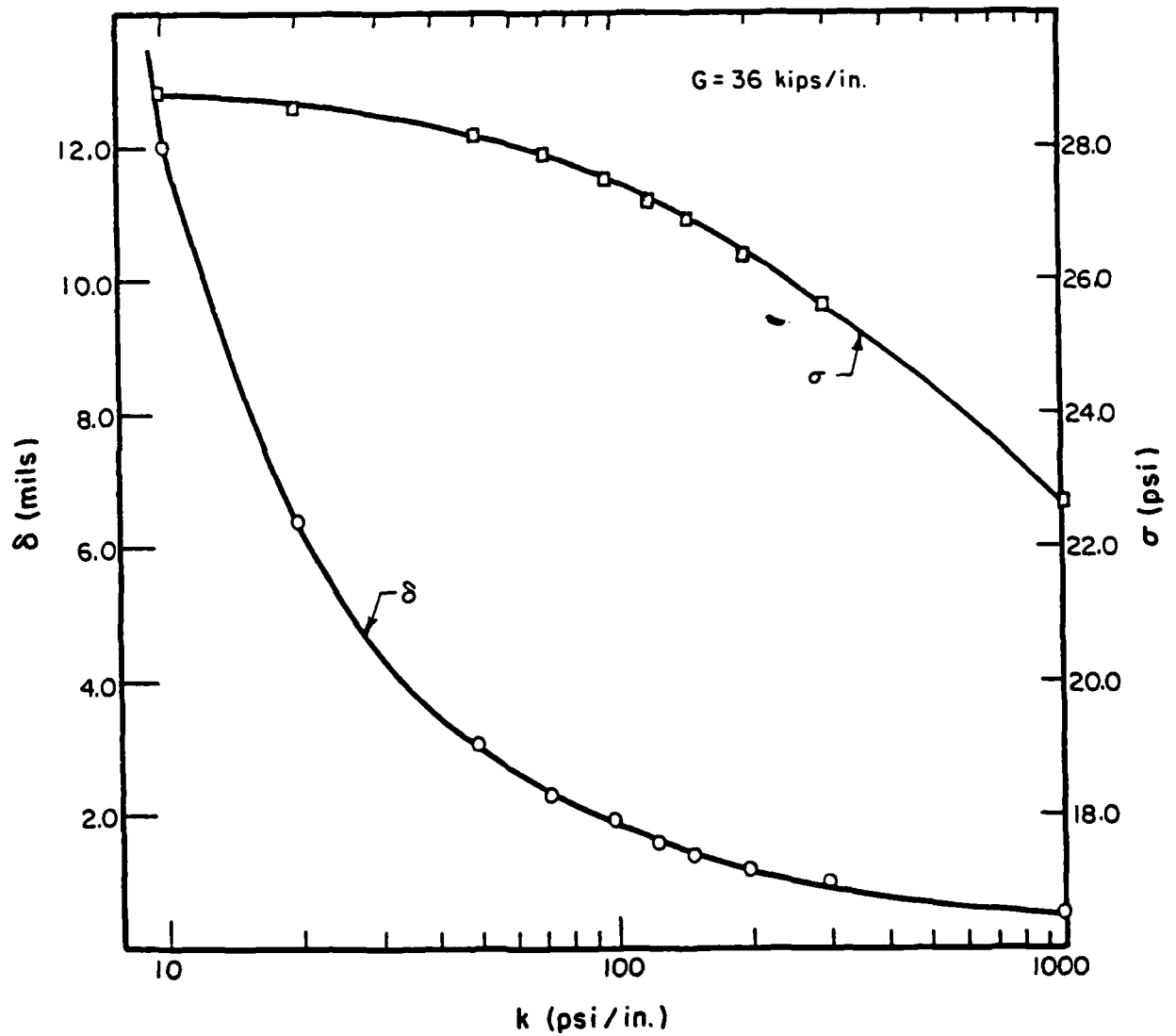


Fig. 11.3 Effect of Subgrade Modulus on Maximum Deflection and Bending Stress

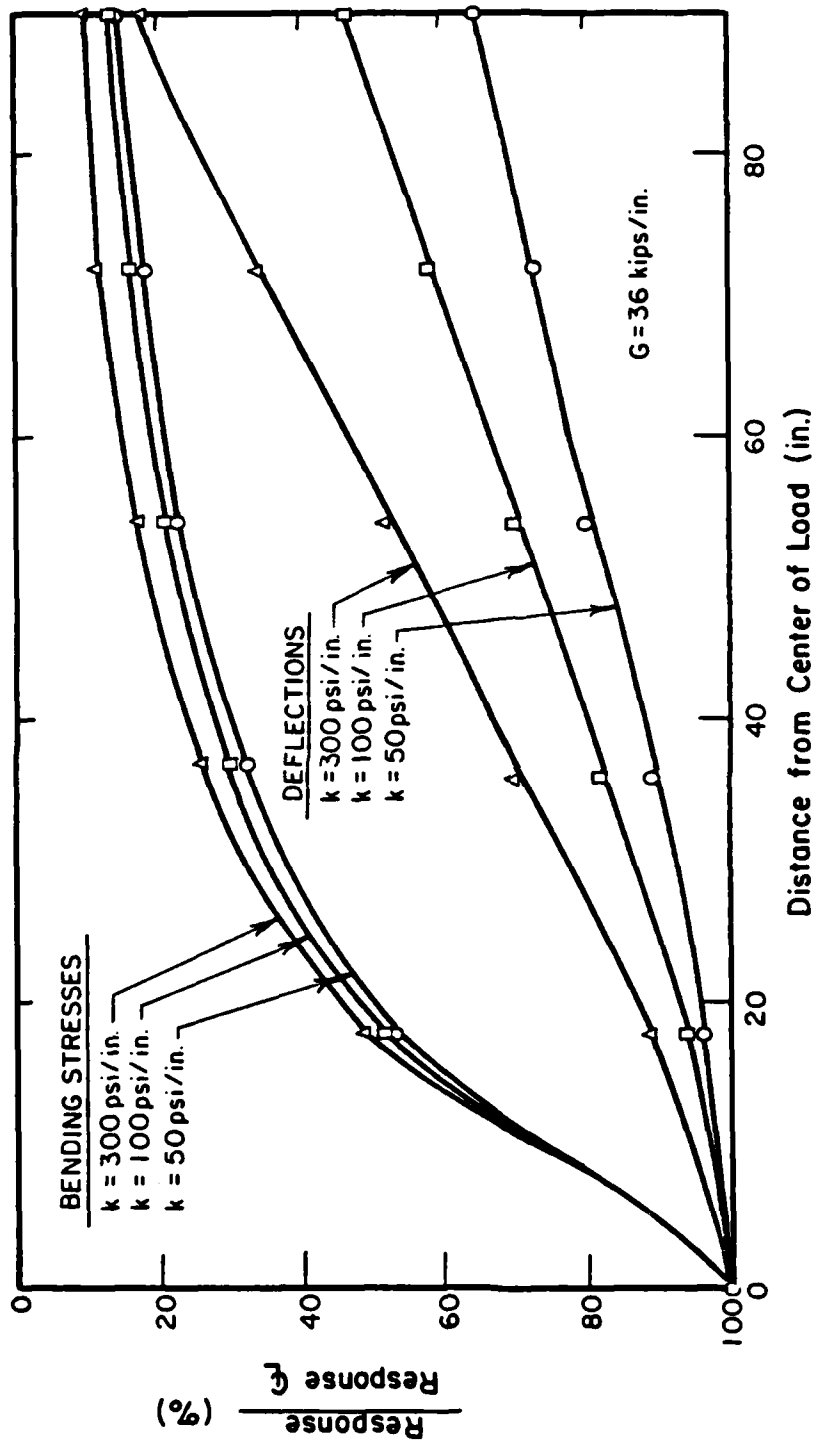


Fig. 11.4 Effect of Subgrade Modulus on Deflection and Bending Stress Profiles

11.7.4 Effect of G for Constant k

In the analyses in this section, the value of the shear parameter, G , is varied, while all other aspects of the runs are kept unaltered. The results from a typical series of such runs are shown in Table 11.6.

Mahanyi [68] had noted that as G increases maximum deflection decreases, and this is confirmed by the results in Table 11.6. Maximum bending stress is also seen to decrease as G increases. On the other hand, the edge deflection (interior loading) increases as G increases, while edge stress decreases. The effect of G on the deflection profile is to flatten it out (Fig. 11.5), confirming both Mahanyi's observation and comments made in the previous section. The effect of increasing G on bending stresses is to increase the relative significance of stresses at the interior, although this effect is very small in magnitude.

An increase in G leads to higher subgrade stresses both at the interior and at the edges of the slab. The increase at the edge, however, is considerably smaller, leading to increased relative significance of interior stresses. This is quite unexpected, and is the opposite of the flattening effect on the deflection profile.

In general, it may be concluded that k and G affect both the shape and the magnitude of the deflection profile. A flatter deflection profile may be obtained by decreasing k or increasing G . A reduction in maximum deflection is achieved by increasing either parameter. These effects are much more pronounced in response to changes in k . To obtain the same changes produced by doubling k , G must be increased by

TABLE 11.6
EFFECT OF SHEAR PARAMETER, G
(a) ON DEFLECTIONS (mils)

G k/in.	Node Number					
	61	62	63	64	65	66
0	2.379	2.253	2.023	1.768	1.519	1.283
1	2.377	2.251	2.021	1.767	1.518	1.284
10	2.361	2.237	2.010	1.761	1.518	1.290
18	2.348	2.224	2.001	1.756	1.518	1.295
25	2.337	2.214	1.993	1.752	1.517	1.299
32	2.326	2.204	1.985	1.747	1.517	1.303
36	2.320	2.199	1.981	1.745	1.517	1.305
40	2.314	2.193	1.977	1.743	1.517	1.307
50	2.300	2.180	1.967	1.737	1.516	1.312
100	2.239	2.124	1.924	1.713	1.515	1.335
300	2.084	1.982	1.817	1.655	1.514	1.393
500	1.997	1.903	1.759	1.625	1.515	1.425
1000	1.882	1.801	1.686	1.590	1.518	1.466

Notes:

See Table 11.5 for system characteristics.

k = 72 psi/in.

TABLE 11.6 (continued)

(b) ON BENDING STRESSES, σ_x (psi)

G k/in.	Node Number					
	61	62	63	64	65	66
0	28.616	15.354	9.360	6.692	5.307	4.628
1	28.593	15.332	9.340	6.674	5.290	4.613
10	28.391	15.141	9.166	6.516	5.145	4.479
18	28.219	14.979	9.018	6.382	5.022	4.365
25	28.073	14.841	8.894	6.269	4.920	4.271
32	27.932	14.708	8.774	6.161	4.821	4.180
36	27.853	14.634	8.707	6.101	4.767	4.129
40	27.776	14.562	8.642	6.042	4.713	4.080
50	27.589	14.386	8.484	5.899	4.584	3.962
100	26.755	13.608	7.792	5.284	4.029	3.454
300	24.475	11.535	6.022	3.762	2.693	2.257
500	23.016	10.265	5.010	2.944	2.008	1.662
1000	20.701	8.365	3.634	1.927	1.212	.998

TABLE 11.6 (continued)

(c) ON SUBGRADE STRESSES, (psi)

G k/in.	Node Number					
	61	62	63	64	65	66
0	.171	.162	.146	.127	.109	.092
36	.243	.186	.158	.134	.115	.100
300	.705	.310	.203	.150	.127	.125
500	1.101	.371	.217	.147	.123	.133

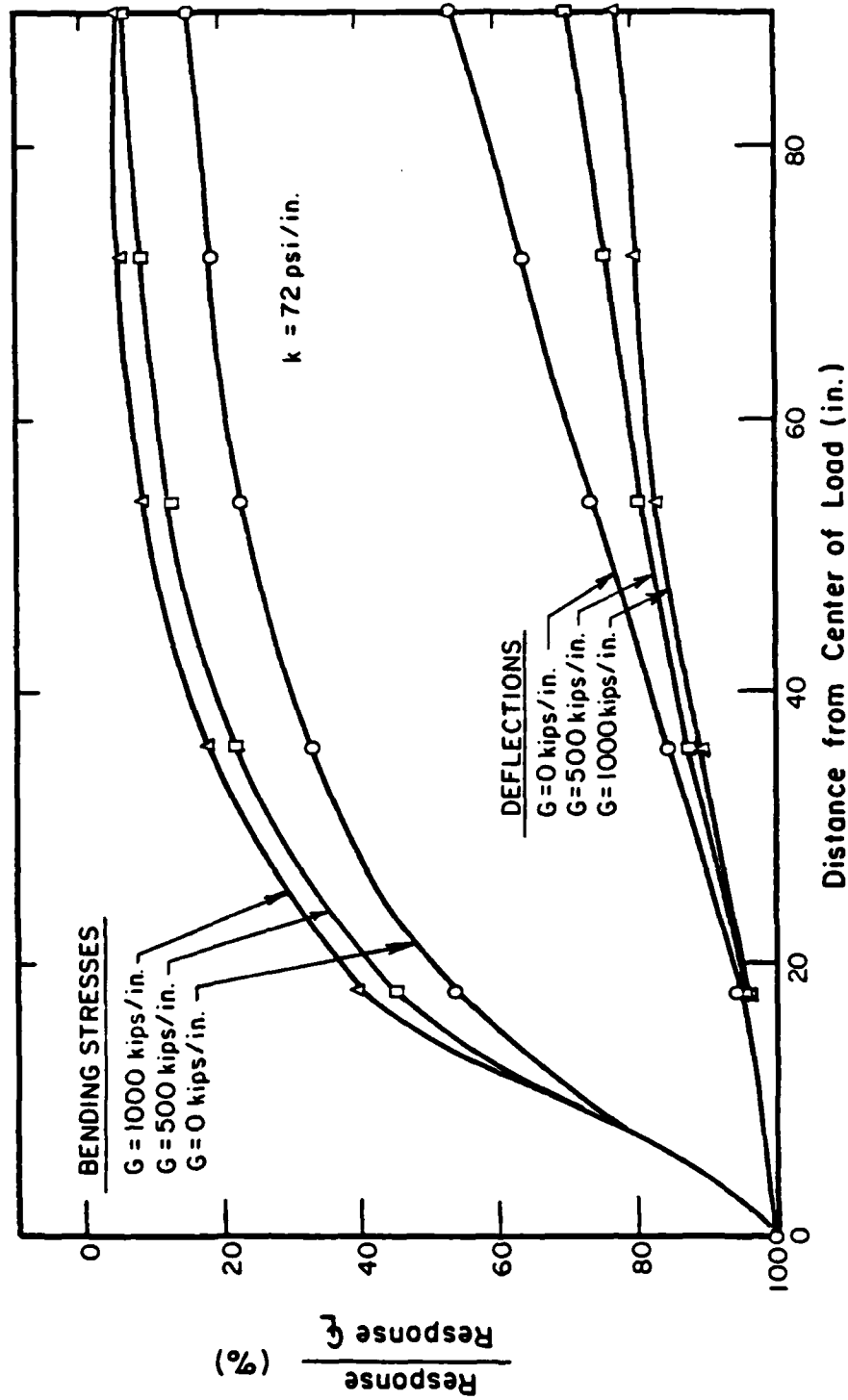


Fig. 11.5 Effect of Shear Parameter on Deflection and Bending Stress Profiles

2 to 3 orders of magnitude. When the two parameters are considered individually, however, a given change in k produces predominantly a magnitude effect; for a given change in G , the shape effect is slightly more important than the magnitude effect.

11.8 COMPARISON OF VLASOV AND ELASTIC SOLID MODELS

It was noted earlier that despite its desirability and a more realistic representation of actual subgrade behavior, the elastic solid model is limited by enormous computer storage requirements. The aim of the analyses presented below is to answer the following questions:

- (i) Can the Vlasov model be used to reproduce the response of the elastic solid subgrade for a given slab and loading configuration?
- (ii) Is there a general relationship between the elastic solid parameters (E_s , μ_s) and the Vlasov parameters (k , G)?
- (iii) Are the Vlasov parameters intrinsic properties of the soil, or do they also depend on characteristics of the slab, such as thickness, length, etc.?

Using a first estimate based on Eqn. (11-38) proposed by Reisner [22] relating the four constants, and a trial-and-error process, the Vlasov and Elastic Solid deflection profiles can be matched. The two cases considered here adequately illustrate the fact that such an exercise is feasible. The resulting profiles are presented in Table 11.7. It is observed that once deflection profiles are matched,

TABLE 11.7

COMPARISON WITH ELASTIC SOLID (I)

(a) CASE A

h= 15 in.; L= 180 in.; 2a= 18 in.

Node	Deflection (mils)		Subgrade Stress (psi)		σ_x (psi)		σ_y (psi)	
	VLASOV	EL.SOLID	VLASOV	EL.SOLID	VLASOV	EL.SOLID	VLASOV	EL.SOLID
61	2.320	2.320	.243	.273	27.853	27.760	27.853	27.760
62	2.199	2.199	.186	.218	14.634	14.572	5.994	6.014
63	1.981	1.981	.158	.162	8.707	8.674	2.334	2.548
64	1.745	1.741	.134	.121	6.101	6.056	.155	.510
65	1.517	1.505	.114	.093	4.767	4.646	-.576	-.240
66	1.305	1.280	.100	.176	4.129	3.857	.000	.000

Node	(VLASOV/EL.SOLID) X 100%			
	Deflection	Subgrade Stress	σ_x	σ_y
61	100	89	100	100
62	100	85	100	100
63	100	98	100	92
64	100	111	101	30
65	101	123	103	240
66	102	57	107	100

Notes:

See Table 11.5 for system characteristics.

VLASOV: $k = 72 \text{ psi/in.}$
 $G = 36,000 \text{ lb/in.}$ EL.SOLID: $E_s = 10,000 \text{ psi}$
 $\nu_s = 0.45$

TABLE 11.7 (continued)

(b) CASE B

h= 15 in.; L= 180 in.; 2a= 18 in.

Node	Deflection (mils)		Subgrade Stress (psi)		σ_x (psi)		σ_y (psi)	
	VLASOV	EL.SOLID	VLASOV	EL.SOLID	VLASOV	EL.SOLID	VLASOV	EL.SOLID
61	1.063	1.067	.712	.531	24.019	24.042	24.019	24.042
62	.964	.968	.337	.376	11.082	11.060	2.798	2.794
63	.806	.809	.221	.234	5.600	5.519	.118	.237
64	.655	.655	.154	.146	3.384	3.253	-1.131	-.839
65	.525	.519	.118	.089	2.348	2.117	-1.110	-.774
66	.414	.396	.102	.059	1.913	1.495	.000	.000

(VLASOV/EL.SOLID) X 100%				
Node	Deflection	Subgrade Stress	σ_x	σ_y
61	100	134	100	100
62	100	90	100	100
63	100	94	101	50
64	100	105	104	135
65	101	133	111	143
66	105	173	128	100

Notes:

See Table 11.5 for system characteristics.

VLASOV: $k = 72 \text{ psi/in.}$
 $G = 275,000 \text{ lb/in.}$ EL.SOLID: $E_s = 30,000 \text{ psi}$
 $\mu_s = 0.45$

bending stress profiles follow closely. Subgrade stress profiles are harder to match. It is also noted that the match is much better at the interior than at the edges, for all three responses. Comparisons of response profiles for the three models (Winkler, Elastic Solid and Vlasov) are shown in Figures 11.6 through 11.9, for one of the two cases analyzed (Case A). These figures indicate that the Vlasov model is an improvement over the Winkler model, in reproducing the elastic half-space response. Computer memory requirements for the three models are compared in Table 11.8. The Vlasov option is substantially less demanding than the Elastic Solid.

To determine whether the relation between (E_s , μ_s) and (k , G) is influenced by the thickness of the slab, comparisons between the Elastic Solid and Vlasov models were repeated for a 7-in. slab, compared to the 15-in. slab used in the original "matching" procedure. Table 11.9 presents the corresponding profiles obtained. There is a general deterioration in the agreement between the two models, confirming the observation by Jones and Xenophontos [176] that the flexural rigidity of the plate (and, therefore, its thickness) affect the value of the Vlasov parameters. This realization substantially reduces the feasibility of reproducing elastic solid results by the Vlasov model on a routine basis.

The effect of a second factor, namely that of slab length, was also investigated. It is already suggested from the thickness effect discussed in the preceeding paragraph, that the relation between the four parameters will also be influenced to some extent by slab length.

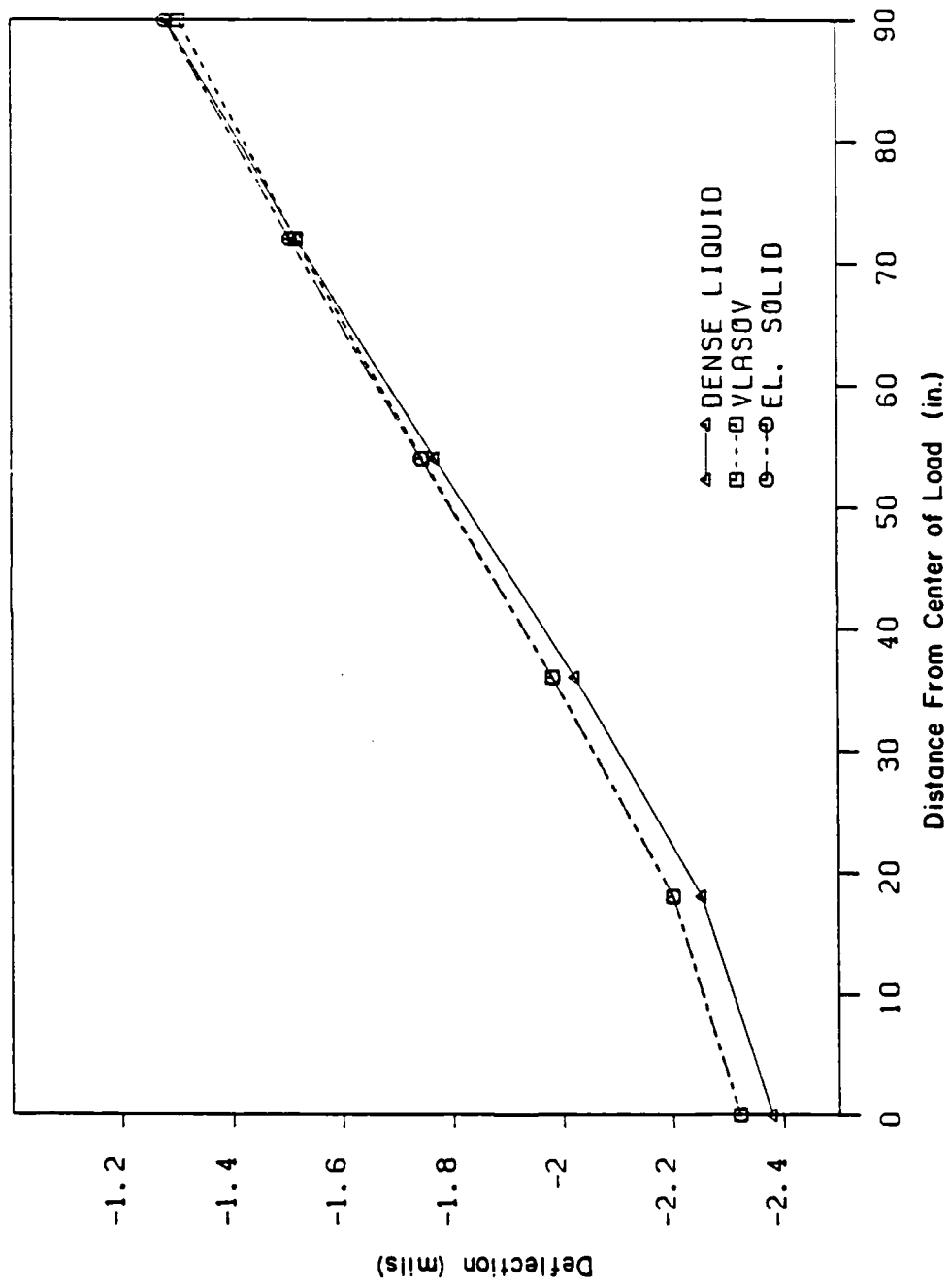


Fig. 11.6 Comparison of Deflection Profiles

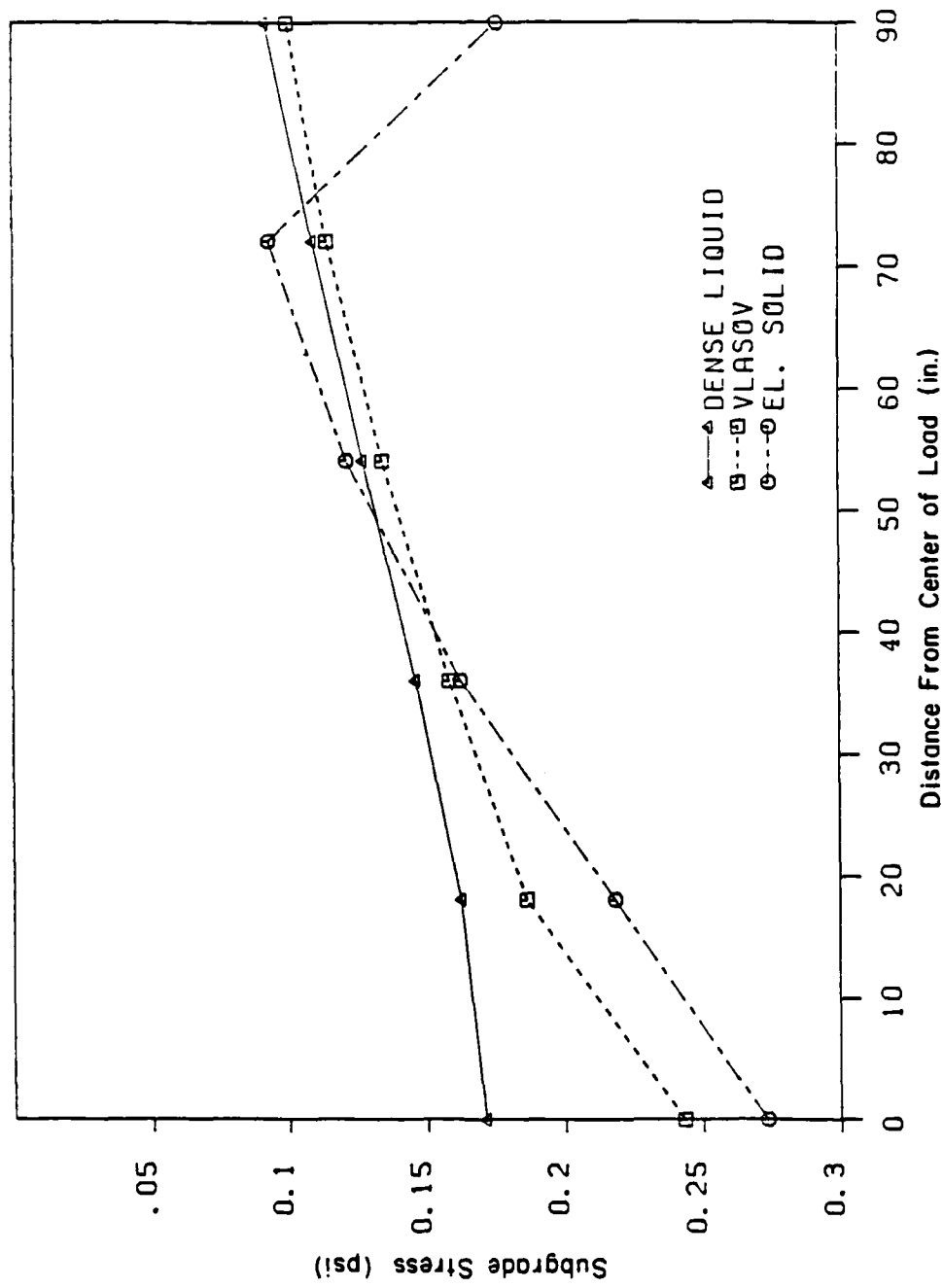


Fig. 11.7 Comparison of Subgrade Stress Profiles

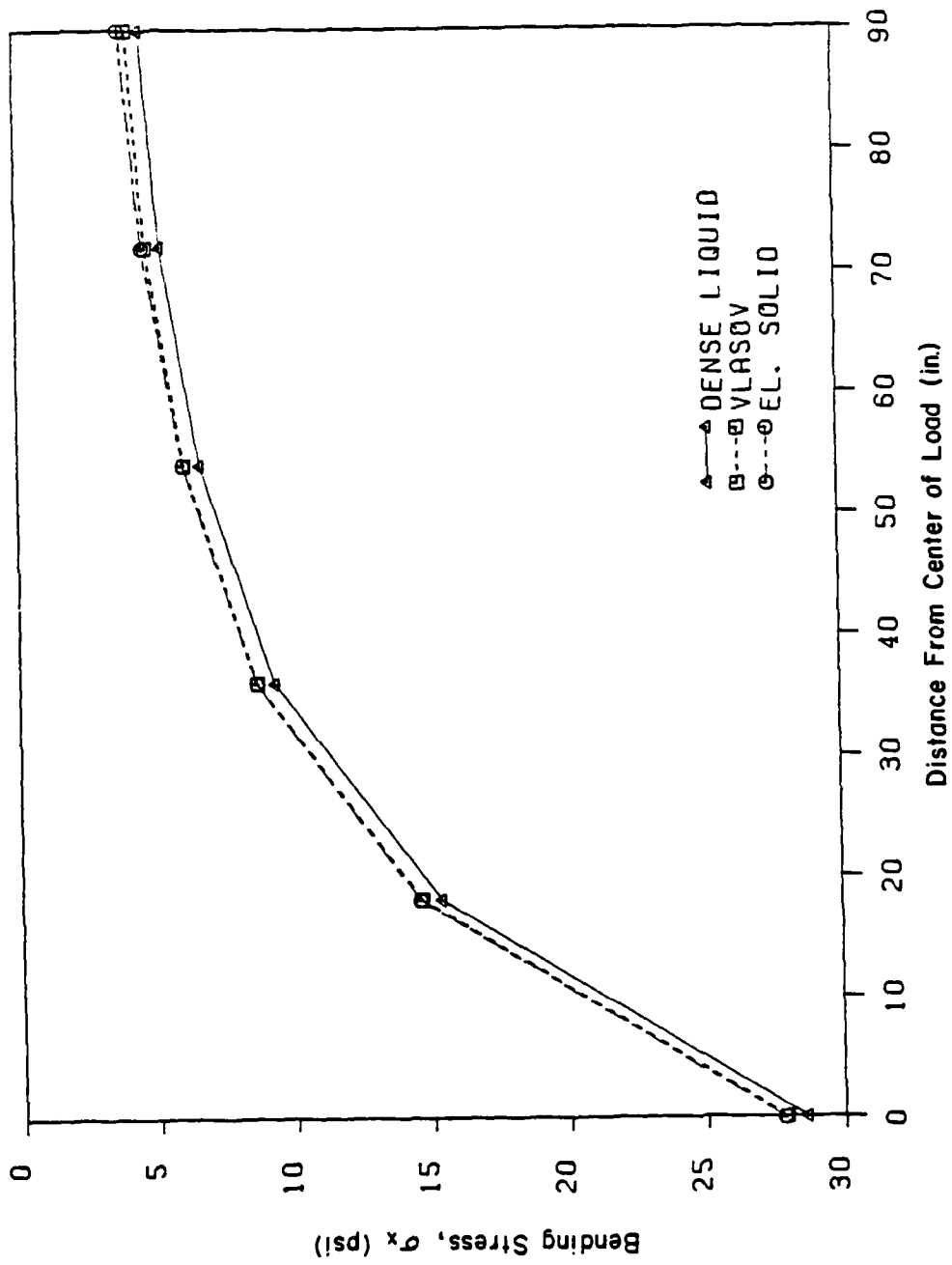


Fig. 11.8 Comparison of Bending Stress, σ_x , Profiles

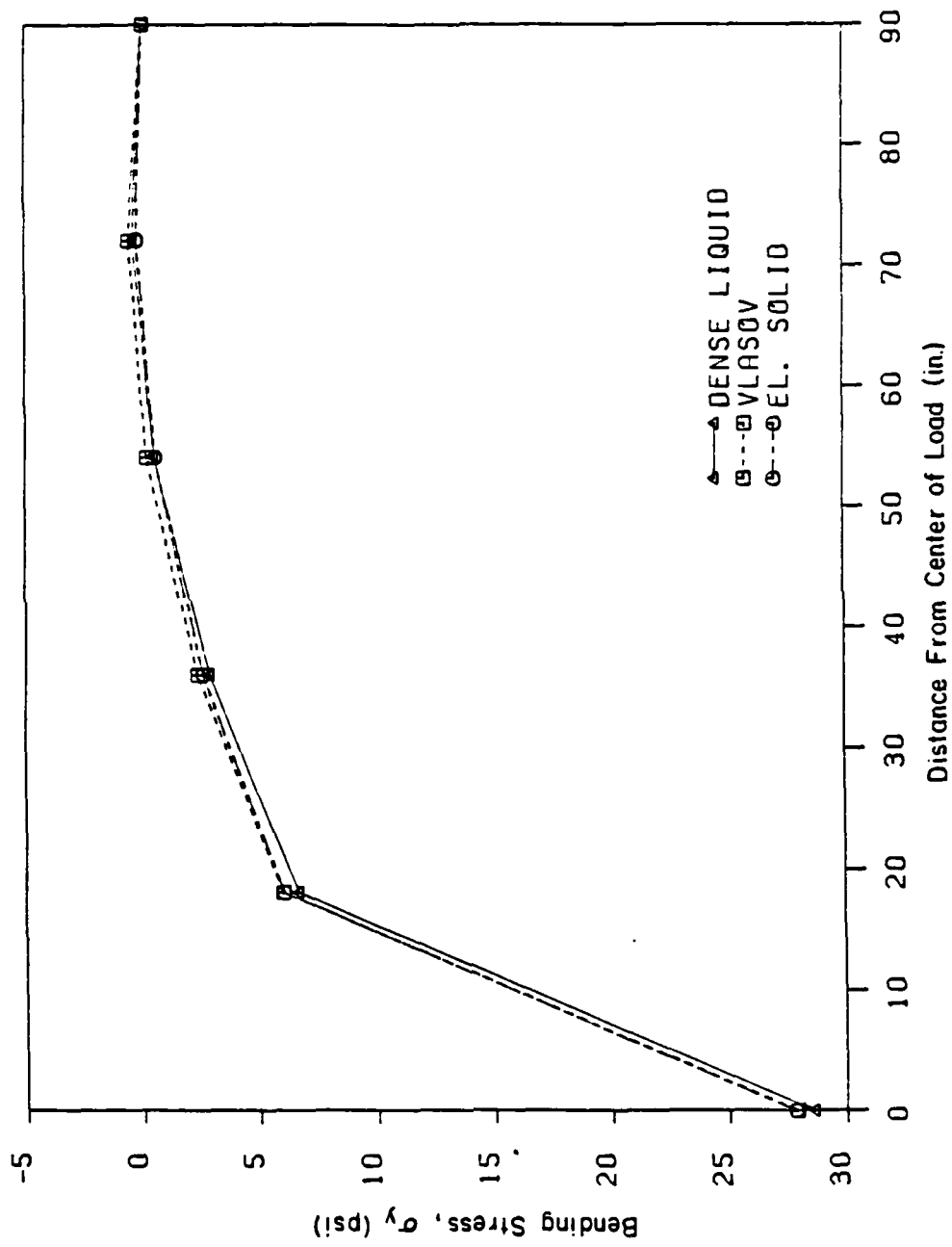


Fig. 11.9 Comparison of Bending Stress, σ_y , Profiles

TABLE 11.8
MEMORY REQUIREMENTS

FOUNDATION TYPE	MESH SIZE	NUMBER OF WORDS OF MEMORY
ELASTIC SOLID	10 x 10	82,380
VLASOV	10 x 10	30,411
WINKLER	10 x 10	30,411
ELASTIC SOLID	20 x 20	980,084
VLASOV	20 x 20	189,811
WINKLER	20 x 20	189,811

TABLE 11.9
COMPARISON WITH ELASTIC SOLID (II)

(a) CASE A

h= 7 in.; L= 180 in.; 2a= 18 in.

Node	Deflection (mils)		Subgrade Stress (psi)		σ_x (psi)		σ_y (psi)	
	VLASOV	EL.SOLID	VLASOV	EL.SOLID	VLASOV	EL.SOLID	VLASOV	EL.SOLID
61	5.237	4.587	.964	1.086	100.733	91.987	100.733	91.987
62	4.377	3.825	.452	.632	42.073	34.843	5.056	-.799
63	3.133	2.822	.267	.285	18.258	13.076	-4.087	-6.170
64	2.064	2.042	.156	.125	9.377	5.851	-6.844	-6.460
65	1.233	1.481	.091	.052	5.548	2.946	-4.904	-3.813
66	.567	1.048	.052	-.058	3.962	1.670	.000	.000

(VLASOV/EL.SOLID) X 100%				
Node	Deflection	Subgrade Stress	σ_x	σ_y
61	114	89	110	110
62	114	72	121	-633
63	111	94	140	66
64	101	125	160	106
65	83	175	188	129
66	54	-90	237	100

See Table 11.7a for system characteristics.

TABLE 11.9 (continued)

(b) CASE B

h= 7 in.; L= 180 in.; 2a= 18 in.

Node	Deflection (mils)		Subgrade Stress (psi)		σ_x (psi)		σ_y (psi)	
	VLASOV	EL.SOLID	VLASOV	EL.SOLID	VLASOV	EL.SOLID	VLASOV	EL.SOLID
61	2.179	2.157	3.698	2.075	73.271	74.342	73.271	74.342
62	1.617	1.583	.630	.928	22.094	22.007	8.344	9.652
63	1.011	.988	.204	.246	6.576	5.649	-6.500	-7.299
64	.627	.641	.067	.052	2.441	1.850	-5.077	-4.560
65	.413	.451	.038	.008	1.103	.767	-3.086	-2.062
66	.295	.332	.075	-.059	.859	.447	.000	.000

Node	(VLASOV/EL.SOLID) X 100%			
	Deflection	Subgrade Stress	σ_x	σ_y
61	101	178	99	99
62	102	68	100	86
63	102	83	116	89
64	98	129	132	111
65	92	475	144	150
66	89	-127	192	100

See Table 11.7b for system characteristics.

For a given slab, altering its thickness, h , automatically changes its radius of relative stiffness, and, therefore, the value of the ratio (L/ℓ) , used on other occasions to characterize the slab length effect. This is confirmed by the profiles presented in Table 11.10, where the slab size is reduced from 180-in. to 126-in. Significant deterioration in the closeness of the "match" between the two models is observed.

Finally, the effect of mesh fineness was considered. Table 11.11 suggests that mesh fineness has practically no effect on the closeness of the "match" between the two models, indicating that both models are affected equally by this factor.

To facilitate any future attempts to match the Vlasov and Boussinesq subgrades, the effect of the subgrade Poisson's ratio was investigated for the latter model. The objective here is to determine whether any trends produced by varying k and/or G in the Vlasov model can be reproduced by changing μ_s in the Elastic Solid model. Table 11.12 shows the response profiles obtained. It is observed that as μ_s increases, maximum deflection and bending stress decrease, while maximum subgrade stress increases (Figures 11.10; 11.11; and 11.12; cf. Table 7.9). The same effects could also be produced by increasing G (see Table 11.6). The influence of μ_s and G on edge responses, however, are not as comparable. Figure 11.13 shows that increasing μ_s causes a decrease in all three responses at the edge of the plate (see also Table 7.9). On the other hand, as G increases edge bending stress decreases, while edge deflection and subgrade stress increase. This indicates that only some of the effects of an increase in μ_s can be

TABLE 11.10
COMPARISON WITH ELASTIC SOLID (III)

(a) CASE A

$h = 15$ in.; $L = 126$ in.; $2a = 18$ in.

Node	Deflection (mils)		Subgrade Stress (psi)		σ_x (psi)		σ_y (psi)	
	VLASOV	EL.SOLID	VLASOV	EL.SOLID	VLASOV	EL.SOLID	VLASOV	EL.SOLID
36	3.515	2.427	.291	.255	13.868	15.557	13.868	15.557
37	3.515	2.427	.291	.255	13.868	15.557	13.868	15.557
38	3.364	2.255	.257	.202	8.662	10.331	2.579	4.131
39	3.181	2.034	.237	.164	5.837	7.425	-.151	.945
40	3.007	1.810	.223	.397	4.781	6.203	.000	.000

Node	(VLASOV/EL.SOLID) X 100%			
	Deflection	Subgrade Stress	σ_x	σ_y
36	145	114	89	89
37	145	114	89	89
38	149	127	84	62
39	156	145	79	-16
40	166	56	77	100

See Table 11.7a for system characteristics.

TABLE 11.10 (continued)

(b) CASE B

h= 15 in.; L= 126 in.; 2a= 18 in.

Node	Deflection (mils)		Subgrade Stress (psi)		σ_x (psi)		σ_y (psi)	
	VLASOV	EL.SOLID	VLASOV	EL.SOLID	VLASOV	EL.SOLID	VLASOV	EL.SOLID
36	1.411	1.051	.520	.459	11.450	12.543	11.450	12.543
37	1.411	1.051	.520	.459	11.450	12.453	11.450	12.543
38	1.287	.914	.336	.310	6.521	7.489	.991	1.993
39	1.151	.752	.262	.205	3.979	4.736	-.869	-.051
40	1.029	.596	.237	.296	3.117	3.537	.000	.000

Node	(VLASOV/EL.SOLID) X 100%			
	Deflection	Subgrade Stress	σ_x	σ_y
36	134	113	91	91
37	134	113	92	91
38	141	108	87	50
39	153	128	84	1704
40	173	80	88	100

See Table 11.7b for system characteristics.

TABLE 11.11
COMPARISON WITH ELASTIC SOLID (IV)

(a) CASE A

$h = 15$ in.; $L = 180$ in.; $2a = 36$ in.

Node	Deflection (mils)		Subgrade Stress (psi)		σ_x (psi)		σ_y (psi)	
	VLASOV	EL.SOLID	VLASOV	EL.SOLID	VLASOV	EL.SOLID	VLASOV	EL.SOLID
21	2.123	2.101	.180	.200	9.870	9.817	9.870	9.817
22	2.123	2.101	.180	.200	9.870	9.817	9.870	9.817
23	1.701	1.676	.130	.115	5.456	5.424	-.101	.350
24	1.269	1.221	.096	.124	3.617	3.305	.000	.000

Node	(VLASOV/EL.SOLID) X 100%			
	Deflection	Subgrade Stress	σ_x	σ_y
21	101	90	101	101
22	101	90	101	101
23	101	113	101	-29
24	104	77	109	100

See Table 11.7a for system characteristics.

TABLE 11.11 (continued)

(b) CASE B

h= 15 in.; L= 180 in.; 2a= 36 in.

Node	Deflection (mils)		Subgrade Stress (psi)		σ_x (psi)		σ_y (psi)	
	VLASOV	EL.SOLID	VLASOV	EL.SOLID	VLASOV	EL.SOLID	VLASOV	EL.SOLID
21	.907	.901	.319	.328	6.607	6.412	6.607	6.412
22	.907	.901	.319	.328	6.607	6.412	6.607	6.412
23	.629	.625	.142	.135	2.890	2.723	-1.366	-1.043
24	.397	.381	.094	.048	1.557	1.137	.000	.000

Node	(VLASOV/EL.SOLID) X 100%			
	Deflection	Subgrade Stress	σ_x	σ_y
21	101	97	103	103
22	101	97	103	103
23	101	105	106	131
24	104	196	137	100

See Table 11.7b for system characteristics.

TABLE 11.12
EFFECT OF μ_s ON ELASTIC SOLID RESPONSES

μ_s	Node Number					
	61	62	63	64	65	66
DEFLECTIONS (mils)						
0.00	2.730	2.604	2.375	2.118	1.861	1.615
0.15	2.685	2.560	2.332	2.076	1.822	1.578
0.30	2.550	2.427	2.202	1.952	1.704	1.467
0.45	2.320	2.199	1.981	1.741	1.505	1.280
0.50	2.220	2.100	1.885	1.651	1.420	1.201
BENDING STRESSES, σ_x (psi)						
0.00	28.469	15.259	9.321	6.664	5.227	4.429
0.15	28.400	15.191	9.257	6.604	5.169	4.371
0.30	28.178	14.977	9.054	6.413	4.985	4.190
0.45	27.760	14.572	8.674	6.056	4.656	3.857
0.50	27.561	14.381	8.495	5.890	4.488	3.703

TABLE 11.12 (continued)

μ_s	Node Number					
	61	62	63	64	65	66
SUBGRADE STRESSES (psi)						
0.00	.238	.193	.147	.114	.091	.194
0.15	.241	.196	.149	.115	.091	.192
0.30	.252	.203	.153	.117	.092	.187
0.45	.273	.218	.162	.121	.093	.176
0.50	.283	.225	.165	.123	.093	.171

Notes:

Slab : 180 X 180 in.
 Mesh : 10 X 10 @ 18 in.
 $E = 3,000,000$ psi
 $\mu = 0.15$
 $h = 15$ in.
 $E_s = 10,000$ psi
 $A = 6 \times 6$ @ 100 psi; interior

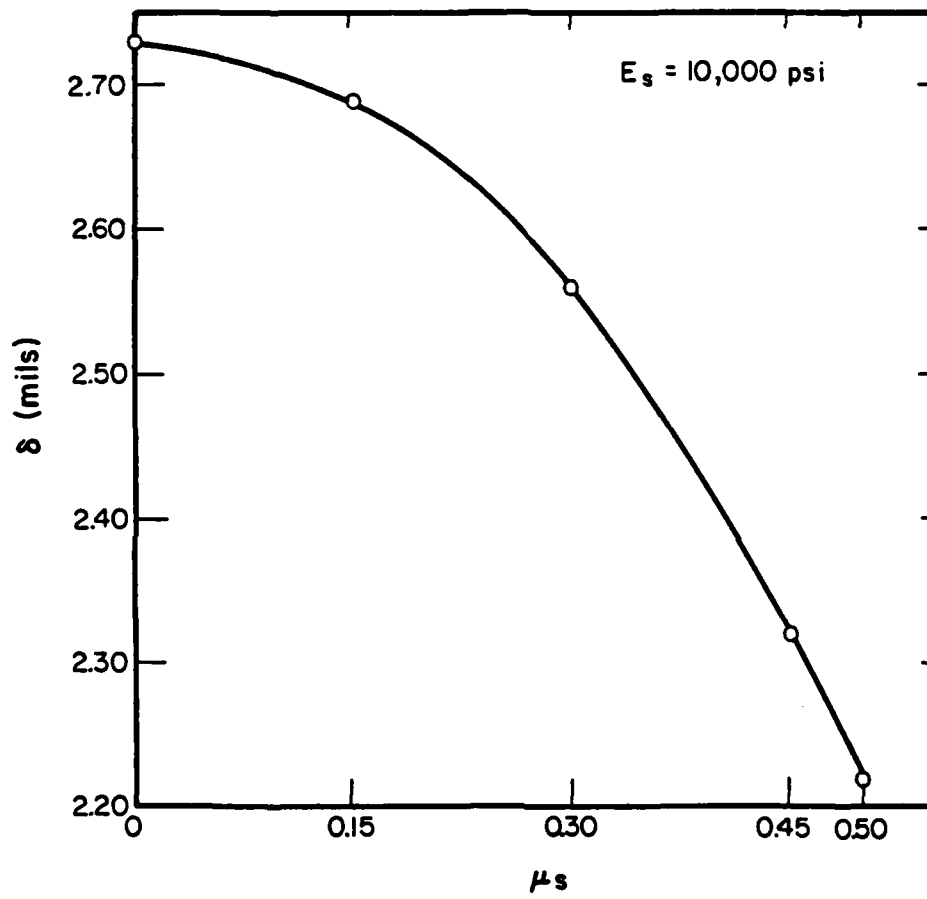


Fig. 11.10 Effect of Elastic Solid Poisson's Ratio on Maximum Deflection

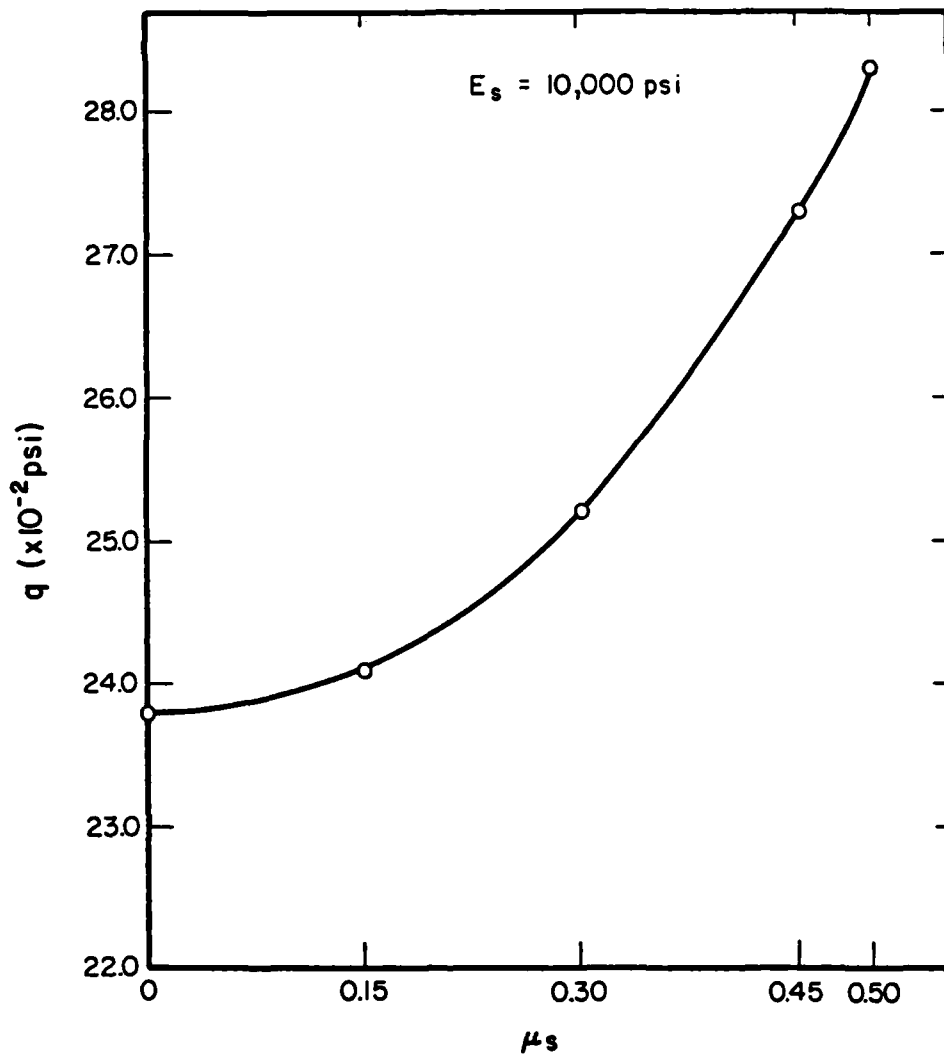


Fig. 11.11 Effect of Elastic Solid Poisson's Ratio on Maximum Subgrade Stress

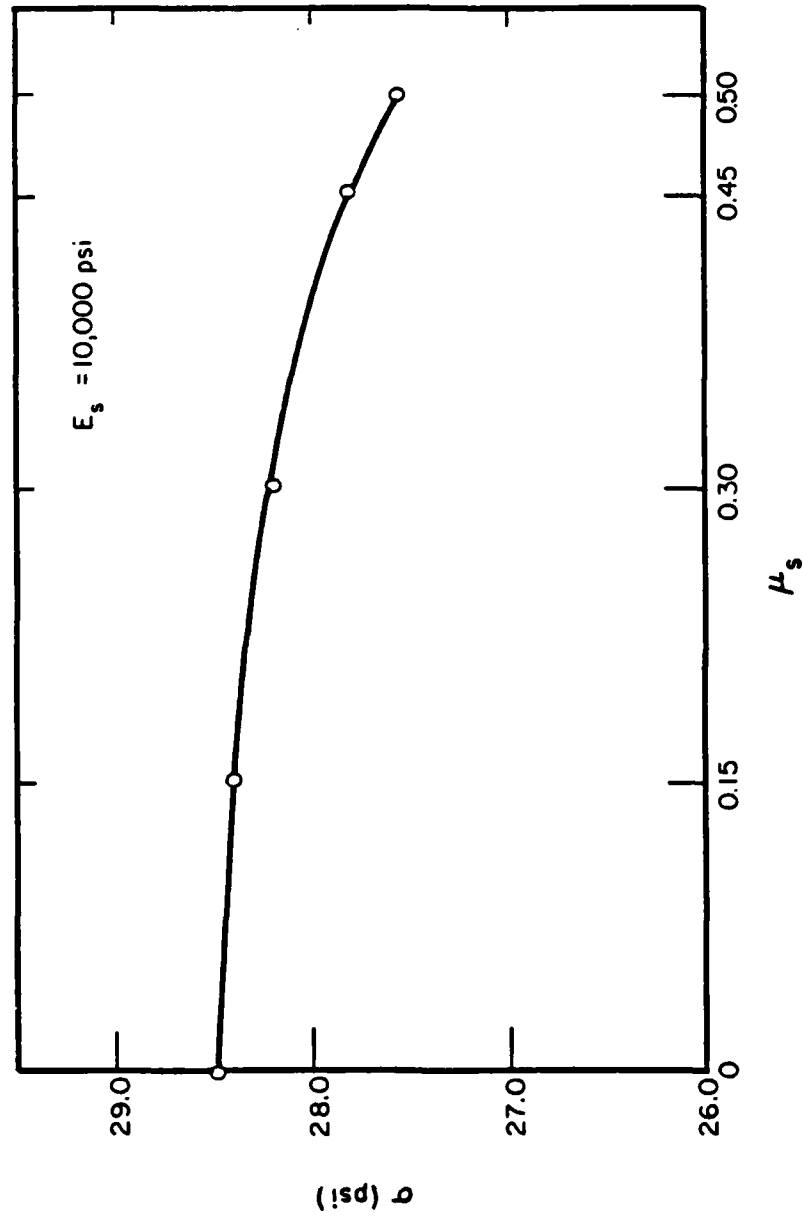


Fig. 11.12 Effect of Elastic Solid Poisson's Ratio on Maximum Bending Stress

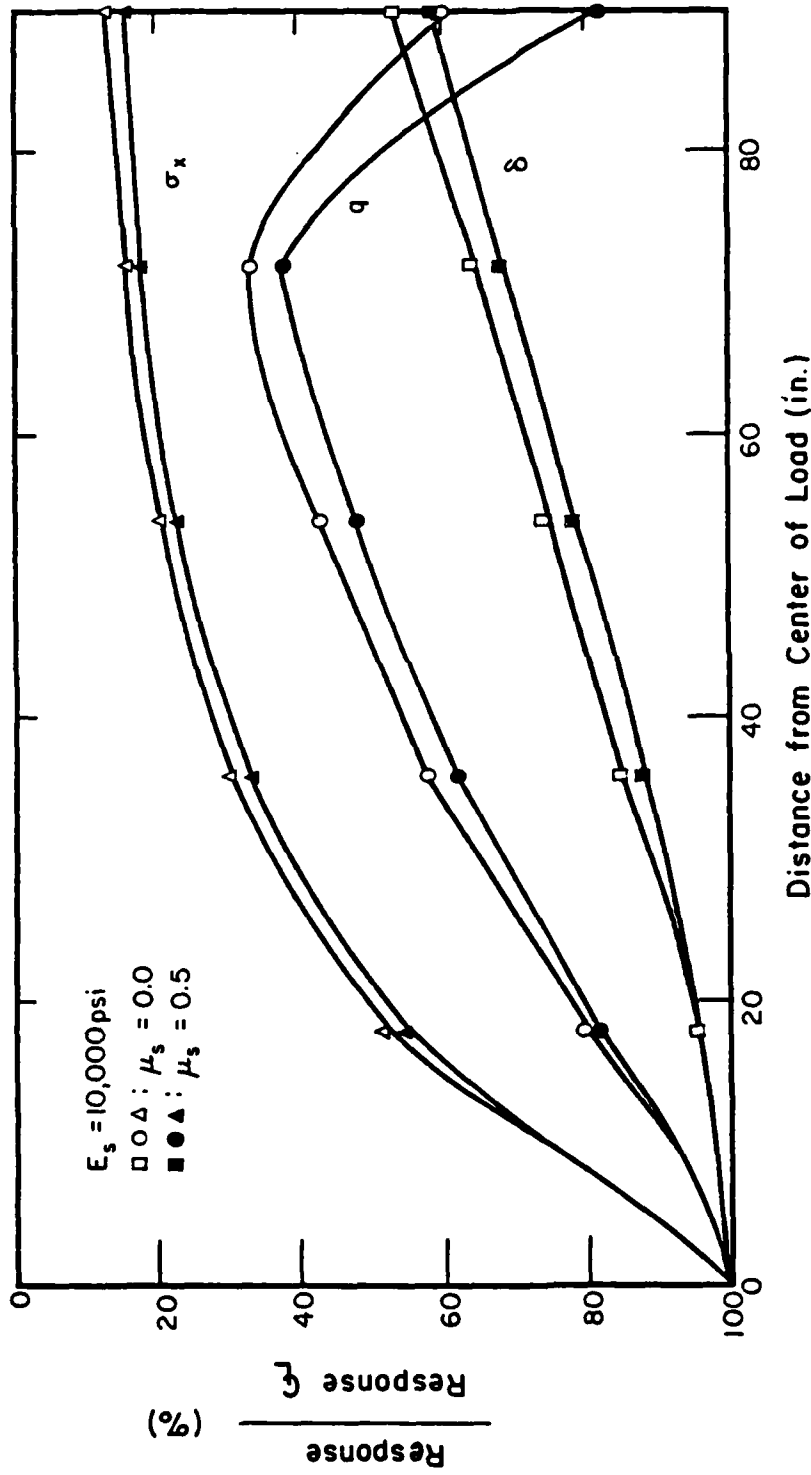


Fig. 11.13 Effect of Elastic Solid Poisson's Ratio on Response Profiles

reproduced by an increase in G . The relative significance of the subgrade stress at the edge, particularly noted in stiff slabs, is diminished as μ_s increases.

The analyses described here do not, of course, exhaust the scope of possible investigations using the Vlasov model. Basic guidelines and conclusions have been reached in this study, however, to improve the chances of future successful applications of this model.

CHAPTER 12

SUMMARY AND CONCLUSIONS

12.1 RESEARCH ACCOMPLISHMENTS

The major goal of this study has been to explore all existing and/or potential tools that may be applied to the analysis of slab-on-grade pavement systems. Within the context of two-dimensional plate theory this has been achieved to a large extent. The major single product of this work is the revised and expanded ILLI-SLAB code. This program was identified at the beginning of this research as a versatile and easy-to-use procedure. Since then, the program's accuracy, ease of application and meaningful result interpretation have been enhanced. In a parallel effort, three new foundation models have now been incorporated into ILLI-SLAB to provide the capability to analyze a slab on a stress dependent (resilient) subgrade, a semi-infinite half-space or a two-parameter foundation. Thus, ILLI-SLAB is currently the first and only computer code that allows these multiple options. Comparative analyses are greatly facilitated, and the whole spectrum of possible subgrade idealizations can be examined, from the entirely discontinuous dense liquid, to the totally continuous elastic solid. The efficient and fruitful utilization of ILLI-SLAB is ensured by adherence to guidelines established during several convergence studies. Thus, a fine mesh ($2a/h=0.8-1.0$) consisting mostly of square elements can be expected to produce accurate results.

The reexamination of Westergaard's pioneering works in the light of the Finite Element Method (F.E.M.) also yielded a number of interesting results. These include the following:

- (1) Several equations ascribed to Westergaard in the literature are erroneous, usually through a series of typographical errors and/or misapplications. The correct form of these equations and their limitations have now been conclusively established;
- (2) Westergaard's original (1926) equation for the edge stress is incorrect. The long ignored equation given in his 1948 paper should be used instead;
- (3) An improved expression for the corner stress has been developed.

The investigation of the problem of a plate on an elastic solid foundation described in this work is, perhaps, the most exhaustive to date. Computer programs have been developed during this research for considering the problem using four different approaches. Independent verification and mutual reinforcement of each program's results is, therefore, feasible. Each of these programs is particularly suitable for a given set of applications, and between them they cover most practical possibilities. Since closed-form solutions for the response of an infinite plate on an elastic solid foundation were only available for the interior loading condition, the programs developed have been used to derive similar predictive expressions for the edge and corner loading conditions. Although these equations are approximate, they are

useful in preliminary designs. Guidelines for the effective use of each of these programs have also been established.

Examination of the two-parameter (Vlasov) foundation has indicated that it is a closer approximation of an elastic solid response than the dense liquid model. Computer memory requirements are identical for the 'VLASOV' and 'WINKLER' options in ILLI-SLAB. Nevertheless, differences between the Vlasov and elastic solid idealizations preclude the existence of a "panacea" for all problems encountered with the latter.

The investigations reported in this work, naturally, do not exhaust the scope of the capabilities of the programs developed. At the same time, the guidelines and conclusions reached during these investigations have potential applications to various soil-structure interaction problems, and structural and geotechnical engineering, in general. The program codes are specially designed to permit easy adaptation, correction and expansion to suit the needs of each individual case considered. Finally, none of the programs developed are particularly expensive to use. Typical execution times on the CDC-CYBER system at the University of Illinois do not exceed 15 CPU seconds. Thus, a large number of analyses can be performed at reasonable expense.

12.2 FUTURE RESEARCH DIRECTIONS

Findings and results from this research clearly indicate that no current procedure can fully model the behavior of a slab of finite

size, supported by a stress dependent fine-grained subgrade extending beyond the slab edges. Consequently, it is sometimes difficult to establish the accuracy and adequacy of the slab-on-grade structural models developed in this study. It is, therefore, highly desirable to develop a three-dimensional finite element model to represent the slab-on-grade problem in more detail. This will help establish base-line structural response data, representative of complex slab boundary and foundation support conditions (stress dependent granular materials and fine-grained soils) encountered in conventional rigid pavement systems.

The following features would be necessary in a three-dimensional finite element model for the analysis of a slab on an elastic solid foundation:

1. Ease of Application: The program must require a minimum amount of input data, thus eliminating potential user pitfalls. It is very frustrating to have such a sophisticated model, but be unable to use it effectively due to the length of data preparation time required;
2. Meaningful Output: The large amount of information generated by such a program must be presented in a way facilitating its interpretation. Methods proven very helpful with the two-dimensional models may be adapted for use here, as well;
3. Flexibility: Although this requirement will be tempered by the complexity of the numerical solution, the three-dimensional model envisaged should be capable of analyzing a pavement system consisting of a slab and base, supported by a uniform or multi-layered elastic

solid foundation. Any number of loads should be allowed at any location on the slab;

4. Stress Dependence: Stress-dependent subgrade moduli can be accommodated through an iterative process similar to that currently used in ILLI-PAVE. Values of the deviator stress for each element should be checked for compatibility against the E_R versus deviator stress algorithms developed by Thompson and Robnett (see Section 2.5). If necessary, element values of E_R should be updated and a new iteration performed until the convergence criteria are satisfied;

5. Effective Machine Implementation: It is now apparent from the two-dimensional investigations in this study, that accurate and meaningful results require a fairly fine finite element mesh, i.e. a large number of elements. This creates a severe problem with respect to computer storage, particularly in the case of the proposed three-dimensional model. Efficient memory core allocation and use of overlays and other advanced techniques will be absolutely essential. The primary objective will be to increase the number of elements that can be accommodated, although this will inevitably prolong execution time. In this day of personal computer networks, the latter problem is becoming less important. As far as possible, the model developed should be adapted for implementation on such a network.

A closer study of the two computer programs with three-dimensional analysis capabilities currently available at the University of Illinois, viz. FINITE and GEOSYS, can provide very useful guidelines as to how these goals may be achieved. Furthermore, trial runs using

these programs can be used to address several questions before the computer code is developed. For example:

1. Which three-dimension finite elements should be used for the slab, the base, and the foundation?
2. How far must the foundation extend beyond and below the rectangular slab to minimize boundary effects?

Other questions pertain to the equation solver to be used and the memory core allocation procedures to be adopted.

APPENDIX A

INPUT GUIDES

FOR PROGRAMS DEVELOPED

INPUT GUIDE FOR ILLI-SLAB(REVISED VERSION: AUGUST 1984)

ILLI-SLAB can be used to calculate deflections and stresses in jointed slab-on-grade pavements, with or without load transfer systems. The program can also accommodate a stabilized base or an overlay, by assuming either perfect bond or no bond between the two layers.

The pavement system can consist of any number of slabs. The program is currently dimensioned to accept up to 10 slabs along each of the x- and y-axes. Elements and nodes are numbered consecutively from bottom to top along the y-axis, and from left to right along the x-axis. Joints are treated as rectangular elements having zero width.

The wheel loads may be applied to any of the slabs, and stresses and deflections at all nodes in the slab, stresses in the stabilized base or overlay, vertical stresses in the subgrade, and transferred loads by the dowel bars are computed.

This revised version incorporates the two-parameter (Vlasov) and the elastic solid (Boussinesq) subgrades (IST=9 and IST=8, respectively). When the latter option is used, only one slab is allowed. This must have a constant thickness and elastic modulus and must consist of only one layer. The symmetry capability is not operable with this option.

The program can accept either fixed-form or free-form type of input. Both types are described below.

AD-A150 965

ANALYSIS OF SLABS-ON-GRADE FOR A VARIETY OF LOADING AND
SUPPORT CONDITION. (U) ILLINOIS UNIV AT URBANA DEPT OF
CIVIL ENGINEERING A M IOANNIDES ET AL. DEC 84

6/7

UNCLASSIFIED

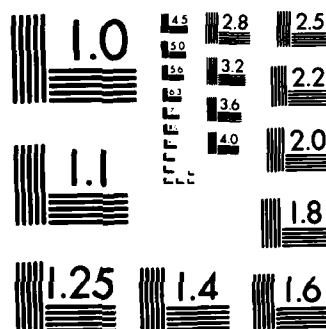
AFOSR-TR-85-0083 AFOSR-87-0143

F/G 13/2

NL

			END										
			110										
			110										

Cont



MICROCOPY RESOLUTION TEST CHART
NATIONAL BUREAU OF STANDARDS-1963-A

CARDS FOR FIXED-FORM INPUT
FOR ILLI-SLAB

Card No. 1.

IFORM

11

IFORM : A numeric flag indicating type of input data type used;
= 0, for free-form input;
= 1, for fixed-form input.

Card No. 2.

TITLE

20A4

TITLE : An 80-column label of alphanumeric characters used to
identify the problem. This label will appear on the
header part of the output.

Card No. 3.

NFOR ISYM

215

NFOR : Number of loaded areas.

ISYM : Numeric flag indicating whether symmetry lines are
used;

= 0, if no symmetry lines are used;

= 1, if x-axis is a line of symmetry;

= 2, if y-axis is a line of symmetry;

= 3, if x-axis and y-axis are lines of symmetry.

Card No. 4.

NNODX(I), I= 1, MAXSLXY

1015

NNODX(I): Number of nodes in slab(s), along the x-axis (MAXSLXY
is set to 10; to change, alter the size of arrays NNODX
and NNODY).

Card No. 5.

NNODY(I), I= 1, MAXSLXY

1015

NNODY(I): Number of nodes in slab(s), along the y-axis (MAXSLXY is set to 10; to change, alter the size of arrays NNODX and NNODY).

Card No. 6.

NLAYER	COMP	CK	E0	PRO
--------	------	----	----	-----

15	15	F10.3	F10.3	F10.3
----	----	-------	-------	-------

NLAYER: Number of layers above subgrade: 1 or 2.

COMP : Composite action factor;

= 0, if no bond exists between the slab and stabilized base or overlay;

= 1, if complete bond.

CK : Subgrade modulus, if subgrade modulus is uniform;

= 0.0, if not (see Card No. 19);

= -1.0, if elastic solid subgrade is used (IST=8).

E0 : Elastic Modulus of subgrade (leave blank if elastic solid solid subgrade is not used);
 = GM, the Vlasov shear parameter when IST=9.
 PR0 : Poisson's Ratio of subgrade (leave blank if elastic solid solid subgrade is not used).

Card No. 7.

IST	ITMAX	TOL1	TOL2	IOT
I5	I5	F5.3	F5.3	I5

IST : A numeric flag for subgrade type:

- = 0, if subgrade type varies (See Card No. 25);
- = 1, for VERY SOFT subgrade;
- = 2, for SOFT subgrade;
- = 3, for MEDIUM subgrade;
- = 4, for STIFF subgrade;
- = 5, for OTHER subgrade (see Card No. 26);
- = 6, for WINKLER energy consistent, uniform subgrade;
- = 7, for SPRINGS subgrade;
- = 8, for BOUSSINESQ subgrade;
- = 9, for VLASOV subgrade.

Recommended values for k in first iteration:

VERY SOFT: $K_R = 300$ psi/in.

SOFT: $K_R = 425$ psi/in.

MEDIUM: $K_R = 725$ psi/in.

STIFF: $K_R = 1000$ psi/in.

OTHER: $K_R = A5/DY$ psi/in.

ITMAX : Maximum number of iterations desired.

TOL1 : Tolerance for K_R (Recommended value= 0.05, ie. 5%).

TOL2 : Tolerance for points exceeding TOL1 (Recommended value= 0.05, i.e. 5%).

IOT : Numeric flag for output type:

= 0, for partial output during intermediate iterations.

= 1, for full output during intermediate iterations.

Note: A new iteration is performed if the ratio of the number of nodes at which the updated K_R is more than TOL1 (%) off the previous K_R , to the total number of nodes, exceeds TOL2 (%).

Card No. 8.

ICON(I), I=1,6	ISTEP
----------------	-------

611	14
-----	----

ICON(I) = A numeric flag indicating which contour plots, if any, are desired;

ICON(1) = 1, if contours of deflection are wanted;
= 0, if not.

ICON(2) = 1, if contours of subgrade stress are wanted;
= 0, if not.

ICON(3) = 1, if contours of x-stress at bottom of Layer 1 are
wanted;
= 0, if not.

ICON(4) = 1, if contours of y-stress at bottom of Layer 1 are
wanted;
= 0, if not.

ICON(5) = 1, if contours of x-stress at bottom of Layer 2 are
wanted;
= 0, if not.

ICON(6) = 1, if contours of y-stress at bottom of Layer 2 are
wanted;
= 0, if not.

NB: ICON(5) and ICON(6) must be set to 0, if NLAYER=1 (see Card
No. 6).

ISTEP : An integer specifying the density of the Virtual Grid
in the contouring routines. The value of 40 produces
pleasing contours. For coarser but quicker lower the
value. For smoother but longer time raise the value.
ISTEP should be less than 200.

Card No. 9 (Read only if there are more than one slabs along x-axis).

LTDX

I5

LTDX : Type of load transfer in x-direction;

= 0, if aggregate intelock or keyway;

= 1, if dowel bars;

= 2, if a combination of dowel bars and aggregate
interlock or dowel bars and keyway.

Card No. 10 (Read only if there are more than one slabs along y-axis).

LTDY

I5

LTDY : Type of load transfer in y-direction;

= 0, if aggregate intelock or keyway;

= 1, if dowel bars;

= 2, if a combination of dowel bars and aggregate
interlock or dowel bars and keyway.

Card No. 11 (Use as many as needed).

 XC(I), I=1,number of nodes along x-axis

8F10.3

XC(I) : x-coordinate of node along the x-axis (read in
 ascending order).

Card No. 12 (Use as many as needed).

 YC(I), I=1,number of nodes along y-axis

8F10.3

YC(I) : y-coordinate of node along the y-axis (read in
 ascending order).

Card No. 13.

 CT1 CE1 V(1)

F10.3 E10.3 F10.3

CT1 : Top layer thickness, if uniform;

= 0.0, if not (see Card No. 14).

CE1 : Modulus of Elasticity for top layer, if uniform;

= 0.0, if not (see Card No. 15).

V(1) : Poisson's ratio of top layer.

Card No. 14 (Read only if CT1=0.0; use as many as needed).

T1(I), I=1,number of nodes

8F10.3

T1(I) : Thickness of the top layer at node I.

Card No. 15 (Read only if CE1=0.0; use as many as needed).

E1(I), I=1,number of nodes

8F10.3

E1(I) : Modulus of Elasticity of the top layer at node I.

Card No. 16 (Read only if NLAYER=2).

CT2	CE2	V(2)
F10.3	E10.3	F10.3

CT2 : Bottom layer thickness, if uniform;

= 0.0, if not (see Card No. 17).

CE2 : Modulus of Elasticity for bottom layer, if uniform;

= 0.0, if not (see Card No. 18).

V(2) : Poisson's ratio of bottom layer.

Card No. 17 (Read only if CT2=0.0; use as many as needed).

T2(I), I=1,number of nodes
8F10.3

T2(I) : Thickness of the bottom layer at node I.

Card No. 18 (Read only if CE2=0.0; use as many as needed).

 E2(I), I=1,number of nodes

8F10.3

E2(I) : Modulus of Elasticity of the bottom layer at node I.

Card No. 19 (Read only if CK=0.0; use as many as needed).

 SUB(I), I=1,number of nodes

8F10.3

SUB(I) : Modulus of subgrade reaction at node I.

Card No. 20 (Read only if LTDX=1 or 2).

 DIN DOUT DE DS DJW DPR DCI

F10.3 F10.3 E10.3 F10.3 F10.3 F10.3 E10.3

DIN : Inside diameter of dowel bars;

= 0.0 for solid round bars.

DOU : Outside diameter of dowel bars.

DE : Modulus of elasticity of dowel bars.

DS : Spacing of dowel bars.

DJW : Joint width.

DPR : Poisson's Ratio of dowel bars.

DCI : Dowel-Concrete Interaction.

DCI for a round steel dowel bar may be determined from either Friberg's dowel analysis or from a relation developed based upon a three-dimensional dowel analysis:

(a) Friberg's Analysis:

$$DCI = \{K^{0.75} D^{2.5}\} / \{0.041 D^{0.75} + 0.0004 K^{0.25} w\}$$

(b) Three-dimensional Analysis:

$$DCI = \{E^{0.75}\} / \{(0.057 - 0.010 D) * (0.810 + 0.013 h) * (1 + 0.414 w)\}$$

where:

E : Concrete modulus of Elasticity, psi;

D : Dowel diameter, in.;

h : Slab thickness, in.;

w : Joint width, in.;

K : Modulus of dowel support, psi/in.

Card No. 21 (Read only if LTDX=0 or 2).

AGGX

E10.3

AGGX : Aggregate Intelock Factor in x-direction.

(Use a large value, eg. AGGX=1.000E+08, for keyways).

Card No. 22 (Read only if LTDY=1 or 2).

DIN DOUT DE DS DJW DPR DCI

F10.3 F10.3 E10.3 F10.3 F10.3 F10.3 E10.3

See Card No. 20 for notations.

Card No. 23 (Read only if LTDY=0 or 2).

AGGY

E10.3

AGGY : Aggregate Intelock Factor in y-direction.

(Use a large value, eg. AGGY=1.000E+08, for keyway).

Card No. 24 (Read NFOR times).

 PRS XX1 XX2 YY1 YY2

F10.3 F10.3 F10.3 F10.3 F10.3

PRS : Tire pressure.

XX1, XX2 : Lower and upper limits of the loaded area in
 x-direction, in global coordinate system.

YY1, YY2 : Lower and upper limits of the loaded area in
 y-direction, in global coordinate system.

Card No. 25 (Read only if IST=0; use as many as needed).

 NST(I), I=1,number of nodes

815

NST(I) : Subgrade Type (IST) under node I. See Card No. 7 for

definition of various subgrade types. IST may take values between 1 and 7, here.

Card No. 26 (Read only if IST=5).

A1	A2	A3	A4	A5	DY
6F10.5					

A1, A2, A3, A4, A5, DY : Parameters for the regression equation defining K_R as a function of w . General form of the equation:

$$K_R = \{A1[1 - \exp\{-A2(w/DY - A3)\}] + A4(w/DY - A3) + 2\} / w$$

$$K_R = A5/DY, \text{ if } w/DY < A3.$$

where

w : deflection, in inches;

K_R : resilient subgrade modulus, in psi/in.

Card No. 27 (Read only if contours are to be plotted).

JCON(I), I=1,6	RATIO
6I1	F10.7

JCON(I) : A numeric flag indicating over which slabs the contours requested in Card No. 8, are to be plotted (Contours can only be plotted over the first 6 slabs);

JCON(I) = 1, if contours over Slab I are to be plotted;
= 0, if not.

RATIO : A factor by which the y-scale is multiplied;
RATIO=1.0 specifies x- and y-scales are equal.

FREE-FORM INPUT GUIDEFOR ILLI-SLABPRELIMINARY REMARKS

Input to the ILLI-SLAB free-form system is in the form of a Problem Oriented Language (POL), designed specifically for structural engineers. This language uses the SCAN package of subroutines developed at the University of Illinois. The following is a description of the conventions used within this Guide to explain the ILLI-SLAB system.

The appearance within an ILLI-SLAB command of a descriptor of the form

< i >

implies that the user is to enter an item of data within that position in the statement, of the class described by the descriptor. In the example above, an integer must be entered. The command

NUMBER OF LAYERS < i >

implies that the word LAYERS is to be followed by an integer, such as 1 or 2, and that the statement entered by the user as input data should be of the form

NUMBER OF LAYERS 2

The following are definitions of the descriptors used in this Guide:

- < i > a series of digits, optionally preceded by a plus or minus sign. Examples are: 123, +500, -56.
- < r > a series of digits with a decimal point included; or a series of digits with a decimal point followed by an exponential indicating a power of 10. Real numbers are optionally signed. Integers are also allowed by this descriptor. Examples are 1.0, -2.5, 4.0E+06, 50, 100.
- < string > is any textual information enclosed within apostrophes. An example is "THIS IS A STRING".
- <list: d> is a notation used to indicate a sequence of integer (d=i), or real (d=r) values, or integer, real pairs of such values (d=i,r). Data in a list consists of a series of the appropriate type of numbers, separated by a comma or blank.

Input to the ILLI-SLAB free-form system is a series of English-like commands. Many of the words or phrases in these commands are optional, and are provided primarily for readability. Optional words are enclosed in parentheses within the command definitions. For example,

NUMBER (OF) LAYERS < i >

can be written as

NUMBER OF LAYERS 2

or

NUMBER LAYERS 2

In the definition of each command in this Guide, words not enclosed in parentheses are absolutely necessary for ILLI-SLAB to properly interpret the command.

In general, only the first four letters in each word need to be entered by the engineer. For example, the phrase

NUMBER (OF) LAYERS 2

can be shortened to

NUMB LAYE 2

if the user so desires.

In many instances, more than one word is acceptable in a given position within a command. The choices are listed one above the other in the command definition. The command definition

SYMMETRY (ABOUT) $\left\{ \begin{array}{l} X \\ Y \\ X \text{ AND } Y \end{array} \right\}$ (AXIS)

indicates that any of the following commands are acceptable:

SYMMETRY ABOUT X AXIS

SYMMETRY Y

SYMM X AND Y

In some commands items may be repeated and/or multiple commands may be combined on one line of data. This is indicated in the command definition by enclosing the repeatable entries within brackets [...]. The command definition

COORDINATES [(OF) (NODES) (IN) $\begin{Bmatrix} X \\ Y \end{Bmatrix}$ (DIRECTION) <string: r >]

implies that the user may enter commands of the form:

COORDINATES OF NODES
IN X DIRECTION 0 10 20 30 40
IN Y 0.0 10. 50. 60.

Continuation of a line of data onto a second line is accomplished by placing a comma (,) at the end of the line to be continued. Comments may be placed in the data. A comment line is defined as a line with C in column 1 and a blank in column 2. Line termination is accomplished in three ways:

- a) The last column examined by the system is column 72;
- b) After encountering the first data item on a card, the system begins counting blank columns between items. If 20 successive blanks

are found, the system assumes the remainder of the line is blank and signals a line termination;

c) A \$ placed on a line indicates end of data on the line. Space remaining on the line may be used for user comments.

Some familiarity with the fixed-form input to ILLI-SLAB will prove very useful in using the free-form option. Symbols used in this part of the Guide have already been defined in the context of fixed-form data, and the user may refer to the appropriate fixed-form card whenever this is necessary. Given below are the command definitions used with the free-form option.

FREE-FORM INPUT COMMANDS

BLOCK 1

These commands must precede those in Block 2 but may be issued in any desired sequence, or may be ignored if the default values are used, or if the commands are not applicable to the problem in question. The default values are listed in Table A.1.

1. TITLE

A title for the problem to be solved may be defined through a command of the form:

TITLE < string >

The title string may contain up to 80 alphanumeric characters enclosed within apostrophes ("..."), and will appear on the header part of the output.

2. NUMBER

Through the use of commands of the following form, the user may specify the number of nodes, layers and loaded areas for the problem under consideration.

TABLE A.1

ILLI-SLAB DEFAULT VALUES FOR FREE-FORM OPTION

DATA GROUP	PARAMETER NAME	DEFAULT VALUE	FIXED-FORM CARD NO.
1. TITLE	TITLE	String of 80 blanks	2
2. NUMBER	NNODX(I), I=1, MAXSLXY	0	4
	NNODY(I), I=1, MAXSLXY	0	5
	NFOR	0	3
	NLAYER	1	6
3. TYPE	IST	1	7
4. CONTOURS	ICONS(I), I=1, 6	0	8
	JCONS(I), I=1, 6	0	27
	RATIO	1.0	27
	ISTEP	50	8
5. COORDINATES	KC(I), I=1, N1X+N2X+N3X	0.0	11
	YC(I), I=1, N1Y+N2Y	0.0	12
6. PROPERTIES	CT1, CE1	0.0	13
	V(1)	0.15	13
	T1(I), I=1, no. of nodes	0.0	14
	E1(I), I=1, no. of nodes	0.0	15
	CT2, CE2	0.0	16
	V(2)	0.0	16
	T2(I), I=1, no. of nodes	0.0	17
	E2(I), I=1, no. of nodes	0.0	18
	COMP	0.0	6
	CK	300.0	6
	SUB(I), I=1, no. of nodes	300.0	19
	IST	1	7
	A1	15.0	26
	A2	0.80	26
	A3	0.1680	26
	A4	0.62	26
	A5	11.9	26
	DY	0.04	26
	NST(I), I=1, no. of nodes	1	25
7. LOADED	PRS(I), XX1(I), XX2(I), YY1(I), YY2(I), I=1, NFOR	0.0	24
8. LOAD		No defaults	20-23
9. ITERATIVE	ITMAX	6	7
	TOL1, TOL2	0.05	7
	IOT	1	7
10. SYMMETRY	ISYM	0	3

$$\text{NUMBER} \left[\begin{array}{l} \text{(OF)} \left\{ \begin{array}{l} \text{NODES (IN) } \left\{ \begin{array}{l} X \\ Y \end{array} \right\} \text{ (DIRECTION) } < \text{list: } i > \\ \text{LOADED (AREAS) } < i > \\ \text{LAYERS } < i > \end{array} \right\} \end{array} \right]$$

3. TYPE

The type of subgrade, and of load transfer (if any) is specified using commands structured as follows:

$$\text{TYPE} \left[\begin{array}{l} \text{(OF)} \left\{ \begin{array}{l} \text{LOAD (TRANSFER) (IN) } \left\{ \begin{array}{l} X \\ Y \end{array} \right\} \text{ (DIRECTION) } \left\{ \begin{array}{l} \text{(AGGREGATE) INTERLOCK} \\ \text{DOWELS} \\ \text{COMBINATION} \end{array} \right\} \\ \text{SUBGRADE } \left\{ \begin{array}{l} \text{VERY (SOFT)} \\ \text{SOFT} \\ \text{MEDIUM} \\ \text{STIFF} \\ \text{OTHER} \\ \text{WINKLER} \\ \text{SPRINGS} \\ \text{BOUSSINESQ} \\ \text{VLASOV} \end{array} \right\} \end{array} \right\} \text{ (EXCEPT) (AT) (NODE) } < i > \left\{ \begin{array}{l} \text{VERY (SOFT)} \\ \text{SOFT} \\ \text{MEDIUM} \\ \text{STIFF} \\ \text{OTHER} \\ \text{WINKLER} \\ \text{SPRINGS} \end{array} \right\} \end{array} \right]$$

4. CONTOURS

These commands are used to indicate the contours requested and are not necessary if such contours are not to be generated.

$$\text{CONTOURS} \left[\begin{array}{l} \text{(REQUEST) (OF) } \left\{ \begin{array}{l} \text{NONE} \\ \text{DEFLECTION} \\ \text{SUBGRADE (STRESS)} \\ \text{XSTRESS} \\ \text{YSTRESS} \end{array} \right\} \text{ (AT) (BOTTOM) (OF) (LAYER) } \left\{ \begin{array}{l} 1 \\ 2 \end{array} \right\} \text{ (OVER) (SLABS) } < \text{list: } i > (,) \end{array} \right]$$

(AND) (WITH) (ASPECT) RATIO $< r >$
RESOLUTION $< i >$

Contours may be requested over slabs 1 through 6, only.

BLOCK 2

These commands must follow those in Block 1 but may be issued in any desired sequence, or may be ignored if the default values are used or the commands are not applicable to the problem in question.

5. COORDINATES

The coordinates of the nodes along the x- and y- axes may be specified using the following commands. The coordinates must be given in ascending order along each axis.

COORDINATES [(OF) (NODES) (IN) $\begin{Bmatrix} X \\ Y \end{Bmatrix}$ (DIRECTION) < string: r >]

6. PROPERTIES

Using commands of this form, the user can specify the properties (E, h, μ) of the top and bottom layers (if applicable), as well as of the subgrade (k, K_R , E_s , μ_s , G, and regression parameters -as appropriate-). SUBGRADE MODULUS may be the value of either k or E_s . COMPOSITE ACTION FACTOR may only be provided as a property of the bottom layer.

PROPERTIES $\left[\begin{array}{l} \begin{array}{l} \text{(OF)} \left\{ \begin{array}{l} \text{TOP} \\ \text{BOTTOM} \end{array} \right\} \text{(LAYER)} \left\{ \begin{array}{l} \text{THICKNESS} \langle r \rangle \\ \text{ELASTIC (MODULUS)} \langle r \rangle \text{ EXCEPT (AT) (NODE) } \langle \text{list: i, r} \rangle \\ \text{POISSON (RATIO)} \langle r \rangle \\ \text{COMPOSITE (ACTION) (FACTOR)} \langle i \rangle \end{array} \right\} \\ \text{SUBGRADE (SUBGRADE)} \left\{ \begin{array}{l} \text{MODULUS} \langle r \rangle \text{ ((EXCEPT) (AT) (NODE) } \langle \text{list: i, r} \rangle) \\ \text{POISSON (RATIO)} \langle r \rangle \\ \text{SHEAR (CONSTANT)} \langle r \rangle \\ \text{PARAMETERS (FOR) (REGRESSION) (EQUATION)} \left\{ \begin{array}{l} A1 \langle r \rangle \\ A2 \langle r \rangle \\ A3 \langle r \rangle \\ A4 \langle r \rangle \\ A5 \langle r \rangle \\ DY \langle r \rangle \end{array} \right\} \end{array} \right\} \end{array} \right]$

7. LOADED

At this stage, the user is ready to specify the loaded areas for the problem to be solved. Each area is defined by its extent in each of the x- and y-directions (global coordinates) and the pressure intensity acting upon it. The form of the command is as follows:

$$\text{LOADED} \left[\begin{array}{c} (\text{AREA}) < i > \left[\begin{array}{c} \left\{ \begin{array}{c} \text{IN } \left\{ \begin{array}{c} X \\ Y \end{array} \right\} (\text{DIRECTION}) \text{ FROM } < r > \text{ TO } < r > (\text{AND}) \\ \hline (\text{WITH}) \text{ PRESSURE } < r > \end{array} \right\} \end{array} \right] \end{array} \right]$$

Note that the full word LOADED must be used here to distinguish this from the following key-word.

8. LOAD

If the problem calls for load transfer between adjacent slabs, the user may use commands of the following form to specify the direction, type and other appropriate parameters for load transfer. If no load transfer is provided this group of commands may be ignored.

$$\text{LOAD} \left[\begin{array}{c} (\text{TRANSFER}) (\text{IN}) \left\{ \begin{array}{c} X \\ Y \end{array} \right\} (\text{DIRECTION}) \left\{ \begin{array}{c} (\text{AGGREGATE}) (\text{INTERLOCK}) (\text{FACTOR}) < r > \\ \left\{ \begin{array}{cc} \begin{array}{l} \text{DINX} \\ \text{DOUTX} \\ \text{DCIX} \\ \text{DEX} \\ \text{DSX} \\ \text{DJWX} \\ \text{DPRX} \\ \text{DCIX} \end{array} & \begin{array}{l} \text{DINY} \\ \text{DOUTY} \\ \text{DCIY} \\ \text{DEY} \\ \text{DSY} \\ \text{DJWY} \\ \text{DPRY} \\ \text{DCIY} \end{array} \end{array} \right\} < r > \end{array} \right\} \end{array} \right]$$

9. ITERATIVE

Associated with the stress dependent subgrade types (IST= 0 through 5) is an iterative scheme for updating K_R values and checking convergence. The user controls this iterative process through commands of the form described below. These commands may be ignored if a stress independent subgrade type is used (IST= 6 or greater).

$$\text{ITERATIVE} \left[\begin{array}{l} \text{(SCHEME)} \left\{ \begin{array}{l} \text{(NUMBER) (OF) ITERATIONS} < i > \\ \text{TOLERANCE} \left[\begin{array}{l} \text{(FOR) } \left\{ \begin{array}{l} \text{SUBGRADE (MODULUS)} < r > \\ \text{(NUMBER) (OF) NODES} < r > \end{array} \right\} \\ \text{OUTPUT (TYPE)} \left\{ \begin{array}{l} \text{FULL} \\ \text{PARTIAL} \end{array} \right\} \end{array} \right\} \end{array} \right] \end{array} \right]$$

10. SYMMETRY

Here the user specifies any symmetry conditions that may exist for the given problem. The following command form is used:

$$\text{SYMMETRY} \left[\begin{array}{l} \text{(ABOUT)} \left\{ \begin{array}{l} \text{X} \\ \text{Y} \\ \text{X AND Y} \\ \text{NONE} \end{array} \right\} \text{(AXIS)} \end{array} \right]$$

ERROR MESSAGES

The free-form subroutines in ILLI-SLAB are set up to issue diagnostic error messages before execution, in the event of improper input data. The general form of these messages is as follows:

ERROR NUMBER n DETECTED

ENTITY: entity

MODE = mode

NCHAR = nchar

NWD = nwd

ICOLMN= icolmn

PROGRAM TERMINATED

where n is the number of the error message detected, as listed in Table A.2. The meaning of the other parameters is explained below:

ENTITY is a vector which contains a left justified alphanumeric copy of the entity found within the input record that caused the error. For MODES 8, 9 and 10 ENTITY is meaningless.

MODE is an integer value indicating the type of entity found in the input record. MODES 3, 4 and 11 are not used in ILLI-SLAB. The values and meanings of MODE are:

TABLE A.2
FREE-FORM DIAGNOSTIC ERROR MESSAGES

Error No.	Explanation
1	Unidentified Statement
2	Title Is Missing
7	Number Of Loaded Areas Must Be An Integer
8	Number of Layers Must Be An Integer
12	Poisson Ratio For Top Layer Missing
14	Poisson Ratio For Bottom Layer Missing
15	Contoured Slab Number(s) Required
16	Contour Aspect Ratio Must Be A Real Number
17	Contour Resolution Must Be An Integer
19	Modulus of Subgrade Missing
20	Type of Subgrade Missing
21	Regression Parameter(s) Missing
22	Loaded Area Must Be Specified In x Or y Direction
23	Loaded Area Limits Must Be Specified From-To
24	Applied Pressure Value Missing
26	Number of Iterations Missing
27	Tolerance Value Missing
28	Composite Action Factor Must Be An Integer
29	Elastic Solid Poisson's Ratio Missing

MODE	TYPE OF ENTITY
1	Integer
2	Real
3	Label
4	Name
5	Anytext
6	Separator
7	String
8	End of Get String Mode
9	End of Line
10	End of File
11	Point

NCHAR is an integer variable giving the number of characters in the entity. The NCHAR count includes all blanks imbedded within a String.

NWD is an integer variable denoting the number of words required to store the entity. The number of storage locations is computed as

$$NWD = (NCHAR + NCPW - 1) / NCPW$$

where NCPW is the number of characters stored per word.

ICOLMN is an integer variable containing the starting input record column number of the current entity.

As a further tip, the user should examine the output file created until the time of the error. An echo of all the commands read and interpreted by the system will appear before the header section, and the last command echoed is the one at fault.

INPUT GUIDE FOR WESTER
A COMPENDIUM OF CLOSED-FORM SOLUTIONS FOR SLABS
ON DENSE LIQUID AND ELASTIC SOLID FOUNDATIONS

Input for each run is provided on a single line as follows:

```

-----
P  PRES  E  PR  SM  H  ES  PRS  FB
-----
  *
-----

```

where:

P : total load (lbs);

PRES : applied pressure (psi);

E : slab modulus (psi);

PR : slab Poisson's ratio;

SM : subgrade modulus, for dense liquid (psi/in.);

H : slab thickness (in.);

ES : soil Young's modulus, for elastic solid (psi);

PRS : soil Poisson's ratio, for elastic solid;

FB : slab flexural strength, for ultimate capacity (psi).

The data items may be provided in any desired format (ie. integer, real, exponential, etc.) and must be separated by one or more blanks from each other.

Data items ES and PRS are used for elastic solid calculations and are optional. The number zero (0), however, must be entered in a line where an optional item is not provided. The default value for PRS is 0.4.

Data item FB is used for ultimate load capacity calculations and is also optional. Again, the number zero (0) must be entered in a line where this optional item is not provided. The default value for FB is 700.

Multiple runs may be performed at a single execution of the program. To do this, simply add extra lines as necessary in the format described above, to the input file. To indicate end-of-file, the last line of every input file must read:

```
-----  
99.99 0 0 0 0 0 0 0 0  
-----
```


INPUT GUIDE FOR CFES
ANALYSIS OF AXISYMMETRIC SLABS OF FINITE EXTENT
ON ELASTIC SOLID FOUNDATION

Input for each run is provided on a single line as follows:

```

-----
PRES ESLAB POISLAB ESOIL POISOIL THIKNS RADTOT RLA NLOAD NUNLOAD
-----
*
-----

```

where:

PRES : applied pressure (psi);
 ESLAB : slab modulus (psi);
 POISLAB : slab Poisson's ratio;
 ESOIL : soil Young's modulus (psi);
 POISOIL : soil Poisson's ratio;
 THIKNS : slab thickness (in.);
 RADTOT : radius of slab (in.);
 RLA : radius of loaded area (in.);
 NLOAD : number of loaded elements;
 NUNLOAD : number of unloaded elements.

The data items may be provided in any desired format (ie. integer, real, exponential, etc.) and must be separated by one or more blanks from each other.

All NUNLOAD unloaded elements are of the same size (ie. ring width). All NLOAD loaded elements are also of the same size, except the central core whose radius is half this size. In general, the size of loaded elements is made smaller than that of the unloaded elements.

Multiple runs may be performed at a single execution of the program. To do this, simply add extra lines as necessary in the format described above, to the input file. To indicate end-of-file, the last line of every input file must read:

```
-----  
99.99 0 0 0 0 0 0 0 0 0 0  
-----
```

INPUT GUIDE FOR H51ES
COMPUTERIZED CHART FOR EDGE STRESS CALCULATION
SEMI-INFINITE SLAB ON DENSE LIQUID OR ELASTIC SOLID

Card No. 1.

 ICM(I),I=1,10

10A6

ICM(I),I=1,10 : A 60-character alphanumeric string giving the
 problem description. This will be printed at the top
 of each output page.

Card No. 2.

 XK G P A XNOH XNOG E XMU

8F10.0

XK : modulus of subgrade reaction (psi/in.) for dense
 liquid. Set XK=-1.0 when elastic solid is used;

G : gear load (lbs);
 P : inflation pressure (psi);
 A : tire contact area (sq. in.);
 XNOH : number of thickness values to be considered (≤ 10);
 XNOG : number of gear positions, rotated with respect to the
 slab edge, to be considered (≤ 10);
 E : slab Young's modulus (psi);
 XMU : slab Poisson's ratio;

Note: When P is given, A is calculated and vice-versa. The value not given should be set to 0.0. Only doubly symmetrical gears can be handled by H51ES.

Card No. 3 (Read Only if XK=-1.0).

 ES XMUS

2F10.0

ES : Elastic modulus for subgrade (psi);
 XMUS : Poisson's ratio for subgrade.

Card No. 4.

XLA XLB XLC XLD XNOD XNOSG

6F10.0

XLA, XLB, XLC, XLD : spacing between tires (a, b, c, d in Fig. A.1);

XNOD : number of positions of gear, translated with respect to the point at which the stress is to be calculated (≤ 10);

XNOSG : number of pairs of stress and gear load for which required thickness is to be calculated (≤ 10).

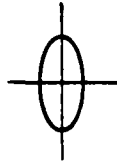
Card No. 5.

XNA XNB XNC XND PHIE

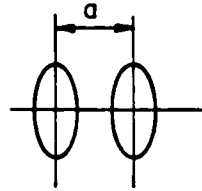
5F10.0

XNA, XNB, XNC, XND : variables describing gear geometry (n_a , n_b , n_c , n_d in Fig. A.1);

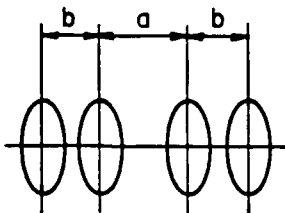
PHIE : ratio of major to minor axis of elliptical tire print(s). The default value is PHIE=5/3.

SINGLE WHEEL

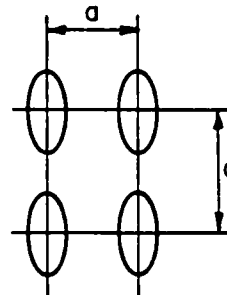
$a = 0$ $n_a = 1$
 $b = 0$ $n_b = 1$
 $c = 0$ $n_c = 1$
 $d = 0$ $n_d = 1$

TWIN

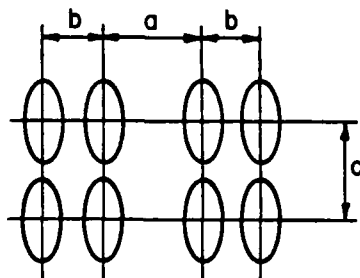
a Shown $n_a = 2$
 $b = 0$ $n_b = 1$
 $c = 0$ $n_c = 1$
 $d = 0$ $n_d = 1$

DUAL TWIN

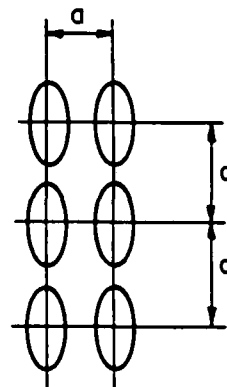
a Shown $n_a = 2$
 b Shown $n_b = 2$
 $c = 0$ $n_c = 1$
 $d = 0$ $n_d = 1$

TWIN TANDEM

a Shown $n_a = 2$
 $b = 0$ $n_b = 1$
 c Shown $n_c = 2$
 $d = 0$ $n_d = 1$

DUAL TWIN TANDEM

a Shown $n_a = 2$
 b Shown $n_b = 2$
 c Shown $n_c = 2$
 $d = 0$ $n_d = 1$

TRIPLE TWIN TANDEM

a Shown $n_a = 2$
 $b = 0$ $n_b = 1$
 c Shown $n_c = 3$
 $d = 0$ $n_d = 1$

Fig. A.1 Definition of Typical Gears

Note:

GEAR FORWARD VIEW: There are n_a groups of tires, spaced a in. apart. Each group has n_b tires, spaced b in. apart.

GEAR SIDE VIEW: There are n_c groups of tires, spaced c in. apart. Each group has n_d tires, spaced d in. apart.

Card No. 6.

```

-----
B   XOP3   BIGX   BIGY   XOP6
-----
F10.0
-----

```

B : number of points used to approximate tire prints;

XOP3 : print option:

= 1.0, if block counts for each wheel are to be printed;

= 0.0, if only the total count for entire gear is to be printed;

BIGX, BIGY : coordinates locating the point at which stress is to be calculated (X,Y in Fig. A.2). These may be used in the "Optional" Method of gear description instead of DELTA;

XOP6 : control specifying the use of BIGX, BIGY or DELTA:

= 1.0, if BIGX, BIGY and GAMMA are used;

= 0.0, if DELTA and GAMMA are used.

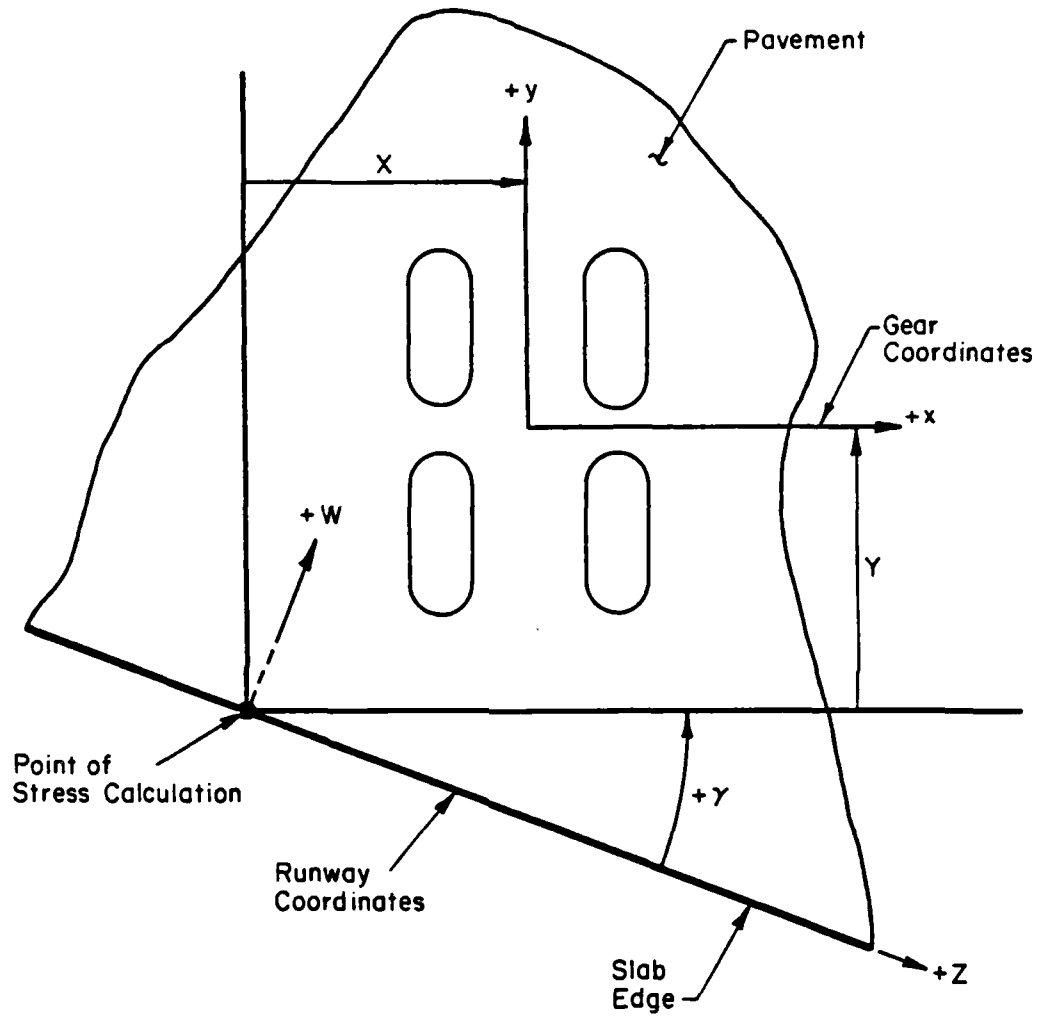


Fig. A.2 Description of Gear - Runway Geometry
("Optional" Method)

Note: X, Y, and GAMMA give the horizontal, vertical and rotational displacements of runway coordinates (Z,W) from gear coordinates (x,y). In Fig. A.2, $X < 0$, $Y < 0$; GAMMA must be between 0 and 90 degrees. The origin of gear coordinates (x,y) is located at the intersection of the two lines of symmetry of the gear.

Card No. 7.

H(I), I=1, XNOH

10F6.0

H(I), I=1, XNOH : thickness of slab (≤ 10). XNOH values must be provided, in inches.

Card No. 8 (Read Only if XNOG is not 0).

GAMMA(I), I=1, XNOG

10F6.0

GAMMA(I), I=1, XNOG : position of gear, rotated with respect to the slab edge (≤ 10). XNOG values must be provided, in

degrees (γ in Figures A.2 and A.3).

Note: GAMMA is measured anticlockwise from the slab edge to the horizontal centerline of the gear (perpendicular to the forward application).

Card No. 9 (Read Only if XNOD is not 0).

 DELTA(I), I=1, XNOD

10F6.0

DELTA(I), I=1, XNOD : position of gear, translated with respect
 to the point at which stress is to be calculated (≤ 10).
 XNOD values must be provided, in inches (Δ in Fig.A.3).

Note: DELTA is measured from the origin in the +Z direction along the slab edge to:

(a) If GAMMA=0°: The projection of the center of the tire in the last row, and column -1;

(b) If GAMMA \neq 0°: The projection of the center of the tire that is on the extreme left and tangent to the edge.

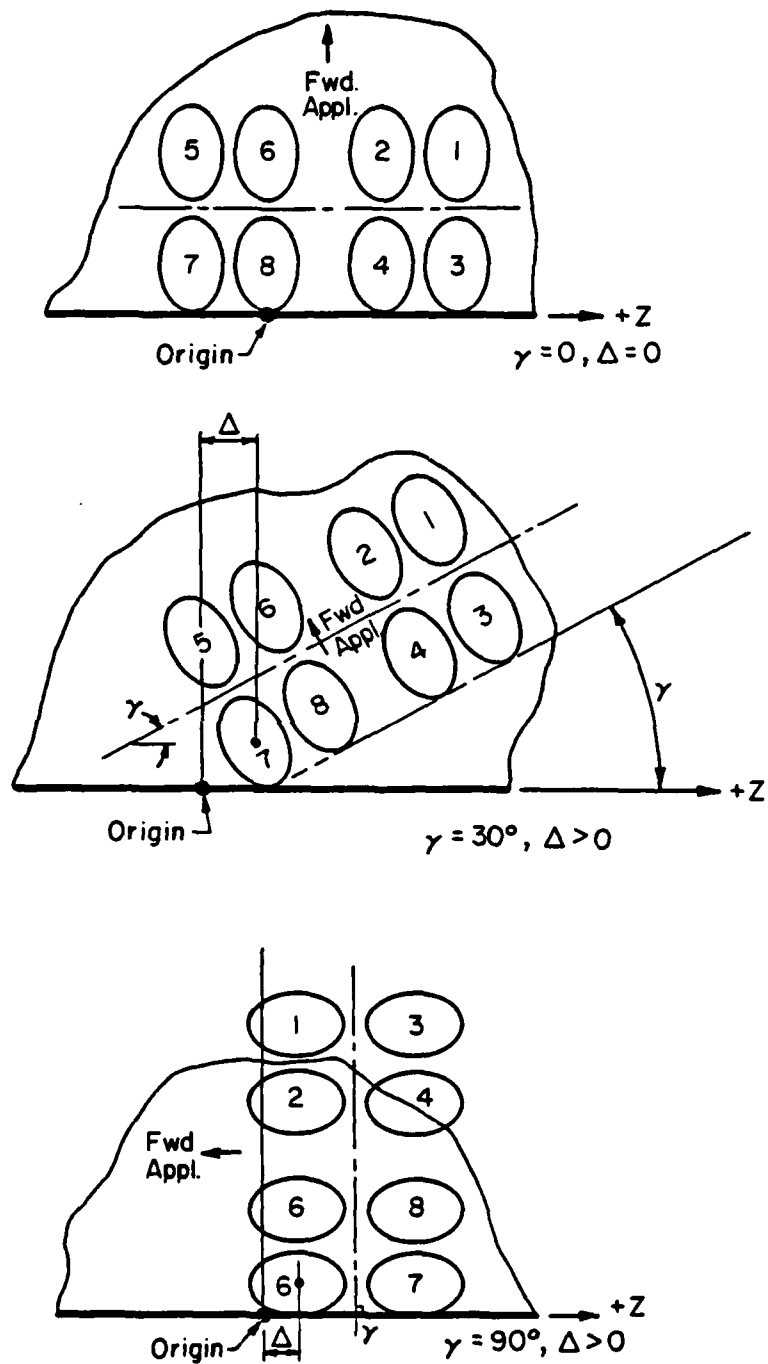


Fig. A.3 Description of Gear - Runway Geometry ("Normal" Method)

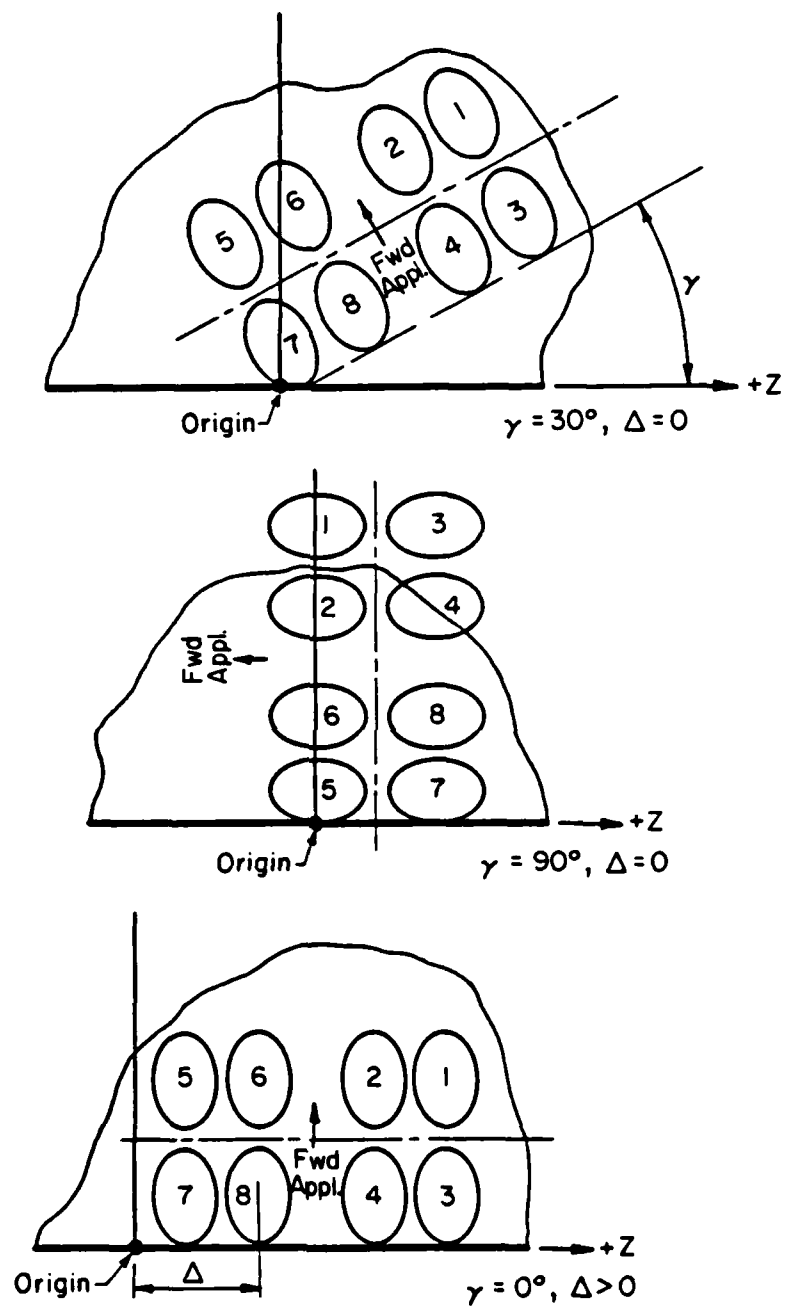


Fig. A.3 (continued)

Card No. 10 (Read Only if XNOSG is not 0; read XNOSG times).

ASIG(I), AG(I), I=1,NOSG

2F10.0

ASIG(I) : prescribed stress for which required thickness is to
be calculated (psi);

AG(I) : prescribed gear load for which required thickness is to
be calculated (lbs).

INPUT GUIDE FOR FIDIES
ANALYSIS OF RECTANGULAR SLABS ON ELASTIC SOLID FOUNDATION
USING THE METHOD OF FINITE DIFFERENCES

Card No. 1.

TITLE

8A10

TITLE : An 80-column string of alphanumeric characters used to
idenfity the problem. This title will appear on the
first page of the output.

Card No. 2.

E PR H ES PRS

5F10.3

E : slab modulus (psi);
PR : slab Poisson's ratio;

H : slab thickness (in.);
ES : soil Young's modulus (psi);
PRS : soil Poisson's ratio (psi).

Card No. 3.

DELTA	NX	NY	NLOAD
F10.3	3	15	

DELTA : finite difference increment in x- and y-direction;
NX : number of elements in x-direction;
NY : number of elements in y-direction;
NLOAD : number of applied loads (global coordinates).

Card No. 4 (Read NLOAD times).

PRES	XX1	XX2	YY1	YY2
5F10.3				

PRES : applied pressure (psi);
XX1, XX2 : lower and upper limits of the loaded area in

x-direction, in global coordinate system;

YY1, YY2 : lower and upper limits of the loaded area in
y-direction, in global coordinate system;

Notes on FIDIES Output:

(a) Sign Convention:

Deflection: Downward is positive;

Bending Stress: Tension is positive (at bottom of slab);

Subgrade Stress: Compression is positive.

(b) Element numbering proceeds from bottom to top, and from left to
right.

APPENDIX B

FINITE ELEMENT MESHES USED

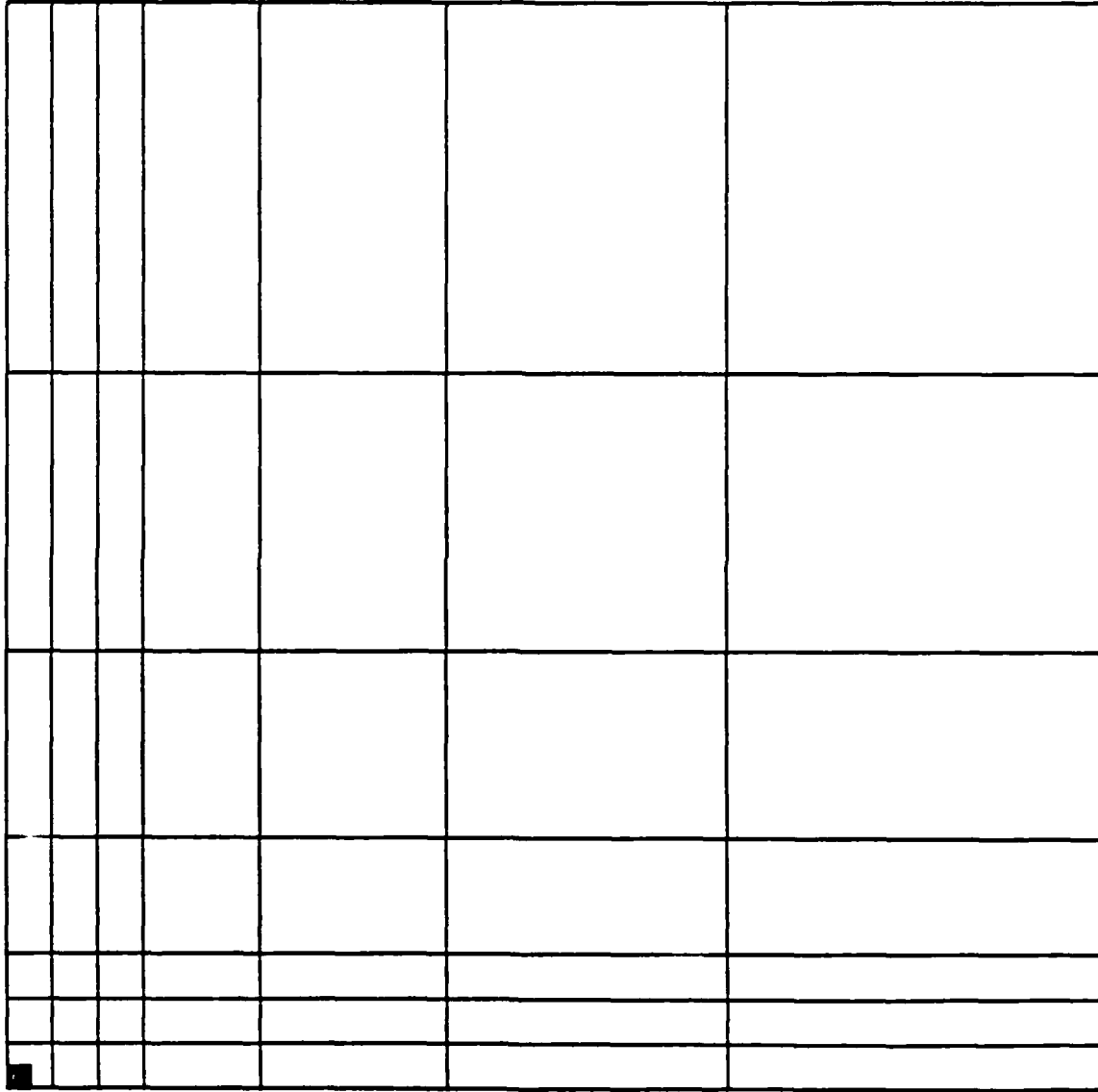


Fig. B.1 Finite Element Mesh II (Corner Loading)

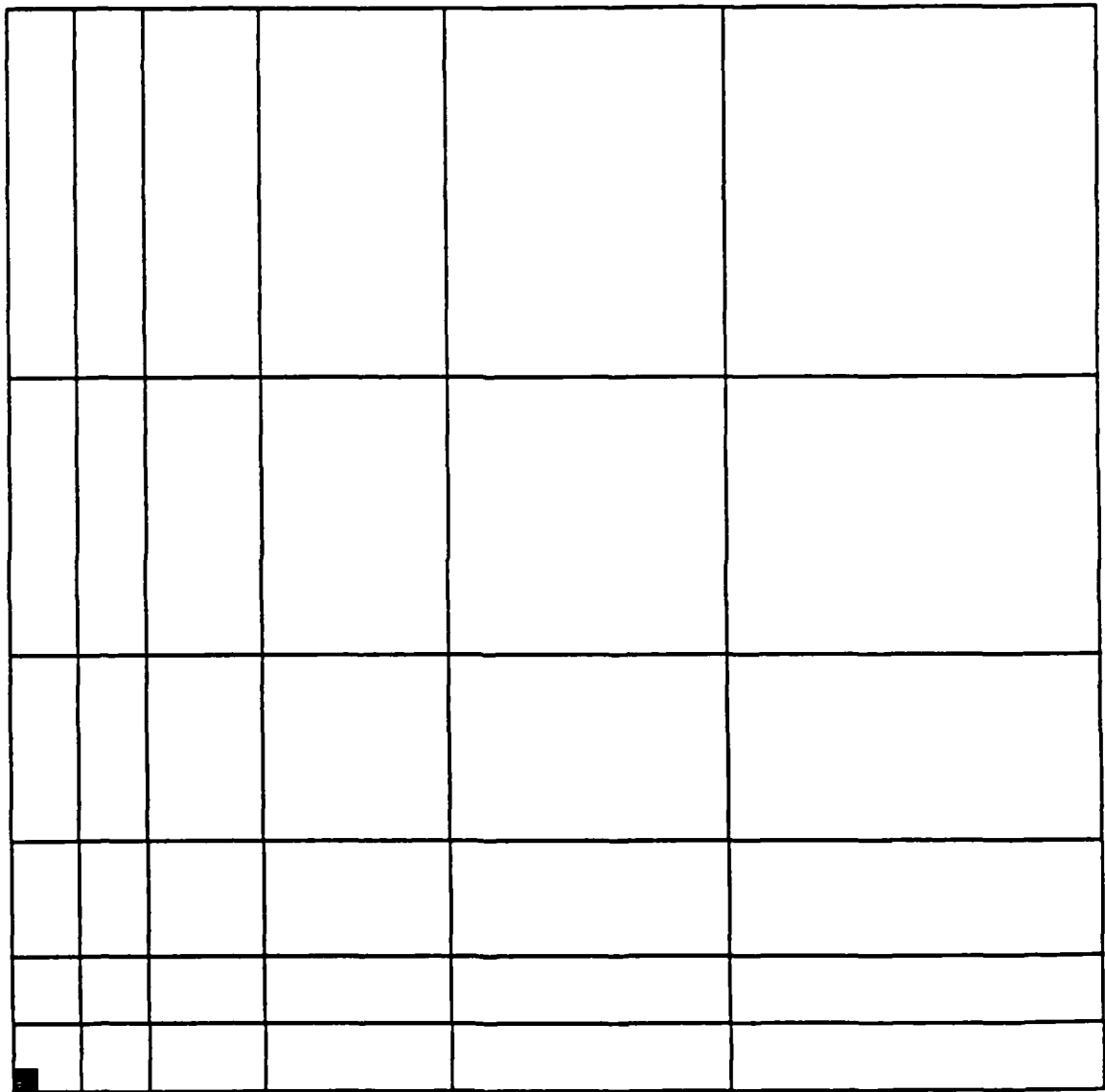


Fig. B.2 Finite Element Mesh III (Corner Loading)

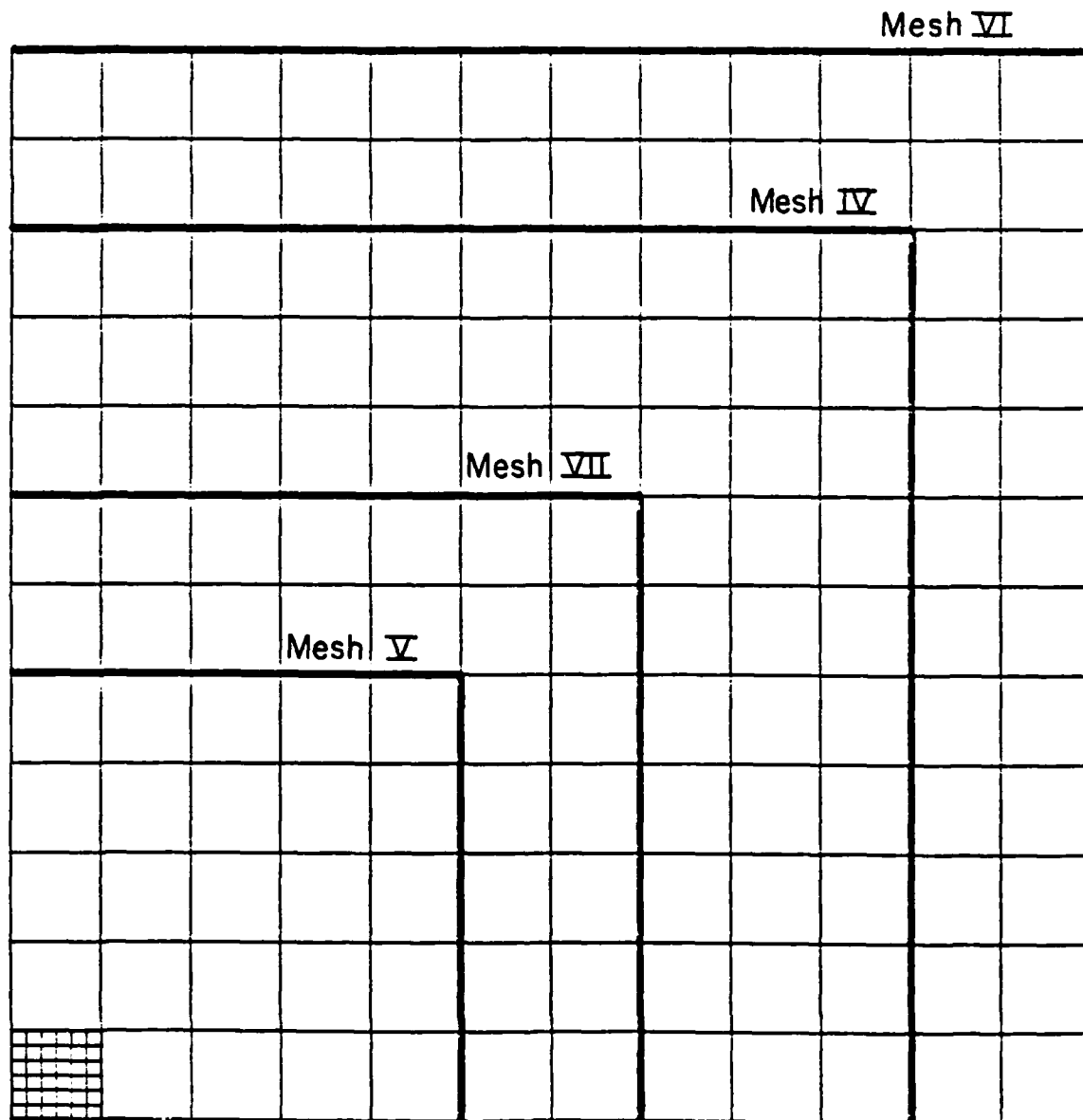


Fig. B.3 Finite Element Meshes IV, V, VI, VII (Corner Loading)

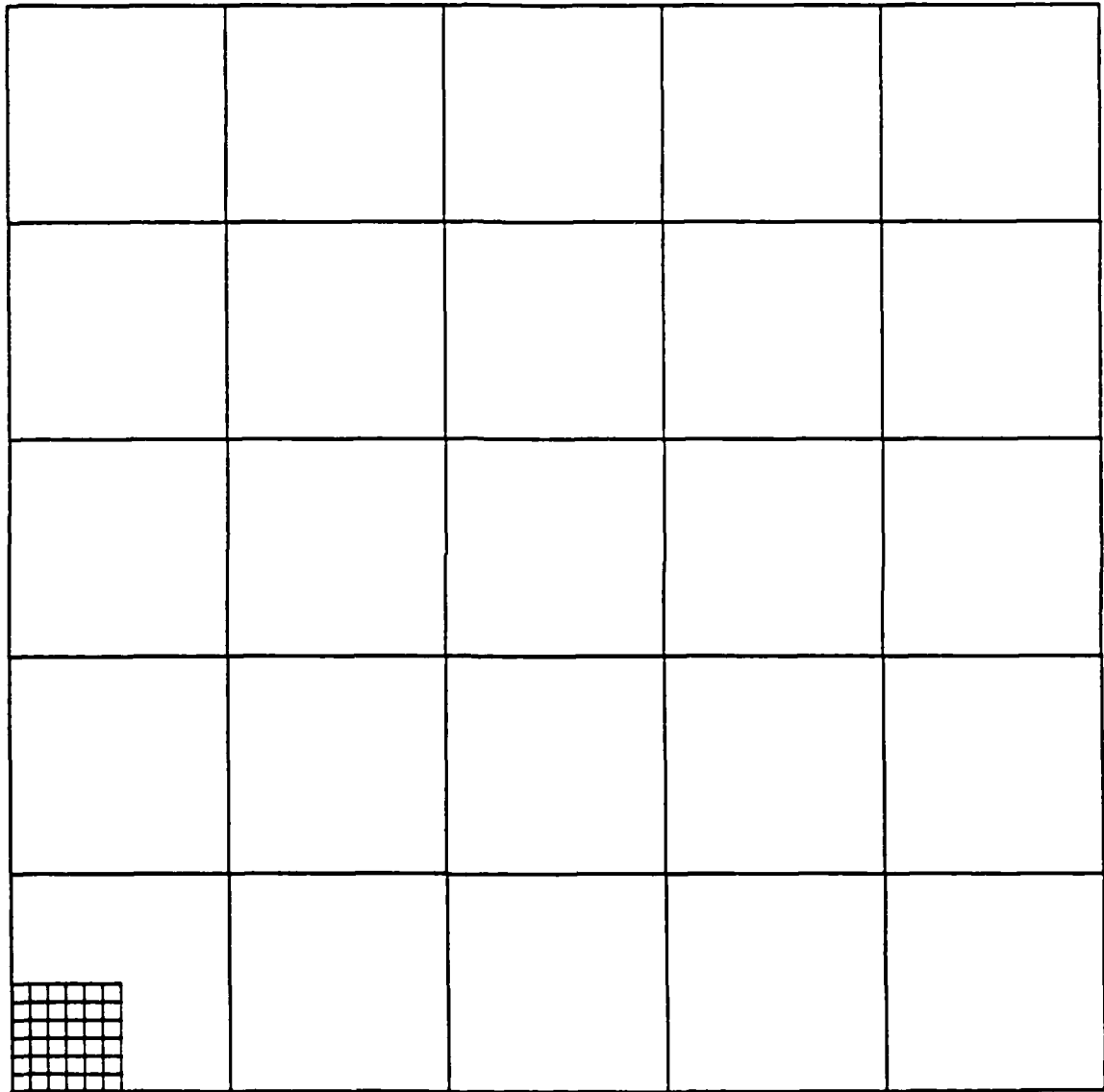


Fig. B.4 Finite Element Mesh VIII (Corner Loading)

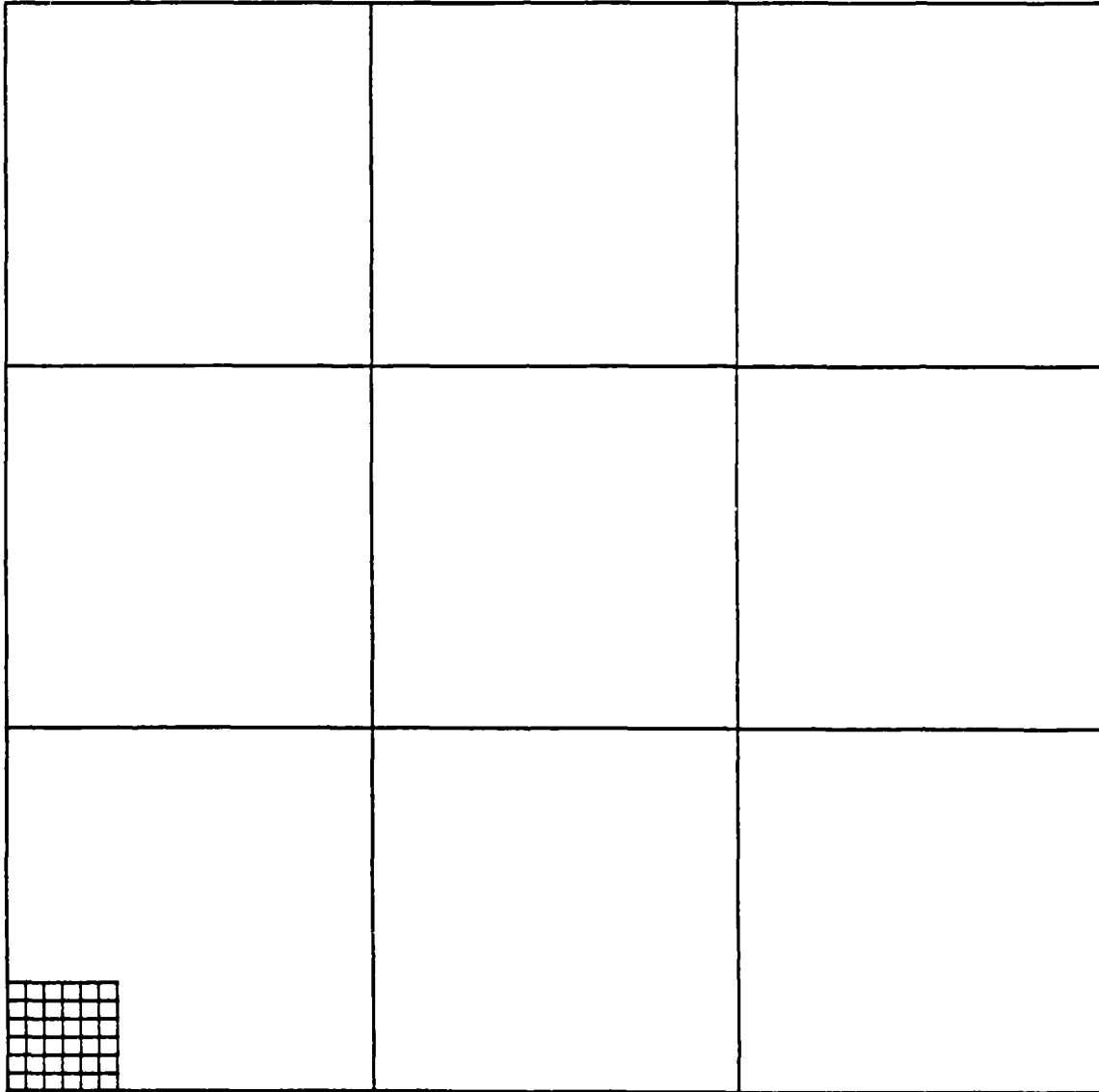


Fig. B.5 Finite Element Mesh IX (Corner Loading)

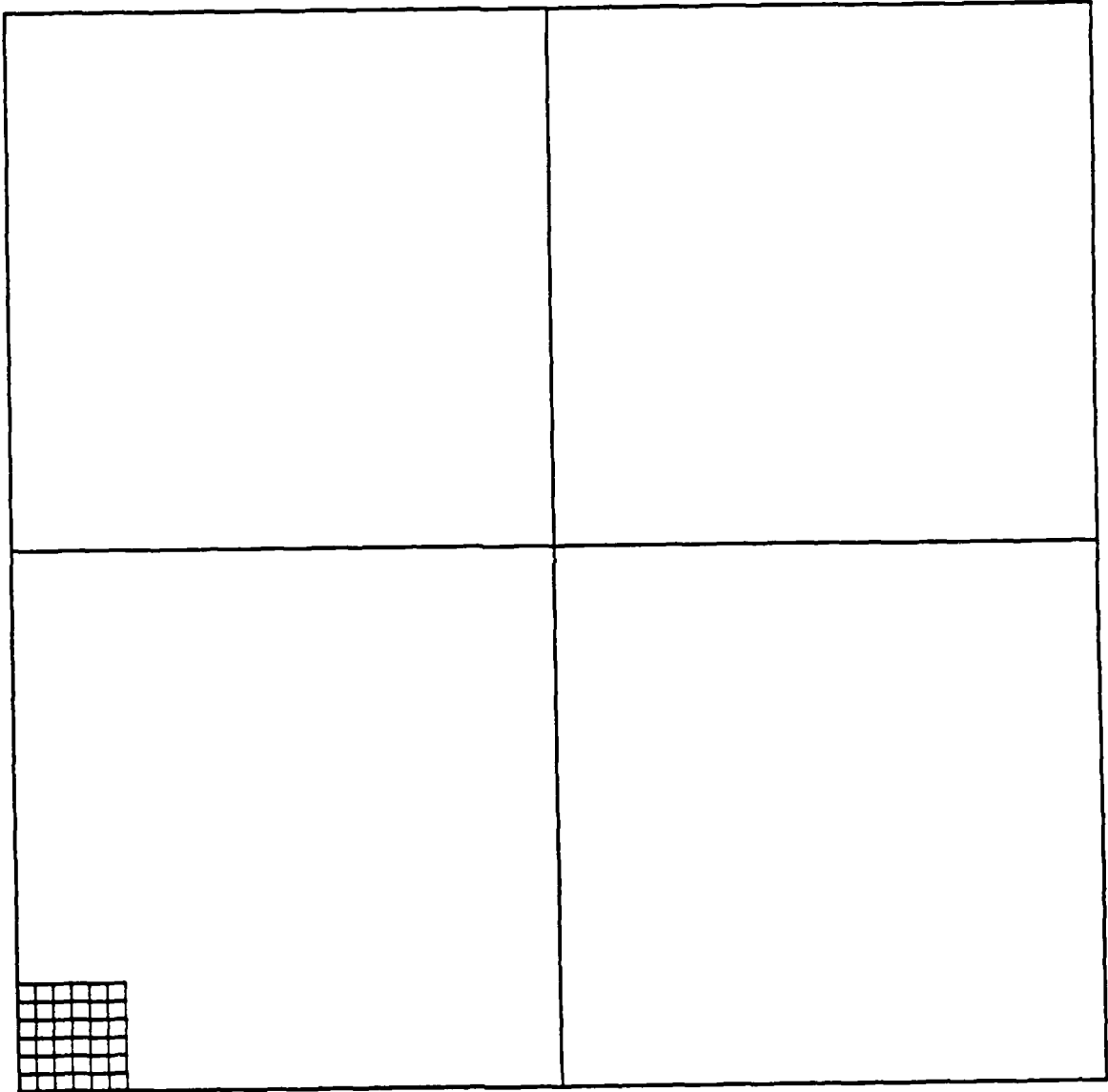


Fig. B.6 Finite Element Mesh X (Corner Loading)

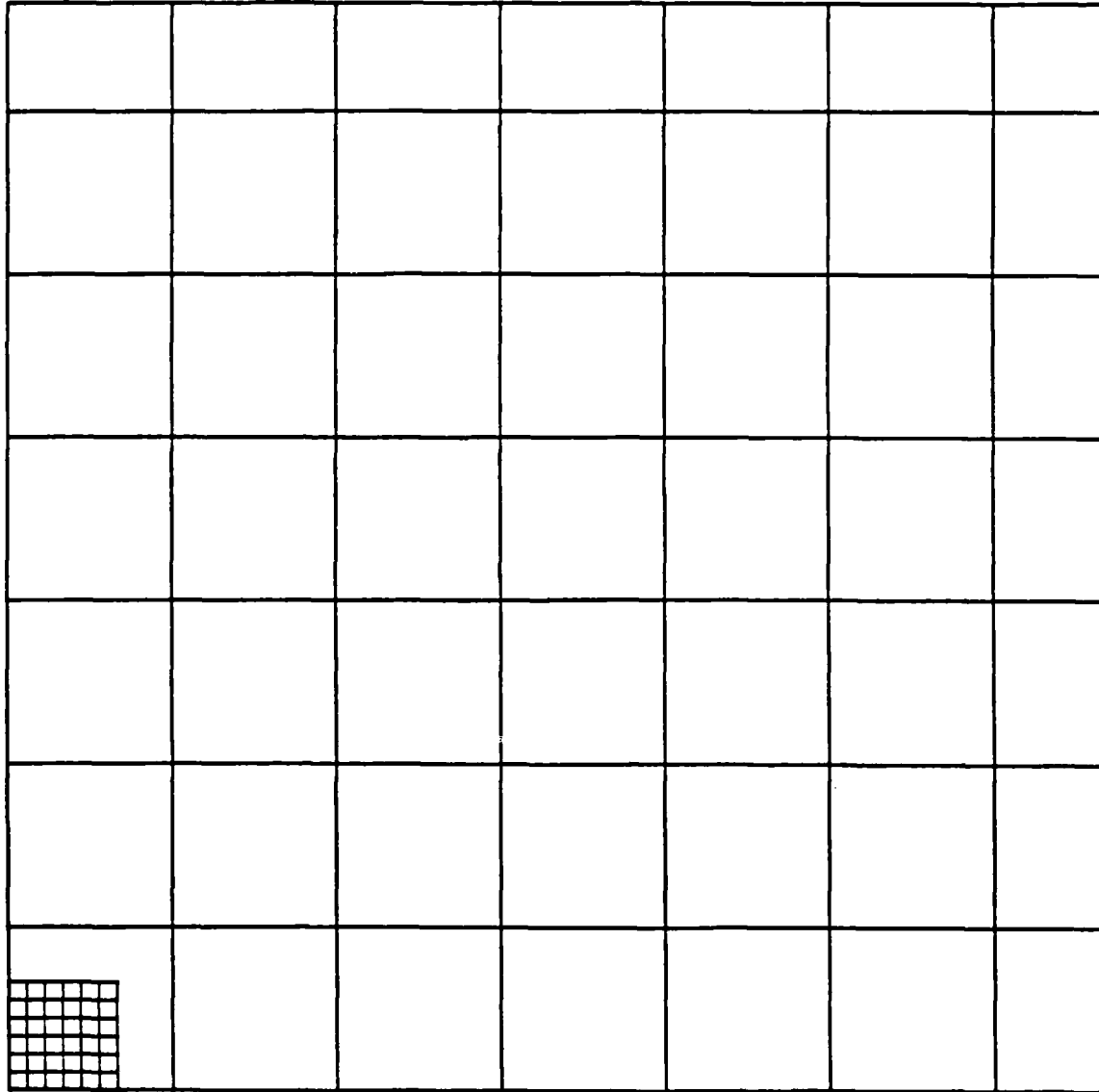


Fig. B.7 Finite Element Mesh XI (Corner Loading)

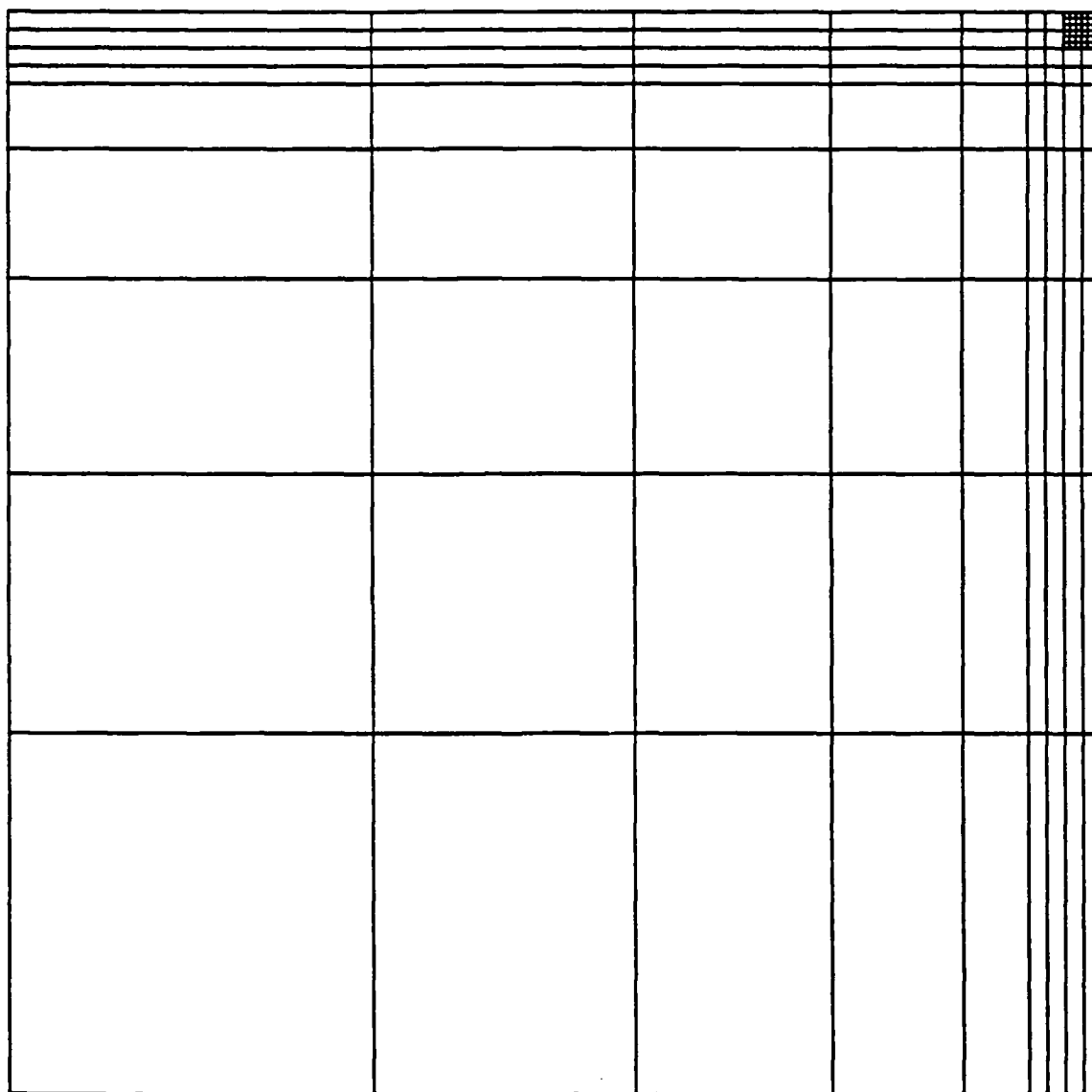


Fig. B.8 Finite Element Mesh XII (Corner Loading)

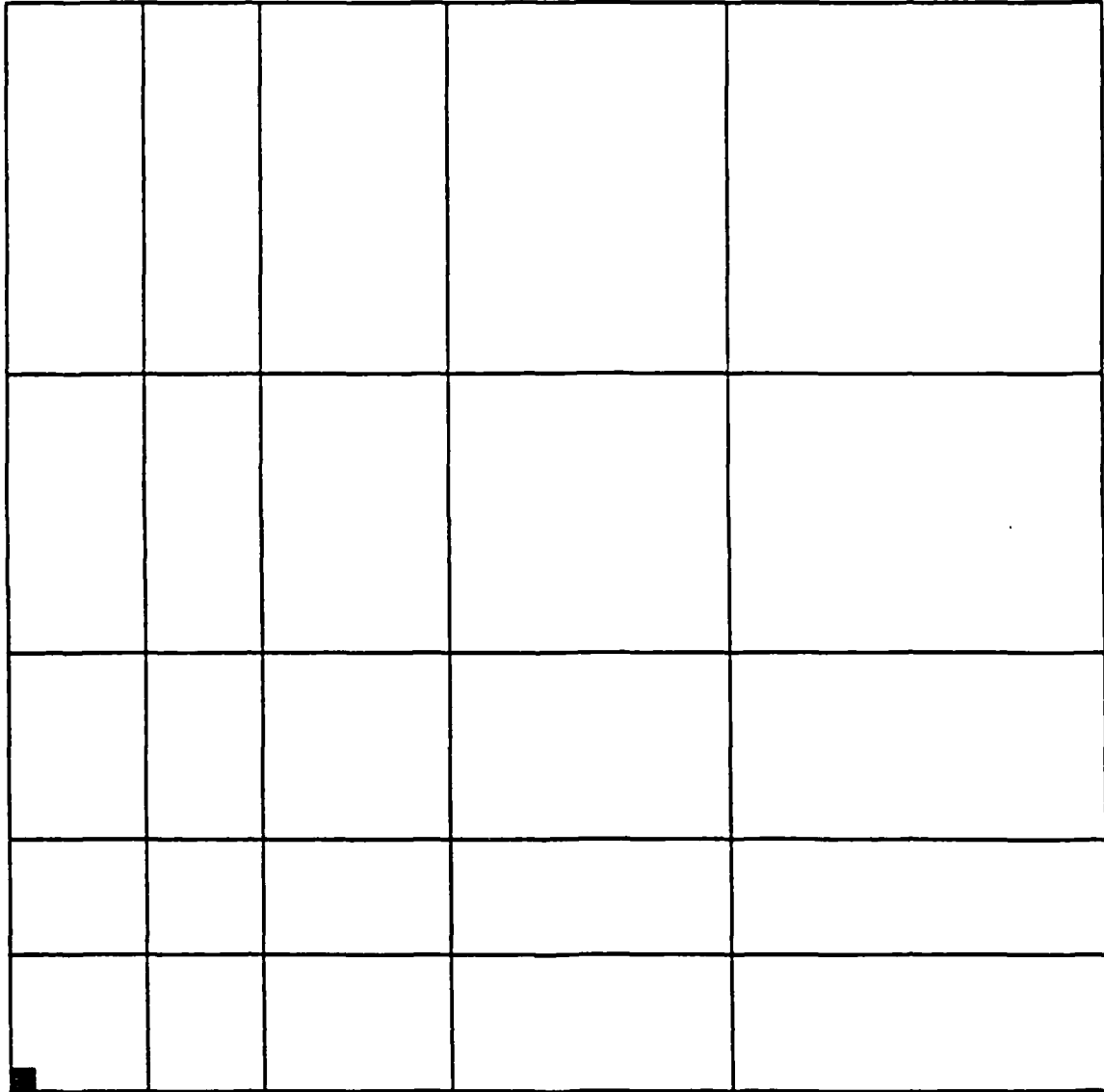


Fig. B.9 Finite Element Mesh XIII (Corner Loading)

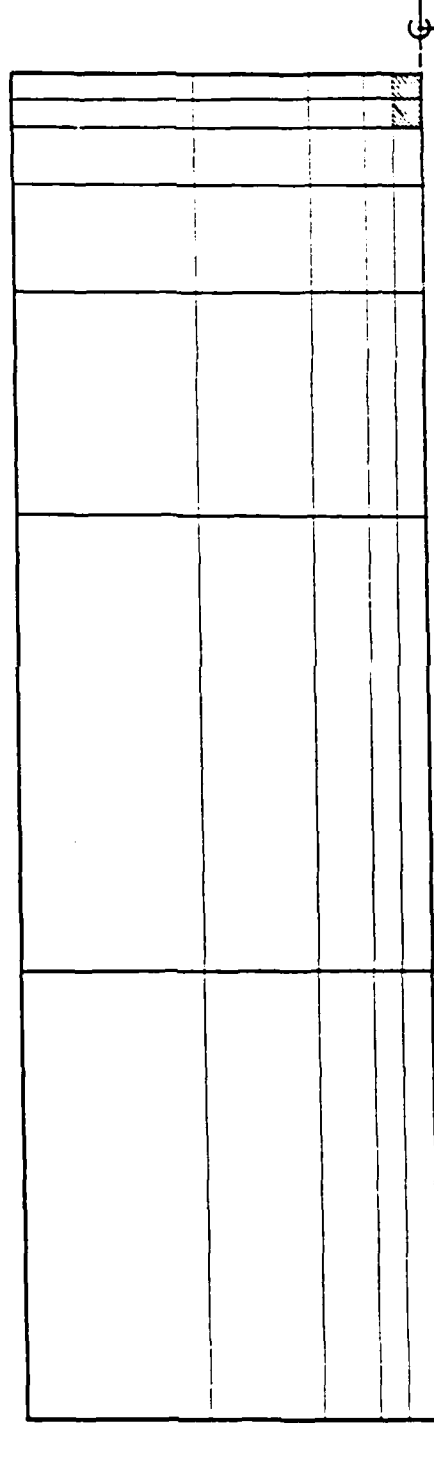


Fig. B.10 Mesh for Highway Load at Edge of PCC Pavement

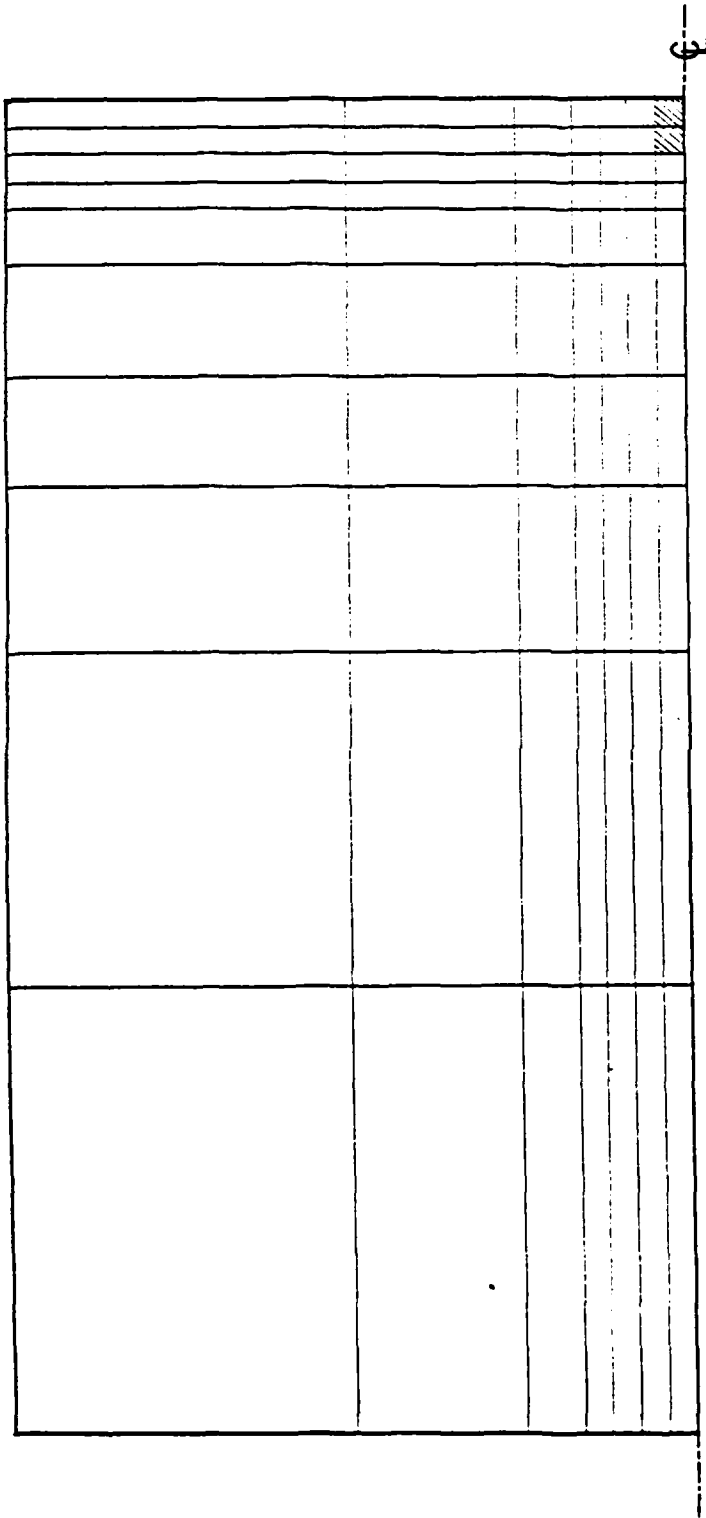


Fig. B.11 Mesh for F-4 at Edge of PCC Pavement

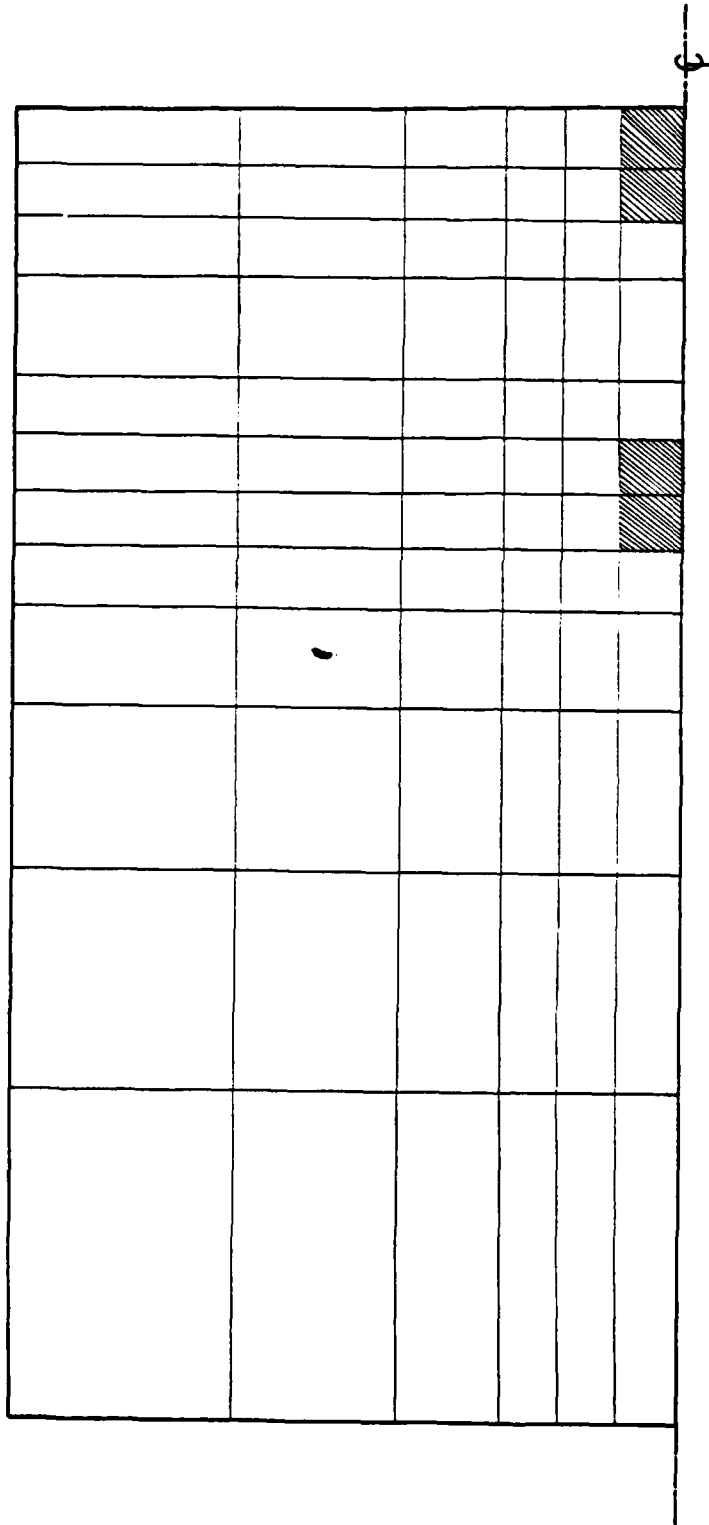


Fig. B.12 Mesh for C-130 at Edge of PCC Pavement

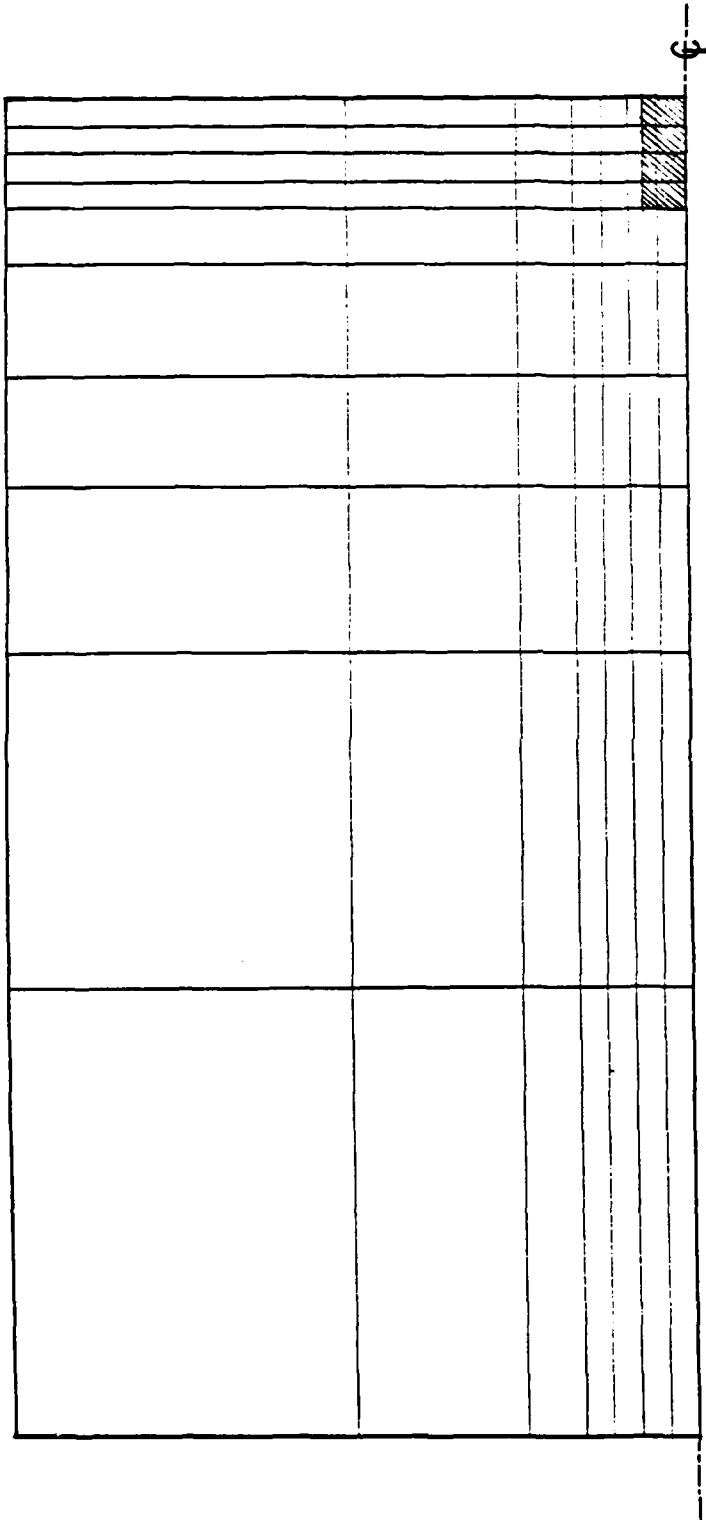


Fig. B.13 Mesh for F-111 at Edge of PCC Pavement

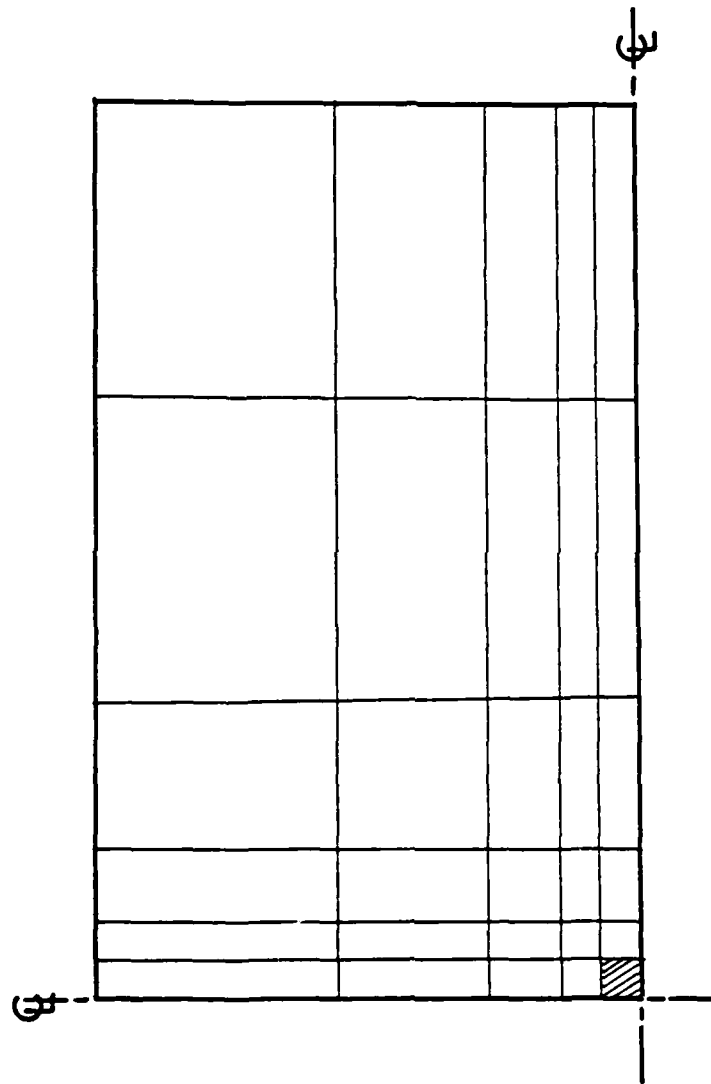


Fig. B.14 Mesh for Highway Load at Interior
of PCC Pavement

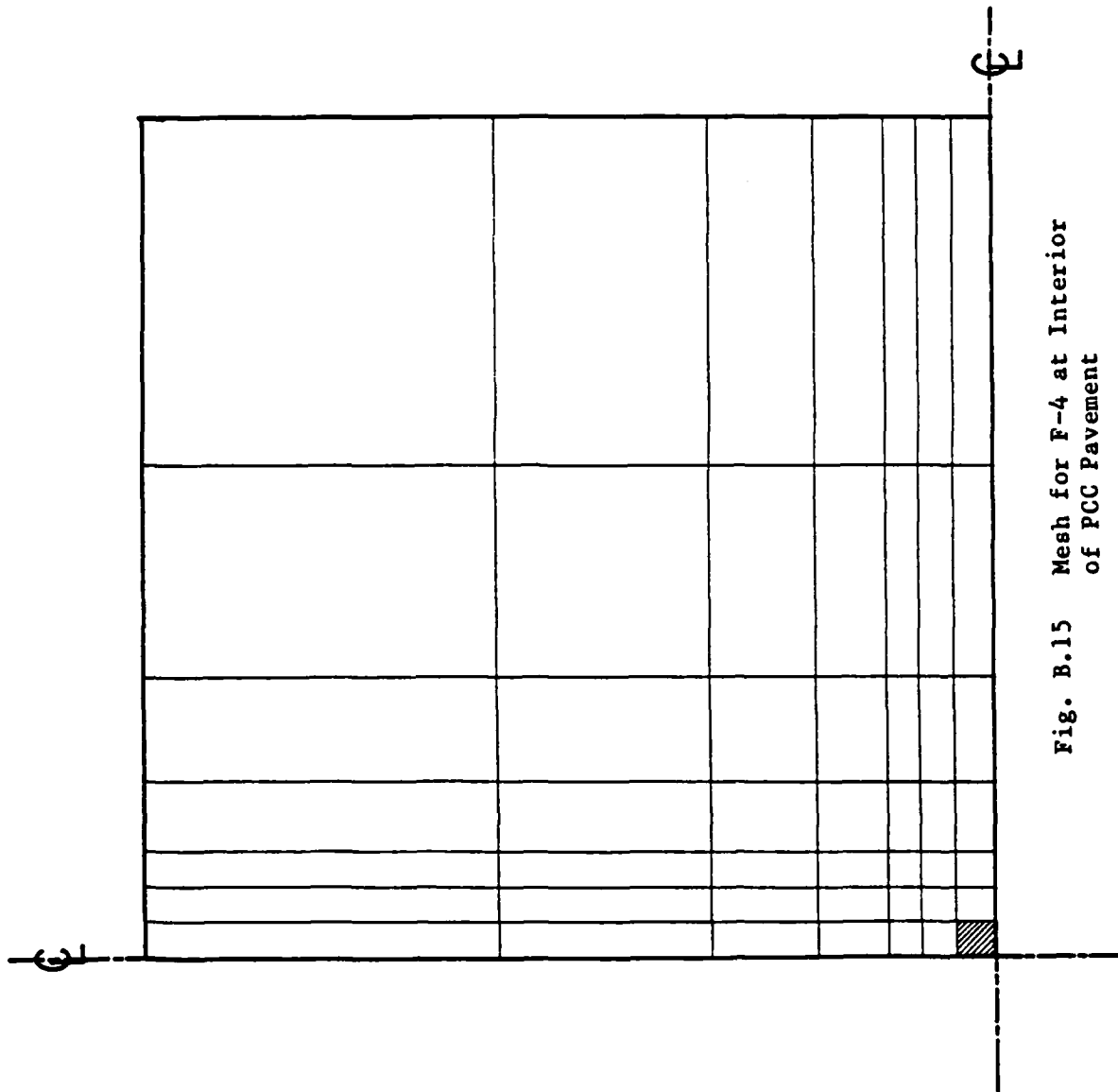


Fig. B.15 Mesh for F-4 at Interior
of PCC Pavement

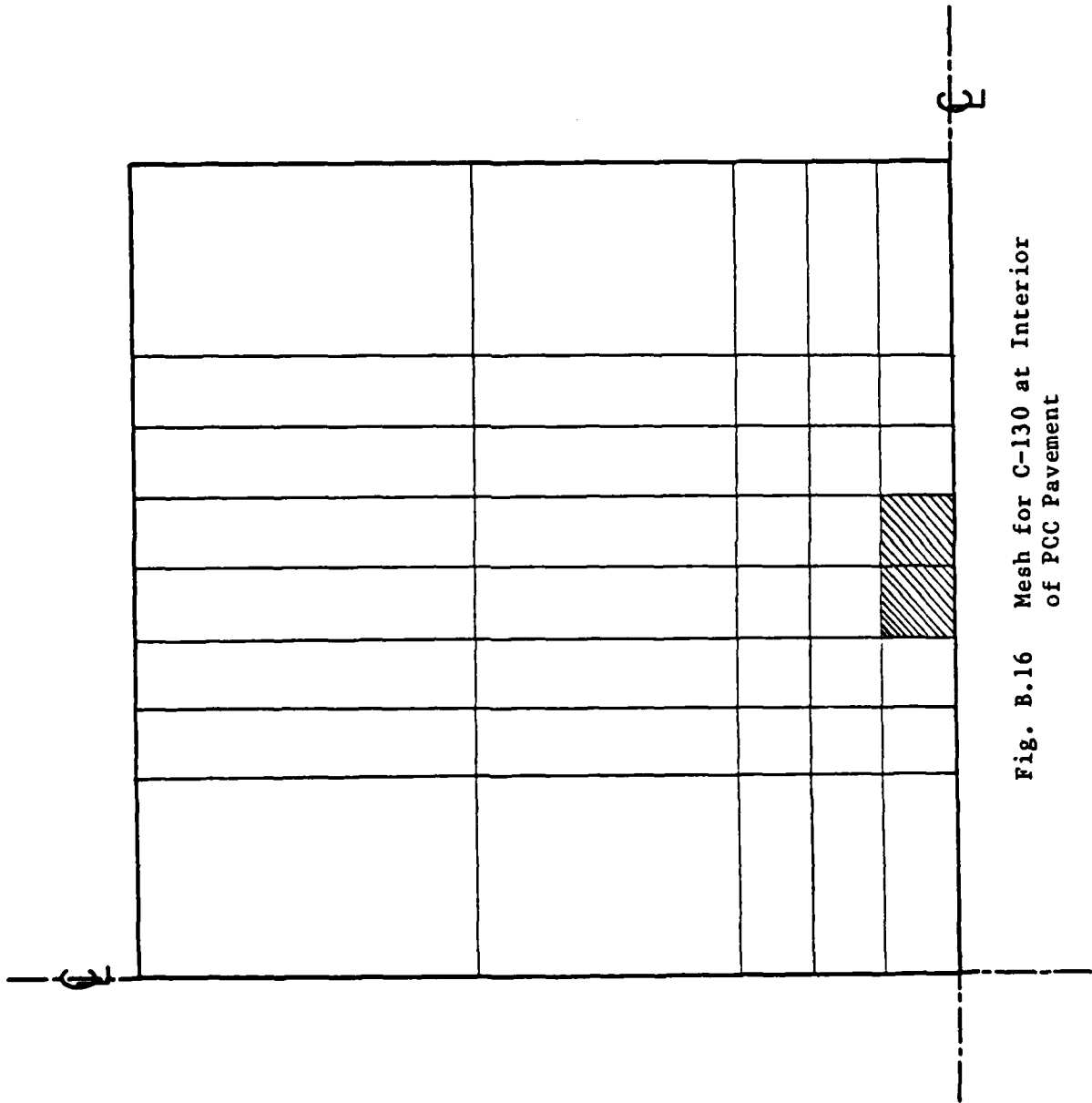


Fig. B.16 Mesh for C-130 at Interior
of PCC Pavement

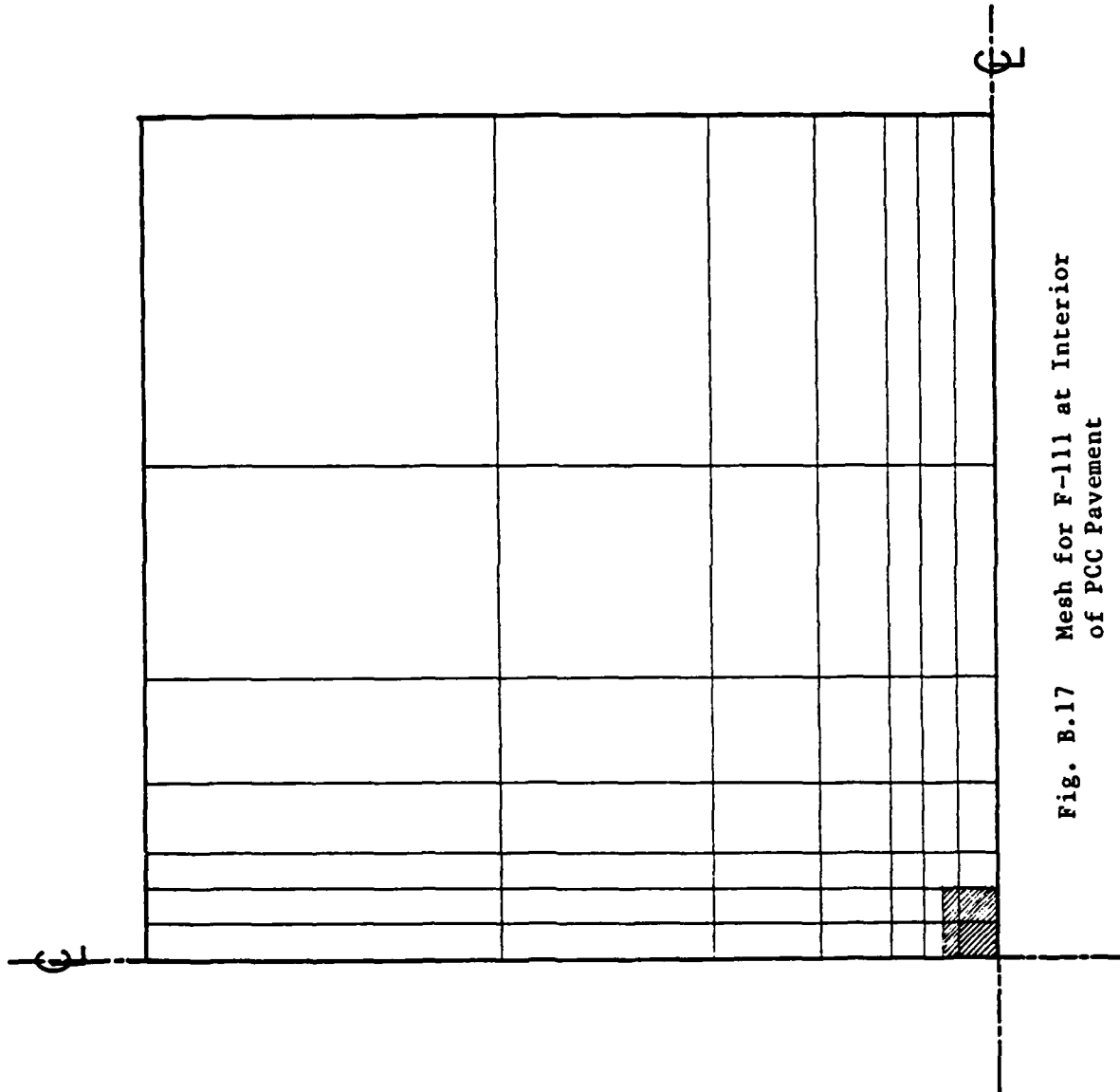


Fig. B.17 Mesh for F-111 at Interior
of PCC Pavement

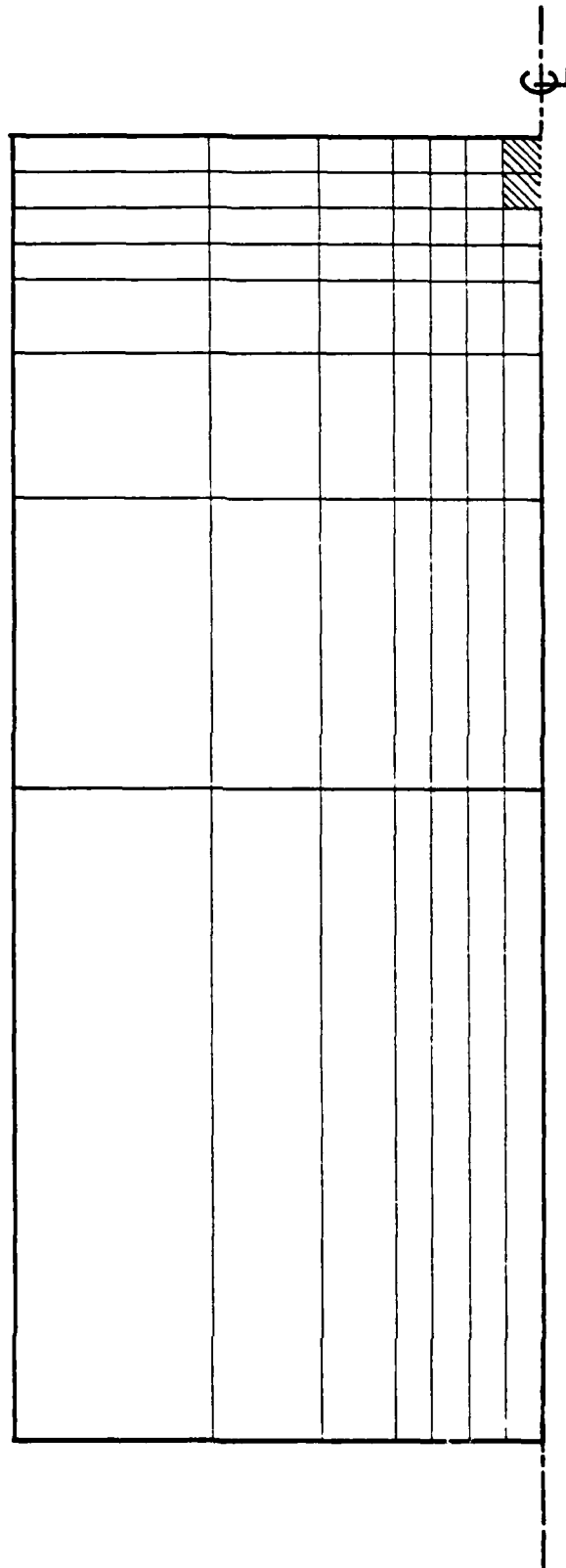


Fig. B.18 Mesh for F-4 at Edge of ALRS Pavement

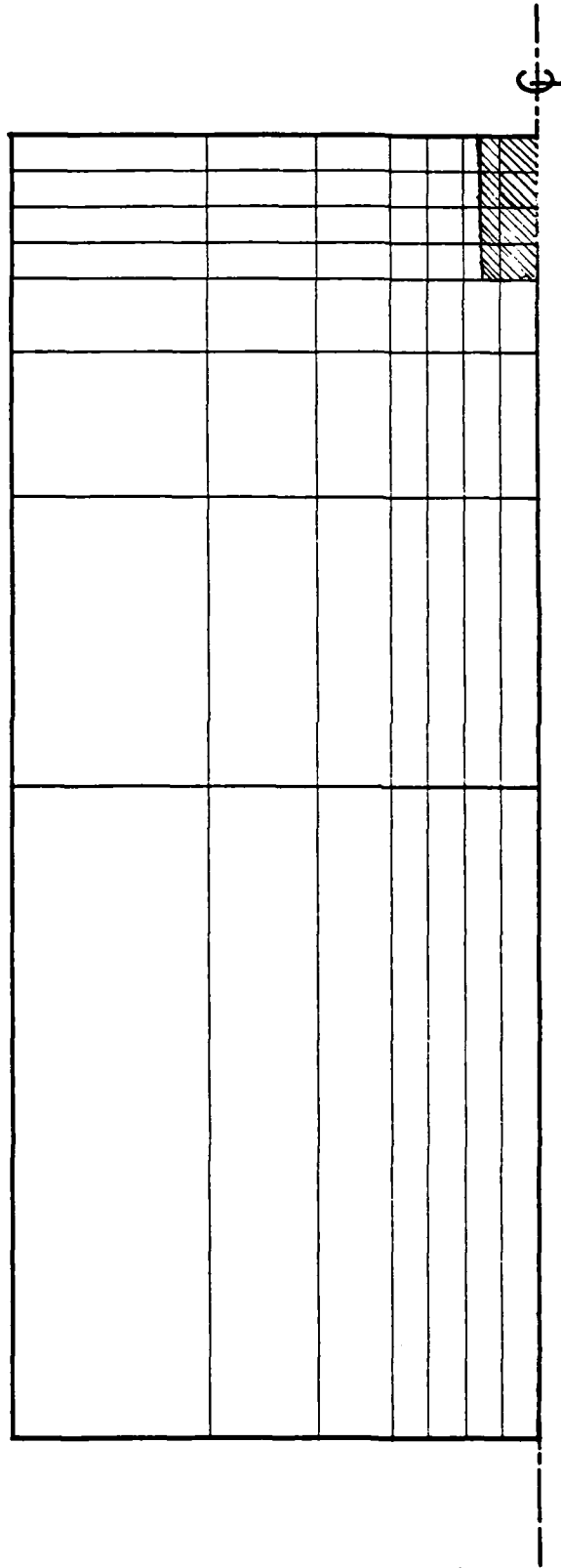


Fig. B.20 Mesh for F-111 at Edge of ALRS Pavement

REFERENCES

1. Winkler, E., "Die Lehre von der Elastizitat und Festigkeit," (The Theory of Elasticity and Stiffness), H. Dominicus, Prague, 1867.
2. Vlasov, V.Z., and Leont'ev, N.N., "Beams, Plates and Shells on Elastic Foundations," translated from the Russian (date of original: 1960), NASA-NSF, NASA TT F-357, TT 65-50135, Israel Program for Scientific Translations, 1966.
3. Selvadurai, A.P.S., "Elastic Analysis of Soil-Foundation Interaction," Developments in Geotechnical Engineering, Vol. 17, Elsevier, 1979.
4. Hertz, H., "Uber das Gleichgewicht schwimmender elastischer Platten," (On the Equilibrium of Floating Elastic Plates), Annalen der Physik und Chemie, Vol. 22, Wiedemann's, 1884.
5. Zimmermann, H., "Die Berechnung des Eisenbahnoberbaues," (Calculation of the Upper Construction Surface for Railway Tracks), Ernst und Korn Verlag, Berlin, 1888; Second Edition: 1930.
6. Schleicher, F., "Kreisplatten auf Elastischer Unterlage," (Circular Plates on Elastic Foundations), Julius Springer, Berlin, 1926.
7. Hetenyi, M., "Beams on Elastic Foundation Theory with Applications in the Fields of Civil and Mechanical Engineering," University of Michigan Press, Ann Arbor, 1946.
8. Westergaard, H.M., "Stresses in Concrete Pavements Computed by Theoretical Analysis," Public Roads, Vol. 7, No. 2, April, 1926. Also in Highway Research Board, Proceedings, 5th Annual Meeting (1925, published 1926), Part I, under title "Computation of Stresses in Concrete Roads."
9. Westergaard, H.M., "Analytical Tools for Judging Results of Structural Tests of Concrete Pavements," Public Roads, Vol. 14, No. 10, December, 1933.
10. Westergaard, H.M., "New Formulas for Stresses in Concrete Pavements of Airfields," ASCE, Transactions, Vol. 113, 1948. Also in ASCE Proceedings, Vol. 73, No. 5, May, 1947.

11. Hogg, A.H.A., "Equilibrium of a Thin Plate, Symmetrically Loaded, Resting on an Elastic Foundation of Infinite Depth," The London, Edinburgh and Dublin Philosophical Magazine and Journal of Science, Series 7, Vol. 25, March, 1938.
12. Holl, D.L., "Equilibrium of a Thin Plate, Symmetrically Loaded, on a Flexible Subgrade," Iowa State College Journal of Science, Vol. 12, No. 4, July, 1938.
13. Losberg, A., "Structurally Reinforced Concrete Pavements," Doktorsavhandlingar Vid Chalmers Tekniska Hogskola, Gotesborg, Sweden, 1960.
14. Arora, M.G., and Khanna, S.K., "Numerical Analysis of Rigid Pavement Resting Over Hookean Subgrade Continuum," Numerical Methods in Geomechanics, C.S. Desai, editor, ASCE, Vol. 1, 1976.
15. Fletcher, D.Q., and Herrmann, L.R., "Elastic Foundation Representation of Continuum," Journal of the Engineering Mechanics Division, ASCE, Vol. 97, No. EM1, February, 1971.
16. Filonenko-Borodich, M.M., "Some Approximate Theories of the Elastic Foundation," (in Russian) Uchenyie Zapiski Moskovskogo Gosudarstvennogo Universiteta (Mekhanika), No. 46, USSR, 1940.
17. Filonenko-Borodich, M.M., "A Very Simple Model on an Elastic Foundation Capable of Spreading the Load," (in Russian) Sb. Tr. Mosk. Elektro. Inst. Inzh. Trans., No. 53, Transzheldorizdat, 1945.
18. Hetenyi, M., "A General Solution for the Bending of Beams on an Elastic Foundation of Arbitrary Continuity," Journal of Applied Physics, Vol. 21, 1950.
19. Pasternak, P.L., "On a New Method of Analysis of an Elastic Foundation by Means of Two Foundation Constants," (in Russian) Gosudarstvennoe Izdatelstvo Literatury po Stroitelstvu i Arkhitekture, Moscow, 1954.
20. Kerr, A.D., "Elastic and Viscoelastic Foundation Models," Journal of Applied Mechanics, Transactions, ASME, Vol. 31, No. 3, 1964.
21. Kerr, A.D., "A Study of a New Foundation Model," Acta Mechanica, Vol. 1, No. 2, 1965.
22. Reissner, E., "A Note on Deflections of Plates on a Viscoelastic Foundation," Journal of Applied Mechanics, Transactions, ASME, Vol. 25, No. 1, March, 1958.

23. Thompson, M.R. and Robnett, Q.L., "Resilient Properties of Subgrade Soils," *Transportation Engineering Journal*, ASCE, Vol. 105, No. TE1, January, 1979.
24. Hoffman, M.S. and Thompson, M.R., "Nondestructive Testing of Flexible Pavements-Field Testing Program Summary," *Civil Engineering Studies, Transportation Engineering Series No. 31*, Illinois Cooperative Highway and Transportation Research Program Series No. 188, University of Illinois at Urbana-Champaign, June, 1981.
25. Thompson, M.R., "Concepts for Developing a Nondestructive Based Asphalt Concrete Overlay Thickness Design Procedure," *Civil Engineering Studies, Transportation Engineering Series No. 34*, Illinois Cooperative Highway and Transportation Series No. 194, University of Illinois at Urbana-Champaign, June, 1982.
26. Rada, G., and Witczak, M.W., "Comprehensive Evaluation of Laboratory Resilient Moduli Results for Granular Material," *Transportation Research Record No. 810*, Transportation Research Board, 1981.
27. American Society for Testing and Materials, "Soil and Rock: Building Stones," *Annual Book of ASTM Standards*, 1982.
28. Departments of the Army, the Navy, and the Air Force, "Materials Testing," *Technical Manual No. 5-530/Navy Publication NAVFAC MO-330/Air Force Manual No. 89-3*, 1971.
29. Teller, L.W., and Sutherland, E.C., "The Structural Design of Concrete Pavements -- Part 5: An Experimental Study of the Westergaard Analysis of Stress Condition in Concrete Pavement Slabs of Uniform Thickness," *Public Roads*, Vol. 23, No. 8, April-May-June, 1943.
30. Packard, R.G., "Design of Concrete Airport Pavement," *Portland Cement Association, Engineering Bulletin EB050.03P*, 1973.
31. Fischer, J.A., Thompson, M.R., Ioannides, A.M., and Barenberg, E.J., " K_R - The Resilient Modulus of Subgrade Reaction," presented at the 63rd Annual Meeting of the Transportation Research Board, Washington, D.C., January, 1984.
32. Kondner, R.L., "Hyperbolic Stress-Strain Response: Cohesive Soils," *Journal of the Soil Mechanics and Foundations Division, ASCE*, Vol. 89, No. SM1, January, 1963.
33. Ramberg, W., and Osgood, W.R., "Description of Stress-Strain Curves by Three Parameters," *Natl. Advis. Comm. Aeronaut., Tech. Note 902*, Washington, D.C., 1943.

34. Butterfield, R., and Georgiadis, M., "New Interpretation of Plate-Bearing Tests," Transportation Research Record No. 810, Transportation Research Board, 1981.
35. Burland, J.B., and Lord, J.A., "The Load-Deformation Behavior of Middle Chalk at Mundford, Norfolk: A Comparison Between Full Scale Performance and In-situ and Laboratory Measurements," In-situ Investigation of Soils and Rocks, British Geological Society, 1970.
36. Engesser, F., "Zur Theorie des Baugrundes," (Toward Subgrade Theory), Zentralblatt der Bauverwaltung, Berlin, Germany, 1893.
37. Butterfield, R. and Georgiadis, M., "Cyclic Plate Bearing Tests," Journal of Terramechanics, Vol. 17, No. 3, 1980.
38. Gibson, R.E., "Some Results Concerning Displacements and Stresses in a Non-Homogeneous Elastic Half-Space," Geotechnique, Vol. 17, No. 1, 1967. Correspondence: Vol. 18, No. 2; Vol. 19, No. 1.
39. Barker, W.R., and Brabston, W.N., "Development of a Structural Design Procedure for Flexible Airport Pavements," US Army Engineer Waterways Experiment Station, Vicksburg, Miss., Techn. Rep. S-75-17 (also, Rep. No. FAA-RD-74-199), September, 1975.
40. Parker, F., Barker, W.R., Gunkel, R.C., and Odom, E.C., "Development of a Structural Design Procedure for Rigid Airport Pavements," US Department of Transportation, Report No. FAA-RD-77-81, Washington, D.C., 1977.
41. Barker, W.R., "Introduction to a Rigid Pavement Design Procedure," Proceedings, Second International Conference on Concrete Pavement Design, Purdue University, April, 1981.
42. Federal Aviation Administration, "Airport Pavement Design and Evaluation," Advisory Circular 150/5320-60, Department of Transportation, Washington, D.C., December 7, 1978.
43. Barenberg, E.J., and Arntzen, D.M., "Design of Airport Pavements as Affected by Load Transfer and Support Conditions," Proceedings, Second International Conference on Concrete Pavement Design, Purdue University, April, 1981.
44. Arntzen, D.M., Barenberg, E.J., and Krauce, R., "Airfield Pavement Demonstration Validation Study," Transportation Engineering Journal, ASCE, Vol. 106, No. TE6, November, 1980.

45. Pickett, G., and Ai, D.K.Y., "Stresses in Subgrade Under Rigid Pavement," Proceedings, 33rd Annual Meeting, Highway Research Board, Washington, D.C., January, 1954.
46. Chou, Y.T., "Subgrade Contact Pressures Under Rigid Pavements," Transportation Engineering Journal, ASCE, Vol. 109, No. TE3, May, 1983. Discussion by A. M. Ioannides, submitted for publication, Transportation Engineering Journal, ASCE.
47. Zienkiewicz, O.C., "The Finite Element Method," 3rd Edition, McGraw-Hill, 1977.
48. Cook, R.D., "Concepts and Applications of Finite Element Analysis," Second Edition, John Wiley and Sons, 1981.
49. Runge, C., "Über eine Methode die partielle Differentialgleichung $Du = \text{Constans}$, numerisch zu integrieren," (On a Method to Numerically Integrate the Partial Differential Equation $Du = \text{Constant}$), Z. Math. Phys., Vol. 56, 1908.
50. Desai, C.S., and Christian, J.T., editors, "Numerical Methods in Geotechnical Engineering," McGraw-Hill, 1977.
51. Southwell, R.V., "Relaxation Methods in Theoretical Physics," Oxford University Press, London, 1946.
52. Allen, D.N. de G., "Relaxation Methods," McGraw-Hill, 1954.
53. Allen, D.N. de G., and Windle, D.W., "The Finite Difference Approach," in "Stress Analysis," O.C. Zienkiewicz and G.S. Holister (editors), John Wiley and Sons, 1965.
54. Morgenstern, D., "Herleitung der aus des dreidimensionalen Elastizitätstheorie," (Derivation from the Three-Dimensional Theory of Elasticity), Arch. Ration. Mech. Anal., Vol. 4, 1959.
55. Tabatabaie, A.M., Barenberg, E.J., and Smith, R.E., "Longitudinal Joint Systems in Slip-Formed Rigid Pavements, Volume II -- Analysis of Load Transfer Systems for Concrete Pavements," U.S. Department of Transportation, Report No. FAA-RD-79-4, II, November, 1979.
56. Wilson, E.L., "Solid SAP, A Static Analysis Program for Three-Dimensional Solid Structures," UC-SESM Report 71-19, Structural Engineering Laboratory, University of California, Berkeley, CA, 1969.

57. Irons, B.M., "Engineering Application of Numerical Integration in Stiffness Methods," Journal of American Institute of Aeronautics and Astronautics, Vol. 4, No. 11, 1966.
58. Wilson, E.L., and Pretorius, P.C., "A Computer Program for the Analysis of Prismatic Solids," UC-SESM Report 70-21, Structural Engineering Laboratory, University of California, Berkeley, CA, 1970.
59. Pretorius, P.C., "Design Considerations for Pavements Containing Soil-Cement Bases," Ph. D. Dissertation, University of California, Berkeley, CA, 1970.
60. Luther, M.S., Majidzadeh, K., and Chang, C.W., "A Mechanistic Investigation of Reflection Cracking," Proceedings, Second Conference on Asphaltic Pavements for South Africa (CAPSA 1974), Durban, South Africa, 1974.
61. Otte, E., "Analysis of a Cracked Pavement Base Layer," Transportation Research Record No. 725, Transportation Research Board, 1979.
62. Fossberg, P.E., Mitchell, J.K., and Monismith, C.L., "Cracking and Edge-Loading Effects on Stresses and Deflections in a Soil-Cement Pavement," Highway Research Record No. 379, Highway Research Board, 1972.
63. Lopez, L.A., "FINITE: An Approach to Structural Mechanics Systems," International Journal for Numerical Methods in Engineering, Vol. 11, 1977.
64. Lopez, L.A., Dodds, R.H., Jr., Rehak, D.R., and Urzua, J., "POLO-FINITE: A Structural Mechanics System for Linear and Nonlinear Analysis," Technical Report, University of Illinois at Urbana-Champaign, and University of Kansas, Lawrence, (no date).
65. Agbabian Associates, "Analytic Modeling of Rock-Structure Interaction," Volumes 1-3, prepared for Advanced Research Projects Agency, Bureau of Mines, Report No. AD-761-648, 649, 650, 1973.
66. Newmark, N.M., "Numerical Methods of Analysis of Bars, Plates, and Elastic Bodies," in "Numerical Methods of Analysis in Engineering," L.E. Grinter, editor, Mc Millan, 1949.
67. Ang, A.H.S., and Newmark, N.M., "A Numerical Procedure for the Analysis of Continuous Plates," Proceedings, Second Conference on Electronic Computation, Structural Division, ASCE, September, 1960.

68. Mahanyi, M.A., "Plates on Elastic Layers," Ph.D. Thesis, University of Illinois, Urbana, 1962.
69. Saxena, S.K., "Pavement Slabs Resting on Elastic Foundation," Highway Research Record No. 466, Highway Research Board, 1973.
70. Saxena, S.K., and Vesic, A.S., "Experimental Study of Slabs Resting on a Silty Clay Subgrade," Proceedings, 52nd Annual Meeting, Highway Research Board, Washington, D. C., 1973.
71. Hudson, W.R., and Matlock, H., "Discontinuous Orthotropic Plates and Pavement Slabs," Research Report 56-6, Center for Highway Research, University of Texas at Austin, May, 1966.
72. Hudson, W.R., and Matlock, H., "Analysis of Discontinuous Orthotropic Pavement Slabs Subjected to Combined Loads," Highway Research Record No. 131, Highway Research Board, 1966.
73. Stelzer, C.F., Jr., and Hudson, W.R., "A Direct Computer Solution for Plates and Pavement Slabs," Research Report 56-9, Center for Highway Research, University of Texas at Austin, 1967.
74. Ayyash, A.A., Hudson, W.R., and Treybig, H.J., "Effects of Cracks on Bending Stiffness in Continuous Pavements," Highway Research Record No. 407, Highway Research Board, 1972.
75. Chou, Y.T., "Structural Analysis Computer Programs for Rigid Multicomponent Pavement Structures with Discontinuities-WESLIQID and WESLAYER; Report 1: Program Development and Numerical Presentations; Report 2: Manual for the WESLIQID Finite Element Program; Report 3: Manual for the WESLAYER Finite Element Program," Technical Report GL-81-6, U. S. Army Engineer Waterways Experiment Station, May, 1981.
76. Huang, Y.H., and Wang, S.T., "Finite-Element Analysis of Concrete Slabs and its Implications for Rigid Pavement Design," Highway Research Record No. 466, Highway Research Board, 1973.
77. Huang, Y.H., and Wang, S.T., "Finite-Element Analysis of Rigid Pavements with Partial Subgrade Contact," Transportation Research Record No. 485, Transportation Research Board, 1974.
78. Tabatabaie, A.M., and Barenberg, E.J., "Finite-Element Analysis of Jointed or Cracked Concrete Pavements," Transportation Research Record No. 671, Transportation Research Board, 1978.

79. Tabatabaie-Raissi, A.M., "Structural Analysis of Concrete Pavement Joints," Ph.D. Thesis, University of Illinois, Urbana, 1977.
80. Timoshenko, S., and Woinowsky-Krieger, S., "Theory of Plates and Shells," Second Edition, McGraw-Hill, 1959.
81. Dawe, D.J., "A Finite Element Approach to Plate Vibration Problems," Journal of Mechanical Engineering Science, Vol. 7, No. 1, 1965.
82. Tabatabaie, A.M., and Barenberg, E.J., "Structural Analysis of Concrete Pavement Systems," Transportation Engineering Journal, ASCE, Vol. 106, No. TE5, September, 1980.
83. Thompson, M.R., Ioannides, A.M., Barenberg, E.J., and Fischer, J.A., "Development of a Stress Dependent Finite Element Slab Model," US Air Force Office of Scientific Research, Report No. TR-83-1061, Air Force Systems Command, USAF, Bolling AFB, D.C. 20332, May, 1983.
84. Pickett, G., Raville, M.E., Janes, W.C., and McCormick, F.J., "Deflections, Moments and Reactive Pressures for Concrete Pavements," Bulletin No. 65, Engineering Experiment Station, Kansas State College, October, 1951.
85. Kreger, W.C., "Computerized Aircraft Ground Flotation Analysis - Edge Loaded Rigid Pavement," Research Report No. ERR-FW-572, General Dynamics Corp., Fort Worth, TX, January, 1967.
86. Pickett, G., and Ray, G.K., "Influence Charts for Concrete Pavements," Transactions, ASCE, Vol. 116, 1951.
87. Huang, Y.H., "Finite Element Analysis of Slabs on Elastic Solids," Transportation Engineering Journal, ASCE, Vol. 100, No. TE2, May, 1974.
88. Cheung, Y.K., and Zienkiewicz, O.C., "Plates and Tanks on Elastic Foundations: An Application of Finite Element Method," International Journal of Solids and Structures, Vol. 1, 1965.
89. Huang, Y.H., and Deng, X.J., "Finite Element Analysis of Jointed Concrete Pavements," Transportation Engineering Journal, ASCE, Vol. 109, No. TE5, September, 1983.
90. Chou, Y.T., "Comparative Analyses of Rigid Pavements," Transportation Engineering Journal, ASCE, Vol. 109, No. TE5, September, 1983.

91. Wilson, E.L., "A Digital Computer Program for the Finite Element Analysis of Solids with Non-Linear Material Properties," Department of Civil Engineering, University of California, Berkeley, CA, 1965.
92. Barksdale, R.D. "Analysis of Layered Systems," School of Civil Engineering, Georgia Institute of Technology, 1969.
93. Duncan, J.M., Monismith, C.L., and Wilson, E.L., "Finite Element Analysis of Pavements," Highway Research Record No. 228, Highway Research Board, 1968.
94. Raad, L. and Figueroa, J.L., "Load Response of Transportation Support Systems," Transportation Engineering Journal, ASCE, Vol. 106, No. TE1, January, 1980.
95. Figueroa, J.L., "Resilient Based Flexible Pavement Design Procedure for Secondary Roads," Ph.D. Thesis, University of Illinois, Urbana, 1979.
96. Hoffman, M.S., and Thompson, M.R., "Mechanistic Interpretation of Nondestructive Pavement Testing Deflections," Civil Engineering Studies, Transportation Engineering Series No. 32, Illinois Cooperative Highway and Transportation Research Program Series No. 190, University of Illinois at Urbana-Champaign, June, 1981.
97. Suddath, L.P. and Thompson, M.R., "Load-Deflection Behavior of Lime-Stabilized Layers," Technical Report M-118, Construction Engineering Research Laboratory, 1975.
98. Traylor, M.R., "Nondestructive Testing of Flexible Pavements," Ph.D. Thesis, Department of Civil Engineering, University of Illinois, Urbana, 1979.
99. Figueroa, J.L. and Thompson, M.R., "Simplified ILLI-PAVE Based Structural Analyses of Flexible Pavement for Secondary Roads," Transportation Research Record No. 766, Transportation Research Board, 1980.
100. Thompson, M.R. and Figueroa, J.L., "Mechanistic Thickness Design Procedure for Soil-Lime Layers," Transportation Research Record No. 754, Transportation Research Board, 1980.
101. SHELL OIL Co., "BISAR: Bitumen Structures Analysis in Roads, User's Manual," Koninklijke/Shell - Laboratorium, Shell Research N.V., Amsterdam, 1978.

102. Peutz, M.G.F., Van Kempen, H.P.M., and Jones, A., "Layered Systems Under Normal Surface Loads," Highway Research Record No. 228, Highway Research Board, 1968.
103. Peutz, M.G.F., Jones, A., and Van Kempen, H.P.M., "Computer Program: Layered Systems Under Normal Surface Loads," Koninklijke/Shell - Laboratorium, Shell Research N.V., Amsterdam, (no date).
104. Michelow, J., "Analysis of Stresses and Displacements in an N-Layered Elastic System Under a Load Uniformly Distributed on a Circular Area," California Research Corporation, Richmond, CA, 1963.
105. Warren, H., and Dieckmann, W.L., "Numerical Computation of Stresses and Strains in a Multiple Layered Asphalt Pavement System," California Research Corporation, Richmond, CA, 1963.
106. Ahlborn, G., "Elastic Layered Systems with Normal Loads," Institute of Transportation and Traffic Engineering, University of California at Berkeley, 1972.
107. Ranck, F., and Barenberg, E.J., "MWELP: Multiple Wheel Elastic Layer Program," University of Illinois, November, 1972 (Unpublished).
108. Majidzadeh, K., Ilves, G.J., and Sklyut, H., "Mechanistic Design of Rigid Pavements - Vol. 1: Development of the Design Procedure, Final Report DTH11-9568 (Draft), November, 1983.
109. Majidzadeh, K., Ilves, G.J., and McComb, R., "Mechanistic Design of Rigid Pavements," Proceedings, Second International Conference on Concrete Pavement Design, Purdue University, April, 1981.
110. Meyerhof, G.G., "Load-Carrying Capacity of Concrete Pavements," Journal of the Soil Mechanics and Foundations Division, ASCE, Vol. 88, No. SM3, June, 1962.
111. Vesic, A.S., and Saxena, S.K., "Analysis of Structural Behavior of AASHO Road Test Rigid Pavements," NCHRP Report No. 97, Highway Research Board, 1970.
112. Ioannides, A.M., Barenberg, E.J., and Thompson, M.R., "Finite Element Model with Stress Dependent Support," presented at the 63rd Annual Meeting of the Transportation Research Board, Washington, D.C., January, 1984.

113. Ioannides, A.M., "ILLI-SLAB Study," Volumes 1-4, University of Illinois, July, 1981 (unpublished).
114. McArthur, G.R., editor, "An Introduction to the SCD Graphics System; The SCD Graphics Utilities; The System Plot Package," Technical Note NCAR-TN/166+IA, Scientific Computing Division, National Center for Atmospheric Research, Boulder, Colorado, 1981.
115. Przemieniecki, J.S., "Theory of Matrix Structural Analysis," McGraw-Hill, 1968.
116. Zienkiewicz, O.C., and Cheung, Y.K., "The Finite Element Method in Structural and Continuum Mechanics," McGraw-Hill, 1967.
117. Tabatabaie, A.M., and Barenberg, E.J., "Longitudinal Joint Systems in Slip-Formed Rigid Pavements, Volume III -- User's Manual," U.S. Department of Transportation, Report No. FAA-RD-79-4, III, November, 1979.
118. Lopez, L.A., "POLO--Problem Oriented Language Organizer," Journal of Computers and Structures, Vol. 2, 1972.
119. Rehak, D.R., and Lopez, L.A., "SCAN: A Tool for Translating Problem Oriented Languages," University of Illinois, CESL, February, 1982.
120. University of Illinois, CESL, "SCAN: User's Manual," September, 1976.
121. Scott, R.F., "Foundation Analysis," Prentice-Hall, 1981.
122. Westergaard, H.M., "Stresses in Concrete Runways of Airports," Proceedings, 19th Annual Meeting, Highway Research Board, Washington, D.C., 1939. Also in "Stresses in Concrete Runways of Airports," Portland Cement Association, Chicago, IL, December, 1941.
123. Westergaard, H. M., "Stress Concentrations in Plates Loaded over Small Areas," ASCE Transactions, Vol. 108, 1943. Also in ASCE Proceedings, Vol. 68, No. 4, April, 1942.
124. Barenberg, E.J., Personal Communication, 1983.
125. Yang, N.C., "Design of Functional Pavements," McGraw-Hill, 1972.
126. Westergaard, H.M., "Om Beregning af Plader paa elastik Underlag med saerligt Henblik paa Sporgsmaalet om Spaendinger i Betoneveje," (On the Design of Slabs on Elastic Foundation with

Special Reference to Stresses in Concrete Pavements), Ingenioren, Vol. 32, Copenhagen, 1923.

127. Bergstrom, S.G., Fromen, E., and Linderholm, S., "Investigation of Wheel Load Stresses in Concrete Pavements," Swedish Cement and Concrete Research Institute, Proceedings No. 13, Royal Institute of Technology, Stockholm, 1949.
128. Carlton, P.F., and Behrmann, R.M., "A Model Study of Rigid Pavement Behavior Under Corner and Edge Loadings," Proceedings, 35th Annual Meeting, Highway Research Board, Washington, D.C., 1956.
129. Westergaard, H.M., "Theory of Stresses in Road Slabs," Proceedings, 4th Annual Meeting, Highway Research Board, Washington, D.C., December, 1924 (published 1925).
130. Goldbeck, A.T., "Thickness of Concrete Slabs," Public Roads, Vol. 1, No. 12, April, 1919.
131. Older, C., "Highway Research in Illinois," Transactions, ASCE, Vol. 87, 1924. Also in Proceedings, ASCE, February, 1924.
132. Westergaard, H.M., "What is Known of Stresses," Engineering News Record, January, 1937.
133. Kelley, E.F., "Application of the Results of Research to the Structural Design of Concrete Pavement," Public Roads, Vol. 20, No. 5, July, 1935; Vol. 20, No. 6, August, 1939. Also in Journal of American Concrete Institute, June, 1939.
134. Pickett, G., "Concrete Pavement Design: Appendix III - A Study of Stresses in the Corner Region of Concrete Pavement Slabs Under Large Corner Loads," Portland Cement Association, 1946; 1951.
135. Bradbury, R.D., "Reinforced Concrete Pavements," Wire Reinforcement Institute, Washington, D.C., 1938.
136. Spangler, M.G., "Stresses in the Corner Region of Concrete Pavements," Bulletin 157, Engineering Experiment Station, Iowa State College, Ames, Iowa, 1942.
137. Frey, P., "Development of a Finite Element Based Expression to Predict Maximum Corner Loading Stresses in a Uniformly Supported Rigid Pavement on an Elastic Subgrade," University of Illinois, Urbana, 1983 (unpublished).
138. Ladd, C.C., and Foott, R., "New Procedure for Stability of Soft Clays," Journal of the Geotechnical Engineering Division, ASCE, Vol. 100, No. GT7, July, 1974.

139. Borowicka, H., "Druckverteilung unter Elastischen Platten," (Pressure Distribution under Elastic Plates), Ingenieur Archiv, Vol. 10, No. 2, 1939.
140. Barden, L., "Distribution of Contact Pressure Under Foundations," Geotechnique, Vol. 12, No. 3, September, 1962.
141. Ramanathan, B., "A New Concept for the Relative Rigidity of Rafts," Numerical Methods in Geomechanics, C.S. Desai, editor, ASCE, Vol. 1, 1976.
142. Holmberg, A., "Cirkulära plattor med jämnt fördelad last på elastiskt underlag," (Circular Plates Under Uniformly Distributed Loads on an Elastic Foundation), Betong, No. 1, 1946.
143. Habel, A., "Die auf dem elastisch-isotropen Halbraum aufruhende zentralsymmetrisch belastete elastische Kreisplatte," (Elastic Circular Plates, Axisymmetrically Loaded, Resting on an Elastic, Isotropic Half-Space), Der Bauingenieur, Vol. 18, No.15/16, 1937.
144. Brown, P.T., "Numerical Analyses of Uniformly Loaded Circular Rafts on Deep Elastic Foundations," Geotechnique, Vol. 19, 1969.
145. Holl, D.L., "Thin Plates on Elastic Foundations," Proceedings, 5th International Congress on Applied Mechanics, Cambridge, Mass., 1938 (published 1939).
146. Hogg, A.H.A., "Equilibrium of a Thin Slab on an Elastic Foundation of Finite Depth," The London, Edinburgh and Dublin Philosophical Magazine and Journal of Science, Series 7, Vol. 35, April, 1944.
147. Barenberg, E.J., "Mathematical Modeling of Pavement Systems: State-of-the-Art," Proceedings, Allerton Park Conference on Systems Approach to Airfield Pavements, March, 1970. Published in CERL, Techn. Report P-5, June, 1973.
148. Pickett, G., and McCormick, F.J., "Circular and Rectangular Plates Under Lateral Load and Supported by an Elastic Solid Foundation," Proceedings, First US National Congress of Applied Mechanics, Illinois Institute of Technology, Chicago, IL, June, 1952.
149. Pickett, G., and Janes, W.C., "Bending Under Lateral Load of a Circular Slab on an Elastic Solid Foundation," Proceedings, First Midwestern Conference on Solid Mechanics, University of Illinois, Urbana, April, 1953.

150. Naghdi, P.M, and Rowley, J.C., "On the Bending of Axially Symmetric Plates on Elastic Foundations," Proceedings, First Midwestern Conference on Solid Mechanics, University of Illinois, Urbana, April, 1953.
151. Poulos, H.G., and Davis, E.H., "Elastic Solutions for Soil and Rock Mechanics," John Wiley and Sons, 1974.
152. Pickett, G., Badaruddin, S., and Ganguli, S.C., "Semi Infinite Pavement Slab Supported by an Elastic Solid Subgrade," Proceedings, First Congress on Theoretical and Applied Mechanics, Indian Institute of Technology, November, 1955.
153. Pickett, G., and Badaruddin, S., "Influence Chart for Bending of a Semi-Infinite Pavement Slab," Proceedings, 9th International Congress on Applied Mechanics, Vol. 6, Universite de Bruxelles, 1956 (published 1957).
154. Svec, O.J., "Thick Plates on Elastic Foundations by Finite Elements," Journal of the Engineering Mechanics Division, ASCE, Vol. 102, No. EM3, June, 1976.
155. Schleicher, F., "Zur Theorie des Baugrundes," (Toward Subgrade Theory), Der Bauingenieur, 1926.
156. Roark, R.J., "Formulas for Stress and Strain," McGraw-Hill, 1938.
157. Costigan, R.R., "Response and Performance of Contingency Airfield Pavements Containing Stabilized Material Layers," Ph.D. Thesis, University of Illinois, Urbana, 1984.
158. Thompson, M.R., and Dempsey, B.J., "Development of Preliminary ALRS Stabilized Material Pavement Analysis System (SPAS)," Technical Report ESL-TR-83-84, USAF Engineering and Services Center, Tyndall AFB, Florida, March, 1984.
159. Boussinesq, M.J., "Application des Potentiels a l'etude de l'equilibre et du mouvement des solides elastiques, principalement au calcul des deformations et des pressions que produisent, dans ces solides, des efforts quelconques exercees sur une petite partie de leur surface ou de leur interieur: Memoire suivi de notes etendues sur divers points de physique mathematique et d'analyse," (Application of Potential to the Study of the Equilibrium and Movement of Elastic Solids, Particularly the Calculation of Deformations and Stresses Produced Within Such Solids, by Some Load Applied Upon a Small Portion of Their Surface or Their Interior: Continuous Paper from Extensive Notes on Diverse Points of Physical Mathematics and Analysis), Gauthier-Villars, Paris, 1885.

160. Giroud, J.P., "Settlement of a Linearly Loaded Rectangular Area," Journal of the Soil Mechanics and Foundations Division, ASCE, Vol. 94, No. SM4, July, 1968.
161. Harr, M.E., "Foundations of Theoretical Soil Mechanics," McGraw-Hill, 1966.
162. Cheung, Y.K., and Nag, D.K., "Plates and Beams on Elastic Foundations - Linear and Non-Linear Behavior," Geotechnique, Vol. 18, No. 2, June, 1968.
163. Wang, S.K., Sargious, M., and Cheung, Y.K., "Advanced Analysis of Rigid Pavements," Transportation Engineering Journal, ASCE, Vol. 98, No. TE1, 1972. Discussion: Vol. 99, No. TE1; Vol. 99, No. TE3.
164. Huang, Y.H., "Rectangular Plates Partially Supported On Elastic Half Space," Proceedings International Conference on Computational Methods in Nonlinear Mechanics, University of Texas at Austin, September, 1974.
165. Cheung, M.S., "A Simplified Finite Element Solution for the Plates on Elastic Foundation," Computers and Structures, Vol. 8, No. 1, February, 1978.
166. Huang, Y.H., "Analysis of Symmetrically Loaded Slab on Elastic Solid," Technical Note, Transportation Engineering Journal, ASCE, Vol. 100, No. TE2, May, 1974.
167. Svec, O.J., and McNeice, G.M., "Finite Element Analysis of Finite Sized Plates bonded to an Elastic Half Space," Computer Methods in Applied Mechanics and Engineering, Vol. 1, 1972.
168. Svec, O.J., and Gladwell, G.M.L., "An Explicit Boussinesq Solution for a Polynomial Distribution of Pressure Over a Triangular Region," Journal of Elasticity, Vol. 1, No. 1, June, 1971.
169. Svec, O.J., and Gladwell, G.M.L., "A Triangular Plate Bending Element for Contact Problems," International Journal of Solids and Structures, Vol. 9, 1973.
170. Svec, O.J., "A Finite Element Approach to the Problem of a Plate on the Elastic Half-Space," Ph.D. Thesis, University of Waterloo at Waterloo, Canada, 1972.
171. Kerr, A.D., "On the Derivation of Well Posed Boundary Value Problems in Structural Mechanics," International Journal of Solids and Structures, Vol. 12, 1976.

- 172. Yang, T.Y., "A Finite Element Analysis of Plates on a Two Parameter Foundation Model," Computers and Structures, Vol. 2, No. 4, 1972.
- 173. Severn, R.T., "The Solution of Foundation Mat Problems by Finite Element Methods," The Structural Engineer, Vol. 44, No. 6, London, June, 1966.
- 174. Yang, H.T.Y., "Flexible Plate Element on Elastic Foundation," Journal of the Structural Division, ASCE, Vol. 96, No. ST10, October, 1970.
- 175. Zhaohua, F., and Cook, R.D., "Beam Elements on Two-Parameter Elastic Foundations," Journal of the Engineering Mechanics Division, ASCE, Vol. 109, No. EM6, December, 1983.
- 176. Jones, R., and Xenophontos, J., "The Vlasov Foundation Model," International Journal of Mechanical Science, Vol. 19, No. 6, 1977.
- 177. Harr, M.E., Davidson, J.L., Ho, D.M., Pombo, L.E., Ramaswamy, S.V., and Rosner, J.C., "Euler Beams on a Two-Parameter Foundation Model," Journal of the Soil Mechanics and Foundations Division, ASCE, Vol. 95, No. SM4, July, 1969.
- 178. Donnelly, J., and Conroyd, J., "Development of Vlasov Subgrade Finite Element Model," University of Illinois, 1984 (unpublished).

END

FL. W. D

4-85

DTIC

Long

AD-A150 985

ANALYSIS OF SLABS-ON-GRADE FOR A VARIETY OF LOADING AND
SUPPORT CONDITION..(U) ILLINOIS UNIV AT URBANA DEPT OF
CIVIL ENGINEERING A M IOANNIDES ET AL. DEC 84
AFOSR-TR-85-0083 AFOSR-82-0143

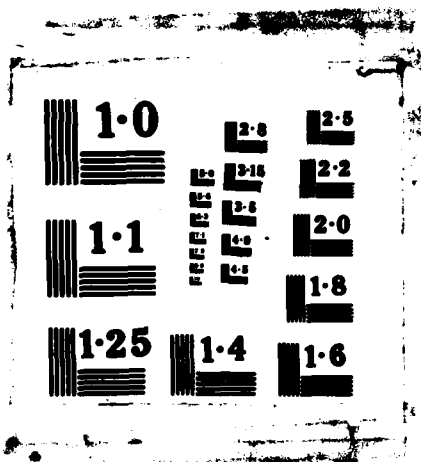
77

UNCLASSIFIED

F/O 13/2

NL

	Supplemental			END DATE 5 86
	Information			



SUPPLEMENTARY

INFORMATION

UNCLASSIFIED

SECURITY CLASSIFICATION OF THIS PAGE

REPORT DOCUMENTATION PAGE

1a. SECURITY CLASSIFICATION UNCLASSIFIED		1b. RESTRICTIVE MARKINGS	
2a. SECURITY CLASSIFICATION AUTHORITY		3. DISTRIBUTION/AVAILABILITY OF REPORT Approved for Public Release; Distribution Unlimited.	
2b. DECLASSIFICATION/DOWNGRADING SCHEDULE		5. MONITORING ORGANIZATION REPORT NUMBER(S) AFOSR-TR- 85-0088	
4. PERFORMING ORGANIZATION REPORT NUMBER(S)		7a. NAME OF MONITORING ORGANIZATION AFOSR/NA	
6a. NAME OF PERFORMING ORGANIZATION UNIVERSITY OF ILLINOIS AT URBANA-CHAMPAIGN		7b. ADDRESS (City, State and ZIP Code) Bolling AFB, DC 20332	
6b. OFFICE SYMBOL (If applicable)		9. PROCUREMENT INSTRUMENT IDENTIFICATION NUMBER AFOSR-82-0143	
8a. NAME OF FUNDING/SPONSORING ORGANIZATION AIR FORCE OFFICE OF SCIENTIFIC RESEARCH		10. SOURCE OF FUNDING NOS. PROGRAM ELEMENT NO. 61102F PROJECT NO. 2307 TASK NO. C1 WORK UNIT NO.	
8b. OFFICE SYMBOL (If applicable) AFOSR/NA		11. TITLE (Include Security Classification) ANALYSIS OF SLABS- ON-GRADE FOR A VARIETY OF SUPPORT CONDITIONS (UNCLASSIFIED)	
8c. ADDRESS (City, State and ZIP Code) BOLLING AFB, DC 20332		12. PERSONAL AUTHOR(S) IC DES, A. M., DONNELLY, J., THOMPSON, M., BARENBERG, E.	
13a. REPORT ANNUAL		14. DATE OF REPORT (Month, Year, Day) December 1984	
13b. TIME COVERED FROM 1 MAY 83 TO 30 SEP 84		15. PAGE COUNT 561	
6. SUPPLEMENTARY NOTATION			

7. COSATI CODES			18. SUBJECT TERMS (Continue on reverse if necessary and identify by block number)	
FIELD	GROUP	SUB GR.	PAVEMENTS SLAB MODEL FINITE ELEMENT SLAB MODEL	
			PAVEMENT ANALYSIS SUBGRADE SUPPORT	

9. ABSTRACT (Continue on reverse if necessary and identify by block number)

This study is concerned with analytical and numerical procedures applied to slab-on-grade pavements, treated as plates on elastic foundation, with particular emphasis on the possibilities offered by the automated digital computer. In the first part of the report, analyses employing the dense liquid foundation are examined. This includes an exhaustive reexamination of Westergaard's work, which established conclusively the correct form of the Westergaard equations and pointed out that the "New" edge stress formula should be used. Closed-form solutions for a plate on a dense liquid or an elastic solid foundation are assembled in a computerized compendium called WESTER.

(Continued)

19. DISTRIBUTION/AVAILABILITY OF ABSTRACT UNCLASSIFIED/UNLIMITED <input checked="" type="checkbox"/> SAME AS RPT. <input type="checkbox"/> DTIC USERS <input type="checkbox"/>		21. ABSTRACT SECURITY CLASSIFICATION UNCLASSIFIED	
22. NAME OF RESPONSIBLE INDIVIDUAL Lt Col Lawrence D Hokanson		23. OFFICE SYMBOL AFOSR/NA	

UNCLASSIFIED

SECURITY CLASSIFICATION OF THIS PAGE

ADDP 150165
TR-85-0083

BLOCK 19 - CONTINUED

The second part of the study focuses on elastic solid analyses of the same problem. Pickett's Chart for edge stress is recalculated using computerized numerical integration, and the result is incorporated in computer program H5IES. Three additional computer codes are developed:

- (i) A method using the concept of concordant deflections for axisymmetric plates (program CFES);
- (ii) A finite difference approach for rectangular plates (program FIDIES);
- (iii) A finite element solution for rectangular plates (incorporated into program ILLI-SLAB).

Formulations for finite element analysis of a plate on a two-parameter foundation and on a stress dependent (resilient) subgrade are also derived and incorporated into ILLI-SLAB. Thus, ILLI-SLAB becomes the first computer program to accommodate several subgrade support characterization models in a usable package. Very interesting comparisons of the behavior of each foundation are presented.

Using the programs developed, predictive expressions for maximum responses under edge and corner loading of a plate on an elastic solid are derived. The efficient and fruitful utilization of these computer codes is ensured by adherence to guidelines established during several convergence studies.

UNCLASSIFIED

SECURITY CLASSIFICATION OF THIS PAGE

DATE
FILMED
-8